Gisela Grupe · Andrea Grigat
George C. McGlynn *Editors*

Across the Alps in Prehistory

Isotopic Mapping of the Brenner Passage by Bioarchaeology

Springer

Across the Alps in Prehistory

Gisela Grupe • Andrea Grigat •
George C. McGlynn
Editors

Across the Alps in Prehistory

Isotopic Mapping of the Brenner Passage by Bioarchaeology

Springer

Editors
Gisela Grupe
LMU München Biozentrum Martinsried
Martinsried, Bayern
Germany

Andrea Grigat
Staatssammlung f. Anthropologie und Paläoanatomie
München, Bayern
Germany

George C. McGlynn
Staatssammlung f. Anthropologie und Paläoanatomie
München, Bayern
Germany

ISBN 978-3-319-41548-2 ISBN 978-3-319-41550-5 (eBook)
DOI 10.1007/978-3-319-41550-5

Library of Congress Control Number: 2017931392

Printed on acid-free paper

This Springer imprint is published by Springer Nature
The registered company is Springer International Publishing AG
The registered company address is: Gewerbestrasse 11, 6330 Cham, Switzerland

Preface

Understanding the history of anatomically modern *Homo sapiens* requires an evaluation of the multiple factors that determine human population development in time and space. This includes insights into processes such as mobility, migration, population admixture and cultural exchange and transfer. While written documentation and the archaeological remains of the material culture both provide clues to these topics, information contained in the bodily remains of the people who once either took an active part in these processes or were merely confronted with them during their lifetime has yet to be fully exploited. The analysis of preserved DNA molecules permits the evaluation of genetic and genealogical relationships, but the genetic make-up of a past people hardly permits access to behavioural aspects of these once-living individuals and their populations.

The majority of human and animal tissues that are preserved over time consists mainly of skeletal remains which are regularly excavated from burial sites, settlements or other places. Inhumations recovered from large civilian, common burial sites are usually representative of a significant proportion of the past local population and permit the reconstruction of demographic parameters such as age- and sex-specific mortality, life expectancy at birth and stature, amongst others. Special burial constructions, grave goods or different burial rites may be due to biological (age at death, sex) or social features, including different provenance and therefore "foreignness". For the majority of the dead on a common burial site however, the material culture does not provide this information or may remain ambiguous. As a result, the extent of population admixture in a settlement chamber mostly remains unknown, let alone the assessment of places of provenance of primarily non-local individuals. With regard to the parameters which are of influence on human population development including potential social, cultural and political implications, extent and direction of immigration and emigration are highly significant.

Humans have always been mobile, and exogamy is only part of this behaviour. Based on numerous historical and pre-industrial population studies and census, palaeodemographic studies consider a proportion of up to 10 % as a reasonable figure for the percentage of non-local individuals buried at a common cemetery. Therefore, this figure may also be assumed for prehistoric times, but is it applicable for all times and different populations and social systems? And how did geographic

barriers such as large rivers and high mountains influence mobility and migration in the past? What were the implications for import, trade and exchange? These questions need answers formulated under consideration of pertinent circumstances such as time, geography, climate, culture, technology and availability of raw materials, just to name some of the influential parameters that can exercise.

Today bioarchaeological sciences have the ability to analyse human and faunal remains at the elemental and molecular level to achieve a better understanding of life histories, spatial movement and population distributions in prehistory. The desire and related scientific efforts for a better understanding of spatial movements and the resulting distribution of humans, animals and cultural features in prehistory stimulated the bioarchaeological sciences to take a closer look at the bodily relics of former populations in an attempt to decipher individual and collective life histories that are hidden in the chemical composition of skeletal finds. In the course of the last decades, substantial research progress has been achieved in the field of radiogenic isotopes, in particular, the $^{87}Sr/^{86}Sr$ isotopic system examined in bones and teeth. The detection of primarily non-local individuals by stable strontium isotopic ratios was regularly employed, and the method enjoyed high status amongst researchers. It was even occasionally viewed as being superior to every other method for the identification of immigrants or imported animals. While researchers involved in this field rapidly became aware of its limitations, it took again some years until it was generally acknowledged that the spatial variability of stable isotopic ratios of a single element such as strontium can be highly redundant. The elemental concentrations and isotopic ratios in the skeleton are highly dependent on a wide variety of environmental and metabolic parameters, yet the fields of archaeology and bioarchaeology were astonishingly slow in accepting this fact. Hypothesis building and the investigation of tracer systems such as stable isotopic ratios benefited substantially from the understanding that such complex issues necessitate an interdisciplinary networking and discourse.

Parallel to this development, attempts were made to overcome the spatial redundancy of single stable isotopic ratios such as the geodependent $^{87}Sr/^{86}Sr$ by measuring more than one isotopic signature in a skeletal find. Stable lead isotopes also rely on geological features, stable oxygen isotopic ratios are related to hydrological cycles, and stable carbon and nitrogen isotopic ratios reflect environmental conditions including dietary preferences and subsistence strategies. Such "multi-isotope fingerprints" are no doubt informative, but it becomes increasingly more difficult to extract the relevant information. The uptake and turnover of elements in organisms are under physiological control. Due to the rather long biological half-life of skeletal and dental tissue, element uptake and incorporation of stable isotopes not only accumulate over years in large mammals but in addition exhibit considerable reservoir effects in the individual body. Therefore, the evaluation of element source, concentration and proportional contribution to a "global" stable isotopic ratio in a skeleton can be very tricky and necessitates mathematical approaches beyond conservative multivariate statistics.

Bioarchaeology is always confronted with the additional problem of tissue decomposition. Element uptake by contamination and element loss by leaching in

the course of long inhumation periods are common processes and may totally obscure the original isotopic signature of a bone or tooth. Mass spectrometers provide very exact measurements, but how can the biological signal be differentiated from the diagenetic one? As long as the research substrate is a biomolecule such as the skeletal structural protein collagen, molecular biological methods such as amino acid sequencing for the purpose of authentication are at hand. Presently, deciphering between local and non-local individuals however is best achieved by stable isotopic signatures in the bioapatite. Methods for the authentication of the mineral integrity of an archaeological skeletal find have been the subject of intense discussion for years, yet still no commonly agreed upon catalogue for quality control criteria exists.

This is an unfortunate knowledge gap, especially with regard to the inhumation practice of cremating the dead, which was performed at different times in prehistory worldwide. On the European continent, cremating the dead was the primary if not exclusive burial custom from the Bronze Age until late Roman Times. The majority of human remains originating from this period, which spans approximately 1500 years are preserved as cremations. Exposure to high temperatures not only leads to a full combustion of all organic skeletal components but at the same time to a high degree of fragmentation and distortion of the remaining mineralized parts. Morphological examinations of cremated bones must be conducted by skilled and experienced osteologists. Archaeometric analyses of cremations still constitute a sort of "terra incognita". Stable isotope analysis of cremated bones and teeth not only requires the differentiation between diagenetic artefacts and original isotopic signals but also an evaluation of possible high temperature artefacts.

In 2012, the project "Transalpine Mobility and Culture Transfer", an interdisciplinary research network, was granted by the German Science Foundation (www.for1670-transalpine.uni-muenchen.de). This project focuses explicitly on some of the pertinent open questions mentioned above: to overcome the spatial redundancy of single isotopic ratios by establishing a multi-isotope fingerprint for archaeological skeletal finds and resolve this multidimensional information in terms of ecogeographic provenance, to subject every sample to an in-depth mineralogical characterization for the authentication of the measured stable isotopic ratios and to specifically investigate the research potential of cremated finds for prehistoric migration research. To accomplish this, a geographical reference area of eminent archaeological importance was chosen, namely, the Inn-Eisack-Adige passage via the Brenner Pass in the European Alps. The multi-isotope fingerprint consists of the following stable isotope ratios measured in the bioapatite of archaeological skeletal finds: $\delta^{18}O_{phosphate}$, $^{87}Sr/^{86}Sr$, $^{206}Pb/^{204}Pb$, $^{207}Pb/^{204}Pb$, $^{208}Pb/^{204}Pb$, $^{208}Pb/^{207}Pb$ and $^{206}Pb/^{207}Pb$. Isotopic mapping was performed by analysis of archaeological bones of large vertebrates, in particular, cattle, pig and red deer, known to have resided in the area. This book summarizes the results achieved after completion of the first three-year phase of this project which are prerequisite for the application of the resulting isotopic map of the specific alpine transect to open questions related to prehistoric mobility and culture transfer. Because of the intended evaluation of the

research potential of cremated finds, the project's archaeological sub-groups are dedicated to periods dating from the Urnfield Period until Imperial Roman Times.

While this project does not claim to solve every problem, the interdisciplinary research group aims at a significant contribution with regard to the reference area chosen. Scientific fields involved include archaeology, archaeozoology, computer sciences, crystallography, geology and physical anthropology, which altogether created a network aiming at the establishment of a large database and computational methods which will be made public by worldwide data sharing. The general structure of this network is visualized by Fig. 1 and is reflected in the structure of this book.

Although the European Alps constitute an imposing geographical boundary separating central Europe and the Mediterranean regions, they have nevertheless been crossed by humans since the Neolithic. The reference area chosen in this project was in use since the ninth millennium BCE, evidenced by numerous finds related to hunter/gatherer populations. The fact that resting places and artefacts were found at altitudes exceeding 1800 m a.s.l., and that stone tools had been manufactured from raw material stemming from different regions, is proof for a successful adaptation of Stone Age human populations to these special ecogeographical regions. Archaeological evidence for transalpine mobility and trade since the Mesolithic is the topic of chapter "Transalpine Mobility and Trade

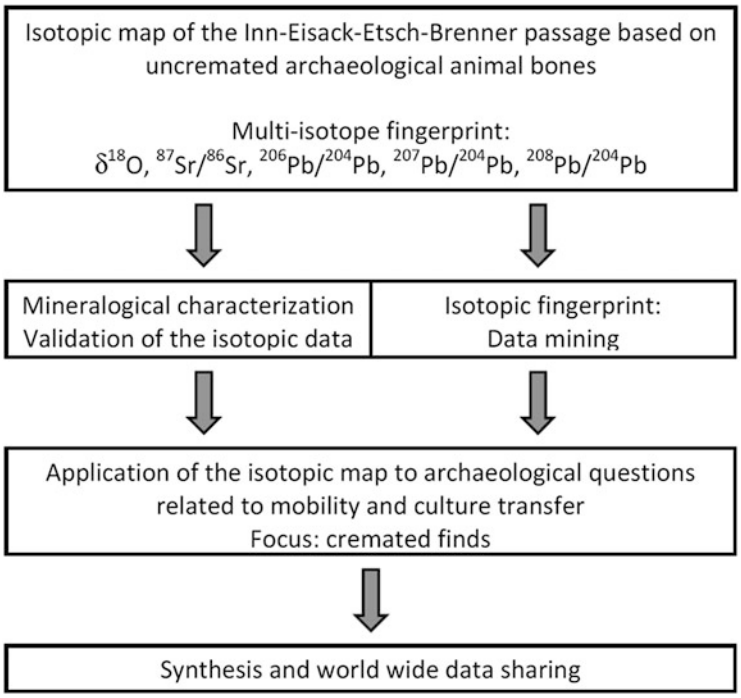

Fig. 1 Contextual and methodological structure of the project

since the Mesolithic". An important and strongly related issue is the archaeological concept distinguishing mobility from migration. Telling local from non-local individuals by stable isotopic signatures in skeletal finds needs to refer to the spatial distribution of geodependent and hydrology-dependent isotopic ratios in the reference area. Isotopic maps give clues to this, but do not yet fulfil the concept of an "isotopic landscape", a valuable tool in modern sciences such as ecogeography, wildlife conservation and others. How modern bioarchaeological research differs from the notion of "isotopic landscapes", and how far bioarchaeology has proceeded to reach this goal, is described in chapter "The Concept of Isotopic Landscapes: Modern Ecogeochemistry versus Bioarchaeology". In our project, isotopic mapping was achieved by stable isotope analysis of contemporary archaeofaunal finds from three different species of large residential vertebra. Drawing upon archaeological and archaeozoological data, chapter "Early Roman Transfer of Animals Across the Alps: Setting the Stage for Interpreting the Results of Isotope Fingerprinting" provides insight into the cultural phenomenon of animal transfer across the Alps in early Roman times. This contribution clearly illustrates that mobility and migration/trade are not only an issue in human population development but are equally important in livestock species valued economically in the northern Alpine foreland. Based on archaeological findings dating to the late first century BCE and the first century CE, the paper also outlines the needs of and the logistical basis for (supra-)regional trade of goods subsequent to the Roman conquest, thereby setting the stage for interpreting the results of isotope fingerprinting scheduled for the second project phase.

Archaeometrical methods such as mass spectrometry produce data which are very exact in terms of measurement precision. As stated above, diagenesis is likely to obscure the original, biological stable isotopic signatures of a find. A mineralogical validation of the quantitative purification of the bioapatite through appropriate sample processing protocols is indispensable. This and the changes induced in the bioapatite by diagenesis and high temperature exposure are addressed in chapter "The Crystalline State of Archaeological Bone Material". A multi-isotope fingerprint necessitates multivariate statistics for its analysis. Chapter "The Isotopic Fingerprint: New Methods of Data Mining and Similarity Search" summarizes the results obtained by application of modern data mining techniques such as EM clustering and its implications for provenance analysis. Such model procedures under consideration of the proxy character of stable isotopic signatures in bioarchaeological finds constitute a valuable tool on the way to the establishment of an "archaeobiological isotopic landscape". Finally, chapter "Isotopic Map of the Inn-Eisack-Adige-Brenner Passage and its Application to Prehistoric Human Cremations" is dedicated to the results achieved after three years of interdisciplinary networking for the isotopic mapping of one of the most important transalpine routes in prehistory. This chapter also shows that cremated skeletal finds, whether human or animal, constitute a suitable substrate for migration research in prehistory. This is the ultimate prerequisite for finding answers to persisting archaeological questions related to human mobility/migration behaviour with or without accompanying culture transfer. How this will be performed, and how the database

established in the frame of the project can be made public for users worldwide, is subject of the closing chapter "Current Synthesis and Future Options".

This project would not have been possible without generous financial support by the Deutsche Forschungsgemeinschaft. Interdisciplinary networking greatly benefited from the specific platform of the ArchaeoBioCenter of the Ludwig Maximilian University in Munich (www.archaeobiocenter.uni-muenchen.de). We are most indebted to Springer Publisher for giving us the opportunity to publish the results achieved in the first phase of our project in the form of this book.

Martinsried, Germany Gisela Grupe
June 2016

Contents

Transalpine Mobility and Trade since the Mesolithic 1
Carola Metzner-Nebelsick, Amei Lang, C. Sebastian Sommer, and Bernd Steidl

The Concept of Isotopic Landscapes: Modern Ecogeochemistry versus Bioarchaeology 27
Gisela Grupe, Stefan Hölzl, Christoph Mayr, and Frank Söllner

Early Roman Transfer of Animals Across the Alps: Setting the Stage for Interpreting the Results of Isotope Fingerprinting 49
Joris Peters, Markus Gschwind, Ferdinand Neuberger, Bernd Steidl, and Simon Trixl

The Crystalline State of Archaeological Bone Material 75
Wolfgang W. Schmahl, Balazs Kocsis, Anita Toncala, Dominika Wycisk, and Gisela Grupe

The Isotopic Fingerprint: New Methods of Data Mining and Similarity Search 105
Markus Mauder, Eirini Ntoutsi, Peer Kröger, and Hans-Peter Kriegel

Isotopic Map of the Inn-Eisack-Adige-Brenner Passage and its Application to Prehistoric Human Cremations 127
Anita Toncala, Frank Söllner, Christoph Mayr, Stefan Hölzl, Karin Heck, Dominika Wycisk, and Gisela Grupe

Current Synthesis and Future Options 229
Gisela Grupe, Martin Grünewald, Markus Gschwind, Stefan Hölzl, Peer Kröger, Amei Lang, Christoph Mayr, George C. McGlynn, Carola Metzner-Nebelsick, Ferdinand Neuberger, Joris Peters, Simone Reuß, Wolfgang Schmahl, Frank Söllner, C. Sebastian Sommer, Bernd Steidl, Simon Trixl, and Dominika Wycisk

Index 251

Contributors

Gisela Grupe Biozentrum, Ludwig-Maximilians-Universität, Martinsried, Germany

Martin Grünewald LVR-Amt für Bodendenkmalpflege im Rheinland, Titz, Germany

Markus Gschwind Bayerisches Landesamt für Denkmalpflege, Munich, Germany

Karin Heck RieskraterMuseum Nördlingen, Nördlingen, Germany

Stefan Hölzl RieskraterMuseum Nördlingen, Nördlingen, Germany

Balazs Kocsis Sektion Kristallographie, Ludwig-Maximilians-Universität, Munich, Germany

Hans-Peter Kriegel Institute for Informatics, Ludwig-Maximilians-Universität München, Munich, Germany

Peer Kröger Lehr- und Forschungseinheit für Datenbanksysteme, Ludwig-Maximilians-Universität, Munich, Germany

Amei Lang Institut für Vor- und Frühgeschichtliche Archäologie und Provinzialrömische Archäologie, Ludwig-Maximilians-Universität München, Munich, Germany

Markus Mauder Institute for Informatics, Ludwig-Maximilians-Universität München, Munich, Germany

Christoph Mayr Institut für Geographie, Friedrich-Alexander-Universität, Erlangen, Germany

GeoBio-Center & Paläontologie und Geobiologie, Ludwig-Maximilians-Universität, Munich, Germany

George C. McGlynn Staatssammlung für Anthropologie und Paläoanatomie, Munich, Germany

Carola Metzner-Nebelsick Institut für Vor- und Frühgeschichtliche Archäologie und Provinzialrömische Archäologie, Ludwig-Maximilians-Universität München, Munich, Germany

Ferdinand Neuberger Institut für Paläoanatomie, Domestikationsforschung und Geschichte der Tiermedizin, Ludwig-Maximilians-Universität, Munich, Germany

Eirini Ntoutsi Faculty of Electrical Engineering and Computer Science, Leibniz Universität, Hannover, Germany

Joris Peters Institut für Paläoanatomie, Domestikationsforschung und Geschichte der Tiermedizin, Ludwig-Maximilians-Universität, Munich, Germany

Simone Reuß Institut für Vor- und Frühgeschichtliche Archäologie und Provinzialrömische Archäologie, Ludwig-Maximilians-Universität München, Munich, Germany

Wolfgang W. Schmahl Sektion Kristallographie, Ludwig-Maximilians-Universität, Munich, Germany

Frank Söllner Department für Geo- und Umweltwissenschaften, Ludwig-Maximilians-Universität, Munich, Germany

C. Sebastian Sommer Bayerisches Landesamt für Denkmalpflege, Munich, Germany

Bernd Steidl Archäologische Staatssammlung, Munich, Germany

Anita Toncala Biozentrum, Ludwig-Maximilians-Universität, Martinsried, Germany

Simon Trixl Institut für Paläoanatomie, Domestikationsforschung und Geschichte der Tiermedizin, Ludwig-Maximilians-Universität, Munich, Germany

Dominika Wycisk Biozentrum, Ludwig-Maximilians-Universität, Martinsried, Germany

Transalpine Mobility and Trade since the Mesolithic

Carola Metzner-Nebelsick, Amei Lang, C. Sebastian Sommer, and Bernd Steidl

Abstract

The European Alps, separating Central Europe from the Mediterranean, were chosen as a reference region for the establishment of an isotopic map and a scientific approach towards bioarchaeological isotopic landscapes. The high ecogeographical diversity of this region constitutes both an opportunity and a challenge for such a project. The geographical boundary has been crossed since the Mesolithic, and ample archaeological evidence is proof for a highly successful adaptation of the Stone Age and later prehistoric human populations to this special environment. Transalpine mobility and trade since prehistory provides the indispensable contextual framework for related migration studies in bioarchaeology.

This chapter provides an overview of the archaeological record in the reference area from the Mesolithic until Roman times, with emphasis on the Inn-Eisack-Adige passage via the Brenner Pass. First exploited for raw materials such as silex and rock crystal, the Alps were increasingly entered and crossed after the beginning of metal working because of their rich ore deposits. In Roman times, the mountains became a busy transition zone connecting the Mediterranean with Central Europe.

Any movement of people is inevitably acompanied by culture transfer to a larger or lesser extent. An important topic is therefore the underlying concept distinguishing human mobility from migration. The journey in time that is

C. Metzner-Nebelsick (✉) • A. Lang
Institut für Vor- und Frühgeschichtliche Archäologie und Provinzialrömische Archäologie, Ludwig-Maximilians-Universität München, Munich, Germany
e-mail: Metzner-Nebelsick@vfpa.fak12.uni-muenchen.de

C.S. Sommer
Bayerisches Landesamt für Denkmalpflege, Munich, Germany

B. Steidl
Archäologische Staatssammlung, Munich, Germany

G. Grupe et al. (eds.), *Across the Alps in Prehistory*,
DOI 10.1007/978-3-319-41550-5_1

provided by this chapter thus starts with a consideration of mobility versus migration and the resulting interpretation of culture transfer.

Introduction

Dealing with mobility in prehistory involves a variety of entities: living beings or things. Being mobile entails various modes of movement in a physical space, be it in a building complex or a vast geographical area covering hundreds of kilometres. Mobility can also be regarded in a social context as mobility between social groups, ranks and classes as well as within gender- or age-related groups to name just a few. Mobility can also effect objects which are moved in the process of various kinds of exchange (gifts, barter, etc.), trade, as bounty or even by chance. Recently mobility of things was widely discussed in the context of object biographies (Kopytoff 1986; Fontijn 2002; Hahn 2008) and as means of representing identity, interaction or complex work processes (Hahn and Weiss 2013). Archaeology in Central Europe traditionally had a very strong focus on material studies. Today a renaissance of material cultural studies in a more global context can be observed (Bintliff and Pearce 2011). However, things, objects and artefacts are being addressed within their own right and not necessarily as a specific and—in archaeological contexts—as a major defining part of a certain culture. As Hans Peter Hahn and Hadas Weiss stressed, this way of looking at things is highly influenced by our modern, globalized world (Hahn and Weiss 2013, p. 6).

Mobility of people is the main factor for the spread not only of goods but most importantly ideas, beliefs and technical innovations. The reasons for various kinds of mobility are manifold and have been addressed extensively in the past. To evaluate historic and social processes and events, a distinction between acts of movement/mobility and migration needs to be made, the latter being understood as vectorized. Migration usually has a starting point and a destination with a connotation of finality of a certain type of movement (Prien 2005). It seems banal to stress that in contrast to mobility, the term migration can only be applied to living beings and more so to humans because of the entailed cultural, i.e. social, components (Anthony 1990).

People migrate from one location to the other in order to stay there at least for a longer period of time. Mobility in contrast involves various kinds of temporary and repeated movement. Traders and sometimes craftsmen exercise mobility by exchanging or selling their goods in distant places. As early as the Bronze Age in the Near East and in Anatolia in the third and second millennium BCE, written accounts exist depicting trading activity taking place over very long distances and on a planned and regular level (Michel 2011). In prehistoric contexts, the distribution of rare objects or so-called imports and the exchange and trade of resources such as metals (copper and tin) or commodities such as the vital salt (Harding 2013) imply human mobility on a minor or larger scale. Exchange patterns are part of social, economic or ritual networks (Knappett 2011).

In contrast to mobility, migration of people is mostly seen in the context of larger groups of people immigrating. In its aggressive form, the term invasion is often applied in historical contexts (Chapman and Hamerow 1997; Burmeister 2000; Prien 2005). Migration events as agents for the transmission of the aforementioned technical innovations, changes in subsistence strategies, lifestyles, ideas and beliefs have a long tradition in European archaeological theory and still remain most prominently connected with V. Gordon Childe's work, who proclaimed migration as a driving force behind European prehistory (Childe 1925, 1929). After a shift towards models of social interaction modes, at the end of the last century, migrationist approaches to interpreting culture have gained growing support (Kristiansen 1989; Anthony 1990). This view has been strengthened by recent aDNA analyses (e.g. Brotherton et al. 2013; Brandt et al. 2014; Haak et al. 2015).

In contrast to projects with an emphasis on population history by means of genetics, the Munich Research Group focusses on the analysis of stable isotopes for determining migratory activity, aiming at contributing to the establishment of bioarchaeological isotopic landscapes (see chapter 'The Concept of Isotopic Landscapes: Modern Ecogeochemistry Versus Bioarchaeology'). Ideally, migratory activity can also be detected by this method. In contrast to aDNA studies, the input of archaeological information is even more essential, since potential geological markers have a wider range of possible fitting accuracy (Montgomery and Mandy 2013 with further quotes). The European Alps have been chosen as a reference area because they constitute a geographical barrier between Central Europe and the Mediterranean which, despite its imposing nature, has been crossed by prehistoric humans since the Mesolithic. In the following, the relevant archaeological finds and topics are reviewed, thereby explaining the choice of this reference region.

The archaeology of the central Eastern Alps and adjacent areas plays an important role in understanding exchange patterns in Europe as a whole. The exchange of resources such as copper, salt or other commodities was responsible for an emerging extensive connectivity especially in the European Bronze Age world starting in the early second millennium BCE (Harding 2013). For a long time and again more recently (see above), the analysis of such exchange networks was mainly focused on objects; the role of the agents however, that is, the people, who provided or embodied various modes of connectivity and created the contexts in which the exchanged objects in question were found and in which they can be interpreted, was often reduced to material studies. The reason behind this can be seen in the fact that archaeological modelling alone could not provide sufficient proof to be decisive in differentiating whether the transfer of goods and objects was caused on the grounds of exchange and cultural appropriation or as a byproduct of migrating people.

Maps illustrating the distribution of various object types (von Uslar 1991) alone provide little insight into the processes which led to certain distribution patterns of object types, and the information needed to help understand how their cultural context can be evaluated is vague at best. The context-based analysis of objects in graves, ritual deposits or settlements offers a series of model-based interpretations of the archaeological record. Non-local objects could have been obtained by means of reciprocity, exchange or trade (i.e. Renfrew and Cherry 1986).

In the context of the project 'Mobility and Social Dynamics in Bavaria and the Eastern Central Alps in the Late Bronze Age (1300-800 BCE)' (see chapter 'Current Synthesis and Future options') for example, the concepts of mobility and migration have offered ways to explain and understand the archaeological record of the eastern central Alps in regard to neighbouring regions. However, for a long time verification of the existence of mobile individuals or migrants as a trigger for innovations, changes in the material culture or the emergence of new customs in areas where they were hitherto not attested, could not be provided. For more than two decades, isotope analyses of human and animal bone material have helped to determine if mobility of individuals took place (Grupe et al. 1997; Price et al. 2004; Montgomery and Mandy 2013), to what extent it occurred and between which areas people were moving during the course of their life.

Transalpine Mobility from the Mesolithic to the Iron Age

In the Eastern Alps, the Inn Valley, Wipp Valley and Eisack and Adige Valleys form a transalpine route that leads over the 1370 m Brenner Pass and connects Upper Bavaria in southern Germany with Venetia in upper Italy. Mesolithic hunters from this area incorporated these valleys and their adjacent mountain ranges in the Alps since the ninth millennium BCE into their living environment. Above the tree line, the high mountain range offered good hunting grounds, and raw materials such as flint and rock crystals were available for producing tools and other implements. Mesolithic hunters set up camps during the warm, dry summers, even at higher elevations. Intensive field surveys have led to the detection of several hundred sites in North Tyrol, South Tyrol and Trentino, some of which have been archaeologically excavated. The mobility of the Mesolithic hunters is determined by the origin of raw materials used for the stone artefacts discovered at the campsites. A good example is the campsite at Ullafelsen in the North Tyrolean Fotscher Valley. Artefacts found there are made of stone originating from the area between southern Bavaria and Trentino (flint, radiolarite, chert) (Schäfer 2011). The late Mesolithic artefacts from the campsite under the abris near Hohlenstein above Vent, BH Imst, North Tyrol, are made primarily from southern alpine stone (Mottes 2002, p. 97). Accordingly, the geographic region in which the hunters moved encompassed the main alpine range both to the north and south. Therefore it can be assumed that certain routes were well known and regularly frequented in order to acquire stone raw material, particularly flint.

Rock crystal is especially useful for constructing arrow points and has been regularly quarried from sources such as the Riepenkar in the Tux Alps in North Tyrol since Mesolithic times (most recently Leitner et al. 2015). The dispersion of artefacts made from this rock crystal indicates that the Inn, Wipp and Eisack Valleys as well as their adjoining mountain sides were travelled. Walter Leitner suggests the existence of a transit route for early trade of goods in this area of this passage (Fig. 1). A map showing the distribution of late Palaeolithic, Mesolithic

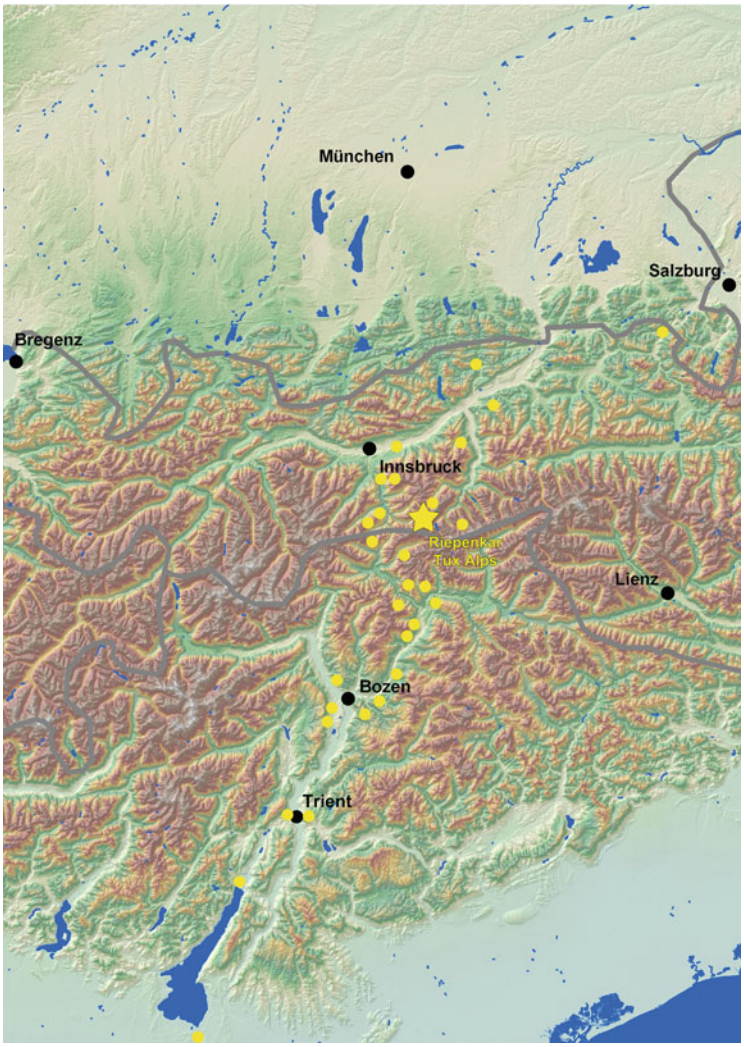

Fig. 1 Map of the possible north-south transit route for early crystal rock trade (Graphic: W. Leitner; IA Innsbruck & G. Hiebel; IGB Innsbruck; ESRI; SRTM-CIAT). After Leitner et al. (2015), p. 67, Fig. 2

and Neolithic/Bronze Age rock crystal artefacts is presented by Töchterle (2015, p. 147, Fig. 12). It is possible that a transalpine supply network for rock crystal existed across the main alpine mountain range. The Wipp and Eisack Valleys, and also the Ziller and Pfitscher Valleys, played an important role in the choice of routes with respect to mobility associated with the supply of raw material.

Mobility along the Inn-Eisack-Adige route started in the middle of the sixth millennium BCE and continued on through the Neolithic (Borrello et al. 2013).

Initially this was documented only by very few finds, such as a single early Neolithic sherd from the upper Italian Gaban Group found at Sistrans, Inn Valley, North Tyrol (Töchterle 2001). Middle Neolithic ceramic fragments exhibiting a southwest German style were discovered in the Eisack and Adige Valleys (a vessel fragment in Hinkelstein and Großgartach style in Brixen-Stufels and a sherd from the Aichbühl culture at the settlement site at Rocca di Rivoli, prov. Verona, Venetien: Tillmann 2002, p. 197). The shoe-last celt (*Schuhleistenkeil*) discovered at the La Vela cemetery in Trentino is also dated to the middle Neolithic (Bagolini and Broglio 1985, Fig. 9.3). These objects of southwest Germany origin probably reached the Eisack-Adige Valley by way of the Lake Constance-Arlberg Pass route.

Mobility along the Inn-Eisack passage increased markedly during the early part of the Neolithic in the fourth millennium BCE. Economic reasons were responsible for this, specifically the transfer of goods. A favourite trade and exchange object was flint from the deposits in the Lessinian Mountains east of the Adige between Rovereto and Verona. It arrived via the Inn-Eisack-Adige route, amongst others, and reached into the northern alpine foreland. During the fourth millennium BCE, Lessinian flint was used there in the making of daggers, status symbols and prestige objects (Tillmann 2002, p. 108; Mottes 2006). The daggers are a documentation of contact between the Altheim culture and the developed Square-Mouthed Pottery culture (Vasi a Bocca Quadrata culture) in upper Italy. In the course of this contact, Vasi a Bocca Quadrata culture ceramics made their way into the North Tyrolean Inn Valley (Kiechlberg near Thaur, Töchterle 2015; Mariahilfberg near Brixlegg, Huijsmans and Krauß 2015). Flint stone from deposits south of the Alps was used in the first copper mining activities in the region around Brixlegg (Huijsmans and Krauß 2015).

Mobility in the opposite direction from north to south along this route is indicated by the discovery of Münchshöfen ceramic in the settlements at Mariahilfberg near Brixlegg (Huijsmans and Krauß 2015) and the Kiechlberg near Thaur in the North Tyrolean Inn Valley (Töchterle 2015). In South Tyrol, Trentino and Venetia, a large number of sites with ceramics with incised-punctated decoration (*Furchenstich* and *Pfeilstich*) are known and can be associated with the Münchshöfen ceramic (distribution map, e.g. by Mottes et al. 2002, p. 125, Fig. 5). Singular pieces of southern Bavarian tabula chert reached the south via the Brenner route (Johanneskofel im Sarntal: Mottes 2002, p. 98).

In addition to the trade of wares and raw material, contacts promote the transfer of nonmaterial goods as well. Annaluisa Pedrotti sees the unique features in northern alpine building construction at the Isera La Toretta settlement not only as a result of transalpine contacts, which catalysed the adaptation of new building techniques, but also as the result of an immigration of north alpine populations (Pedrotti 2001, pp. 141, 152, 158), who at least in part must have utilized the Inn-Eisack-Adige route. This also applies to stylistic elements of Pfyn and Altheim ceramics seen in early Neolithic ceramics from Trentino (Marzatico 2002, p. 26). 'In particular the mixing of ceramic styles from both sides of the Alps suggests a give and take during the Neolithic, not only of goods but also of parts of the population as well' (Mottes 2002, p. 130). Marzatico also associates the adaptation of stylistic elements of the

Pfyn and Altheim ceramics seen on early Neolithic ceramics in Trentino with the immigration of population groups (Marzatico 2002, p. 26). The fortuitous geographic location of settlements situated along the Inn-Eisack-Adige passage functioned as a turning point for long-distance trade relationships. Accordingly, the first copper artefacts show up at these settlements (Rocca di Rivoli, Isera La Toretta [Trentino], the Kiechlberg near Thaur and Mariahilfberg near Brixlegg [Nordtirol]: Mottes 2002, p. 97 ff.; Töchterle 2015, p. 421).

As could be shown so far in this chapter, the region of the Eastern Alps has been the focus of intensive archaeological research for a long time. This especially holds true for the Bronze Age and later periods. The abundant deposits of copper were indispensable for the manufacture of copper wares and since the second millennium BCE also bronze objects. This special condition made the Alps and immediate surroundings an important area on a European scale, comparable with the Middle East today in regard to oil. Thus the impact of alpine or immediately adjacent areas on Europe as a whole was tremendous. Mining activities had a significant influence on local communities (Stöllner and Oeggl 2015) and fostered exchange and attracted migrating groups in the search of copper. After an experimental phase in the fourth millennium BCE, significant traces of metal processing activities in the Inn Valley around Schwaz-Brixlegg in Tyrol were discovered from the beginning of the Bronze Age around 2100 BCE (Bartelheim et al. 2002; Töchterle 2015). So-called fahlore copper but also small amounts of oxidic copper (azurite, malachite) were exploited and processed here and in turn exchanged with communities especially to the north in what is now modern Bavaria and beyond (Martinek and Sydow 2004; Kienlin 2013). Connectivity in Bronze Age Europe was mainly based on the exchange of resources and finished goods. Therefore, the geography of the Alps as one of Europe's ore-rich regions played a crucial role in connecting people and whole communities with far-reaching areas along the trade and exchange routes along the valleys of the Inn, Salzach and other rivers as well as through mountain passes in a predominantly north-south direction (Tomedi and Töchterle 2012, p. 588).

Especially the Inn Valley was of significant importance, since it provided the Bavarian piedmont zone with copper (Möslein and Winghart 2002, p. 139, Fig. 2), which was cast into ring-shaped ingots there, the most prominent ingot type of the Early Bronze Age in Central Europe (Lenerz-de Wilde 1995).

The route across the Brenner was also used during the Early Bronze Age. The stations along this route are marked by a row of settlements on the northern and southern Wipp Valley (von Uslar 1991). Finds such as upper Italian ceramics and the loaf of bread idol (*Brotlaibidol*) from Gschleiersbühl near Matrei in North Tyrol (Bankus 2004, p. 417 Nr. 18) and the *Brotlaibidole* from Albanbühel near Brixen as well as from Wallburg Nössing near Vahrn in South Tyrol (Bankus 2004, 418 Nr. 45.68), ceramics from Nössingbühl that are similar in form to the Straubing culture (Tecchiati in preparation), a Horkheim-type pin and also the casting mould of the Straubing culture from Albanbühel and finally very Early Bronze Age ceramics ornamented with half-moon stamped edges, are all witness to cross regional trade routes. The fortified high altitude settlements at Patsch and Matrei Gschleiersbühl

in the Wipp Valley form important places along the path of this route (most recently Jaeger 2016). A fragment belonging to a flanged axe from Steinach on the Brenner may possibly be considered a hoard find along the Brenner route. Steiner and Tecchiati assume that travelling craftsmen might possibly have used this route (Steiner and Tecchiati 2015, p. 145).

Mobility along the Brenner route satisfied the supply of raw materials and the trade of material goods. Contact between the population groups on both sides of the Brenner resulted in a transfer of knowledge, ideas, etc. The beginning of sacrificial sites for burnt offerings (*Brandopferplätze*) in North Tyrol is likely connected to this. In the Early Bronze Age, a sacrificial site was erected at Goldbichl near Igls in North Tyrol (ca. 2200 BCE; abandoned in the Middle Bronze Age at around 1600 BCE, Tomedi and Nicolussi Castellan 2007). The Goldbichl is situated at a geographically important thoroughfare along the Inn-Eisack passage across the Brenner at the point where the Wipp Valley connects with the Inn Valley (Tomedi and Nicolussi Castellan 2007). The sacrificial site at Goldbichl is the oldest known alpine site for burnt offerings. A forerunner of this type of ritual practice is the Copper Age deposition of copper axes, partially burned flint tools, broken ceramics and burned animal bones in a rock crevasse on the Pigloner Kopf above Pfatten in the Adige Valley (2600–2400 BCE; Oberrauch 2000). It can be assumed that a transfer of ideas across time (Copper Age to Middle Bronze Age) and through the Brenner route between the Pigloner Kopf and the Goldbichl actually took place, although those activities cannot be supported by archaeological evidence so far. The sacrifical site with burnt offerings at Weer-Stadlerhof in the Inn Valley (1610–1250 BCE; Töchterle 2013) lies on the route in the direction of the Middle Bronze Age sacrificial sites of similar type in the alpine foreland (Weiss 1997), which includes the Wasserfeldbühl in Oberaudorf on the Inn River.

Tetrahedrites (fahlore) from the Schwaz region lost its economic importance in the first part of the Early Bronze Age and Middle Bronze Age. In its place, chalocpyrite (*Kupferkies*) from the quarries at Mitterberg and Salzachpongau became the main components for metallurgy, and the area gained importance as suppliers. A regional centre for bronze production developed during the middle Bronze Age in Tyrol's upper Inn Valley in the area around Fliess. Even though small deposits of chalocpyrite exist in the area, local bronze metal workers used this type of copper originating from Bischofshofen in the Pongau, which is about 250 km away. This was determined by metal analysis of a bronze hoard find in Piller-Moosbruckschrofen in the district of Fliess (Tomedi et al. 2013, p. 59; Tomedi and Töchterle 2012, p. 591). The variety and richness of the bronze hoard inventory at Piller-Moosbruckschrofen (Tomedi 2004, 2012), the presence of a sacrificial site with burnt offerings on the Pillerhöhe during the Middle Bronze Age (Bz C2) (Stefan 2010), and the fortified Middle Bronze Age settlement at Wenns-Spielkopf at the crossroad to Pillerhöhe reflect a regional elite and widespread relationships that were associated with corresponding mobility (Tomedi 2004, p. 2012).

For the region of Fliess, the connection to the south was most likely provided over the Reschen Pass, through which the Adige River flows and eventually leads into the

Vinschgau. A prominent hub for the transfer of goods along this route was the fortified settlement on the Ganglegg near Schluderns. Ceramic with chip-carved (*Kerbschnitt*) and grain-shaped incised ornaments from the Middle Bronze Age and early Late Bronze Age, a Middle Bronze Age disc ornament (*Stachelscheibe*) and a dagger (Steiner 2007, 2010a, p. 462, Fig. 4) from this archaeological site were all imported from the northern Alps. The southern alpine influence is shown by local ceramics from Ganglegg with ansa cornuta handles (Steiner 2007, 2010a, p. 463).

The Brenner still remained in use in addition to the route over the Reschen Pass. Northern alpine artefacts are characterized by chip-carved decorated (*kerbschnittverzierte*) ceramic from Zieglmühlegg near Sterzing and ceramic with grain-shaped incised decoration (*Kornstichverzierung*) from Plabach and Albanbühel (Steiner and Tecchiati 2015, p. 145). The settlements at Thumburger Hill, Burgstall-Möders, Burgstall-Wiesen as well as Pflastererhof south of Gossensass marks the route south of the Brenner. North of the Brenner Pass, a number of settlements forming the transalpine connection over the Brenner are located at the Gschleiersbühl near Matrei, the Patscherhügel near Patsch, the Muiggensbichl in the Stubai Valley near Telfs and the Sonnenburger Bichl near Natters where the route pans out into the Inn Valley near Innsbruck (von Uslar 1991).

As will be shown in greater detail in chapter 'Current Synthesis and Future Options', after the decline of mining and metal working activities in the Schwaz-Brixlegg area and the increasing importance of the mega copper-producing mining district at the Mitterberg (Stöllner and Oeggl 2015), the Late Bronze Age or Urnfield period is a period characterized by substantial mobility and indeed a time when migration events into the North Tyrolean Inn Valley very likely took place (Staudt and Tomedi 2015; Sölder 2015; Sperber 1997, 1999).

The newly founded cremation grave cemeteries display a major change in burial customs as well as a remarkable appearance of artefact types originating in the northern alpine piedmont zone in southern Bavaria (Müller-Karpe 1959; Sperber 1992). Thus, Lothar Sperber and others have stated that local communities were joined by newly arriving people coming in from the latter area, who settled the North Tyrolean Inn Valley not only in the search of copper but probably in order to control the exchange routes. The exchange of copper along the previously mentioned routes is proven by a hoard find of raw copper and bun ingots (Winghart 1998, p. 105, Fig. 2) which was found at the foot of the Rachelburg at Flintsbach near Rosenheim. The Rachelburg is an Urnfield period hilltop settlement which towers over the Inn at a particularly narrow part of the valley (Möslein 1998/1999; Möslein and Winghart 1998/1999, 2002). Its steep edges and the position on a prominently isolated hill underline its strategically crucial position. The metal analysis of the deposited ingots revealed that they were cast out of fahlore copper from the North Tyrolean deposits. In addition to the widely discussed northern connection, the late Bronze Age in the central Eastern Alps is also characterized by intensive contacts to the south.

The first inner alpine cultural group, the Laugen culture (Luco culture) appeared in the western part of the Eastern Alps, in Trentino and South Tyrol, in the late

Bronze Age at around the 13th century BCE. The most characteristic feature is their ceramic: jugs with beak-shaped spout (*Schneppenkannen*) biconical jugs (Marzatico 2012), with which the area of this cultural group was redefined (Fig. 2). From the Brixen basin, the group spread out over the Puster Valley into East Tyrol. Another group belonging to the Laugen culture settled in Graubünden. Routes from the Adige Valley in the Vinschgau lead there, and as it was the case during the Middle Bronze Age, the settlement on the Ganglegg near Schluderns represented a central place on the way to Graubünden. Steiner assumes that population groups belonging to the Laugen culture in South Tyrol migrated into Engadin (Steiner 2007, p. 256); they probably used the route through the Vinschgau into Unterengadin. The cross regional importance of the settlement at Ganglegg is reflected in the bronze and ceramic objects from the northern alpine foreland (Steiner 2010a, p. 476, Fig. 13).

The Laugen culture pottery style can also be found in the Engadin; however, the Eisack route leading from the Brixen basin across the Brenner to North Tyrol seems to have been used only occasionally. Laugen ceramic is rather rare in the region around Innsbruck where a separate Urnfield cultural group in the Inn Valley was established. It is unclear whether the few Laugen jugs represent imported ceramic from the Southern Alps or stylistic adaptations.

As indicated by von Uslar's archaeological site map of the Wipp and Eisack Valleys, the appearance of the Laugen culture did not significantly change mobility across the Brenner (von Uslar 1991, maps 40, 41). The winged axe from the Brenner Pass (von Uslar 1991, p. 300 Nr. 10) is a typical hoard find at pass elevation along a transit route.

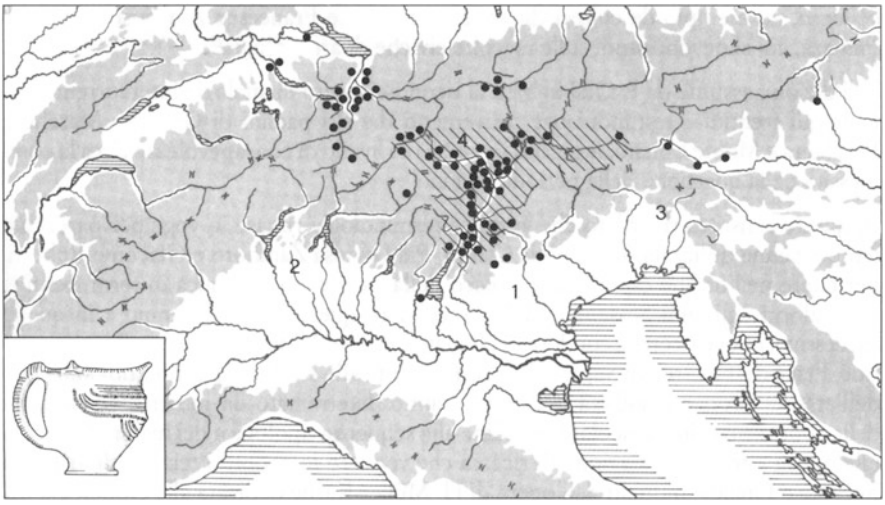

Fig. 2 Distribution of the Laugen jugs with beak-shaped spout (*Schneppenkannen*) (*dots*) and main area of distribution of the Laugen culture (*chequered*). After Marzatico (2001a), p. 171, Fig. 2

In the southern alpine area, the Laugen culture style transformed into the Melaun culture pottery style at the beginning of the Iron Age (Marzatico 2001b); a separate Hallstatt period cultural group developed north of the Alps in North Tyrol. The two cultural groups in Trentino/South Tyrol and North Tyrol are connected to each other at different levels. Both continue to practise the Urnfield traditional burial ritual of cremating the dead. They also shared common attributes such as the cult of sacrificial sites for burnt offerings. The ritual of burning animal offerings, ritual feasting activities including the consumption of food and the sacrificial offering of material goods were anchored in the religious life to the north and south of the Brenner and also the Reschen Pass (Steiner 2010b).

Ceramics in the material culture each exhibit local attributes. Melaun jugs constitute a further development of the Laugen jugs with beak-shaped spout (*Schneppenkannen*) (Marzatico 2001b). Form and ornamentation of Hallstatt period ceramic in the Inn Valley clearly show some similarities with ceramics from the Bavarian alpine foreland (Lang 1998). Metal grave goods in some of the richly furnished burials at the cemetery in Wörgl, which consist of several hundred Hallstatt and early Latène period burials (8th-4th centuries BCE), indicate contact with upper Italy. Women wore Italic belt plates and the men carried daggers of upper Italian type with parallels in the Este culture (Egg 2016). At the cemetery in Kundl (BH Kufstein) near Wörgl, men were also equipped with upper Italian type daggers (Lang 1998). Specific types of fibulae, i.e. dress fasteners and costume accessories, show a connection between southern Bavaria and upper Italy over the Inn-Eisack-Adige passage. Florian Hauser documented this based on an example of east alpine double button fibulae (*Zweiknopffibeln*) (Hauser 2012, 2014). A revealing observation is that the distribution terminates at the northern alpine edge, which suggests that this was the border of communication networks (Hauser 2012, p. 89, 2014). Certain forms of serpentine fibulae (*Dragofibel*) and fibulae with decorated end (*Fußzierfibel*) clearly demarcate the Inn-Eisack-Adige passage (Hauser 2012, p. 90, 2014), as Anne-Marie Adam stated (Adam 1996, p. 38, Fig. 2). Figure 3 shows the potential routes which Hauser connected with the Brenner Pass.

Mobility across the Brenner gained a new quality with the onset of the Iron Age. The wearing of similar fibula types between upper Italy and southern Bavaria and the use of upper Italian belt plates and daggers in North Tyrol indicate regular communication within an area across and beyond the main alpine range.

The hoard finds from Fliess allows the detection of a Hallstatt period elite, whose clothing, weapons, tools and drinking vessels evidence the existence of cross regional relationships (Sydow 1995; Tomedi 2008). This represents the same development as was seen with the Middle Bronze Age hoard find at Piller (see above; Tomedi 2004). Gerhard Tomedi suggests that the inhabitants of the region around Fliess profited from the long-distance trade across the Alps (Tomedi 2008, p. 46); a prerequisite for this is organized mobility. For the region Fliess, the route across the Reschen Pass into the Adige Valley and Venetia would be closest, but also to pass trough the Inn Valley upstream and over the mountain passes into the area of the Golasecca culture can be assumed.

This type of contact and communication lasted until around 500/450 BCE at the transition from the Early to Younger Iron Age. This represented a fundamental

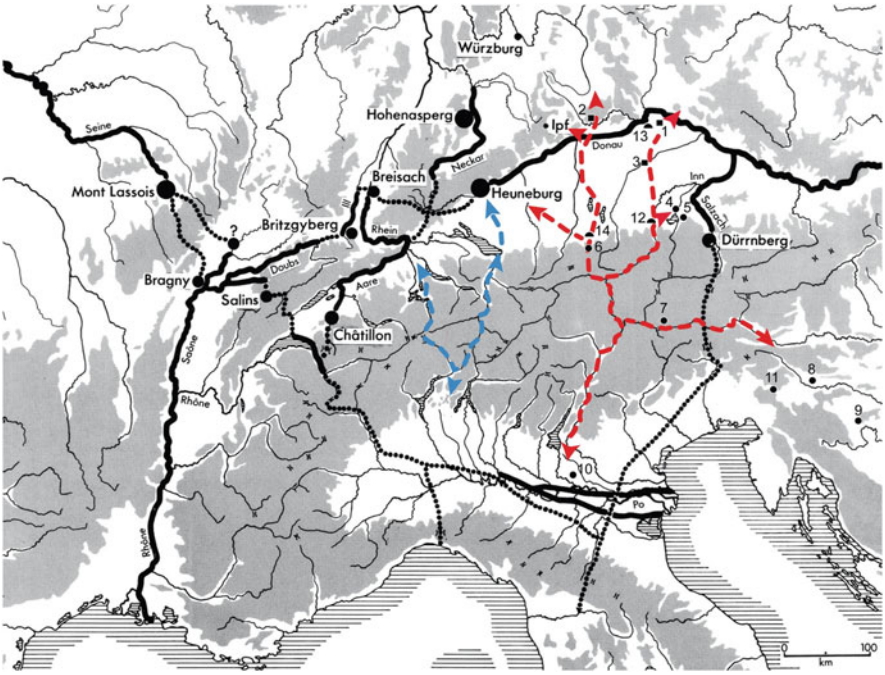

Fig. 3 Late Hallstatt period travel routes according to B. Schmid Sikimić (*blue route*) and F. Hauser with the passage across the Adige, Eisack and Inn (*red*). After Hauser (2012), p. 86, Fig. 3

change because for the first time, a fairly unified culture was established in the North Tyrolean Inn Valley, South Tyrolean Eisack and Adige Valleys and adjoining valleys, as well as in Trentino: the Fritzens-Sanzeno culture, named after a characteristic archaeological site in North Tyrol—Fritzens—and one in Trentino, Sanzeno in Nonsberg (Fig. 4) (Lang 1998; Marzatico 2001c, d). The Fritzens-Sanzeno culture lasted for about 500 years and disappeared following Roman occupation in the middle alpine area.

The cultural area was characterized by similar features at different levels. For example, religious beliefs involved the cult at sacrifical sites for burnt offerings where various material goods were sacrificed and of course the burial ritual of cremating the dead. In the northern and southern alpine regions, the material culture exhibits strong similarities in ceramics, costume accessories, iron tools and objects as well as weapons. The characteristic house construction is the so-called casa retica, a house built on a stone foundation possessing an angled entrance way. Some parts of the house also had more than one level. The use of scripture (Schumacher 2004) and figurative decoration in the so-called Situla style (Kern et al. 2009; Wamers 2010) are shared features of the whole Fritzens-Sanzeno cultural area. Writing and figurative art originated from the Venetian-Etruscan culture circle;

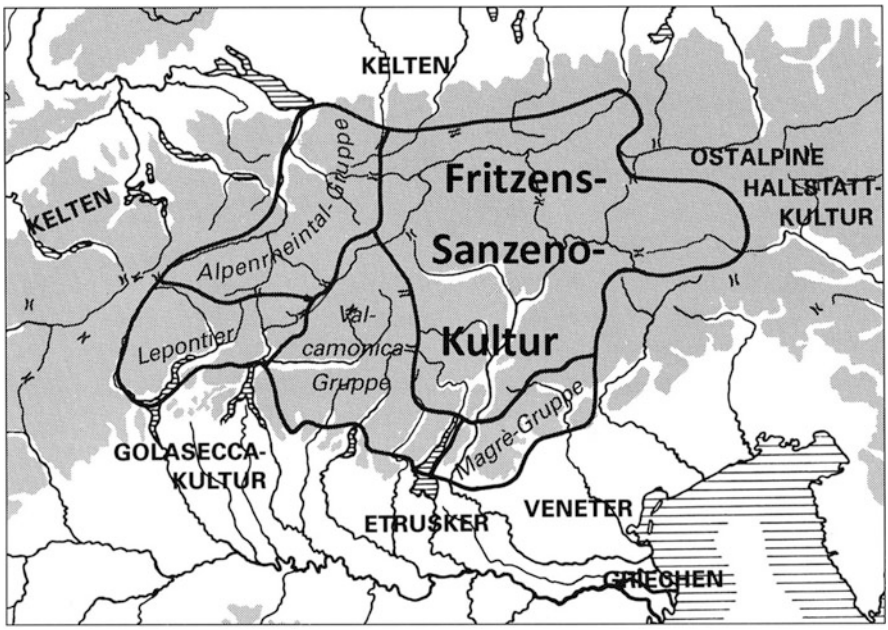

Fig. 4 Distribution of the Fritzens-Sanzeno culture and neighbouring cultural groups. After Gleirscher (1991), p. 16, Fig. 6

south of the Brenner Pass they were much more intensively adopted than in North Tyrol.

Distribution maps depicting types characteristic for the Fritzens-Sanzeno culture clearly illustrate the utilization of the Adige-Eisack-Brenner passage. This is best illustrated by the Fritzens pottery bowls and the pressed S-shaped bowls with comb-stamped ornamentation (*Kammstempeldekor*) (Fig. 5), and for costume accessories by the fibulae of the late Early La Tène and Middle La Tène period (4th-2nd centuries BCE) (Adam 1996, p. 149, Fig. 23, p. 156, Fig. 24, p. 165, Fig. 25). Also the widespread type of Eastern alpine animal head fibulae (*ostalpine Tierkopffibeln*) of the fifth century BCE indicate communication and exchange along the Brenner pass route (Adam 1996, p. 91, Fig. 14).

It can be assumed that people of the Fritzens-Sanzeno culture were regularily engaged in mobility along the Inn-Eisack-Brenner route. In comparison to the 12th-6th century BCE (Laugen and Melaun cultures), the Eisack Valley has a significantly greater number of archaeological sites (Pisoni 2009, p. 227, Fig. 2; p. 228, Figs. 3 and 4). In order to sustain continuous mobility, infrastructure along the route is necessary. This includes controlled modes of transportation and rest stops situated at geographically strategic spots. They also functioned as centres and market places.

Based on the topography and sometimes lavish and high-quality finds, a number of rest stops are postulated (Lang 2002; Tomedi et al. 2006; Tomedi 2010). It starts with the Burgberg near Oberaudorf on the northern alpine rim (6th-1st centuries

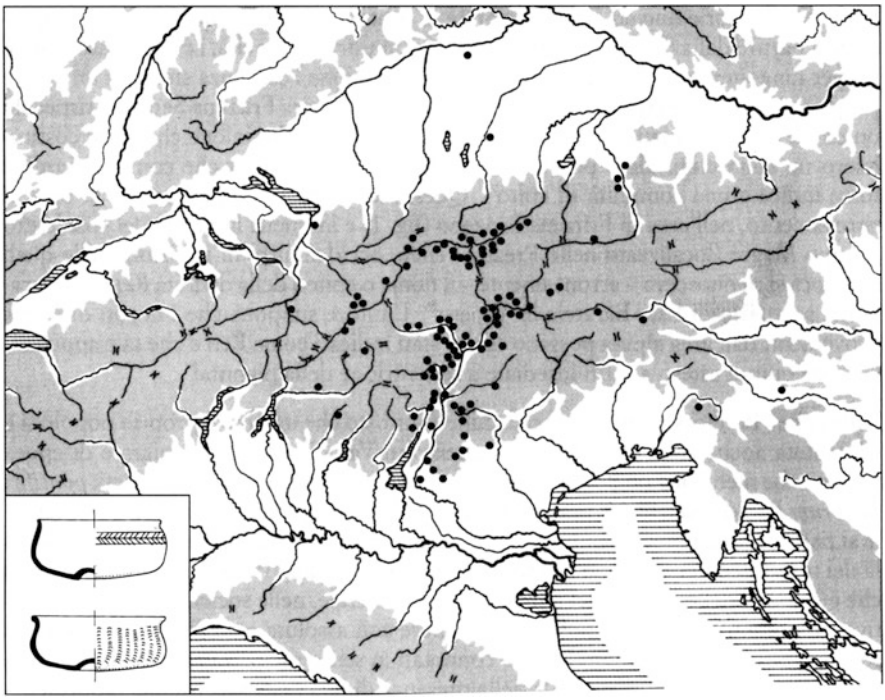

Fig. 5 Distribution of the Fritzens bowl and pressed s-shaped bowls with comb-stamped ornamentation. After Marzatico (2001c), p. 481, Fig. 1

BCE; Pietsch 1998). The next station is located near Wörgl on the east side of the Inn at the entrance to Brixen Valley (documented by the richly furnished 8th-4th centuries BCE graves; Egg 2016). This is replaced by a station near Kundl in approximately 300 BCE, which the author surmises based on the wealth of finds and iron production there (Lang 1998). The next station is represented by the Buchberg near Wiesing at the mouth of the Ziller Valley. This leads up to the Achen Lake, over the Isar Valley and on to southern Bavaria. A fortified settlement belonging to the Fritzens-Sanzeno culture was located at the Buchberg (Sydow 1984). The next place upstream along the Inn River was probably the fortified settlement situated on the Himmelreich near Wattens (Sinnhuber 1949; Kasseroler 1957). The settlement which was built in the late part of the Early La Tène period and destroyed at the beginning of the Late La Tène period is exemplified by a rich fundus of bronze and iron artefacts as well as high-quality ceramics. Iron finds include farming tools and wagon parts. However, the apparent prosperity of the settlement cannot be linked to an agrarian surplus production, but rather to the geographical location near the ore-rich Schwaz region and the old passage leading from Ampass in the direction of the Brenner. The next station is Ampass (Töchterle 2009; Töchterle 2013). Pfaffenhofen and Stams are located in the upper Inn Valley where the road turns off to the north towards the Fern Pass. The settlements Karres, Wenns and Faggen

were apparently rest stops along the way in the direction of the Reschen Pass (Tomedi et al. 2006).

South of the Brenner, the settlement Brixen-Stufels in the Eisack Valley formed a centre and junction, the cross regional importance of which is exemplified by archaeological findings (Dal Ri 1985; Tecchiati et al. 2010). This is where the path turns off into the Puster Valley in the direction of Carinthia. For the rest of the way, another junction in the Bolzano basin is presumed (Zanforlin and Tecchiati 2010). The settlement and cemetery at Pfatten (Lunz 1991; Dal Ri and Evans 1992; Alberti 2007) indicate the existence of a central site at the edge of the Adige Valley with a connecting road over the Kreither Saddle into the Adige.

With regard to mobility in river valleys, the question of boat transport always arises. Shipping played an important role in Iron Age transportation; for example, this could clearly be shown for the Rhône, Saône (Pauli 1993, pp. 110 ff.), the Neckar (Wieland 2000) and the Salzach, Inn and Traun rivers (Stöllner 2002) as well as for the Elbe river (Salač 1998). Even though the Inn river possesses a flow intensity and an enormous difference in summer and winter water tables typical for high alpine rivers, its alpine section was doubtlessly used (Plaseller 1936/37; Gritsch 1987). Due to its strong currents and numerous shallows, the river was not easy to navigate after passing Telfs, which lies west of Innsbruck. According to Gritsch, ship travel was restricted to the time between May and September because of heavy shifts in water depth. Because the Inn was wild and had side branches, new passable routes along the river had to be found following each high water event. Upstream near Telfs goods had to be unloaded and carried by pack animals for the route leading over the Reschen Pass. If the route across the Brenner was chosen, it was necessary to use pack animals beginning in the area around Wattens-Hall. The old assent, which was later used as the Roman road, led over Ampass, Igls, Patsch and Ellbögen in the direction of the Brenner. South of the Alps, the Adige forms a wide meandering river after it flows into the Eisack south of Bolzano (Tengler 1991). Before the river was regulated in modern times, it was used for shipping in the lower Inn Valley near Pfatten. The ships used on the Inn and Adige were probably the same type of barge that is in use today: flat, no keel, about 12 m long and 4 m wide and with a carrying capacity of approximately 30 tons (Tremel 1970).

In conclusion the following can be said. The passage routes through the valleys of the rivers Inn, Eisack and Adige have been used since the Mesolithic period. Mobility was connected to hunting territories on the one hand and the supply of raw materials on the other. The mining of rock crystal and supplying of certain stone material such as flint during the Mesolithic and Neolithic, as well as mining and metallurgy since the Bronze Age, were all reasons for mobility within interregional and often far ranging exchange and travel networks. Another factor was the alpine pastoral activity (*Almwirtschaft* - a specific form of transhumance) which gained momentum in the Bronze Age. In general transhumance in the alpine area led to mobility.

In the early Iron Age and with the intensification of contacts with the Mediterranean world the transit routes across the Alps continued to be used. The Brenner and Reschen passes both functioned as connecting passages to upper Italy. The

formation of the Fritzens-Sanzeno culture in the early Iron Age in around 500–450 BCE was associated with continuous mobility over the Brenner and Reschen passes. It can be assumed that settlements along the route acted as rest stops, and if the geographical position in regard to trade or mobility in general was suitable, also as centres for the distribution of goods when the geographic location was fortuitous. This network of routes was used by the Romans at the end of the first century BCE for their military campaign across the Alps (*Alpenfeldzug* 15 BCE).

Transalpine Mobility in the Roman Period

The Roman period can be considered as a time of migration par excellence. With the expansion of the Roman influence through military action beyond the Alps from Caesar onwards, Gaul, Germany and the Danube region experienced various influxes of legionary soldiers, originally drafted somewhere in Italy. After the respective wars, which led to the conquest of considerable tracts of land, many of these soldiers were settled in these regions after they were released as veterans. Their new settlements, often so-called coloniae, must have originated as towns with an almost exclusively Roman population often of several thousand men.

From Augustus onwards more and more troops were drafted in the newly conquered areas, now as provinces under direct Roman rule (auxiliaries). At the beginning, many of them seem to have been formed exclusively with men from a particular region (e.g. cohors Batavorum, cohors Raetorum), often commanded by members from the leading class of that region, sometimes even named after their first commanding officer (e.g. cohors Indiana; see e.g. Holder 1980). Others were named after the Roman official, under whom they were established (e.g. ala Pansiana; see e.g. Farkas 2015, also for the newest account on the Roman army in Raetia/southern Germany). Usually, these units of approximately 500 men were not employed close to where they originated but far away somewhere in the still expanding Roman Empire. This led to a considerable shuffling around of people within the Empire, extending in its high days in the second century CE from the Atlantic in the west to the Euphrates in the east and from Britain in the north to the northern fringes of the Sahara in the south.

In respect to the study region of the central Alps and its northern fringes down towards the Danube in southern Germany, we know from written as well as archaeological sources that the region was brought under direct Roman influence with the so-called alpine war of Augustus or rather his stepsons Drusus and Tiberius in 15 BCE (Strobel 2009; Zanier 2010). Whereas the alpine region never experienced long-term garrisoning of Roman military, we find indications of a gradual construction of Roman forts in the foothills of the Alps down to the southern bank of the Danube in the first century CE from the first years of CE onwards.

Indicated by some written sources but mainly from archaeological excavations, we know that Roman soldiers almost never moved around and were stationed alone. They were followed even on campaigns by substantial numbers of sutlers—people who lived off and with the military and soldiers as traders, craftsmen, and people in

various services including prostitution, religious services, etc. These civilians are labelled in the English literature as camp followers (Sommer 1984; for the system behind and the settlements see Czysz 2013; Sommer 1988, 1999, 2006, 2009, 2015a). Wherever a Roman unit would be stationed for a longer period of time, i.e. when its soldiers started building more permanent structures, the camp followers would settle in the vicinity of these military installations (fortresses, forts). Their settlements—canabae next to legions, military vici next to auxiliaries—can be traced archaeologically. They extended usually for much larger areas than the originating military installations. In their planning and layout, they appear in a fairly regular fashion with a clear orientation towards 'their' fort.

Of particular importance are, on the one hand, that the civilian settlements started archaeologically contemporary with 'their' forts and, on the other hand, that quite a number of places were evacuated more or less at the same time the soldiers were moved away. Additionally, cemeteries, which according to Roman law were supposed to be separated from settlements, were planned by the military in such a way that between them and the military installations, enough space was left for the civil settlements (Fig. 6).

Consequently, we have to assume that the camp followers were attached fairly strongly to 'their' soldiers and moved with them. Ample proof is given through the so-called military diplomas, which give evidence of the grant of Roman citizenship to an auxiliary soldier on his release from the army after 25 years of service. According to these bronze tablets, citizenship was often also granted to a wife, 'in case the soldier had one', and for a short period of time also to children, if there were any. This was despite that a Roman soldier was not allowed to be married while in service. However, the procedure apparently acknowledged the facts of male-female relationship and the possible results thereof, i.e. offspring.

If we follow the chain of soldiers and their dependents movement to the beginning, we end with a view that the origin of the majority of camp followers should be the place(s) of the origin of the soldiers. Only gradually there seem to have been additions from the regions where the soldiers were stationed. Problematic is that we rarely know a continuous sequence of the places where a unit was stationed and/or its origin. As many of the units experienced far-reaching movements, this resulted in a particular military culture which shows a certain similarity across the Roman provinces. Only gradually, with a stabilization of the garrisons from the second century CE onwards, can we expect more and more 'local' reproduction within the military, resulting in an increasingly local appearance of the soldiers and their followers.

Highly controversial is the question of the extent and nature of the people in the conquered territories south of the Danube north of the Alps, i.e. natives living there before the Roman appearance. Whereas we have for the alpine valleys historical knowledge of various groups (tribes) mostly through a victory monument with the mentioning of conquered people situated above Monaco (Tropaeum Alpium) and also archaeological knowledge of their settlements and occasionally their burial grounds (Strobel 2009; Zanier 2004), nothing of that seems to be certain further north. Only a few names of groups may be linked with that region, and

Fig. 6 Magnetogram of Ruffenhofen in the UNESCO World Heritage, Frontiers of the Roman Empire. In the north the fort (c 4 ha), in the south and east along a bypassing road the military vicus, in the continuation towards the northeast the cemetery (BLfD; H. Becker/J. Faßbinder)

archaeologically there seems to be a gap between the last people living here before the Roman conquest (i.e. the late La Tène period, Celtic people, ending sometime in the second half of the first century BCE) and settlements or graves which contain datable Roman material (from the late 20s or 30s of the first century CE onwards). The dispute sees on the one side the possibility that there is a problem in dating these places. People living continuously in the region after the La Tène period might not have used material which was preserved in the ground to a large extent. Only after the Roman conquest persistent and datable material would have found its way into much older settlements. As some of these native-looking settlements and adjoining graves contain also material which shows a connection to older Celtic stuff, there is the theory of nativist behaviour, i.e. the remembrance, celebration and use of long-forgotten ideas or ideals and material in some kind of silent opposition to the Romans (Steidl and Will 2005; Zanier 1999, 2004, 2007).

On the other side stands the view that southern Germany experienced an interruption in its settlement at the end of the first century BCE. Only after the Roman conquest either people were settled in the empty lands or attracted to move there by incentives like free land, tax exemption for some time or military pressure. As many were coming from a partially Romanized Gaul, which had a Celtic background itself, their material culture appears to us 'native' (Sommer 2015b).

This is the background for the archaeological subprojects 'Population and livestock in the Raetian Alps and alpine foreland of the first century CE' and 'Gontia as a melting pot?—The composition of the population during Günzburg's Roman military period, as reflected by its graves. A model for Raetia' of our project (see chapter 'Current Synthesis and Future options'). Can the population of southern Germany living in native-appearing settlements at the beginning of the Roman occupation in the beginning of the first century BCE be determined as indigenous, or does it have its roots somewhere else outside the region? If the latter, are there indications as from where they were moving and under what circumstances did they migrate to our area? Can we determine from where the Roman soldiers were coming and is the model of camp followers from previous places of garrison or original place of recruitment correct? In other words, how small or large was the interaction with a possible surrounding population, as the forts provided a well-defined market, not least because of the regular instalments which the soldiers received? We hope that the detailed archaeological analysis features and finds in relation to the isotopic analysis will provide further insights into the settlement history of the Roman times.

Acknowledgements This research project would not have been possible without the support of a number of people. We would like to sincerely thank the following institutions for their cooperation and assistance: Arbeitskreis für Vor- und Frühgeschichte—Gruppe Augsburg Süd; AschheiMuseum, Aschheim; Autonome Provinz Bozen—Südtirol, Amt für Bodendenkmäler, Bozen; Bayerisches Landesamt für Denkmalpflege; Bundesdenkmalamt Österreich, Landeskonservatorat für Tirol, Innsbruck; Kreisarchäologie Deggendorf; Museum Erding; Pfarrmuseum Flintsbach; Salzburg Museum; Soprintendenza per i Beni Librari, Archivistici ed Archeologici, Trento; Staatssammlung für Anthropologie und Paläoanatomie München; Stadt Günzburg; Tiroler Landesmuseum Ferdinandeum, Innsbruck; and everyone else who helped this project to succeed.

References

Adam A (1996) Le fibule di tipo celtico nel Trentino. Patrimonio Storico e Artistico del Trentino 19. Ufficio Beni Archeologici, Trento

Alberti A (2007) La necropoli protostorica di Vadena. Tesi di laurea in protostorica europea. Unpublished thesis, Università di Roma La Sapienza, Roma

Anthony D (1990) Migration in Archaeology. The baby and the bath water. Am Anthropol 92:895–914

Bagolini B, Broglio B (1985) Il ruolo delle Alpi nei tempi preistorici (dal Paleolitico al Calcolitico). In: Liverani M et al (eds) Studi di Paletnologia in onore di Salvatore M. Puglisi. Universita di Roma "La Sapienza", Roma, pp 663–705

Bankus M (2004) Der Freisinger Domberg und sein Umland. Untersuchungen zur prähistorischen Besiedlung. Freisinger Archäologische Forschungen 1. Verlag Marie Leidorf, Rahden

Bartelheim M, Eckstein K, Huijsmans M, Krauß R, Pernicka E (2002) Kupferzeitliche Metallgewinnung in Brixlegg, Österreich. In: Bartelheim M, Krause R, Pernicka E (eds) Die Anfänge der Metallurgie in der Alten Welt. Freiberger Forschungen zur Archäometrie und Kulturgeschichte 1, pp 33–82

Bintliff J, Pearce M (eds) (2011) The death of archaeological theory? Oxbow Books, Oxford

Borrello MA, Mottes E, Schlichtherle H (2013) Traverser les Alpes au Néolithique. In: Borrello MA (ed) Les hommes préhistoriques et les Alpes. BAR International Series 2476, pp 27–40

Brandt G, Szécsényi-Nagy A, Roth C, Alt KW, Haak W (2014) Human paleogenetics of Europe—the known knowns and the known unknowns. J Hum Evol 30:1–20

Brotherton P et al (2013) Neolithic mitochondrial haplogroup H genoms and the genetic origins of Europeans. Nat Commun 4:1764

Burmeister S (2000) Archaeology and migration: approaches to an archaeological proof of migration. Curr Anthropol 41:539–567

Chapman J, Hamerow H (eds) (1997) Migrations and invasions in archaeological explanations. BAR International Series 664

Childe VG (1925) The dawn of European civilization. K. Paul, London

Childe VG (1929) The danube in prehistory. Oxford University Press, Oxford

Czysz W (2013) Zwischen Stadt und Land—Gestalt und Wesen römischer *Vici* in der Provinz Raetien. In: Heising A (ed) Neue Forschungen zu zivilen Kleinsiedlungen (*vici*) in den römischen Nordwest-Provinzen. Akten der Tagung Lahr 21–23.10.2010, Bonn, pp 261–377

Dal Ri L (1985) Scavo di una casa dell'Età del Ferro a Stufles, quartiere di Bressanone (Stufles B). Denkmalpflege in Südtirol—Tutela dei Beni Culturali in Alto Adige 1985:195–237

Dal Ri L, Evans S (1992) Note sull'insediamento e sulla necropoli di Vadena (Alto Adige). Bemerkungen über die Siedlung und das Gräberfeld von Pfatten (Südtirol). In: Metzger I, Gleirscher P (eds) Die Räter/I Reti. Schriften der Arbeitsgemeinschaft Alpenländer. Athesia, Bozen, pp 475–525

Egg M (2016) Das eisenzeitliche Gräberfeld von Wörgl in Nordtirol—Leben in einer Grenzregion. http://web.rgzm.de/forschung/schwerpunkte-und-projekte/a/article/das-eisenzeitliche-graeberfeld-von-woergl-in-nordtirol-leben-in-einer-grenzregion. Accessed 10 June 2016

Farkas IG (2015) The dislocation of the roman army in Raetia. BAR International Series 2733

Fontijn D (2002) Sacrificial landscapes. Cultural biographies of persons, objects and "natural places" in the Bronze Age of the southern Netherlands, c. 2300–600 BC. Analecta Praehistorica Leidensia 33/34. Leiden University Press, Leiden

Gleirscher P (1991) Die Räter. Rätisches Museum Chur

Gritsch H (1987) Schiffahrt auf Etsch und Inn. In: Lindgren U (ed) Alpenübergänge vor 1850. Landkarten, Straßen, Verkehr. Symposium am 14./15. Februar 1986 in München. Vierteljahresschrift für Sozial - und Wirtschaftsgeschichte, Beiheft 83:47

Grupe G, Price TD, Schröter P, Söllner F, Johnson CM, Beard BL (1997) Mobility of Bell Beaker people revealed by strontium isotope ratios of tooth and bone: a study of southern Bavarian skeletal remains. Appl Geochem 12:517–525

Haak W, Lazaridis J, Patterson N et al (2015) Massive migration from the steppes is a source for Indo-European languages in Europe. Nature 522:207–211

Hahn HP (2008) Diffusion appropriation and globalization some remarks on current debates in anthropology. Anthropos 103:191–202

Hahn HP, Weiss H (2013) Introduction: biographies, travels and itineraries of things. In: Hahn HP, Weiss H (eds) Mobility, meaning & transformation of things shifting contexts of material culture through time and space. Oxbow Books, Oxford, pp. 1–14

Harding A (2013) Trade and exchange. In: Harding A, Fokkens H (eds) The Oxford Handbook of the European Bronze Age. Oxford University Press, Oxford, pp. 370–381

Hauser F (2012) Anmerkungen zur Rekonstruktion des Verkehrsnetzes der Hallstattzeit. In: Tappert C, Later C, Fries-Knoblach J, Ramsl P, Trebsche P, Wefers S, Wiethold J (eds) Wege und Transport. Beiträge zur Sitzung der AG Eisenzeit während der 80. Verbandstagung des West - und Süddeutschen Verbandes für Altertumsforschung e.V. in Nürnberg 2010. Beiträge zur Ur - und Frühgeschichte Mitteleuropas 69, pp 83–94

Hauser F (2014) Der Ipf bei Bopfingen und das Nördlinger Ries im überregionalen Verkehrsnetz der Hallstatt - und Frühatènezeit. In: Krause R (ed) Neue Forschungen zum frühkeltischen Fürstensitz auf dem Ipf. Frankfurter Archäologische Schriften 24:213–224

Holder PA (1980) Studies in the auxilia of the Roman army from Augustus to Trajan. BAR International Series 70

Huijsmans M, Krauß R (2015) 6.000 Jahre Brixlegg. Archäologische Untersuchungen auf den Fundstellen Mariahilfbergl und Hochkapelle am Mehrnstein. Fundberichte aus Österreich, Materialien, Reihe A, 22

Jaeger M (2016) Bronze age fortified settlements in central Europe. Studien zur Archäologie in Osteuropa 17. Rudolf Habelt Verlag, Bonn

Kasseroler A (1957) Die vorgeschichtliche Niederlassung auf dem “Himmelreich” bei Wattens. Schlern-Schriften 166. Wagner, Innsbruck

Kern A, Guichard V, Cordie R, David W (eds) (2009) Situlen—Bilderwelten zwischen Etruskern und Kelten auf antikem Weingeschirr. Schriften des Kelten Römer Museums Manching 2

Kienlin T (2013) Copper and Bronze: Bronze age metalworking in context. In: Fokkens A, Harding A (eds) The Oxford Handbook of the European Bronze Age. Oxford University Press, Oxford, pp. 414–436

Knappett C (2011) An archaeology of interaction. Network perspectives on material culture and society. Archaeological Press, Oxford

Kopytoff I (1986) The cultural biography of things: commoditization as process. In: Appaduri A (ed) The social life of things: commodities in cultural perspective. Cambridge University Press, Cambridge, pp. 64–91

Kristiansen K (1989) Prehistoric migrations—the case of the single grave and corded ware cultures. J Danish Archaeol 8:211–225

Lang A (1998) Das Gräberfeld von Kundl im Tiroler Inntal. Studien zur vorrömischen Eisenzeit in den zentralen Alpen. Frühgeschichtliche und provinzialrömische Archäologie; Quellen und Forschungen 2. Verlag Marie Leidorf, Rahden

Lang A (2002) Das Inntal als Route für Verkehr und Handel in der Eisenzeit. In: Schnekenburger G (ed) Über die Alpen. Menschen—Wege—Waren. Archäologisches Landesmuseum, Stuttgart, pp. 49–57

Leitner W, Brandl M, Bachnetzer T (2015) Die Ostalpen als Abbaugebiet und Versorgungsregion für Silex und Bergkristall in der Prähistorie. In: Stöllner T, Oeggl K (eds) Bergauf Bergab. 10.000 Jahre Bergbau in den Ostalpen. Wissenschaftlicher Beiband zur Ausstellung im Deutschen Bergbau-Museum Bochum vom 31.10.2015–24.04.2016, im Vorarlberg Museum Bregenz vom 11.06.2016–26.10.2016. Veröffentlichung aus dem Deutschen Bergbau-Museum Bochum 207, pp 59–69

Lenerz-de Wilde M (1995) Prämonetäre Zahlungsmittel in der Kupfer - und Bronzezeit Mitteleuropas. Fundberichte Baden-Württemberg 20:229–327

Lunz R (1991) Ur - und Frühgeschichte des Pfattener Raumes. In: Tengler G (ed) Pfatten. Landschaft und Geschichte. Komitee Dorfbuch Pfatten, Pfatten, pp. 53–179
Martinek KP, Sydow W (2004) Frühbronzezeitliche Kupfermetallurgie im Unterinntal (Nordtirol)—Rohstoffbasis, archäologische und archäometallurgische Befunde. In: Weisgerber G, Goldenberg G (eds) Alpenkupfer—Rame delle Alpi. Der Anschnitt, Beiheft 17. Deutsches Bergbaumuseum, Bochum, pp 119–211
Marzatico F (2001a) Letà del Bronzo Recente e Finale. In: Lanzinger M, Marzatico F, Pedrotti A (eds) Storia del Trentino I: La Preistoria e la Protostoria. Il Mulino, Bologna, pp. 367–416
Marzatico F (2001b) La prima età del Ferro. In: Lanzinger M, Marzatico F, Pedrotti A (eds) Storia del Trentino I: La Preistoria e la Protostoria. Il Mulino, Bologna, pp. 417–477
Marzatico F (2001c) La seconda età del ferro. In: Lanzinger M, Marzatico F, Pedrotti A (eds) Storia del Trentino I: La Preistoria e la Protostoria. Il Mulino, Bologna, pp. 479–573
Marzatico F (2001d) Il Trentino-Alto Adige/Südtirol tra il VI secolo e la romanizzazione. In: Vitri S, Oriolo F (eds) I Celti in Carnia e nell'arco alpino centro-orientale. Atti della Giornata di studio. Tolmezzo 30 Aprile 1999. Editreg, Trieste, pp 227–239
Marzatico F (2002) "Mobilität" entlang des Etschtals vor der Romanisierung. Mobilità lungo la Valle dell' Adige prima della romanizzatione. In: Schnekenburger G (ed) Über die Alpen. Menschen—Wege—Waren. Archäologisches Landesmuseum, Stuttgart, pp 23–37
Marzatico F (2012) La Cultura di Luco/Laugen, aggiornamenti e problemi aperti. In: Angelini A, Leonardi G (eds) Il castelliere di Castel de Pedena. Un sito di frontiera del II e I millenio a.C. Atti del Convegno Sabato 6 giugno 2009. Fondazione Angeolini, Feltre, pp 177–204
Michel C (2011) The Kārum period on the plateau. In: Steadman SR, McMahon G (eds) The Oxford handbook of ancient anatolia 10,000–323 B. C. E. Oxford University Press, Oxford, pp. 313–336
Möslein S (1998/1999) Siedlung, Depotfund und Gräberfeld der Urnenfelderzeit auf der Innterrasse am Fuße der Rachelburg bei Flintsbach a. Inn, Lkr. Rosenheim. Berichte der Bayerischen Bodendenkmalpflege 39/40:331
Möslein S, Winghart S (1998/1999) Die Rachelburg bei Flintsbach a. Inn, Lkr. Rosenheim—Eine vor - und frühgeschichtliche Höhensiedlung und mittelalterliche Burg am Alpenrand. Berichte der Bayerischen Bodendenkmalpflege 39/41:145
Möslein S, Winghart S (2002) Produktion, Verarbeitung und Verteilung von Kupfer—Die Beziehungen der alpinen Lagerstätten und der Handel in Südbayern. In: Über die Alpen—Menschen, Wege, Waren. Archäologisches Landesmuseum, Stuttgart, pp. 137–143
Montgomery J, Mandy J (2013) The contribution of skeletal isotope analysis to understanding the Bronze age in Europe. In: Harding A, Fokkens H (eds) The Oxford Handbook of the European Bronze Age. Oxford University Press, Oxford, pp. 179–196
Mottes E (2002) Südalpiner Silex im nördlichen Alpenvorland. Handel und Verbreitung in vorgeschichtlicher Zeit. In: Schnekenburger G (ed) Über die Alpen. Menschen—Wege—Waren. Archäologisches Landesmuseum, Stuttgart, pp. 95–105
Mottes E (2006) Les lames de poignards bifaciaux en silex de l'Italie septentrionale: sources d'approvisionnement, technologie et diffusion. In: Vaquer J, Briois F (eds) La fin de l'âge de Pierre en Europe du Sud. Actes de la table ronde Carcassonne 5–6 septembre 2003. Archives d'écologie préhistorique, Toulouse, pp 25–42
Mottes E, Nicolis F, Schlichtherle H (2002) Kulturelle Beziehungen zwischen den Regionen nördlich und südlich der Zentralalpen während des Neolithikums und der Kupferzeit. In: Schnekenburger G (ed) Über die Alpen. Menschen—Wege—Waren. Archäologisches Landesmuseum, Stuttgart, pp 119–135
Müller-Karpe H (1959) Beiträge zur Chronologie der Urnenfelderzeit nördlich und südlich der Alpen. Römisch-Germanische Forschungen 22. de Gruyter, Berlin
Oberrauch H (2000) Ein Depotfund von vier Kupferäxten am Pigloner Kopf (Südtirol). Archäologisches Korrespondenzblatt 30:481–498

Pauli L (1993) Hallstatt - und Latènezeit. Der Münsterberg im überregionalen Verkehrsnetz. In: Bender H, Pauli L, Stork I (eds) Der Münsterberg bei Breisach II. Münchner Beiträge zur Vor - und Frühgeschichte 40. C.H. Beck, München, pp 110–170

Pedrotti A (2001) Il Neolitico. In: Lanzinger M, Marzatico F, Pedrotti A (eds) Storia del Trentino I: La Preistoria e la Protostoria. Il Mulino, Bologna, pp. 119–181

Pietsch M (1998) Der Burgberg bei Oberaudorf—Eine Höhensiedlung der Späthallstatt - und Latènezeit. Das archäologische Jahr in Bayern 1998:52–55

Pisoni L (2009) Aspetti e problemi dell'occupazione del territorio, dell'organizzazione sociale e dell'economia agro-pastorale nell'età del ferro atesina: un'introduzione allo studio dei sistemi alimentari. Preistoria Alpina 44:225–243

Plaseller F (1936/1937) Die tirolische Innschiffahrt. Tiroler Heimat 9/10:62

Price TD, Knipper C, Grupe G, Smrcka V (2004) Strontium isotopes and prehistoric human migration: the bell beaker period in central Europe. Eur J Archaeol 7:9–40

Prien R (2005) Archäologie und Migration. Universitätsforschungen zur Prähistorischen Archäologie 120. Rudolf Habelt Verlag, Bonn

Renfrew C, Cherry JF (eds) (1986) Peer polity interaction and sociopolitical change. Cambridge University Press, Cambridge

Salač V (1998) Die Bedeutung der Elbe für die böhmisch-sächsischen Kontakte in der Latènezeit. Germania 76:573–617

Schäfer D (2011) Das Mesolithikum-Projekt Ullafelsen—Landschaftlicher Rahmen und archäologische Befunde. Arbeitsstand 2009/2010. In: Schäfer D (ed) Das Mesolithikum-Projekt Ullafelsen (Teil 1). Mensch und Umwelt im Holozän Tirols 1. Philipp von Zabern, Darmstadt [u.a.], pp 245–351

Schumacher S (2004) Die rätischen Inschriften. Geschichte und heutiger Stand der Forschung. 2. Aufl. Innsbrucker Beiträge zur Kulturwissenschaft, Sonderheft 79, Innsbruck

Sinnhuber A (1949) Die Altertümer vom "Himmelreich" bei Wattens. Schlern-Schriften 60. Wagner, Innsbruck

Sölder W (2015) Das Brandgräberfeld Vomp—Fiecht-Au im Unterinntal und die Nordtiroler Urnenfelderzeit. In: Stöllner T, Oeggl K (eds) Bergauf Bergab. 10.000 Jahre Bergbau in den Ostalpen. Wissenschaftlicher Beiband zur Ausstellung im Deutschen Bergbau-Museum Bochum vom 31.10.2015–24.04.2016, im Vorarlberg Museum Bregenz vom 11.06.2016–26.10.2016. Veröffentlichung aus dem Deutschen Bergbau-Museum Bochum 207, pp 273–277

Sommer CS (1984) The military vici in Roman Britain. BAR British Series 129

Sommer CS (1988) Kastellvicus und Kastell Untersuchungen zum Zugmantel im Taunus und zu den Kastellvici in Obergermanien und Rätien. Fundberichte aus Baden-Württemberg 13:457–707

Sommer CS (1999) The Roman army in SW Germany as an instrument of colonisation: the relationship of forts to military and civilian vici. In: Goldsworthy A, Haynes I (eds) The Roman army as a community. J Roman Archaeol Suppl. Ser. 32 (Portsmouth), pp 81–93

Sommer CS (2006) Canabae et vici militaires. In: Reddé M et al (eds) Les fortifications militaires. Documents d'archéologie française 100 (Bordeaux), pp 131–136

Sommer CS (2009) Soldiers on the move. In: Morillo A, Hanel N, Martìn E (eds) LIMES XX. XXth International Congress of Roman Frontier Studies. León (España), Septiembre 2006. Anejos de Gladius 13 (Madrid), pp 807–812

Sommer CS (2015a) Civilian settlements. In: LeBohec Y (ed) The Encyclopedia of the Roman army. Wiley, Hoboken, pp. 122–276

Sommer CS (2015b) Hat der Auerberg sein Geheimnis gelüftet?—Überlegungen zur Funktion des Auerberg in (der Provinz) Raetien. In: Ulbert G, Der Auerberg IV. Die Kleinfunde mit Ausnahme der Gefäßkeramik sowie die Grabungen von 2001 und 2008. Münchner Beiträge zur Vor - und Frühgeschichte 63, pp 487–526

Sperber L (1992) Zur Spätbronzezeit im alpinen Inn - und Rheintal. In: Metzger I, Gleirscher P (eds) Die Räter/I Reti. Schriftenreihe der Arbeitsgemeinschaft Alpenländer. Athesia, Bozen, pp. 53–90

Sperber L (1997) Zur Demographie des spätbronzezeitlichen Gräberfeldes von Volders in Nordtirol. In: Rittershofer KF (ed) Demographie der Bronzezeit. Paläodemographie—Möglichkeiten und Grenzen. Verlag Marie Leidorf, Espelkamp, pp. 105–124

Sperber L (1999) Zu den Schwertträgern im westlichen Kreis der Urnenfelderkultur: profane und religiöse Aspekte. In: Kilian-Dirlmeier I, Egg M (eds) Eliten in der Bronzezeit. Ergebnisse zweier Kolloquien in Mainz und Athen. Römisch-Germanisches Zentralmuseum, Mainz, pp. 605–659

Staudt M, Tomedi G (2015) Zur Besiedlungsgeschichte der Ostalpen in der Mittel - bis Spätbronzezeit: Bestand, Kolonisation und wirtschaftlicher Neuanfang in der mittleren und späten Bronzezeit in Nordtirol. In: Stöllner T, Oeggl K (eds) Bergauf Bergab. 10.000 Jahre Bergbau in den Ostalpen. Wissenschaftlicher Beiband zur Ausstellung im Deutschen Bergbau-Museum Bochum vom 31.10.2015–24.04.2016, im Vorarlberg Museum Bregenz vom 11.06.2016–26.10.2016. Veröffentlichung aus dem Deutschen Bergbau-Museum Bochum 207, pp 135–143

Stefan W (ed) (2010) Der Brandopferplatz auf der Piller Höhe in Fließ. Begleitband zur Dauerausstellung im Archäologiemuseum. Schriften Museum Fliess, Fliess

Steidl B, Will M (2005) Römer und Bajuwaren—Ausgrabungen auf der Trasse der A 99, Autobahnring München-West. Das archäologische Jahr in Bayern 2004:113–116

Steiner H (2007) Die befestigte bronze - und urnenfelderzeitliche Siedlung am Ganglegg im Vinschgau—Südtirol. Ergebnisse der Ausgrabungen 1997–2001 (Bronze-/Urnenfelderzeit) und naturwissenschaftliche Beiträge. Forschungen zur Denkmalpflege in Südtirol 3. Temi Editrice, Trento

Steiner H (2010a) Archäologische Untersuchungen am Ganglegg bei Schluderns in den Jahren 1997–2001. In: Dal Ri L, Gamper P, Steiner H (eds) Höhensiedlungen der Bronze - und Eisenzeit. Kontrolle der Verbindungswege über die Alpen. Forschungen zur Denkmalpflege in Südtirol 6. Temi Editrice, Trento, pp 454–485

Steiner H (2010b) Alpine Brandopferplätze. Archäologische und naturwissenschaftliche Untersuchungen. Roghi Votivi Alpini. Archeologia e scienze naturali. Forschungen zur Denkmalpflege in Südtirol 5. Temi Editrice, Trento

Steiner H, Tecchiati U (2015) Bronzezeitliche Siedlungsgeschichte in Südtirol. In: Stöllner T, Oeggl K (eds) Bergauf Bergab. 10.000 Jahre Bergbau in den Ostalpen. Beibuch zur Ausstellung im Deutschen Bergbau-Museum Bochum vom 31.10.2015–24.04.2016, im Vorarlberg Museum Bregenz vom 11.06.2016–26.10.2016. Veröffentlichung aus dem Deutschen Bergbau-Museum Bochum 207. Bochum, pp 145–149

Stöllner T (2002) Salz als Fernhandelsgut in Mitteleuropa während der Hallstatt - und Latènezeit. In: Lang A, Salač V (eds) Fernkontakte in der Eisenzeit. Konferenz Liblice 2000. Archeologický Ùstar, Prag, pp 47–71

Stöllner T, Oeggl K (eds) (2015) Bergauf Bergab. 10.000 Jahre Bergbau in den Ostalpen. Beibuch im zur Ausstellung im Deutschen Bergbau-Museum Bochum vom 31.10.2015–24.04.2016, im Vorarlberg Museum Bregenz vom 11.06.2016–26.10.2016. Veröffentlichung aus dem Deutschen Bergbau-Museum Bochum 207, pp 99–105

Strobel K (2009) Augustus und die Annexion des Alpenbogens. Die Einrichtung der Provinzen Raetia und Noricum. Germania 87:437–509

Sydow W (1984) Die prähistorische Wehranlage auf dem Buchberg, OG Wiesing, Tirol. Fundberichte aus Österreich 23:179–207

Sydow W (1995) Der hallstattzeitliche Bronzehort von Fließ im Oberinntal, Tirol. Fundberichte aus Österreich Materialhefte. Reihe A, 3. Wien

Tecchiati U (in preparation) Die Wallburg Nössing bei Vahrn (Brixen, Südtirol) und die frühe Bronzezeit im oberen Etschgebiet. Professorial dissertation, University Innsbruck

Tecchiati U, Morandi A, Negri P (2010) Archeologia, Epigrafia, Archeobotanica e Archeozoologia di una casa delle Media Età del Ferro (V–IV sec. A.C.) scavata a Bressanone, Stufles (BZ), nella proprietà Russo (Stufles 16). Annali Museo Civico Rovereto 26:3–103

Tengler G (1991) Beiträge zur Dorfgeschichte. In: Tengler G (ed) Pfatten. Landschaft und Geschichte. Komitee Dorfbuch Pfatten, Pfatten, pp. 181–391

Tillmann A (2002) Transalpiner Handel in der jüngeren Steinzeit. In: Schnekenburger G (ed) Über die Alpen. Menschen—Wege—Waren. Archäologisches Landesmuseum, Stuttgart, pp 107–110

Töchterle U (2001) Ein Keramikfragment der jungsteinzeitlichen Gaban-Gruppe aus Ampass im Tiroler Landesmuseum Ferdinandeum in Innsbruck. In: Zeisler J, Tomedi G (ed) Archaeo Tirol. Kleine Schriften 3. Wattens, pp 23–32

Töchterle U (2009) Archäologische Topographie der Siedlungskammer Ampass. Ikarus 4, Innsbruck

Töchterle U (2013) Ein Vorbericht zu den laufenden Auswertungen der bronzezeitlichen Brandopferplatzdeponie Weer-Stadlerhof (Tirol). In Stadler H, Leib S, Gamon T (eds) Brandopferplätze in den Alpen. Der Scheibenstuhl in Nenzing. Prearchos, 3/Nenzing 6. Innsbruck, pp 113–122

Töchterle U (2015) Der Kiechlberg bei Thaur als Drehscheibe zwischen den Kulturen nördlich und südlich des Alpenhauptkammes: ein Beitrag zum Spätneolithikum und zur Früh- und Mittelbronzezeit in Nordtirol. Universitätsforschungen zur prähistorischen Archäologie 261. Rudolf Habelt Verlag, Bonn

Tomedi G (2004) Der bronzezeitliche Schatzfund von Piller. Schriften des Museums Fliess 1, Fliess

Tomedi G (2008) Der hallstattzeitliche Schatzfund von Fliess, Gemeinde Fliess, Nordtirol. Schriften des Museums Fliess 2, Fliess

Tomedi G (2010) Eisenzeitliche Höhensiedlungen entlang der Transitroute des Tiroler Inntals. In: Dal Ri L, Gamper P, Steiner H (eds) Höhensiedlungen der Bronze - und Eisenzeit. Kontrolle der Verbindungswege über die Alpen. Forschungen zur Denkmalpflege in Südtirol 6. Temi Editrice, Trento, pp 560–569

Tomedi G (2012) Der mittelbronzezeitliche Schatzfund vom Piller. Eine kulturhistorische Lokalisierung. In: Hansen S, Neumann D, Vachta T, (eds) Hort und Raum. Aktuelle Forschungen zu bronzezeitlichen Deponierungen in Mitteleuropa. de Gruyter, Berlin, pp 151–168

Tomedi G, Hye S, Nicolussi Castellan S (2006) Die Räter in Stams. Neue Forschungen an der eisenzeitlichen Siedlung am Glasbergl bei Stams. Archaeo Tirol, Kleine Schriften 5. Wattens, pp 107–115

Tomedi G, Nicolussi Castellan S (2007) Ein Heiligtum der Bronze - und Eisenzeit am Goldbichl bei Igls. In: Meighörner W (ed) Ur - und Frühgeschichte von Innsbruck. Katalog zur Ausstellung im Tiroler Landesmuseum Ferdinandeum. Innsbruck, pp 69–77

Tomedi G, Staudt M, Töchterle U (2013) Zur Bedeutung des prähistorischen Bergbaus auf Kupfererze im Raum Schwaz-Brixlegg. In: Oeggl K, Schaffer V, Montanwerke Brixlegg AG (eds) Cuprum Tyrolense. 5550 Jahre Bergbau und Kupferverhüttung in Tirol. Edition Tirol, Brixlegg, pp. 55–70

Tomedi G, Töchterle U (2012) Der Kupferbergbau als Movens für die früh- und mittelbronzezeitliche Aufsiedlung Nordtirols. In: Anreiter P, Banffy E, Bartosiewicz L, Meid W, Metzner-Nebelsick C (eds) Archaeological, cultural and linguistic heritage. Festschrift für Elisabeth Jerem in honour of her 70th birthday. Archaeolingua Main Series 25. Archaeolingua, Budapest, pp 587–600

Tremel F (1970): Der Floß - und Plättenbau. In: Weidacher F, Smola G (eds) Das steirische Handwerk. Katalog zur 5. Landesausstellung Graz, Graz, pp 441–448

von Uslar R (1991) Vorgeschichtliche Fundkarten der Alpen. Römisch-Germanische-Forschungen 48. Zabern, Mainz

Wamers E (ed) (2010) Fürsten Feste Rituale. Bilderwelten zwischen Kelten und Etruskern. Archäologisches Museum Frankfurt

Weiss RM (1997) Prähistorische Brandopferplätze in Bayern. Internationale Archäologie 35. Verlag Marie Leidorf, Espelkamp

Wieland G (2000) Keltische Flussschifffahrt in Südwestdeutschland. In: Einbaum, Lastensegler, Dampfschiff. Frühe Schifffahrt in Südwestdeutschland. ALManach 5/6:77–92

Winghart S (1998) Produktion, Verarbeitung und Verteilung. Überlegungen zur Bedeutung metallischer Rohstoffe bei der Ausbildung politischer Systeme im südbayerischen Alpenvorland während der Bronzezeit. Vorträge 16. Niederbayerischer Archäologentag 1998:99–113

Zanforlin L, Tecchiati U (2010) Topografia archeologica della Bassa Atesina (prov. Bolzano). In: Dal Ri L, Gamper P, Steiner H (eds) Höhensiedlungen der Bronze - und Eisenzeit. Kontrolle der Verbindungswege über die Alpen. Forschungen zur Denkmalpflege in Südtirol 6. Temi Editrice, Trento, pp 597–646

Zanier W (1999) Der Alpenfeldzug 15 v. Chr. und die Eroberung Vindelikiens. Bilanz einer 100jährigen Diskussion der historischen, epigraphischen und archäologischen Quellen. Bayer Vorgeschbl 64:99–132

Zanier W (2004) Gedanken zur Besiedlung der Spätlatènezeit und frühen römischen Kaiserzeit zwischen Alpenrand und Donau. Eine Zusammenfassung mit Ausblick und Fundstellenlisten. In: Hüssen C-M, Irlinger W, Zanier W (eds) Spätlatènezeit und frühe römische Kaiserzeit zwischen Alpenrand und Donau. Akten des Kolloquiums in Ingolstadt am 11. und 12. Oktober 2001. Kolloquien zur Vor - und Frühgeschichte 8. Bonn, pp 237–264

Zanier W (2007) Vindeliker—Archäologisch. RGA 35:448–458

Zanier W (2010) Der römische Alpenfeldzug unter Tiberius und Drusus im Jahre 15 v. Chr. Übersicht zu den historischen und archäologischen Quellen. In: Asskamp R, Esch T (eds) IMPERIUM—Varus und seine Zeit. Beiträge zum internationalen Kolloquium des LWL-Römermuseums am 28. und 29. April 2008 in Münster. Veröffentlichungen der Altertumskommission für Westfalen, Landschaftsverband Westfalen-Lippe 18. Münster, pp 73–96

The Concept of Isotopic Landscapes: Modern Ecogeochemistry versus Bioarchaeology

Gisela Grupe, Stefan Hölzl, Christoph Mayr, and Frank Söllner

Abstract

The term "isotopic landscape" or "isoscape" is used to indicate a map depicting isotopic variation in the environment. The spatial distribution of isotopic ratios in environmental samples is an indispensable prerequisite for generating an isotopic landscape yet represents more than simply an assessment of this distribution. An isotopic landscape also includes the fundamental parameters of prediction and modelling, thus providing estimated isotopic signatures at sites for which no values are known. When calibrated, such models are very helpful in assessing the origin of geological and biological materials. Reconstructing the place of origin of primarily non-local archaeological finds is a major topic in bioarchaeology because it gives clues to major driving forces for population development through time such as mobility, migration, and trade. These are fundamental aspects of the past human behaviour. For decades, stable isotope analysis has been the method of choice, but still has its limitations. Bioarchaeological sciences have adopted "isoscapes" mainly as a term, but not as a contextual concept.

This chapter briefly introduces the research substrate of bioarchaeology, which mainly consists of human and animal skeletal finds, provides a concise

G. Grupe (✉)
Biozentrum, Ludwig-Maximilians-Universität, Martinsried, Germany
e-mail: G.Grupe@lrz.uni-muenchen.de

S. Hölzl
RieskraterMuseum Nördlingen, Nördlingen, Germany

C. Mayr
Institut für Geographie, Friedrich-Alexander-Universität, Erlangen, Germany

GeoBio-Center & Paläontologie und Geobiologie, Ludwig-Maximilians-Universität, Munich, Germany

F. Söllner
Department für Geo- und Umweltwissenschaften, Ludwig-Maximilians-Universität, Munich, Germany

G. Grupe et al. (eds.), *Across the Alps in Prehistory*,
DOI 10.1007/978-3-319-41550-5_2

overview of selected stable isotopic ratios in these remains, and explains their research potential for migration research. State of the art in bioarchaeology, including efforts towards the generation of predictive models, is discussed within the framework of existing isotopic maps and landscapes relevant to bioarchaeology. The persisting challenges in this field of research, which gave rise to research efforts summarized in this book, are also addressed.

Introduction

Stable isotopes are very useful and indispensable markers for the monitoring of the flow of matter through biogeochemical cycles. Isotopes of an element differ in the number of neutrons and are generated, e.g. by the decay of parent isotopes or by reactions with subatomic particles in the environment. Differences in the atomic mass of isotopes of the same element lead to differences in molecular bond strength and vibration energies, whereby the vibrational frequency of a molecule is inversely related to the atomic masses of its compounds. This, and the different thermodynamic reactivity of light and heavy isotopes or molecules consisting of light or heavy isotopes, leads to isotopic fractionation, i.e. uneven partitioning of isotopes between source and product. Isotopic fractionation is mostly considered for non-radiogenic isotopes of light elements because these effects are often difficult to distinguish from decay effects in radiogenic isotopes (Porcelli and Baskaran 2012) and decrease with increasing atomic mass. In general, three fractionation processes are possible and do occur in nature: In the course of equilibrium fractionation, isotopes are separated between the source and reaction products in the form of a chemical or physical equilibrium such as the reversible exchange of molecules between two phases (e.g. water vapour and liquid water). Kinetic fractionation describes mass-dependent isotopic splitting in the course of a unidirectional process such as an enzymatic reaction (e.g. photosynthesis), and diffusion fractionation occurs in the gas phase only, which is due to the slower diffusion velocity of molecules containing or consisting of heavy isotopes.

Isotopic fractionation and mixing in an ecosystem, thus, can generate compartments with characteristic isotopic signatures (see, e.g. Fry 2006). For instance, evaporation and condensation in the course of hydrological processes lead to predictable distributions of hydrogen and oxygen isotopes in the atmosphere and in precipitation, while photosynthesis is the crucial process of carbon isotope fractionation on the level of the primary producers. Isotopic labels shared by certain ecological components such as soil, water, plants, microbia and animals are successfully used for the generation of isotopic maps for the investigation of landscape ecology. Source inputs such as wastewater discharge into rivers or changing floral communities in time and space are tracked this way (Fry 2006). Such isotopic maps are empirically generated by sampling the relevant environmental components and by subsequent analyses of their isotopic signatures. However, isotopic maps differ substantially from an “isotopic landscape”.

The term "isotopic landscape" or "isoscape" emerged around the turn of the millennium and describes "maps of isotopic variation produced by iteratively applying (predictive) models across regions of space using gridded environmental data sets", whereby one "common use of isoscapes is as a source of estimated isotopic values at unmonitored sites, which can be an important implementation for both local- and global-scale studies if the isoscape is based on a robust and well-studied model" (Bowen 2010). In April 2008, a conference on isoscapes was held in Santa Barbara, California, where research interests in the fields of ecology, climate change, biogeochemistry, hydrology, forensic sciences, anthropology, atmospheric chemistry and trade regulation were addressed in an attempt to better understand and quantify the distributions of stable isotopic ratios in time and space. The conference proceedings were published by West et al. (2010a) as a monograph and received high international attention.

Bioarchaeological sciences adopted the measurement and interpretation of stable isotopes in preserved archaeological finds rapidly after their potential as ecological markers became evident and long before the concept of "isotopic landscapes" was developed. Early studies concerned the reconstruction of palaeodiet and ancient food webs by stable carbon and nitrogen isotopes in bone collagen (e.g. Vogel and van der Merwe 1977; Bumsted 1981; Schoeninger et al. 1983; Norr 1984; Schwarcz et al. 1985; DeNiro 1985) and provenance analysis by stable strontium and lead isotopic ratios in bone minerals (Ericson 1985; Molleson et al. 1986). Decades later, "isoscapes" have been adopted by bioarchaeologists, but mainly just as a term and not as a contextual concept (Grupe and McGlynn 2016). The vast majority of stable isotope studies in this field lack the fundamental parameters of prediction and modelling and are still restricted to the evaluation of the spatial variability of isotopic data. To quote Bowen et al. (2009), "the underlying premise behind isoscapes is that isotopic composition can be predicted as a function of time, location, and spatially explicit variables describing isotope-discriminating processes" and that "well calibrated models also help predict patterns of environmental isotope variation that can be used to 'fingerprint' the origin of geological and biological materials". Bioarchaeology cannot claim to use this concept before these prerequisites are fulfilled. To identify the origin of humans, animals or goods in prehistory, existing gaps in empirical data sets have to be filled, and continuous predictions of isotope distributions in time and space are needed (Bowen 2010).

In the beginning, stable isotopes in bioarchaeological finds were measured and simply compared to the known spatial distribution of the isotopic system under study such as $^{87}Sr/^{86}Sr$ in geological maps or the climate and habitat-dependent distribution of C_3 and C_4 plants which is reflected in the $\delta^{13}C$ values of the consumers' tissues. Outliers, detectable by univariate statistics (e.g. Grupe et al. 1997), were readily interpreted as immigrant individuals. Soon it became obvious, however, that the use of stable isotopes for the reconstruction of migration and trade in bioarchaeology is not an end in itself but frequently necessitates accompanying data (e.g. analysis of not only human but also animal bones or soil sampled from the same site) for the assessment of ecogeographical baseline values to account for the

small-scale variability in time and space. The deliberate a priori establishment of maps of bioavailable stable isotopes in modern environments or archaeological strata was a first approximation to "archaeological isotopic landscapes" and was developed only slowly in the course of the last decade (see below). The accumulating knowledge on the distribution of stable isotopes in the environment in time and space was followed by a refinement of the simplified notion that outliers necessarily represent primarily non-local individuals. Growing insights into the small-scale variability in isotopically characterized ecogeographical compartments gave rise to more fruitful discussions on mobility versus migration/trade in the past. In the case of individual or collective residence change, as depicted by "non-local" stable isotope signatures in the skeletal remains, distance travelled is a crucial aspect. A single micro-region might be patchy in terms of stable isotopic signatures, and simple mobility within such a region can be easily mistaken as migration and trade.

Brief Introduction into the Research Substrate: Archaeological Skeletal Remains

Bioarchaeological finds are preserved organic remains, either the remnants of former beings or preserved artefacts manufactured from organic material. Soft tissue preservation requires special burial conditions (e.g. bog bodies, fossils) or post-mortem treatments such as intended mummification. While stable isotope analysis is also applied to such remains, this will not be considered in this book because the vast majority of bioarchaeological research substrates are made up of mineralized tissues such as bones, teeth and shells. Biominerals are formed by living organisms and are under genetic control, permitting for sizes and shapes that do not occur in the course of inorganic mineralization (e.g. dissymmetry). Also, biominerals are primarily composite materials consisting of minerogenic nanocrystals that are surrounded and penetrated by organic material. In the living being, the structured composition of organic and inorganic components guarantees for material properties such as pressure and tension resistance. Since the research efforts that led to this book concentrate on how to evaluate migration and culture transfer in a defined reference area, focus is on vertebrate skeletal remains because both humans and many non-human vertebrates are mobile by nature. Recovered shells are not considered because they are either the remnants of the local fauna or were transported to the site of their recovery by their owners or as trade goods.

With the exception of cell-free tissue, such as mature dental enamel, the major constituents of the vertebrate skeleton are the elastic structural protein collagen (type I) and the pressure-resistant calcium phosphate mineral. Mature human bone consists of about 70 % mineral and 21 % collagen, mature enamel of >96 % mineral and a few weight percentages of non-collagenous proteins, while tooth dentine largely resembles bone in its gross composition (Grupe et al. 2015). The minerogenic fraction corresponds to hydroxyapatite ($Ca_{10}(PO_4)_6(OH)_2$), but is both calcium deficient and carbonated and is therefore named "bioapatite". Calcium

lattice positions may be substituted by trace elements such as the non-essential elements strontium and lead that are sequestered into the skeleton after assimilation. As a result, the calcium/phosphate ratio in bioapatite is somewhat lower than the respective ratio in the ideal hydroxyapatite (1.4–1.6 opposed to 1.67, Pate 1994). Both the phosphate and the hydroxyl group are substituted by carbonate anions in vivo (Peroos et al. 2006) but do not amount to more than 2–4 % in the living being. Bone mineral crystals are extremely small and thin platelets in vivo with an average size of only 50 × 25 nm and a thickness of 1.5–4.0 nm (Berna et al. 2004; Schmahl et al. 2017). This size and shape guarantees for a high reactive surface that is a necessity for an active metabolic organ, but requires a constant energy supply for its maintenance. After death, energy supply ceases and the crystals readily start growing in size. At the same rate as the surrounding organic material is degraded in the course of dead bone decomposition, this growth will continue until all intracrystalline porosities are filled and the bone turns into a closed system (Trueman et al. 2008). Mineral crystals of dental enamel are much larger and of µm size and are combined into bundles with a diameter of about 4 µm (Hillson 1996).

Collagen type I is responsible for the elasticity of bone and makes up about 90 % of all organic molecules in the living skeleton. It is a highly conservative structural protein that occurs in all connective tissues that have to stand tension forces. Mature collagen type I is a triple helix consisting of two α1(I) and one α2(I) chain, each made up of 338 tripeptides corresponding to 1014 amino acids of the glycine-X–Y type. Being the smallest of all physiological amino acids, the presence of glycine at every third position of the helix permits for a particularly tightly twisted chain. The triple helix is stabilized by a high abundance of the amino acid hydroxyproline by forming hydrogen bonds and pyridinoline cross-links which are specific for bone collagen (Grupe et al. 2015). While the single collagen molecule has an average length of about 300 nm and a thickness of about 1.5 nm, its combination into fibrils leads to bundles that can reach a length of several millimetres and a thickness of several hundred nanometres (Weiner and Wagner 1998; Persikov et al. 2000). Bone collagen is therefore a highly stable and hardly soluble molecule. These properties and its embedding into the bioapatite are the reasons why this organic molecule is at all capable of surviving hundreds and thousands of years after death in the soil and may serve as a substrate for several archaeometric methods such as radiocarbon dating, among others. This does not imply that bone collagen is infinitely stable and not subject to dead bone decomposition, but its state of integrity after purification from a bioarchaeological find is securely and easily assessable by its amino acid profile. This availability of a routine molecular biological method for the assessment of the molecule's state of integrity contrasts with the definition of the state of preservation of archaeological bone and tooth mineral (see Schmahl et al. 2017).

Stable Isotopes in Archaeological Skeletons and Their Research Potential for Migration Research

Stable isotopes in vertebrate skeletal remains which are suitable for an ecogeographical isotope mapping concern on the one hand the light elements hydrogen (H), carbon (C), nitrogen (N) and sulfur (S) in bone collagen, whereby carbon, hydrogen and in addition oxygen isotopic ratios are also measurable in the bone mineral (phosphate and structural carbonate groups), and on the other hand the heavy elements strontium (Sr) and lead (Pb) that substitute for calcium lattice positions in the bioapatite (Fig. 1). Since the mass differences of isotopes of light elements are relatively large with regard to the element's atomic weight, stable isotope abundances are expressed by the δ-notation as $\delta = [(R_{\text{sample}} - R_{\text{standard}})/R_{\text{standard}}]*1000$ in ‰ with R being the molar ratio of the heavy to the light isotope. A quasi-linear relationship exists between the δ-value and the abundance of the heavy isotope in a natural sample. For heavy elements with an atomic mass exceeding about 50 mass units, absolute abundance ratios are used (e.g. $^{87}Sr/^{86}Sr$) because fractionation is negligible. While this has long been assumed for logical reasons, it has been verified experimentally only very recently (Flockhart et al. 2015). *Per definition*, the fractionation factor α between source x and product y is expressed as $\alpha_{x-y} = R_x/R_y$. In most bioarchaeological publications, this fractionation factor is expressed in a simplified way as the mere difference of the δ-values between source and product $\Delta_{x-y} = \delta_x - \delta_y$ although this is not mathematically correct. However, Δ is suitable for an empirical assessment of the amount of isotopic partitioning during element

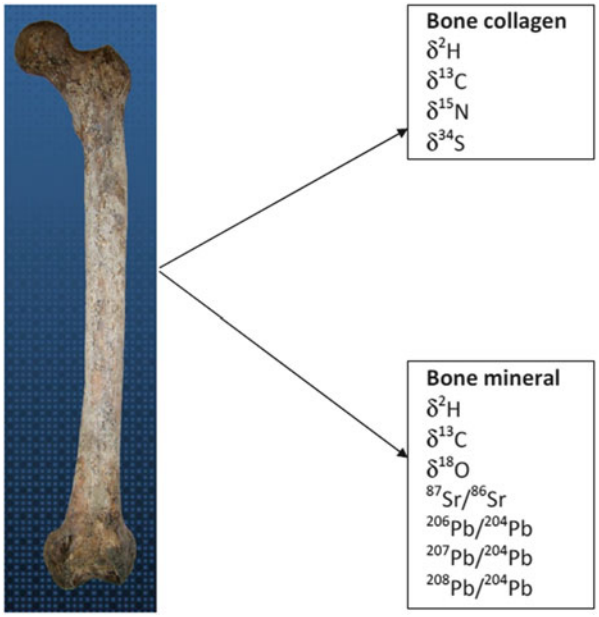

Fig. 1 Isotopic ratios routinely measured in archaeological skeletal remains

Table 1 Average atomic fraction (abundance %) of selected isotopes, and standard reference material for analysis. Abundance data from Hobson (1999), Ben-David and Flaherty (2012), and West et al. (2010b)

Element	Isotope	Abundance (%)	Standard
Hydrogen	^{1}H	99.985	V-SMOW
	^{2}H (=D)	0.015	
Carbon	^{12}C	98.90	V-PDB
	^{13}C	1.10	
Nitrogen	^{14}N	99.63	AIR
	^{15}N	0.37	
Oxygen	^{16}O	99.76	V-SMOW
	^{18}O	0.20	
Sulfur	^{32}S	95.02	CDT
	^{34}S	4.21	
Strontium	^{86}Sr	9.86	SRM 987
	^{87}Sr	7.0	
Lead	^{204}Pb	1.4	SRM 981
	^{206}Pb	24.1	
	^{207}Pb	22.1	
	^{208}Pb	52.4	

transport, e.g. through the food chain. As long as Δ does not exceed about 10 ‰, it constitutes a reasonable approximation for α because $\Delta_{x-y} \approx 10^3 \ln \alpha_{x-y}$ (West et al. 2010b). An overview of the average abundance of stable isotopes in elements which are suitable for bioarchaeological purposes is given in Table 1.

Stable isotope ratios in archaeological skeletal finds that are frequently used for the reconstruction of migration and trade in prehistory concern the radiogenic strontium and lead isotopes and $\delta^{18}O_{phosphate}$ in bioapatite. The radiogenic isotopes are related to the overall geochemistry at a site, while $\delta^{18}O$ is dependent on hydrological cycles and therefore on ecogeographical parameters. $\delta^{13}C$ and $\delta^{15}N$ in bone collagen are strongly related to diet and may serve as additional markers for provenance analysis in cases where the presumed place of origin of the finds and the site of their recovery are likely to differ in terms of the spectrum of edible plants and animals (see Fry 2006; Ben-David and Flaherty 2012). $\delta^{34}S$ in bone collagen mainly differentiates between marine/coastal and inland environments (Richards et al. 2001; Fry 2006) and is also related to diet. $\delta^{2}H$ can be measured both in bone collagen and the bioapatite. It is again governed by hydrological cycles and therefore strongly coupled with $\delta^{18}O$. Normally, a deuterium excess d is observed in stable isotopes in precipitation ($d = \delta^{2}H - \delta^{18}O \times 8$, Dansgaard 1964). However, $\delta^{2}H$ is still rather infrequently used for bioarchaeological purposes. First, a strong interference of ecogeography and diet is evident (Reynard and Hedges 2008; Petzke et al. 2010), and, second, hydrogen in both bone collagen and apatite is subject to exchange processes in the course of decomposition rendering the authentication of $\delta^{2}H$ in bone very difficult.

Isotope Maps and Isotopic Landscapes of Relevance for Bioarchaeology

The most advanced isotopic landscapes that are augmented on a regular basis concern the global hydrological cycles. The "Global Network of Isotopes in Precipitation" (GNIP) arose from a joint cooperation of the International Atomic Energy Agency (IAEA) and the World Meteorological Organization (WMO) that started a worldwide survey of the oxygen and hydrogen isotopic composition in precipitation (Dansgaard 1964; Aggarwal et al. 2010). Since the year 2007, the "Global Network of Isotopes in Rivers" (GNIR) is operated by the IAEA Water Resources Programme and monitors the isotopic composition of large river run-offs (Vitvar et al. 2007). Other projects initiated and supported by the IAEA are the "Moisture Isotopes in the Biosphere and Atmosphere" (MIBA, launched in 2004) and "Isotope Composition of Surface Waters and Groundwaters" (IAEA-TWIN, launched in 2003) networks (Aggarwal et al. 2010). For a prediction of stable isotope ratios in water, soils and plants, the IsoMAP modelling tool was first released in 2011 (Bowen et al. 2014). With regard to the global climate change, these networks are of outstanding importance for a deep understanding of the water flux in the course of environmental processes.

Empirical local maps of $\delta^{18}O$ in precipitation exist worldwide, of relevance for the transalpine passage investigated in this book are, e.g. the publications by Humer et al. (1995), Longinelli and Selmo (2003) and Kern et al. (2014). Bioarchaeology tries to make use of these existing isotopic landscapes and isotope maps by transforming stable oxygen (and to a far lesser extent also hydrogen) isotopes in the bioapatite of human and animal skeletal remains to $\delta^{18}O$ in precipitation in an attempt to gain insights into palaeoclimates and individual place of origin. Longinelli and Nuti (1973) were the first to relate $\delta^{18}O_{phosphate}$ to water and temperature and gave way to numerous studies using archaeological bones and teeth as substrate for the reconstruction of palaeoclimate proxies (e.g. Fricke et al. 1998; Luz and Kolodny 1985, 1989; Shemesh et al. 1983, 1988). Technical and methodological progress, as well as corrections with regard to the standard reference material NBS 120c, led Pucéat et al. (2010) to publish a revised regression between $\delta^{18}O_{phosphate}$, $\delta^{18}O_{water}$ and temperature (T):

$$T(^{\circ}C) = 118.7 - 4.22\left[\left(\delta^{18}O_{phosphate} + \left(22.6 - \delta^{18}O_{NBS120c}\right)\right) - \delta^{18}O_{water}\right],$$

with the result that previously published applications of $\delta^{18}O_{phosphate}$ for the reconstruction of past climates underestimated the palaeotemperature of water by 4–8 °C. But still, stable oxygen isotopic ratios prove to be accepted climate proxies.

Closely linked with climatic conditions are stable carbon isotope ratios in vegetation. Terrestrial plants preferentially assimilate the $^{12}CO_2$ over the $^{13}CO_2$ molecule in the course of photosynthesis, whereby plants using the photosynthetic C_3 and C_4 pathways differ in their isotopic fractionation leading to significantly different plant $\delta^{13}C$ values (Farquhar et al. 1989). The majority of terrestrial vegetation in the temperate climates follows the C_3 photosynthesis, while the C_4

pathway is largely restricted to herbaceous plants that prefer open, warmer and more arid environments. The overall higher flexibility towards different growth conditions in addition leads to a smaller variability of C_4 plant $\delta^{13}C$ values (about −15 ‰ to −11 ‰) compared to those of C_3 plants (on average −27 ‰ to −22 ‰, but with much lower values under closed canopies; Still and Powell 2010; Ben-David and Flaherty 2012). These isotopic differences in the primary producers are transferred into the consumer's tissues and are therefore frequently used by bioarchaeologists for the reconstruction of palaeodiets from the skeleton (with consideration of some *caveats*; see Grupe et al. 2015). $\delta^{13}C$ values of aquatic primary producers can differ from terrestrial ones, but are highly variable and related to the assimilation of different inorganic carbon species (bicarbonate versus dissolved CO_2, Mook et al. 1974; Keeley and Sandquist 1992), water temperature, salinity, amount of solubilized CO_2, water depth, etc. (Fry 2006). Differences in $\delta^{13}C$ of human bone collagen from the same archaeological site are basically indicators of different dietary preferences of the consumers and can give clues to the general past subsistence economy such as fishing versus farming (e.g. Grupe et al. 2013) and can assist in identifying immigrated human or animal individuals which originated from regions with a different vegetation cover. Because of a fairly constant offset between $\delta^{13}C_{collagen}$ and $\delta^{13}C_{carbonate}$ in the skeleton (Passey et al. 2005), also $\delta^{13}C$ in the bone structural carbonate can be successfully measured for the scope of palaeodiet reconstruction and migration research. The creation of vegetation $\delta^{13}C$ isotopic landscapes that will be of great benefit for bioarchaeological research is straightforward (Still and Powell 2010).

Stable isotope ratios in bone collagen are related to the growth metabolism of a vertebrate and mirror the respective isotopic composition of the protein part of the diet. While $\delta^{34}S_{collagen}$ reliably differentiates between terrestrial and marine environments and is therefore also a useful isotopic system for palaeodietary and potentially related migration research in bioarchaeology (Privat et al. 2007), the relationship of $\delta^{15}N$ and diet can be rather variable and less useful for migration research despite an overall enrichment of proteins with ^{15}N in marine environments. Since heavy isotopes prefer the stronger molecular bonds, ^{14}N is enriched in excreta in the course of protein metabolism, leaving the consumer's tissues enriched with ^{15}N. This leads to a significant trophic level effect in the course of the food chain (Caut et al. 2008), but the nitrogen cycle as such is complex. As a result, nitrogen uptake by the primary producers and the soil properties in terrestrial environments can be highly variable and dependent on former land use, among other factors (Pardo and Nadelhoffer 2010). $\delta^{15}N_{collagen}$ therefore does not contribute much to bioarchaeological migration research, with the exception of special scenarios related to mobility and residence change between coastal and inland sites.

Stable strontium isotope ratios ($^{87}Sr/^{86}Sr$) have long been used in ecological and bioarchaeological studies for the reconstruction of place of origin and migration of modern and past humans and animals (e.g. Bentley 2006; Crowley et al. 2015). ^{87}Sr is a radiogenic isotope and the decay product of ^{87}Rb, which has a half-life of 48.8×10^9 years which by far exceeds the age of our planet. In the course of our

earth's history, stable strontium isotopes with the masses 84, 86 and 88 gained constant ratios, while the abundance of ^{87}Sr in rocks is a function of the initial ^{87}Rb concentration in rock and its age. Therefore, geochemistry has greatly benefited from the $^{87}Sr/^{86}Sr$ ratio for dating rocks (Faure 1986). Since soil is largely generated from weathering rock, $^{87}Sr/^{86}Sr$ in terrestrial ecosystems is related to parent rocks, whereby oceanic basalts and young volcanic rocks typically exhibit $^{87}Sr/^{86}Sr$ isotopic ratios around 0.7036, while Rb-rich continental rocks have much higher ratios such as around 0.737 (Faure 1986). Due to global mixing, modern ocean water has a relative constant $^{87}Sr/^{86}Sr$ isotopic ratio of 0.7092, however, with some variability dependent on the salinity (e.g. Andersson et al. 1992). Today, a geological map exists for nearly every place on the planet that gives clues to the smaller and larger scale variability of stable strontium isotope ratios in bedrock. While such empirically generated maps may be helpful in defining expected $^{87}Sr/^{86}Sr$ values in bioarchaeological finds, they can at the same time be very misleading because the bioavailable strontium which enters the biosphere can significantly differ in its isotopic composition from the respective bedrock (Sillen et al. 1998). Let alone that some soils are not at all related to local parent rock such as glacial till introduced into carbonate-dominated regions in the North German Plain in the course of the last glaciation, most rocks do not have a uniform mineral composition. First, some constituents of parent rock weather faster than others. Beard and Johnson (2000) have already pinpointed that carbonates are both rich in strontium and weather fast, and therefore, bioavailable strontium from a region characterized by, e.g. both carbonates and siliciclastics, is heavily biased towards the carbonate portion in terms of its isotopic signature. Second, in contrast to Rb, which is an alkali metal, Sr is an alkaline earth element and behaves differently in geological reactions. Resulting differences in the Rb/Sr ratio of rocks are accordingly reflected in variations of $^{87}Sr/^{86}Sr$ isotopic ratios in ecosystems (Capo et al. 1998; Porcelli and Baskaran 2012) what basically permits the routing of $^{87}Sr/^{86}Sr$ to its geological source.

However, discerning local from non-local $^{87}Sr/^{86}Sr$ isotopic ratios in bioarchaeological finds necessitates both some geological variability between place of origin and place of recovery and at the same time a relative geological homogeneity at the latter (Slovak and Paytan 2012). This prerequisite is rarely met: The worldwide variability of archaeological human dental enamel is significantly compressed compared to the geological variability at any site (Burton and Hahn 2016) because consumer $^{87}Sr/^{86}Sr$ ratios are dependent from a finite number of calcium-rich food items (Meiggs 2007; Fenner and Wright 2014). 95 % of $^{87}Sr/^{86}Sr$ isotopic ratios of 4885 human dental enamel samples originating from six continents fall within the narrow range between 0.7047 and 0.7190 (Burton and Price 2013). Definition of the typical "local" bioavailable $^{87}Sr/^{86}Sr$ isotopic ratio is therefore far from easy. Several methods for the assessment of local strontium isotope ratios in archaeological strata have been suggested, such as the accompanying analysis of archaeological remains of the residential fauna (Price et al. 2002), sampling of modern reference material such as soil, water, snails and flora (Frei and Frei 2011; Maurer et al. 2012) or simply by referring to the majority

of measured $^{87}Sr/^{86}Sr$ isotopic ratios in an archaeological human population under the assumption that the majority of individuals should have been local to the site (Wright 2005). While the latter is a plausible assumption for any settlement chamber, it may however lead to circular conclusions and will be misleading in case of pioneering populations (Grupe and McGlynn 2010). Also, imported food such as salt (Fenner and Wright 2014) or the reliance on marine resources may obscure the data.

As a result, isotopic mapping for a detection of immigrant people or imported animals is still mainly performed by gathering as many data as possible from the finds themselves and from accompanying archaeological or modern ecological samples to get an overview of the isotopic variability in the region of interest. Without doubt, such empirical data are the indispensable prerequisite for model predictions. Geological maps can be used for a gross estimation of expected isotopic ratios to assess possible places of origin of finds which do not fit into the "regional" isotopic range. A list of major such radiogenic strontium isotope studies in bioarchaeology with regard to Europe, the Mediterranean and the Americas is provided by Slovak and Paytan (2012, pp 756–757). Such isotopic maps however do not fulfil the requirements for a definition of an "isotopic landscape". Primarily non-local individuals are readily identified by the exclusion principle, but their possible place of origin remains ambiguous because of the spatial redundancy of isotopic ratios. Slovak and Paytan (2012) are therefore right in claiming that "scientists should formulate hypotheses and devise their sampling strategy", because "the interpretation of $^{87}Sr/^{86}Sr$ data is hardly straight forward". Bioarchaeological strontium isotope maps are thus useful for supporting or rejecting any archaeological hypothesis about possible place of origin of immigrants to a site, but still cannot predict it with a certain probability.

Meanwhile, the simple amount of accumulated data resulted in regional archaeological isotopic maps covering several regions worldwide (e.g. Sillen et al. 1998; Porder et al. 2003; Hodell et al. 2004; Hedman et al. 2009; Maurer et al. 2012; Evans et al. 2010). Alternatively, an a priori isotopic mapping of suitable material can be performed for a defined region of interest for a subsequent application to bioarchaeological finds to come to answer precise questions related to migration and trade. Several such studies already exist, but are still the exception to the rule (e.g. Price and Gestsdóttir 2006; Gillmaier et al. 2009; Nafplioti 2011; Voerkelius et al. 2010; Frei and Frei 2011; Brems et al. 2013; Willmes et al. 2014). This latter procedure was chosen for the study of transalpine mobility in our project (see Toncala et al. 2017). A few years ago, a major step towards strontium isotopic landscapes was made by Bataille and Bowen (2012) by the development of a "local water model" capable of predicting $^{87}Sr/^{86}Sr$ in surface waters. Essentially this prediction relies on the relationship of bedrock with a weathering model and the resulting contributions of dissolved strontium in water. Shortly thereafter, Bataille et al. (2014) issued an independent sub-model for siliciclastic sediments. Crowley et al. (2015) undertook large efforts in compiling hundreds of published $^{87}Sr/^{86}Sr$ ratios of surface water, soil, vegetation, fish and mammalian bone across the USA and compared the accuracy of predictability by the use of the aforementioned local

water model. Besides the expected outcome that the predictability is higher in geologically homogenous regions compared to more complex ones, one result is of particular interest for bioarchaeology, namely, the fact that mammalian skeletons were most accurately predicted. This led the authors to conclude that at least in their study, mammal bone and the local water model "integrated Sr in similar ways"…"making mammal tissues particularly well suited for the model" (Crowley et al. 2015). Larger mammals (>100 kg) exhibited lower offsets between modelled and empirically measured isotopic ratios than smaller mammals, possibly because they integrate Sr "across broader spatial scales" (Crowley et al. 2015). In a small pilot study performed in the frame of the transalpine project, Söllner et al. (2016) had modelled and predicted local $^{87}Sr/^{86}Sr$ isotopic ratios in archaeological skeletons of cattle, pig and red deer from modern ecological reference samples. While at some sites, soil $^{87}Sr/^{86}Sr$ in the archaeological horizons had greatly influenced the respective isotopic ratio in mammalian bones, skeletal $^{87}Sr/^{86}Sr$ was almost exclusively related to the isotopic ratio of available Sr in water at a single site. It is apparent that soil/water/atmosphere/vegetation interdependencies resulting in bioavailable strontium for the vertebrate consumer are more complex than expected and that the spatial distribution of $^{87}Sr/^{86}Sr$ in bioarchaeological samples has been too focussed on the underlying bedrock and overlying soil properties. These interdependencies need much more research efforts in the future, but the development of "strontium isotopic landscapes" for bioarchaeological purposes is straightforward.

Like strontium, lead becomes fixed into the skeletal hydroxyapatite at calcium lattice positions. Therefore, lead and strontium are not independent in terms of mineral metabolism. More than 90 % of lead that is not excreted is stored in the skeleton where it has a particular long biological half-life of up to 10 years in compact bone (Smith et al. 1996). Basically, lead isotopes in the mammalian skeleton can therefore be used as a georeferencing tool (Kamenov and Gulson 2014). Compared to $^{87}Sr/^{86}Sr$, however, lead isotopic ratios have less frequently been used for provenance studies in bioarchaeology (e.g. Carlson 1996; Yoshinga et al. 1998; Åberg et al. 1998; Chiaradia et al. 2003; Bower et al. 2005; Montgomery et al. 2005; Turner et al. 2009; Fitch et al. 2012). The often very low lead content in archaeological finds and in particular the technical difficulties in accurately measuring the least abundant isotope ^{204}Pb constituted only one limiting factor (Albarède et al. 2012; see below). It has been strongly advised that all four stable lead isotopes need to be taken into account for any georeferencing purpose (Kamenov and Gulson 2014; Villa 2016).

In general, lead isotopes should be very promising for provenance studies because radiogenic lead is the product of three different decay series: $^{238}U \rightarrow {}^{206}Pb$, $^{235}U \rightarrow {}^{207}Pb$ and $^{232}Th \rightarrow {}^{208}Pb$. Only ^{204}Pb is not a radiogenic isotope. Therefore, the variability of lead isotopic ratios in rocks is far higher than for $^{87}Sr/^{86}Sr$ (Bullen and Kendall 1998). Just as in the case of $^{87}Sr/^{86}Sr$, stationary and bioavailable lead and its respective isotopic ratios need to be distinguished from each other. While lead is absorbed tighter to mineral surfaces than strontium and therefore only

soluble at low pH values, it can also be transported in the form of organic lead complexes and is highly mobile in nature. Consequently, the assessment of a typical "local" stable lead isotopic ratio is much more difficult. In addition to the lithological sources, the atmospheric introduction of lead into a certain catchment area is also of crucial importance (Bullen and Kendall 1998). While such airborne lead is concentrated in the topsoil layers, lead and its respective isotopic ratios in groundwater are largely a function of rock weathering. Both lead sources will mix in stream water accordingly. Ombrotrophic bogs are to a large extent fed with water and nutrients from the atmosphere and are considered "long-term traps of airborne particles" (Dunlap et al. 1999). Early metal working by humans already had a measurable impact on atmospheric lead, and bog analyses indicate that since at least 2.300 years, atmospheric lead over Europe "has not had a natural background lead isotope signature" (Shotyk et al. 1996; Dunlap et al. 1999). According to several relevant studies, preindustrial lead isotopic ratios should fall into the following ranges: $^{206}Pb/^{207}Pb$, 1.21 ± 0.05; $^{206}Pb/^{204}Pb$, 18.90 ± 0.86; $^{207}Pb/^{204}Pb$, 15.66 ± 0.10; and $^{208}Pb/^{204}Pb$, 38.74 ± 0.57 (Shotyk et al. 1996; Kylander et al. 2010; Breitenlechner et al. 2010; Kamenov and Gulson 2014). With regard to the topic of this book, typical ratios for ore deposits in the Alps are $^{206}Pb/^{204}Pb$, 18.3–18.5; $^{207}Pb/^{204}Pb$, 15.6–15.7; and $^{208}Pb/^{204}Pb$, 38.3–38.7 (Villa 2016). Due to the impact of industrial lead sources such as leaded gasoline and their worldwide distribution, modern lead isotopic signatures are significantly different (Bollhöfer and Rosman 2001).

With regard to bioarchaeological applications of lead isotopes for the assessment of mobility and migration, it is logical to expect that residential vertebrates will also best reflect the local lead isotopic ratios at a site. But in contrast to Sr, lead sources and lead uptake may significantly differ in humans and animals. In general, lead enters the organism through the ingestion of food and drinking water, but also through the skin and lungs. While soil ingestion is a major source of lead in herbivores (the bones of which should therefore reflect local isotopic signatures), leachable Pb released from soil and dust dominates over dietary intake in modern humans (Kamenov and Gulson 2014; Keller et al. 2016). Since vertebrates also discriminate against ingested lead in favour of calcium, the lead content of mineralized tissues is by far lower than environmental lead contents. Only in recent times, the global heavy metal contamination led to more similar lead contents in tissues and the surrounding habitat (Elias et al. 1982). Neolithic human skeletons exhibit typical lead concentrations between <1 and 3 ppm only (Grupe 1991), a level that was named "physiological zero level" by Drasch (1982). Modern human skeletons in contrast may exhibit lead concentrations up to 70 ppm without any accompanying symptoms of lead intoxication (Fergusson 1990). But lead exposure can have been particularly high also during several epochs in human history which is of relevance for bioarchaeological studies. Ore smelting for the purification of, e.g. silver by the process known as *cupellation* leads to the formation of lead oxide that is highly toxic because of its solubility in body fluids (Waldron 1988). Extensive metal working in antiquity has resulted in the generation of regional anthropogenic "hot spots" which are contaminated to an extent that they were no

longer suitable for agriculture until modern times (Thornton and Abrahams 1984). Since it takes a particularly long time until soils are generated by weathering of rocks and sediments, soils belong to the non-renewable resources and are an important topic in the frame of modern efforts for environment protection (Reimann et al. 2012). But also daily life in history offered many opportunities for lead exposure, such as the lead contamination of acidic food that was cooked or otherwise prepared in lead vessels by formation of lead acetate. Because of its sweet taste (synonymous "lead sugar"), preparation of *sapa*, a concentrated fruit juice widely used both as sweetener and as preservative in Roman antiquity, was preferably performed in leaden cooking ware. *Sapa* should have been a major lead source for the population at that time (Alföldi-Rosenbaum 1984). With regard to stable isotope mapping, lead isotopes from such utensils of daily life are likely to overprint the isotopic ratios of locally occurring lead. Lead ores are characterized by fairly typical isotopic fingerprints which are reflected in manufactured artefacts and are helpful in provenancing items belonging to the material culture, whereby the isotopic ratios are often augmented by trace element analysis (Frotzscher et al. 2007; Fabian and Fortunato 2010; Ling et al. 2014; Villa 2016). The custom of reusing metals by smelting broken or otherwise useless artefacts introduces an additional problem because this will lead to mixed isotopic fingerprints that are not easy to resolve. With regard to the reconstruction of human mobility and migration, primarily local individuals may therefore exhibit stable lead isotopic signatures that are no longer compatible with the respective local ratios in their native environment simply because of daily contact with traded and therefore non-local lead artefacts.

Provenancing metal objects by lead isotopic ratios has a long history in archaeometry, and extensive isotopic data bases do exist (for Europe, e.g. Durali-Mueller et al. 2007; Stos-Gale 1993; Stos-Gale and Gale 2009). Reimann et al. (2012) published a lead isotopic map of European agricultural soils a few years ago. Recently, Albarède et al. (2012) suggested to additionally focus on the geological age of the tectonic provinces where the ores have been generated and presented a model to evaluate a "geological model age" and the necessary U/Pb (μ) and Th/U (κ) ratios from lead isotopic ratios, thereby reorganizing existing Pb isotopic databases to better decipher these measurements for provenance studies of metals. But still, most provenance studies relying on lead isotopes make use of the normal "isotopic fingerprint" provided by the raw measurement data (Klein 2007). In this field, archaeometry is probably much further away from the generation of an isotopic landscape compared with stable strontium and oxygen isotope analyses. While prehistoric, historic and modern lead isotopic signatures are significantly different from each other, telling the place of origin is still not easily achieved because of the geological redundancy and the quite large catchment area of airborne lead. Villa (2016) is therefore right in claiming that archaeometry should rely on "Occam's razor: the nearest ore source, as small as it may be is the most likely choice of origin".

Persistent Challenges

In contrast to archaeological finds of artefacts manufactured from inorganic materials, stable isotope ratios in bioarchaeological finds were generated in the course of individual metabolism and have been under physiological control. When it comes to provenance analyses, these physiological parameters need to be taken into account, but still, they are largely unknown or at least known in insufficient detail. This is probably the largest obstacle for the generation of bioarchaeological isotopic landscapes.

Considering the most frequently used isotopic systems for provenance analysis, namely, oxygen, strontium and lead isotopes in the skeleton, $\delta^{18}O$ is independent from lead and strontium isotope ratios, but the latter two are not independent in terms of mineral metabolism because strontium and lead compete over calcium lattice positions in the bone/tooth mineral (see above). Reconstructing human mobility is more complex than residence change of herbivorous mammals, since omnivores assimilate a variety of different food items and the measured isotopic ratio in any tissue is made up of the weighted average of the respective dietary isotopic signatures. The first challenge therefore lies in the definition of the most important element sources which automatically implies that although stable isotope ratios are important data with a high explanatory value, they will always remain approximations. The question is how closely a past reality can be approximated at all.

Accompanying analyses of animal bone finds still are the main clue for defining the most probable local isotopic signatures for humans. Since humans and animals have different water and food sources, the human isotopic fingerprints should be similar to those of the animals (provided that all animals were in fact local to a site and not imported), but not identical. With regard to $\delta^{18}O$, average ambient humidity may have a considerable impact on animal bone $\delta^{18}O$ depending on the species (Kohn 1996). Humans are known to seldom drink surface water but rather prefer water from springs, wells or cisterns. Standing water is in constant exchange with the atmosphere, and $H_2{}^{16}O$ molecules will preferably evaporate, opening up the possibility of generating a $\delta^{18}O$ value of drinking water that significantly differs from $\delta^{18}O$ in precipitation. Another issue that has been raised early by Luz and Kolodny (1989) but has not received much attention afterwards is the fact that the residence time of phosphate in a skeleton varies between different types of bone. In the event that people migrate across climatic boundaries and ingest water of a different stable oxygen isotopic composition, the bones of the skeleton will respond to this at different rates. The resulting heterogeneous isotopic composition of a single skeleton can be very useful for the reconstruction of past migration, but necessitates a standardized sampling procedure. This holds also for the analysis of stable strontium and lead isotopes because of a strong reservoir effect in the mammalian body (Montgomery et al. 2010) and the faster turnover rate of trabecular opposed to compact bone.

It took many years until the significant impact of dietary preferences on consumer $^{87}Sr/^{86}Sr$ isotopic ratio was accepted (Burton and Hahn 2016), and still, this

important topic is often neglected in relevant publications. With regard to the variety of lead sources in the environment, sourcing the accumulated lead isotopic signatures in a skeleton is still in its infancy. In other words, while it is at present technically possible to measure original stable lead isotopic ratios in bioarchaeological finds after application of appropriate laboratory protocols, the information hidden in the measurement data is far from being deciphered. This constitutes a big obstacle especially in any attempt to generate lead isotopic landscapes.

The spatial variability of oxygen, strontium and lead isotopes in a given region of interest is mostly at hand or can be generated for archaeological strata. It has also been accepted that the spatial redundancy of all three isotopic systems necessitates the establishment of a "multi-isotope fingerprint" for each individual. Such multi-isotope studies are gaining importance, but frequently, the measured stable isotopic ratios are still compared and related to each other one by one (e.g. Müller et al. 2003). Modern mathematical tools are seldom applied, such as the hierarchical clustering of Pb, Sr and O isotopic parameters by Turner et al. (2009) or clustering of lead and oxygen isotopic ratios by Keller et al. (2016). Since the isotopic ratios $\delta^{18}O$, $^{87}Sr/^{86}Sr$, $^{206}Pb/^{204}Pb$, $^{207}Pb/^{204}Pb$, $^{208}Pb/^{204}Pb$, $^{208}Pb/^{207}Pb$ and $^{206}Pb/^{207}Pb$ may be taken as seven different, partly dependent and partly independent features capable of characterizing an individual bone find, data mining methods such as Gaussian mixture model clustering and application of an expectation-maximization algorithm have been tested in our transalpine project with a promising outcome (Mauder et al. 2016, 2017).

Resolving isotopic mixtures in geological systems is not trivial, but mixing in the biosphere and the evaluation of the involved metabolic processes is even more difficult. Many efforts have been and still are undertaken to generate bioarchaeological isotopic landscapes, and there is a strong reason to believe that the information hidden in multi-isotopic fingerprints of biominerals is far from being fully exploited. The isotopic mapping of one of the most frequently used Alpine passages, which demonstrates that a geographical obstacle does not prevent culture transfer and population admixture, is just one of the ongoing research efforts in the field.

References

Åberg G, Fosse G, Stray H (1998) Man, nutrition and mobility: a comparison of teeth and bone from the medieval era and the present from Pb and Sr isotopes. Sci Total Environ 224:109–119

Aggarwal PK, Araguás-Araguás LJ, Groening M, Kulkarni KM, Kurttas T, Newman BD, Vitvar T (2010) Global hydrological isotope data and data networks. In: West JB, Bowen GJ, Dawson TE, Tu KP (eds) Isoscapes. Understanding movement, pattern, and process on earth through isotope mapping. Springer, Dordrecht, pp. 33–50

Albarède F, Desaulty A-M, Blichert-Toft J (2012) A geological perspective on the use of Pb isotopes in archaeometry. Archaeometry 54:853–867

Alföldi-Rosenbaum E (1984) Das Kochbuch der Römer. Rezepte aus der "Kochkunst" des Apicius. 7. Aufl. Artemis & Winkler, Zürich

Andersson PS, Wasserburg GJ, Ingri J (1992) The sources and transport of Sr and Nd isotopes in the Baltic Sea. Earth Planet Sci Lett 113:459–472

Bataille CP, Bowen GJ (2012) Mapping $^{87}Sr/^{86}Sr$ variations in bedrock and water for large scale provenance studies. Chem Geol 304/305:39–52

Bataille CP, Brennan SR, Hartmann J, Moosdorf N, Wooller MJ, Bowen GJ (2014) A geostatistical framework for predicting variability in strontium concentrations and isotope ratios in Alaskan rivers. Chem Geol 389:1–15

Beard BI, Johnson CM (2000) Strontium isotope composition of skeletal material can determine the birth place and geographic mobility of humans and animals. J Forensic Sci 45:1049–1061

Ben-David M, Flaherty EA (2012) Stable isotopes in mammalian research: a beginner's guide. J Mammal 93:312–328

Bentley RA (2006) Strontium isotopes from the earth to the archaeological skeleton: a review. J Archaeol Method Theory 13:135–187

Berna F, Matthews A, Weiner S (2004) Solubilities of bone mineral from archaeological sites: the recrystallization window. J Archaeol Sci 31:867–882

Bollhöfer A, Rosman KJR (2001) Isotopic source signatures for atmospheric lead: the Northern Hemisphere. Geochim Cosmochim Acta 65:1727–1740

Bowen GJ (2010) Isoscapes: spatial pattern in isotopic biogeochemistry. Annu Rev Earth Planet Sci 38:161–187

Bowen GJ, Liu Z, Vander Zanden HB, Zhao L, Takahasi G (2014) Geographic assignment with stable isotopes in IsoMAP. Methods Ecol Evol 5:201–206

Bowen GJ, West JB, Vaughn BH, Dawson TE, Ehleringer JR, Fogel ML, Hobson K, Hoogewerff J, Kendall C, Lai C-T, Miller CC, Noone D, Schwarcz HP, Still CJ (2009) Isoscapes to address large-scale earth science challenges. Eos 90:109–116

Bower NW, Getty SR, Smith CP, Simpson ZR, Hoffman JM (2005) Lead isotope analysis of intra-skeletal variation in a 19th century mental asylum cemetery: diagenesis versus migration. Int J Osteoarchaeol 15:360–370

Breitenlechner E, Hilber M, Lutz J, Kathrein Y, Unterkircher A, Oeggls K (2010) The impact of mining activities on the environment reflected by pollen, charcoal and geochemical analyses. J Archaeol Sci 37:1458–1467

Brems D, Ganio M, Latruwe K, Balcaen L, Carremans M, Gimeno D, Silvestri A, Vanhaecke F, Muchez P, Degryse P (2013) Isotopes on the beach, Part 1: Strontium isotope ratios as provenance indicator for lime as raw materials used in Roman glass-making. Archaeometry 55:214–234

Bullen TD, Kendall C (1998) Tracing of weathering reactions and water flowpaths: a multi-isotope approach. In: Kendall C, Mc Donnell JJ (eds) Isotope tracers in catchment hydrology. Elsevier, Amsterdam, pp. 611–646

Bumsted M (1981) The potential of stable carbon isotopes in bioarchaeological anthropology. In: Martin D, Bumsted M (eds) Biocultural adaptation—comprehensive approach to skeletal analyses. Department of Anthropology Research Reports, Amherst, MA, pp. 108–126

Burton JH, Hahn R (2016) Assessing the "local" $^{87}Sr/^{86}Sr$ ratio for humans. In: Grupe G, McGlynn GC (eds) Isotopic landscapes in bioarchaeology. Springer, Berlin, pp. 113–121

Burton JH, Price TD (2013) Seeking the local $^{87}Sr/^{86}Sr$ ratio to determine geographic origins of humans: no easy answers. In: Armitage RA, Burton JH (eds) Archaeological chemistry VIII. American Chemical Society, Washington, DC, pp. 309–320

Capo RC, Stewart BW, Chadwick OA (1998) Strontium isotopes as tracers of ecosystem processes: theory and methods. Geoderma 82:197–225

Carlson AK (1996) Lead isotope analysis of human bone for addressing cultural affinity: a case study from Rocky Mountain House, Alberta. J Archaeol Sci 23:557–567

Caut S, Angulo E, Courchamp F (2008) Discrimination factors (Delta N-15 and Delta C-13) in an omnivorous consumer: effect of diet isotopic ratio. Funct Ecol 2:255–263

Chiaradia M, Gallay A, Todt W (2003) Different contamination styles of prehistoric human teeth at a Swiss necropolis (Sion, Valais) inferred from lead and strontium isotopes. Appl Geochem 18:353–370

Crowley BE, Miller JH, Bataille CP (2015) Strontium isotopes ($^{87}Sr/^{86}Sr$) in terrestrial ecological and palaeoecological research: empirical efforts and recent advances in continental-scale models. Biol Rev. doi:10.1111/brv.12217

Dansgaard W (1964) Stable isotopes in precipitation. Tellus 16:436–468

DeNiro M (1985) Postmortem preservation and alteration of in vivo bone collagen isotope ratios in relation to palaeodietary reconstruction. Nature 317:806–809

Drasch GA (1982) Lead burden in prehistorical, historical, and modern human bones. Sci Total Environ 24:99–231

Dunlap CE, Steinnes E, Flegal AR (1999) A synthesis of lead isotopes in two millennia of European air. Earth Planet Sci Lett 167:81–88

Durali-Mueller S, Brey GP, Wigg-Wolf D, Lahaye Y (2007) Roman lead mining in Germany: its origin and development through time deduced from lead isotope provenance studies. J Archaeol Sci 34:1555–1567

Elias RW, Hirao Y, Patterson CC (1982) The circumvention of natural biopurification of Ca along nutrient pathways by atmospheric inputs of industrial lead. Geochim Cosmochim Acta 46:2561–2580

Ericson J (1985) Strontium isotope characterization in the study of prehistoric human ecology. J Hum Evol 14:503–514

Evans JA, Montgomery J, Wildman G, Boulton N (2010) Spatial variations in biosphere $^{87}Sr/^{86}Sr$ in Britain. J Geol Soc Lond 167:1–4

Fabian D, Fortunato G (2010) Tracing white: a study of lead white pigments found in seventeenth-century paintings using high precision lead isotope abundance ratios. In: Kirby J, Nash S, Cannon J (eds) Trade in artists' materials: markets and commerce in Europe to 1700. Archetype, London, pp. 426–443

Farquhar GD, Ehleringer JR, Hubick KT (1989) Carbon isotope discrimination and photosynthesis. Annu Rev Plant Physiol Plant Mol Biol 40:503–537

Faure G (1986) Principles of isotope geology. Wiley, New York

Fenner JN, Wright LE (2014) Revisiting the strontium contribution of sea salt in the human diet. J Archaeol Sci 44:99–103

Fergusson JE (1990) The heavy elements: chemistry, environmental impact and health effects. Pergamon, Oxford

Fitch A, Grauer A, Augustine L (2012) Lead isotope ratios: tracking the migration of European-Americans to Grafton, Illinois in the 19th century. Int J Osteoarchaeol 22:305–319

Flockhart DTT, Kyser TK, Chipley D, Miller NG, Norris DR (2015) Experimental evidence shows no fractionation of strontium isotopes ($^{87}Sr/^{86}Sr$) among soil, plants, and herbivores: implications for tracking wildlife and forensic science. Isot Environ Health Stud 51:372–381

Frei KM, Frei R (2011) The geographic distribution of strontium isotopes in Danish surface waters—a base for provenance studies in archaeology, hydrology and agriculture. Appl Geochem 26:326–240

Fricke HC, Clyde WC, O'Neil JR, Gingerich PD (1998) Evidence for rapid climate change in North America during the latest Paleocene thermal maximum oxygen isotope composition of biogenic phosphate from the Bighorn Basin (Wyoming). Earth Planet Sci Lett 160:193–208

Frotzscher M, Borg G, Pernicka E, Höppner B, Lutz J (2007) Lead isotope and trace element patterns of German and Polish Kupferschiefer—a provenance study of bronze artifacts. In: Andrews CJ (ed) Mineral exploration and research: digging deeper. Millpress, Rotterdam, pp. 531–534

Fry B (2006) Stable isotope ecology. Springer, New York

Gillmaier N, Kronseder C, Grupe G, von Carnap-Bornheim C, Söllner F, Schweissing M (2009) The strontium isotope project of the International Sachsensymposion. Beitr Archäozool Prähist Anthropol VII:133–142

Grupe G (1991) Anthropogene Schwermetallkonzentration in menschlichen Skelettfunden als Monitor früher Umweltbelastungen. USW-Z Umweltchem Ökotox 3:226–229
Grupe G, Harbeck M, McGlynn GC (2015) Prähistorische Anthropologie. Springer, Berlin
Grupe G, McGlynn GC (2010) Anthropologische Untersuchung der Skelettfunde von Unterhaching. In: Wamser L (ed) Karfunkelstein und Seide. Neue Schätze aus Bayerns Frühzeit. Pustet, München, pp. 30–39
Grupe G, McGlynn GC (eds) (2016) Isotopic landscapes in bioarchaeology. Springer, Berlin
Grupe G, Price TD, Schröter P, Söllner F, Johnson CM, Beard BL (1997) Mobility of Bell Beaker people revealed by strontium isotope ratios of tooth and bone: a study of southern Bavarian skeletal remains. Appl Geochem 12:517–525
Grupe G, von Carnap-Bornheim C, Becker C (2013) Rise and fall of a medieval trade centre: economic change from Viking Haithabu to medieval Schleswig revealed by stable isotope analysis. Eur J Archaeol 16:137–166
Hedman KM, Curry BB, Johnson TM, Fullagar PD, Emerson TE (2009) Variation in strontium isotope ratios of archaeological fauna in the midwestern United States: a preliminary study. J Archaeol Sci 36:64–73
Hillson S (1996) Dental anthropology. Cambridge University Press, Cambridge
Hobson KA (1999) Tracing origins and migration of wildlife using stable isotopes: a review. Oecologia 120:314–326
Hodell DA, Quinn RL, Brenner M, Kamenov G (2004) Spatial variation of strontium isotopes ($^{87}Sr/^{86}Sr$) in the Maya region: a tool for tracking ancient human migration. J Archaeol Sci 31:585–601
Humer G, Rank D, Stichler W (1995) Niederschlagsisotopennetzwerk Österreich. Monographien des Bundesministeriums für Umwelt, Band 52, Wien
Kamenov GD, Gulson BL (2014) The Pb isotopic record of historical to modern human lead exposure. Sci Total Environ 490:861–870
Keeley JE, Sandquist DR (1992) Carbon: freshwater plants. Plant Cell Environ 15:1021–1035
Keller AT, Regan LA, Lundstrom CC, Bower NW (2016) Evaluation of the efficacy of spatiotemporal Pb isoscapes for provenancing human remains. Forensic Sci Int 261:83–92
Kern Z, Kohán B, Leuenberger M (2014) Precipitation isoscape of high reliefs: interpolation scheme designed and tested for monthly resolved precipitation oxygen isotope records of an Alpine domain. Atmos Chem Phys 14:1897–1907
Klein S (2007) Dem Euro der Römer auf der Spur—Bleiisotopenanalysen zur Bestimmung der Metallherkunft römischer Münzen. In: Wagner GA (ed) Einführung in die Archäometrie. Springer, Berlin, pp. 143–152
Kohn MJ (1996) Predicting animal $\delta^{18}O$. Accounting for diet and physiological adaptation. Geochim Cosmochim Acta 60:4811–4829
Kylander ME, Klaminder J, Bindler R, Weiss DJ (2010) Natural lead isotope variations in the atmosphere. Earth Planet Sci Lett 290:44–53
Ling J, Stos-Gale Z, Grandin L, Billström K, Hjärthner-Holdar E, Persson P-O (2014) Moving metals II: provenancing Scandinavian Bronze Age artefacts by lead isotope and elemental analysis. J Archaeol Sci 41:106–132
Longinelli A, Nuti S (1973) Revised phosphate-water isotopic temperature scale. Earth Planet Sci Lett 19:373–376
Longinelli A, Selmo E (2003) Isotopic composition of precipitation in Italy: a first overall map. J Hydrol 270:75–88
Luz B, Kolodny Y (1985) Oxygen isotope variation in phosphate of biogenic apatites IV. Mammal teeth and bones. Earth Planet Sci Lett 75:29–36
Luz B, Kolodny Y (1989) Oxygen isotope variation in bone phosphate. Appl Geochem 4:317–323
Mauder M, Ntoutsi E, Kröger P, Kriegel H-P (2016) Towards predicting places of origin from isotopic fingerprints—A case study on the mobility of people in the Central European Alps. In: Grupe G, McGlynn G (eds) Isotopic landscapes in bioarchaeology. Springer, Berlin, pp. 219–231

Mauder M, Ntoutsi E, Kröger P, Kriegel H-P (2017) The isotopic fingerprint: new methods of data mining and similarity search. In: Grupe G et al (eds) Across the Alps in prehistory: isotopic mapping of the Brenner passage by bioarchaeology. Springer, Cham, pp. 105–125

Maurer A-F, Galer SJG, Knipper C, Beierlein I, Nunn EV, Peters D, Tütken T, Alt KW, Schöne BR (2012) Bioavailable $^{87}Sr/^{86}Sr$ in different environmental samples. Effects of anthropogenic contamination and implications for isoscapes in past migration studies. Sci Total Environ 433:216–229

Meiggs DC (2007) Visualizing the seasonal round: a theoretical experiment with strontium isotope profiles in ovicaprine teeth. Anthropozoologica 42:107–127

Molleson TI, Eldridge D, Gale N (1986) Identification of lead sources by stable isotope ratios in bones and lead from Poundbury Camp, Dorset. Oxford J Archaeol 5:249–253

Montgomery J, Evans JA, Horstwood MSA (2010) Evidence for long-term averaging of strontium in bovine enamel using TIMS and LA-MC-ICP-MS strontium intra-molar profiles. Environ Archaeol 15:32–42

Montgomery J, Evans JA, Powlesland D, Roberts CA (2005) Continuity or colonization in Anglo-Saxon England? Isotope evidence for mobility, subsistence practice, and status at West Heslerton. Am J Phys Anthrop 126:123–138

Mook WG, Bommerson JC, Staverman WH (1974) Carbon isotope fractionation between dissolved bicarbonate and gaseous carbon dioxide. Earth Planet Sci Lett 22:169–176

Müller W, Fricke H, Halliday AN, McCulloch MT, Wartho J-A (2003) Origin and migration of the Alpine Iceman. Science 302:862–866

Nafplioti A (2011) Tracing population mobility in the Aegean using isotope geochemistry: a first map of locally bioavailable $^{87}Sr/^{86}Sr$ signatures. J Archaeol Sci 38:1560–1570

Norr L (1984) Prehistoric subsistence and health status of coastal peoples from the Panamanian Isthmus of lower Central America. In: Cohen M, Armelagos G (eds) Paleopathology at the origins of Agriculture. Academic Press, Orlando, FL, pp. 463–480

Pardo LH, Nadelhoffer KJ (2010) Using nitrogen isotope ratios to assess terrestrial ecosystems at regional and global scales. In: West JB, Bowen GJ, Dawson TE, Tu KP (eds) Isoscapes. Understanding movement, pattern, and process on earth through isotope mapping. Springer, Dordrecht, pp. 221–249

Passey BH, Robinson TF, Ayliffe LK, Cerling TE, Sponheimer M, Dearing MD, Roeder BL, Ehleringer JR (2005) Carbon isotope fractionation between diet, breath CO_2, and bioapatite in mammals. J Archaeol Sci 32:1459–1470

Pate FD (1994) Bone chemistry and paleodiet. J Archaeol Method Theory 1:161–209

Peroos S, Du Z, de Leeuw NH (2006) A computer modeling study of the uptake, structure and distribution of carbonate defects in hydroxyapatite. Biomaterials 27:2150–2161

Persikov AV, Ramshaw JAM, Kirkpatrick A, Brodsky B (2000) Amino acid propensities for the collagen triple-helix. Biochemistry 39:14960–14967

Petzke KJ, Fuller BT, Metges CC (2010) Advances in natural stable isotope ratio analysis of human hair to determine nutritional and metabolic status. Curr Opin Clin Nutr Metab Care 13:532–540

Porcelli D, Baskaran M (2012) An overview of isotope geochemistry in environmental studies. In: Baskaran M (ed) Handbook of environmental isotope geochemistry. Springer, Berlin, pp. 11–32

Porder S, Paytan A, Hadly EA (2003) Mapping the origin of faunal assemblages using strontium isotopes. Palaeobiology 29:197–201

Price TD, Burton JH, Bentley RA (2002) The characterization of biologically available strontium isotope ratios for the study of prehistoric migration. Archaeometry 44:117–135

Price TD, Gestsdóttir H (2006) The first settlers of Iceland: an isotopic approach to colonization. Antiquity 80:130–144

Privat KL, O'Connell TC, Hedges REM (2007) The distinction between freshwater- and terrestrial-based diets: methodological concerns and archaeological applications of sulphur stable isotope analysis. J Archaeol Sci 34:1197–1204

Pucéat E, Joachimski MM, Bouilloux A, Monna F, Bonin A, Motreuil S, Morinière P, Hénard S, Mourin J, Dera G, Quesna D (2010) Revised phosphate-water fractionation equation reassessing paleotemperatures derived from biogenic apatite. Earth Planet Sci Lett 298:135–142

Reimann C, Flem B, Fabian K, Birke M, Ladenberger A, Négrel P, Demetriades A, Hoogewerff J, The GEMAS Project Team (2012) Lead and lead isotopes in agricultural soils of Europe—the continental perspective. Appl Geochem 27:532–542

Reynard LM, Hedges REM (2008) Stable hydrogen isotopes in bone collagen in palaeodietary and palaeoenvironmental reconstruction. J Archaeol Sci 35:1934–1942

Richards MP, Fuller BT, Hedges REM (2001) Sulphur isotopic variation in ancient bone collagen from Europe: implications for human palaeodiet, residence mobility, and modern pollutant studies. Earth Planet Sci Lett 191:185–190

Schmahl WW, Kocis B, Toncala A, Wycisk D, Metzner-Nebelsick M, Grupe G (2017) The crystalline state of archaeological bone material. In: Grupe G et al (eds) Across the Alps in prehistory: isotopic mapping of the Brenner passage by bioarchaeology. Springer, Cham, pp. 75–104

Schoeninger MJ, DeNiro M, Tauber H (1983) Stable nitrogen isotope ratios of bone collagen reflects marine and terrestrial components of prehistoric human diet. Science 220:1380–1383

Schwarcz HP, Melbye J, Katzenberg MA, Knyf M (1985) Stable isotopes in human skeletons of southern Ontario: reconstructing paleodiet. J Archaeol Sci 12:187–206

Shemesh A, Kolodny Y, Luz B (1983) Oxygen isotope variations in phosphate of biogenic apatites. II. Phosphorite rocks. Earth Planet Sci Lett 64:405–416

Shemesh A, Kolodny Y, Luz B (1988) Isotope geochemistry of oxygen and carbon in phosphate and carbonate phosphorite francolite. Geochim Cosmochim Acta 52:2565–2572

Shotyk W, Cheburkin AK, Appleby P, Fankhauser A, Kramers JD (1996) Two thousand years of atmospheric arsenic, antimony, and lead deposition recovered in ombrotrophic peat bog profile, Jura mountains, Switzerland. Earth Planet Sci Lett 145:E1–E7

Sillen A, Hall G, Richardson S, Armstrong R (1998) $^{87}Sr/^{86}Sr$ ratios in modern and fossil foodwebs of the Sterkfontein valley: implications for early hominid habitat preference. Geochim Cosmochim Acta 62:2463–2478

Slovak NM, Paytan A (2012) Applications of Sr isotopes in archaeology. In: Baskaran M (ed) Handbook of environmental isotope geochemistry. Springer, Berlin, pp. 743–768

Smith DR, Osterloh JD, Flegal AR (1996) Use of endogenous, stable lead isotopes to determine the release of lead from the skeleton. Environ Health 104:60–66

Söllner F, Toncala A, Hölzl S, Grupe G (2016) Determination of geo-dependent bioavailable $^{87}Sr/^{86}Sr$ isotopic ratios for archaeological sites from the Inn Valley (Austria): a model calculation. In: Grupe G, McGlynn GC (eds) Isotopic landscapes in bioarchaeology. Springer, Berlin, pp. 123–140

Still CJ, Powell RL (2010) Continental-scale distributions of vegetation stable carbon isotope ratios. In: West JB, Bowen GJ, Dawson TE, Tu KP (eds) Isoscapes. Understanding movement, pattern, and process on earth through isotope mapping. Springer, Dordrecht, pp. 179–193

Stos-Gale ZA (1993) Lead isotope provenance studies—do they work? Archaeolog Polona 31:149–180

Stos-Gale ZA, Gale NH (2009) Metal provenancing using isotopes and the Oxford archaeological lead isotope database (OXALID). Archaeol Anthrop Sci 1:195–213

Thornton I, Abrahams P (1984) Historical records of metal pollution in the environment. In: Nriagu JO (ed) Changing metal cycles and human health. Springer, Berlin, pp. 7–25

Toncala A, Söllner F, Hölzl S, Mayr C, Heck K, Wycisk D, Grupe G (2017) Isotopic map of the Inn-Eisack-Etsch-Brenner passage. In: Grupe G (eds) Across the Alps in prehistory: isotopic mapping of the Brenner passage by bioarchaeology. Springer, Cham, pp. 127–227

Trueman CN, Privat K, Field J (2008) Why do crystallinity values fail to predict the extent of diagenetic alteration of bone mineral? Palaeogeogr Palaeoclimatol Palaeoecol 266:160–167

Turner BL, Kamenov GD, Kingston JD, Armelagos GJ (2009) Insights into immigration and social class at Macchu Picchu, Peru based on oxygen, strontium, and lead isotopic analysis. J Archaeol Sci 36:317–332

Villa IM (2016) Provenancing bronze: exclusion, inclusion, uniqueness, and Occam's razor. In: Grupe G, McGlynn GC (eds) Isotopic landscapes in bioarchaeology. Springer, Berlin, pp. 141–154

Vitvar T, Aggarwal PK, Herczeg AL (2007) Global network is launched to monitor isotopes in rivers. Eos 88:325–326

Voerkelius S, Lorenz GD, Rummel S, Quétel CR, Heiss G, Baxter M, Brach-Papa C, Deters-Itzelberger P, Hölzl S, Hoogewerff J, Ponzevera E, VanBocxstaele M, Ueckermann H (2010) Strontium isotopic signatures of natural mineral waters, the reference to a simple geological map and its potential for authentication of food. Food Chem 118:993–940

Vogel J, van der Merwe N (1977) Isotopic evidence for early maize cultivation in New York State. Am Antiq 42:238–242

Waldron T (1988) The heavy metal burden in ancient societies. In: Grupe G, Herrmann B (eds) Trace elements in environmental history. Springer, Berlin, pp. 125–133

Weiner S, Wagner HD (1998) The material bone: structure-mechanical function relations. Annu Rev Mater Sci 28:271–298

West JB, Bowen GJ, Dawson TE, Tu KP (eds) (2010a) Isoscapes. Understanding movement, pattern, and process on earth through isotope mapping. Springer, Dordrecht

West JB, Bowen GJ, Dawson TE (2010b) Preface: Context and background for the topic and book. In: West JB, Bowen GJ, Dawson TE, Tu KP (eds) Isoscapes. Understanding movement, pattern, and process on earth through isotope mapping. Springer, Dordrecht, pp v–xi

Willmes M, McMorrow L, Kinsley L, Armstrong R, Aubert M, Eggins S, Falguères C, Maureille B, Moffat I, Grün R (2014) The IRHUM (Isotopic Reconstruction of Human Migration) database—bioavailable strontium isotope ratios for geochemical fingerprinting in France. Earth Sys Sci Data 6:117–122

Wright LE (2005) Identifying immigrants to Tikal, Guatemala: defining local variability in strontium isotope ratios of human tooth enamel. J Archaeol Sci 32:555–566

Yoshinga J, Yoneda M, Morita M, Suzuki T (1998) Lead in prehistoric, historic, and contemporary Japanese: stable isotopic study by ICP mass spectrometry. Appl Geochem 13:403–413

Early Roman Transfer of Animals Across the Alps: Setting the Stage for Interpreting the Results of Isotope Fingerprinting

Joris Peters, Markus Gschwind, Ferdinand Neuberger, Bernd Steidl, and Simon Trixl

Abstract

Although the Alps represent a major ecological barrier separating two distinct biomes, cultural exchange between the Mediterranean Basin and Central Europe across this formidable region can be evidenced since prehistory. However, the influx of goods, humans and animals to the newly founded province *Raetia* achieved an unprecedented level subsequent to the Roman conquest and the integration of the northern Alpine forelands into the *Imperium Romanum*. Analysing the provenance of that material culture and also the immigrated humans and imported animals associated with it represents a significant challenge to research. To improve our understanding of sociocultural changes triggered by the Romanisation of the northern Alpine foreland and of human exploitation of animals and developments in livestock breeding practices in particular, our approach combines archaeological, zooarchaeological and stable isotope evidence from contexts dating between 100 BCE and 100 CE. Based on the archaeological record, it can be concluded that a large part of Mediterranean and Mediterranean-style supplies for early Roman *Raetia* was shipped via or from Gaul, whereas the via *Claudia Augusta* witnessed the transportation of significantly fewer goods from Northern Italy across the Alpine divide. This spatial framework provides the basis for defining possible regions of origin of draught and pack animals, mounts, breeding stock and pets. Since Augustan/Tiberian times, animal husbandry in *Raetia* benefitted from breeding measures

J. Peters (✉) • F. Neuberger • S. Trixl
Institut für Paläoanatomie, Domestikationsforschung und Geschichte der Tiermedizin, Ludwig-Maximilians-Universität, Munich, Germany
e-mail: joris.peters@palaeo.vetmed.uni-muenchen.de

M. Gschwind
Bayerisches Landesamt für Denkmalpflege, Munich, Germany

B. Steidl
Archäologische Staatssammlung, Munich, Germany

G. Grupe et al. (eds.), *Across the Alps in Prehistory*,
DOI 10.1007/978-3-319-41550-5_3

aimed at improving performance. This was accomplished by importing sires or sometimes even small founder flocks, but details about such practices are missing from Roman writings. By applying isotope fingerprinting, the issue of animal transfers will be tested and possible regions of origin defined. However, using georeferenced isotope signatures (Sr, Pb and O) to document distant transfers of animals is not unproblematic. Limitations are linked not only to the geological/geographical complexity of the Alps and its forelands but also to the diversity in husbandry systems (e.g. vertical transhumance) as well as fast and multiple animal transfers.

Introduction

Separating the warm temperate Mediterranean basin from cool temperate Central Europe, the Alps represent a major ecogeographical and at the same time cultural barrier between (pre)historic communities inhabiting the regions north and south of the main Alpine divide. Nonetheless, human migration and the transfer of material culture and valuable goods across the Alps have a long tradition (e.g. Schnekenburger 2002; see chapter "Transalpine Mobility and Trade since the Mesolithic"). Cultural exchange however, took place via few Alpine passages already frequented since ancient times. One major passage connecting the Po River valley with the northern Alpine foreland crossed the Raetian Alps following the valleys of the rivers Etsch (with its source near the Reschen-Scheideck Pass), Eisack (with its source near the Brenner Pass), Inn and Lech.

The Roman conquest of the Alps and the northern Alpine foreland 15 BCE was accomplished by a pincer movement, whereby Tiberius marched one army group from Gaul to the High Rhine River and then eastwards, whereas Drusus assembled a second army group in Northern Italy and used *Tridentum*/Trento as base for an advance across the Alpine divide. Conceivably, the Roman conquest and subsequent integration of the northern Alpine forelands into the *Imperium Romanum* represents one of the most significant incursions into the development of the cultural landscape north of the Alpine divide. Under the influence of the novel Mediterranean lifestyle, the political and sociocultural system as well as many aspects of everyday life witnessed profound changes affecting domains as diverse as, e.g. agriculture, urban architecture and infrastructure. Since early Roman times, the influx of cultural assets and goods was essentially determined by three factors, namely, (1) dislocation of Roman military units, (2) private economy and (3) autochthonous regional trade.

A first dislocation of military units in the region concerned the Roman legions invading the country during the Alpine war ('Alpenfeldzug'). They stayed in or near Augsburg until 9/16 CE. The *legionarii* at this time consisted of Italics, people from southern France and possibly from Spain (Nuber 2015; Scholz 2015; Zanier 1999), with a pronounced Mediterranean lifestyle and consumer behaviour. These legions were reinforced by auxiliary units initially derived from Gaulish tribes

stationed permanently in *Raetia* after the withdrawal of the legions. During the process of occupation, the army had already started building up an infrastructure of road networks, certainly out of strategic and administrative considerations, but, more importantly, to ensure the transport of supplies (Fig. 1). These measures included planning the location and building and completing of roads from the Po Valley in Northern Italy to the most important military base at *Augusta Vindelicum*/Augsburg (via *Augusta*, later called via *Claudia Augusta*) and from Gaul via Lake Geneva, *Aventicum*/Avenches, *Brigantium*/Bregenz, into the Alpine forelands, with connections to Italy from Lake Geneva via *Summus Poeninus*/Great St. Bernard Pass to *Augusta Praetoria*/Aosta, respectively, from the Alpine Rhine Valley to *Comum*/Como. In the eastern part of north Alpine *Raetia*, the road from Gaul led to *Iuvavum*/Salzburg in the Province *Noricum* with a branch to *Lentia*/Linz on the Danube and another one southwards via Radstädter Tauern Pass to *Aquileia* at the *Caput Adriae* (Solano 2011; Steidl 2016).

Immediately after the onset of Roman occupation, the supply of troops and immigrating colonists, particularly in the urban settlements, was ensured or quickly furnished by private enterprise companies. Especially foodstuffs of Mediterranean origin, such as wine, olive oil, fish sauce and fruits as well as table- and kitchenware

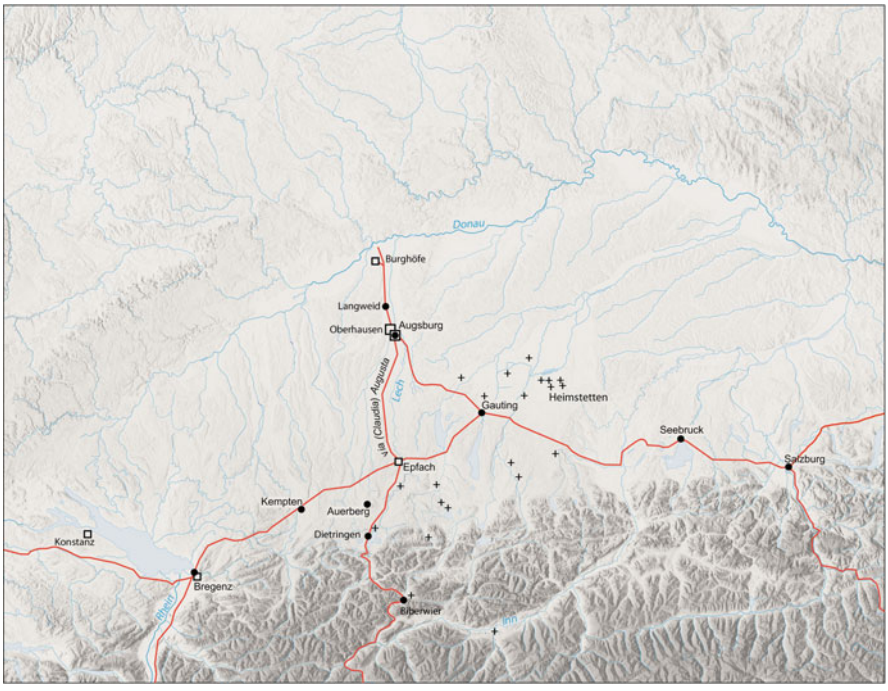

Fig. 1 Legionary base (*large square*), castella (*small square*), civil settlements (*filled circle*) and the main roads in Roman Raetia at the beginning of the first century AD. Settlements, graves and ritual places of the autochthonous Heimstetten group (+) of about the mid-first century AD

and special handicraft products, were in high demand. Long-distance transport was carried out by a network of investors, trading companies, contractors and distributors (Schlippschuh 1974; Walser 1994) creating an effective set-up by using public infrastructure facilities including roads, *mansiones*, harbours, etc.

Apart from new supply ways introduced by Roman merchants and companies, certain forms of autochthonous regional trade already in use for centuries may have been continued. The small-scale trade and transfer of Mediterranean prestige items such as metal vessels, formerly distributed from the south by local tribes, likely came to an end, but regional trade with agricultural products, livestock, hunting and fishing products and slaves likely persisted. This is suggested by singular finds pointing to the use in Roman times of Alpine passes of secondary importance that had not been upgraded to accommodate vehicles (Mallnitzer Tauern: Lippert and Dembski 2000, 2013; Theodul Pass: Thüry 2011; Hochtor Pass: Harl 2014).

Obviously, the Roman conquest of *Raetia* coincided with the introduction of larger numbers of animals of Mediterranean origin north of the Alps. Osseous and dental remains in refuse pits of the military camp at Dangstetten erected 20/15 BCE by *Legio XIX* and auxiliary troops (Martin-Kilcher 2011; Nuber 2015) illustrate the presence of pack and draught animals as well as mounts that are morphologically distinct from pre-Roman local populations of the same species. These animal imports obviously formed part of the baggage trains employed to transport heavy military equipment, bulk foods and other army supplies. Following the occupation of the northern Alpine foreland, the administration of the newly founded Province *Raetia* was installed and a standing army deployed. However, the question still remains for the period during the first century following the Roman conquest, whether traditional local agriculture rather than Mediterranean mixed farming practices (*pastio villatica*) fulfilled the dietary needs of the military, the provincial population and immigrants inhabiting the newly founded urban centres e.g. at *Cambodunum*/Kempten and *Augusta Vindelicum*/Augsburg.

Previous work already illustrated that melioration of livestock populations was a major consequence of Romanisation north of the Alpine divide (Boessneck 1958; Peters 1998). Since Tiberian times animal husbandry in the northern Alpine foreland demonstrably benefitted from breeding measures aiming at improving performance. To this extent, sires or sometimes even small founder flocks that were, for instance, reputed for their endurance, stature or weight were imported to *Raetia*, but details about such practices are missing from Roman writings. This explains why tangible evidence for the geographic origins of imported stock can only be obtained by a detailed study of the material culture and the faunal remains from archaeological sites dating to 100 BCE–100 CE. In addition, the routes used by immigrants, merchants and other foreign persons or for trading goods from the Mediterranean to *Raetia* could help in tracing the direction of stock imports (Fig. 2). Ideally, archaeological finds allow defining favoured regions of origin or at least directions of less probability. Of course, it cannot be excluded that sometimes the desire for a particular breed of animal from a particular region initiated transfers from areas beyond the usual flow of goods.

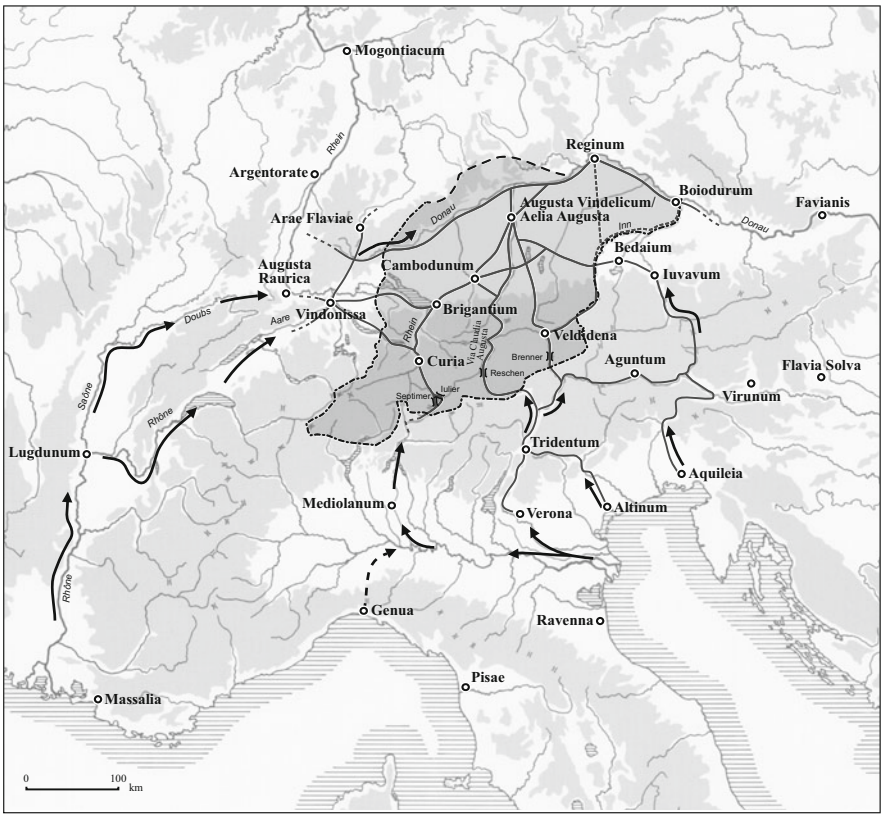

Fig. 2 Main communication lines and trade routes to *Raetia* in the first and second centuries CE according to Schimmer 2009), Abb. 10

Since trade and transport with animals will be in focus of our project 'Across the Alps', the paper considers the primary species involved and the zooarchaeological parameters used to identify potential candidates of such actions among faunal remains in early Roman contexts. This is followed by a concise overview of Mediterranean merchandise evidenced in early Roman sites in *Raetia*, together with an assessment of their possible regions of origin. The resulting geographic framework provides the archaeological basis for defining possible regions of origin of draught and pack animals, mounts, breeding stock and pets, which is currently tested applying isotope fingerprinting. However, using isotope signatures to document distant transfers of animals and mobility patterns of stock on the hoof in particular is not unproblematic, as explained in some detail below. The paper thus sets the stage for tracing animal imports across the Alps based on the isotope map presented in chapter "Isotopic Map of the Inn-Eisack-Adige-Brenner Passage and its Application to Prehistoric Human Cremations".

Archaeozoology of Roman Imports

The distinction between introduced and local stock using morphological and osteometrical criteria is based on the morphology of the skull (teeth, horncores) and size and proportions of the long bones, the latter representing parameters associated with shoulder height and body mass. Relative to the **horse**, for instance, the marked increase in shoulder height noted previously in early Roman mounts and pack animals (Boessneck 1958; Peters 1998; Peters and Manhart 2004) is currently analysed at higher resolution with the aid of equid bones from early Roman Biberwier, Cambodunum/Kempten, Langweid and Aislingen. The results obtained clearly illustrate that from Augustan/Tiberian times onwards, horses rendering service in the catchment area of the via *Claudia Augusta* had on average higher statures than their relatives bred in the northern Alpine foreland during the preceding La Tène period. One possible explanation for this development is the need for horses that met the requirements of the Roman military. Because the notable increase in shoulder height seems difficult to explain exclusively by improved husbandry conditions, we conclude that some larger-sized horses represent imports.

To satisfy local demand sustainably, however, breeding facilities probably had to be installed. Although written information about such infrastructure is lacking, it can be safely assumed that autochthonous Raetian lineages were the result of deliberate horse breeding since they were well-adapted to local conditions of climate, food and the landscape. However, it is difficult to identify such practices osteologically. As such, shoulder height estimates in horses are based on long bone lengths, which unfortunately do not allow geldings to be distinguished from propagable animals (stallions, mares). Having said that, it is irrefutable that by the end of the first century CE, small-sized horse breeds typical for the study area since the early Iron Age had been largely replaced by horse populations averaging about 15–20 cm higher at the withers.

In addition to horses, another major development in livestock husbandry concerns **cattle**. Beginning with the small-sized, short-horned Iron Age breeds, increased variability in size and proportions of Romanised cattle in the Alps and the northern Alpine foreland was already noted by Schlosser (1887) nearly 130 years ago. Since then, this conclusion has been reinforced through the study of faunal remains from several Mediterranean-influenced sites located in western *Raetia*, such as *Abodiacum*/Epfach, *Cambodunum*/Kempten, Auerberg, Langweid, etc. (Boessneck 1957, 1958, 1964; Peters 1998; Riedel 1986; Trixl et al. in press; von den Driesch 1994). Compared to La Tène cattle, average size increase in early Roman Raetian animals is quite moderate, suggesting melioration efforts on the one hand and at the same time breeding continuity from the late Iron Age into Roman times on the other. In first-century CE western *Raetia*, Roman cattle populations thus illustrate the coexistence of small- and large-sized individuals. Although the latter mainly represent draught oxen, some very robust bones also suggest the presence of bulls. Crossbred with Raetian lineages well-adapted to the constraints imposed by the local environment, autochthonous cattle breeds could be improved. Arguably, breeding efforts aimed at producing powerful animals were motivated by the necessity posed by the pulling of heavily loaded wheeled carriages and the

large-scale ploughing of arable land. Osteopathologies observed at the base of the horncores due to harnessing using withers yokes and at the tendon and ligament insertions of the lower extremities confirm the animals' use in heavy labour. Interestingly, local cattle of small stature did not disappear entirely in early Roman times and are likely associated with milk production. This assumption garners support in the fact that first-century CE Alpine and Germanic cattle were reported as prolific dairy breeds (Plinius, *Naturalis historia* 8, 179), yet cattle breeders in the Mediterranean basin considered this performance uninteresting since milk production was based on sheep and goats (Boessneck 1958; Peters 1998; Peters and Manhart 2004; Riedel 1986).

Cultural developments in eastern *Raetia*, which was inhabited by people belonging to the Heimstetten Group (~30–60 CE), obviously differed from populations living in the western part of the province. Distinguishing features of the Heimstetten Group include their burial customs, material culture clothing and settlement structure (Keller 1984; Steidl and Will 2005). Another characteristic discovered recently is the fact that at the middle of the first century CE, farmers of the Heimstetten Group already raised large-sized cattle. The animals recorded from sites like Heimstetten and Aubing exhibit limited intrapopulation variability, implying morphologically homogeneous populations. This observation clearly contrasts with the aforementioned osteological findings from western *Raetia* and suggests either replacement of local cattle by animals introduced from abroad or systematic upgrading through continuous inbreeding (Trixl et al. in press). Why developments in cattle husbandry in eastern and western *Raetia* are so different cannot be answered satisfactorily at present.

A third species exhibiting increased morphological variability in Roman times is the **dog**. Classical writings and iconography demonstrate that its Mediterranean breeding history differs from that north of the Alps: in addition to dogs used for guarding (*Canis villaticus*), herding (*Canis pastoralis*) and hunting (*Canis venaticus*), the Classical World already reared companion and even lap dogs (Peters 1997, 2005; Toynbee 1973), and it would therefore be very surprising if in the context of Romanisation, local canine populations inhabiting *Raetia* would not have been affected at all by this process.

Being normally proportioned and exhibiting shoulder heights varying between ca. 30 and 65 cm, late Iron Age canid remains reflect essentially small- and medium-sized dogs. Based on dog remains excavated at *Vitudurum*/Oberwinterthur (Morel 1991), *Augusta Vindelicum*/Augsburg (Pöllath 2012) and *Cambodunum*/Kempten, this picture does not change markedly in the northern Alpine foreland during the first decades of Roman occupation. Thus, early first-century CE dog remains strongly suggest continuity in breeding (Peters and Manhart 2004), despite sporadic evidence for phenotypically different individuals. One example of this is a tiny dog found at Langweid. With an estimated shoulder height of only 25 cm, this dog must be attributed a non-local status. So far its geographic origin is unknown, but the fact that such lap and other companion dogs could easily travel with their owners might imply the transfer of such animals over considerable distances (Boessneck 1958). To which extent such sporadic imports affected canine breeding practices in early Roman *Raetia* is unclear, but it is a fact that dog remains from

Flavian contexts (69–96 CE) illustrate a considerable increase in morphological variability (e.g. Manhart and Peters 1995).

One species of particular economic interest in the Mediterranean mixed farming practice was the **chicken**. Its introduction north of the Alps can be dated to the late Hallstatt period (Thesing 1977), whereby trade connections suggest that domestic fowl may have been introduced to southern Germany from the Mediterranean coast via the Rhône Valley and the Belfort Gap. However, the infrequency of *Gallus* remains in pre-Roman faunal assemblages supports the conclusion that chicken husbandry was only slowly adopted in Iron Age food economies (Benecke 1994). Soon after the Roman conquest, however, poultry farming intensified visibly. Besides an increase in the relative frequency of their remains in Mediterranean-influenced settings, e.g. at Auerberg (von den Driesch 1994) and *Cambodunum*/Kempten, chickens from Roman contexts were also larger sized on average and therefore heavier than their pre-Roman relatives. Since size increase already took effect soon after the Roman conquest, upgrading local lineages by means of crossbreeding with imported cocks seems the most likely explanation for this phenomenon (Peters and Manhart 2004). Whereas the presence of some extraordinary large cocks in early Roman contexts might point to birds intended for breeding (Benecke 1994; von den Driesch 1994), the possibility cannot be entirely ruled out that their presence relates to cockfighting, a practice widespread throughout the Mediterranean in antiquity. Written sources mention Greek and Medan breeds that were considered suitable for crossbreeding with local hens (Columella, *De re rustica* 8,2,13 f.), but the geographic origin of early Roman large-sized cocks in *Raetia* still needs to be determined.

Roman animal imports to *Raetia* also included taxa previously unrecorded from the study area. This category of 'exotic' species includes for instance the domestic **cat**, conceivably the most steady and successful Roman introduction north of the Alps. Another striking example is the **mule**, the much valued (but usually infertile) offspring produced by crossing a jackass with a mare. Well-adapted to perform in mountainous terrain, this frugal, strong hybrid with its even temperament must have been indispensable as an army mount and pack animal (Benecke 1994). However, it should be noted that faunal analysts face difficulties separating horses from mules in faunal assemblages. Few morphological and dental characteristics have been described in the literature (e.g. Arloing 1882; Chaveau 1879; Farello 2006; Johnstone 2005; Peters 1998; von den Driesch and Peters 2002; Uerpmann and Uerpmann 1994), but we noted that their manifestation is variable, probably because—morphologically speaking—hybrids can exhibit a morphological tendency to either to their mother, thus showing close resemblance to horses, or to their father, implying donkey-like characters. In the latter case, the chances of identifying mules are better. This explains why it is difficult to estimate the proportion of hybrids in equid assemblages that remain undetected when applying morphological analyses. It can therefore be suggested that mules were likely important in Roman army service and a preferred draught animal for passenger carriages in *Raetia*. We deduce this from an equid assemblage of 23 individuals found in a large refuse ditch located just outside of the Middle Roman frontier fort

of *Biriciana*/Weißenburg: dating ~150 CE the ratio horse to mule in this assemblage is about 5 to 1 (Peters 1998, footnote 163).

Apart from five mules identified in the refuse pits of the middle Augustan legionary camp at Dangstetten (Uerpmann and Uerpmann 1994), their presence is noted in the early and middle Roman vicus of *Vitudurum*/Oberwinterthur (Morel 1991, 88), the middle Roman settlement of Munich-Aubing and a series of middle Roman forts and associated vici, e.g. *Abusina*/Eining (Lipper 1981/82), *Quintana*/Künzing (Pöllath 2011; von den Driesch and Cartajena 2001), Oberstimm (Stettmer 1997) and *Biriciana*/Weißenburg (Peters 1998). Conversely, in early Roman sites such as Auerberg (von den Driesch 1994), *Augusta Vindelicum*/Augsburg (Pöllath 2012), *Cambodunum*/Kempten, Langweid or Aislingen, mules are apparently lacking, in spite of the fact that in some cases (small) military units were stationed here as well. Finally, the notable absence of remains of (male) donkeys in Roman archaeofaunas does not support the assumption that the breeding of mules took place in *Raetia* (Peters 1998). The thermophile nature of both donkeys and mules makes a Mediterranean origin likely.

Regions of Trade Disclosed by the Early Roman Material Culture

From the very beginning of the Roman conquest, the main routes of military advance functioned as lines of communication for supplies and linked new territories to the already existing infrastructure. Archaeological finds from early occupation sites, like olive oil, wine and fish sauce amphorae, mainly from the south of the Iberian Peninsula, but also from Italy, the eastern Mediterranean and Gaul, clearly show that the Roman army provided its forces deployed in the Alps and the northern Alpine foreland with food supplies from distant Mediterranean production centres (Ehmig 2010; Martin-Kilcher 2003; Schimmer 2009; Fig. 2). Together with the import of tablewares, these food supplies enabled the Roman military and their civilian associates to keep up a Mediterranean lifestyle even in recently conquered areas in central Europe. Midden deposits yielding very large amounts of domestic refuse are a regular feature of early Roman sites in *Raetia*. The sheer quantity of discarded ceramics and other rubbish and the fact that even objects made of copper alloy were not recycled but also dumped implies that the imported goods must have been affordable and available in large quantities (Ettlinger and Simonett 1952; Gschwind 2015).

For many of the fine wares and amphorae exhibiting wide, supra-regional distributions, the combined analysis of fabric, form and potter stamps (if available) enables us to determine the place or at least the geographic region of their production (Martin-Kilcher 1987, 1994a, b; Oxé et al. 2000; Schucany et al. 1999). Being essentially functional transport containers, amphorae show limited typological development. Conversely, tablewares were subjected to fashion trends, with frequent changes in shape, appearance and composition. This applies to the Julio-Claudian period in particular (27 BCE–68 CE). After Octavius had concluded the civil wars and established the Principate in 27 BCE, the Roman Empire under

his rule as Emperor Augustus witnessed a period of internal peace, characterised by prolific artistic and economic development almost unparalleled in its vitality and with wide-reaching impact (Freyberger 1998; Zanker 1987). At the same time, Rome's foreign policy strove for expansion, resulting in the conquest and occupation of new territories. With the gradual advance of the Roman army into new territories in western and southern Germany, frequent dislocations of military units occurred. Suppliers of the army gradually followed the troops into the newly conquered areas and met their demands by establishing new workshops and making changes in supply routes.

A relatively well understood case for the establishment of workshops closer to their markets concerns the production of Italian red slipped Terra Sigillata. In Arezzo, for example, several large workshops have been reported producing top quality red Terra Sigillata from approximately 30 BCE onwards. Around 20 BCE, some of these workshops had already established branches in Pisa and less than a decade later also at *Lugdunum*/Lyon in order to bring the production centres closer to the numerous consumers living in Gaul, along the Rhine River and in *Raetia* (Ettlinger et al. 1990; Mees 2011; Oxé et al. 2000).

In Gaul, however, additional pottery workshops were established that were independent from Italian investors. From the reign of Emperor Augustus onwards, these workshops successfully met local, regional and supra-regional demands for tablewares, a key requirement for a Roman or Romanised lifestyle. At La Graufesenque in southern Gaul, potters initially copied the type and decoration of Italian Sigillata. Soon thereafter, however, they created new vessel shapes with unique decorative styles and a characteristic standardized high-quality fabric with a glossy sintered slip. At the same time they organized their workshops in a way that enabled them to consistently produce large numbers of vessels of high quality. Consequently they succeeded in forcing Italian Sigillata out of the market in the entire northwest of the Roman Empire (Genin 2007; Mees 2011; Polak 2000; Schaad 2007). During the first half of the first century CE, additional Gaulish pottery workshops were established that specialized in other classes of fine wares intended for supra-regional trade as well. In *Raetia*, for instance, cups, beakers and lamps showing the characteristic fabric reported from *Lugdunum*/Lyon are commonly found in archaeological contexts of the Tiberian to Neronian periods. Glazed wares originating from central Gaul were regularly found as well, but in significantly smaller numbers (Greene 1979).

It is obvious that all imports from Gaulish pottery production centres reached *Raetia* via the main trading routes running north of the Alps from west to east, but the question arises whether the merchandise travelled via the Swiss Midlands or the Belfort Gap. Based on the distribution of Central Gaulish glazed wares in Roman Switzerland, it was noted that this distinct class of fine ware obviously reached the legionary camp of *Vindonissa*/Windisch via the latter route (Hochuli-Gysel 1998). In contrast, for imports originating from Italian workshops, it is much more difficult to determine the trade routes used for their transfer. Since Terra Sigillata from Arezzo and 'Pompeian Red' Ware produced in central Italy are commonly found in Gaul, *Germania superior*, Northern Italy and *Noricum* (Flügel 1999; Heger 1986;

Schindler-Kaudelka 1986; Schucany et al. 1999), it is not possible to decide whether vessels of this kind excavated in *Raetia* travelled via the Rhône Valley or via Northern Italy and across the Alps.

The analysis of tens of thousands of potter stamps on Italian Terra Sigillata is of particular interest as well, since it could be demonstrated that workshops producing in the same region had market areas in different regions. Obviously, different trade networks were employed for the distribution of the respective productions (Ettlinger et al. 1990; Mees 2011; Oxé et al. 2000). The series of stamps on Italian Terra Sigillata reported from *Iuvavum*/Salzburg in northwest *Noricum*, for example, resembles closely the spectrum found at Magdalensberg in Carinthia, but differs significantly from stamp series excavated in Raetian sites (Gschwind, in prep.). In contrast, analysis of the stamps on Italian Terra Sigillata reported from *Brigantium*/Bregenz suggests that the site was supplied mainly from the west, whilst finds from the Alpine Rhine Valley indicate differences in the supply with Italian Terra Sigillata compared to *Brigantium*/Bregenz (Schimmer 2005), rendering it unlikely that in the early Imperial periods, trade between Northern Italy and the Alpine Rhine Valley played a significant role to forwarding goods to the Raetian Alpine foreland.

The foregoing observations suggest that neither the routes across the Grison Alps nor the ones across the Tauern were of major economic importance for supplying the early Imperial inhabitants of the Raetian Alpine forelands with goods from Northern Italy. This in turn suggests that the via *Claudia Augusta* was indeed essential for supplying the northern Alpine foreland with Mediterranean commodities from Northern Italy, as—according to the epigraphic and archaeological evidence—this route was economically much more important during the first centuries of Roman Rule in *Raetia* than the one via the Brenner Pass (Flügel 2007; Grabherr 2006). In this respect, an inscription on a milestone commemorating the consolidation of the via *Claudia Augusta* in 46 CE (IBR 465 = CIL V 8003 = HD039394) mentions road works carried out under the command of Drusus in the context of his military campaign of 15 BCE. Thus, by the time of Rome's conquest, the route via the Reschen-Scheideck Pass had already been converted into a major axis connecting Northern Italy with the northern Raetian foothills of the Alps. For that reason it is not unlikely that the road works initiated by Drusus already served to optimise the route for ox carts and other wheeled transport.

Although the foregoing considerations point to the via *Claudia Augusta* as the main supply route for certain goods across the Alps, it still remains difficult to securely identify the region of origin of the merchandise brought to *Raetia*. From sites in *Raetia* that were occupied in the Augustan and early Tiberian periods, for instance, a whole series of fine and tablewares is known, which for good reasons are thought representing imports from Northern Italy (Flügel 1999; Mackensen 1978; Sieler 2009; Ulbert 1965). Verification of this assumption is nonetheless difficult, simply because the major northern Italian pottery production centres could not be located yet. Even for well-studied categories of finds, such as Terra Sigillata Padana, Aco-beakers or Sarius-bowls, the production centres that also supplied transalpine markets could not be identified yet. Independent thereof, chemical

analyses confirm the archaeological hypothesis that the production of the aforementioned groups took place in Northern Italy. The results moreover show, that we have to assume a whole series of production centres for Terra Sigillata and other fine wares in Northern Italy. On the other hand, chemical analyses remind us that occasionally similar vessels have been produced in other regions of Italy as well (Oxé et al. 2000; Schneider 2000; Schneider and Daszkiewicz 2006). Finally, it should be considered that workshops in Gaul also made Italian style fine wares such as Aco-beakers, e.g. at *Lugdunum*/Lyon (Desbat et al. 1996; Lemaître and Batigne Vallet 2015).

Turning to other early Imperial materials of Mediterranean origin found in *Raetia*, the methodological problems noted with Terra Sigillata also apply to glass. As such, the colourful high-quality glass vessels typically found in early Roman sites (Rottloff 2015) have traditionally been considered to originate from Italian workshops. Although it can be postulated that most of these finds were indeed imported from Italy, this is again difficult to verify, since glass workshops with a similar range of products were discovered in the Rhône Valley as well (Fünfschilling 2015). But even if an Italian origin can be determined, the via *Claudia Augusta* would be the most probable route of transportation only for glass vessels made in northern Italian workshops.

For early Imperial common and kitchenwares including jugs and *mortaria*, the region of origin cannot be determined so far, except for a special group of marble tempered blackware known as 'Auerberg pots'. In this case, the combined results of archaeological and natural-scientific analyses allowed concluding that the pots functioned as transport containers for mutton meat confit produced in southwest *Noricum*. Preserved this way the mutton was shipped via the Puster Valley and the via *Claudia Augusta* to sites with early Roman military occupation in *Raetia* (Flügel 2015). Because the black marble tempered 'Auerberg pots' clearly illustrate direct trade between the regions south of the Alpine divide and the northern Alpine foreland via the via *Claudia Augusta*, it can be assumed that this itinerary was also used for other goods including animals.

Further evidence for major trade across the Alps rather than via the Rhône Valley comes from the distribution of Histrian amphorae. Whereas this might not be unequivocal for the wine or fish sauce amphorae Dressel 6 A found in Dangstetten, the distribution of Histrian oil amphorae Dressel 6B strongly indicates that vessels of this type found in sites located in the Raetian Alpine foreland were introduced across the Alps (Ehmig 2010, 2011/12, 2015; Martin-Kilcher 1994a; Mees 2011; Schimmer 2009). Despite the fact that corresponding evidence from sites along this route is extremely scanty for the early Imperial period, general considerations support the conclusion that the via *Claudia Augusta* served as the main route for supplying *Raetia* with Histrian oil (Schimmer 2009). Using archaeological evidence published so far, however, it is not yet possible to quantify the role Histrian products played for the oil supply of the Alpine foreland. Interestingly, fragments of Baetian amphorae Dressel 20 show that the regular supply of olive oil had already begun by 15 BCE. Thus, whereas olive oil from the south of Spain was already being imported to *Raetia* in the late first century BCE and continued at least

until the mid-third century CE, Histrian oil imported in amphorae Dressel 6B complemented this supply to some extent only from the late Tiberian till the Neronian or early Flavian period (Schimmer 2009).

Taken together, provenance analysis of tablewares (especially of Italian Terra Sigillata) and amphorae (respectively of their contents) clearly show that *Raetia* was 'sandwiched' between two large regions with relatively homogenous supply patterns, namely, the Swiss Midlands and the Rhine Region in the west and the Eastern Alps of *Noricum* in the east (Ehmig 2011/12; Schimmer 2009). Our analysis of the literature and own data clearly illustrates that *Raetia* received supplies via and/or from Gaul and thus from the west as well as from the south, i.e. from or via Northern Italy following the via *Claudia Augusta*. However, the proportion of the different kinds of supplies varied considerably in the different subregions of *Raetia*. In addition, supply patterns may have changed quickly, not only through time but also as a function of the military or civilian character of a site and the varying composition and degree of Romanization of its inhabitants. In this respect, the aforementioned outstanding dynamics typical for the Julio-Claudian period are also reflected by shifting patterns in the supply of goods, but due to their quick succession the archaeological material can only reflect these changes in rough outlines.

Stamped Italian Terra Sigillata is of particular interest for our project since it is chronologically sensitive, often allocable to regions of production, and easily accessible thanks to the work by Philip Kenrick (Oxé et al. 2000). With production centres in central Italy, Gaul and Northern Italy, it certainly is the category of archaeological finds most suitable for the analysis of shifting trade patterns in the northern Alpine foreland during the decades before and after the beginning of the Common Era. Nevertheless, the evidence published so far can only shed some patches of light on the subject in question.

So far, the earliest Terra Sigillata ensemble comes from the early military base of Augsburg-Oberhausen, where more than half of the stamped vessels originated from *Lugdunum*/Lyon (Oxé et al. 2000; Schimmer 2005; Ulbert 1960). Together with Baetian oil amphorae, these findings underscore the importance played by Gaul for supplying the army at the beginning of the Roman occupation. In contrast to this, products from central Italian workshops form the majority of the stamped vessels in other early Imperial sites located in the Raetian Alpine foreland, such as *Brigantium*/Bregenz, *Cambodunum*/Kempten, *Abodiacum*/Epfach, the Auerberg and *Augusta Vindelicum*/Augsburg (Schimmer 2005; Sieler 2009, 2015). Even if the transport routes to *Raetia* are not clear due to the wide distribution of Arretine products in Gaul as well as in Northern Italy, the fact that products from Pisa form a considerable portion of the central Italian Terra Sigillata found in *Raetia* strongly suggests that at least these vessels were first shipped by sea and then forwarded to *Raetia* via the Rhône and Rhine rivers. This confirms once more that in early Roman times trade from central Italy via the Rhône Valley to *Raetia* was well established.

Another significant feature of all sites mentioned is the very small number of Terra Sigillata vessels imported from workshops situated in the Po Valley (Oxé

et al. 2000; Schimmer 2005; Sieler 2015). Since the via *Claudia Augusta* is the most likely import route, these finds corroborate the picture already drawn for other fine wares from Northern Italy as well as for Auerberg pots and Histrian oil amphorae.

To conclude, as far as we can judge on the basis of archaeological material surviving in archaeological contexts, most supplies for early Imperial *Raetia* were shipped from or via Gaul, whereas the via *Claudia Augusta* witnessed the transportation of significantly fewer goods from Northern Italy across the Alpine divide. However, even if the analysis of the material culture surviving in archaeological contexts sheds light on the importance of the different main routes for the supply of early Roman *Raetia*, it has to be pointed out that this concerns goods transported in large quantities. To which extent these findings can be extended to merchandise that met rare or exquisite demands for extraordinary products or exotic breeding stock remains to be seen.

Isotope Analysis and Animal Transfers

To discern patterns of mobility in livestock and long-distance transfer of individual animals, stable isotope analysis of strontium (Sr), lead (Pb) and oxygen (O) preserved in animal tissues is useful. Because these isotopes serve as proxies for both the local geological context and environment (Frei et al. 2015; Turner et al. 2009), they can help in distinguishing non-local from autochthonous individuals (e.g. Bentley and Knipper 2005a, b; Frei et al. 2015; Price et al. 2000, 2015; Scheeres et al. 2014; Schweissing and Grupe 2003; Wunder and Norris 2008). To understand patterns of mobility and transfer of animals, however, it is important to link the different geographic regions frequented consecutively including place of origin, last place of residence and intermediate stopover sites (Hobson 1999). The challenge of any study applying stable isotopes therefore is not only to evidence which individual could have been transferred but also what would have been its most likely region of provenance. Thus, in order to gain insight into the lifetime of individual animals, selection of hard tissues yielding the different isotopic signatures of the abodes throughout an individual's lifetime is essential (Tütken 2010).

Stable isotope signatures measured in animal bone usually reflect the region where that particular individual spent most of its life. As such, local isotopic signals are primarily incorporated by nutrition (Sr), dust ingestion (Pb) and drinking water (O), but bone remodelling during lifetime results in ongoing adaptation to local isotopic composition (Kamenov and Gulson 2014; Sealy et al. 1991). Contrary to bone, tooth crown formation begins shortly after birth and is usually completed during adolescence. Therefore, isotope analysis of dental enamel produces a signal of the place where this individual had spent its childhood. Consequently, differences between osseous and dental signatures are indicative of residential changes during lifetime and hence of an individual of non-local origin (Grupe and Peters 2007; Price et al. 2000). Divergent bone values moreover allow for delineation of individuals that are not in equilibrium with their current isotopic

environment and thus help in recognizing new arrivals to an area as well (Hobson 1999).

Previous work already pointed out that interpretation of Sr and Pb isotope signatures is complex and not always straightforward (Burton and Hahn 2016). In this respect, isotope ratios in tooth enamel only help identifying migrated individuals (Price et al. 2004). Relative to the geology of the study area, considerable variability has been noted in the inner Alpine region (Castellarin et al. 2006), whereas certain areas of its southern and northern foreland might be difficult to distinguish (see chapter "Isotopic Map of the Inn-Eisack-Adige-Brenner Passage and its Application to Prehistoric Human Cremations"). Moreover, as Alpine formations are composed of different kinds of rocks, run-off and erosion by rivers, glaciers and mudflows as well as rock fall will cause transportation of materials and soil admixture, thereby causing small-scale variability (Berger et al. 2010). This circumstance may well obscure larger-scale differences in the isotopic ratios of the locally available strontium (and lead) isotopes (Grupe and Peters 2007; Price et al. 2004). In geologically heterogeneous regions, an animal's diet will reflect a mixture of isotope ratios proportionate to the amount of food from each zone (Price et al. 2004).

Previous research also noted the complexity of interpretation of oxygen isotope ratios (Mayr et al. 2016, see also chapter "Isotopic Map of the Inn-Eisack-Adige-Brenner Passage and its Application to Prehistoric Human Cremations"). Influenced by temperature, humidity, altitude, distance from the coast and other aspects of the environment, sources of drinking water in the Alps and its southern and northern foreland may yield quite divergent oxygen isotope ratios (Turner et al. 2009). Moreover, whereas sources of drinking water fed by nearby wells or rainwater will reflect conditions of the local environment, drinking water in mountainous regions and their piedmonts may be distantly sourced by melting water or rivers fed by glaciers (Longinelli 1984). These sources take along the isotopic values of the mountain range from where the water originates and can result in small-scale isotopic variability (Mayr et al. 2016) similar to the geological variability explained above.

Any isotope study of biogenous materials invariably requires adequate scientific questions and robust hypotheses (Grupe and Peters 2007). This implies extensive collection of relevant information about local geology, climatic and environmental conditions as well as detailed knowledge about the feeding behaviour and physiology of the vertebrate taxa intended for analysis. One obvious challenge will be to understand isotopic patterns in nature on the one hand and processes contributing to their spatial and temporal variation on the other (Burton and Hahn 2016; Hobson 1999). Understandably, close cooperation between different disciplines is essential in projects like ours. Apart from identification of potential allochthonous individuals (s. above), zooarchaeological research needs addressing species-specific food requirements, pasturing areas and possible annual rounds in that particular ecological setting as well. Equally prerequisite are patterns of mobility in (pre)historic groups deduced from the archaeological record as well as material

and written evidence for ancient trade connections and long-distance exchange in order to discern possible source areas for animals.

Naturally identifying possible regions of provenance in humans and animals alien to a particular landscape requires systematic mapping of isotopic ratios of oxygen and bioavailable strontium and lead of the latter as well as the presumed trading area(s) (Bentley 2006; Eerkens et al. 2014; Hodell et al. 2004). As detailed in chapter "Isotopic Map of the Inn-Eisack-Adige-Brenner Passage and its Application to Prehistoric Human Cremations", a map has been generated for a major ancient passage across the Raetian Alps using dental and osseous remains of domestic cattle (grazer), domestic pig (omnivore) and red deer (mixed grazer/browser) found in pre-Iron Age sites located north and south of the Alpine divide and in the central Alps. This approach presupposes that in pre-Iron Age times, pigs and most of the cattle lived near the farmsteads for most of the year (Mayr et al. 2016; Söllner et al. 2016, see chapter "Isotopic Map of the Inn-Eisack-Adige-Brenner Passage and its Application to Prehistoric Human Cremations"). Given their omnivorous feeding behaviour, domestic pigs were likely fed on agricultural by-products and kitchen refuse, which may even have included whey (Werner 1995). Cattle played a key role in the economies north of the Alps and were involved in labour, supplied dung, and produced milk and offspring during their lifetime and were the source of primary products such as meat, fat, hides, etc., which explains why valued animals were taken care of by their owners. In the Alps and their piedmont regions, however, selected animals may have been involved in vertical transhumance and Alpine pasturing as well, explaining why from the Neolithic period onwards, patterns of seasonal mobility might complicate interpretation of isotopic composition in faunal remains (e.g. Haas 2004; Jacomet et al. 2004; Kühn and Hadorn 2004). In contrast to pigs and cattle managed by humans, red deer (*Cervus elaphus*) were roaming freely at all times and therefore more flexible in terms of mobility, food intake and access to sources of drinking water.

As mentioned before, patterns of mobility and trading of animals have been addressed in previous research projects, but most studies published so far dealt with local patterns or short-distance trade (Bentley and Knipper 2005a, b; Price et al. 2006; Stephan et al. 2012). Whereas the results of these studies are extremely valuable and beneficial from a methodological and interpretational viewpoint, it is clear that the isotope study intended here is on a different scale and therefore perhaps more challenging.

Discussion

From the archaeological inventories studied so far, it is obvious that from the very beginning of the Roman occupation in 15 BCE onwards, trade via and possibly with Gaul was of key importance to supplying *Raetia* with merchandise necessary for cultivating a Mediterranean lifestyle. Whereas from early occupation onwards the via *Claudia Augusta* linking the northern Alpine foreland with Northern Italy was used for the transportation of goods across the Alpine divide as well, it is beyond

question that this trade route only played a secondary role in terms of supplying goods to the provincial population. Routes further east across the Tauern were well established for supplying civil and military settlements in *Noricum* but—according to the distribution of fine and coarse wares—were of no significance for the supply of *Raetia*.

Together with other finds from early Roman sites in *Raetia*, the numerous remains from first century CE refuse deposits of the roadside settlement at Langweid, located on the via *Claudia Augusta* 15 km north of *Augusta Vindelicum*/Augsburg, also illustrate that supply and consumption patterns changed significantly in the course of the first century CE. During the reign of Tiberius, for instance, regular imports of Italian tablewares ceased and—with the exception of small groups like 'Pompeian Red' Ware plates—were fully replaced by fine wares produced in Gaul or in the wider region. From the Flavian period onwards regional products not only became more important, our analysis of the fine wares also illustrates that with the exception of southern Gaulish Terra Sigillata, there was no longer a major demand for imported fine wares (Gschwind 2015).

Since the archaeological findings point to Gaul as the major region of trade for early Roman table- and kitchenwares, amphorae etc., it is possible that draught and pack animals arrived in *Raetia* from the west as well, unless transportation occurred by rotation, with animals being exchanged at stopping places along the road. However, archaeozoological findings point to the long-distance transfer of mounts, pack animals, breeding stock and pets, and conceivably the via *Claudia Augusta* played an important role in this kind of trade. Whether the patterns emerging for the material culture also apply to animal trade remains to be seen.

Having said that, each method used for documenting the transfer of animals across the Alps has its limitations, and isotope analysis is no exception to this. A first issue relates to the long-distance transfer of large breeding stock (horse, cattle) early in life. To avoid problems of handling, this kind of transfer would ideally take place well before the animals reached sexual maturity, i.e. at an age when the process of bio-mineralisation of the high-crowned permanent dentition might not be concluded yet. In such individuals only the upper (older) part of the tooth crown retained the primary isotopic signature indicative of the animal's provenance, whereas enamel and dentine generated during the final phase of tooth formation would produce a second, distinct signature characteristic of the region of destination, provided the individual's transfer did not take months. Since animals exploited as mounts and sires or for pulling ploughs and carts usually exhibited considerable longevity, the crown section corresponding isotopically to the animal's early stages of food intake might have disappeared through abrasion. Consequently, difficulties will be faced tracing the provenance of horses and cattle imported for breeding and labour purposes when introduced to their final destination as young animals.

Another problem concerns animals that witnessed multiple transfers during life. Indeed, valuable long-living animals like mules and horses employed in military may have rendered service in different ecological settings, e.g. after cavalry and other army units were relocated due to the changing geopolitical situation. In such cases, isotope values in bone (in the absence of tooth samples) will reflect a

combination of the original place of residence, length of stay in other settings during life and number of years of residence prior to death (Price et al. 2004). Considerable mobility can also be assumed for pack animals and mounts serving in the *cursus publicus*, the official state run postal system for speedy communication along the roads to distant provinces. Associated with this infrastructure were relay stages (*mansiones*) at regular intervals, where injured animals received medical treatment by *mulomedici* whilst exhausted ones could be replaced. Ambiguous signatures in bones and teeth can also be expected in mobile livestock herds that had been pastured in isotopically distinct landscapes. This applies to the populations inhabiting the Alps and their southern and northern piedmonts, which witnessed exploitation of pasture land at higher altitude since prehistory (e.g. Career 2013; Deschler-Erb et al. 2015; Mandl 2006; Marzatico 2007; Reitmaier 2010) and its continuity into the Roman period (e.g. Donat et al. 2006; Segard 2009; Staudt et al. 2014). Provided meat supply of larger urban centres in *Raetia* (e.g. *Cambodunum*/Kempten) fell back on individuals that were integrated in transhumance in the northern Alpine region, isotopic signatures will represent a mixture of different seasonal parameters (Bentley and Knipper 2005a; Stephan et al. 2012), explaining why the map intended by the project is highly relevant.

Thirdly, most models discussing transfer of animals across rugged hostile terrain like high mountain ranges tacitly assume unidirectional events. As mentioned before, isotopic signatures in the enamel of adult animals would ideally be indicative of the place of birth and those in bone of the region of exploitation until it died. Whereas in stock introduced for local breeding or in comparably short-living species like the chicken this supposition seems justified, the possibility of multiple crossings should not be discounted entirely. Of course, the speedy crossing of mountain barriers such as the Alps will remain undetected (Berger et al. 2010), but provided after crossing phases of recovery north and south of the Alps were scheduled, for instance, during the winter months when major passages were closed due to heavy rain and snowfall, back and forth movements can be evidenced. Prominent examples of this are the mules that died in the battle of Kalkriese 9 CE (Uerpmann and Uerpmann 1994). However, questions like this can only be answered by applying sequential isotope analysis of molar teeth.

Finally, as indicated above, isotope analysis in this project largely depends on the ability of zooarchaeology to recognise possible outliers in faunal assemblages. However, breeding with imported sires likely already resulted in morphologically divergent offspring since the first generation. From a statistical viewpoint, it can therefore be expected that isotope analysis of specimens selected essentially by applying osteological criteria could catch primarily individuals resulting from local breeding efforts rather than founder individuals transferred to *Raetia* for this purpose. In addition, the exclusive use of morphology and size to sort out specimens might result in non-local individuals being overlooked, simply because it cannot be excluded that some animals introduced showed close resemblance to autochthonous breeds. According to us, any attempt aiming at quantifying this kind of methodological bias seems futile, even if large samples were screened systematically. Some additional challenges may be introduced by the overall small number of samples

analysed and the fact that the assemblage only represents a minor segment of the original deposit.

Concluding Remarks

This project combines archaeological, zooarchaeological and stable isotope evidence from contexts dating between the first century BCE and the first century CE to improve our understanding of human exploitation of animals and developments in livestock breeding practices in *Raetia* in the course of Romanisation. Supposedly representing a region nearly void of inhabitants at the time of the Roman conquest (Sommer 2008), archaeological finds uncovered recently from first century BCE contexts (e.g. Müller 2008) and excavations of burials and settlements belonging to the Heimstetten Group (~30–60 CE) (e.g. Volpert and Früchtl 2012) revealed architecture and material culture possibly indicative of cultural persistence from the La Tène culture into the first century CE (Steidl and Will 2005). New archaeological and faunal data also suggest that Romanisation of eastern and western *Raetia* may have occurred at a different pace and intensity (Trixl et al. in press). Conceivably, proximity to the province of *Gallia* and infrastructure measures such as the opening up of the via *Claudia Augusta* for wheeled transport speeded up the process in the western part of the province. Central questions in our study, therefore, are the timing and extent of Mediterranean influence on Raetian society and its animal world north of the Alpine divide on the one hand and the issue of continuity versus discontinuity in local cultural traditions and husbandry practices on the other.

As explained elsewhere (chapter 'Isotopic Map of the Inn-Eisack-Adige-Brenner Passage and Its Application to Prehistoric Human Cremations'), georeferenced isotope signatures (Sr, Pb, O) from ancient and modern locations across the study area are essential to tackle the question of human migration and transfer of animals across the Alps (Grupe et al. 2015). Notwithstanding the potential of stable isotope analysis for evidencing individuals of non-local origin in the Roman northern Alpine foreland that were introduced for reasons as different as military operations and melioration of livestock and poultry lineages or simply as companion animals, expectations should probably be attenuated with respect to the number of animal imports that can be positively evidenced at all, not to mention their geographic origin. Complicating factors are the use of long-living mounts and pack animals by the Roman army and *cursus publicus*, considerably enhancing the probability that these beasts of burden had been relocated more than once in life, thus blurring isotope signatures. Moreover, although it is uncontested that Roman know-how about animal breeding and husbandry was introduced north of the Alps together with suitable (Mediterranean?) founder stock (Peters 1998; Peters and Manhart 2004), detecting the latter applying stable isotope analysis might be like looking for a needle in a haystack. Notwithstanding these obvious limitations, isotope fingerprinting of larger series of early Roman finds not only promises unique insight into the human-induced mobility of several animal species but also

into human decision-making concerning husbandry practices in the different parts of *Raetia*. Needless to say that similar work in other provinces of the Roman Empire will help improve our knowledge about long-range movements of animals as well as the intention behind these transfers.

Acknowledgements The financial support of the German Research Foundation (DFG, PE 424/11-1,2) to the authors is gratefully acknowledged. We are grateful to Dr. Florian Schimmer, Römisch-Germanisches Zentralmuseum, Mainz, for comments on an earlier version of our contribution to this publication. In addition, we are very grateful to Dr. Hannes Napierala for selecting mammalian teeth and bone samples suitable for stable isotope analysis and recording of primary data of these specimens in the database OssoBook. These samples proved essential for the analyses reported in the chapters "The Crystalline State of Archaeological Bone Material" and "Isotopic Map of the Inn-Eisack-Adige-Brenner Passage and its application to Prehistoric Cremations". We kindly thank the editors of this volume for their help.

References

Arloing MJ (1882) Caractères ostéologiques différentiels de l'âne, du cheval et de leurs hybrides. Bull Soc Anthr Lyon 2:1–48

Benecke N (1994) Archäozoologische Studien zur Entwicklung der Haustierhaltung in Mitteleuropa und Südskandinavien von den Anfängen bis zum ausgehenden Mittelalter. Schr zur Ur- u Frühgesch 46, Berlin

Bentley RA (2006) Strontium isotopes from the earth to the archaeological skeleton: a review. J Archaeol Method Theory 13(3):135–187

Bentley RA, Knipper C (2005a) Geographical patterns in biologically available strontium, carbon and oxygen isotope signatures in prehistoric SW Germany. Archaeometry 47(3):629–644

Bentley RA, Knipper C (2005b) Transhumance at the early Neolithic settlement at Vaihingen (Germany). Antiquity 79(306):1–3

Berger T, Peters J, Grupe G (2010) Life history of a mule (c. 160 AD) from the Roman fort Biriciana/Weißenburg (Upper Bavaria) as revealed by serial stable isotope analysis of dental tissues. Int J Osteoarchaeol 20(2):158–171

Boessneck J (1957) Die Tierknochen. In: Krämer W (ed) Die Ausgrabung von Holzhäusern zwischen der 1. und 2. Querstraße. Cambodunumforschungen 1 = Materialhefte zur bayerischen Vorgeschichte 9. Kallmünz, pp 103–116

Boessneck J (1958) Zur Entwicklung vor- und frühgeschichtlicher Haus- und Wildtiere Bayerns im Rahmen der gleichzeitigen Tierwelt Mitteleuropas. Stud vor- u frühgesch Tierreste Bayern 2, München

Boessneck J (1964) Die Tierknochen aus den Grabungen 1954–1957 auf dem Lorenzberg bei Epfach. In: Werner J (ed) Studien zu Abodiacum-Epfach. Münchner Beiträge zur Vor- und Frühgeschichte 7. C.H. Beck, München, pp 213–261

Burton JH, Hahn R (2016) Assessing the "local" $^{87}Sr/^{86}Sr$ ratio for humans. In: Gupe G, McGlynn GC (eds) Isotopic landscapes in bioarchaeology. Springer, Heidelberg, pp. 131–121

Career F (2013) Archeologia della pastorizia nelle Alpi: nuovi dati e vecchi dubbi. Preistoria Alpina 47:49–56

Castellarin A, Nicolich R, Fantoni R, Cantelli L, Sella M, Selli L (2006) Structure of the lithosphere beneath the Eastern Alps (southern sector of the TRANSALP transect). Tectonophysics 414(1):259–282

Chaveau A (1879) Traité d'Anatomie comparée des animaux domestiques 3, Paris

Desbat A, Genin M, Lasfargues J (eds) (1996) Les productions des ateliers de Potiers antiques de Lyon. 1. Les ateliers précoces. Gallia 53:1–249

Deschler-Erb S, Ginella F, Hüster Plogmann H (2015) Archäozoologische Untersuchungen zu den prähistorischen und mittelalterlichen Funden vom Kiechlberg. In: Töchterle U (ed) Der Kiechlberg bei Thaur als Drehscheibe zwischen den Kulturen nördlich und südlich des Alpenhauptkammes. Ein Beitrag zum Spätneolithikum und zur Früh- und Mittelbronzezeit in Nordtirol. Universitätsforschungen zur Prähistorischen Archäologie 261, Bonn, pp 361–396

Donat P, Chr F, Petrucci G (2006) Fleischkonserven als Produkte römischer Almwirtschaft. Schwarze Auerbergkeramik vom Monte Sorantri bei Raveo (Friaulisch-Julisch-Venetien, Nordostitalien). Bayer Vorgeschichtsbl 71:209–232

Eerkens JW, Barfod GH, Jorgenson GA, Peske C (2014) Tracing the mobility of individuals using stable isotope signatures in biological tissues: "locals" and "non-locals" in an ancient case of violent death from Central California. J Archeol Sci 41:474–481

Ehmig U (2010) Dangstetten IV. Die Amphoren. Untersuchungen zur Belieferung einer Militäranlage in augusteischer Zeit und den Grundlagen archäologischer Interpretation von Fund und Befund. Forsch u Ber Vor- u Frühgesch 117, Stuttgart, BW

Ehmig U (2011/2012) Über alle Berge. Früheste mediterrane Warenlieferungen in den römischen Ostalpenraum. Röm. Österreich 34/35:13–35

Ehmig U (2015) Die Amphorenfunde aus dem römischen Gauting, Lkr. Starnberg. Bayer Vorgeschbl 80:155–168

Ettlinger E, Hedinger B, Hoffmann B, Kenrick PM, Pucci G, Roth-Rubi K, Schneider G, von Schnurbein S, Wells CM, Zabehlicky-Scheffenegger S (1990) Conspectus formarum terrae sigillatae italico modo confectae. Mat. Röm.-Germ. Keramik 10. Rudolf Habelt Verlag, Bonn

Ettlinger E, Simonett Ch (1952) Römische Keramik aus dem Schutthügel von Vindonissa. Veröff. Ges. Pro Vindonissa 3, Basel

Farello P (2006) Equidi dalla fogna di Classe (RA)—(IV–V secolo d.C.). In: Tecchiati U, Sala B (eds) Archaeozoological studies. In honour of Alfredo Riedel, Bozen, pp. 269–284

Flügel Ch (1999) Der Auerberg III. Die römische Keramik Münchner Beitr Vor- u Frühgesch 47

Flügel C (2007) Cenni sulle importazioni italiche nella Raetia. Quad Friulani Arch 17:83–95

Flügel Ch (2015) Fleischkonserven für Raetien. Archäometrische Untersuchungen an schwarzen Auerbergtöpfen mit Marmormagerung. In: Ulbert G (ed) Der Auerberg IV. Kleinfunde mit Ausnahme der Gefäßkeramik sowie die Grabungen von 2001 und 2008. Münchner Beitr Vor- u Frühgesch 63, pp 383–392

Frei KM, Mannering U, Kristiansen K, Allentoft ME, Wilson AS, Skals I, Tridico S, Nosch ML, Willerslev E, Clarke L (2015) Tracing the dynamic life story of a Bronze Age female. Sci Rep 5

Freyberger KSt (1998) Die frühkaiserzeitlichen Heiligtümer der Karawanenstationen im hellenisierten Osten. Zeugnisse eines kulturellen Konflikts im Spannungsfeld zweier politischer Formationen Damaszener Forsch 6

Fünfschilling S (2015) Die römischen Gläser aus Augst und Kaiseraugst. Kommentierter Formenkatalog und ausgewählte Neufunde 1981–2010 aus Augusta Raurica, Forsch, Augst 51

Genin M (2007) La Graufesenque (Millau, Aveyron). 2. Sigillées lisses et autres productions. Éditions de la Fédération Aquitania, Pessac

Grabherr G (2006) Die Via Claudia Augusta in Nordtirol—Methode, Verlauf, Funde. In: Walde E, Grabherr G (Hrsg) Via Claudia Augusta und Römerstraßenforschung im östlichen Alpenraum. Ikarus 1, pp 35–336

Greene K (1979) Report on the excavations at Usk 1965–1976. The Coins, Inscriptions and Graffiti, Cardiff

Grupe G, Grünewald M, Gschwind M, Hölzl S, Kocsis B, Kröger P, Lang A, Mauder M, Mayr C, McGlynn G, Metzner-Nebelsick C, Ntoutsi E, Peters J, Renz M, Reuß S, Schmahl W, Söllner F, Sommer S, Steidl B, Toncala A, Trixl S, Wycisk D (2015) Networking in bioarchaeology: the example of the DFG research group for 1670 "transalpine mobility and culture transfer". In: Grupe G, McGlynn GC, Peters J (eds) Documenta Archaeobiologiae 13. Verlag Marie Leidorf, Rahden, pp. 13–51

Grupe G, Peters J (2007) Molecular biological methods applied to Neolithic bioarchaeological remains: research potential, problems, and pitfalls. In: Larsson L, Lüth F, Terberger T (eds) Innovation and continuity—non-megalithic mortuary practices in the Baltic. New methods and research into the development of stone age society. Internationaler Workshop at Schwerin on 24–26 March 2006. Bericht der Römisch-Germanischen Kommission 88, Mainz, von Zabern, pp 275–306

Gschwind M (2015) Langweid—eine frühe römische Straßensiedlung an der via Claudia Augusta. Bayer Arch 3:30–33

Haas JN (2004) Mikroskopische Analyse von Schaf−/Ziegenkoprolithen. In: Jacomet S, Leuzinger U, Schibler J (eds): Die jungsteinzeitliche Seeufersiedlung Arbon Bleiche 3. Umwelt und Wirtschaft. Archäologie im Thurgau 12. Frauenfeld, pp 351–357

Harl O (2014) Hochtor und Glocknerroute. Ein hochalpines Passheiligtum und 2000 Jahre Kulturtransfer zwischen Mittelmeer und Mitteleuropa. Sonderschr. Österr. Arch. Inst. 50, Wien

Heger N (1986) Frührömische Amphoren aus der Stadt Salzburg (Mozartplatz 4). Bayer Vorgeschbl 51:131–161

Hobson KA (1999) Tracing origins and migration of wildlife using stable isotopes: a review. Oecologia 120(3):314–326

Hochuli-Gysel A (1998) Die bleiglasierte Keramik. In: Rey-Vodez V, Hochuli-Gysel A, Raselli-Nydegger L (eds) Beiträge zum römischen Oberwinterthur—Vitudurum 8. Ausgrabungen im Unteren Bühl. Les fibules, keramische Sondergruppen: Bleiglasierte Keramik, Terrakotten, Lampen. Monogr. Kantonsarch. Zürich 30. Egg, Zürich, pp 63–81

Hodell DA, Quinn RL, Brenner M, Kamenov G (2004) Spatial variation of strontium isotopes ($^{87}Sr/^{86}Sr$) in the Maya region: a tool for tracking ancient human migration. J Arch Sci 31 (5):585–601

Jacomet S, Leuzinger U, Schibler J (2004) Synthesis. In: Jacomet S, Leuzinger U, Schibler J (eds) Die jungsteinzeitliche Seeufersiedlung Arbon Bleiche 3. Umwelt und Wirtschaft. Archäologie im Thurgau 12. Frauenfeld, pp 381–416

Johnstone C (2005) Those elusive mules: investigating osteometric methods for their identification. In: Mashkour M (ed): Equids in time and space. Proceedings of the 9th conference of the international council of zooarchaeology. Oxbow, Oxford, pp 183–191

Kamenov GD, Gulson BL (2014) The Pb isotopic record of historical to modern human lead exposure. Sci Total Environ 490:861–870

Keller W (1984) Die frühkaiserzeitlichen Körpergräber von Heimstetten bei München und die verwandten Funde aus Südbayern. Münchner Beitr Vor- u Frühgesch 37, München

Kühn M, Hadorn P (2004) Pflanzliche Makro- und Mikroreste aus Dung von Wiederkäuern. In: Jacomet S, Leuzinger U, Schibler J (eds) Die jungsteinzeitliche Seeufersiedlung Arbon Bleiche 3. Umwelt und Wirtschaft. Archäologie im Thurgau 12. Frauenfeld, pp 327–350

Lemaître S, Batigne Vallet C (eds) (2015) Abécédaire pour un archéologue lyonnais: Mélanges offerts à Armand Desbat Arch et Hist Romaine 31

Lipper E (1981/1982) Die Tierknochenfunde aus dem römischen Kastell Abusina-Eining, Stadt Neustadt a. d. Donau, Ldkr. Kelheim. Ber der Bayer Bodendenkmalpflege 22/23:81–160

Lippert A, Dembski G (2000) Keltische und römische Passopfer am Mallnitzer Tauern. Archäologisches Korrespondenzblatt 30:252–268

Lippert A, Dembski G (2013) Ein weiterer keltischer Münzopferplatz am Mallnitzer Tauern (Salzburg/Kärnten). Archäologisches Korrespondenzblatt 43:523–534

Longinelli A (1984) Oxygen isotopes in mammal bone phosphate: a new tool for paleohydrological and paleoclimatological research? Geochim Cosmochim Acta 48 (2):385–390

Mackensen M (1978) Das römische Gräberfeld auf der Keckwiese in Kempten. I. Gräber und Grabanlagen des 1. und 4. Jahrhunderts. Cambodunumforsch. 4. Materialh Bayer Vorgesch A 34

Mandl F (2006) Almen und Salz. Hallstatts bronzezeitliche Dachsteinalmen. Jahrbuch des Oberösterreichischen Musealvereines 151:7–36

Manhart H, Peters J (1995). Acht Hundeskelette aus einem flavischen Wehrgraben in Augsburg, Heilig-Kreuz-Strasse. Schwaben. Das Archäologische Jahr in Bayern, pp 106–109
Martin-Kilcher St (1987) Die römischen Amphoren aus Augst und Kaiseraugst. Ein Beitrag zur römischen Handels- und Kulturgeschichte. 1: Die südspanischen Ölamphoren (Gruppe 1), Forsch, Augst 7,1
Martin-Kilcher St (1994a) Die römischen Amphoren aus Augst und Kaiseraugst. Ein Beitrag zur römischen Handels- und Kulturgeschichte. 2: Die Amphoren für Wein, Fischsauce, Südfrüchte (Gruppen 2–24) und Gesamtauswertung. Forsch, Augst 7,2
Martin-Kilcher St (1994b) Die römischen Amphoren aus Augst und Kaiseraugst. Ein Beitrag zur römischen Handels- und Kulturgeschichte. 3: Archäologische und naturwissenschaftliche Tonbestimmungen und Katalog und Tafeln (Gruppen 2–24). Forsch, Augst 7,3
Martin-Kilcher St (2003) Wein—Olivenöl—Fischsaucen: Amphoren aus den stratifizierten Befunden der 1. und 2. Holzbauperiode. In: Hagendorn A, Doppler H W, Huber A, Plogmann H, Jacomet St, Meyer-Freuler Ch, Pfäffli B, Schibler J (eds) Zur Frühzeit von Vindonissa. Veröff Ges Pro Vindonissa 18, pp 351–361
Martin-Kilcher S (2011) Römer und gentes Alpinae im Konflikt—archäologische und historische Zeugnisse des 1. Jahrhunderts v. Chr. In: Moosbauer G, Wiegels R (eds) Fines imperii—imperium sine fine? Römische Okkupations- und Grenzpolitik im frühen Principat. Beiträge zum Kongress 'Fines imperii—imperium sine fine?' in Osnabrück vom 14. bis 18. September 2009. Verlag Marie Leidorf, Rahden, pp. 27–62
Marzatico F (2007) La frequentazione dell'ambiente montano nel territorio atesino fra l'età del Bronzo e del Ferro: alcune considerazioni sulla pastorizia transumante e "l'economia di malga". Preistoria Alpina 42:163–182
Mayr M, Grupe G, Toncala A, Lihl CM (2016) Linking oxygen iosotopes of animal-bone phosphate with altimetry: results from archaeological finds from a transect in the alps. In: Grupe G, McGlynn GC (eds) Isotopic landscapes in bioarchaeology. Springer, Heidelberg, pp. 157–172
Mees AW (2011) Die Verbreitung von Terra Sigillata aus den Manufakturen von Arezzo, Pisa, Lyon und La Graufesenque. Die Transformation der italischen Sigillata-Herstellung in Gallien. RGZM Monogr. 93, Verlag, des Römisch-Germanischen Zentralmuseums, Mainz
Morel P (1991) Untersuchung des osteologischen Fundgutes aus dem Vicus Vitudurum-Oberwinterthur. In: Etter H, Fellmann Brogli R, Fellmann R, Martin-Kilcher S, Morel Ph, Rast A (eds) Beiträge zum römischen Oberwinterthur-VITUDURUM 5. Zürich, pp 79–189
Müller S (2008) Die Viereckschanzen von Sallach, Gde. Geiselhöring, Lkr. Straubing-Bogen, Niederbayern im Spiegel keltischer Besiedlung des Kleinen Labertales. Regensburg
Nuber HU (2015) P. Quinctilius Varus siegte . . . als legatus Augusti in Süddeutschland. In: Seitz G (ed) Hans Ulrich Nuber. Ausgewählte Schriften. Verlag Marie Leidorf, Rahden, pp. 301–310
Oxé A, Comfort H, Kenrick P (2000) Corpus vasorum Arretinorum^2. Antiquitas III 41
Peters J (1997) Der Hund in der Antike aus archäozoologischer Sicht. Anthropozoologica 25/26:511–552
Peters J (1998) Römische Tierhaltung und Tierzucht. Eine Synthese aus archäozoologischer Untersuchung und schriftlich-bildlicher Überlieferung. Passauer Universitätsschriften zur Archäologie 5. Verlag Marie Leidorf, Rahden
Peters J (2005) Ein Hundeleben in der Antike. Antike Welt 5:8–16
Peters J, Manhart H (2004) ". . . und jegliches heimische Rind ist weit besser als ein auswärtiges. . ." Zur Frage der Kontinuität keltischer Viehwirtschaft im süddeutschen Raum. In: Hüssen CM, Irlinger W, Zanier W (eds) Spätlatène- und frühe römische Kaiserzeit zwischen Alpenrand und Donau. Akten des Kolloquiums in Ingolstadt am 11- und 12. Oktober 2001, Kolloquien zur Vor- und Frühgeschichte, vol 8. Rudolf Habelt Verlag, Bonn, pp. 39–52
Pöllath N (2011) Old horses, stray dogs and butchering refuse—the faunal remains from the amphitheatre at the Roman military station Quintana/Künzing. In: Grupe G, McGlynn GC, Peters J (eds) Archaeobiodiversity—a European perspective, Documenta Archaeobiologiae, vol 8. Verlag Marie Leidorf, Rahden, pp. 235–274

Pöllath N (2012) Von Hornschnitzern und Schweinehaltern. Tierknochen aus dem frührömischen Vicus von Augsburg. In: Tremmel B (ed) Der Kastellvicus des 1. Jahrhunderts n. Chr. von Augusta Vindelicum/Augsburg. Augsburger Beitr Arch 6. Augsburg

Polak M (2000) South Gaulish Terra Sigillata with Potters' Stamps from Vechten. RCRF Acta Suppl 9

Price TD, Burton JH, Fullagar PD, Wright LE, Buikstra JE, Tiesler V (2015) Strontium isotopes and the study of human mobility among the ancient Maya. Archaeology and bioarchaeology of population movement among the Prehispanic Maya. Springer International Publishing, Switzerland, pp. 119–132

Price TD, Knipper C, Grupe G, Smrcka V (2004) Strontium isotopes and prehistoric human migration: the Bell Beaker period in Central Europe. Eur J Arch 7(1):9–40

Price TD, Manzanilla L, Middleton WD (2000) Immigration and the ancient city of Teotihuacan in Mexico: a study using strontium isotope ratios in human bone and teeth. J Arch Sci 27 (10):903–913

Price TD, Wahl J, Bentley RA (2006) Isotopic evidence for mobility and group organization among Neolithic farmers at Talheim, Germany, 5000 BC. Eur J Archaeol 9(2–3):259–284

Reitmaier Th (2010) Auf der Hut—Methodische Überlegungen zur prähistorischen Alpwirtschaft in der Schweiz. In: Mandl F, Stadler H (eds) Archäologie der Alpen. Gröbming, pp 219–238

Riedel A (1986) Ergebnisse von archäozoologischen Untersuchungen im Raum zwischen Adriaküste und Alpenhauptkamm (Spätneolithikum bis zum Mittelalter). Padusa 22:1–220

Rottloff A (2015) Die Gläser vom Auerberg. In: Ulbert G (ed) Der Auerberg IV. Kleinfunde mit Ausnahme der Gefäßkeramik sowie die Grabungen von 2001 und 2008. Münchner Beitr Vor- u Frühgesch 63, pp 261–351

Schaad D (Hrsg) (2007) La Graufesenque (Millau, Aveyron). 1. Condatomagos. Une agglomération de confluent en territoire rutène IIe s. a.C.–IIIe s. p.C., Pessac

Scheeres M, Knipper C, Hauschild M, Schönfelder M, Siebel W, Pare C, Alt KW (2014) "Celtic migrations": fact or fiction? Strontium and oxygen isotope analysis of the Czech cemeteries of Radovesice and Kutná Hora in Bohemia. Am J Phys Anthropol 155(4):496–512

Schimmer F (2005) Die italische Terra Sigillata aus Bregenz (Brigantium). Schr Vorarlberger Landesmus A 8, Bregenz, 2005

Schimmer F (2009) Amphoren aus Cambodunum/Kempten. Ein Beitrag zur Handelsgeschichte der römischen Provinz Raetia. Münchner Beitr Provinzialröm Arch 1 (Wiesbaden 2009)

Schindler-Kaudelka E (1986) Die Backplatten vom Magdalensberg. In: Vetters H, Piccottini G (Hrsg) Die Ausgrabungen auf dem Magdalensberg 1975 bis 1979. Magdalensberg-Grabungsbericht 15 (Klagenfurt 1986), pp 279–337

Schlippschuh O (1974) Die Händler im Römischen Kaiserreich in Gallien, Germanien und den Donauprovinzen Rätien, Noricum und Pannonien. Amsterdam

Schlosser M (1887) Ueber Säugethier- und Vogelreste aus den Ausgrabungen in Kempten stammend. Correspondenz-Blatt der Deutschen Gesellschaft für Anthropologie. Ethn und Urgesch 19:17–22

Schneider G (2000) X-ray fluorescence analyses of vernice nera, sigillata and Firmlampen from north Italy. In: Brogiolo GP, Olcese G (eds) Produzione ceramica in area padana tra il II secolo a.C. e il VII secolo d.C.: Nuovi dati e prospettive di ricerca. Convegno internazionale. Desenzano del Garda 8–10 aprile 1999 (Mantova 2000), pp 103–106

Schneider G, Daszkiewicz M (2006) Chemical analysis of Italian Sigillata from Italy and from the Northern Provinces. In: Malfitana D, Poblome J, Lund J (Hrsg) Old pottery in a new century. Innovating perspectives on roman pottery studies. Atti del Convegno Internazionale di Studi, Catania, 22–24 Aprile 2004. Monogr. Istituto Beni Archeologici e Monumentali 1 (Catania 2006), pp 537–543

Schnekenburger G (ed) (2002) Über die Alpen. Menschen—Wege—Waren, Stuttgart

Scholz M (2015) Die legio II (Augusta) in Rätien?—Die Botschaft eines goldenen Fingerrings aus Augsburg-Oberhausen (Bayern/D). In: NON SOLUM . . . SED ETIAM. Festschrift für Thomas Fischer zum 65. Geburtstag. Rahden, pp 399–406.

Schucany C, Martin-Kilcher S, Berger L, Paunier D (eds) (1999) Römische Keramik in der Schweiz, Antiqua, vol 31. Verlag Schweizerische Gesellschaft für Ur- und Frühgeschichte, Basel

Schweissing M, Grupe G (2003) Tracing migration events in man and cattle by stable strontium isotope analysis of appositionally grown mineralized tissue. Int J Osteoarchaeol 3(1–2):96–103

Sealy JC, van der Merwe NJ, Sillen A, Kruger FJ, Krueger HW (1991) $^{87}Sr/^{86}Sr$ as a dietary indicator in modern and archaeological bone. J Archaeol Sci 18(3):399–416

Segard M (2009) Pastoralism, rural economy and landscape evolution in the western Alps. J Roman Archaeol 22:171–182

Sieler M (2009) Die frühkaiserzeitlichen Holzbauten im Bereich der kleinen Thermen von Cambodunum-Kempten. Cambodunumforsch. 8. Materialh Bayer Vorgesch A 93

Sieler M (2015) Bemerkungen zur Provenienz der italischen Terra Sigillata vom Auerberg. In: Ulbert G (ed) Der Auerberg IV. Kleinfunde mit Ausnahme der Gefäßkeramik sowie die Grabungen von 2001 und 2008. Münchner Beitr Vor- u Frühgesch 63:373–382

Solano S (2011) Viaggiatori e strade nel mondo romano. In: Marzatico F, Gebhard R, Gleirscher P (eds) Le grandi vie delle civiltà. Relazioni e scambi fra Mediterraneo e il centro Europa dalla Preistoria alla Romanità. Mostra Trento, Castello del Buonconsiglio, monumenti e collezioni provinciali, 1 luglio—13 novembre 2011, Trento, pp 375–377

Söllner F, Toncala A, Hölzl S, Grupe G (2016) Determination of geo-dependent bioavailable $^{87}Sr/^{86}Sr$ isotopic ratios for archaeological sites from the inn valley (Austria): a model calculation. In: Grupe G, McGlynn GC (eds) Isotopic landscapes in bioarchaeology. Springer, Heidelberg, pp. 123–140

Sommer CS (2008) Die Anfänge der Provinz Raetien. In: Piso I (ed) Die römischen Provinzen. Begriff und Gründung. Colloquium Cluj-Napoca, 28. September–1. Oktober 2006. Cluj-Napoca, pp 207–224

Staudt M, Klocker C, Flatscher E, Stadler H (2014) KG Alkus, OG Ainet. Fundberichte aus Österreich 52, pp 350–351

Steidl B (2016) Einige Aspekte zur Verkehrsinfrastruktur und zu den Vici in Raetien. In: Römische Vici und Verkehrsinfrastruktur in Raetien und Noricum. Colloquium Bedaium Seebruck 26–28 März 2015. Inhalte—Projekte—Dokumentationen. Schriftenreihe des Bayerischen Landesamtes für Denkmalpflege 15, pp 68–83

Steidl B, Will M (2005) Römer und Bajuwaren—Ausgrabungen auf der Trasse der A 99, Autobahnring München-West Das archäologische Jahr in Bayern, pp 113–116

Stephan E, Knipper C, Schatz K, Price T, Hegner E (2012) Strontium isotopes in faunal remains: evidence of the strategies for land use at the Iron Age site Eberdingen Hochdorf (Baden-Württemberg, Germany). Population dynamics in prehistory and early history. New approaches using stable isotopes and genetics. Topoi 5:265–286

Stettmer A (1997) Tierknochenfunde aus dem römischen Kastell Oberstimm, Ldkr. Ingolstadt/Bayern. Diss. München

Thesing R (1977) Die Größenentwicklung des Haushuhns in vor- und frühgeschichtlicher Zeit. Diss. med. vet. München

Thüry GE (2011) Edward Whymper und die römischen Münzen vom Theodulpass. Schweizer Münzbl 244:103–115

Toynbee J (1973) Animals in Roman life and art. Thames and Hudson, London

Trixl S, Steidl B, Peters J (in press) Archaeology and zooarchaeology of the late Iron Age-Roman transition in the Province Raetia (100 BC–100 AD). Eur J Archaeol

Turner BL, Kamenov GD, Kingston JD, Armelagos GJ (2009) Insights into immigration and social class at Machu Picchu, Peru based on oxygen, strontium, and lead isotopic analysis. J Archaeol Sci 36(2):317–332

Tütken T (2010) Die Isotopenanalyse fossiler Skelettreste–Bestimmung der Herkunft und Mobilität von Menschen und Tieren. Anthropologie, Isotopie und DNA–biografische Annäherung an namenlose vorgeschichtliche Skelette. Tagungsband 2:33–51

Uerpmann HP, Uerpmann M (1994) Maultiere in der römischen Armee zur Zeit der Eroberungsfeldzüge in Germanien. In: Kokabi M, Wahl J (eds) Beiträge zur Archäozoologie und Prähistorischen Anthropologie. 8. Arbeitstreffen der Osteologen Konstanz 1993 im Andenken an Joachim Boessneck. Forsch u Ber Vor- u Frühgesch 53, pp 353–357

Ulbert G (1960) Die römische Keramik aus dem Legionslager Augsburg-Oberhausen. Materialh Bayer Vorgesch 14

Ulbert G (1965) Der Lorenzberg bei Epfach. Die frührömische Militärstation Epfach III Münchner Beitr Vor- u Frühgesch 9

Volpert HP, Früchtl S (2012) Römische Holzbaubefunde des 1. Jahrhunderts n. Chr. im Gewerbegebiet "Hasenheide Nord" in Fürstenfeldbruck. Das archäologische Jahr Bayern 27:77–79

von den Driesch A (1994) Tierknochenfunde vom Auerberg. In: Ulbert G (ed) Der Auerberg I. Topographie, Forschungsgeschichte und Wallgrabungen. Münchner Beiträge zur Vor- und Frühgeschichte. C.H. Beck, München, pp 213–230

von den Driesch A, Cartajena I (2001) Geopfert oder verscharrt? Tierskelette aus dem römischen Künzing. In: Schmotz K (ed) Vorträge des 19. Niederbayerischen Archäologentages. Verlag Marie Leidorf, Rahden, pp 81–107

von den Driesch A, Peters J (2002) Frühe Pferde- und Maultierskelette aus Auaris (Tell el-Dab'a), östliches Nildelta. Ägypten und die Levante 11:301–311

Walser G (1994) Corpus mercatorum cisalpinorum et transalpinorum. In: Studien zur Alpengeschichte in antiker Zeit. Historia Einzelschr. 86. Stuttgart

Werner P, 1995. Almen. Bäuerliches Wirtschaftsleben in der Gebirgsregion. Georg D. W. Callwey, München

Wunder MB, Norris DR (2008) Analysis and design for isotope-based studies of migratory animals. In: Hobson KA, Wassenaar LI (eds) Tracking animal migration with stable isotopes. Academic Press, Amsterdam, pp. 107–128

Zanier W (1999) Der Alpenfeldzug 15 v. Chr und die Eroberung Vindelikiens. Bayer Vorgeschbl 64:99–132

Zanker P (1987) Augustus und die Macht der Bilder (München 1987)

Classical Sources

Columella (1972) De re rustica. Über Landwirtschaft. Aus dem Lateinischen übersetzt, eingeführt und erläutert von K. Ahrens. Schriften zur Geschichte und Kultur der Antike 4. Akademie-Verlag, Berlin

Plinius der Ältere (1974–1979) Naturalis historia. Naturkunde. Herausgegeben und übersetzt von R. König in Zusammenarbeit mit G. Winkler und J. Hopp (Buch 37). Heimeran, München

The Crystalline State of Archaeological Bone Material

Wolfgang W. Schmahl, Balazs Kocsis, Anita Toncala, Dominika Wycisk, and Gisela Grupe

Abstract

Isotope studies on archaeological bone mineral require a validation of the investigated sample material. Diagenetic alteration or contaminated bone mineral should be recognized as such and not be used for conclusions requiring pristine material. X-ray diffraction (XRD) and Fourier Transform Infrared Spectroscopy (FTIR) provide two complementary tools to characterize the state of the bone mineral. While IR measurements are easy and rapid, their interpretation is still largely empirical. Modern XRD analysis is more demanding with respect to experiment and data evaluation, but it is based on rigorous theoretical modelling of the observed data. Our study involved both uncremated animal bone samples from the alpine region covering ages from 7600 to 550 years before present, as well as cremated human bone remains in comparison with experimentally cremated bovine bone. All samples were mechanically cleaned to remove soil, and inner and outer periosteal surfaces were mechanically removed. We avoided visually decomposed bones completely. The mineralogic state of the thus cleaned, uncremated samples showed only minor systematic changes with archaeologic age. The changes are most pronounced for the lattice parameter and crystalline domain size in the short dimension of the original bone-apatite platelets. The long direction corresponding to the crystallographic c-axis of the apatite appears almost unaffected. We conclude that in the investigated samples, there is only a minor diagenetic alteration of the original bone mineral, possibly related to exchange of carbonate by hydroxyl or fluorine.

W.W. Schmahl (✉) • B. Kocsis
Sektion Kristallographie, Ludwig-Maximilians-Universität, Munich, Germany
e-mail: Wolfgang.W.Schmahl@lrz.uni-muenchen.de

A. Toncala • D. Wycisk • G. Grupe
Biozentrum, Ludwig-Maximilians-Universität, Martinsried, Germany

G. Grupe et al. (eds.), *Across the Alps in Prehistory*,
DOI 10.1007/978-3-319-41550-5_4

From annealing experiments with bovine femur bone material at different temperatures for 1 h annealing time, we established calibration curves to be used to estimate cremation temperatures of bones based on FTIR spectra and X-ray diffractograms. While the evaluation of the diffractograms is rigorously based on a physical model, the evaluation of spectral components in FTIR spectra is empirical. The experiments indicate that original bone apatite contains little–if any–OH^- such that it is carbonate-H_2O-apatite (rather than hydroxyapatite), and with increasing temperature, water and carbonate leave the material, and from 600 °C, hydroxyapatite is formed with increasing purity and crystallite size with increasing temperature. The analysis of some cremated bones from Urnfield Culture sites of Eching and Zuchering, southern Bavaria, clearly indicated that the archaeological cremated bones are inhomogeneous materials where different parts of the samples were subjected to different cremation temperatures and/or times at temperature within fractions of centimetres. This can be attributed to the conditions in the pile of burning logs and burning tissue. Nevertheless, a fair estimation of cremation temperatures is certainly possible even where the FTIR approach and the XRD approach still do not have a full mutual consistency. Future work needs to address the anatomical variability of original bone material within and between species in much more detail than is known at present. Beyond the well-defined temperature/time conditions in furnace annealing experiments, cremation experiments with bone material analyses must also be done in more realistic conditions as they occur in a funeral pyre.

Introduction

The creation of a map of isotope signatures of archaeological vertebrate bone finds excavated along the Inn-Eisack-Adige passage via the Brenner Pass in the European Alps has been at the core of the initial period of the DFG Forschergruppe FOR1670 (see Introduction). This map is intended to function as a basis to reconstruct ancient migration, trade and culture transfer across this region by geochemical analysis of human bone remains. Certainly, any reliable interpretation of isotopic or microchemical signatures of archaeologic bone samples relies on the assumptions that the analysed material is the uncontaminated original material and that this material has been chemically preserved as it was during the life of the individual. The bioapatite bone mineral, however, represents a biogenic tissue component with a specific chemistry and nanostructure that is quite different from that of nominally similar inorganic apatite minerals that are in equilibrium with the ambient conditions where the bone is buried. This, aside from the trivial possibility of contamination with soil particles and the effects of the decomposition of the organic component of the bone, makes bioapatite susceptible to chemical and structural alterations occurring after the death of the individual as the material reacts towards equilibrium with the environment. To take precautions against these possible sources of error in isotope data, FOR1670 decided to screen the

archaeologic bone finds by mineralogic analysis based on X-ray diffraction and infrared spectroscopy. In a time period of about 1500 years in the investigated area, from the Bronze Age until Imperial Roman Times, i.e. 60 generations, cremating the deceased was the dominant burial custom (Grupe et al. 2015). Thus, we performed some initial analyses on cremated bones to prepare for a deeper study in the second funding period of FOR1670.

The Bone Mineral

Bone is a composite material of nearly equal volumes of collagen and nanometre scale crystallites of a carbonated apatite mineral (Peters et al. 2000). The geologic mineral hydroxyapatite is rarely found, as the geologic apatite tends to incorporate F^- and Cl^- ions instead of OH^- to give an approximate formula $Ca_{10}(PO_4)_6(F_{1-x-y}, Cl_x, OH_y)_2$. Bone has a complex hierarchical structure (Wegst et al. 2015; Reznikov et al. 2014; Schwarcz et al. 2014; Weiner et al. 1999; Rho et al. 1998) where the platelike nanocrystals of ~ 2 × 30 × 40 nm size (Cuisinier et al. 1987; Alexander et al. 2012) provide stiffness and compressive strength to the hybrid composite.

The formation of the apatite mineral phase is a complex, biologically controlled process, where the mechanisms of nucleation, growth and growth limitation of the small crystallites are not yet clear. There are several models, including other calcium phosphate phases as precursors and growth from an amorphous phase (Landis and Jacquet 2013).

Chemically, the apatite mineral component of the mammal bone can be approximated as

$$[Ca_{1-u-v}Na_u]_{10}\left[(PO_4)_{1-x-y}(CO_3)_x(HPO_4)_y\right]_6\left[OH_{1-z-w},(CO_3)_z,(H_2O)_w\right]_2$$

where the small potential vacancy concentration v on Ca-sites is
$v = 3(x+y) - z + w - \frac{1}{2}u\,;\,(x, y, z, u, v, w \geq 0)$.

Carbonate (5–8 wt.%) is an essential component of the bone mineral, mostly substituting for $[PO_4]^{3-}$, but also for $[OH]^-$ to a much lesser degree (LeGeros et al. 1967, 1968; Rey et al. 1989, 1990, 1995; Yi et al. 2013). The two different variants of $[CO_3]^{2-}$ substitution in the crystal structure (type A $[CO_3]^{2-} \leftrightarrow [PO_4]^{3-}$, type B $[CO_3]^{2-} \leftrightarrow [OH]^-$) (Wopenka and Pasteris 2005) can be distinguished by IR spectroscopy (Balan et al. 2011). The presence of the acidic phosphate species $[HPO_4]^{2-}$ is also important in the biomineral (Wang et al. 2013; Rey et al. 2014). For bone apatite, the presence of OH^- is low (Pasteris et al. 2004), and water may reside in the OH position. A multitude of different schemes of coupled exchange to maintain charge balance can be suggested (e.g. Wopenka and Pasteris 2005; de Leeuw 2010). In mammal bioapatite, small amounts of F^- replace OH^- (notably in tooth enamel), and on the Ca^{2+} cation position voids (Wilson et al. 2005), Na^+ and Mg^{2+} can be substituted as well as traces of Sr^{2+} and Ba^{2+} (e.g. Elliot 2002; Turner-

Walker 2008). Sponheimer et al. (2005) report that herbivores accumulate higher levels of Sr^{2+} und Ba^{2+} than carnivores and omnivores.

Nuclear magnetic resonance investigations of Jäger et al. (2006) and Wang et al. (2013) indicate the existence of an amorphous surface layer of water-bearing carbonated Ca-phosphate (amorphous calcium carbonate, ACC) which coats a bioapatite nano-crystallite core. Together with the collagen and other organic/cellular components, the mineral nanoparticles compose, right from the supramolecular scale, a hierarchical hybrid composite (Wegst et al. 2015; Reznikov et al. 2014; Schwarcz et al. 2014; Weiner et al. 1999; Rho et al. 1998). As long as this compound structure remains intact, both the inorganic and the organic components are stabilized against chemical and biochemical attack (Gernaey et al. 2001; Turner-Walker 2008). The taphonomic (biological postmortem) decomposition of the about 30 wt.-% organic components of the bone (Peters et al. 2000) creates a high porosity and internal surface in the remaining mineral. This internal surface is reactive and promotes adsorption of ions and molecules from solutions in the soil. The triangular $[CO_3]^{2-}$ groups which are substituted into the crystal structure for the tetrahedral $[PO_4]^{3-}$ complex or for the essentially spherical OH^- induce structural disorder related to the geometric mismatch and charge compensation mechanism. Both this structural misfit and the high surface/interface area increase the free energy of the bioapatite, and thus it has an increased solubility compared to inorganic hydroxyapatite, which is fairly insoluble (Hedges 2002; Berna et al. 2004; Wopenka and Pasteris 2005; de Leeuw 2010). In vivo this enhanced solubility plays a substantial role in the continual physiologic reconstruction of bone. Similarly, the increased free energy provides a driving force for diagenetic recrystallization (Nielsen-Marsh and Hedges 2000; Nielsen-Marsh et al. 2000) and formation of larger crystals. Thus, secondary minerals may form such as newly grown abiotic inorganic hydroxyapatite (which is free of carbonate) and calcite, $CaCO_3$, taking up the $[CO_3]^{2-}$ and associated Ca^{2+} from the former bioapatite.

$$[Ca_{1-u-v}Na_u]_{10}\left[(PO_4)_{1-x-y}(CO_3)_x(HPO_4)_y\right]_6\left[OH_{1-z-w},(CO_3)_z,(H_2O)_w\right]_2$$

Bioapatite (Carbonate-Hydro-Hydroxyapatite)

$$\rightarrow\sim s\,\underset{\text{Hydroxyapatite}}{Ca_{10}(PO_4)_6(OH)_2} + (6x+2z-6y)\,\underset{\text{Calcite}}{CaCO_3} + 10u\,NaCaPO_4 + 2w\,H_2O + 6y\,CO_2$$

with $s \approx (1-2u-v-0.6\,x-0.2z+0.6y)$.

The $NaCaPO_4$ phase here is a nominal phase to account for the sodium. Those secondary minerals potentially incorporate ions present in the soil solution, such as Sr^{2+}, Pb^{2+}, etc. (Tütken et al. 2008), which changes the trace elements signatures of the sample.

While the bone mineral is comparatively stable against exposures at temperatures reached by cooking, boiling, or roasting, conditions above ca. 500 °C profoundly change the bulk chemistry and crystalline consistence of the bioapatite (Rogers and Daniels 2002; Enzo et al. 2007; Munro et al. 2008; Piga et al. 2008, 2009a, b, 2013;

Harbeck et al. 2011; Galeano and Garcia-Lorenzo 2014). From about 500 °C, a significant recrystallization of the bioapatite and crystallite growth of hydroxyapatite sets in. Prehistoric cremation pyres could reach temperatures up to 1000 °C (McKinley 2016). Ratios of stable isotopes of light elements contained in the atmosphere change considerably during heat treatment (Olsen et al. 2008; Schurr et al. 2008), while those of elements such as strontium and lead do not appear to be altered as long as there are no reactions with surrounding materials (Harbeck et al. 2011).

The selected techniques for mineralogical characterization of the bone materials, X-ray diffraction (XRD) and Fourier Transform Infrared Spectroscopy (FT IR), are essentially complementary. To characterize the diagenetic recrystallization of bone apatite, Person et al. (1995) defined their classical empirical "crystallinity index" (CI) on the basis of the width of X-ray diffraction lines. This index number became widely used (e.g. Hedges 2002). Another popular empirical index number is the infrared splitting factor (IRSF) by Weiner et al. (1993) (see, e.g. Surovell and Stiner 2001). The utility of the simple IRSF to describe complex spectral features is debated in the literature (Sillen 1989; Shemesh 1990; Weiner and Bar-Yosef 1990; Wright and Schwarcz 1996; Trueman et al. 2008; Tütken et al. 2008). According to Shinomiya et al. (1998), the IRSF indicated chemical alterations already a few years after death. Sample preparation for XRD or FTIR measurement certainly has an influence on the CI/IRSF results (Surovell and Stiner 2001). The simplifying indices for a "crystallinity" of the bone mineral do not correlate with modifications of chemical composition and also not with stable isotope data of the structural carbonate (e.g. Lee-Thorp and Sponheimer 2003; Pucéat et al. 2004; Trueman et al. 2008; Tütken et al. 2008). Moreover, physiological differences in bioapatite characteristics between different species, different skeletal elements and different age groups of the population can be expected and need to be considered in the future (Rey et al. 1991, 2009; Yerramshetty and Akkus 2008). To put the IRSF on a more physical basis, Lebon et al. (2008) suggested spectral decomposition by curve-fitting procedures on the relevant part of the infrared spectrum; these procedures were later improved by Vandecandelaere et al. (2012) and Grunenwald et al. (2014). Pedone et al. (2007) and Yi et al. (2014) contributed more rigorous considerations on the theory of phosphate and carbonate vibrations to be expected in bioapatite.

The X-ray diffraction (XRD) technique takes advantage of the periodic lattice-like structure of crystalline materials, as it measures interference patterns of the X-ray waves scattered from the atoms or molecules in the material. Crystals are objects with a spatially periodic arrangement of the constituting atoms, ions or molecules, and for such materials, the interference maxima become sharp if the spatial range of the periodic order is wide. The concept of a crystal is an array of building blocks (called unit cells, Fig. 1) which are periodically repeated in a space-filling, lattice-like fashion. The positions of the X-ray diffraction peaks are defined by the unit-cell dimensions, the so-called lattice parameters. The peak intensities, explained in a nutshell, are related to the electron density distribution pattern in the unit cell averaged over time and space in the crystal. This pattern reflects the positions and electron densities of all the individual atoms or molecules in the crystal, superimposed by the space and time average (cf. for details e.g. to

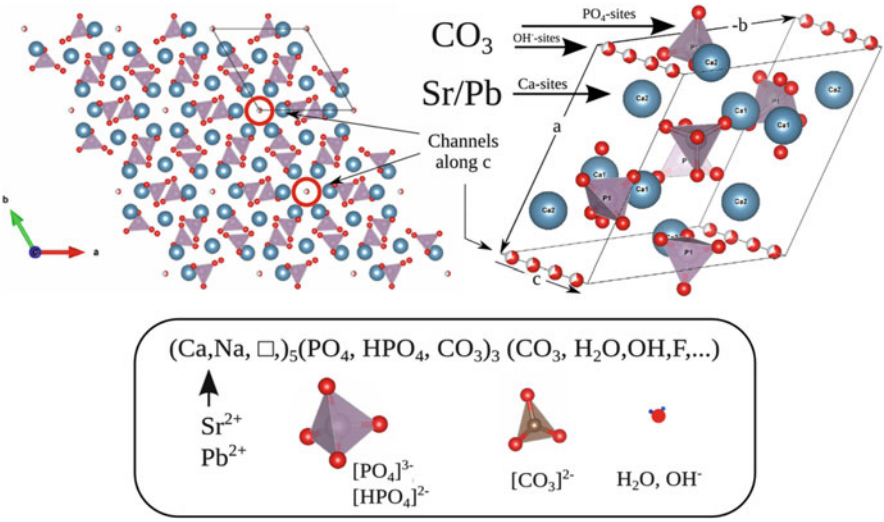

Fig. 1 Crystal structure of hydroxyapatite in hexagonal setting after Wilson et al. (1999) and Tonegawa et al. (2010). Some authors (Ikoma et al. 1999; Tonegawa et al. 2010) believe that monoclinic symmetry (space group $P2_1/c$) gives a better description for well-crystalline hydroxyapatite. In bioapatite, the $[PO_4]^{3-}$ is exchanged by $[CO_3]^{2-}$ and $[HPO_4]^{2-}$, while the channel sites (OH^- location of hydroxyapatite) contain $[CO_3]^{2-}$, H_2O, OH^- and other ions. The Ca-sites are also occupied by minor amounts of Na^+ and by vacancies (*white square*). It is here where trace elements such as Sr^{2+} and Pb^{2+} reside

Pecharsky and Zavalij 2003 and Mittemeijer and Welzel 2012). For small crystallites, as is the case for bioapatite, there are fewer atoms contributing to the interference phenomenon, and thus the diffraction maxima widen inversely proportional to the coherence length of the periodic crystalline order (de Keijser et al. 1982). The width and shape of the X-ray diffraction peak related to a particular lattice plane depend both on this coherence length (i.e. in the simplest case the crystallite size) perpendicular to that plane and on the variance of the lattice parameters in the sample, the so-called microstrain. Microstrain results from inhomogeneities in chemical composition, other lattice defects, and from mechanical strains on the scale of the crystallite size. In the case of bone, such mechanical strains can result from the composite structure with collagen. Note that the frequently used term "crystallinity" (Rogers et al. 2010) is a notion mingling effects of crystallite size, microstrains, random chemical substitution and presence of amorphous phases in a rather undefined way.

Deviations from the average structure give a very small intensity contribution in XRD, which we neglect here. Amorphous substances do not have a periodic structure; their diffraction pattern consists of diffuse intensity halos with maxima related to peaks in the spatial probability density distribution of the constituting atoms. In any case, amorphous, crystalline or "in between", the diffraction signal is the Fourier transform of the electron density self correlation function, which is straightforward to calculate (see Schmahl et al. 2016 for more information). Thus,

modern XRD analysis is based on a rigorous calculation of the diffraction profile and algorithms fitting the model parameters to obtain the best-possible agreement with the observed diffraction profile (so-called Rietveld refinement method, Rietveld 1969; Rodriguez-Carvajal 1993; Rodriguez-Carvajal and Roisnel 2004; Pecharsky and Zavalij 2003; Mittemeijer and Welzel 2012).

This quantitative treatment of the X-ray diffraction profile led to assessments of the crystallographic characteristics of archaeological and paleontological bone materials (Stathopoulou et al. 2008; Piga et al. 2008, 2009a, b, 2013; Harbeck et al. 2011). Stathopoulou et al. (2008) examined Miocene and Pleistocene samples from the Aegean with the Rietveld technique and arrived at the conclusion that "Diagenetic trends, common to all these sites include a subtle but systematic decrease of the unit-cell volume and a-axis of carbonate hydroxylapatite, as well as a parallel increase of the coherence length along the c-axis". Stathopoulou et al. (2008) also established a correlation of X-ray diffraction data with IR data. Enzo et al. (2007), Piga et al. (2008, 2009a, b, 2013), Harbeck et al. (2011), and Galeano and Garcia-Lorenzo (2014) applied modern full-profile analysis of X-ray diffractograms to evaluate effects of cremation on the bone mineral. From about 500 °C, a significant recrystallization of the bioapatite and crystallite growth of hydroxyapatite sets in. Piga et al. (2008, 2009a) experimented with varying cremation times at different temperatures and found that between 600 °C and 850 °C, the transformation of the bioapatite to hydroxyapatite occurs essentially within the first 20 min of the heat treatment.

X-ray diffraction is less well suited to probe local molecular environments. Infrared spectroscopy, however, can distinguish, e.g. the two different variants of $[CO_3]^{2-}$ substitution in the crystal structure (type A $[CO_3]^{2-} \leftrightarrow [PO_4]^{3-}$, type B $[CO_3]^{2-} \leftrightarrow [OH]^{-}$) (Wopenka and Pasteris 2005). Infrared spectroscopy (IR) probes the frequencies of molecular scale vibrations in the material. Infrared photons are absorbed if their frequency is in resonance with a frequency of a molecular scale vibration in the sample. The frequency characteristics of the vibration depend on the precise local structural configuration of the vibrating entity in the sample. In a crystallographically well-ordered material, the vibrations in neighbouring unit cells are identical. In this case, the IR absorption peaks are well developed and rather sharp. In a disordered or amorphous material, the IR absorption signal is still present, but it broadens as the molecular vibration frequencies become locally different due to different molecular environments in the structure. This interaction is complex, however, as the frequencies shift both with changing chemical bond strengths and masses of vibrating bodies in different configurations or environments, but the signal also broadens in relation to the fading (damping) of the vibration after its initial excitation.

In any case, the IR spectrum reflects the time structure of local molecular scale environments of the vibrating entities in the sample, while the X-ray diffraction signal reflects the spatial periodicity in the atomistic structure. Accordingly, the two methods give complementary information. Atoms and molecules vibrate around their equilibrium configuration in all materials, regardless if the materials structure is crystallographically ordered or not. This gives an advantage to IR spectroscopy for the investigation of materials which are not spatially ordered. On the other hand,

IR probes periodic long-range order ("crystallinity") only indirectly: by the effect of the crystal structure on the time structure of the vibrations. So far, there is no straightforward general way to calculate this indirect influence.

Materials and Methods

Among the uncremated archaeological animal bone samples which were prepared for isotope studies in FOR1670 (see chapter "Isotopic Map of the Inn-Eisack-Adige-Brenner Passage and its Application to Prehistoric Human Cremations"), we selected 63 random samples for screening by X-ray diffraction. The samples were from the species *Bos taurus*, *Sus domesticus* and *Cervus elaphus*. Fresh bovine bone samples and fossil samples of a Miocene hippopotamus from Bavaria were obtained for comparison. A piece of compact bone was cut from the skeletal element, and the endosteal and periosteal surfaces were mechanically removed by grinding off. The sample was then ultrasonically washed in deionized H_2O (35 kHz), where the water was changed every 5 min. The washing was repeated until the water remained clear. After drying in air, the bone piece was defatted for 5 h with diethylether in a Soxhlet and air dried again. Finally, the sample was homogenized to a fine powder.

For experimental cremation, we used thus prepared bovine femur powder and subjected it to heat treatment in air in a muffle. The samples were put into the preheated furnace for an exposure time of 1 h, after which they were removed and left to cool in air.

For an investigation archaeological bone samples from burials which were subjected to cremation as a burial rite, we selected long bones from the Bronze Age (Urnfield Culture) site of Eching (1300–800 BC) and a skull from the Zuchering site of the same culture, both in in southern Bavaria. All cremated bones were buried in urns; the urns were found in a broken state.

X-ray diffractograms were collected on a General Electric 3003 powder diffractometer in Bragg-Brentano reflection geometry. Cu-Kα_1 radiation was selected with a focussing monochromator in the primary beam. Data collection time for a complete diffractogram from 5 to 100 degrees 2θ amounted to 240 min with a 1D Meteor detector and exposure time of 1000 s for each frame. The instrumental resolution function was experimentally determined with a NIST LaB_6 standard. For data evaluation and Rietveld refinement, the FULLPROF code (Rodriguez-Carvajal 1993; Rodriguez-Carvajal and Roisnel 2004) was employed. The Thompson-Cox-Hastings method for convolution of sample effects such as anisotropic size and isotropic microstrain broadening (Thompson et al. 1987) with instrumental resolution (as determined with a NIST LaB_6 standard) was applied.

Infrared spectra were measured on a Bruker Equinox FTIR instrument with a resolution of 4 cm^{-1}. A total of 128 scans was averaged resulting in a 2 min acquisition time per sample. The bone powder (as described above for XRD) was sieved through a 100 μm mesh, and 1 mg of resulting sample powder was manually mixed with 200 mg of KBr in a mortar and pelletized subsequently. Spectral decomposition into seven bands was performed in the range 400–800 cm^{-1}. The seven bands were fitted with a Gaussian-Lorentzian sum function with fixed ratio of

3:7 each. For each band, the center position, the full width at half maximum (FWHM) and the peak area were fitted. Background was described with a cubic polynomial, but the function remained essentially flat.

Results and Discussion

The Uncremated Mammal Bones

Due to the nanoscale dimension of the bone bioapatite particles, the diffraction peaks of original bone material are significantly broadened (Fig. 2). The broadening is anisotropic, as the (002) peak, corresponding to the crystallographic c-axis of the crystallites, is comparatively sharp while the peaks corresponding to the a- and b-directions are significantly broader. We parameterized the size as a second rank tensor, corresponding to an ellipsoid. The agreement between observed and calculated diffraction profile is excellent in view of the complexity of the system. Due to

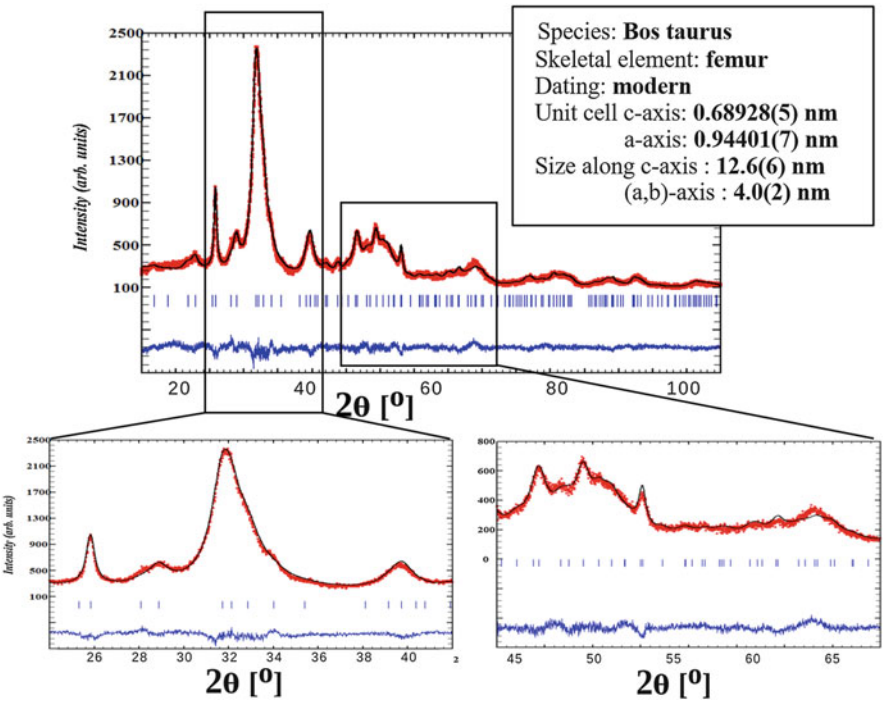

Fig. 2 X-ray diffraction trace of the bone mineral from the femur of modern domestic cattle (*Bos taurus*) taken with Cu-kα_1 radiation. *Red dots*: observed data points; *black line*: calculated XRD profile; *blue line on bottom*: difference of observed and calculated data. *Blue vertical bars*: positions of the diffraction peaks. The two enlarged regions show the most featured parts of the diffractogram. The XRD profile was fitted with an anisotropic size model for the coherently diffracting domain

the hexagonal symmetry, the XRD peaks which would have been able to discriminate different crystallite sizes in a- and b-directions directly overlap, so that a distinction is not possible with the current method. Correspondingly, quoted crystallite sizes correspond to an average of the directions in the a-b plane. For the fresh bovine bone, we arrive at 12.6 nm for the c-direction and 3.9 nm for the a-b plane. The estimated precision of these numbers from the Rietveld least-squares fit is in the order of 5 %. Most of the archaeological samples show a slightly reduced broadening such that the 211, 121, 112 and 030 peaks become more distinct (Fig. 3). This may indicate grain growth and/or dissolution of the finest-scaled fraction during burial. Most importantly, we observe calcite as a secondary phase in about 20 % of the investigated archaeological sample. Note that all investigated samples had visually very good quality to be selected for isotope analysis, and their surfaces were cleaned away to avoid contamination by soil. There is no indication of typical soil minerals such as clay minerals or quartz, other than calcite, such that the selection and cleaning procedure was effective. Only in 3 samples out of 63, the determined calcite fraction was $\geq$ 2 wt.%, with the maximum at 5 wt%. The

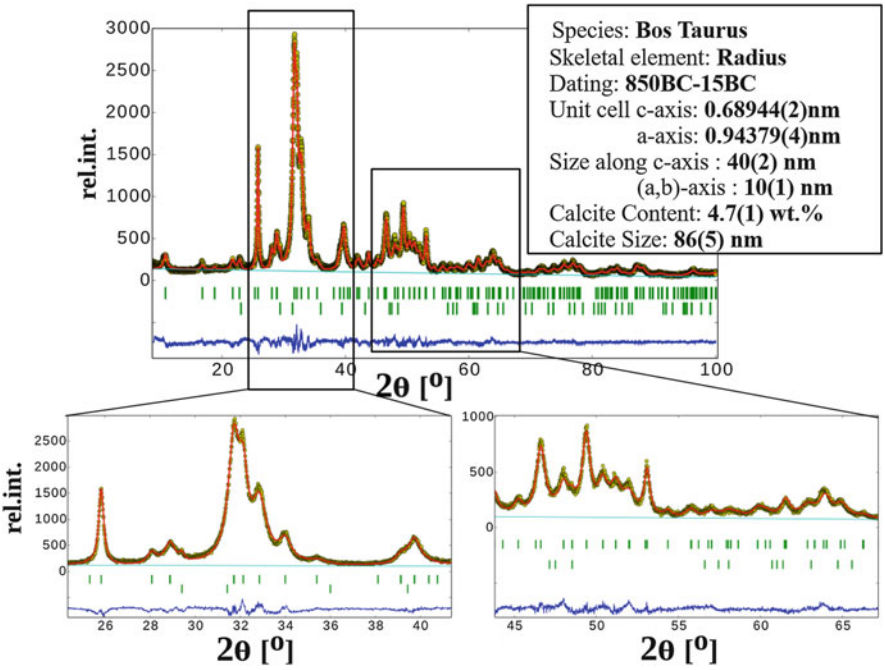

Fig. 3 X-ray diffraction trace of an archaeologic animal bone sample (*Bos taurus*, radius) from the Brixen Stufels, Hotel Dominik site. Cu-kα_1 radiation. *Red dots*: observed data points; *black line*: calculated XRD profile; *blue line on bottom*: difference of observed and calculated data. *Green vertical bars*: positions of the diffraction peaks; *top row*: bone apatite; *bottom row*: calcite. The two enlarged regions show the most featured parts of the diffractogram. The XRD profile was fitted with an anisotropic size model for the coherently diffracting domain. In the enlarged region the different broadening of the 002 and the 030 peaks can be clearly seen (c.f. Fig. 5)

observed calcite itself shows a diffraction line broadening which indicates a crystallite size on the scale of 100 nm, which is a strong indicator that this calcite is not simply due to crystallization from infiltrating soil solution, for which micrometre-sized crystals would be expected. We examined an archaeological deer bone (metatarsus) in the SEM after careful deproteination (Fig. 4). The calcite is contained inside the bone fabric in the form of ideal rhombohedral crystals of the 100–500 nm size range.

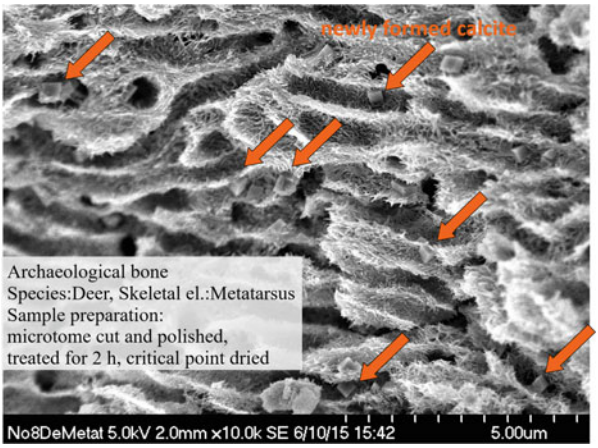

Fig. 4 SEM micrograph of deproteinated archaeological deer bone (metatarsus) from the Brixen-Stufels "Hotel Dominik" 4856 archaeological site (~ 5th century BC). Note the ideal rhombohedral crystals of secondary calcite (*arrows*) distributed in the bone fabric

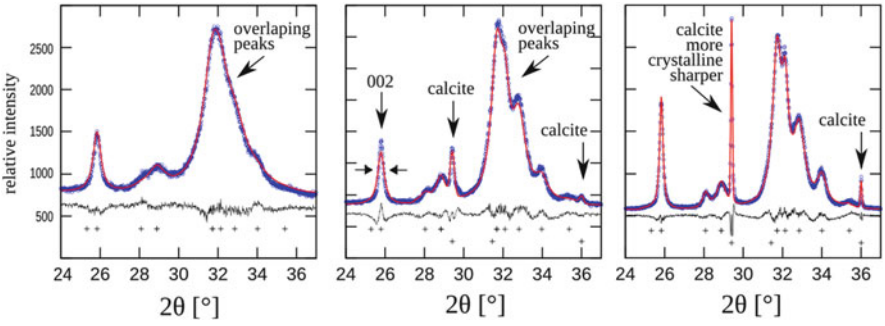

Fig. 5 Comparison of the 25°-42° 2θ range of X-ray diffractograms of fresh bone (*Bos taurus*, femur) and two archaeological bones (*Sus domesticus*, mandibula, *Cervus elaphus*, metatarsus III +IV). Cu-kα_1 radiation. *Blue dots*: observed data points; *red line*: calculated XRD profile; *black line on bottom*: difference of observed and calculated data. *crosses*: positions of the diffraction peaks; *top row*: bone apatite; *bottom row*: calcite

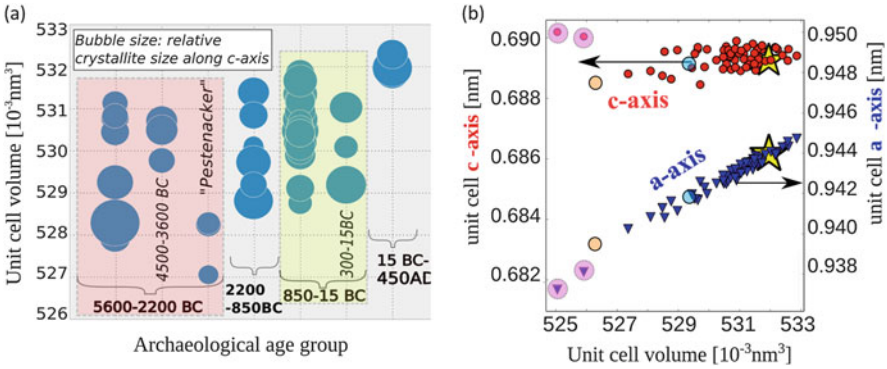

Fig. 6 Overview on crystallographic parameters of the uncremated archaeological samples of animal bones. (**a**) Unit-cell volume vs. archaeological (cultural) age group. The bubble size indicates the size along c of the coherently diffracting domain. There is only a weak correlation with archaeological age. (**b**) Lattice constants (unit-cell axes) vs. unit-cell volume. *Red dots and blue triangles*: unit cell c-axis and a-axis, respectively, of the archaeological bones. *Yellow stars*: modern bovine femur. *Pink circles*: Miocene (~20 million year old) fossil hippopotamus from Bavaria. *Light blue circles*: hydroxyapatite. *Orange circles*: fluorapatite

A closer comparison of the 25°–42° diffraction angle (2θ) range is shown in Fig. 5. There is a small but detectable sharpening of the XRD peaks of the archaeological material compared to the fresh bovine femur.

Figure 6 gives an overview on crystallographic parameters of the 63 examined archaeological samples. Figure 6a compares the apatite unit-cell volume and the crystallite size along the c-axis with the archaeological age group. We observe only a vague correlation of unit-cell volume decreasing with archaeological age, and the crystallite size shows no correlation with age. Clearly, this indicates that there are other factors contributing to the measured lattice parameter than just changes with age, related to possible loss of carbonate. These other factors may include humidity and soil pH at the archaeological site, which might affect the alteration reaction, and also intraspecies and across-species variations of the crystallographic parameters of the bone mineral, which still need to be examined in the future. Figure 6b displays the lattice parameters and unit-cell volume. The star in Fig. 6b marks the lattice parameters of the fresh bovine femur bone material. The pinkish circles mark the lattice parameters of a bone fragment of a fossil Miocene hippopotamus from Bavaria (~ 20 million years old). The plot of Fig. 6b allows to conclude that the c-axis of the archaeological bone mineral is fairly constant while the a-axis lattice parameter varies in a systematic way. The data lie on a pseudo-linear trend (because the unit-cell volume V scales with the lattice parameters as $V = a^2 c \sin 120°$, and the parabolic relation between V and a is approximately linear in a small range of data), but interestingly, this trend line connects the fresh bone with the fossil bone. Synthetic hydroxyapatite also lies on this trend line (light-blue circle) and fluorapatite (orange circles) as well. We infer that the bone mineral undergoes a chemical alteration during burial, possibly by exchange of the carbonate with hydroxyl and fluorine. But this interpretation needs to be confirmed with future studies.

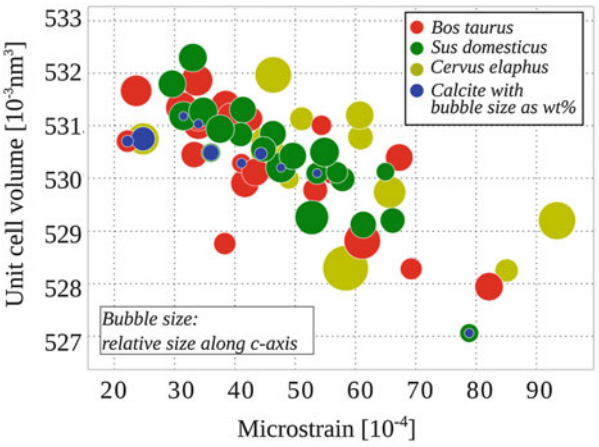

Fig. 7 Correlation of unit-cell volume with microstrain broadening. Microstrain is the statistical variation of the lattice parameters due to chemical or mechanical inhomogeneity in the sample. Smaller unit-cell volumes, indicative of higher degree of diagenesis, are associated with larger inhomogeneity of the lattice parameters in the sample

Figure 7 plots the unit-cell volume vs. the distribution width of the statistical variation of lattice parameters within each single sample (the so-called microstrain), which also gives a diffraction line broadening, which can be distinguished, however, from the size broadening to its different dependence on the scattering angle ($\tan\theta$) compared to the size broadening $(\cos\theta)^{-1}$. There is a correlation indicating that smaller unit cells, which appear to occur due to alteration by loss of carbonate, as discussed above, have a more inhomogeneous distribution of lattice parameters. This can be explained by an inhomogeneity in the progress of the alteration reaction within each bone sample. However, the plot also indicates that the three different species which were examined show different characteristic, with the wild form (*Cervus elaphus*) displaying a larger spread than the domesticated species (*Sus* and *Bos*).

Figure 8 displays a compilation of crystallographic parameters and $^{87}S/^{86}Sr$ isotope values for the 63 samples. It shows that the data set is fairly uniform with any correlations occurring in a quite random manner. We interpret this situation as due to the successful cleaning procedure, which removed potential contamination, and that in the selected material, the isotope ratios do not show any trends with the crystallographic parameters of the bone apatite.

Furnace Annealing (Experimental Cremation)

To simulate the effect of heat treatment on bone material, we performed annealing experiments with bovine femur material. Figure 9a gives an overview of the change of the bone mineral diffractograms as a function of annealing temperature; Fig. 9b and c show sections of the diffractograms as difference plots between measured and calculated profile. Below 400 °C, the width of the peaks reduces only little, but we see small but significant changes of the lattice parameters (Fig. 10). These could be the result of the breakdown of the collagen and the changes in the composite structure of the bone occurring accordingly. Between 400 °C and 600 °C, the trend in the lattice parameters is reversed compared to the lower temperatures, indicating that a different and so far unknown structural process sets in. From about 600 °C upwards, there is a marked

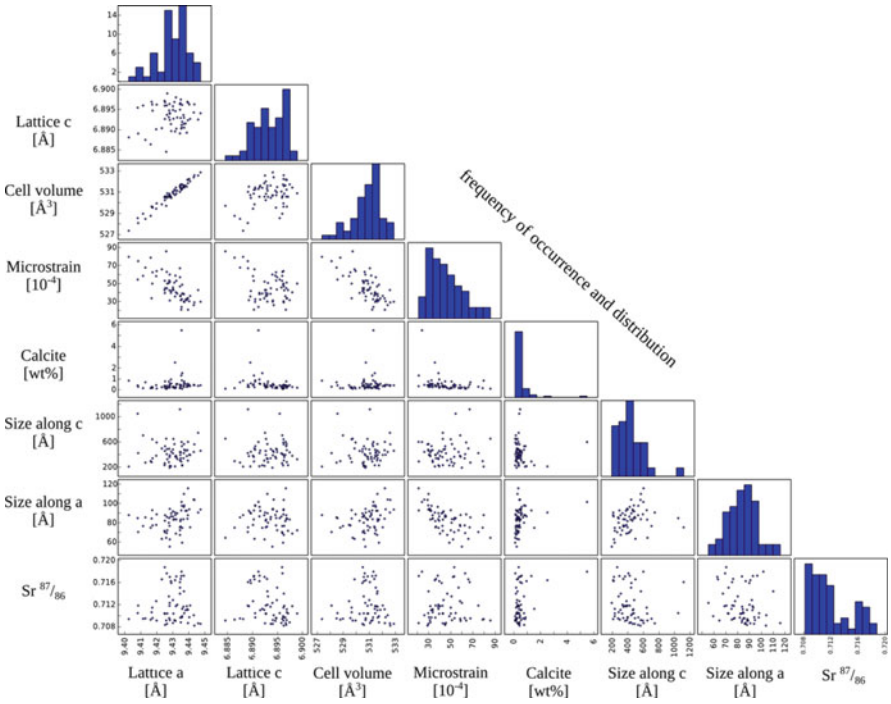

Fig. 8 Scattergram of the most relevant crystallographic parameters (from Schmahl et al. 2016)

increase in sharpness of the XRD peaks, which is related to a dramatic increase of the crystallite size and a progressive transformation from carbonated apatite to hydroxyapatite as a function of annealing temperature (Fig. 10; Table 1). Similar results have been obtained by Rogers and Daniels (2002). CaO forms as a further reaction product of the bioapatite decomposition at 800 °C and above.

Infrared spectra of the cremated bioapatite are shown in Figs. 11, 12 and 13. Figure 11 compares a typical IR spectrum of archaeological bone with those of two selected experimentally annealed bones. The archaeological bone–like fresh bone–shows carbonate vibration bands. Their intensity decreases with heat treatment, and they are absent in the material annealed at 1000 °C, which shows the spectrum of hydroxyapatite. In Fig. 12, spectral changes with heat treatment are shown, in particular, the development of the OH^- stretching vibration at 3568 cm^{-1} and the OH^- libration near 633 cm^{-1} as a function of heat treatment. It is very evident that the contributions of OH^- to the spectra of untreated bone are quite insignificant and that they rise with heat treatment. This can also be seen in the FTIR spectra of Stiner et al. (1995). Further, the deproteinated untreated bone shows an intense contribution of H_2O, which diminishes with heat treatment and which is practically absent in the sample treated at 1000 °C. This all points to the assumption that the bioapatite is a carbonate-H_2O-apatite with little OH^- (Rey et al. 1995; Loong et al. 2000; Pasteris et al. 2004) and it becomes hydroxyapatite with

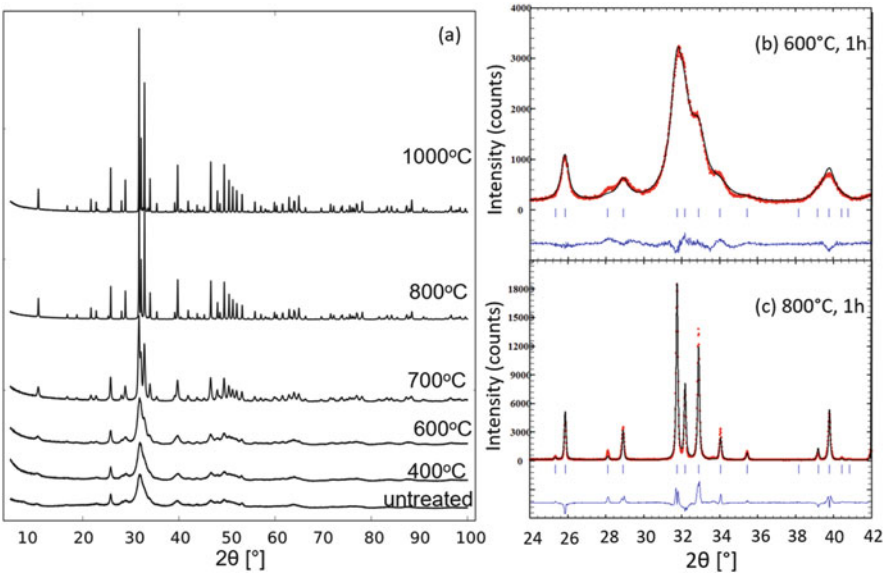

Fig. 9 Overview of X-ray diffractograms of bovine femur bone mineral samples annealed for 1 h at different temperatures (experimental cremation). Note the dramatically increasing sharpness of the XRD peaks with annealing temperatures above 600 °C corresponding to increasing crystallite size. Exemplary Rietveld fits are shown in (**b**) and (**c**) for treatment at 600 °C and 800 °C

heat treatment, losing CO_2 and perhaps some H_2O ($CO_3^{2-} + H_2O \rightarrow CO_2 + 2OH^-$). At the same time, the high temperatures lead to an increased crystallite size by Ostwald-ripening, driven by the reduction of free energy by lowering the internal surface. The excess free energy due to the surface is proportional to $(2\gamma/r)$ where γ is the specific surface energy and r is the crystallite size; thus, large crystallites grow at the expense of smaller crystallites.

Figure 13 displays the spectral decomposition based on seven peaks in the 400–800 cm^{-1} range which covers the v_4 phosphate group bending modes and the mode at 633 cm^{-1} which is attributed to OH^- libration (Gonzalez-Diaz and Hidalgo 1976; Gonzalez-Diaz and Santos 1977; Vandecandelaere et al. 2012). The most robust spectral parameter useful to correlate with cremation temperature is the full width at half maximum (Balan et al. 2011) of the band at 603 cm^{-1}. It correlates linearly with cremation temperature (Fig. 14). For uncremated bones and for low temperatures of heat treatment, the FTIR peaks are poorly developed and show a large overlap of the spectral features (Figs. 13a and 14). As the material gets more ordered while it approaches more stoichiometric chemistry with increasing sintering temperature, the peaks get increasingly narrower and well defined. The calibration equation is

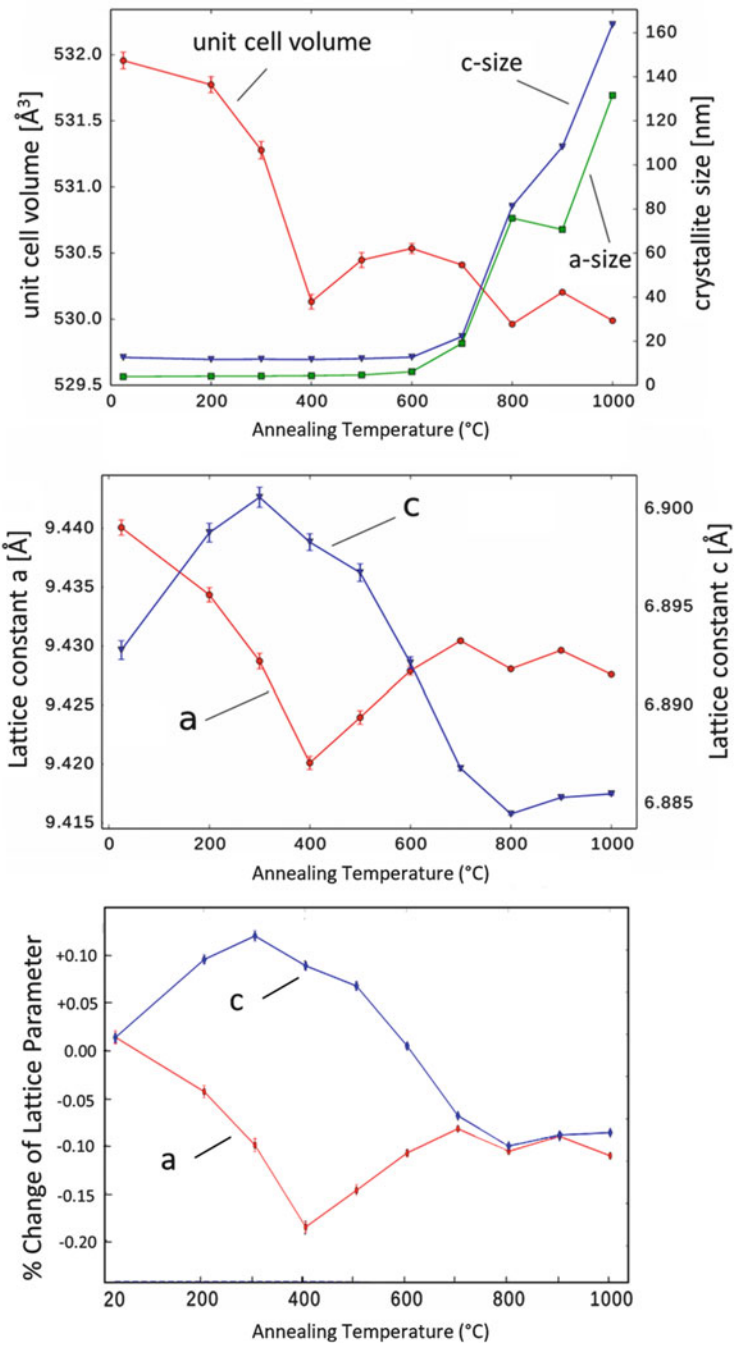

Fig. 10 Size of the coherently diffracting domains in c- and a- and b-direction (crystallite sizes labelled "c-size" and "a-size", respectively) and lattice parameters for the experimentally annealed samples as a function of annealing temperature. Annealing time is 1 h

Table 1 X-ray diffraction results on experimentally annealed samples and cremated archaeological samples

Experimentally annealed samples				
Annealing temperature (°C)	*c* (Å)	*a* (Å)	*c*-size (nm)	(*a*,*b*)-size (nm)
21	6.8854(5)	9.4318(7)	12.7	3.9
200	6.8876(5)	9.4234(7)	11.7	4.1
300	6.8932(5)	9.4218(7)	11.8	4.2
400	6.8912(4)	9.4161(6)	11.7	4.3
500	6.8921(4)	9.4231(5)	12.1	4.6
600	6.8899(3)	9.4266(4)	12.7	6.1
700	6.88718(11)	9.4303(12)	22.1	19.0
800	6.88486(5)	9.42865(6)	81.2	75.8
900	6.88616(6)	9.43106(7)	108.2	70.6
1000	6.88601(5)	9.42822(5)	163.7	131.5
Eching samples				
8_Eching_247	6.891953(18)	9.41861(20)	104	93
10_Eching_626	6.8836(7)	9.44582(9)	128	44
14_Eching_727	6.89629(12)	9.41812(17)	22.5	11.5
17_Eching_346	6.88568(3)	9.42397(3)	113	101
18_Eching_140	6.88682(3)	9.42269(4)	143	98
19_Eching_219	6.88686(2)	9.42079(3)	188	130
20_Eching_222	6.89439(14)	9.4198(2)	22.5	10.2
Zuchering skull				
Outer_1	6.89796(6)	9.42178(8)	69	60
Inner_1	6.89727(14)	9.4221(2)	36	22
Outer_2	6.89857(4)	9.42311(5)	139	147
Inner_2	6.89603(5)	9.42419(6)	173	108
Outer_3	6.89873(5)	9.4215(6)	73	63
Inner_3	6.89832(16)	9.4211(2)	35	21
Outer_4	6.89772(11)	9.42127(14)	36	27
Inner_4	6.89885(18)	9.4185(2)	23	13
Outer_5	6.89797(8)	9.42159(11)	42	32
Inner_5	6.9004(2)	9.4206(3)	22	12

Numbers in brackets are standard deviations referring to the last digit(s). The estimated standard deviation for crystallite sizes is estimated as 5 %

$$FWHM = -0.0231\left[\frac{\mathrm{cm}^{-1}}{^{\circ}\mathrm{C}}\right]{*}T + 37.9\left[\mathrm{cm}^{-1}\right] \quad (1)$$

where T is the cremation temperature in °C.

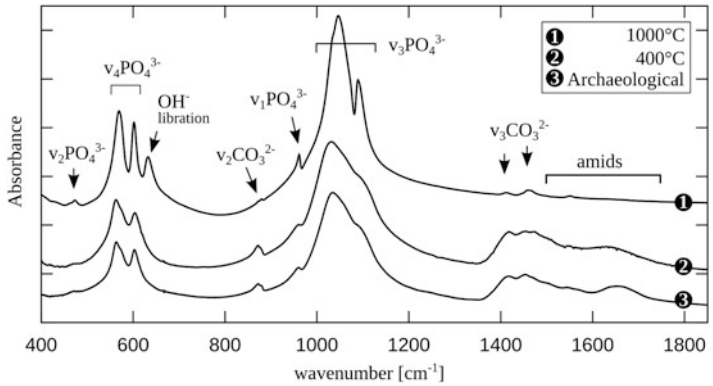

Fig. 11 Comparison of FTIR spectra of uncremated archaeological and experimentally annealed samples with the most important vibrational bands indicated. Note the absence of carbonate bands in the 1000 °C annealed samples and the absence of OH^- libration in the uncremated sample and the 400 °C annealed sample

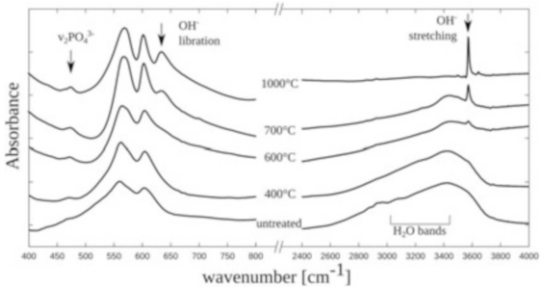

Fig. 12 Change of the FTIR spectra of degreased and deproteinated bovine (femur) bone material as a function of experimental annealing temperature (annealing time 1 h). Note the pronounced increase of the OH^- signals and the decrease of the H_2O signal with increasing treatment temperature

Cremated Archaeological Samples

We exemplify results on cremated archaeological bone remains from the Bronze Age (Urnfield Culture) of southern Bavaria with long bones from the Eching site and a skull from the Zuchering site.

Figure 15 shows the Fourier transform infrared spectra of seven samples from the Eching locality in the spectral range of the ν_4 phosphate group bending modes and the OH^- libration mode at 633 cm^{-1}. The seven samples can be separated into two groups. The first group consists of the samples 20_Eching (black trace) and 14_Eching (red trace) which show fairly similar FTIR spectra. Their ~567 cm^{-1} band is at lower frequencies than that of the second group, and the width of both the 567 cm^{-1} band and the 603 cm^{-1} band is broad; further, they do not show a well-

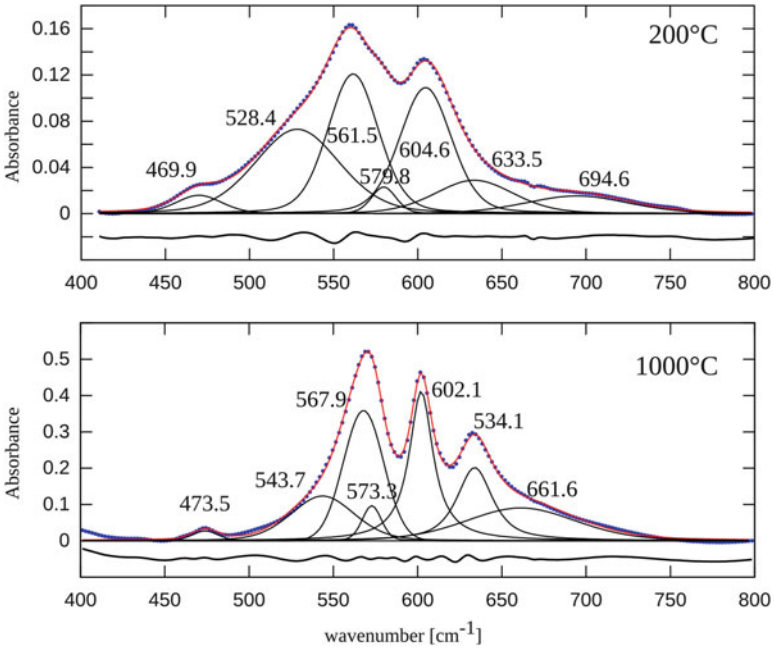

Fig. 13 Spectral decomposition of the FTIR signal of the ν_4 $[PO_4]^{3-}$ vibration bands and the OH^- libration band in the 400 cm^{-1} to 800 cm^{-1} range into seven contributions for two exemplary states of experimental annealing of bovine femur bone mineral

differentiated hydroxyl libration peak at 632 cm^{-1}. The second group consists of the remaining five samples with narrower peaks for the phosphate bands and a well-differentiated OH^- libration band. Correspondingly, the group 2 samples have seen higher cremation temperatures than the group 1 samples.

Table 2 lists the results for the estimated cremation temperature based on Eq. (1) from the spectral decomposition of the P–O bands. For group 1, we estimate a cremation temperature around 750 °C, while the group 2 samples are placed between 1000° and 1150 °C.

As the XRD of the Eching samples (see below) gave strong indications that cremated bones are typically inhomogeneous with respect to the cremation state, we also investigated a cremated skull from the Zuchering site for which we had visually observed colour differences between the inner and outer side of the cranium. Five samples from the cranium were divided into the inner compact bone layer and the outer compact bone layer (the spongiosa was thus lost). Infrared spectra of the skull sample are shown in Fig. 16; FWHM values of the ~603 cm^{-1} band and corresponding calculated cremation temperatures are given in Table 2. First of all, the IR data for the single skull are quite variant and indicate a range of cremation temperatures between 834 °C ± 45 °C and 1016 °C ± 20 °C, and there are significant differences between corresponding inner and outer layers, which are just millimetres apart. In contrast, the estimation of the cremation temperature

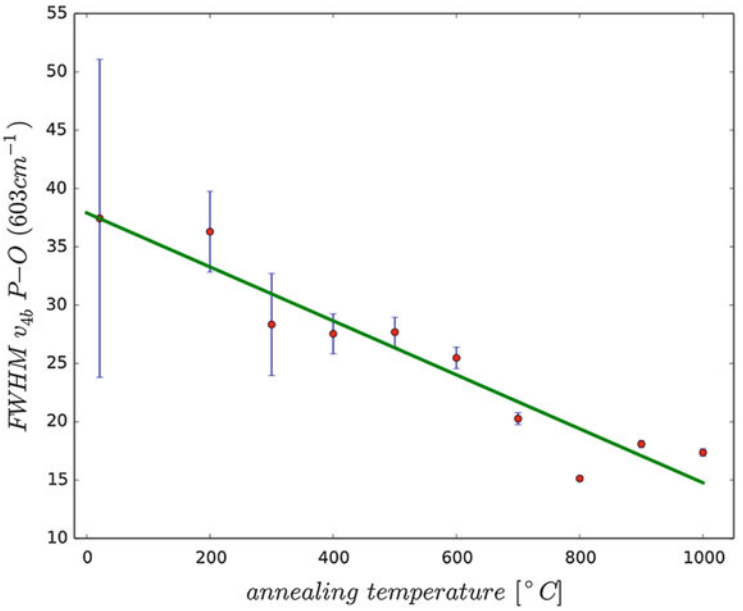

Fig. 14 Correlation of the full width at half maximum (FWHM) of the 603 cm^{-1} band vs. annealing temperature of experimental cremation (annealing time 1 h)

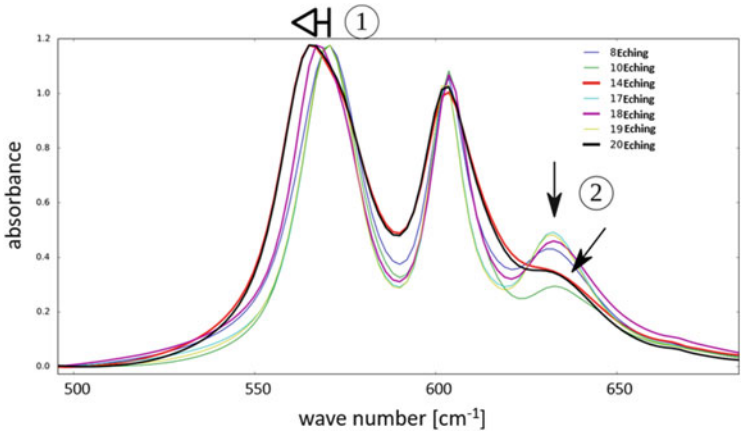

Fig. 15 FTIR spectra of archaeological cremated samples from the Urnfield Culture site of Eching (1300–800 BC). The phosphate ν_4 bending modes are highlighted with changes in the frequency (1) of the ~567 cm^{-1} band, and the appearance and broadening of the OH^- libration mode at 633 cm^{-1} are indicated (2)

Table 2 Full width at half maximum of the ~603 cm^{-1} ν_4 [PO_4] infrared absorption band for the archaeological cremated samples from the Eching and Zuchering Urnfield Culture sites, the corresponding calculated cremation temperature from Eq. (1), the cremation temperature estimated from XRD crystallite size (Table 1; Fig. 10) and the cremation temperature estimate from the colour of the specimen on the basis of (Wahl 1981)

Sample	FWHM of the 603 cm^{-1} P–O band (cm^{-1})	Calculated cremation temperature from Eq. 1 (°C)	Estimated cremation temperature from XRD line width (°C)	Estimated cremation temperature after Wahl (1981) (°C)
20_Eching_222	20.1(1.2)	769(100)	700	
14_Eching_727	20.7(1.3)	743(100)	700	
8_Eching_247	14.4(3)	1015(15)	840	
10_Eching_626	14.3(2)	1020(10)	920	
17_Eching_346	11.6(7)	1136(100)	900	
18_Eching_140	12.74(1.8)	1087(10)	950	
19_Eching_219	11.6(2)	1136(10)	1030	
Zuchering skull				
Outer 1	16.6(7)	920(30)	780	550
Inner 1	18.6(0.98)	834(45)	750	550
Outer 2	15.12(81)	985(35)	920	>800
Inner 2	14.4(4)	1016(20)	1020	>800
Outer 3	15.12(57)	984(25)	800	550–600
Inner 3	15.0(5)	989(25)	740	550–600
Outer 4	17.6(8)	877(35)	740	500–550
Inner 4	20(3)	773(167)	700	500–550
Outer 5	16.5(7)	925(30)	750	550
Inner 5	20(3)	773(130)	700	550

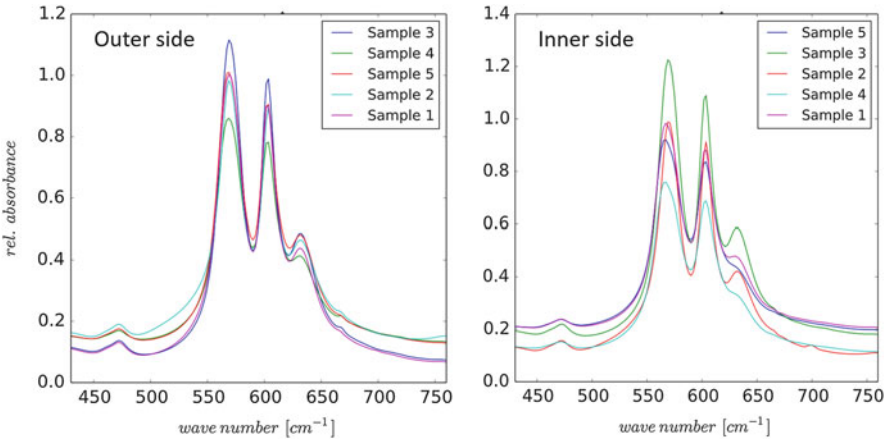

Fig. 16 FTIR spectra of archaeological cremated skull from the Urnfield Culture site of Zuchering (1300–800 BC) covering the phosphate ν_4 bending modes and the OH^- libration mode near 633 cm^{-1}

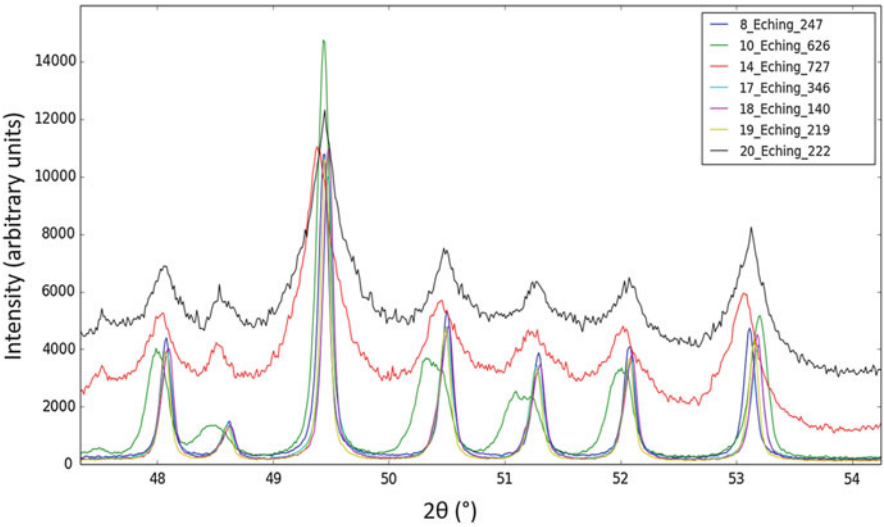

Fig. 17 XRD patterns of the cremated archaeological samples of the Urnfield Culture Eching locality. Cu-Kα_1 radiation. The group 1 samples 14_Eching and 20_Eching show broad peaks, indicating smaller crystallize sizes and thus lower cremation temperatures than the other samples (group 2). The diffractogram of the 10_Eching sample indicates a completely different material state than the other group 2 samples

based on the colour of the sample (Wahl 1981) gives much lower temperatures. The estimate of the cremation temperature based on the FWHM of the ~603 cm^{-1} band may give slightly overestimated values as the correlation in Fig. 14 may not really be linear and flatten off at temperatures >700 °C. However, even a simple interpolation between the data points in Fig. 14 with the FWHM values of the cremated samples indicates temperatures in excess of those based on the method of (Wahl 1981).

The X-ray diffractograms of the Eching samples are compiled in Fig. 17. Here three groups can be distinguished. Like in the FTIR data above, the samples 14_Eching and 20_Eching experienced lower cremation temperatures as their XRD peaks are broad. Rietveld refinement (Fig. 18) puts their crystallite sizes to 22 nm (Table 1), which corresponds to 700 °C cremation temperature, within limits of error well corresponding to the estimate derived from FTIR above. The group 2 samples have sharper lines with the exception of 10_Eching. The latter forms a very particular case which cannot be treated with our temperature calibration for XRD (see below). The group 2 samples excluding 10_Eching show crystallite sizes in the order of 100–190 nm which puts them into the 800–1000 °C range, again corresponding to the FTIR within bounds of error. A representative Rietveld analysis is shown in Fig. 19. The apatite in the 10_Eching sample appears to have an entirely different structure from what has been encountered so far in fresh, uncremated archeologic and experimentally cremated bone samples. The observed diffraction trace can be fitted with a monoclinic apatite structure (Ikoma et al. 1999), which is able to produce the flat-topped XRD peaks encountered here

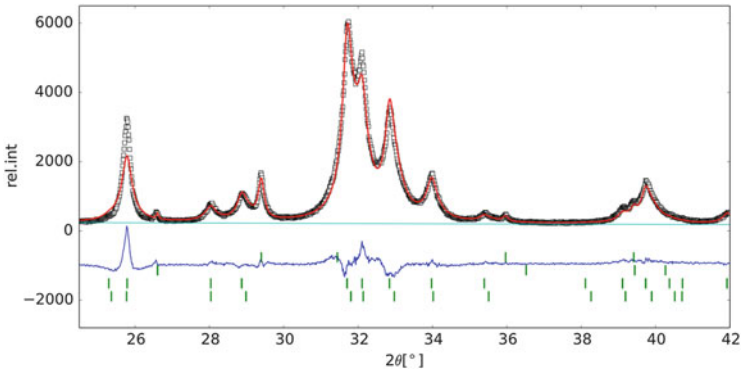

Fig. 18 Section of the X-ray diffractogram of the 14_Eching sample. *Red*: observed profile. Cu-Kα_1 radiation. *Black*: calculated profile. *Blue*: difference curve. *Green*: markers for reflection positions. *From top to bottom*: calcite, quartz, apatite-I and apatite-II. To fit the observed profile with reasonable quality, two apatite phases with slightly different lattice parameters and different microstructural characteristics had to be used

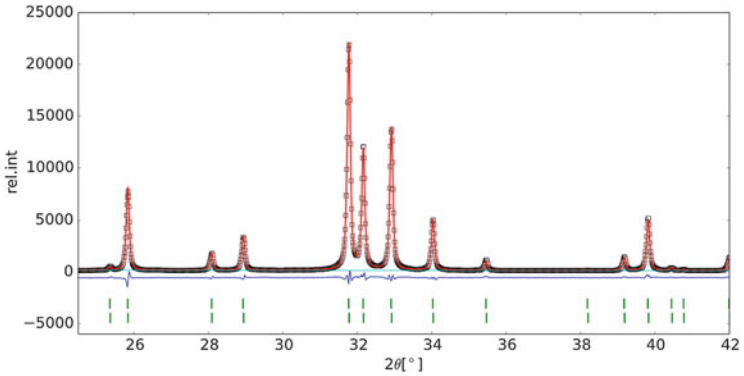

Fig. 19 Section of the X-ray diffractogram of the 8_Eching sample. *Red*: observed profile. Cu-Kα_1 radiation. *Black*: calculated profile. *Blue*: difference curve. *Green*: markers for reflection positions. To fit the observed profile with reasonable quality, two apatite phases with slightly different lattice parameters and different microstructural characteristics had to be used

(Fig. 20). Quartz and calcite impurities from the sediment are also present, which were included in the fit. A possibility to explain the occurrence of the monoclinic symmetry of apatite may be a reaction with ashes or other materials at high temperature in the burning funeral pile. What is clear from the Rietveld refinements of the archaeological sample is that we get pathologic XRD profiles which are not as clearly interpretable as the profiles from fresh or experimentally annealed bone materials. The diffractograms clearly indicate an inhomogeneity in the sample in the sense that apatites with different lattice parameters, different crystallite sizes,

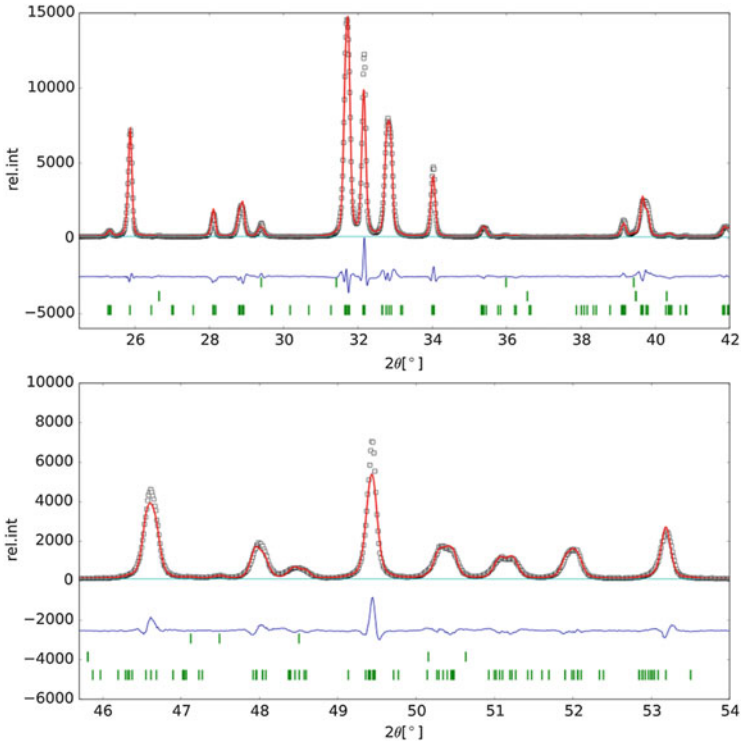

Fig. 20 Section of the X-ray diffractogram of the 10_Eching sample. *Red*: observed profile. Cu-Kα_1 radiation. *Black*: calculated profile. *Blue*: difference curve. *Green*: markers for reflection positions. *From top to bottom*: calcite, quartz, monoclinic apatite. To fit the observed profile with reasonable quality, monoclinic symmetry for apatite had to be used

and microstrain values are needed to model the diffractograms. The origin of inhomogeneity can be attributed to different degrees of cremation intensity. These can result from inhomogeneous temperatures produced by the burning wood logs and tissues, and also from differing lengths of time to which certain bone segments were exposed to the highest cremation temperatures. A similar observation has been made by Stiner et al. (1995) on paleolithic bone material.

Finally, we turn to the XRD results on the Zuchering skull samples. Diffractograms are shown in Fig. 21. The inner parts of samples 4 and 5 have the broadest lines corresponding to the lowest treatment temperatures. From the corresponding crystallite size of 22–23 nm obtained from Rietveld refinement (Table 1), we estimate the cremation temperatures as 700° or slightly above, which is quite consistent with the IR data discussed above. Sample 2 has certainly experienced the highest cremation temperatures, and here we also have fair agreement between FTIR and XRD results. On the whole, we see that the IR calibration overestimates the cremation temperature compared to XRD; for the skull sample 3, we have the greatest discrepancies. There are several potential origins of

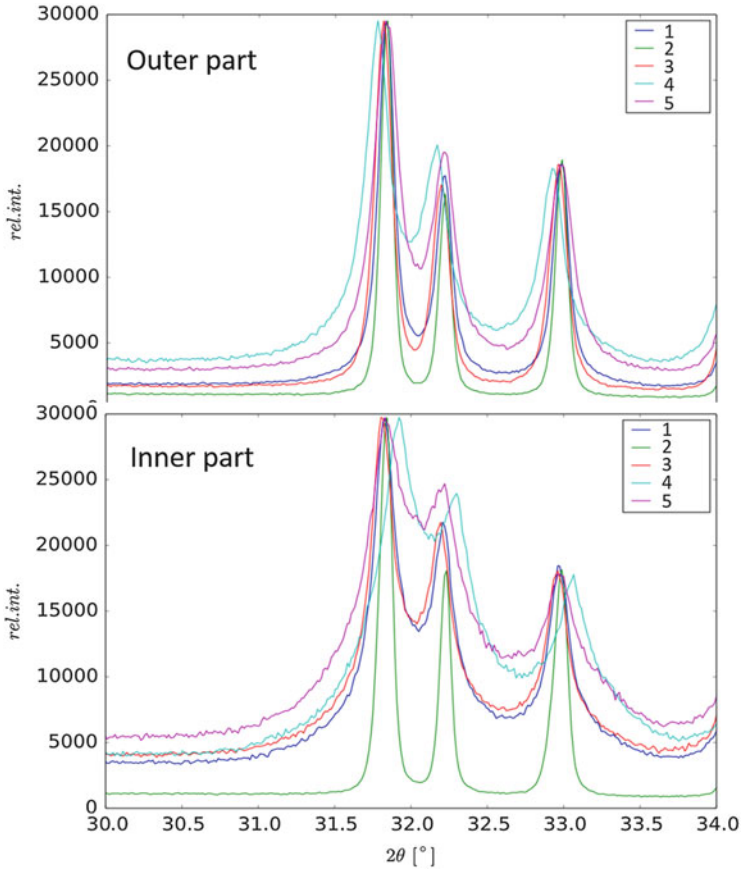

Fig. 21 Section of the X-ray diffractograms of the Zuchering skull sample comparing outer and inner compact bone layers of the cranium. Cu-Kα_1 radiation

difference obtained in cremation temperature when applied to archaeological cremated samples. First, our IR calibration is based on the assumption of a linear relationship between the FWHM of the ~603 cm^{-1} phosphate vibration (Fig. 14) and the annealing temperature. From the XRD evaluation of the experimentally annealed samples, we clearly see that the microstructural change in the material is strongly nonlinear in temperature, with a drastic change between the regimes below and above 600–700 °C (Fig. 10). Second, the archaeological cremated bones are clearly inhomogeneous, and the calibration so far assumes a well-defined average state. However, both the IR and the XRD data are at odds with the cremation temperatures estimated from the colour of the specimens after Wahl (1981).

Concluding Discussion

Our study of uncremated mammal bone samples from the alpine region covers ages from 7600 to 550 years before present. Only those samples which were of the best quality selected for the isotope studies within FOR1670 were analysed. Visually decomposed bones were avoided completely, and also the surfaces of the bones were mechanically cleaned by grinding away soil and/or decomposed material. The mineralogic state of the thus prepared samples showed only minor signs of diagenetic alteration, and beside bone apatite, the only secondary phase was calcite. The most pronounced change with archeologic age resides in the lattice parameter and in the crystalline domain size in the short dimension of the original bone-apatite platelets; the long direction corresponding to the crystallographic c-axis of the apatite appears almost unaffected. From the data, it is clear that other factors such as anatomic variation of the original materials and conditions in the soil play a major role in the diagenetic change of the bone material, masking the changes with burial time. As judged from the lattice parameters, the diagenetic alteration of the original bone mineral, apart from the sight increase in crystallite size, is possibly related to exchange of carbonate by hydroxyl and fluorine.

We established calibration curves from annealing experiments with bovine femur bone material at different temperatures for 1 h annealing time, which were subsequently used to estimate cremation temperatures of archaeological bones based on FTIR spectra and X-ray diffractograms. The experiments indicate that the original bone apatite contains little–if any–OH^- while carbonate and H_2O are present. Thus, the bone mineral is a carbonate-hydro-apatite rather than hydroxy-apatite. With increasing annealing temperature, water and carbonate leave the material, and from 600 °C, the bone mineral progressively reacts to form hydroxy-apatite with increasing purity and crystallite size with increasing temperature. We analysed some cremated bones from the Urnfield Culture sites of Eching and Zuchering, southern Bavaria. The analyses clearly indicate that the archaeological cremated bones are inhomogeneous materials, where within fractions of centimetres, the different parts of the samples experienced different cremation temperatures and/or times at temperature. Thus, compared to annealing experiments in furnaces, the conditions within the pile of burning logs and burning tissue are strongly variable locally, in particular towards the outside of the pyre. As the urns typically contain only a small fraction of the skeleton, the selection of bone fragments for burial in the urn might preferentially pick such items which experienced inhomogeneous conditions. The estimated cremation temperatures based on the FTIR and XRD analytical approaches tentatively agree but are still not fully mutually consistent. The IR and XRD data are consistently at odds with the cremation temperatures estimated from the colour of the specimens after Wahl (1981). To discuss the discrepancies between the FTIR and the XRD approaches, we first need to consider that the archaeological cremated bones are clearly inhomogeneous and the calibration so far assumes that a well-defined average state exists. Secondly, our IR calibration so far assumes a linear model relation (Eq. 1) between the FWHM of the ~603 cm^{-1} phosphate vibration (Fig. 14) and the

cremation temperature. From the XRD evaluation of the experimentally annealed samples, however, we clearly see that the microstructural change in the material is not simply proportional to temperature: there is a drastic change between the regimes below and above 600–700 °C (Fig. 10). Below this temperature, the IR signal is more sensitive to the change in material state, while in the temperature range above 600 °C, it is the XRD signal which is more sensitive. In the future, more refined models can be produced on the basis of more annealing experiments made to obtain better statistics. Further, cremation experiments must be done in the conditions that exist in a funeral pyre to gain experience on temperature and burning time inhomogeneity. While the evaluation of the diffractograms today is rigorously based on a physical model, the evaluation of spectral components in FTIR spectra is still empirical, and results depend very much on empirical assumptions made on the spectral shape of any single band and the number of bands contributing to the spectral range of overlapping peaks. Future work also definitely needs to address the chemistry and anatomical variability of original bone material within and between species in much more detail than is known at present.

Acknowledgement We thank the Deutsche Forschungsgemeinschaft, DFG, for financial support in Forschergruppe FOR1670, projects SCHM930/12-1 and GR959/21-1 and 20-1.

References

Alexander B, Daulton TL, Genin GM, Lipner J, Pasteris JD, Wopenka B, Thomopoulos S (2012) The nanometre-scale physiology of bone: steric modelling and scanning transmission electron microscopy of collagen–mineral structure. J Royal Soc Interface 9:1774–1786

Balan E, Delattre S, Roche D, Segalen L, Morin G, Guillaumet M, Blanchard M, Lazzeri M, Brouder C, Salje EKH (2011) Line-broadening effects in the powder infrared spectrum of apatite. Phys Chem Miner 38:111–122

Berna F, Matthews A, Weiner S (2004) Solubilities of bone mineral from archaeological sites: the recrystallization window. J Archaeol Sci 31:867–882

Cuisinier F, Bres EF, Hemmerle J, Voegel JC, Frank RM (1987) Transmission electron microscopy of lattice planes in human alveolar bone apatite crystals. Calcif Tissue Int 40:332–338

de Keijser TH, Langford JI, Mittemeijer EJ, Vogels ABP (1982) Use of the Voigt function in a single-line method for the analysis of X-ray diffraction line broadening. J Appl Crystallogr 15:308–314

de Leeuw NH (2010) Computer simulations of structures and properties of the biomaterial hydroxyapatite. J Mater Chem 20:5376–5389

Elliot JC (2002) Calcium phosphate biominerals. In: Kohn MJ, Rakovan J, Hughes JM (Hrsg) Phosphates: geochemical, geobiological and material importance. Reviews in mineralogy and geochemistry, vol 48. Mineralogical Society of America, Washington, DC, pp 631–672

Enzo S, Bazzoni M, Mazzarello V, Piga G, Bandiera P, Melis P (2007) A study by thermal treatment and X-ray powder diffraction on burnt fragmented bones from tombs II, IV and IX belonging to the hypogeic necropolis of “Sa Figu” near Ittiri, Sassari (Sardinia, Italy). J Archaeol Sci 34:1731–1737

Galeano S, García-Lorenzo ML (2014) Bone mineral change during experimental calcination: an X-ray diffraction study. J Forensic Sci 59:1602–1606

Gernaey AM, Waite ER, Collins MJ, Craig OE, Sokol RJ (2001) Survival and interpretation of archaeological proteins. In Brothwell DR, Pollard AM (Hrsg) Handbook of archaeological science. Wiley, Chichester: 323–329

Gonzalez-Diaz PF, Hidalgo A (1976) Infrared spectra of calcium apatites. Spectrochim Acta A Mol Spectrosc 32A:1119–1124

Gonzalez-Diaz PF, Santos M (1977) On the hydroxyl ions in apatites. J Solid State Chem 22:193–199

Grunenwald A, Keyser C, Sautereau AM, Crubézy E, Ludes B, Drouet C (2014) Novel contribution on the diagenetic physicochemical features of bone and teeth minerals, as substrates for ancient DNA typing. Anal Bioanal Chem 406:4691–4704

Grupe G, Harbeck M, McGlynn GC (2015) Prähistorische Anthropologie. Springer, Berlin

Harbeck M, Schleuder R, Schneider J, Wiechmann I, Schmahl WW, Grupe G (2011) Research potential and limitations of trace analyses of cremated remains. Forensic Sci Int 204:191–200

Hedges REM (2002) Bone diagenesis: an overview of precesses. Archaeometry 44:319–328

Ikoma T, Yamazaki A, Nakamura S, Akao M (1999) Preparation and structure refinement of monoclinic hydroxyapatite. J Solid State Chem 144:272–276

Jäger C, Welzel T, Meyer-Zaika W, Epple M (2006) A solid-state NMR investigation of the structure of nanocrystalline hydroxyapatite. Magn Reson Chem 44:573–580

Landis WJ, Jacquet R (2013) Association of calcium and phosphate ions with collagen in the mineralization of vertebrate tissues. Calcif Tissue Int 93:329–337

Lebon M, Reiche I, Frohlich F, Bahain J, Falgueres C (2008) Characterization of archaeological burnt bones: contribution of a new analytical protocol based on derivative FTIR spectroscopy and curve fitting of the ν_1 and ν_3 PO_4. Anal Bioanal Chem 392:1479–1488

Lee-Thorp J, Sponheimer M (2003) Three case studies used to reassess the reliability of fossil bone and enamel isotope signals for paleodietary studies. J Anthropol Archaeol 23:208–216

LeGeros RZ, Trautz OR, Legeros JP, Klein E, Shirra WP (1967) Apatite crystallites: effects of carbonate on morphology. Science 155:1409–1411

LeGeros RZ, Trautz OR, Legeros JP, Klein E (1968) Carbonate substitution in the apatite structure. Bull Soc Chim Fr 4:1712–1718

Loong CK, Rey C, Kuhn LT, Combes C, Wu Y, Chen SH, Glimcher MJ (2000) Evidence of hydroxyl-ion deficiency in bone apatites: an inelastic neutron-scattering study. Bone 26:599–602

McKinley J (2016) Complexities of the ancient mortuary rite of cremation: an osteoarchaeological conundrum. In: Grupe G, McGlynn GC (eds) Isotopic landscapes in bioarchaeology. Springer, Berlin, pp. 17–41

Mittemeijer EJ, Welzel U (eds) (2012) Modern diffraction methods. Wiley-VCH, Weinheim, 528p

Munro LE, Longstaffe FJ, White CD (2008) Effects of heating on the carbon and oxygen-isotope compositions of structural carbonate in bioapatite from modern deer bone (Beyond documenting diagenesis: the fifth international bone diagenesis workshop). Palaeogeogr Palaeoclimatol Palaeoecol 266:142–150

Nielsen-Marsh CM, Hedges REM (2000) Patterns of diagenesis in bone I: the effects of site environments. J Archaeol Sci 27:1139–1150

Nielsen-Marsh CM, Gernaey A, Turner-Walker G, Hedges REM, Pike A, Collins MJ (2000) The chemical degradation of bone. In: Cox M, Mays S (eds) Human osteology in archaeology and forensic science. Greenwich Medical Media, London, pp. 439–454

Olsen J, Heinemeier J, Bennike P, Krause C, Hornstrup KM, Thrane H (2008) Characterisation and blind testing of radiocarbon dating of cremated bone. J Archaeol Sci 35:791–800

Pasteris JD, Wopenka B, Freeman JJ, Rogers K, Valsami-Jones E, van der Houwen AM, Silva MJ (2004) Lack of OH in nanocrystalline apatite as a function of degree of atomic order: implications for bone and biomaterials. Biomaterials 25:229–238

Pecharsky VK, Zavalij PY (2003) Fundamentals of powder diffraction and structural characterization of materials. Springer, New York, 741p

Pedone A, Corno M, Civalleri B, Malavasi G, Menziani C, Segrea U, Ugliengo P (2007) An ab initio parameterized interatomic force field for hydroxyapatite. J Mater Chem 17:2061–2068

Person A, Bocherens H, Saliege JF, Paris F, Zeitoun V, Gerard M (1995) Early diagenetic evolution of bone phosphate—an X-ray diffractometry analysis. J Archaeol Sci 22:211–221

Peters F, Schwarz K, Epple M (2000) The structure of bone studied with synchrotron X-ray diffraction, X-ray absorption spectroscopy and thermal analysis. Thermochim Acta 361:131–138

Piga G, Malgosa A, Thompson TJU, Enzo S (2008) A new calibration of the XRD technique for the study of archaeological burned human remains. J Archaeol Sci 35:2171–2178
Piga G, Thompson TJU, Malgosa A, Enzo S (2009a) The potential of X-Ray diffraction in the analysis of burned remains from forensic contexts. J Forensic Sci 54:3534–3539
Piga G, Santos-Cubedo A, Moya Sola S, Brunetti A, Malgosa A, Enzo S (2009b) An X-ray diffraction (XRD) and X-ray fluorescence (XRF) investigation in human and animal fossil bones from Holocene to Middle Triassic. J Arch Sci 36:857–1868
Piga G, Solinas G, Thompson TJU, Brunetti A, Malgosa A, Enzo S (2013) Is X-ray diffraction able to distinguish between animal and human bones? J Archaeol Sci 40:778–785
Pucéat E, Reynard B, Lécuyer C (2004) Can crystallinity be used to determine the degree of chemical alteration of biogenic apatites? Chem Geol 205:83–97
Rey C, Collins B, Goehl T, Dickson IR, Glimcher MJ (1989) The carbonate environment in bone mineral: A resolution-enhanced fourier transform infrared spectroscopy study. Calcif Tissue Int 45:157–164
Rey C, Combes C, Drouet C, Glimcher MJ (2009) Bone mineral: update on chemical composition and structure. Osteoporos Int 20:1013–1021
Rey C, Combes C, Drouet C, Cazalbou S, Grossin D, Brouillet F, Sarda S (2014) Surface properties of biomimetic nanocrystalline apatites; applications in biomaterials. Prog Cryst Growth Charact Mater 60:63–73
Rey C, Miquel JL, Facchini L, Legrand AP, Glimcher MJ (1995) Hydroxyl groups in bone mineral. Bone 16:583–586
Rey C, Renugopalakrishnan V, Collins B, Glimcher MJ (1991) Fourier transform infrared spectroscopic study of carbonate ions in bone mineral during aging. Calcif Tissue Int 49:251–258
Rey C, Shimizu M, Collins B, Glimcher MJ (1990) Resolution-enhanced fourier transform infrared spectroscopy study of the environment of phosphate ions in the early deposits of a solid phase of calcium-phosphate in bone and enamel, and their evolution with age. I: Investigations in the v4PO4 domain. Calcif Tissue Int 46:384–394
Reznikov N, Shahar R, Weiner S (2014) Three-dimensional structure of human lamellar bone: the presence of two different materials and new insights into the hierarchical organization. Bone 59:93–104
Rho J-Y, Kuhn-Spearing L, Zioupos P (1998) Mechanical properties and the hierarchical structure of bone. Med Eng Phys 20:92–102
Rietveld H (1969) A profile refinement method for nuclear and magnetic structures. J Appl Crystallogr 2:65–71
Rodriguez-Carvajal J (1993) Recent advances in magnetic structure determination by neutron powder diffraction. Phys B Condens Matter 192:55–69
Rodriguez-Carvajal J, Roisnel T (2004) Line broadening analysis using FullProf: determination of microstructural properties. Mater Sci Forum 443:123–126
Rogers KD, Beckett S, Kuhn S, Chamberlain A, Clement J (2010) Contrasting the crystallinity indicators of heated and diagenetically altered bone mineral. Palaeogeogr Palaeoclimatol Palaeoecol 296:125–129
Rogers KD, Daniels P (2002) An X-ray diffraction study of the effects of heat treatment on bone mineral microstructure. Biomaterials 23:2577–2585
Schmahl WW, Kocis B, Toncala A, Grupe GJ (2016) Mineralogic characterisation of archaeologic bone. In: Grupe G, McGlynn GC (eds) Isotopic landscapes in bioarchaeology. Springer, Berlin, pp. 17–41
Schurr MR, Hayes RG, Cook DC (2008) Thermally induced changes in the stable carbon and nitrogen isotope ratios of charred bones. In: Schmidt CW, Symes SA (eds) The analysis of burned human remains. Academic Press, London, pp 95–108
Schwarcz HP, McNally EA, Botton GA (2014) Dark-field transmission electron microscopy of cortical bone reveals details of extrafibrillar crystals. J Struct Biol 188:240–248
Shemesh A (1990) Crystallinity and diagenesis of sedimentary apatites. Geochim Cosmochim Acta 54:2433–2438
Shinomiya T, Shinomiya K, Orimoto C, Minami T, Tohno Y, Yamada MO (1998) In- and out-flows of elements in bones embedded in reference soils. Forensic Sci Int 98:109–118

Sillen A (1989) Diagenesis of the inorganic phase of cortical bone. In Price TD (Hrsg) The chemistry of prehistoric human bone. Cambridge University Press, New York, pp 211–229
Sponheimer M, de Ruiter D, Lee-Thorp J, Späth A (2005) Sr/Ca and early hominin diets revisited: new data from modern and fossil tooth enamel. J Hum Evol 48:147–156
Stathopoulou ET, Psycharis V, Chryssikos GD, Gionis V, Theodorou G (2008) Bone diagenesis: new data from infrered spectroscopy and X-ray diffraction. Palaeogeogr Palaeoclimatol Palaeoecol 266:168–174
Stiner MC, Kuhn SL, Weiner S, Bar-Yosef O (1995) Differential burning, recrystallization, and fragmentation of archaeological bone. J Archaeol Sci 22:223–237
Surovell TA, Stiner M (2001) Standardizing infra-red measures of bone mineral crystallinity: an experimental approach. J Archaeol Sci 28:633–642
Thompson P, Cox DE, Hastings JB (1987) Rietveld refinement of Debye-Scherrer synchrotron X-ray data from Al_20_3. J Appl Crystallogr 20:79–83
Tonegawa T, Ikoma T, Yoshioka T, Hanagata N, Tanaka J (2010) Crystal structure refinement of A-type carbonate apatite by X-ray powder diffraction. J Mater Sci 45:2419–2426
Trueman CN, Privat K, Field J (2008) Why do crystallinity values fail to predict the extent of diagenetic alteration of bone mineral? Palaeogeogr Palaeoclimatol Palaeoecol 266:160–167
Tütken T, Vennemann TW, Pfretzschner H-U (2008) Early diagenesis of bone and tooth apatite in fluvial and marine settings: constraints from combined oxygen isotope, nitrogen and REE analysis. Palaeogeogr Palaeoclimatol Palaeoecol 266:254–268
Turner-Walker G (2008) The chemical and microbial degradation of bones and teeth. In Pinhasi R, Mays S (Hrsg) Advances in human paleopathology. Wiley, Chichester, pp 3–29
Vandecandelaere N, Rey C, Drouet C (2012) Biomimetic apatite-based biomaterials: on the critical impact of synthesis and post-synthesis parameters. J Mater Sci Mater Med 23:2593–2606
Wahl J (1981) Beobachtungen zur Verbrennung menschlicher Leichname. Archäologisches Korrespondenzblatt 11:271–279
Wang Y, Von Euw S, Fernandes FM, Cassaignon S, Selmane M, Laurent G, Pehau-Arnaudet G, Coelho C, Bonhomme-Coury L, Giraud-Guille M-M, Babonneau F, Azaïs T, Nassif N (2013) Water-mediated structuring of bone apatite. Nat Mater 12:1144–1153
Wegst UGK, Bai H, Saiz E, Tomsia AP, Ritchie RO (2015) Bioinspired structural materials. Nat Mater 14:23–36
Weiner S, Bar-Yosef O (1990) State of preservation of bones from the prehistoric sites in the near East: a survey. J Archaeol Sci 17:187–196
Weiner S, Goldberg P, Bar-Yosef O (1993) Bone preservation in Kebara Cave, Israel using on-site Fourier-transform infrared spectroscopy. J Archaeol Sci 20:613–627
Weiner S, Traub W, Wagner HD (1999) Lamellar bone: structure-function relations. J Struct Biol 126:241–255
Wilson RM, Elliot JC, Dowker SEP (1999) Rietveld refinement of the crystallographic structure of human dental enamel apatites. Am Mineral 84:1406–1414
Wilson RM, Elliton JC, Dowker SEP, Rodriguez-Lorenzo LM (2005) Rietveld refinements and spectroscopic studies of the structure of Ca-deficient apatite. Biomaterials 26:1317–1327
Wopenka B, Pasteris JD (2005) A mineralogical perspective on the apatite in bone. Mater Sci Eng C 25:131–143
Wright LE, Schwarcz HP (1996) Infrared and isotopic evidence for diagenesis of bone apatite at Dos Pilas, Guatemala: palaeodietary implications. J Archaeol Sci 23:933–944
Yerramshetty JS, Akkus O (2008) The associations between mineral crystallinity and the mechanical properties of human cortical bone. Bone 42:476–482
Yi H, Balan E, Gervais C, Ségalen L, Blanchard M, Lazzeri M (2014) Theoretical study of the local charge compensation and spectroscopic properties of B-type carbonate defects in apatite. Phys Chem Miner 4:347–359
Yi H, Balan E, Gervais C, Segalen L, Fayon F, Roche D, Person A, Morin G, Guillaumet M, Blanchard M, Lazzeri M, Babonneau F (2013) A carbonate-fluoride defect model for carbonate-rich fluorapatite. Am Mineral 98:1066–1069

The Isotopic Fingerprint: New Methods of Data Mining and Similarity Search

Markus Mauder, Eirini Ntoutsi, Peer Kröger, and Hans-Peter Kriegel

Abstract

The generation of an isotopic map of the reference region featuring local stable isotopic fingerprints requires the application of data mining methods due to the heterogeneity and complexity of the generated data. In this chapter, we explore new techniques to process isotopic data with the ultimate goal of constructing a map of locally characteristic isotopic fingerprints that help predict the places of origin of particular findings and, thus, supports archaeologists in deriving and testing hypotheses. In particular, we propose a new method for feature selection and apply it to a sample dataset of animal bones from the reference region. This application confirms that a multivariate fingerprint is clearly superior over univariate analysis and that the impact of oxygen on the reliability of the fingerprints is not very prominent. These findings confirm that it is possible to explore cremated human material for provenance analysis. Based on these results, we also propose a new spatial clustering method for detecting spatially consistent areas of homogeneous isotopic fingerprints resulting in an isotopic map of the reference region.

Mrs. Ntoutsi was with Ludwig-Maximilians-Universität when the presented work was done.

M. Mauder (✉) • P. Kröger • H.-P. Kriegel
Institute for Informatics, Ludwig-Maximilians-Universität München, Munich, Germany
e-mail: mauder@dbs.ifi.lmu.de; kroeger@dbs.ifi.lmu.de; kriegel@dbs.ifi.lmu.de

E. Ntoutsi
Faculty of Electrical Engineering and Computer Science, Leibniz Universität Hannover, Hannover, Germany
e-mail: ntoutsi@kbs.uni-hannover.de

G. Grupe et al. (eds.), *Across the Alps in Prehistory*,
DOI 10.1007/978-3-319-41550-5_5

Introduction

The term *isotopic landscape* or *isoscape* emerged around the turn of the millennium and describes *maps of isotopic variation produced by iteratively applying (predictive) models across regions of space using gridded environmental datasets*, whereby one *common use of isoscapes is as a source of estimated isotopic values at unmonitored sites, which can be an important implementation for both local- and global-scale studies if the isoscape is based on a robust and well-studied model* (Bowen 2010). In bioarchaeology, the variation of isotopes is used to predict patterns that can be utilized to "fingerprint" the origin of geological and biological materials at a small spatial scale. Such isotopic maps are empirically generated by sampling the relevant environmental components and measuring their isotopic signatures. The samples typically come from human and animal remains found at designated spatial locations, i.e., archaeological sites. Early studies concerned the reconstruction of paleodiet and ancient food webs by stable carbon and nitrogen isotopes in bone collagen (e.g., Vogel and van der Merwe 1977; Bumsted 1981; Schoeninger et al. 1983; Norr 1984; Schwarz et al. 1985; DeNiro 1985) and provenance analysis by stable strontium and lead isotopic ratios in bone mineral (Ericson 1985; Molleson et al. 1986). However, the vast majority of stable isotope studies in this field are small-scale projects that lack the fundamental capabilities of prediction and modeling.

This study rather aims at the construction of a large-scale isotopic map of the reference region, the Inn-Eisack-Adige transect via the Brenner pass in the European Alps. This area covers a long distance from northern Italy (around Bolzano) to southern Germany (around Munich) and, thus, requires a large collection of data from approximately 30 sites along that route. A geographic map of the reference region including the sample sites is visualized in Fig. 1. The envisioned isotopic map will represent the common, local isotopic signatures (or fingerprints) characteristic for a given spatial region, e.g., north/middle/south of the Alps. The application of this map will help to differentiate between local finds and nonlocal finds and for the definition of the place of origin of the latter in order to answer the aforementioned scientific questions regarding mobility, trade, as well as cultural transfer. The reason behind this application is that knowledge of the spatial distribution of stable isotopes in the environment allows identifying outliers that represent primarily nonlocal individuals and predict places of origin of samples.

Historically, stable isotopes in bioarchaeological finds were measured and simply compared to the known spatial distribution of the isotopic system under study such as $^{87}Sr/^{86}Sr$ in geological maps or the climate- and habitat-dependent distribution of C3- and C4-plants which is reflected in the ^{13}C-values of the consumers' tissues. Outliers, detectable by conservative statistics (e.g., Grupe et al. 1997), were readily interpreted as immigrant individuals. Very often, this was simply done by measuring one specific isotopic system, e.g., $\delta^{18}O$ from phosphate in bones and then manually determining local models and outliers in the univariate plots of the resulting values. However, growing insights into small-scale variabilities in isotopically characterized ecogeographical compartments gave

Fig. 1 The reference region: sampling sites across the transalpine Inn-Eisack-Adige passage

rise to more fruitful discussions on mobility versus migration/trade in the past. Pretty soon it became obvious that measurement of stable isotopes for the reconstruction of migration and trade in bioarchaeology cannot be looked at in isolation but rather necessitates collecting a lot of accompanying data (e.g., analysis of not only human but also animal bones or soil sampled from the same site) for the assessment of ecogeographical baseline values to account for the small-scale variability in time and space.

A common approach of analyzing isotopic data for these purposes used by domain experts is visual inspection of 1D/2D scattered plots. These approaches

are obviously limited to univariate and bivariate analyses only. This makes the standard visual analysis approaches not applicable anymore. Instead, multivariate analysis using data mining algorithms is required to define small-scale spatial regions with their respective characteristic isotopic fingerprints.

From the very beginning of this study, the intention was to derive an isotopic map not only based on animal bones but also based on human remains. However, human remains of the relevant time periods in this area are typically cremated. Cremated material, however, does not allow the measurement of certain isotopic systems such as oxygen, which has recently been very popular in deriving isotopic fingerprints (see above).

As a consequence, one first application for data mining to the problem of isoscaping in the reference region is to carefully analyze isotopic features and their impact on the construction of a reliable map of isotopic fingerprints. This will not only support choosing the best features for isoscaping but will in turn also help in deciding whether or not a certain isotopic feature (such as oxygen) is needed. In the end, these results will leverage the decision if certain available materials can be utilized or not, e.g., if cremated material that lacks oxygen values is eligible for fingerprinting.

Here, we address this problem in a generalized way: we focus on the question which isotopic systems should be measured in order to generate a reliable data source for map construction. We describe a framework that was developed to solve this problem in general and, thus, supports any domain experts in making decisions before or during data generation. As mentioned above, we are particularly interested in the impact of oxygen when generating local fingerprints. For that purpose, we used a preliminary sample dataset consisting of non-cremated bones. Based on the experience of the domain experts, seven isotopic systems from three elements (oxygen, strontium, and lead) were identified as being potentially relevant for the differentiation between local and nonlocal finds and the definition of the place of origin of the latter, i.e., the construction of the envisioned map. From the sites displayed in Fig. 1, sample findings were picked, and for each of these bones, seven isotopic values were derived. The data mining task was to discover which of the isotopic systems (oxygen, strontium, lead) was the most relevant or the most redundant and therefore irrelevant isotopic ratio for provenance analysis in this reference region. The results reveal the impact of single features, in particular oxygen, and supports the claim stated above that a multivariate approach clearly outperforms a univariate approach in terms of reliability of the resulting map.

With the design of a suitable data source for map construction, the derivation of the isotopic map is also challenging. Multivariate data can no longer be analyzed manually, but local isotopic fingerprints need to be identified by means of clustering algorithms that can identify groups of findings having similar isotopic values. However, even though clustering is a very well-studied problem in the data mining community, the particular task of isotopic fingerprinting is still far from trivial.

A cluster in the sense employed here is a set of samples, which when grouped maximize the samples' similarity in isotope space, while minimizing the similarity between clusters. As an "unsupervised" task, clustering will produce a model for the presented data regardless of the underlying real-world implications. This has

several drawbacks: First, the resulting clustering does not account for spatial coherence, i.e., clusters might be spread all over the reference region with heavily overlapping covering area. Second, we have to expect that not all findings within a small area are indeed originating from this location. On the one hand, these nonlocal samples will disrupt the local models. On the other hand, since we do not exactly know the ground truth, i.e., which sample is nonlocal and which sample is local, all we can do is treat all samples as equally important.

In this chapter, we present a variation of a classical probabilistic clustering algorithm (Gaussian Mixture Models with expectation maximization) that takes spatial information of samples into account. This approach not only solves the first of the abovementioned problems but also eases out the negative impact of local outliers in the data. We apply this spatial clustering approach to the isotopic measures of the reference region in order to derive a reliable map of local isotopic fingerprints.

In summary, the contributions of this chapter are as follows:

- We present a new framework for feature selection that evaluates the impact of features on the identification of local fingerprints (cf. section "Feature Selection for Isotopic Mapping").
- We provide a preliminary case study that uses our new framework for feature selection with a set of non-cremated material from the reference region (cf. section "A Case Study on Feature Selection in the Reference Region").
- We detail the lessons learned from this case study in section "Lessons Learned from the First Case Study" including two important conclusions: First, oxygen can be omitted leveraging the use of cremated material. Second, the traditional univariate approach using one or two isotopic features only is not sufficient to derive a reliable isotopic map of the reference region.
- We present a novel spatial clustering solution for defining characteristic isotopic fingerprints at small spatial scale that supports the prediction of places of origin and, thus, leverages archaeological studies on mobility, cultural transfer, trade, etc. (cf. section "Spatial Clustering for Identifying Local Isotopic Fingerprints: Towards an Isotopic Map of the Reference Region").
- Based on this new spatial clustering algorithm, we present the first version of an isotopic map of the reference region (also cf. in section "Spatial Clustering for Identifying Local Isotopic Fingerprints: Towards an Isotopic Map of the Reference Region"). The map is based on six isotopic features from two isotopic systems (strontium and lead).

Feature Selection for Isotopic Mapping

Feature selection aims at identifying the most relevant features for a given data mining task. In the context of this study, we aim at identifying those isotopic ratios that are most relevant or most redundant and therefore most irrelevant for provenance analysis in this reference region.

We present a general framework based on a technique that explores the relevance and redundancy of individual variables to a clustering in comparison to a reference clustering. There is no obvious reference clustering, because no ground truth is known and none can be derived by domain experts. However, we can use domain-specific knowledge and assumptions to generate several *plausible* reference clusterings that are estimations of a ground truth. Thus, the general idea is to explore how the relevance and the redundancy of single features behave under different ground truth assumptions.

In our approach, the quality of a feature, or feature subset, is assessed based on its contribution to a reference data structure. In particular, we assess how stable (i.e., unchanged) the data structure is while applying feature space projections. Our assumption is that a highly relevant projection will result in a data structure that resembles the reference data structure. There are many approaches for supervised feature evaluation (Guyon and Elisseeff 2003), which however require class information, i.e., the data structure is inferred from the classes. Since we have no class labels, we rely on unsupervised learning to learn the data structure. That is, the data structure is actually the clusters extracted upon the data. To assess the effect of a projection on the data structure, we compare the projection-based partitioning to the reference data partitioning.

The proposed unsupervised feature evaluation framework consists of three steps:

1. The data structure extraction step
2. The data structure comparison step
3. The feature ranking step

Before explaining each of these steps, let us introduce some notation: Let D be a dataset described upon a feature space F. Let $F_0 \subset F$ be the feature set upon which a reference data structure, i.e., clustering, is extracted; we refer to Θ^{F_0} as the *reference clustering* and to F_0 as the *reference feature space*. Let $F_v \subset F$ be a set of features to investigate w.r.t. their quality for the reference data structure, Θ^{F_0}. Note that F_v and F_0 are treated as being independent from each other even though they need not to be disjunct.

To extract structure from the data, we use a clustering approach. Domain knowledge suggests continuous values for the measurements, which can be best modeled as a mixture model of continuous distributions, like a Gaussian Mixture Model. To extract a robust indication of the data's structure in an unsupervised way, we applied the expectation-maximization (EM) algorithm (Dempster et al. 1977). EM fits a number of multivariate normal distributions over the given dataset. The result is a soft clustering; in our dataset though, the assignment is typically fairly hard. A typical run over an isotope dataset results in a standard deviation of 0.115 for the maximum likelihood cluster labels. As an example, Fig. 2 depicts the membership and spatial structure of a sample clustering done on the set of 217 bones where only the seven isotopic features are used.

For easier handling, we convert the cluster probabilities to hard cluster assignment by their maximum likelihood. The result of the clustering is a set of partitions,

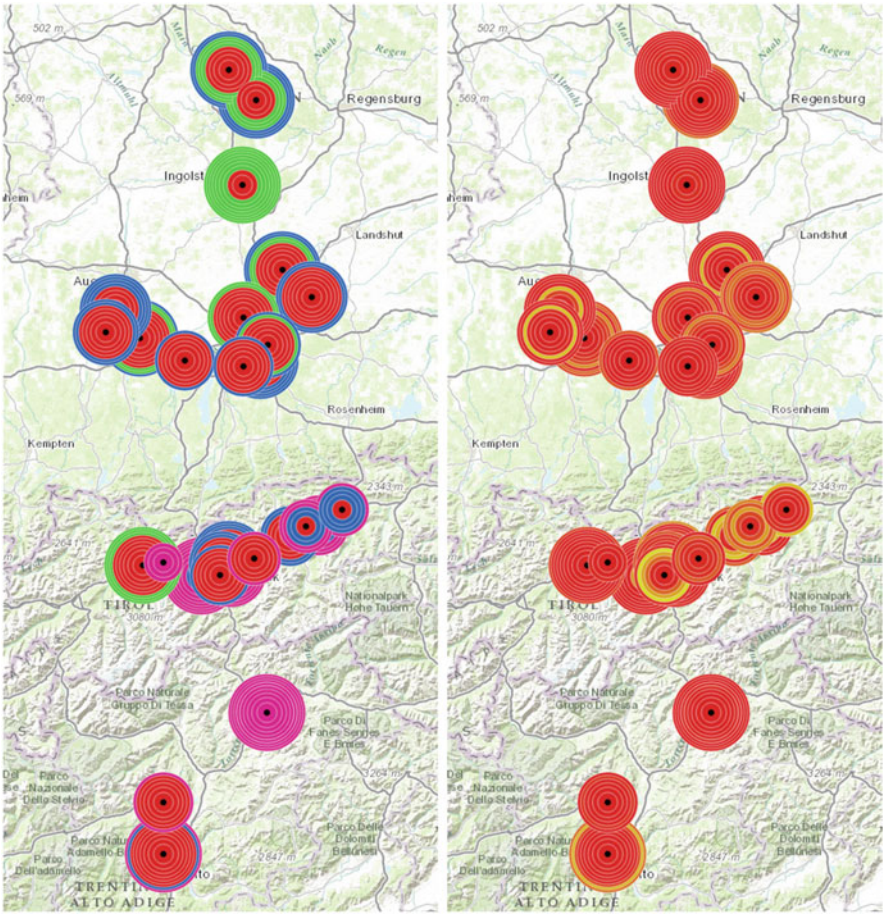

Fig. 2 Example of EM clustering on isotope data. Image best viewed in color. *Left*: spatial projection of maximum likelihood cluster. *Right*: membership likelihood (*red* is 100 %, *yellow* 50 %)

$\Theta^F = \{\theta_1, \theta_2, \ldots, \theta_k\}$, where k is the number of clusters (optimized by cross-validation, see below).

To compare how well a clustering Θ^{F_v} extracted upon an under-investigation feature projection F_v reflects the structure of a reference clustering Θ^{F_v}, we employ the *Adjusted Rand Index* (ARI) (Hubert and Arabie 1985) of the two clustering partitionings:

$$s(F_0, F_v) := \mathrm{ARI}\left(\Theta^{F_0}, \Theta^{F_v}\right)$$

ARI evaluates the agreement between two clusterings by counting pairs assigned to the same cluster under both clusterings and pairs assigned to different clusters

versus the total number of pairs in the dataset. ARI (Hubert and Arabie 1985) was proposed to reduce the influence of randomness on the traditional Rand Index (RI) (Rand 1971) and has been proven to perform better when the number of clusters in the two clusterings is not the same (Milligan and Cooper 1987; Vinh et al. 2010). ARI has a maximum value of 1 and takes the value 0 when the index equals its expected value. Negative values are also possible and indicate less than expected agreement between two clusterings.

Not all attributes are equally important for a given analysis task: a feature may be unnecessary to describe the result of a given analysis, or the data reflected in the feature may be noise or encompassed by other attributes. By selecting a suitable comparison feature space, we investigate the *structural relevance* of a feature (i.e., how well it captures the structure in isolation) for a clustering as well as its *structural redundancy* (i.e., if the clustering becomes unstable without this particular feature).

To generate these scores, we extract a single-feature $f \in F_v$. Let D_f be our original dataset projected onto dimension f, and let Θ^f be the clustering over $D_f : \Theta^f = \{\theta_1, \theta_2, \ldots, \theta_{k'}\}$, where k' is the number of clusters. We refer to Θ^f as the *univariate clustering*. Let $f_- = F_v \backslash f$ be the complementary feature space, that is, all dimensions in F_v except for the investigated feature f. Let D^{f_-} be the complementary dataset, i.e., the dataset projected onto the complementary feature space f_-. Applying EM on D^{f_-} generates a clustering $\Theta^{f_-} = \left\{\theta_1, \theta_2, \ldots, \theta_{k''}\right\}$ where k'' is the number of clusters. We refer to Θ^{f_-} as the *complementary clustering*.

To calculate the structural relevance of f, we compare the univariate clustering Θ^f derived from the specific feature f to the reference clustering Θ^{F_0}:

$$s_{\text{relevance}}(f, F_0) := \mathrm{ARI}\left(\Theta^f, \Theta^{F_0}\right)$$

To calculate the structural redundancy of f, we compare the complementary clustering Θ^{f_-} derived from the complementary feature space f_- to the reference clustering Θ^{F_0}:

$$s_{\text{redundancy}}(f, F_0) := \mathrm{ARI}\left(\Theta^{f_-}, \Theta^{F_0}\right)$$

The first comparison evaluates the structural relevance of f for Θ^{F_0}, whereas the second evaluates whether f's contribution can be reproduced by some other feature (s) in the feature space. In that sense, the first score derives the specific feature's structural relevance and the second score its structural redundancy due to the existence of other feature(s) in the feature space.

Combining structural relevance and structural redundancy scores in a single score is not straightforward, due to their complimentary semantics. We characterize each feature f in terms of both structural relevance and structural redundancy. To help a domain expert glance the effect a feature may have on their analysis, we combine the two scores in one plot where the x-axis reflects the structural relevance score and the y-axis the structural redundancy. In other words, the x-axis represents

the degree to which the reference clustering structure is evident in a single-dimension f, while the y-axis shows whether the reference clustering structure can be captured by the rest of the dimensions. We present such plots in the next section.

A Case Study on Feature Selection in the Reference Region

We apply our general framework for evaluating feature relevance and feature redundancy described above as a first step toward the establishment of the final map of the reference region. The goal of this case study is to decide which isotopic features should be considered for the construction of isotopic fingerprints. It should be stressed that the results presented in this section only hold for the specific reference region of the study, i.e., the Inn-Eisack-Adige passage. However, our framework is quite generic and is most likely applicable to other reference regions and/or other isotopic systems.

The case study was done with a small set of 217 non-cremated animal samples derived from 30 investigated sites. From each investigated specimen, seven isotopes were measured: ^{18}O, ^{86}Sr, ^{87}Sr, ^{204}Pb, ^{206}Pb, ^{207}Pb, and ^{208}Pb. Due to technical particularities of isotope measuring, the strontium (Sr) and lead (Pb) isotopes were measured and recorded as fractions of isotopes of the same element, yielding the fractions $^{87}Sr/^{86}Sr$, $^{208}Pb/^{204}Pb$, $^{207}Pb/^{204}Pb$, $^{206}Pb/^{204}Pb$, $^{208}Pb/^{207}Pb$, and $^{206}Pb/^{207}Pb$. The oxygen isotope was normalized against ocean water isotope levels and recorded as $\delta^{18}O$. This yields a seven-dimensional feature vector for each recovered sample. In addition to these isotope measurements, each sample was annotated with a spatial description (latitude, longitude, altitude) based on the discovery area. Also, each sample was recognized as one of the three animal species (pig, cattle, and red deer).

Due to the aforementioned reasons, we first focused on oxygen as a marker to distinguish between local and nonlocal finds. A preliminary manual analysis of the $\delta^{18}O$ of 118 of the 217 animal bone samples by a domain expert revealed a highly significant correlation ($r = -0.68$) between $\delta^{18}O$ and altitude, whereby the averaged $\delta^{18}O$ values plotted exactly on the regression between altitude and $\delta^{18}O$ in precipitation in the Alps as published by Kern et al. (2014). However, although the $\delta^{18}O$ values behaved as expected and, thus, are potentially suitable for provenance analysis as a single marker, in this study, it proved impossible to distinguish even rough spatial compartments (such as north, center, and south of the Alps). The same observation was made when considering species-specific fractionation factors. Interindividual variability remained high and did not permit for a firm assignment of individual animals to spatial regions. The histogram of $\delta^{18}O$ values shown in Fig. 3 illustrates this variability. The samples from the three very coarse compartments north, center, and south derived from a hypothesis of the domain experts are marked in different colors.

These results confirm that deeper insights in the reliability of oxygen and the other isotopic features are needed. Thus, we applied our framework for isotopic feature selection to the set of 217 non-cremated animal remains.

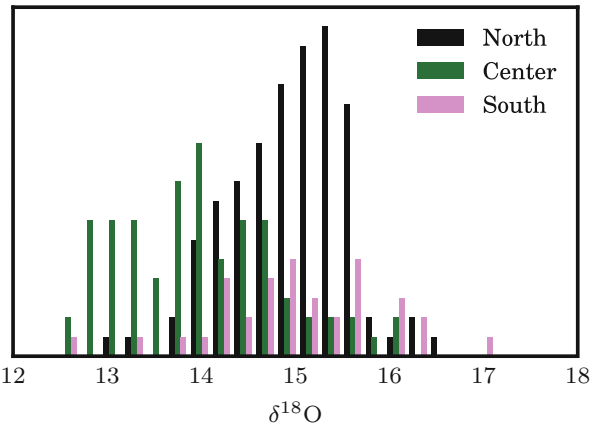

Fig. 3 Distribution of δ^{18}O by region. Although very large regions were picked, there is only a very weak correlation observable

The definition of the reference clustering is crucial for our ARI-based feature evaluation presented in the previous section. However, there is no ground truth reference clustering available for the region under inspection nor for the dataset at hand. A purely data-driven approach is also not possible since we cannot be sure about the originality of each finding, i.e., we do not know if a bone found at a specific site s in fact originates from s or is a nonlocal outlier. As a consequence, even if we explore local isotopic outliers within each site, we are not sure if the outliers are the nonlocal finds or the local ones. However, the domain experts have some assumptions and hypothesis available about possible spatial compartments that could be used to derive potentially plausible approximations of the ground truth. Thus, we follow a mixture between data-driven approaches enriched by domain expertise (Table 1).

Instead of using just one potential reference clustering, we investigated several possible definitions for the reference clustering based on the available features, in close collaboration with the domain experts. In other words, we generated reference clusterings in a data-driven way using clustering but rely on the domain experts for deciding on which feature space the clustering was done. In particular, we varied the feature space from containing all isotope and spatial features to containing only single-domain features, i.e., isotopes or spatial coordinates to generate a reference clustering. In the following, the set $I = \{^{87}Sr/^{86}Sr,\ ^{208}Pb/^{204}Pb,\ ^{207}Pb/^{204}Pb,\ ^{206}Pb/^{204}Pb,\ ^{208}Pb/^{207}Pb,\ ^{206}Pb/^{207}Pb,\ \delta^{18}O\}$ denotes all isotopic features, and $I^{-O} = \{^{87}Sr/^{86}Sr,\ ^{208}Pb/^{204}Pb,\ ^{207}Pb/^{204}Pb,\ ^{206}Pb/^{204}Pb,\ ^{208}Pb/^{207}Pb,\ ^{206}Pb/^{207}Pb\}$ denotes all isotopic features except oxygen. In addition, we use $S = \{altitude, latitude, longitude\}$ for all spatial attributes, and $S^{-lon} = \{\text{altitude, latitude}\}$ refers to the spatial attributes without longitude (see Table 1 for an overview). We list the different setups for the feature spaces that we used to generate the reference clusterings based on the input of the domain experts below. For this first set of experiments, the set of features under investigation is always the set of isotopic features, i.e., $F_v = I$.

Table 1 Notations for the different subsets of features used to derive reference clusterings

Notation	Description
I	All seven isotopic features
I^{-O}	All isotopic features except oxygen
S	All three spatial attributes
$S^{-\text{lon}}$	All spatial features except longitude

$F_0 = I \cup S$ **(Isotopes + Spatial)** The feature space consists of all available isotopic features and spatial features. This is the most information we have and, thus, serves as the starting point of the study.

$F_0 = I \cup S^{-\text{lon}}$ **(Isotopes + (latitude, altitude))** From the spatial attributes, only those that has been found to have an effect on the isotopes are retained, namely, altitude and latitude. Since the passage under inspection is mostly north/south, the domain experts expect that longitude does have only minor influence on the spatial compartments.

$F_0 = I$ **(Isotopes only)** The feature space consists only of the isotopic features. There is no spatial influence. Such a feature space is typically used for fingerprinting and predicting the origin of new samples (with unknown spatial coordinates).

In a second analogously conducted series of reference clusterings, oxygen was removed from the isotopic features at all since the domain experts wanted to test the hypothesis that oxygen is much less relevant in this reference region and for this sample selection as it seems to be in other existing provenance studies. Especially the sample selection using a mix of three different species may have a blurring impact on the δ^{18}O-values according to the domain experts. Analogously, the set of features under investigation is always the set of isotopic features without oxygen, i.e., $F_v = I^{-\text{O}}$. The resulting configurations are similar to the four alternatives listed above:

$F_0 = I^{-\text{O}}S$ **(Isotopes (except oxygen) + Spatial)** The feature space consists of all isotopes minus oxygen and all spatial features.

$F_0 = I^{-\text{O}}$ **(Isotopes only (except oxygen))** Only the isotope description, without the oxygen feature.

$F_0 = I^{-\text{O}} \cup S^{-\text{lon}}$ **(Isotopes (except oxygen) + (latitude + altitude))** Isotope description, without the oxygen feature and spatial coordinates except longitude.

A supplementary feature space to be used as a reference clustering is purely spatial:

$F_0 = S$ **(Spatial only)** The feature space consists only of spatial coordinates. Isotopic values do not play any role, and findings from spatially close sites are considered as being in the same cluster (compartment). This ground truth scenario must be complemented by a corresponding set of investigated features, i.e., $F_v = I$ and $F_v = I^{-\text{O}}$.

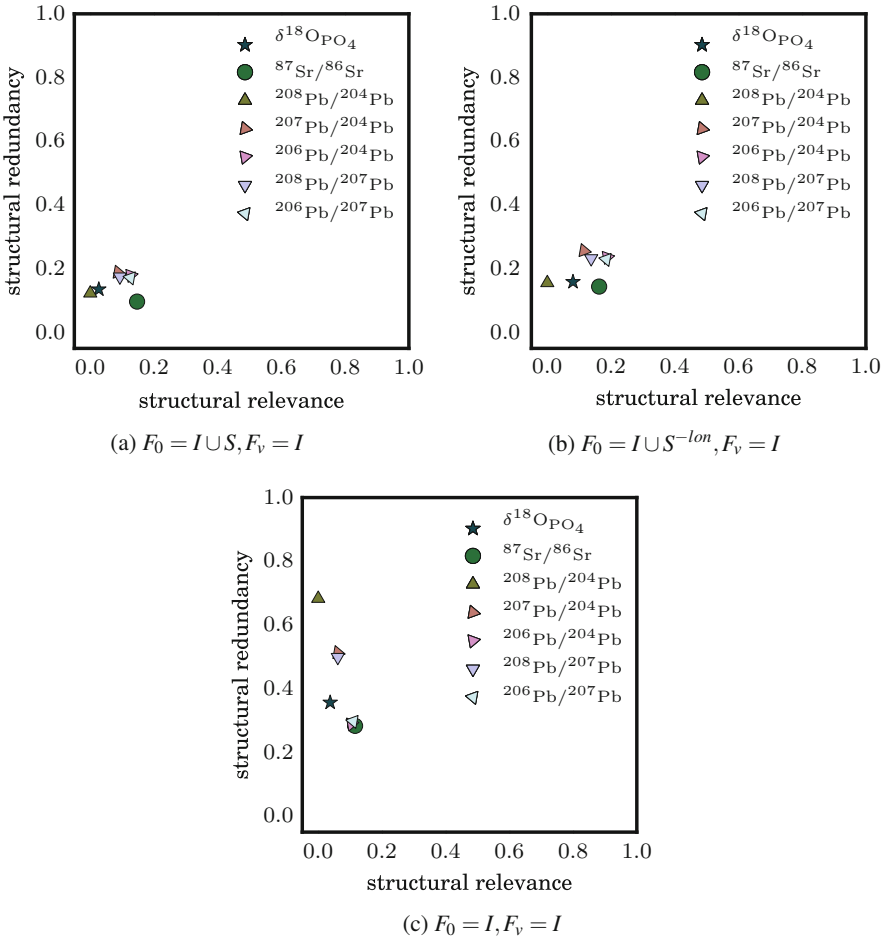

(a) $F_0 = I \cup S, F_v = I$

(b) $F_0 = I \cup S^{-lon}, F_v = I$

(c) $F_0 = I, F_v = I$

Fig. 4 Structural relevance-vs-structural redundancy plots using reference clusterings with all isotope features

For each of the feature spaces described above, we apply EM to derive the reference clustering, and we evaluate how each isotope attribute "contributes" to the corresponding reference clustering. We illustrate these results in the structural relevance-vs-structural redundancy plots presented in the previous section. For the EM, the number of clusters was selected by cross-validation as in the Weka data mining framework (Hall et al. 2015). When examining the presented reference attribute sets, we chose $F_v = I$ or $F_v = I^{-O}$ to reflect the isotopes in the reference attributes. That is, where F_0 contains I, F_v becomes I, where F_0 contains only I^{-O}, $F_v = I^{-O}$. A special case is $F_0 = S$, which does not contain any isotopes to compare with. In these scenarios, we investigated both $F_v = I$ and $F_v = I^{-O}$ for completeness.

The results of reference clusterings containing isotopes including oxygen are presented in Fig. 4, experiments with isotopes excluding oxygen are presented in

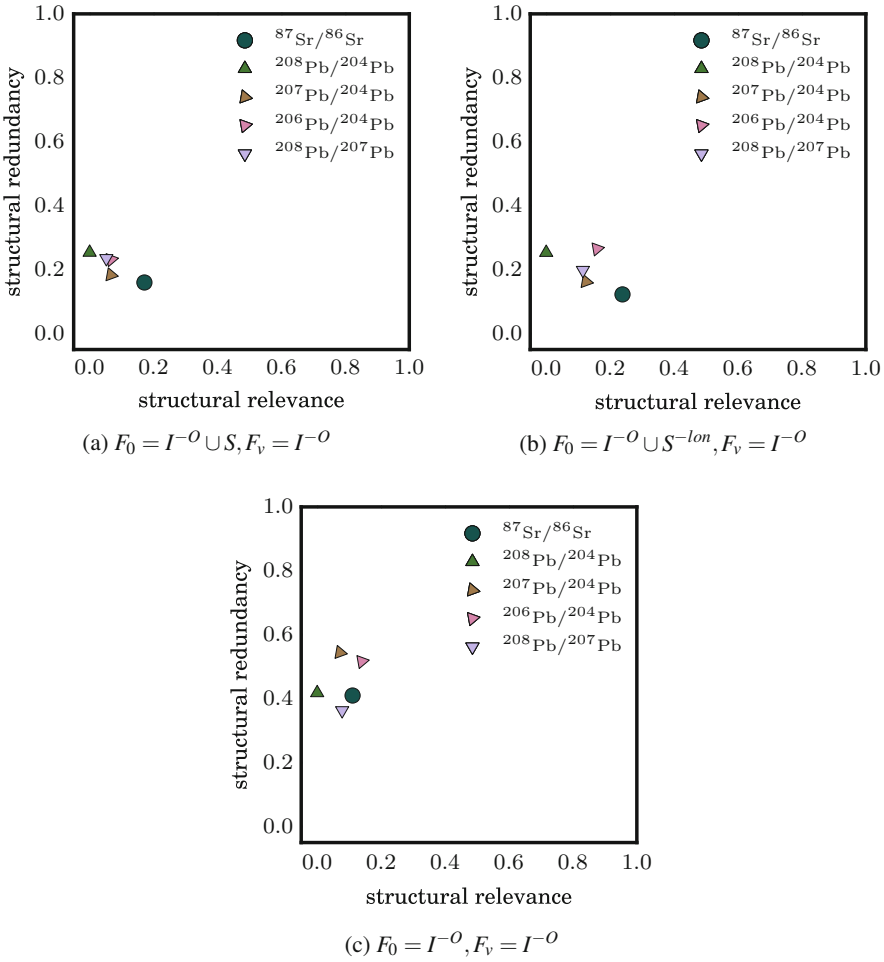

(a) $F_0 = I^{-O} \cup S, F_v = I^{-O}$

(b) $F_0 = I^{-O} \cup S^{-lon}, F_v = I^{-O}$

(c) $F_0 = I^{-O}, F_v = I^{-O}$

Fig. 5 Structural relevance-vs-structural redundancy plots using reference clusterings with all isotopes except oxygen

Fig. 5, and those with only spatial attributes are presented in Fig. 6. Regarding the ARI values, a score of zero indicates random behavior, while a score of one indicates identical clusterings.

In the following, we discuss the individual experiments showing structural redundancy and structural relevance for all described reference feature sets and discussing potential explanations for the observed values.

$F_0 = I \cup S$, $F_v = I$ (see Fig. 4a)

Strontium is the most prominent attribute as it has the highest structural relevance score and the lowest structural redundancy score. *Lead* isotopes depict a similar behavior, scoring average relevance and redundancy scores. An exception is ^{208}Pb/

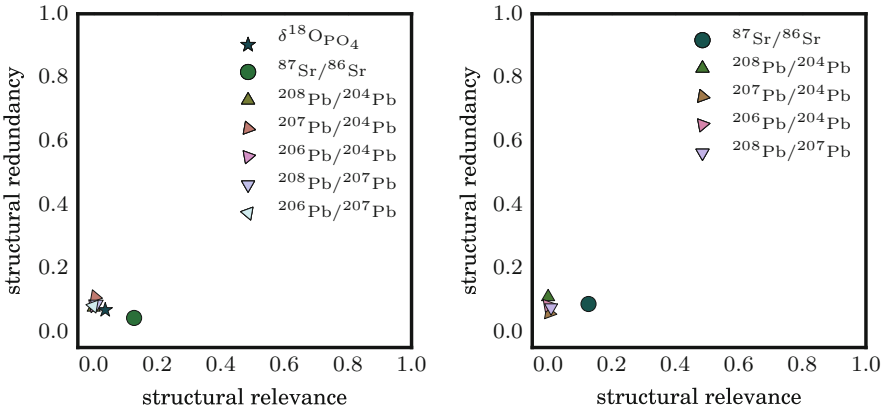

Fig. 6 Structural relevance-vs-structural redundancy plot: reference clustering upon S (**a**), So (**b**)

^{204}Pb, which has a very low relevance; a closer inspection of the results shows that a clustering based on ^{208}Pb/^{204}Pb only places all instances in the same cluster, i.e., the values in this feature follow one Gaussian distribution. *Oxygen* has also a very low relevance score.

***$F_0 = I \cup S^{-lon}$, $F_v = I$* (see Fig. 4b)**
F_0 now includes no longitude information. There is no much difference in the rankings comparing to the *IS* case, although the scores are higher. An interesting change is the repositioning of oxygen: its redundancy became lower and relevance became higher.

***$F_0 = I$, $F_v = I$* (see Fig. 4c)**
The removal of all spatial information from F_0 pits the isotopes against each other. This might be due to the better quality clusterings we obtain by also employing spatial information. Strontium is still the top relevant isotope; however, two lead isotopes score very close, namely, ^{206}Pb/^{207}Pb and ^{206}Pb/^{204}Pb. Both isotopes repositioned in the plot after the removal of the spatial information from the reference clustering. In particular, they became more relevant and less redundant. Also, the redundancy of oxygen increased.

***$F_0 = S$, $F_v = I$* (see Fig. 6a)**
This scenario tests how well the isotope's structure lines up with the spatial structure. We expect very little alignment as the spatial structure will be dominated by the density of sample sites, which the isotope values reflect indirectly at best. The lead isotopes have very low redundancy and relevance scores, indicating that they neither reflect the spatial structure nor does their complimentary feature space do so. Strontium seems to reflect all the structure: the sets of isotopes that contain

strontium achieve a median score of 0.08, and strontium by itself achieves a score of 0.13. All other isotopes have relevance scores around zero (oxygen scoring highest at 0.04).

$F_0 = I^{-O} \cup S$, $F_v = I^{-O}$ (see Fig. 5a)
Without oxygen, strontium is again the most prominent attribute, whereas the relevance of lead decreases.

$F_0 = I^{-O} \cup S^{-lon}$, $F_v = I^{-O}$ (see Fig. 5b)
Compared with the previous scenario containing the entire set of spatial attributes, strontium retains very similar scores, but some lead isotopes' relevance increases. This indicates a stronger role of those lead isotopes in the formation of the structure, possibly because longitude supports other structural elements that are now being expressed less strongly.

$F_0 = I^{-O}$, $F_v = I^{-O}$ (see Fig. 5c)
Removal of all spatial information (and oxygen) affects the ranking of strontium. Lead isotopes are now more relevant comparing to strontium, but still more redundant than strontium.

$F_0 = S$, $F_v = I^{-O}$ (see Fig. 6b)
If oxygen is omitted, the situation changes only marginally compared to the original setup with $F_v = I$. This indicates that oxygen had little influence on the structure of the isotope space, consistent with the analysis above.

Lessons Learned from the First Case Study

We already pointed out that each experiment refers to a specific reference clustering, and therefore it is not straightforward to compare scores based on different reference clusterings. However, we can draw some conclusions about the dataset from the interpretation of all experiments.

First of all, it is clear that the choice of the reference clustering influences the ranking of the different isotopes w.r.t. their structural relevance and structural redundancy to that reference clustering. There are however some "trends" which are repeated across the different configurations. In particular, there is a much better separation in the rankings when the spatial coordinates are considered, cf. Fig. 4a, b. A possible explanation is that the reference clustering is much more differentiated when considering the complete feature space of isotopes and spatial features. A similar observation holds when we remove oxygen from the feature space, cf. Fig. 5. The worst distinction is manifested when we consider all isotopes, including oxygen, cf. Fig. 4c.

Regarding the behavior of the different isotopes, *strontium* and *lead* are the top *structural relevant* isotopes, i.e., they display higher values in the structural relevance axis. This implies that in isolation, these isotopes manage to capture most of

the reference clustering structure. *Oxygen* depicts a low structure relevance score, meaning that oxygen alone is not a good indicator of the reference clustering.

With respect to *structural redundancy*, the lead isotopes display high redundancy as expected since we have five different lead isotopes in our dataset. Strontium has the lowest redundancy, implying that the information in strontium is not replicated by some other isotope or combination of isotopes in the dataset.

It is noteworthy that two of the lead isotopes, $^{206}Pb/^{207}Pb$ and $^{206}Pb/^{204}Pb$, behave similarly across all the different experiments. The domain experts have no direct explanation for this observation. However, the result inspired them to further investigate these isotopes' connection since this may be an indication that stable lead isotopes can be very promising for provenance studies.

Overall low relevance scores indicate that no isotope alone reflects the full structure of the data. This supports our hypothesis that univariate analysis is not powerful enough to draw meaningful conclusions.

The bad scores achieved by all isotopes against the reference clustering including only spatial coordinates illustrate that there is no trivial correspondence between the two domains, isotope and spatial. Domain knowledge suggests a connection, but it is not pronounced enough to be automatically reflected by the isotope feature set. Therefore, the combination of both domains to extract a spatially coherent isotope map is also not trivial and will require more complex models.

In summary, our study resulted in the two major insights that were previously uncertain and represented major added values for the domain experts.

Insight 1 A multivariate isotopic fingerprint is indeed needed instead of a univariate analysis relying on oxygen only.

Our analysis showed that despite its popularity, oxygen does not provide exceptional structure to the dataset (average structural relevance), nor are they unique in the role they play (no exceptionally low structural redundancy values). Thus, at least in this reference region, provenance studies based solely on oxygen is bound to fail. On the other hand, the implication from our results is that the envisioned isotopic map can benefit strongly from a multi-isotopic fingerprint that includes strontium and lead isotopes as well.

Insight 2 The omission of oxygen in the isotopic fingerprint does not considerably decrease the quality of the fingerprinting.

Oxygen did not show a particularly low redundancy. Where spatial information was included (IS, $IS^{-\mathrm{lon}}$), the redundancy was close to 70 % while it decreased to about 35 % in I. The latter scenario has less relevance for the fingerprinting of regions, because it omitted the spatial component. This indicates that the other isotopes can provide much the same information as oxygen, i.e., they can be substituted for oxygen where it is not available. Its low relevance score indicates that oxygen does not dominate the structure (i.e., other isotopes are needed). While the redundancy was not 100 %, it was definitely not outstanding and never the lowest value in the analysis.

The fact that oxygen seems not very relevant to provenance analysis in the reference region opens up the opportunity to use cremated material for isotopic mapping.

Spatial Clustering for Identifying Local Isotopic Fingerprints: Toward an Isotopic Map of the Reference Region

In this section, we present a new clustering algorithm for deriving an isotopic map addressing the following challenges: First, the dataset may contain nonlocal outliers which are hard to be identified as such. Second, the resulting clusters should be spatially coherent.

As before, we use a Gaussian Mixture Model as basic clustering model, i.e., a set of k Gaussian distributions are iteratively fit to the data. Gaussian models are powerful and versatile models that suit many kinds of scientific data. Their strength is in the ubiquitous natural distributions that can be modeled well using the simple Gaussian formulation. Efficient algorithms like expectation-maximization exist that allow building Gaussian (Mixture) Models quickly. Also, the resulting Gaussian distributions are well suited for predicting class memberships for new samples, i.e., using the maximum likelihood decision principle.

In a spatial domain, Gaussian Mixture Models have a shortcoming in that the best fit for a feature dataset must not necessarily align with a best spatial fit. This has a number of interesting consequences:

- Clustering using both the spatial and feature domains as equals may be dominated by one or the other, resulting in a suboptimal model.
- Clustering based on only one of the domains can result in a particularly bad model for the domain.

It is fairly simple to calculate the probability density for each point in the modeled domain and construct a new model by applying the normalized density onto measurements from the other domain. The result is a projection of the original model into another domain. If the first law of geography holds (and a "correct" model was built), there should be little discrepancy between the fit of the original model and the derived model. Given this case, a projection of the data will be concise and can be treated as equally "correct."

To be able to visualize a feature model in a spatial domain, we must generate a spatial projection of the model. Given the data upon which the feature model is based and associated spatial dimension, we can calculate the membership probability of each point and use this information combined with the spatial information to derive a corresponding model in the spatial domain. This model can then be used to determine the spatial extent of each model. In addition, the feature model can be used to determine colors that represent the feature domains. This color can be

applied to the spatial extent of each feature to visualize the semantical connection between the models and their influence on the spatial projection.

Given a feature model Σ, feature data f, and corresponding spatial coordinates s, we can determine a spatial model Σ_s. If $\Sigma = (\mu^{(k)}, \sigma^{(k)})$ is a Gaussian Mixture Model, the normalized probability density function p can be used to determine the probability of cluster membership for each cluster $c_{(k)}$. These probabilities can then be applied to s to determine the spatial projection of the model. This approach works for various different forms of Gaussian model, e.g., without a measure of variance, a variance vector, or a covariance matrix.

Given a suitable model for the data, the results must be presented in a way that allows domain experts to understand and interpret the results. Spatial projections lend themselves much better to visual presentation than feature models. In addition, the spatial distribution of a Gaussian model is necessary for some application domains like provenance analysis. Given a two-dimensional geo-projection of the spatial distribution, we require an intuitive representation of the (possibly multidimensional) underlying feature model. One remaining visual domain is color. The LUV color model is designed to preserve perceptual differences proportional to the Euclidean distance between the color vectors. Given its three-dimensional nature, we require a three-dimensional input. If the feature space is higher dimensional, its three strongest principal components are used. Normalization of the feature space yields a set of three-dimensional vectors that can be interpreted as LUV vectors as given below:

$$v = \frac{\mathrm{PCA}_3(x|d) - \min(\mathrm{PCA}_3(d|d))}{\max(\mathrm{PCA}_3(d|d)) - \min(\mathrm{PCA}_3(d|d))}$$
$$\mathrm{col} = \mathrm{RGB}_{\mathrm{LUV}}(v_0 \cdot 100, v_1 \cdot 200 - 100, v_2 \cdot 200 - 100)$$

where d is the training data, $\mathrm{PCA}_3(x|\,d)$ transforms x according to d's three principal components, and $\mathrm{RGB}_{\mathrm{LUV}}$ is a function that transforms LUV colorspace to RGB. The scaling of the values of v is chosen to approximate the LUV color space's limits, but due to LUV's design being modeled after human perception, it is possible for this formula to yield invalid (but approximately correct) RGB values. This problem can be addressed by normalizing the resulting values to valid RGB feature ranges in a final step. This weakens the perceptual distance between the points but is limited to the small range that was not expressible as LUV values.

Given the presented color model, it becomes possible to express the expected feature values in the region of interest. The Gaussian Mixture Model over the feature space allows predicting the value generated by the mixture of the feature means. This allows assigning any given point an appropriate feature value and corresponding color.

We used the described spatial EM clustering algorithm in combination with the proposed coloring schema and applied it to the isotopic data of the reference region derived from the project partners. The dataset contains six isotopic features from two isotopic systems (strontium and lead) omitting oxygen including human and animal remains.

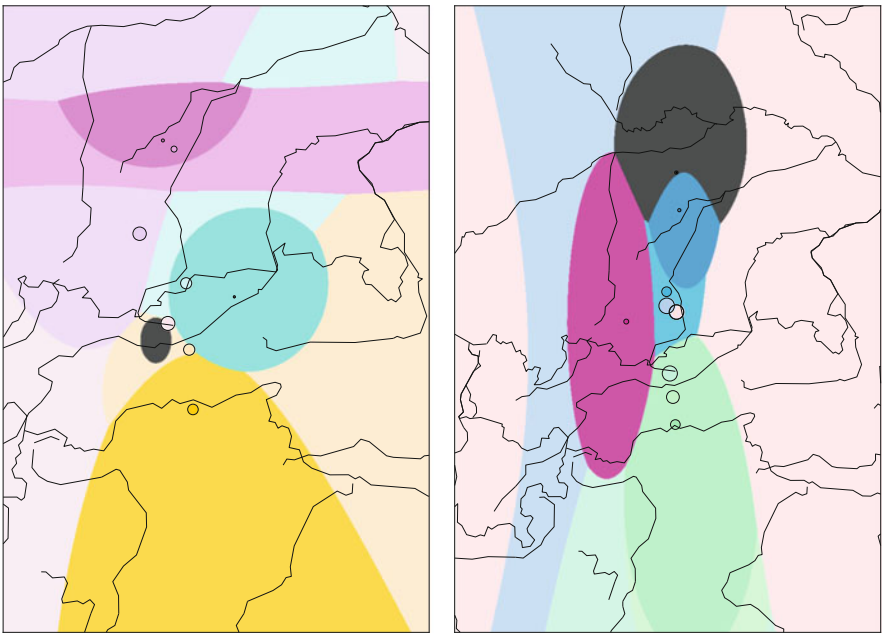

(a) Humans (b) Animals

Fig. 7 Map of isotopic fingerprints for the reference region using animal data and human data

Figure 7 (best seen in color) displays the resulting map both for using only the animal data and using only the human data. Both maps have a clear tendency: while the fingerprints in the south (northern Italy around Bolzano) and the north (Munich stone plain) of the Alps are similarly stable, the isotopic values measured for the inner alpine area (basically the Inn valley) are very heterogeneous and are hard to group into small-scale characteristic fingerprints.

Conclusions

In this section, we presented two novel data mining methods that may contribute to the generation of isotopic maps in general and are particularly used to derive a map of isotopic fingerprints for the reference region of this study, the Inn-Eisack-Adige transect in the European Alps.

The first method deals with feature selection and can be used to evaluate the impact of isotopic features on provenance analysis in a reference region. It can support domain experts to decide about the necessity of single features for their particular study. We applied this method to a preliminary dataset of animal remains and could derive important insights that were used later on for the construction of the final map: First, the results confirm that a multivariate approach using more than

only one or two isotopic features is much more stable and will most likely produce a more reliable map. Second, the popularity of oxygen as a marker could not be supported. Rather, oxygen seems to be rather redundant for provenance analysis in the reference region. This also confirms that cremated material can be used for map isotopic fingerprinting which leverages the use of massive data on human findings.

The second method addresses the construction of the map by clustering the isotope data into groups of similar isotopic features that are spatially coherent. This algorithm is a variant of the classical Gaussian Mixture Model clustering on the isotopic features using the spatial coordinates of the findings as an additional (independent) domain for validation. We also propose a coloring model to display the results.

The resulting maps for animals and humans (similar maps are available for each animal species as well as a combined map; the results are mostly redundant) depict a clear picture: while the isotopic fingerprints derived for the areas in the south and in the north of the alps are rather stable, there is a quite heterogeneous area in the inner alps. The models behind the clustering algorithm are probabilistic and allow for predicting the places of origin of a new sample based on its isotopic values.

It should be pointed out that while the data mining methods presented here are generic in the sense that they can be applied to virtually any data from any reference region, the concrete results of the case study (e.g., the relevancy of single features) do only hold for this particular reference region. However, due to the generality of the methods, it is easy to integrate more data in the future or even open the focus of this study to other parts of the Alps like Switzerland and France in the west or the other parts of Austria in the east.

References

Bowen GJ (2010) Isoscapes: spatial pattern in isotopic biogeochemistry. Annu Rev Earth Planet Sci 38:161–187

Bumsted M (1981) The potential of stable carbon isotopes in bioarchaeological anthropology. Biocultural adaptation—comprehensive approaches to skeletal analyses, pp 108–127

Dempster AP, Laird NM, Rubin DB (1977) Maximum likelihood from incomplete data via the EM algorithm. J R Stat Soc Ser B Methodolol 39:1–38

DeNiro M (1985) Postmortem preservation and alteration of in vivo bone collagen isotope ratios in relation to palaeodietary reconstruction. Nature 317:806–809

Ericson J (1985) Strontium isotope characterization in the study of prehistoric human ecology. J Hum Evol 14:503–514

Grupe G, Price TD, Schröter P, Söllner F, Johnson CM, Beard BL (1997) Mobility of Bell Beaker people revealed by strontium isotope ratios of tooth and bone: a study of southern Bavarian skeletal remains. Appl Geochem 12:517–525

Guyon I, Elisseeff A (2003) An introduction to variable and feature selection. J Mach Learn Res 3:1157–1182

Hall M, Frank E, Holmes G, Pfahringer B, Reutemann P, Witten IH (2015) EM. http://weka.sourceforge.net/doc.dev/weka/clusterers/EM.html. Accessed 10 Mar 2015

Hubert L, Arabie P (1985) Comparing partitions. J Classif 2(1):193–218

Kern Z, Kohán B, Leuenberger M (2014) Precipitation isoscape of high reliefs: interpolation scheme designed and tested for monthly resolved precipitation oxygen isotope records of an Alpine domain. Atmos Chem Phys 14:1897–1907

Milligan GW, Cooper MC (1987) Methodology review: clustering methods. Appl Psychol Meas 11(4):329–354

Molleson TI, Eldridge D, Gale N (1986) Identification of lead sources by stable isotope ratios in bones and lead from Poundbury Camp, Dorset. Oxf J Archaeol 5:249–253

Norr L (1984) Prehistoric subsistence and health status of coastal peoples from the Panamanian Isthmus of lower Central America. Paleopathology at the origins of agriculture, pp 463–480

Rand WM (1971) Objective criteria for the evaluation of clustering methods. J Am Stat Assoc 66 (336):846–850

Schoeninger MJ, DeNiro M, Tauber H (1983) Stable nitrogen isotope ratios of bone collagen reflects marine and terrestrial components of prehistoric human diet. Science 220:1380–1383

Schwarz HP, Melbye J, Katzenberg MA, Knyf M (1985) Stable isotopes in human skeletons of southern Ontario: reconstructing paleodiet. J Archaeol Sci 12:187–206

Vinh NX, Epps J, Bailey J (2010) Information theoretic measures for clusterings comparison: variants, properties, normalization and correction for chance. J Mach Learn Res 11:2837–2854

Vogel J, van der Merwe N (1977) Isotopic evidence for early maize cultivation in New York state. Am Antiq 42:238–242

Isotopic Map of the Inn-Eisack-Adige-Brenner Passage and its Application to Prehistoric Human Cremations

Anita Toncala, Frank Söllner, Christoph Mayr, Stefan Hölzl, Karin Heck, Dominika Wycisk, and Gisela Grupe

Abstract

This chapter summarizes the results achieved in an attempt to contribute to bioarchaeological research aiming at the reconstruction of migration and culture transfer in a region of eminent archaeological importance in Europe, namely, the Inn-Eisack-Adige passage via the Brenner Pass in the European Alps. 219 archaeological animal bone samples of three residential species (*Bos taurus*, *Sus scrofa*, *Cervus elaphus*) from 30 archaeological sites covering the transalpine passage have been analysed in terms of $\delta^{18}O_{phosphate}$, $^{87}Sr/^{86}Sr$, $^{208}Pb/^{204}Pb$, $^{207}Pb/^{204}Pb$, $^{206}Pb/^{204}Pb$, $^{208}Pb/^{207}Pb$ and $^{206}Pb/^{207}Pb$, thus generating a multi-isotope fingerprint. All measurement data and the laboratory processing methods are reported in detail. The isotopic map based on the spatial distribution of isotopic signatures in the bone finds is augmented by modern reference samples (water, soil, vegetation) to verify whether the choice of animal skeletal samples was appropriate and to perform a pilot study leading to a predictive model for $^{87}Sr/^{86}Sr$ isotopic ratios in local bioarchaeological specimens. Univariate statistics for each single isotopic signature and the related maps with the respective spatial distribution are presented.

A. Toncala (✉) • D. Wycisk • G. Grupe
Biozentrum, Ludwig-Maximilians-Universität, Martinsried, Germany
e-mail: anita-tank@gmx.de

F. Söllner
Department für Geo- und Umweltwissenschaften, Ludwig-Maximilians-Universität, Munich, Germany

C. Mayr
Institut für Geographie, Friedrich-Alexander-Universität, Erlangen, Germany

GeoBio-Center & Paläontologie und Geobiologie, Ludwig-Maximilians-Universität, Munich, Germany

S. Hölzl • K. Heck
RieskraterMuseum Nördlingen, Nördlingen, Germany

G. Grupe et al. (eds.), *Across the Alps in Prehistory*,
DOI 10.1007/978-3-319-41550-5_6

This isotopic map is a prerequisite for the quantification of human population movement in the reference region and for defining direction of migration. Information based on single isotopic ratios that is necessary for understanding whether migration took place in a north-to-south direction or vice versa is limited. In addition, cremating the dead was the major if not exclusive burial rite during several periods in European history. Since stable isotopic ratios of light elements such as oxygen are thermally less stable than the isotopic ratios of the heavy elements strontium and lead, migration research based on isotope analysis of fully cremated finds is restricted to the latter. In a pilot study, 184 human cremations from the Urnfield period and the Fritzens-Sanzeno culture recovered in the reference area were analysed for strontium and lead isotopic ratios, and the spatial distribution for each ratio was also mapped. Subsequent GMM clustering (see chapter "The Isotopic Fingerprint: New Methods of Data Mining and Similarity Search") resulted in a clear definition of micro-regions to the north and south of the Alps.

Introduction

To contribute to bioarchaeological research aiming at the reconstruction of migration, trade and culture transfer in a region that experienced considerable population dynamics through time (see chapter "Transalpine Mobility and Trade Since the Mesolithic"), a map has been established for the Inn-Eisack-Adige passage via the Brenner Pass in the European Alps (Fig. 1). This isotopic map is based primarily on archaeological vertebrate bone finds excavated along this Alpine transect and augmented with modern reference material. In addition to the routinely measured $^{87}Sr/^{86}Sr$ isotopic ratio in the bioapatite of the skeletons, lead and oxygen isotopic ratios of the bone mineral were also determined to generate a multi-isotope fingerprint (see chapter "The Concept of Isotopic Landscapes: Modern Ecogeochemistry Versus Bioarchaeology"). This way, the differentiation between a "local" and "non-local" multi-isotopic signature including the migratory direction of primarily non-local individuals is achieved. While isotopic ratios of heavy elements such as strontium and lead are not altered by exposure to high temperatures (Harbeck et al. 2011), stable isotopic ratios of light elements such as oxygen do change considerably (Olsen et al. 2008; Schurr et al. 2008). Therefore, $\delta^{18}O_{phosphate}$ does not provide reliable information for the detection of non-local individuals in cremated finds. While common cooking, roasting and boiling temperatures will not corroborate apatite $\delta^{18}O$ (Harbeck et al. 2011), prehistoric cremation pyres could easily reach temperatures up to 1000 °C (see below). For a time period of about 1500 years in human prehistory (from the Bronze Age until Imperial Roman Times), cremating the dead was the major if not exclusive burial custom (Grupe et al. 2015). Although recent work by Snoeck et al. (2015) suggests that cremations could also be a suitable substrate for migration research by the use of stable isotope analysis, a systematic evaluation of this special research substrate has yet to be attempted. This implies that for about 60 human generations, the extent of population admixture and

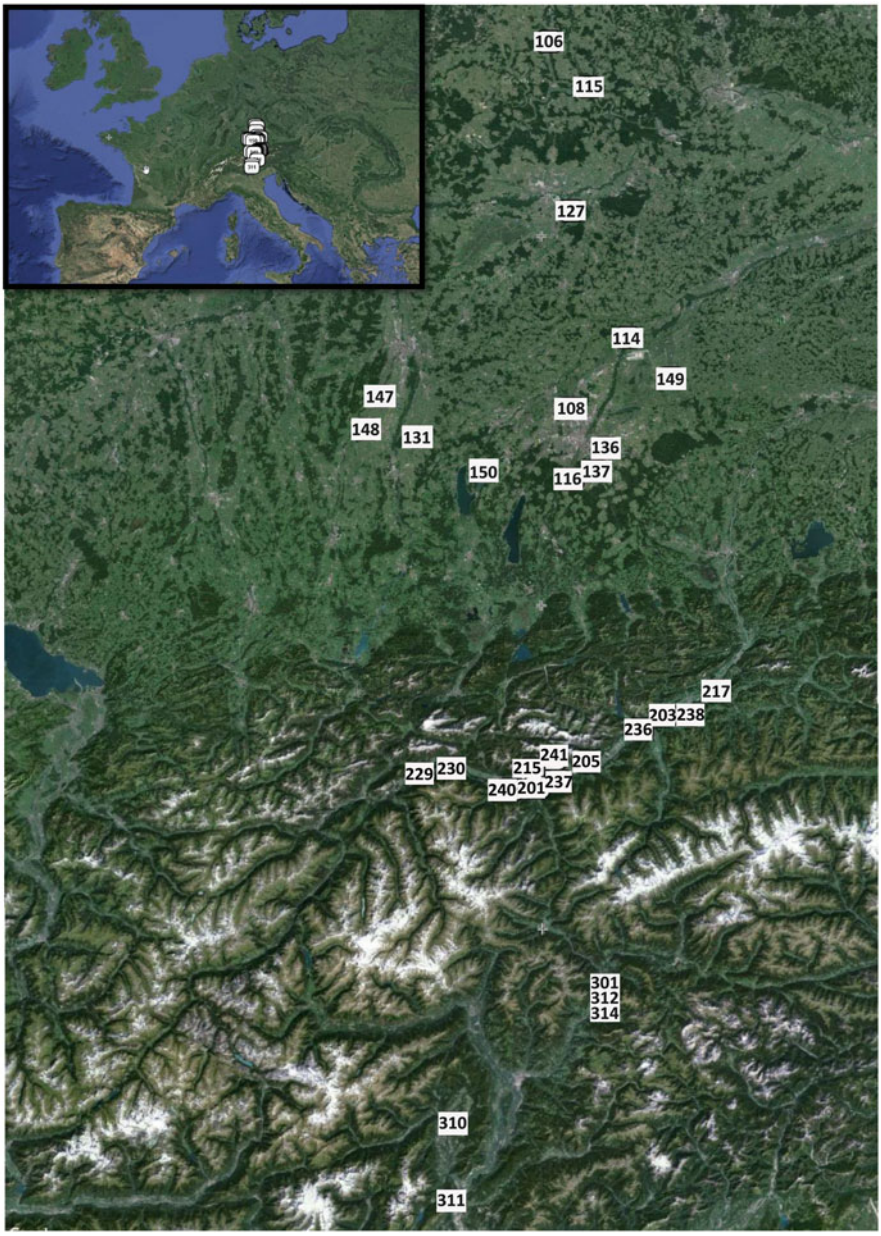

Fig. 1 Geographical location of the European Alps and magnification of the Inn-Eisack-Adige passage. Sites sampled along this transect are marked with site codes. Figure by A. Toncala, created by the use of scribblemaps http://www.scribblemaps.com

cultural exchange is still insufficiently exploited. Our study aims at initiating the closure of this knowledge gap.

Isotopic mapping of the Alpine transect is challenging in two ways: (1) The region is characterized by significant geological and ecological diversity and small-scaled isotopic patterning where considerable isotopic mixing occurs, and (2) the isotopic methodology for uncremated archaeological bones consisting of lead, strontium and oxygen stable isotopic ratios needs to be reduced to a fingerprint consisting of stable strontium and lead isotopic ratios only, when applied to cremated finds. The subsequent comparison of the spatial specificity will open up the possibility for a systematic inclusion of cremated finds into bioarchaeological migration research. The ultimate goal of our research is the establishment of a high-resolution isotopic fingerprint for archaeological contexts in the regions of northern Italy, the inner Alpine regions and the northern Alpine foothills. While it is necessary to stress at this point that the results outlined in this chapter are related to this specific reference area only, the general methodological and interpretive procedure can be adopted to other regions of interest.

With regard to the multifaceted sociocultural and historical research contexts, the choice of a specific region in the European Alps is understandable. However, since both the northern and the southern Alpine foothills are dominated by carbonate soils, a regional differentiation based on the commonly applied $^{87}Sr/^{86}Sr$ isotopic system only is very limited. Migration from the carbonate-dominated areas in the north to the carbonate-rich areas of the south or vice versa will largely remain undetected. The establishment and appropriate interpretation of a multi-isotope fingerprint for bioarchaeological migration research are requisite.

In a climatological sense, every alpine region is vertically stratified due to the ambient atmospheric conditions. The altitudinal changes in condensation temperature and humidity, however, also have an influence on the isotopic composition of the rain water. This is the reason why stable oxygen isotopic ratios ($\delta^{18}O$) in the skeleton of residential vertebrates are correlated to the altitude of the habitat. While the unweighted global gradient of $\delta^{18}O$ in precipitation averages −0.16 ‰ per 100 m altitude, the northern slopes of the European Alps exhibit a slightly larger such gradient (−0.18 ‰) than the southern ones (−0.08 ‰ per 100 m; Humer et al. 1995). Local $\delta^{18}O_{precipitation}$ is, however, also influenced by additional parameters, e.g. when a site is situated at the leeward side of a high mountain chain (Mayr et al. 2007).

The general hydrological difference in the Alps is mainly due to the origin of precipitating air masses from the Atlantic and the Mediterranean, enhanced by the continental effect which results from the different distances travelled by the air masses originating from the north or south. When $\delta^{18}O$ is measured in bone which is remodelled throughout the lifetime of an individual, temporary short-term climatic fluctuations are integrated. With regard to the reference area, publications on the variability of $\delta^{18}O$ in precipitation in southern Germany and northern Italy are already available (Humer et al. 1995; Longinelli and Selmo 2003; Tütken et al. 2004; see also the "Global Network of Isotopes in Precipitation" (GNIP) database, Aggarwal et al. 2010).

Geologically, the Alps exhibit a complex make-up and are subdivided into the Western, Eastern and Southern Alps. The Inn-Eisack-Adige passage belongs to the Eastern Alps (Fig. 2a, b). A molasse basin that developed at the northern foothills

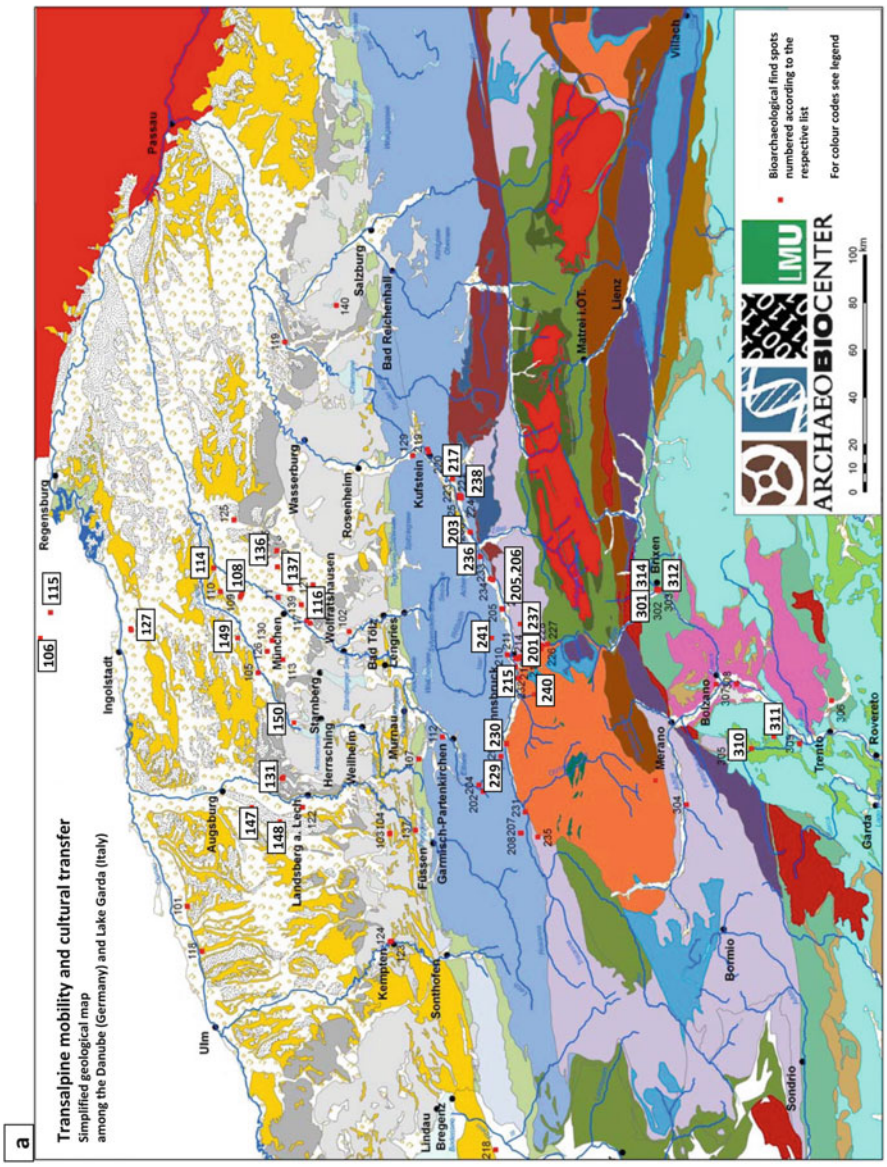

Fig. 2 Geological map of the European Alps (**a**) with colour codes (**b**). Figure by F. Söllner

b

No. geol map	running No.	colour in map	RGB	regional geology of the Eastern Alps	age of series	rock type	Sr-isotopic ratio	
	Legend of the geological map of the FOR 1670 project: Transalpine mobility and cultural transfer							
				Northern Alpine zone (NAZ) calcareous series and its crystalline basement				
				quaternary cover of the Alpine foreland				
0	1		R:255, G:255, B:255	fluviatile erosion detritus of the Northern Calcareous Alps (NCA)	Quaternary	glacial river pavement	carbonate ratio	<0.708
	2		R:225, G:225, B:225	glacial erosion detritus of the NCA	Quaternary	young moraines (Würm glacial stage)	carbonate ratio	<0.708
	3		R:178, G:178, B:178	glacial erosion detritus of the NCA	Quaternary	old moraines (pre-Würm glacial stage)	carbonate ratio	<0.708
	4		R:255, G:225, B:255	aeolian erosion detritus of the NCA	Quaternary	loess	mixed ratio	~0.71
				Tertiary cover of the Alpine foreland				
21	5		R:255, G:207, B:0	Molasse	Tertiary	mainly sand and sandstone	mixed ratio	~0.71
				Mesozoic underground of the Alpine foreland and Northern Bavaria				
35	6		R:194, G:214, B:154	Rheno-danubic flysch (Alps and Northern Bavaria)	Cretaceous/Tertiary	sand, sandstone, quarzite (limestone)	mixed ratio	~0.71
	7		R:0, G:112, B:255	limestone, northern Bavaria	White Jura (Malm)	limestone	carbonate ratio	<0.707
				Northern Calcareous Alps (NCA) and its crystalline basement				
14	10		R:219, G:229, B:241	Helvetikum	Jura/Kreide	limestone, dolomite, marl	carbonate ratio	<0.708
8+9	11		R:141, G:180, B:227	limestone of the NCA (Bavarikum/Tirolikum)	Trias/Jura/Cretaceous	limestone, dolomite, marble	carbonate ratio	<0.708
7	12		R:55, G:96, B:145	limestone of the Graywacke zone	Silurian/Devonian	dolomite, marble	carbonate ratio	0.7075–0.7085
6	13		R:149, G:55, B:53	Graywacke zone (crystalline basement of the NCA)	Palaeozoic	gneiss, mica schist, acid and basic (minor) mata-volcanics	crystalline, crustal-affine	>0.71
				Central Alpine zone (CAZ) crystalline basement and its calcareous cover				
2	20		R:0, G:176, B:240	Mesozoic cover of the CAZ (Karawanken, Ortler)	Mesozoic	limestone, dolomite, marble	carbonate ratio	<0.708
19	21		R:255, G:117, B:53	high-grade metamorphic sediments (Ötztal-Stubai crystalline complex)	Early Palaeozoic	gneiss, mica schist, acid meta-igneous rocks	crystalline, crustal-affine	>0.71
	22		R:0, G:115, B:76			basic meta-igneous rocks	crystalline, mantle-affine	<0.705

3	**23**		R:151, G:72, B:7	multiple high-grade metamorphic sediments (Schneeberger Zug, Kor-u. Saualpe)	Early Palaeozoic	gneiss, mineral-rich mica schists, marble, basic meta, igneous rocks	mixed ratio	~0.71
1	**24**		R:96, G:73, B:123	unmetamorphic sediment series (Grazer Paläozoikum, Gurktal nappe, Steinach nappe, Basement Drauzug)	Early Palaeozoic	sandstone, marl, clay	mixed ratio	~0.71
4+5	**25**		R:204, G:192, B:218	low metamorphic sediment series (Innsbrucker & Landecker quarzphyllite, Campo-Sesvenne crystalline complex, Schladminger-, Seckauer-, Radstätter Tauern, Err-Bernina nappe)	Early Palaeozoic	phyllite and mica schist	mixed ratio	~0.71
				Penninikum (Central Alpine zone) Mesozoic oceanic series and its cystalline basement				
11+12	**30**		R:117, G:146, B:60	Penninikum (outer covering series of the Tauern window, Engadin window (Bünden Schists))	Trias - Cretaceous	ophiolite, marble, schist, volcanic rocks	mixed ratio	~0.71
24	**31**		R:79, G:98, B:40	basement of the Penninikum (inner covering series of the Tauern window, Greiner series)	Palaeozoic (early Variscan)	black schist, amphibolite, hbl-gneiss, metavolcanics	crystalline, mantle-affine	<0.71
13	**32**		R:255, G:0, B:0	Variscan intrusiva	Tauern window (Alps) and Moldanubian zone (Northern Bavaria)	granite, tonalite, diorite, gabbros gneiss, amphibolite	crystalline, crustal- and mantle-affine	0.707–0.71
				South Alpine zone (SAZ) mesozoic-tertiary series and its crystalline basement				
0	**40**		R:255, G:255, B:255	fluviatile erosion detritus of the SAZ	Quaternary	glacial gravel and moraines	carbonate ratio	<0.708
18	**41**		R:146, G:208, B:80	Mesozoic - Tertiary cover	Cretaceous/Early Tertiary	flysch (sandstone, limestone)	mixed ratio	~0.71
				Southern Calcareous Alps (SCA) and its crystalline basement				
17A	**42**		R:102, G:255, B:255	calcareous series of the Mesozoic	Trias-Jura	limestone, dolomite	carbonate ratio	<0.708
	43		R:205, G:170, B:102	sandstones of the Permian	Permian	Gröden sandstone	mixed ratio	~0.71
17	**44**		R:255, G:102, B:204	acid volcanics of the Permian	Permian	Bozen quarz-porphyry	crystalline, crustal-affine	>0.71
	45		R:169, G:112, B:0	unmetamorphic Early Palaeozoic series	Silurian -Devonian	clay shale and limestone	mixed ratio	~0.71
16	**46**		R:197, G:190, B:151	cystalline basement of the SCA	Early Palaeozoic	quarz-phyllite	crystalline, crustal-affine	>0.71
10	**47**		R:192, G:0, B:0	young intrusiva	peri-adriatic Intrusiva (Tertiary)	tonalite, granite	crystalline, mantle-affine	0.704–0.709
				Dinaric Alps				
20	**50**		R:191, G:191, B:191	External Dinaric Alps		limestone	carbonate ratio	<0.708

Fig. 2 (continued)

has been filled mainly with debris of the Northern Calcareous Alps; therefore, soils developed on carbonate-rich substrate dominate the region north of the mountain chains up to the Danube River. In the inner Alpine regions, from the Inn Valley to the city of Brixen in the south, the mountains consist of crystalline and siliciclastic rocks (Moebus 1997; Henningsen and Katzung 1998; Park 2014). With regard to the north-to-south transalpine transect, the northern and southern Alpine foothills are geologically indistinguishable from each other. The central regions are, however, very diverse because of extensive sediment mixtures created through erosion and material transport by mudslides, rivers and glaciers, generating a mixture of different rock varieties with primarily distinct stable strontium isotopic ratios. In addition, multiple ore deposits in the Alps have generated provinces with characteristic stable lead isotope patterns (e.g. Kovach 1968; Köppel and Schroll 1988; Schroll 1990; Schroll et al. 2006). In sum, the European Alps are a region with a large potential for reconstructing the place of origin of bioarchaeological finds on a small scale given the prerequisite that the multi-isotope fingerprint is appropriately deciphered.

Material

Archaeological Animal Bone Finds

Following the suggestion of Price et al. (2002) for the establishment of a map of spatial variability of bioavailable stable isotopes within the scope of archaeological migration research, and also according to our own experience, uncremated skeletal remains of vertebrates from archaeological contexts were sampled for analysis. Three mammalian taxa in particular were selected for two reasons. First, the species should be available at the majority of sites. Second, the larger the animal, the better it integrates local stable isotopic signatures into its tissues, which are incorporated by feeding and drinking across broader spatial scales (Crowley et al. 2015). The taxa chosen for this project are cattle (*Bos taurus*), domesticated pig (*Sus scrofa domestica*) and red deer (*Cervus elaphus*). Bioapatite was purified, and $^{87}Sr/^{86}Sr$, $^{208}Pb/^{204}Pb$, $^{207}Pb/^{204}Pb$, $^{206}Pb/^{204}Pb$, $^{208}Pb/^{207}Pb$, $^{206}Pb/^{207}Pb$ and $\delta^{18}O_{phosphate}$ were measured. For comparative reasons, $\delta^{18}O_{carbonate}$ was also measured in a subsample of the bones.

All three species are assumed to be fairly residential, a logical assumption for the domesticated pigs and cattle since they were likely kept in close proximity to the human settlements. However, herd management for cattle and pigs could have been different because the practice of a transhumant economic system in alpine regions was developed very early in prehistory. It cannot be excluded that cattle spent several months of the year at higher altitudes grazing in meadows of the mountain slope, while pigs may have been kept within the settlement. The catchment area of red deer, a species which is also known for its seasonal migration, should have been considerably larger in prehistory compared to modern times. However, the size of catchment areas and hunting grounds in prehistory is for the most part unknown.

Therefore, the term "residential" is relative, and it cannot be expected that all three species integrate the local isotopic signals of their environment in the same way. Moreover, species-specific metabolic peculiarities have a further influence on average $\delta^{18}O_{phosphate}$. $\delta^{18}O$ in the body is related to the respective isotopic ratio in drinking water, which is in turn related to $\delta^{18}O$ of precipitation. While both cattle and pigs drink daily and are diurnal species, red deer are crepuscular animals which cover their water demands mostly by dew and succulent green fodder. Diet is also species-specific: pigs are omnivores, while both cattle and red deer are herbivores and ruminants. Cattle are grazers and folivores preferring open meadowlands, while red deer live in forests and grasslands where they feed on leaves and bark. Due to their different drinking behaviour and regular leaf eating, red deer $\delta^{18}O$ can be significantly enriched in ^{18}O compared to cattle in a given micro-region (see, e.g. Fricke et al. 1998). Furthermore, the type of thermoregulation of a species (e.g. sweating versus panting) can play a major role in the oxygen isotope balance of a mammal body.

Any isotopic map generated by the use of local vertebrate bone finds will therefore rely on similar but not identical isotopic fingerprints. The same holds for human skeletal isotopic fingerprints which are later related to this "faunal isotopic map". Therefore, in several ways isotopic signatures constitute "data with some uncertainties". First, every isotope value obtained has an analytical error that also comprises the quantitative decontamination of a bone that was subjected to soil conditions during centuries or even millennia of burial (see chapter "The Crystalline State of Archaeological Bone Material"). Second, individual physiological and metabolic peculiarities frequently exert an unknown influence on the isotopic signature. Third, species specificity and the environmental variability of isotopic fingerprints render the definition of cut-off values between "local" and "non-local" quite complex and can hardly be achieved using univariate statistics alone. This necessitates new efforts for the extraction of the relevant information from the fingerprint (see chapter "The Isotopic Fingerprint: New Methods of Data Mining and Similarity Search"). Finally, after establishing this environmentally defined cut-off value, the notion of "foreignness" in relation to the size of a micro-region and distance travelled, in other words the differentiation between "mobility" and "migration/trade/import", must be discussed in relation to the particular archaeological context. An additional difficulty is introduced by the fact that an archaeological bone find may plausibly be assumed to be local to a site, but it can often not be assessed a priori whether certain animal individuals, or parts of them, have been imported to the site of their recovery as food or raw material. Since the Alpine transect studied in this project was a transition zone, it cannot be firmly excluded that, for example, cadavers of draught animals such as oxen were disposed of in the vicinity of a settlement.

The faunal specimens considered for the isotopic map are housed at the Bavarian State Collection for Anthropology and Palaeoanatomy in Munich and have been analysed osteologically according to international archaeozoological standards. The assemblages under study essentially consist of butchering refuse and meat consumption but occasionally comprise whole carcasses as well. Prior to isotope

analysis, key archaeozoological parameters including skeletal element, taxon, bone weight, size, sex, age at death and butchering marks were recorded and the data entered into the research database OssoBook (http://xbook.vemed.uni-muenchen.de), together with the relevant archaeological information. Relative to isotopic mapping, remains of cattle, red deer and pigs from pre-Roman contexts were selected.

Analysing archaeological animal bone finds for the establishment of an isotopic map is not an end in itself. The possibility that some of the animals which had been assumed to be local exhibit an isotopic fingerprint which is not shared by the other individuals of the same species instead can be of great historic significance. As will be shown below, this actually happened in our data set. The question about the underlying motive for the transfer of animals is automatically raised – was this done to improve local breeds, were these animals in accompaniment during population movements or even military manoeuvres, or was this an outcome of normal trade? This way, the isotopic map may serve as a design for future archaeozoological projects (see chapter "Early Roman Transfer of Animals Across the Alps: Setting the Stage for Interpreting the Results of Isotope Fingerprinting").

Animal bones excavated from 30 archaeological sites of the Alpine transect were sampled. Sites were selected according to the archaeological relevance, quality of the documentation and availability of appropriate material. Sites and bones were labelled with site codes. Sites labelled between 100 and 199 are located north of the Alps, inner Alpine sites are labelled between 200 and 299, and southern Alpine sites have labels $\geq$300 (Fig. 1). Whenever possible, compact bone of three adult animals per species and site were sampled to ensure that the measured isotopic ratios are integrated over several years or even the total lifetime of the individual in question.

Selection of Archaeological Sites

The map of bioavailable isotopic ratios in vertebrate bone finds constitutes the necessary framework and supplies the background data for answering archaeological questions related to mobility, trade, migration and culture transfer in the reference area. It is not uncommon that the settlements belonging to prehistoric burial grounds are not known. Therefore, the archaeological sites from which the animal bones were sampled were chosen according to the following reasons: The sites should cover the Inn-Eisack-Adige passage as good as possible, well-preserved bones of the three vertebrate species chosen should be available, and the sites of animal bone recovery should be located as close as possible to archaeological sites containing human cremations used in isotopic fingerprinting for provenance analysis. It should be emphasized that the archaeological dating of the archaeofaunal remains (see Table 1) is not necessarily identical with the dating of the human cremations. This is in part due to the availability of material but was also performed on purpose because this permits the monitoring of possible changes in isotopic ratios through time. The best case scenario is when the isotopic map, which records bioavailable isotopic ratios in consumer tissues and are unbiased by modern

Table 1 Individual animal bones analysed for the isotopic map, place of recovery with geographical coordinates, and all measurement data (the latter established by authors Toncala, Mayr, Heck and Hölzl)

Site code, site name	Dating	°N	°E	m a.s.l.	Species	Bone/tooth	$\delta^{18}O$	$^{87}Sr/^{86}Sr$	2SE [%]	$^{208}Pb/^{204}Pb$	2SE [%]	$^{207}Pb/^{204}Pb$	2SE [%]	$^{206}Pb/^{204}Pb$	2SE [%]	$^{208}Pb/^{207}Pb$	$^{206}Pb/^{207}Pb$
106 Berching Pollanten	250–80/50 BC	49.14	11.45	399.9	Cattle	Mandible	14.3	0.70931	0.0033	38.3957	0.2005	15.6076	0.1506	18.6140	0.1007	2.4601	1.1926
	250–80/50 BC	49.14	11.45	399.9	Cattle	Mandible	15.1	0.71060	0.0043	38.1878	0.2064	15.8570	0.1583	21.3966	0.1104	2.4081	1.3492
	250–80/50 BC	49.14	11.45	399.9	Cattle	Mandible	14.6	0.71034	0.0051	38.5544	0.2014	15.6417	0.1514	18.8441	0.1018	2.4649	1.2047
	250–80/50 BC	49.14	11.45	399.9	Pig	Mandible	15.2	0.71082	0.0027	38.7605	0.2014	15.6813	0.1509	19.0414	0.1011	2.4719	1.2143
	250–80/50 BC	49.14	11.45	399.9	Pig	Mandible	14.8	0.71123	0.0020	38.4401	0.2007	15.6071	0.1509	18.6775	0.1013	2.4631	1.1968
	250–80/50 BC	49.14	11.45	399.9	Pig	Mandible	15.6	0.71044	0.0033	38.4837	0.2005	15.6138	0.1506	18.6352	0.1009	2.4646	1.1935
	250–80/50 BC	49.14	11.45	399.9	Red deer	Radius	14.8	0.71029	0.0032	38.5919	0.2015	15.6940	0.1515	19.0785	0.1016	2.4591	1.2157
	250–80/50 BC	49.14	11.45	399.9	Red deer	Tibia	15.5	0.71060	0.0044	38.4105	0.2012	15.6162	0.1511	18.6928	0.1014	2.4598	1.1970
	250–80/50 BC	49.14	11.45	399.9	Red deer	Tibia	15.6	0.71037	0.0042	38.4667	0.2003	15.6459	0.1505	19.0057	0.1006	2.4585	1.2147
115 Griesstetten	3300–2800/ 2700 BC	49.03	11.6	390.9	Pig	Humerus	15.0	0.71060	0.0034	38.5002	0.2004	15.6216	0.1505	18.7473	0.1007	2.4646	1.2001
	3300–2800/ 2700 BC	49.03	11.6	390.9	Pig	Humerus	15.4	0.71148	0.0056	38.5781	0.2005	15.6422	0.1504	18.9399	0.1006	2.4662	1.2108
	3300–2800/ 2700 BC	49.03	11.6	390.9	Pig	Humerus	15.2	0.71145	0.0037	38.6165	0.2014	15.6473	0.1514	18.9677	0.1018	2.4680	1.2122
	3300–2800/ 2700 BC	49.03	11.6	390.9	Red deer	Metacarpus	15.4	0.71046	0.0043	38.4776	0.2011	15.6332	0.1514	18.7952	0.1018	2.4612	1.2023
	3300–2800/ 2700 BC	49.03	11.6	390.9	Red deer	Metacarpus	14.9	0.71106	0.0041	38.4884	0.2017	15.6218	0.1524	18.7972	0.1029	2.4638	1.2032
	3300–2800/ 2700 BC	49.03	11.6	390.9	Red deer	Metacarpus	15.2	0.71168	0.0054	38.6386	0.2064	15.7222	0.1587	19.4937	0.1128	2.4576	1.2399
	3300–2800/ 2700 BC	49.03	11.6	390.9	Cattle	Phalanx 1	15.4	0.71182	0.0017	38.4603	0.2008	15.6248	0.1509	18.7541	0.1013	2.4615	1.2003
	3300–2800/ 2700 BC	49.03	11.6	390.9	Cattle	Phalanx 1	15.4	0.70708	0.0044	38.6520	0.2010	15.6591	0.1510	19.0047	0.1015	2.4684	1.2137
	3300–2800/ 2700 BC	49.03	11.6	390.9	Cattle	Phalanx 1	13.7	0.71088	0.0043	38.6447	0.2012	15.6390	0.1514	18.8615	0.1022	2.4710	1.2060

(continued)

Table 1 (continued)

Site code, site name	Dating	°N	°E	m a.s.l.	Species	Bone/tooth	$\delta^{18}O$	$^{87}Sr/^{86}Sr$	2SE [%]	$^{208}Pb/^{204}Pb$	2SE [%]	$^{207}Pb/^{204}Pb$	2SE [%]	$^{206}Pb/^{204}Pb$	2SE [%]	$^{208}Pb/^{207}Pb$	$^{206}Pb/^{207}Pb$
127 Manching Pfaffenhofen Ilm	250–15 BC	48.72	11.53	379.4	Red deer	Phalanx 1	15.3	0.70912	0.0042	38.4928	0.2033	15.7827	0.1525	20.4403	0.1032	2.4394	1.2950
	250–15 BC	48.72	11.53	379.4	Red deer	Phalanx 1	15.7	0.70901	0.0037	38.5028	0.2009	15.7600	0.1511	20.1306	0.1016	2.4431	1.2773
	250–15 BC	48.72	11.53	379.4	Red deer	Phalanx 1	14.9	0.70957	0.0033	38.5909	0.2042	15.7321	0.1529	19.8473	0.1027	2.4531	1.2617
	250–15 BC	48.72	11.53	379.4	Cattle	Mandible	14.8	0.71027	0.0047	38.4109	0.2026	15.7637	0.1535	20.0858	0.1052	2.4366	1.2741
	250–15 BC	48.72	11.53	379.4	Cattle	Mandible	15.8	0.71069	0.0052	38.6177	0.2022	15.6664	0.1530	18.8252	0.1043	2.4650	1.2016
	250–15 BC	48.72	11.53	379.4	Cattle	Mandible	15.2	0.70967	0.0047	38.3586	0.2006	15.6107	0.1508	18.7192	0.1010	2.4571	1.1991
	250–15 BC	48.72	11.53	379.4	Pig	Mandible	15.0	0.71084	0.0037	38.5245	0.2030	15.6541	0.1518	18.7651	0.1018	2.4609	1.1987
	250–15 BC	48.72	11.53	379.4	Pig	Mandible	14.9	0.71349	0.0047	38.4124	0.2026	15.7543	0.1521	20.0609	0.1020	2.4383	1.2734
	250–15 BC	48.72	11.53	379.4	Pig	Mandible	15.0	0.71096	0.0048	38.6585	0.2040	15.7457	0.1535	19.8442	0.1044	2.4551	1.2603
114 Freising Domberg	1700/ 1650–1500 BC	48.4	11.75	459.4	Cattle	Mandible	14.4	0.71147	0.0056	38.5233	0.2012	15.6534	0.1511	19.0154	0.1015	2.4610	1.2148
	1700/ 1650–1500 BC	48.4	11.75	459.4	Cattle	Mandible	15.6	0.71104	0.0052	38.3923	0.2010	15.6134	0.1513	18.7251	0.1019	2.4591	1.1993
	No secure date	48.4	11.75	459.4	Cattle	Mandible	15.7	0.71066	0.0052	38.5462	0.2002	15.6606	0.1502	18.9413	0.1002	2.4613	1.2095
	No secure date	48.4	11.75	459.4	Pig	Mandible	15.2	0.71042	0.0059	38.3556	0.2021	15.7914	0.1525	20.6645	0.1043	2.4290	1.3088
	No secure date	48.4	11.75	459.4	Pig	Mandible	15.7	0.71007	0.0046	38.4423	0.2020	15.7654	0.1523	20.4420	0.1029	2.4386	1.2966
	2200–780 BC	48.4	11.75	459.4	Pig	Mandible	15.7	0.71076	0.0022	38.6361	0.2004	15.6604	0.1506	18.8308	0.1010	2.4672	1.2024
	1350/ 1300–780 BC	48.4	11.75	459.4	Red deer	Radius	15.5	0.71123	0.0056	38.3531	0.2024	15.6340	0.1527	19.0062	0.1035	2.4532	1.2157
	1700/ 1650–1500 BC	48.4	11.75	459.4	Red deer	Metatarsus	14.6	0.71186	0.0037	38.5702	0.2017	15.6577	0.1511	18.8750	0.1015	2.4635	1.2055
	500 AD	48.4	11.75	459.4	Red deer	Mandible	15.4	0.71059	0.0021	38.4336	0.2004	15.6343	0.1506	18.6266	0.1008	2.4583	1.1914
149 Erding-Altenerding	3800–3400 BC	48.3	11.91	466.4	Pig	Mandible	15.1	0.70956	0.0022	38.4863	0.2022	15.6710	0.1515	18.7847	0.1018	2.4559	1.1987
	3800–3400 BC	48.3	11.91	466.4	Pig	Humerus		0.70989	0.0030	38.5846	0.2097	15.6597	0.1619	18.9855	0.1159	2.4640	1.2124
	3800–3400 BC	48.3	11.91	466.4	Pig	Tibia	14.8	0.70981	0.0030	38.4314	0.2005	15.6530	0.1506	18.7943	0.1007	2.4552	1.2006
	3800–3400 BC	48.3	11.91	466.4	Cattle	Mandible	15.6	0.70980	0.0034	38.5370	0.2018	15.6424	0.1526	18.8408	0.1041	2.4636	1.2046
	3800–3400 BC	48.3	11.91	466.4	Cattle	Mandible	16.5	0.70973	0.0030	38.5115	0.2042	15.6463	0.1551	18.8908	0.1068	2.4611	1.2072
	3800–3400 BC	48.3	11.91	466.4	Cattle	Mandible	16.3	0.70983	0.0033	38.4597	0.2012	15.6449	0.1514	18.6865	0.1019	2.4583	1.1945
	3800–3400 BC	48.3	11.91	466.4	Red deer	Radius	14.8	0.70947	0.0016	38.3778	0.2012	15.6400	0.1510	18.9696	0.1013	2.4538	1.2129
	3800–3400 BC	48.3	11.91	466.4	Red deer	Calcaneus	15.4	0.71016	0.0057	38.4482	0.2025	15.6543	0.1534	19.0287	0.1048	2.4562	1.2155
	3800–3400 BC	48.3	11.91	466.4	Red deer	Metatarsus	15.3	0.70968	0.0022	38.4018	0.2009	15.6439	0.1509	18.5282	0.1012	2.4548	1.1844

147 Wehringen-Hochfeld	780–15 BC	48.25	10.81	537.1	Pig	Ulna	15.4	0.70881	0.0044	38.4913	0.2002	15.6429	0.1502	18.7201	0.1003	2.4607	1.1967
	780–15 BC	48.25	10.81	537.1	Pig	Humerus	14.7	0.70832	0.0056	38.4209	0.2010	15.6161	0.1513	18.6079	0.1016	2.4603	1.1916
	780–15 BC	48.25	10.81	537.1	Pig	Scapula	14.0	0.70883	0.0030	38.4290	0.2002	15.6221	0.1501	18.6018	0.1002	2.4599	1.1907
	780–15 BC	48.25	10.81	537.1	Cattle	Metacarpus	15.3	0.70895	0.0044	38.5390	0.2008	15.6544	0.1507	18.7056	0.1007	2.4619	1.1949
	780–15 BC	48.25	10.81	537.1	Cattle	Radius +ulna		0.70971	0.0027	38.5104	0.2069	15.6509	0.1569	19.0086	0.1102	2.4604	1.2146
	780–15 BC	48.25	10.81	537.1	Red deer	Femur	14.3	0.70965	0.0038	38.4109	0.2014	15.6314	0.1509	18.4794	0.1010	2.4573	1.1822
	780–15 BC	48.25	10.81	537.1	Red deer	Cranium	15.0	0.71016	0.0029	38.5364	0.2026	15.6463	0.1531	18.9500	0.1041	2.4630	1.2111
	780–15 BC	48.25	10.81	537.1	Red deer	Ulna	14.0	0.70843	0.0024	38.5475	0.2037	15.6609	0.1526	18.7254	0.0224	2.4613	1.1957
	780–15 BC	48.25	10.81	537.1	Cattle	Humerus	15.2	0.70852	0.0022	38.4779	0.2040	15.6417	0.1550	18.9179	0.0374	2.4599	1.2095
108 Eching-IKEA Freising	120–15. BC	48.22	11.53	482.7	Red deer	Cranium	14.3	0.70885	0.0023	38.6633	0.2006	15.7215	0.1506	20.0275	0.1006	2.4592	1.2739
	1500–1300/ 1350 BC	48.22	11.53	482.7	Cattle	Humerus	15.6	0.70888	0.0035	38.6898	0.2005	15.7184	0.1504	19.8617	0.1005	2.4613	1.2636
	1500–1300/ 1350 BC	48.22	11.53	482.7	Cattle	Humerus	14.9	0.70906	0.0043	38.5804	0.2047	15.6587	0.1542	19.1030	0.1053	2.4639	1.2199
	1500–1300/ 1350 BC	48.22	11.53	482.7	Cattle	Tibia	16.3	0.70957	0.0013	38.6593	0.2007	15.6786	0.1507	18.8863	0.1010	2.4657	1.2046
	1500–1300/ 1350 BC	48.22	11.53	482.7	Pig	Humerus	14.3	0.70908	0.0061	38.5605	0.2005	15.6739	0.1504	19.4533	0.1006	2.4602	1.2411
	1500–1300/ 1350 BC	48.22	11.53	482.7	Red deer	Metacarpus	15.6	0.70846	0.0035	38.6644	0.2084	15.7085	0.1606	19.2899	0.1147	2.4614	1.2281
	1500–1300/ 1350 BC	48.22	11.53	482.7	Pig	Humerus	13.0	0.70955	0.0029	38.7769	0.2073	15.7113	0.1601	19.1887	0.1138	2.4679	1.2212
	1500–1300/ 1350 BC	48.22	11.53	482.7	Pig	Ulna	15.0	0.70874	0.0035	38.6419	0.2013	15.6901	0.1516	19.3662	0.1022	2.4628	1.2343
148 Schwabmünchen	4500–3800 BC	48.17	10.76	566.3	Pig	Mandible	14.8	0.71087	0.0023	38.5867	0.2032	15.6688	0.1537	19.1307	0.1049	2.4626	1.2209
	4500–3800 BC	48.17	10.76	566.3	Pig	Mandible	15.4	0.71088	0.0020	38.3831	0.2006	15.6314	0.1506	18.4210	0.1007	2.4555	1.1785
	4500–3800 BC	48.17	10.76	566.3	Pig	Mandible	13.8	0.71290	0.0026	38.5765	0.2021	15.6546	0.1520	18.8731	0.1031	2.4642	1.2055
	4500–3800 BC	48.17	10.76	566.3	Cattle	Mandible	15.5	0.70964	0.0036	38.5573	0.2003	15.6377	0.1502	18.8441	0.1003	2.4656	1.2050
	4500–3800 BC	48.17	10.76	566.3	Cattle	Mandible	15.1	0.70921	0.0037	38.6960	0.2020	15.6891	0.1523	19.1196	0.1031	2.4665	1.2186
	4500–3800 BC	48.17	10.76	566.3	Cattle	Mandible	15.3	0.70922	0.0036	38.6753	0.2016	15.6616	0.1510	18.9670	0.1009	2.4694	1.2110
	4500–3800 BC	48.17	10.76	566.3	Red deer	Metacarpus	15.4	0.70906	0.0023	38.3701	0.2002	15.6225	0.1503	18.6501	0.1005	2.4561	1.1938

(continued)

Table 1 (continued)

Site code, site name	Dating	°N	°E	m a.s.l.	Species	Bone/tooth	$\delta^{18}O$	$^{87}Sr/^{86}Sr$	2SE [%]	$^{208}Pb/^{204}Pb$	2SE [%]	$^{207}Pb/^{204}Pb$	2SE [%]	$^{206}Pb/^{204}Pb$	2SE [%]	$^{208}Pb/^{207}Pb$	$^{206}Pb/^{207}Pb$
131 Pestenacker am Lech	3800–3400 BC	48.15	10.95	571.5	Red deer	Radius +ulna	14.5	0.70928	0.0059	38.4788	0.2021	15.6599	0.1513	19.1105	0.1016	2.4569	1.2203
	3800–3400 BC	48.15	10.95	571.5	Red deer	Radius +ulna	14.3	0.70918	0.0057	38.4173	0.2018	15.6349	0.1512	18.7886	0.1015	2.4570	1.2017
	3800–3400 BC	48.15	10.95	571.5	Red deer	Radius	15.3	0.70960	0.0030	38.4936	0.2015	15.6454	0.1513	18.8879	0.1016	2.4603	1.2072
	3800–3400 BC	48.15	10.95	571.5	Cattle	Mandible	14.4	0.70936	0.0026	38.3424	0.2011	15.6688	0.1517	19.2868	0.1024	2.4470	1.2309
	3800–3400 BC	48.15	10.95	571.5	Cattle	Mandible	14.2	0.70900	0.0038	38.4575	0.2079	15.7916	0.1587	19.9644	0.1122	2.4353	1.2643
	3800–3400 BC	48.15	10.95	571.5	Cattle	Mandible	15.0	0.70949	0.0023	38.5969	0.2043	15.6685	0.1529	18.9548	0.1032	2.4634	1.2097
	3800–3400 BC	48.15	10.95	571.5	Pig	Mandible	14.4	0.70938	0.0043	38.3318	0.2011	15.6666	0.1508	19.3903	0.1009	2.4467	1.2377
	3800–3400 BC	48.15	10.95	571.5	Pig	Mandible	14.3	0.70927	0.0032	38.4052	0.2011	15.6932	0.1512	19.5820	0.1016	2.4473	1.2478
	3800–3400 BC	48.15	10.95	571.5	Pig	Mandible	14.0	0.70978	0.0031	38.5244	0.2019	15.6979	0.1530	19.5108	0.1044	2.4539	1.2429
136 München-Trudering	650–250 BC	48.12	11.67	532.5	Pig	Mandible	16.1	0.70809	0.0022	38.6115	0.2043	15.6835	0.1550	19.5438	0.1058	2.4619	1.2462
	650–250 BC	48.12	11.67	532.5	Pig	Humerus	15.2	0.70836	0.0023	38.6269	0.2013	15.6825	0.1516	19.6985	0.1025	2.4631	1.2561
	650–250 BC	48.12	11.67	532.5	Pig	Humerus	14.6	0.70834	0.0023	38.5675	0.2022	15.6686	0.1522	19.3565	0.1032	2.4614	1.2353
	650–250 BC	48.12	11.67	532.5	Cattle	Mandible	15.5	0.70868	0.0030	38.4463	0.2072	15.6137	0.1591	18.8463	0.1127	2.4623	1.2071
	650–250 BC	48.12	11.67	532.5	Cattle	Mandible	15.4	0.70845	0.0021	38.4703	0.2072	15.6418	0.1585	19.2203	0.1111	2.4594	1.2288
	650–250 BC	48.12	11.67	532.5	Cattle	Mandible	15.5	0.70899	0.0019	38.5198	0.2015	15.6502	0.1519	19.2897	0.1027	2.4614	1.2326
	650–250 BC	48.12	11.67	532.5	Red deer	Cranium	15.3	0.70870	0.0034	38.4382	0.2032	15.6473	0.1536	18.9405	0.1057	2.4565	1.2104
137 Unterhaching Am Rodelberg	1350/ 1300–780 BC	48.06	11.63	560.9	Cattle	Mandible	14.7	0.70820	0.0033	38.3958	0.2006	15.6225	0.1508	18.6991	0.1017	2.4577	1.1969
	1350/ 1300–780 BC	48.06	11.63	560.9	Cattle	Mandible	14.9	0.70871	0.0047	38.3214	0.2008	15.6043	0.1511	18.5680	0.1019	2.4559	1.1899
	1350/ 1300–780 BC	48.06	11.63	560.9	Cattle	Mandible	14.8	0.70824	0.0016	38.4839	0.2013	15.6477	0.1516	19.0461	0.1023	2.4595	1.2172
	1350/ 1300–780 BC	48.06	11.63	560.9	Red deer	Coxa	13.2	0.70854	0.0036	38.3724	0.2020	15.6105	0.1528	18.7861	0.1035	2.4581	1.2034
	1350/ 1300–780 BC	48.06	11.63	560.9	Red deer	Radius	14.1	0.70860	0.0040	38.4090	0.2022	15.6438	0.1533	18.6253	0.1047	2.4554	1.1907
	1350/ 1300–780 BC	48.06	11.63	560.9	Red deer	Metacarpus	13.9	0.70854	0.0046	38.4501	0.2010	15.6609	0.1511	18.8849	0.1014	2.4552	1.2059
	1350/ 1300–780 BC	48.06	11.63	560.9	Pig	Mandible	14.6	0.70938	0.0041	38.5932	0.2055	15.6753	0.1566	19.2736	0.1105	2.4622	1.2297
	1350/ 1300–780 BC	48.06	11.63	560.9	Pig	Humerus	14.6	0.70852	0.0034	38.5809	0.2057	15.6712	0.1567	19.1758	0.1083	2.4619	1.2236
	1350/ 1300–780 BC	48.06	11.63	560.9	Pig	Humerus	14.3	0.70854	0.0028	38.5454	0.2002	15.6512	0.1502	19.1174	0.1002	2.4628	1.2215

150 Wörthsee-Steinebach	250–80 BC	48.06	11.2	574.9	Pig	Mandible	15.0	0.70917	0.0018	38.6351	0.2020	15.6634	0.1522	19.0546	0.1031	2.4664	1.2165
	250–80 BC	48.06	11.2	574.9	Pig	Mandible	14.8	0.70876	0.0026	38.6539	0.2046	15.6606	0.1565	19.1417	0.1103	2.4683	1.2223
	250–80 BC	48.06	11.2	574.9	Pig	Tibia	14.3	0.71029	0.0022	38.7122	0.2021	15.6877	0.1522	19.0082	0.1026	2.4678	1.2117
	250–80 BC	48.06	11.2	574.9	Cattle	Scapula	14.7	0.70856	0.0025	38.5355	0.2037	15.6483	0.1543	19.0264	0.1070	2.4627	1.2160
	250–80 BC	48.06	11.2	574.9	Cattle	Mandible	15.3	0.70886	0.0028	38.4820	0.2002	15.6390	0.1502	18.5730	0.1002	2.4607	1.1876
	250–80 BC	48.06	11.2	574.9	Cattle	Cranium	14.5	0.70858	0.0029	38.7234	0.2005	15.6681	0.1505	18.8047	0.1007	2.4716	1.2002
116 Grünwald-Parkgarage	1350/ 1300–780 BC	48.04	11.53	599.2	Cattle	Mandible	15.7	0.70865	0.0030	38.6796	0.2012	15.6797	0.1509	19.1010	0.1009	2.4668	1.2182
	1350/ 1300–780 BC	48.04	11.53	599.2	Cattle	Mandible	14.8	0.70874	0.0023	38.5427	0.2005	15.6559	0.1506	19.0141	0.1006	2.4618	1.2145
	1350/ 1300–780 BC	48.04	11.53	599.2	Cattle	Metacarpus	15.2	0.70892	0.0059	38.4357	0.2002	15.6234	0.1502	18.7253	0.1003	2.4601	1.1985
	1350/ 1300–780 BC	48.04	11.53	599.2	Pig	Mandible	14.1	0.70887	0.0035	38.4872	0.2014	15.6377	0.1520	19.0609	0.1027	2.4612	1.2189
	1350/ 1300–780 BC	48.04	11.53	599.2	Pig	Tibia	14.3	0.70867	0.0032	38.6095	0.2007	15.6691	0.1508	19.4191	0.1011	2.4641	1.2393
	1350/ 1300–780 BC	48.04	11.53	599.2	Pig	Tibia	14.5	0.70868	0.0029	38.5411	0.2015	15.6564	0.1518	19.2013	0.1030	2.4617	1.2265
217 Kirchbichl bei Wörgl Grattenbergl Mixed	780–250 BC	47.5	12.08	587.4	Pig	Tibia	13.7	0.71197	0.0022	38.5828	0.2040	15.6683	0.1550	19.1392	0.0363	2.4625	1.2216
	780–250 BC	47.5	12.08	587.4	Pig	Humerus	15.2	0.71197	0.0019	38.4263	0.2030	15.6393	0.1537	18.7401	0.0331	2.4571	1.1983
	780–250 BC	47.5	12.08	587.4	Cattle	Femur	15.7	0.71201	0.0030	38.4098	0.2007	15.6278	0.1508	18.4909	0.0137	2.4579	1.1832
	780–250 BC	47.5	12.08	587.4	Cattle	Metatarsus	14.6	0.71306	0.0016	38.5891	0.2023	15.6571	0.1529	18.8833	0.0292	2.4646	1.2060
	780–250 BC	47.5	12.08	587.4	Cattle	Radius	14.1	0.71212	0.0043	38.4638	0.2018	15.6391	0.1522	18.7005	0.1031	2.4595	1.1958
238 Radfeld-Mauken	1200–1000 BC	47.44	11.95	1020	Pig	Humerus	14.0	0.71334	0.0035	38.5789	0.2017	15.7048	0.1523	18.4661	0.1035	2.4563	1.1758
	1200–1000 BC	47.44	11.95	1020	Cattle	Metacarpus	14.9	0.71605	0.0042								
	1200–1000 BC	47.44	11.95	1020	Pig	Humerus	12.8	0.71230	0.0022	38.3521	0.2027	15.6314	0.1522	18.4906	0.1025	2.4533	1.1829
	1200–1000 BC	47.44	11.95	1020	Pig	Humerus	12.8	0.71238	0.0028	38.3875	0.2055	15.6269	0.1539	18.4679	0.1039	2.4567	1.1818
	1200–1000 BC	47.44	11.95	1020	Cattle	Metacarpus	16.1	0.71035	0.0019	38.5044	0.2066	15.6412	0.1595	18.7273	0.1125	2.4617	1.1973
	1200–1000 BC	47.44	11.95	1020	Cattle	Tibia	15.5	0.71701	0.0043	38.3804	0.2149	15.6287	0.1697	18.3525	0.1289	2.4558	1.1743
203 Brixlegg Inn Mariahilfbergl	4500–3800 BC	47.43	11.88	630.6	Cattle	Costa	14.9	0.71498	0.0033	38.4470	0.2044	15.6414	0.1549	18.5432	0.1070	2.4580	1.1856
	4500–3800 BC	47.43	11.88	630.6	Cattle	Humerus	13.0	0.70992	0.0021	38.4744	0.2002	15.6435	0.1503	18.5277	0.1003	2.4595	1.1844
	4500–3800 BC	47.43	11.88	630.6	Cattle	Femur	13.6	0.70990	0.0014	38.5677	0.2057	15.6556	0.1556	18.6120	0.1068	2.4634	1.1889
	4500–3800 BC	47.43	11.88	630.6	Red deer	Mandible	13.7	0.71298	0.0025	38.5296	0.2022	15.6672	0.1519	18.5418	0.1024	2.4593	1.1835
	4500–3800 BC	47.43	11.88	630.6	Red deer	Femur	13.7	0.71398	0.0022	38.3270	0.2005	15.6230	0.1505	18.7200	0.1008	2.4533	1.1982

(continued)

Table 1 (continued)

Site code, site name	Dating	°N	°E	m a.s.l.	Species	Bone/tooth	$\delta^{18}O$	$^{87}Sr/^{86}Sr$	2SE [%]	$^{208}Pb/^{204}Pb$	2SE [%]	$^{207}Pb/^{204}Pb$	2SE [%]	$^{206}Pb/^{204}Pb$	2SE [%]	$^{208}Pb/^{207}Pb$	$^{206}Pb/^{207}Pb$
236 Wiesing bei Jenbach Buchberg	2200–1500 BC	47.4	11.79	614.4	Cattle	Mandib. sin	14.1	0.71114	0.0025	38.4456	0.2006	15.6416	0.1505	18.8916	0.1006	2.4578	1.2077
	2200–1500 BC	47.4	11.79	614.4	Cattle	Mandib. sin	13.3	0.71238	0.0017	38.5136	0.2002	15.6370	0.1502	18.7251	0.1003	2.4630	1.1975
	2200–1500 BC	47.4	11.79	614.4	Cattle	Mandib. sin	13.7	0.70983	0.0022	38.5837	0.2032	15.6707	0.1524	18.9299	0.1020	2.4620	1.2079
		47.4	11.79	614.4	Pig	Mandib dex	13.9	0.71172	0.0021	38.4702	0.2029	15.6849	0.1537	19.2541	0.1055	2.4526	1.2277
	2200–1500 BC	47.4	11.79	614.4	Pig	Mandib dex	14.8	0.71287	0.0035	38.6430	0.2004	15.6608	0.1506	18.8935	0.1008	2.4676	1.2064
	2200–1500 BC	47.4	11.79	614.4	Pig	Mandib dex	14.4	0.71152	0.0032	38.3917	0.2105	15.6046	0.1642	18.8025	0.1191	2.4598	1.2048
205, 206 Fritzens Pirchboden	780–15 BC	47.31	11.59	805	Cattle	Coxa	14.2	0.71418	0.0031	38.6074	0.2003	15.6666	0.1504	18.5401	0.1005	2.4643	1.1834
	780–15 BC	47.31	11.59	805	Cattle	Costa	15.0	0.71171	0.0021	38.5431	0.2020	15.6630	0.1519	18.7770	0.1020	2.4607	1.1988
	780–15 BC	47.31	11.59	805	Pig	Scapula	12.5	0.71089	0.0017	38.5945	0.2005	15.6593	0.1506	18.6892	0.1008	2.4646	1.1935
	780–15 BC	47.31	11.59	805	Pig	Mandible	13.8	0.71318	0.0015	38.5316	0.2004	15.6643	0.1504	19.1612	0.1005	2.4599	1.2232
	780–15 BC	47.31	11.59	805	Pig	Tibia	13.9	0.71099	0.0017	38.6257	0.2002	15.6536	0.1502	18.6866	0.1002	2.4675	1.1938
241 Thaur "Kiechlberg"	ca. 4200–3600 BC	47.3	11.45	1026.3	Pig	Femur	13.6	0.70953	0.0016	38.5430	0.2015	15.6514	0.1519	18.6739	0.1029	2.4626	1.1931
	ca. 4200–3600 BC	47.3	11.45	1026.3	Pig	Humerus	13.0	0.71000	0.0021	38.4732	0.2011	15.6527	0.1511	18.9383	0.1018	2.4579	1.2099
	ca. 4200–3600 BC	47.3	11.45	1026.3	Pig	Scapula	14.2	0.71068	0.0036	38.4858	0.2040	15.6484	0.1544	18.5478	0.1061	2.4594	1.1853
	ca. 4200–3600 BC	47.3	11.45	1026.3	Cattle	Humerus	14.6	0.70941	0.0037	38.5858	0.2008	15.6705	0.1508	19.1146	0.1008	2.4624	1.2197
	ca. 4200–3600 BC	47.3	11.45	1026.3	Cattle	Metacarpus	14.2	0.70919	0.0024	38.4956	0.2010	15.6614	0.1509	18.6576	0.1012	2.4580	1.1913
	ca. 4200–3600 BC	47.3	11.45	1026.3	Cattle	Metatarsus	14.5	0.71110	0.0048	38.5692	0.2011	15.6538	0.1514	18.7849	0.1020	2.4637	1.2000
	ca. 4200–3600 BC	47.3	11.45	1026.3	Red deer	Metatarsus	13.2	0.71282	0.0044	38.4268	0.2007	15.6298	0.1510	18.5719	0.1017	2.4586	1.1882
	ca. 4200–3600 BC	47.3	11.45	1026.3	Red deer	Metatarsus	13.3	0.70992	0.0041	38.5520	0.2010	15.6556	0.1511	18.7131	0.1014	2.4625	1.1953
	ca. 4200–3600 BC	47.3	11.45	1026.3	Red deer	Phalanx	13.6	0.70940	0.0024	38.3982	0.2056	15.6138	0.1579	18.7464	0.1107	2.4593	1.2006

230 Pfaffenhofen am Inn	400/350–250/ 200 BC	47.29	11.08	860.2	Cattle	Humerus	13.5	0.71441	0.0025	38.7016	0.2011	15.6916	0.1511	19.1467	0.1010	2.4664	1.2203
	450–250 BC	47.29	11.08	860.2	Cattle	Scapula	14.2	0.71524	0.0049	38.6977	0.2018	15.6619	0.1524	18.9930	0.1035	2.4708	1.2127
	450–15 BC	47.29	11.08	860.2	Cattle	Calcaneus	13.0	0.71644	0.0026	38.6938	0.2026	15.6321	0.1537	18.8393	0.1059	2.4752	1.2051
215 Innsbruck Kalvarienberg	1600 BC–300 AD	47.29	11.41	625.9	Pig	Mandible	14.0	0.70944	0.0026	38.5216	0.2008	15.6492	0.1509	18.9101	0.1012	2.4616	1.2084
	1600 BC–300 AD	47.29	11.41	625.9	Pig	Humerus	14.0	0.71014	0.0016	38.4645	0.2008	15.6423	0.1510	19.0409	0.1013	2.4590	1.2173
	1600 BC–300 AD	47.29	11.41	625.9	Pig	humerus	12.8	0.71316	0.0016	38.2927	0.2008	15.6215	0.1508	18.4302	0.1013	2.4514	1.1798
	1600 BC–300 AD	47.29	11.41	625.9	Cattle	Radius	16.1	0.70993	0.0028	38.6348	0.2034	15.6475	0.1541	18.8543	0.1058	2.4691	1.2049
	1600 BC–300 AD	47.29	11.41	625.9	Cattle	Radius	14.7	0.71096	0.0018	38.6566	0.2005	15.6620	0.1506	19.0055	0.1008	2.4682	1.2135
	1600 BC–300 AD	47.29	11.41	625.9	Cattle	Radius	13.1	0.70927	0.0040	38.4979	0.2008	15.6359	0.1509	18.9940	0.1015	2.4621	1.2148
	1600 BC–300 AD	47.29	11.41	625.9	Red deer	Metacarpus	13.4	0.71191	0.0024	38.5043	0.2015	15.6223	0.1519	18.6161	0.1029	2.4646	1.1916
229 Mieming	450–15 BC	47.28	10.96	792	Cattle	Mandible	13.4	0.71020	0.0033	38.4350	0.2001	15.6441	0.1501	18.7340	0.1003	2.4569	1.1975
	650–250 BC	47.28	10.96	792	Cattle	Mandible	13.9	0.71022	0.0042	38.3879	0.2039	15.6452	0.1557	19.2316	0.1083	2.4535	1.2292
	650–250 BC	47.28	10.96	792	Cattle	Mandible	13.3	0.71060	0.0033	38.6477	0.2006	15.6985	0.1507	19.0883	0.1010	2.4618	1.2159
	1300/ 1350–450 BC	47.28	10.96	792	Pig	Humerus	14.0	0.71039	0.0034	38.6145	0.2009	15.6451	0.1508	18.8954	0.1014	2.4682	1.2077
	No secure date	47.28	10.96	792	Pig	Humerus	13.9	0.71081	0.0044	38.6884	0.2003	15.6756	0.1505	19.0020	0.1008	2.4681	1.2122
	2200–780 BC	47.28	10.96	792	Pig	Humerus	15.7	0.71028	0.0023	38.6798	0.2015	15.6789	0.1511	18.8524	0.1009	2.4669	1.2024
	450–15 BC	47.28	10.96	792	Red deer	Phalanx 1	14.6	0.71236	0.0036	38.2745	0.2057	15.6497	0.1580	19.4565	0.1107	2.4457	1.2433
	No secure date	47.28	10.96	792	Red deer	Metatarsus	14.5	0.71041	0.0020	38.2659	0.2014	15.6880	0.1519	19.7480	0.1031	2.4392	1.2588
	No secure date	47.28	10.96	792	Red deer	Metacarpus	14.4	0.71021	0.0017	38.4224	0.2031	15.6392	0.1543	18.5811	0.1064	2.4568	1.1881

(continued)

Table 1 (continued)

Site code, site name	Dating	°N	°E	m a.s.l.	Species	Bone/tooth	$\delta^{18}O$	$^{87}Sr/^{86}Sr$	2SE [%]	$^{208}Pb/^{204}Pb$	2SE [%]	$^{207}Pb/^{204}Pb$	2SE [%]	$^{206}Pb/^{204}Pb$	2SE [%]	$^{208}Pb/^{207}Pb$	$^{206}Pb/^{207}Pb$
237 Ampass-Widumfeld	650–450 BC	47.26	11.46	636	Cattle	Mandible	14.3	0.71665	0.0047	38.7254	0.2045	15.6747	0.1537	18.7758	0.1037	2.4706	1.1979
	650–450 BC	47.26	11.46	636	Cattle	Mandible	14.3	0.71643	0.0044	38.3984	0.2049	15.6115	0.1566	18.6339	0.1101	2.4597	1.1936
	650–450 BC	47.26	11.46	636	Cattle	Mandible	14.8	0.71663	0.0045	38.6221	0.2020	15.6902	0.1511	18.6490	0.1010	2.4615	1.1886
	650–450 BC	47.26	11.46	636	Pig	Mandible	14.4	0.71636	0.0046	38.6707	0.2055	15.6520	0.1573	18.7415	0.1107	2.4705	1.1973
	650–450 BC	47.26	11.46	636	Pig	Mandible	13.4	0.71654	0.0057	38.6054	0.2044	15.6996	0.1537	19.2494	0.1042	2.4589	1.2261
	650–450 BC	47.26	11.46	636	Pig	Mandible	15.5	0.71658	0.0028								
	650–450 BC	47.26	11.46	636	Red deer	Cranium	14.6	0.71607	0.0047	38.4534	0.2020	15.6525	0.1516	18.6858	0.1017	2.4566	1.1939
	650–450 BC	47.26	11.46	636	Pig	Mandible	15.3	0.71672	0.0034	38.4408	0.2060	15.6416	0.1571	18.8916	0.1103	2.4575	1.2077
201 Bergisel IBK	650–15 BC	47.25	11.4	725.3	Cattle	Mandible	12.8	0.71162	0.0029	38.6002	0.2005	15.6435	0.1505	18.7201	0.1007	2.4674	1.1967
	650–15 BC	47.25	11.4	725.3	Cattle	Scapula	14.7	0.71306	0.0027	38.4535	0.2006	15.6253	0.1505	18.7078	0.1006	2.4609	1.1972
	650–15 BC	47.25	11.4	725.3	Cattle	Scapula	14.6	0.71204	0.0034	38.5756	0.2200	15.6681	0.1758	18.9931	0.1349	2.4621	1.2124
	650–15 BC	47.25	11.4	725.3	Pig	Ulna	12.5	0.71067	0.0029	38.4792	0.2045	15.6878	0.1556	19.2719	0.1078	2.4528	1.2285
	650–15 BC	47.25	11.4	725.3	Pig	Tibia	13.1	0.71183	0.0021	38.5596	0.2084	15.6324	0.1602	18.7881	0.1166	2.4665	1.2018
	650–15 BC	47.25	11.4	725.3	Pig	Coxa	13.7	0.71147	0.0034	38.3380	0.2088	15.6806	0.1611	19.4369	0.1167	2.4449	1.2395
240 Hohe Birga	250–15 BC	47.24	11.3	855.3	Cattle	Humerus	13.4	0.71909	0.0026	38.3811	0.2012	15.6358	0.1510	18.6967	0.1010	2.4547	1.1957
	250–15 BC	47.24	11.3	855.3	Cattle	Metatarsus	14.1	0.71380	0.0028	38.4949	0.2013	15.6368	0.1512	18.6036	0.1015	2.4619	1.1897
	250–15 BC	47.24	11.3	855.3	Red deer	Metatarsus	14.0	0.72043	0.0036	38.6417	0.2027	15.6724	0.1521	18.6126	0.1021	2.4656	1.1876
	250–15 BC	47.24	11.3	855.3	Cattle	Radius	12.7	0.71766	0.0020	38.5651	0.2179	15.6403	0.1709	18.7984	0.1305	2.4654	1.2018
	250–15 BC	47.24	11.3	855.3	Red deer	Metacarpus	13.1	0.71507	0.0014	38.4868	0.2029	15.6590	0.1537	19.0504	0.1055	2.4576	1.2166
	250–15 BC	47.24	11.3	855.3	Pig	Radius	13.6	0.71325	0.0029	38.4430	0.2025	15.6343	0.1520	18.6095	0.1020	2.4589	1.1903
	250–15 BC	47.24	11.3	855.3	Pig	Humerus	12.8	0.71876	0.0020	38.6371	0.2077	15.6494	0.1595	18.7086	0.1123	2.4687	1.1955
	250–15 BC	47.24	11.3	855.3	Pig	Ulna	12.8	0.71800	0.0024	38.6263	0.2041	15.6518	0.1540	18.7899	0.1054	2.4680	1.2005
	250–15 BC	47.24	11.3	855.3	Red deer	Phalanx 1	13.9	0.71440	0.0018	38.5644	0.2019	15.6540	0.1523	18.6779	0.1039	2.4634	1.1931
314 Brixen-Stufels Villa Kranebit	450–120 BC	46.72	11.66	553	Cattle	Mandible	15.5	0.71717	0.0045	38.7500	0.2012	15.6544	0.1514	18.6599	0.1021	2.4754	1.1920
	450–120 BC	46.72	11.66	553	Cattle	Mandible	15.6	0.71524	0.0034	38.5441	0.2027	15.6245	0.1537	18.7560	0.1051	2.4672	1.2004
	450–120 BC	46.72	11.66	553	Cattle	Mandible	15.7	0.71695	0.0021	38.8265	0.2003	15.6773	0.1504	18.6337	0.1005	2.4766	1.1886
	450–120 BC	46.72	11.66	553	Pig	Maxilla	14.4	0.71695	0.0035	38.7724	0.2028	15.6585	0.1539	18.6734	0.1053	2.4762	1.1925
	450–120 BC	46.72	11.66	553	Red deer	Humerus	15.0	0.71710	0.0044	38.6668	0.2013	15.6324	0.1514	18.6522	0.1022	2.4736	1.1932

312 Brixen-Stufels "Russo"	450–250 BC	46.72	11.66	573.6	Cattle	Metacarpus	16.3	0.71336	0.0017	38.3899	0.2036	15.6371	0.1535	18.3299	0.1048	2.4553	1.1722
	450–250 BC	46.72	11.66	573.6	Cattle	Metatarsus	15.0	0.71719	0.0021	38.6517	0.2023	15.6635	0.1519	18.4672	0.1027	2.4678	1.1790
	450–250 BC	46.72	11.66	573.6	Pig	Femur	14.5	0.71179	0.0030	38.4555	0.2071	15.6249	0.1597	18.5546	0.1157	2.4612	1.1873
	450–250 BC	46.72	11.66	573.6	Cattle	Humerus	13.3	0.72068	0.0021	38.4867	0.2008	15.6577	0.1508	18.5685	0.1011	2.4580	1.1859
	450–250 BC	46.72	11.66	573.6	Pig	Metatarsus iv	15.3	0.71694	0.0015	38.6324	0.2011	15.6623	0.1508	18.4743	0.1011	2.4667	1.1796
	450–250 BC	46.72	11.66	573.6	Pig	Metatarsus iii	16.0	0.71635	0.0016	38.5991	0.2010	15.6543	0.1508	18.6383	0.1010	2.4658	1.1906
301 Brixen-Stufels Hotel Dominik I +II	650–250 BC	46.72	11.66	572	Red deer	Metatarsus	17.1	0.71796	0.0048	38.5822	0.2002	15.6444	0.1503	18.5790	0.1004	2.4662	1.1876
	650–250 BC	46.72	11.66	572	Red deer	Radius	15.6	0.71772	0.0040	38.6825	0.2043	15.6573	0.1554	18.9279	0.1082	2.4704	1.2089
	650–250 BC	46.72	11.66	572	Red deer	Radius	14.9	0.71834	0.0032	38.5913	0.2013	15.6232	0.1514	18.7069	0.1020	2.4703	1.1975
	650–250 BC	46.72	11.66	572	Pig	Mandible	15.7	0.71585	0.0022	38.5571	0.2014	15.6470	0.1518	18.5156	0.1026	2.4642	1.1833
	650–250 BC	46.72	11.66	572	Pig	Mandible	15.1	0.71641	0.0036	38.5988	0.2005	15.6370	0.1507	18.6710	0.1011	2.4684	1.1940
	650–250 BC	46.72	11.66	572	Pig	Mandible	14.7	0.71645	0.0045	38.6605	0.2008	15.6413	0.1509	18.6233	0.1015	2.4717	1.1906
	650–250 BC	46.72	11.66	572	Cattle	Mandible	15.1	0.71625	0.0057	38.6860	0.2012	15.6523	0.1513	18.6340	0.1019	2.4714	1.1904
	650–250 BC	46.72	11.66	572	Cattle	Mandible	15.1	0.71616	0.0031	38.5877	0.2012	15.6160	0.1516	18.7388	0.1018	2.4710	1.2000
	650–250 BC	46.72	11.66	572	Cattle	Metacarpus	16.1	0.71302	0.0034	38.4874	0.2024	15.6135	0.1533	18.7445	0.1047	2.4650	1.2005
310 Sanzeno	450–120 BC	46.37	11.08	683	Pig	Mandible	14.0	0.70879	0.0042	38.4489	0.2001	15.6262	0.1501	18.7292	0.1001	2.4605	1.1986
	450–120 BC	46.37	11.08	683	Pig	Mandible	14.8	0.70898	0.0033	38.5451	0.2068	15.6568	0.1591	18.8774	0.1122	2.4619	1.2056
	450–120 BC	46.37	11.08	683	Pig	Mandible	14.2	0.70872	0.0028	38.6121	0.2086	15.6904	0.1611	19.0877	0.1156	2.4611	1.2165
	450–120 BC	46.37	11.08	683	Cattle	Radius	14.9	0.71591	0.0036	38.6088	0.2007	15.6446	0.1506	18.7849	0.1009	2.4679	1.2007
	450–120 BC	46.37	11.08	683	Cattle	Radius	14.3	0.70984	0.0037	38.6353	0.2005	15.6705	0.1506	18.9902	0.1011	2.4655	1.2118
	450–120 BC	46.37	11.08	683	Cattle	Humerus	14.7	0.71154	0.0042	38.5546	0.2006	15.6471	0.1506	18.8171	0.1008	2.4640	1.2026
311 Zambana	450–250 BC	46.17	11.08	193.8	Pig	Ulna	13.7	0.70930	0.0050	38.6812	0.2009	15.6743	0.1509	18.6385	0.1010	2.4678	1.1891
	450–250 BC	46.17	11.08	193.8	Pig	Radius	14.2	0.70929	0.0039	38.7221	0.2004	15.6768	0.1504	18.7859	0.1007	2.4699	1.1983
	450–250 BC	46.17	11.08	193.8	Pig	Tibia	14.1	0.71262	0.0039	38.6987	0.2001	15.6667	0.1501	18.5918	0.1001	2.4701	1.1867
	450–250 BC	46.17	11.08	193.8	Cattle	Metatarsus	14.9	0.70962	0.0042	38.5400	0.2007	15.6554	0.1507	18.8480	0.1010	2.4617	1.2039
	450–250 BC	46.17	11.08	193.8	Cattle	Tibia	15.7	0.70941	0.0033	38.5899	0.2011	15.6632	0.1510	18.7079	0.1014	2.4637	1.1944
	450–250 BC	46.17	11.08	193.8	Cattle	Tibia	16.2	0.70851	0.0053	38.5522	0.2005	15.6435	0.1506	18.6784	0.1008	2.4644	1.1940
	450–250 BC	46.17	11.08	193.8	Red deer	Maxilla and m3	16.4	0.70960	0.0068	38.4705	0.2029	15.6790	0.1535	18.9945	0.1053	2.4536	1.2114
	450–250 BC	46.17	11.08	193.8	Red deer	m3 sup.	14.6	0.70922	0.0037	38.5796	0.2087	15.6962	0.1605	18.6804	0.1148	2.4581	1.1901
	450–250 BC	46.17	11.08	193.8	Red deer	m3 sup.	12.6	0.70951	0.0037	38.3550	0.2004	15.6249	0.1504	18.6491	0.1006	2.4546	1.1935

The authors are very grateful to Dr. H. Napierala for selecting specimens for isotope analysis from a large number of faunal assemblages in the study area. The detailed recording of these in the Database Ossobook was essential to the project and financed by the DFG in the frame of FOR 1670, Project J. Peters, DFG PE 424/11-1

industrialisation, will be suitable for the majority if not all archaeological strata. In the following listing, the sites are ordered by latitude (see Figs. 1 and 2).

Archaeological Sites to the North of the Alps

- *Berching-Pollanten* (site code 106); coordinates: 49.14°N, 11.45°E, 400 m a.s.l.
- *Griesstetten* (site code 115); coordinates: 49.03°N, 11.6°E, 390 m a.s.l.
- *Manching, Pfaffenhofen/Ilm* (site code 127); coordinates: 48.72°N, 11.53°E, 379 m a.s.l.
- *Freising Domberg* (site code 114); coordinates: 48.4°N, 11.75°E, 459 m a.s.l.
- *Erding-Altenerding* (site code 149); coordinates: 48.3°N, 11.91°E, 467 m a.s.l.
- *Wehringen-Hochfeld* (site code 147); coordinates: 48.25°N, 10.81°E, 537 m a.s.l.
- *Eching-IKEA* (site code 108); coordinates: 48.22°N, 11.53°E, 483 m a.s.l.
- *Schwabmünchen* (site code 148); coordinates: 48.17°N, 10.86°E, 566 m a.s.l.
- *Pestenacker/Lech* (site code 131); coordinates: 48.15°N, 10.95°E, 572 m a.s.l.
- *München-Trudering* (site code 136); coordinates: 48.12°N, 11.67°E, 533 m a.s.l.
- *Unterhaching* "Am Rodelberg" (site code 137); coordinates: 48.06°N, 11.63°E, 561 m a.s.l.
- *Wörthsee-Steinebach* (site code 150); coordinates: 48.06°N, 11.20°E, 575 m a.s.l.
- *Grünwald-Parkgarage* (site code 116); coordinates: 48.04°N, 11.53°E, 599 m a.s.l.

Inner Alpine Sites

- *Kirchbichl/Wörgl* "Grattenbergl" (site code 217); coordinates: 47.5°N, 12.08°E, 587 m a.s.l.
- *Radfeld-Mauken* (site code 238); coordinates: 47.44°N, 11.95°E, 1020 m a.s.l.
- *Brixlegg/Inn* "Mariahilfbergl" (site code 203); coordinates: 47.43°N, 11.88°E, 631 m a.s.l.
- *Wiesing/Jenbach Buchberg* (site code 236); coordinates: 47.4°N, 11.79°E, 614 m a.s.l.
- *Fritzens Pirchboden* (site code 205, 206); coordinates: 47.31°N, 11.59°E, 805 m a.s.l.
- *Thaur* "Kiechlberg" (site code 241); coordinates: 47.3°N, 11.45°E, 1026 m a.s.l.
- *Pfaffenhofen/Inn* (site code 230); coordinates: 47.29°N, 11.08°E, 860 m a.s.l.
- *Innsbruck* "Kalvarienberg" (site code 215); coordinates: 47.29°N, 11.41°E, 626 m a.s.l.
- *Mieming* (site code 229); coordinates: 47.28°N, 10.96°E, 792 m a.s.l.
- *Ampass-Widumfeld* (site code 237); coordinates: 47.26°N, 11.46°E, 636 m a.s.l.
- *Bergisel-IBK* (site code 201); coordinates: 47.25°N, 11.40°E, 725 m a.s.l.
- *Hohe Birga* (site code 240); coordinates: 47.24°N, 11.30°E, 855 m a.s.l.

Archaeological Sites to the South of the Alps

- *Brixen-Stufels* "Villa Kranebit" (site code 314); coordinates: 46.72°N, 11.66°E, 553 m a.s.l.
- *Brixen-Stufels* "Russo" (site code 312); coordinates: 46.72°N, 11.66°E, 574 m a.s.l.
- *Brixen-Stufels* "Hotel Dominik I+II" (site code 301); coordinates: 46.72°N, 11.66°E, 572 m a.s.l.
- *Sanzeno* (site code 310); coordinates: 46.37°N, 11.08°E, 683 m meters a.s.l.
- *Zambana* (site code 311); coordinates: 46.17°N, 11.08°E, 194 m a.s.l.

Modern Reference Samples

An isotopic map suitable for archaeological strata must be free of modern contaminants, e.g. introduced by mineral fertilizers or industrial lead. To control for this, the map based on animal bone finds was augmented with modern reference samples which had been gathered in the course of several field excursions in the years 2013 and 2015. Soil samples were taken from the archaeological horizons of the sites and were subjected to a leaching step prior to analysis afterwards (after Drouet et al. 2005, see methods' section). Groundwater was taken from the bottom of neighbouring springs or wells at the closest distance to the archaeological site. Accordingly, these water samples consist of both precipitation and surface water enriched with soil components. Since no archaeobotanical material was available, modern vegetation was sampled from trees which develop deep-reaching roots well below the agricultural horizon. Preference was on hazelnut branches (*Corylus avellana*) because of the frequent availability of this plant species (Göhring et al. 2015).

In a pilot study, local $^{87}Sr/^{86}Sr$ isotopic ratios of archaeological strata were modelled for five selected sites in the Inn Valley, a region where small-scale mixed isotopic composition is expected (Söllner et al. 2016). The specific sites and samples for the model calculations are:

- *Fritzens, Pirchboden* (site code 206): soil developed on argillaceous sand, light brown with crystalline components of boulder pavement of varying size, definitely of moraine origin ($^{87}Sr/^{86}Sr = 0.714$, profile depth = 100–110 cm); hazelnut wood; spring water from a nearby well.
- *Innsbruck-Mühlau, Kalvarienberg* (site code 215): soil consisting of brown rendzina with calcareous fragments and some crystalline pebbles, covered by landslide material interspersed with carbonate fragments only ($^{87}Sr/^{86}Sr = 0.70876$, profile depth = 25–30 cm); hazelnut wood; water from a well next to the church at the Kalvarienberg.
- *Pfaffenhofen/Inn, Hörtenberg* (site code 230): soil developed on grey soft clay ($^{87}Sr/^{86}Sr = 0.72533$, profile depth = 100–130 cm), whereby the whole fine-

grained loamy profile intercalated with chalk bands suggests a lacustrine sequence (see also Fig. 11); hazelnut wood; spring water from a well inside the "Maierhof" farm.
- *Wiesberg, Buchberg* (site code 236): soil developed on sandy silt ($^{87}Sr/^{86}Sr = 0.71081$, profile depth = 50–60 cm); hazelnut wood; spring water from the nearby village of Jenbach.
- *Ampass, Widumfeld* (site code 237): soil containing small pebbles of quartz-phyllite, probably related to an argillaceous sandy valley or lake filling from post-Roman times, it is assumed that the sediment source remained similar during postglacial times with no fundamental change of strontium isotopic ratios of the reservoir ($^{87}Sr/^{86}Sr = 0.71736$, profile depth = 50–60 cm); hazelnut wood; spring water from the nearby forest (Söllner et al. 2016).

Finally, to monitor the altitudinal gradient of $\delta^{18}O$ in precipitation, α-cellulose was purified from 24 wood samples of nine plant species (*Acacia sp.*, *Corylus avellana*, *Fraxinus excelsior*, *Juglans regia*, *Malus sp.*, *Prunus sp.*, *Quercus sp.*, *Ribes sp.*, and *Sambucus nigra*) from selected sites (Göhring et al. 2015). Bulk analyses were performed instead of annual tree ring analyses to integrate over the growth period of the trees. Seventeen groundwater and three river water samples were taken for comparison (Göhring et al. 2015).

Methods

Stable Oxygen Isotopes in the Bone Apatite Structural Carbonate ($\delta^{18}O_{carbonate}$)

The endosteal and periosteal surfaces of small pieces of compact bone were removed manually by the use of tweezers and tongs to avoid any heat generation through grinding. One-way gloves were worn all time. The remaining compact bone core was homogenized to a fine powder with a ball mill (ZrO_2 beakers). About 100 mg of bone powder was incubated into 5 mL of 4 % NaOCl for deproteination, and the solution was kept under constant motion for at least two full days. On the third day latest, the solution was replaced with fresh NaOCl, and incubation continued until effervescence ceased. The powder was then washed with deionized water by centrifuging at 5000 rpm for 5 min each. When a pH between 5 and 6 was reached, the pellet was suspended in 5 mL 1 M calcium-acetate-acetic acid buffer (pH 4.5) and kept under constant motion for at least one full day. The sample was then washed as described before and lyophilized. Stable isotope analysis was performed by a coupled analysing system GasBench II/Delta Plus (Thermo Finnigan), where the sample reacts with orthophosphoric acid at 72 °C and the resulting CO_2 is transferred in He (4.6) as carrier gas into the mass spectrometer. A laboratory standard was calibrated against the IAEA NBS 19 and NBS 20 standards, and isotopic ratios were expressed in the conventional δ-notation against the VPDB standard. Measurement error did not exceed 0.1 ‰.

Stable Oxygen Isotopes in the Bone Apatite Phosphate ($\delta^{18}O_{phosphate}$)

The samples were deproteinated according to the protocol for the purification of the apatite structural carbonate. 3 mg of deproteinated apatite powder was then placed into a 2 mL Eppendorf cup and dissolved in 115 µL 2 M HF. The solution was kept under constant motion for at least 4 h. To neutralize the solution, 115 µL 2 M KOH were added followed by centrifuging at 3000 rpm for 15 min. The supernatant was pipetted into a new Eppendorf cup, and 1500 µL $AgNO_3$ solution (pH 10–11) was added for the precipitation of silver phosphate. The open tube was kept overnight at 60 °C. On the following day, the supernatant (pH between 6 and 7) was discarded. The crystallized silver phosphate was washed carefully with distilled water, whereby the Eppendorf cups were placed five times for 3 min each into an ultrasonic bath to loosen all crystals still adherent to the tube walls. Next, as much liquid as possible was pipetted away, and the crystals were dried in the open tubes at 60 °C to a constant weight and homogenized.

For the mass spectrometry, three times 0.93 mg each of the silver phosphate powder (triplicate measurements) was weighted into tin capsules and vacuum dried at 60 °C for 48 h. The samples were then immediately transferred to an autosampler flushed with helium and pyrolyzed in a HEKAtech HT Oxygen Analyser. Quantitative pyrolysis was achieved in a SiC reaction tube at 1490 °C in the presence of glassy carbon covered with granulated carbon. The resulting carbon monoxide was transferred in a continuous He flow via a trap filled with Carbosorb and $MgClO_4$ and a gas chromatography column (GC, 70 °C) to the mass spectrometer (Delta V Advantage, Thermo Fisher Scientific). Stable oxygen isotopic ratios are reported as $\delta^{18}O_{phosphate}$ (*VSMOW*). Analytical precision was 0.2 ‰.

The oxygen isotopic ratio was calculated from the m/z ratios 30 and 28 in the mass spectrometer and by the use of the benzoic acid standards IAEA 601 ($\delta^{18}O = 23.3$ ‰) and 602 ($\delta^{18}O = 71.4$ ‰). Two additional standards were processed in the same way as the samples, namely, a phosphorite rock standard (NBS 120c, $\delta^{18}O = 22.6$, $n = 21$) and bone ash (SRM 1400, $\delta^{18}O = 17.1$ ‰, $n = 23$). The $\delta^{18}O$ value of the NBS 120c standard is in agreement with previously reported values (22.6 ± 0.1 ‰, Vennemann et al. 2002, and 22.4 ± 0.2 ‰, Fischer et al. 2013, respectively) but disagrees with lower values reported elsewhere (see Fischer et al. 2013 for discussion). Such differences are due to different calibration standards, phosphate extraction protocols or methods and facilities for isotope analyses (Vennemann et al. 2002). Triplicate analyses of 24 bone phosphate samples had an average standard deviation of 0.12 ‰. Oxygen concentration per sample was determined from the m/z ratios related to the weight used in the isotope analysis certified standards for elemental analyses and was used to check the purity of the extracted phosphate (Mayr et al. 2016).

Stable Oxygen Isotopes in the α-Cellulose of Modern Wood ($\delta^{18}O_{cellulose}$)

After manual removal of the bark, the wood samples were air-dried and homogenized to a fine powder in a ball mill. This powder was passed through a 125 μm sieve, and the remaining particles filled into polyester filter bags with a pore size of 25 μm. α-cellulose was purified according to Jayme (1942) and Gaudinski et al. (2005): A 24 h Soxhlet extraction with a mixture of toluene and ethanole (2:1) was followed by a second 24 h Soxhlet extraction with 95 % ethanole. Samples were then air-dried and boiled for a minimum of 4 h in distilled H_2O, whereby the water was changed until no further changes in colour occurred. For the following extraction steps, the filter bags must not be allowed to dry. Bleaching was achieved ultrasonically at 70 °C by the use of a solution made up of 7 g $NaClO_2$ dissolved in 500 mL distilled water, acidified with 3 mL glacial acetic acid. Every 2 h, another 7 g of sodium chlorite and 3 mL glacial acetic acid were added, and after 8 h total, the samples remained in the solution overnight at room temperature. After being washed four times ultrasonically with 70 °C distilled water for 15 min each, both the bleaching and washing step were repeated a second time. During the last wash in hot water, the water needs to be replaced every 15 min until the pH does not change any more. The filter bags were then placed into a filter flask in an ultrasonic bath (70 °C) and washed for another 4 h under continuous water flow. The remaining holocellulose was then washed four times ultrasonically for 15 min each with 2 L of cold water (about 4 °C).

For the solubilization of hemicellulose, the samples were then stirred in 500 mL 17 % NaOH solution for 1 h at room temperature. Afterwards, the samples were washed four times for 15 min each, and then for another 2 h under continuous water exchange. Sugars and sugar residues were then removed by an ultrasonical treatment of the samples in a solution made up of 450 mL distilled H_2O and 50 mL glacial acetic acid for 1 h. Finally, the filter bags with the purified α-cellulose were dried to a constant weight at 50 °C. 300 μg of α-cellulose each were weighed for mass spectrometry. α-cellulose standard C8002 (Sigma) was used for quality control. The purification protocol was validated by FTIR (Göhring 2014; Göhring et al. 2015). The oxygen isotope analysis was performed with the same device as reported for the bone apatite phosphate.

Stable Strontium and Lead Isotopes in the Bioapatite

The endosteal and periosteal surfaces of compact bone pieces (2–4 g) and all trabecular bone parts were removed by the use of a diamond-tipped saw. The sample was then divided into two parts, whereby one fragment was processed further for stable strontium and one for lead isotope analysis. To remove all remaining bone powder generated by the grinding process, the bone pieces were washed two times each ultrasonically with deionized H_2O for 5 min and air-dried. From now on, samples were manipulated wearing one-way gloves. Uncremated

bones were defatted for 5 h with diethylether in a Soxhlet reflux device and air-dried.

To also remove the inner sample surfaces, the bone/tooth pieces were etched ultrasonically at 35 kHz for 5 min in concentrated HCOOH* (98 %) for stable strontium isotope analysis and for 10 min in concentrated HCl** (37 %) for stable lead isotope analysis. Next, the specimens were washed ultrasonically with deionized H_2O until a pH between 5 and 6, air-dried, and the dry weight was recorded. The samples were then ashed for 12 h at 800 °C in a muffle furnace, and the weight of the ash was also recorded after cooling to room temperature for a calculation of the apatite yield. Last, the specimens were homogenized to a fine powder in a ball mill (ZrO_2 beakers).

For $^{87}Sr/^{86}Sr$ determination, a maximum of 50 mg homogenized apatite was wet ashed in 1 mL concentrated HNO_3*** (65 %) in closed Teflon cubes for 24 h on a hotplate at 100 °C, and the remaining liquid was evaporated at the same temperature overnight. For the following column separation, the sample was solubilized for a minimum of 20 min on a hotplate at 100 °C in 1 mL 10 N HNO_3*** and forwarded to the column separation (after Pin et al. 2003, modified by Vohberger 2011).

Column cleaning and conditioning was performed as follows: About 75 µL Sr-spec solubilized in H_2O** are loaded, divalent ions are removed with 0.8–1 mL 6 N HNO_3***, the column is rinsed with 0.8–1 mL H_2O**, Pb is removed with 0.8–1 mL 6 N HCl**, the column is rinsed with 0.8–1 mL H_2O**, and the column is finally conditioned with 100 µL 10 N HNO_3***. Next, 300 µL of the sample is loaded and flushed into the resin by adding 100 µL 10 N HNO_3*** followed by 200 µL, 600 µL and again 200 µL 10 N HNO_3 (elution of Rb and binding of Sr to the resin). Purified Sr is eluted by adding 1000 µL 0.05 N HNO_3***, and the liquid is evaporated on a hotplate at 100 °C. The sample is then again solubilized in 1000 µL 10 N HNO_3***, and the loading process is repeated with the complete 1000 µL sample volume. After evaporation of the remaining liquid, the sample was forwarded to mass spectrometry.

$^{87}Sr/^{86}Sr$ was analysed with a thermal ionisation mass spectrometer Finnigan MAT 261.5 on single tungsten filaments. Significant extant Rb was evaporated from the loaded filament by controlled preheating before the isotopic Sr composition was measured. A certified reference material served for quality control ($SrCO_3$, NIST SRM 987, $^{87}Sr/^{86}Sr$: 0.710219 ± 0.000059 STD, $n = 80$). Isotope mass fractionation during analysis was corrected by referencing to an invariant $^{88}Sr/^{86}Sr$ value of 8.37521. Total analytical uncertainty (precision + accuracy) for $^{87}Sr/^{86}Sr$ on natural samples was estimated to be <50 ppm. In addition, Standard Reference Material (SRM) 1400 "Bone Ash" (NIBS, Washington DC) was used with regard to the wet ashing and Rb-Sr separation ($^{87}Sr/^{86}Sr$: 0.713091 ± 0.000081, $n = 43$). Measurement precision was ± 0.00001 (Söllner et al. 2016).

For lead isotope analysis ($^{208}Pb/^{204}Pb$, $^{207}Pb/^{204}Pb$, $^{206}Pb/^{204}Pb$, $^{208}Pb/^{207}Pb$, $^{206}Pb/^{207}Pb$), 200 (± 1) mg homogenized bone/tooth sample was solubilized in 1 mL concentrated HNO_3***, evaporated for about 2 h under red light and wet ashed in closed quartz vessels for 4 h at 800 °C. The ashed sample was then moisturized with concentrated HBr, evaporated for 30 min under red light and

solubilized ultrasonically in 0.45 mL 0.5 N HBr for 1 minute at 35 kHz. The solution was then centrifuged for 3 min at 13,400 rpm and the supernatant forwarded to the column separation, which was performed in two steps (separation of Pb followed by a "clean-up").

For element separation columns were loaded with 40 μL Dowex (1×8) anion exchange resin which has been cleaned before by replicate flushing with 1 N HNO_3 and H_2O***. After cleaning columns were conditioned by adding 100 μL 0.5 N HBr. Next, the complete supernatant was loaded and Pb was purified by adding three times 200 μL 0.5 N HBr. After converting to chloride form by adding 250 μL 2 N HCl, Pb was eluted by adding two times 150 μL 6 N HCl. Then the sample was evaporated to dryness.

For the "Pb clean-up", the same resin was used after cleaning as described above. After conditioning with 100 μL 2 N HCl, samples were loaded in 100 μL 2 N HCl. Then Pb was cleaned by flushing the resin two times with 100 μL 2 N HCl. The purified Pb was eluted into PFA containers by adding two times 150 μL 6 N HCl. Before eluating, 1 μL $HClO_4$ was added to the beakers to destroy remaining organics during evaporation of the samples under red light. All reagents were of ultrapure grade, and equipments were thoroughly cleaned before using. The blanks of the complete analytical procedure were far below 1 ng Pb, which was regarded to be insignificant. Lead samples were loaded on precleaned rhenium filaments using the silica gel technique. Lead isotopic ratios were measured with a MAT Finnigan 261.5 mass spectrometer in static mode. Isotope mass fractionation during analysis was corrected with -0.1 ± 0.05 % per atomic mass unit, which was deduced from repeated analyses of the NBS 982 international standard. NIST Standard Reference Material NBS 982 served for quality control ($^{206}Pb/^{204}Pb = 36.75842 \pm 0.03473$, $^{206}Pb/^{207}Pb = 2.14129 \pm 0.00087$, $n = 83$) of the measurement. In addition, Standard Reference Material SRM 1400 "Bone Ash" (NIBS, Washington DC) was analysed with regard to test the laboratory processing protocol ($^{206}Pb/^{204}Pb = 18.36663 \pm 0.01188$, $^{206}Pb/^{207}Pb = 1.17229 \pm 0.00047$, $n = 132$).

Strontium Stable Isotopes in Soil

Soil samples were sieved through a 0.5 μm mesh. 300 mg of the sample was treated with 2 mL 35 % HCl** overnight at 120 °C. After evaporation of the acid, 1 mL of 65 % HNO_3** was added, and the sample was dissolved overnight at the same temperature. Remaining minerogenic particles were removed by centrifuging for 10 min at 11,000 rpm. The supernatant was transferred into Teflon cubes and inspissated overnight. In case the sample exhibited a conspicuous brown colour or appeared semi-fluid, an additional solubilization in 1 mL 65 % HNO_3** overnight was necessary. After evaporation of the acid prior to column separation, the sample was collected for a minimum of 20 min in 1 mL 6 N HNO_3*** on a hotplate at 100 °C. 300 μL sample was forwarded to the column separation (see above).

Results and Discussion

Isotopic Map of the Inn-Eisack-Adige Passage based on uncremated Archaeological Vertebrate Skeletons, augmented by modern Environmental Reference Samples

All measurement data obtained on animal skeletal finds are listed in Table 1. For very few individuals only, the amount was not sufficient for reliable measurements of lead or oxygen isotopes. Therefore, the complete data set consists of 219 samples for $^{87}Sr/^{86}Sr$, and 217 individuals for $\delta^{18}O_{phosphate}$ and lead isotopes, respectively. A summary of univariate statistics of all animals and all sites is given in Table 2. When the complete data set without differentiation per site of recovery is considered, no significant differences in any of the five isotopic ratios per species exist. Statistically, cattle, pig and red deer share the same data population in terms of their single isotopic signatures.

Since both strontium and lead are non-essential trace elements which are taken up in food and drinking water, these elements are mostly excreted. Atoms that remain in the body are sequestered into the bone mineral at calcium lattice positions. With regard to oxygen, however, species-specific metabolic and dietary peculiarities need to be taken into account. For animals, the primary oxygen source should be surface water, but the raw measurement data of $\delta^{18}O_{phosphate}$ are strongly biased by these aforementioned peculiarities. To account for that, species-specific regressions between $\delta^{18}O_{phosphate}$ and $\delta^{18}O_{water}$ have been established, namely:

$$\delta^{18}O_{phosphate,\,cattle} = (1.01 \pm 0.04) \times \delta^{18}O_{water} + 24.90 \text{ (D'Angela and Longinelli 1990)}, \quad (1)$$

$$\delta^{18}O_{phosphate,\,pig} = (0.86 \pm 0.05) \times \delta^{18}O_{water} + 22.71 \text{ (Longinelli 1984)}, \quad (2)$$

and

$$\delta^{18}O_{phosphate,\,deer} = (1.13 \pm 0.14) \times \delta^{18}O_{water} + 25.55 \text{ (D'Angela and Longinelli 1990)}. \quad (3)$$

After transformation of the $\delta^{18}O_{phosphate}$ into $\delta^{18}O_{water}$ data, the univariate statistics exhibit slight changes and so does the Kernel density plot (see below), but still, no species-specific differences are detectable: For cattle, $\delta^{18}O_{water}$ varies between −12.1 and −7.6 ‰ with a mean of −9.9 ± 0.93 ‰ and a median of −9.9 ‰; for pigs, variation is −11.9 to −7.7 ‰ with a mean of −9.7 ± 0.99 ‰ and a median of −9.7 ‰; and for red deer, variation is −11.5 to −7.5 ‰, with a mean of −9.6 ± 0.80 ‰ and a median of −9.6 ‰.

A relationship between isotopic signatures and spatial coordinates (latitude, longitude and altitude in meters a.s.l.) as indicated by the R^2 values remained mostly undetectable. Weak such relationships exist for $\delta^{18}O_{phosphate}$ and altitude in all species and for $\delta^{18}O_{phosphate}$ and latitude in pigs, for $^{87}Sr/^{86}Sr$ and latitude in

Table 2 Number of specimens (n), minimum, maximum and mean isotopic ratios with one standard deviation (sd) and median isotopic ratios for all animals and all sites, differentiated per species

	Cattle	Pig	Red deer
$\delta^{18}O_{phosphate}$			
n	88	81	48
Minimum	12.7	12.5	12.6
Maximum	16.5	16.1	17.1
Mean	14.8	14.4	14.7
sd	0.1	0.1	0.1
Median	14.9	14.4	14.7
$^{87}Sr/^{86}Sr$			
n	89	82	48
Minimum	0.70708	0.70809	0.70843
Maximum	0.72068	0.71876	0.72043
Mean	0.71154	0.71134	0.71128
sd	0.00305	0.00237	0.00301
Median	0.71034	0.71072	0.71019
$^{208}Pb/^{204}Pb$			
n	88	81	48
Minimum	38.1878	38.2927	38.2659
Maximum	38.8265	38.7769	38.6825
Mean	38.5376	38.5473	38.4848
sd	0.1118	0.1095	0.1037
Median	0.5414	38.565	38.4782
$^{207}Pb/^{204}Pb$			
n	88	81	48
Minimum	15.6043	15.6046	15.6105
Maximum	15.857	15.7914	15.7827
Mean	15.6547	15.6624	15.6573
sd	0.0359	0.0328	0.0375
Median	15.648	15.6585	15.6468
$^{206}Pb/^{204}Pb$			
n	88	81	48
Minimum	18.3299	18.421	18.4794
Maximum	21.3966	20.6645	20.4403
Mean	18.8843	18.9816	18.9453
sd	0.3968	0.4272	0.4447
Median	18.8109	18.8916	18.7919
$^{208}Pb/^{207}Pb$			
n	88	81	48
Minimum	2.4081	2.429	2.4392
Maximum	2.4766	2.4762	2.4736
Mean	2.4617	2.4611	2.4581
sd	0.0086	0.0078	0.0069
Median	2.4619	2.4619	2.4583

(continued)

Table 2 (continued)

	Cattle	Pig	Red deer
$^{206}Pb/^{207}Pb$			
n	88	81	48
Minimum	1.1722	1.1758	1.1822
Maximum	1.3492	1.3088	1.295
Mean	1.2063	1.2119	1.2099
sd	0.0229	0.0250	0.0259
Median	1.2017	1.2064	1.2028

all species and for $^{87}Sr/^{86}Sr$ and altitude in cattle and red deer, for $^{206}Pb/^{204}Pb$ and latitude in all species, for $^{208}Pb/^{207}Pb$ and latitude for cattle and for $^{206}Pb/^{207}Pb$ and latitude in all species (Table 3). In the reference area studied, variability of isotopic ratios by longitude obviously produced no valuable information with regard to provenance analysis, a result that is compatible with the negligible role of this spatial feature in the structural ranking of features in the course of the cluster analysis (see chapter "The Isotopic Fingerprint: New Methods of Data Mining and Similarity Search"). A variability of $\delta^{18}O$ by altitude meets expectations (see below), and also the spatial variability of isotopic ratios by latitude is informative especially with regard to $^{87}Sr/^{86}Sr$, $^{206}Pb/^{204}Pb$ and $^{206}Pb/^{207}Pb$. After transformation of $\delta^{18}O_{phosphate}$ into $\delta^{18}O_{water}$, the relationships between the isotopic signatures and coordinates are maintained ($R^2_{altitude} = 0.17$ for cattle, 0.26 for pigs, 0.23 for red deer; $R^2_{latitude} = 0.11$ for pigs).

In the following sections, the spatial distribution of isotopic signatures is mapped in the traditional way one by one. Mathematically, one or more of the isotope values of individual animals were outliers ($n = 21$, Table 4), but not a single individual represents such a statistical outlier with regard to all its isotopic signatures. In the traditional way of interpreting isotope values, either by comparing them one by one or in bivariate plots, these mathematical outliers would be considered indicators for "non-local" individuals on the site of their recovery. But since the specimens in this data set constitute statistical outliers either with regard to stable strontium isotopic ratios or to lead isotopic ratios, yet not a single specimen exhibits outliers for both strontium and lead, such a ready conclusion is possibly not justified. Mathematical outliers may have several underlying reasons whereby mobility is only one. The usually applied univariate statistical procedure can evaluate the structure of an existing data set but cannot take into account the small-scale variability of geological and soil conditions. Also species-specific home ranges or herding practices of domesticates will be of influence on the measurement data.

Boxplots and histograms are useful tools in univariate statistics for a graphic representation of data distributions, but the limitations, especially of the latter, are well known. Therefore, Kernel density estimates, which are of major benefit in

Table 3 R^2 values of regressions between isotopic ratios and spatial coordinates per species

	Cattle	Pig	Red deer
$\delta^{18}O_{phosphate}$			
n	88	81	48
Latitude	0.02	0.11	0.07
Longitude	0.04	0.04	0.02
Altitude	0.16	0.26	0.24
$^{87}Sr/^{86}Sr$			
n	89	82	48
Latitude	0.26	0.14	0.22
Longitude	0.04	0.04	0.05
Altitude	0.13	0.04	0.11
$^{208}Pb/^{204}Pb$			
n	88	81	48
Latitude	0.07	0.02	0.00
Longitude	0.05	0.00	0.03
Altitude	0.00	0.04	0.01
$^{207}Pb/^{204}Pb$			
n	88	81	48
Latitude	0.03	0.02	0.04
Longitude	0.04	0.01	0.00
Altitude	0.01	0.06	0.08
$^{206}Pb/^{204}Pb$			
n	88	81	48
Latitude	0.15	0.15	0.11
Longitude	0.05	0.01	0.00
Altitude	0.05	0.07	0.05
$^{208}Pb/^{207}Pb$			
n	88	81	48
Latitude	0.11	0.05	0.05
Longitude	0.00	0.01	0.02
Altitude	0.01	0.00	0.02
$^{206}Pb/^{207}Pb$			
n	88	81	48
Latitude	0.16	0.16	0.12
Longitude	0.05	0.00	0.00
Altitude	0.03	0.07	0.04

analytical chemistry, have been performed for each isotopic data population. A Kernel estimate visualizes the density function of a data population without the necessity of making a previous assumption on the data distribution (e.g. normal distribution; see Thompson 2006). It is conspicuous that additional peaks in the Kernel density plots (see below) are nearly exclusively related to the domesticated species and less frequently depicted in the stable isotopic ratios of free-ranging red deer. As mentioned in the introduction, the notion of an "isotopically local" sample

Table 4 Individual bone samples with mathematically outlying isotopic ratios (indicated in bold) according to univariate statistics

Site code, site name	Species	Bone/tooth	$^{87}Sr/^{86}Sr$	$^{208}Pb/^{204}Pb$	$^{207}Pb/^{204}Pb$	$^{206}Pb/^{204}Pb$	$^{208}Pb/^{207}Pb$	$^{206}Pb/^{207}Pb$
106, Berching-Pollanten	Cattle	Mandible	0.71060	**38.1878**	**15.8570**	**21.3966**	**2.4081**	**1.3492**
115, Griesstetten	Red deer	Metacarpus	0.71168	38.6386	**15.7222**	19.4937	2.4576	1.2399
127, Manching	Red deer	Phalanx 1	0.70912	38.4928	**15.7827**	**20.4403**	**2.4394**	**1.2950**
127	Red deer	Phalanx 1	0.70901	38.5028	**15.7600**	**20.1306**	**2.4431**	**1.2773**
127	Red deer	Phalanx 1	0.70957	38.5909	**15.7321**	**19.8473**	2.4531	1.2617
127	Cattle	Mandible	0.71027	38.4109	**15.7637**	**20.0858**	**2.4366**	**1.2741**
127	Pig	Mandible	0.71349	38.4124	**15.7543**	**20.0609**	**2.4383**	**1.2734**
114, Freising	Pig	Mandible	0.71042	38.3556	**15.7914**	**20.6645**	**2.4290**	**1.3088**
114	Pig	Mandible	0.71007	38.4423	**15.7654**	**20.4420**	**2.4386**	**1.2966**
108, Eching-IKEA	Red deer	Cranium	0.70885	38.6633	15.7215	**20.0275**	2.4592	1.2739
108	Cattle	Humerus	0.70888	38.6898	**15.7184**	**19.8617**	2.4613	1.2636
131, Pestenacker	Cattle	Mandible	0.70900	38.4575	**15.7916**	**19.9644**	**2.4353**	**1.2643**
229, Mieming	Red deer	Metatarsus	0.71041	38.2659	15.6880	**19.7480**	**2.4392**	**1.2588**
240, Hohe Birga	Red deer	Metatarsus	**0.72043**	38.6417	15.6724	18.6126	2.4656	1.1876
240	Pig	Humerus	**0.71876**	38.6371	15.6494	18.7086	2.4687	1.1955
240	Pig	Ulna	**0.71800**	38.6263	15.6518	18.7899	2.4680	1.2005
314, Brixen-Stufels Hotel Dominik	Red deer	Humerus	**0.71710**	38.6668	15.6324	18.6522	2.4736	1.1932
312, Brixen-Stufels "Russo"	Cattle	Humerus	**0.72068**	38.4867	15.6577	18.5685	2.4580	1.1859
301, Brixen-Stufels Hotel Dominik	Red deer	Metatarsus	**0.71796**	38.5822	15.6444	18.5790	2.4662	1.1876
301	Red deer	Radius	**0.71772**	38.6825	15.6573	18.9279	2.4704	1.2089
301	Red deer	Radius	**0.71834**	38.5913	15.6232	18.7069	2.4703	1.1975

is not exactly defined, and the exploitation of different microhabitats by free-ranging and domesticated vertebrates, thereby integrating different bioavailable isotopic ratios, is plausible. Therefore, while the simple spatial distribution of bioavailable isotopic ratios in the generated maps includes the 21 individual animals with statistically outlying measurement data in the first instance, these outliers were no longer included into the data set forwarded to data mining. In a second step, the outliers were plotted on the geographical map to evaluate whether a different place of provenance would indeed be the most plausible interpretation (see chapter "The Isotopic Fingerprint: New Methods of Data Mining and Similarity Search").

Stable Oxygen Isotopes

The distribution of the $\delta^{18}O_{phosphate}$ raw measurement data, and the transformation of these raw data into estimated $\delta^{18}O_{water}$ to account for species-specific metabolic peculiarities and drinking behaviour, is visualized both by boxplots (quartiles) and Kernel density plots (Figs. 3a–d). Not a single bone sample exhibits a statistically outlying isotopic ratio. As expected, the Kernel density is smoother in case of $\delta^{18}O_{water}$. It is conspicuous that only in the free-ranging red deer, the data are normally distributed with a very high probability ($\delta^{18}O_{phosphate}$, $p(\text{normal}) = 0.9990$ and 0.9993, Jarque-Bera and Monte Carlo tests, respectively; $\delta^{18}O_{water}$, $p(\text{normal}) = 0.9982$ and 0.9986, Jarque-Bera and Monte Carlo). The probability for a normal data distribution is only 0.05537 for $\delta^{18}O_{water}$ in cattle (Jarque-Bera) and is insignificant for all other oxygen isotope data sets. Additional peaks in the Kernel density are evidenced in the domesticated species only. Figure 4a, b shows the spatial distribution of $\delta^{18}O_{phosphate}$ and $\delta^{18}O_{precipitation}$ of the whole data set along the Alpine transect. Especially the northern Alpine foothills appear very uniform in terms of both isotopic ratios, and the inner Alpine regions exhibit the most ^{18}O-depleted values. It is conspicuous that $\delta^{18}O_{precipitation}$ values <-11.5 are restricted to the inner Alpine regions and only occasionally occur to the south of the Alps, which is indicative of individual drinking water sources that are probably related to the herd management of domesticates (see below).

A look at the raw measurement data reveals that total variability of $\delta^{18}O_{phosphate}$ ranges from 12.5 ‰ (site code 201) to 17.1 ‰ (site code 301). Median values are 15.0 ‰ for both Germany and Italy, while the inner Alpine median of 13.9 ‰ is significantly lower. Total variability per country is largest in Italy (12.6–17.1 ‰, $\Delta = 4.5$ ‰) despite the relative paucity of sampled archaeological sites, while the ranges are nearly identical in Austria (12.5–16.1 ‰, $\Delta = 3.6$ ‰) and Germany (13.0–16.5 ‰, $\Delta = 3.5$ ‰). Within one archaeological site, variability of $\delta^{18}O_{phosphate}$ is relatively stable around 1.9 ‰, although three different species are lumped together. Only at five sites (site codes 311, 215, 238, 108 and 312) is variability ≥ 3 ‰ and <1 ‰ at three other sites (site codes 310, 127 and 150). Overall, the relation of oxygen isotopic ratios with geographical location allows

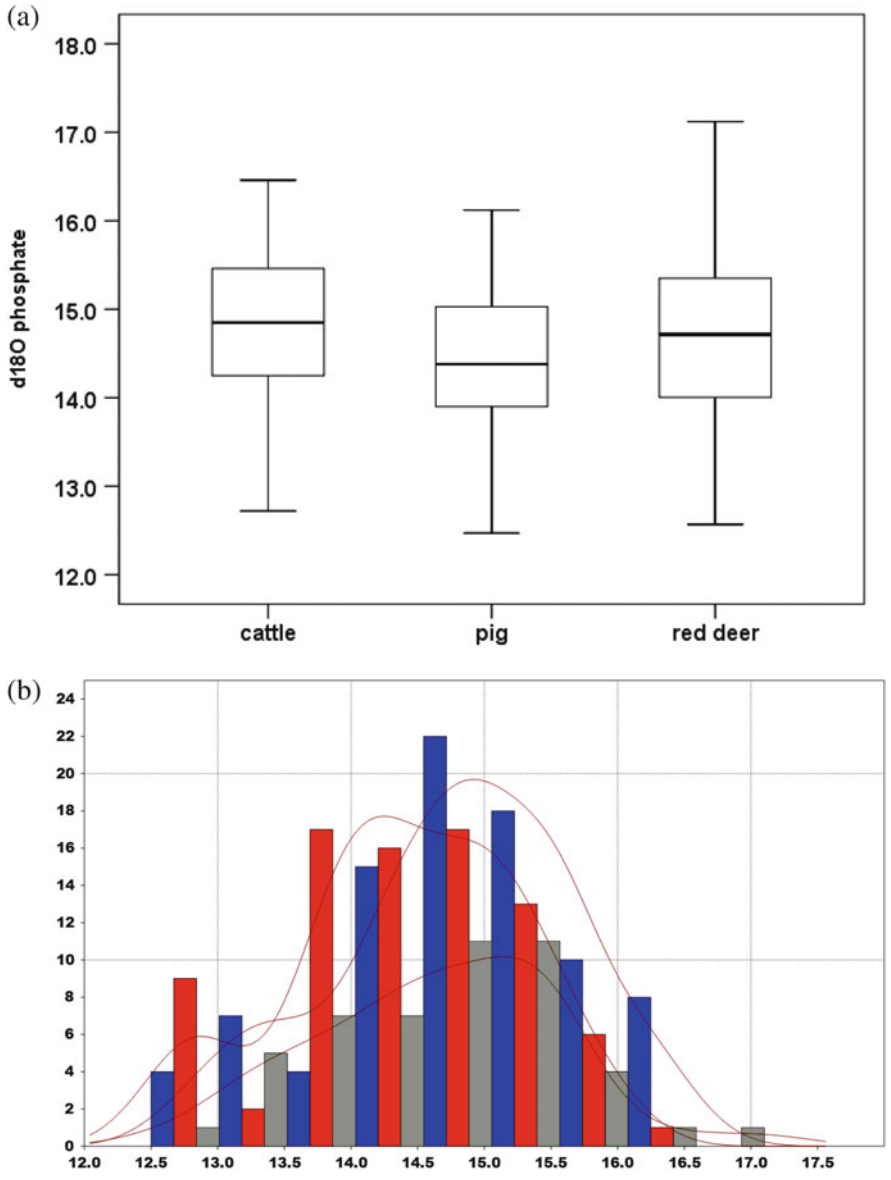

Fig. 3 Measurement data of $\delta^{18}O_{phosphate}$ and isotopic values transformed into $\delta^{18}O_{precipiation}$. (**a**) Boxplot (quartiles) of $\delta^{18}O_{phosphate}$ per species and (**b**) $\delta^{18}O_{phosphate}$ Kernel density plot. *Red*: cattle, *blue*: pig, *grey*: red deer; (**c**) Boxplot (quartiles) of $\delta^{18}O_{precipiation}$ per species and (**b**) $\delta^{18}O_{precipiation}$ Kernel density plot. *Red*: cattle, *blue*: pig, *grey*: red deer

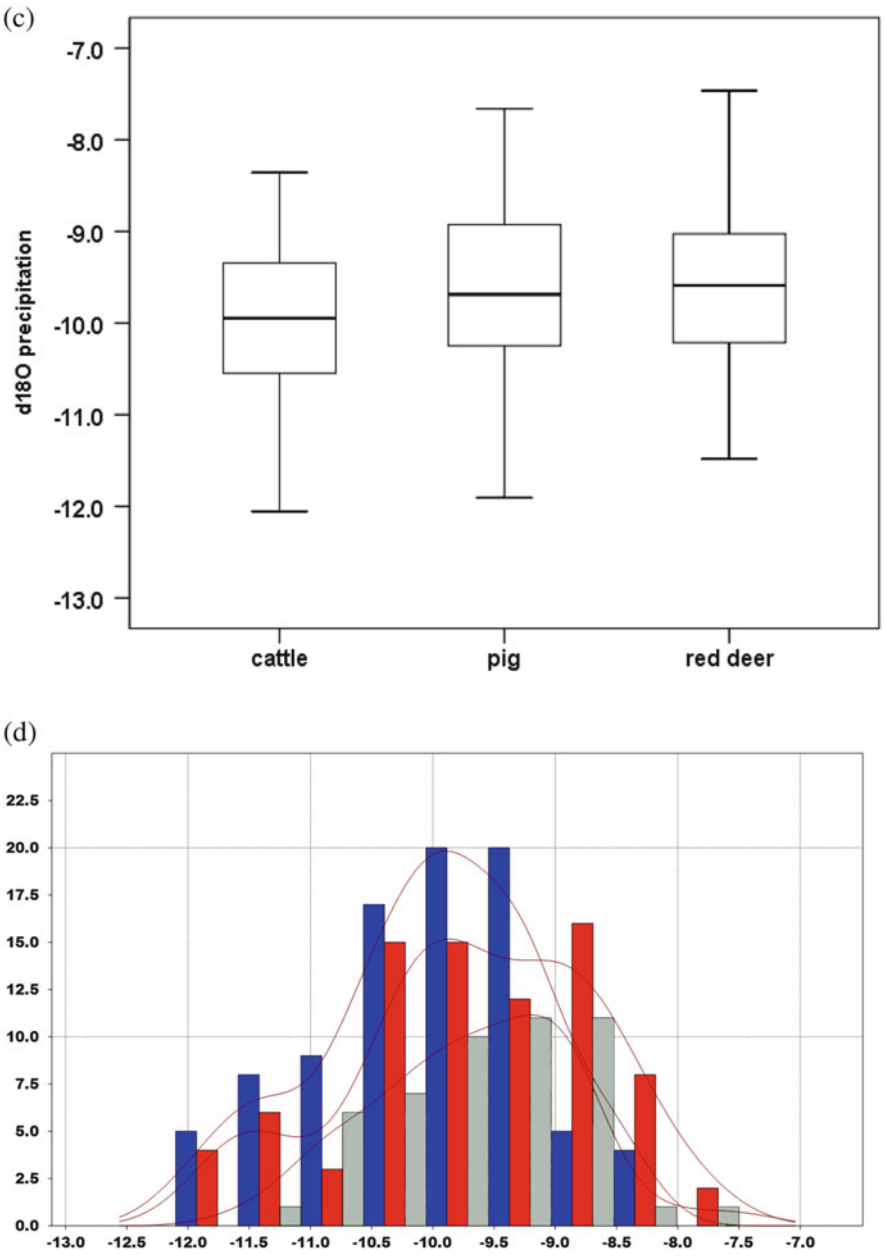

Fig. 3 (continued)

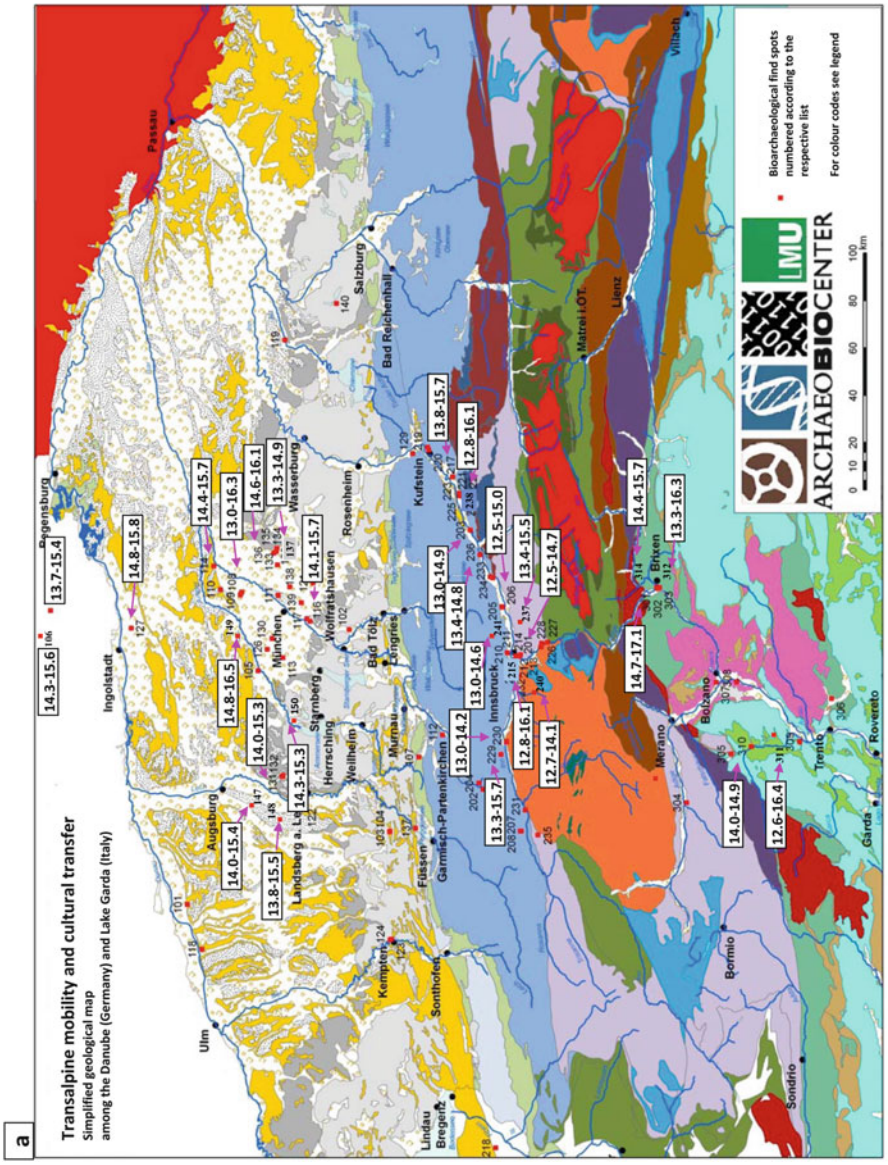

Fig. 4 Spatial distribution of stable oxygen isotopic ratios, complete data set. (**a**) $\delta^{18}O_{phosphate}$, (**b**) isotopic ratios transformed into $\delta^{18}O_{precipiation}$

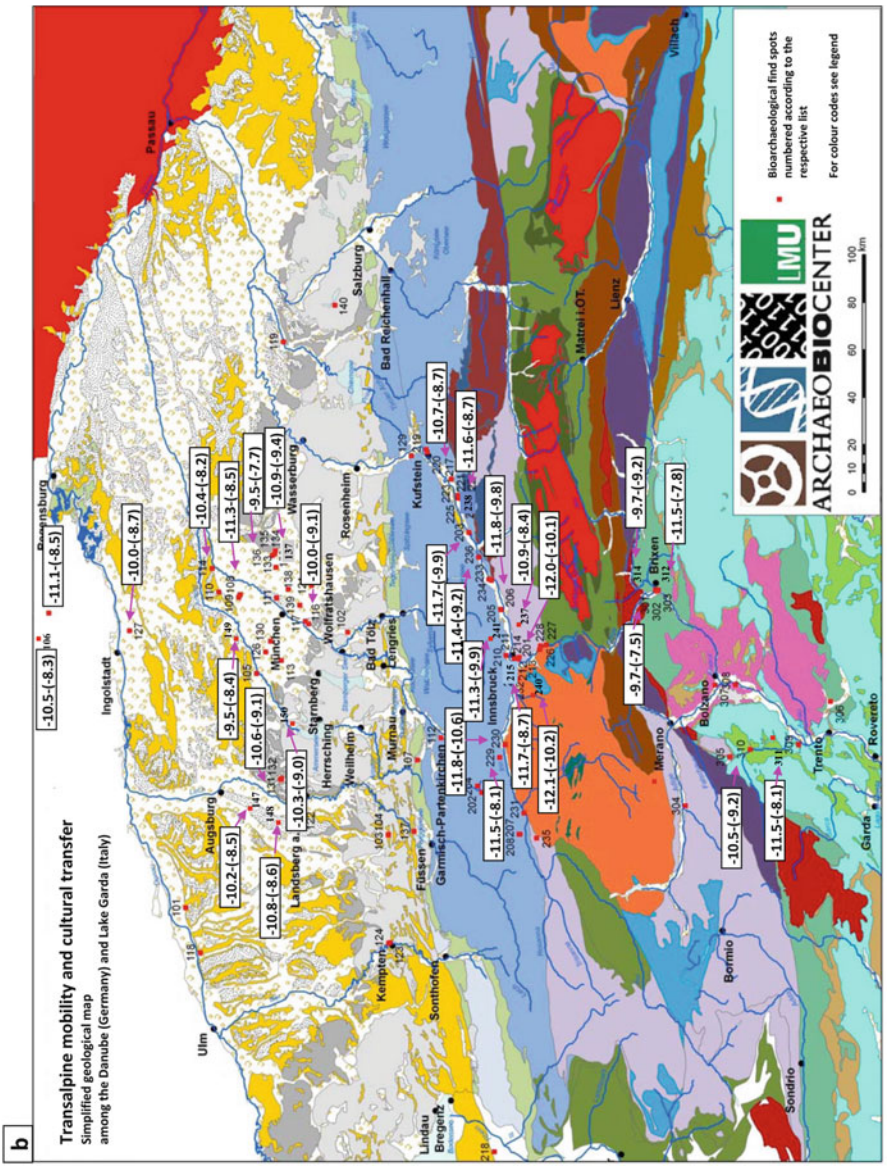

Fig. 4 (continued)

depicting general spatial gradients, but the data set does not permit a fine-scaled spatial resolution.

Altitude Effect of $\delta^{18}O_{phosphate}$

It was expected that any spatial information hidden in the $\delta^{18}O_{phosphate}$ values of the archaeological animal bones in the Alpine environment should largely relate to the altitude effect (see chapter "The Concept of Isotopic Landscapes: Modern Ecogeochemistry versus Bioarchaeology"). To test whether this was indeed the case, what would at the same time imply that the animal bone samples were appropriately chosen for the establishment of an isotopic map, a subsample of 118 specimens, namely, 26 deer, 47 cattle and 45 pig bones, was analysed with regard to this essential aspect at a relatively early stage of the project (Mayr et al. 2016). The samples originate from 16 sites and different archaeological horizons: Late Neolithic (115, Griesstetten; 131, Pestenacker), Bronze Age (114, Freising; 108, Eching; 236, Wiesing), Iron Age (106, Berching-Pollanten; 114, Freising; 127, Manching; 116, München-Grünwald; 229, Mieming; 237, Ampass-Widumfeld; 201, Bergisel; 312/314, Brixen-Stufels; 310, Sanzeno; 311, Zambana) and Roman Times (137, München-Unterhaching; 237, Ampass-Widumfeld). The Alpine transect is thus covered from north to south from Berching-Pollanten to Zambana with geographical coordinates from 49.14°N to 46.17°N and from 11.45°E to 11.08°E, spanning altitudes between 193 m a.s.l. (Zambana) and 792 m a.s.l. (Mieming). No consistent relationship between $\delta^{18}O_{phosphate}$ and time was detectable. Comparison with the geographical coordinates showed that the variation of oxygen isotopic ratios was mainly due to altitude (Mayr et al. 2016), a result that is maintained in the complete data set made up of 217 specimens (see Table 3). To erase the species effect, $\delta^{18}O_{phosphate}$ values were transformed into $\delta^{18}O_{water}$ by the use of the regressions published by Longinelli (1984) and D'Angela and Longinelli (1990) (Eqs. 1–3).

Slopes of the regression lines between $\delta^{18}O_{water}$ and altitude were -0.0026 ± 0.0007 for cattle, -0.00036 ± 0.0010 for pigs and -0.0018 ± 0.0010 for red deer, but interindividual variability per species remained too high to permit a firm allocation of specific individuals to a certain altitude (Mayr et al. 2016). This is not unexpected, because an archaeofaunal assemblage accumulates over many years. Therefore, individuals of the same taxon should have hardly lived under the same conditions, including access to drinking water sources, herding practices and small-scale fluctuations in climate and precipitation. To minimize such differences, all calculated $\delta^{18}O_{water}$ values per site were averaged. Only the pigs from the southernmost Zambana site were significantly depleted with ^{18}O and did not fit into the new regression, which strongly supports our assumption of the underlying reasons for the considerable interindividual variability observed. Zambana is located at the lowest altitude of the Alpine transect in the Adige River valley. Field observations during the collection of modern reference samples suggest that until today wells at this site are fed by groundwater infiltrating from the

river, the catchment of which is reaching considerably higher altitudes. Therefore, local water sources of the pigs may have been influenced by the river water and thus do not mirror the actual altitude of the site. Excluding the Zambana pigs, a significant correlation following the equation

$$\delta^{18}O_{water} = (-0.0030 \pm 0.0014) \times \text{altitude} - (7.95 \pm 0.77) \quad (4)$$

was found (Mayr et al. 2016). It is noteworthy that the average calculated $\delta^{18}O_{water}$ values plot perfectly on the regression between $\delta^{18}O_{precipitation}$ and altitude that has recently been published by Kern et al. (2014). The authors evaluated the stable oxygen isotopic signature in precipitation at 39 stations in Switzerland between 1995 and 2000 and found a relationship between altitude (below 2000 m a.s.l.) and annual amount-weighted $\delta^{18}O_{precipitation}$ values following the equation

$$\delta^{18}O \text{ meteoric water} = -0.0034 \times \text{altitude} - 7.79 \quad (5)$$

(Kern et al. 2014). Within errors of slopes and intercepts, the equations provided by Mayr et al. (2016) and Kern et al. (2014) are indistinguishable from each other. We conclude that the general altitude effect of $\delta^{18}O$ in precipitation of the Alpine transect studied in our project is adequately integrated by the $\delta^{18}O_{phosphate}$ of archaeological vertebrates transformed into $\delta^{18}O_{water}$, and that the choice of samples for the isotopic map was appropriate with regard to $\delta^{18}O$.

Still, some lessons are to be learned from these results. First, it is clearly demonstrated that quite a large amount of data needs to be available for approximating palaeo-altitudes by the use of bioarchaeological finds. Only 26 red deer specimens were available for this subproject, and we cannot exclude that this small sample size is responsible for the considerably weaker correlation between reconstructed $\delta^{18}O_{water/precipitation}$ (red deer) and altitude compared to the regressions for pigs and cattle. But large home ranges and seasonal migration might also have been responsible for this. The example of the pigs from the Zambana site suggests that these animals either spent their lives at a place different from the one where the slaughter remains had been deposited or that their drinking water sources originated from much higher altitudes and did not reflect local meteoric water $\delta^{18}O$ (Mayr et al. 2016).

Comparison of $\delta^{18}O_{phosphate}$ with $\delta^{18}O_{carbonate}$ in Animal Bones

$\delta^{18}O$ in skeletal apatite can be either measured in the phosphate group or in the structural carbonate that substitutes for both the hydroxyl and the phosphate group in vivo. In the course of measuring stable isotopes of light elements such as carbon for the purpose of reconstructing palaeodiet, $\delta^{18}O_{carbonate}$ is usually measured together with $\delta^{13}C_{carbonate}$. In addition, the purification of structural carbonate does not need much more than a deproteination of the sample, while phosphate is purified by the use of a silver phosphate precipitation method that affords many

more laboratory steps including the manipulation of dangerous chemicals such as hydrofluoric acid. Many researchers make use of these analytical benefits to gain information on the drinking water source of the individuals in question by measuring $\delta^{18}O_{carbonate}$, which is related to ecogeographical features (see chapter "The Concept of Isotopic Landscapes: Modern Ecogeochemistry versus Bioarchaeology"). Although "reasonable" information can be obtained this way, the reliability of $\delta^{18}O_{carbonate}$ was questioned early on and claimed inferior to $\delta^{18}O_{phosphate}$ because the P–O bonds in the apatite crystals are stronger and less prone to diagenesis (Lee-Thorp 2002). Shortly thereafter, Zazzo et al. (2004) were able to show that this assumption only holds as long as no biogenic decomposition processes are involved, which is readily explained by the microbial phosphate metabolism. Bacteria are important vectors within the geochemical phosphate cycle (Blake et al. 1998) because most of them can take up inorganic phosphorus only. This P_i is released from phosphate molecules by enzymatic reactions that necessarily happens outside the cell and hence under open-system conditions (Blake et al. 1997). In temperate climates, biogenic bone decomposition plays a major role. Therefore, the question arises whether the spatial information hidden in bone apatite $\delta^{18}O$ is best derived from $\delta^{18}O_{phosphate}$ or $\delta^{18}O_{carbonate}$.

To answer this question with regard to the specimens analysed in the frame of the transalpine study, both $\delta^{18}O_{carbonate}$ and $\delta^{18}O_{phosphate}$ were measured in a subsample of 91 animal bones (Table 5). Total variability of all $\delta^{18}O$ values was considerably higher in the structural carbonate (17.32–23.44 ‰, $\Delta = 6.12$ ‰) compared to the apatite phosphate (12.47–17.12 ‰, $\Delta = 4.65$ ‰). This holds also for a separate consideration per species: while $\delta^{18}O_{phosphate}$ varies between 3.22 and 3.89 ‰, variability of $\delta^{18}O_{carbonate}$ reaches values up to 5.84 ‰ in cattle. A look at the data by site reveals that an individual of a certain taxon that, for example, exhibits the highest $\delta^{18}O_{phosphate}$ value at a particular site does not necessarily also exhibit the highest $\delta^{18}O_{carbonate}$ value. If both $\delta^{18}O$ signatures were equally reliable ecogeographical indicators, the order from minimum to maximum isotopic ratio in individuals of the same species per site should have been maintained. This was, however, only the case for 5 out of 12 sites, namely, Freising (site code 114), Pestenacker (site code 131), Unterhaching (site code 137), Bergisel (site code 201) and Zambana (site code 311) (Lihl 2014).

This result contradicts the seminal publications by Iacumin et al. (1996), Pellegrini et al. (2011) and Chenery et al. (2012) who all found a very strong linear correlation between $\delta^{18}O_{carbonate}$ and $\delta^{18}O_{phosphate}$ and an offset between these two data of around 9 ‰ within the same skeletal sample. Accordingly, such a strong correlation was not found in the data set of the transalpine project (Lihl 2014). We explain the higher stability of the $\delta^{18}O_{phosphate}$ signals in our data set as mainly resulting from physiological reasons. Bryant et al. (1996) emphasized that different enzymes, namely, ATPases in the case of phosphate and carbonic anhydrases in the case of carbonate, mediate the oxygen exchange between the stoichiometric groups in the apatite and body water. Also Pellegrini et al. (2011) admitted that the strong linear relationship postulated between the $\delta^{18}O$ values needs not hold in every instance because phosphate and carbonate might precipitate from different body

Table 5 Comparison of $\delta^{18}O_{carbonate}$ with $\delta^{18}O_{phosphate}$ in a subsample of 91 archaeological animal bones

Site code	Site name	Lab no.	Species	$\delta^{18}O_{carbonate}$	$\delta^{18}O_{phosphate}$	$\Delta\delta_{carb\text{-}phos}$
106	Berching	106.1	Cattle	22.3	14.3	8.0
		106.2	Cattle	22.5	15.1	7.1
		106.4	Cattle	22.2	14.6	7.6
		106.5	Pig	22.4	15.2	7.3
		106.7	Pig	22.0	14.8	7.2
		106.9	Pig	22.8	15.6	7.2
		106.13	Red deer	22.0	14.9	7.1
		106.14	Red deer	23.4	15.5	8.0
		106.15	Red deer	22.1	15.6	6.5
115	Griesstetten	115.11	Cattle	20.6	15.4	5.2
		115.14	Cattle	18.9	15.4	3.5
		115.15	Cattle	17.3	13.7	3.6
		115.2	Pig	21.6	15.0	6.5
		115.3	Pig	22.1	15.4	6.7
		115.4	Pig	21.6	15.2	6.4
		115.7	Red deer	21.9	15.4	6.5
		115.8	Red deer	22.0	14.9	7.1
		115.9	Red deer	22.0	15.2	6.9
114	Freising	114.1	Cattle	22.5	14.4	8.0
		114.3	Cattle	22.8	15.6	7.2
		114.5	Cattle	23.0	15.7	7.3
		114.6	Pig	22.6	15.2	7.4
		114.7	Pig	23.3	15.7	7.7
		114.8	Pig	22.7	15.7	7.1
		114.11	Red deer	23.3	15.5	7.7
		114.12	Red deer	22.2	14.6	7.7
		114.13	Red deer	22.6	15.5	7.2
131	Pestenacker	131.6	Cattle	19.9	14.4	5.5
		131.7	Cattle	20.6	14.2	6.4
		131.9	Cattle	20.2	15.0	5.2
		131.11	Pig	19.8	14.4	5.4
		131.12	Pig	20.3	14.3	6.0
		131.14	Pig	19.1	14.0	5.1
		131.1	Red deer	20.7	14.5	6.2
		131.2	Red deer	20.3	14.3	6.1
		131.5	Red deer	22.8	15.3	7.6
137	Unterhaching	137.1	Cattle	22.4	14.7	7.7
		137.4	Cattle	22.5	14.9	7.6
		137.5	Cattle	22.7	14.9	7.8
		137.6	Pig	22.0	14.6	7.3
		137.14	Pig	22.0	14.6	7.4
		137.15	Pig	21.7	14.3	7.5
		137.11	Red deer	10.3	13.2	6.1
		137.12	Red deer	21.8	14.1	7.7
		137.13	Red deer	20.1	13.9	6.2

(continued)

Table 5 (continued)

Site code	Site name	Lab no.	Species	$\delta^{18}O_{carbonate}$	$\delta^{18}O_{phosphate}$	$\Delta\delta_{carb\text{-}phos}$
236	Wiesing	236.1	Cattle	21.4	14.1	7.4
		236.2	Cattle	20.7	13.4	7.4
		236.3	Cattle	21.3	13.7	7.6
		236.6	Pig	20.2	13.9	6.3
		236.7	Pig	21.5	14.8	6.6
		236.8	Pig	21.6	14.4	7.3
237	Ampass	237.1	Cattle	20.9	14.3	6.6
		237.2	Cattle	21.4	14.3	7.1
		237.4	Cattle	20.9	14.8	6.1
		237.6	Pig	20.5	14.4	6.1
		237.7	Pig	20.3	13.4	6.9
		237.8	Pig	21.8	15.5	6.3
		237.11	Red deer	21.0	14.6	6.4
201	Bergisel	201.1	Cattle	20.9	12.8	8.0
		201.3	Cattle	22.2	14.7	7.5
		201.5	Cattle	22.4	14.7	7.8
		201.6	Pig	20.6	12.5	8.1
		201.7	Pig	21.4	13.1	8.2
		201.8	Pig	21.4	13.7	7.7
301	Brixen Hotel Dominik	301.9	Cattle	20.1	15.1	5.0
		301.10	Cattle	21.5	15.1	6.4
		201.12	Cattle	21.1	16.1	6.1
		301.5	Pig	21.9	15.7	6.2
		301.7	Pig	21.2	15.1	6.1
		301.8	Pig	20.2	14.7	5.6
		301.1	Red deer	22.0	17.1	4.8
		301.2	Red deer	22.3	15.6	6.7
		301.3	Red deer	20.6	14.9	5.8
314	Siebeneich	314.1	Cattle	22.1	15.5	6.6
		314.2	Cattle	21.8	15.6	6.2
		314.3	Cattle	21.9	15.7	6.3
		314.6	Pig	21.1	14.4	6.7
		314.7	Red deer	20.1	15.0	5.1
310	Sanzeno	310.7	Cattle	21.4	14.9	6.6
		310.8	Cattle	21.5	14.3	7.3
		310.9	Cattle	22.2	14.8	7.5
		310.3	Pig	21.3	14.0	7.3
		310.4	Pig	21.8	14.8	7.0
		310.6	Pig	22.4	14.2	8.2
311	Zambana	311.6	Cattle	23.2	14.9	8.3
		311.7	Cattle	22.2	15.7	6.5
		311.9	Cattle	23.2	16.2	7.0
		311.2	Pig	20.9	13.7	7.2
		311.3	Pig	21.1	14.2	6.9
		311.4	Pig	21.5	14.1	7.3

water components. This assumption is strongly supported by the fact that carbonate occurs in the form of solubilized bicarbonate in blood and is therefore in constant isotopic equilibrium with dissolved CO_2 (Podlesak et al. 2008), while phosphate is involved in a variety of metabolic reactions and therefore maintains a constant exchange with the body fluids (Blake et al. 1997). Luz and Kolodny (1989) emphasized that different turnover rates of skeletal elements are responsible for varying biological half-lives of the phosphate groups, but this developmental aspect does not account for our results because $\delta^{18}O_{carbonate}$ and $\delta^{18}O_{phosphate}$ were measured from one and the same skeletal sample (Lihl 2014).

It cannot be firmly decided at this stage whether the lack of a correlation between the $\delta^{18}O$ signatures in the apatite phosphate and structural carbonate in the transalpine data set is due to special burial conditions at the sampling sites or due to the considerably reduced spatial distribution of the sampling sites and the different archaeological dates compared to the earlier publications mentioned above. The conclusion that has to be drawn from this comparative study is that for the scope of an isotopic mapping of bioarchaeological finds in the reference region, $\delta^{18}O_{phosphate}$ has to be preferred over $\delta^{18}O_{carbonate}$. But even without consideration of possible sampling biases, the fact remains that bioapatite is a carbonated hydroxylapatite (see chapter "The Crystalline State of Archaeological Bone Material"). Therefore, the stoichiometric phosphate group is always an integral part of the bone mineral, while the structural carbonate is always a substitute for either the hydroxyl or the phosphate group which involves different and additional metabolic processes.

$\delta^{18}O$ in Modern α-Cellulose and Water Reference Samples

To further test whether $\delta^{18}O$ in archaeological animal bone apatite reliably reflects the ecogeographical variability of stable oxygen isotopes in precipitation of the reference area, both modern groundwater and spring water ($n = 20$) and $\delta^{18}O_{cellulose}$ of wood ($n = 24$, 9 species) were analysed (Table 6).

$\delta^{18}O_{cellulose}$ values were significantly higher in the Italian samples compared to wood from the Austrian sites ($p = 0.0031$; Fig. 5), but no clear altitude effect was detectable. At best, a tendency to more positive stable oxygen isotopic ratios >28 ‰ at lower altitudes was evident (Table 5, Fig. 6) (Göhring et al. 2015). Species-specific differences in α-cellulose can be significant (e.g. Song et al. 2014) and were indeed as large as 3.78 ‰ between hazelnut and apple tree wood at the Sanzeno site (site code 310). Considering the most abundant wood species in our sample only, namely, hazelnut (*Corylus avellana*, $n = 15$), the correlation between $\delta^{18}O_{cellulose}$ and latitude becomes much stronger and rises from $r = -0.55$ ($p = 0.0071$, complete data set) to $r = -0.80$ ($p = 0.0004$, hazelnut only) (Fig. 7; Göhring et al. 2015).

Only three spring water samples as representatives for meteoric water were available opposed to 17 groundwater samples. The latter were significantly depleted in ^{18}O ($p = 0.02$). In contrast to the isotopic ratios measured in α-cellulose, no general relationship between longitude and latitude was detected.

Table 6 $\delta^{18}O$ of modern reference samples (water, α-cellulose) (Göhring et al. 2015)

Site name	Latitude (°N)	Longitude (°E)	Meter a.s.l.	Site code-lab no.	Water	$\delta^{18}O_{water}$ (*VSMOW*)	Site code-lab no.	Cellulose wood	$\delta^{18}O_{cellulose}$ (*VSMOW*)
Kirchbichl	47.49	12.08	531	217–2	Groundwater	−11.6			
Kundl	47.45	12.01	573	224–3	Precipitation	−10.6			
Brixlegg	47.43	11.8	606	203–2	Groundwater	−10.4	203–4	*Corylus*	26.7
Ehrwald	47.39	10.91	998	204–3	Groundwater	−12.8			
Ehrwald	47.4	10.92	1001				204–4	*Corylus*	27.7
Wiesing	47.39	11.79	614				236–3	*Corylus*	26.7
Bieberwier	47.38	10.89	1001	202–3	Groundwater	−11.3	202–2	*Corylus*	27.9
Fritzens	47.31	11.58	805				206–2	*Corylus*	26.4
Fritzens (valley)	47.31	11.59	816	206–4	Groundwater	−11.3			
Fritzens (valley)	47.3	11.58	613	205–2	Groundwater	−11.8			
Pfaffenhofen	47.29	11.07	822	230–6	Groundwater	−10.3			
Pfaffenhofen	47.29	11.07	860				230–3	*Corylus*	26.6
Hötting	47.28	11.41	630	215–2	Groundwater	−12.9			
Hötting	47.26	11.41	625	215–3	Groundwater	−13	215–4	*Corylus*	28.5
Mieming	47.28	10.06	792				229–2	*Corylus*	28.2
Ampass	47.26	11.46	658				237–103	*Corylus*	26.8
Völs	47.25	11.35	587				232–6	*Juglans*	25.5
Völs	47.24	11.38	636				232–11	*Corylus*	27.2
Wilten	47.24	11.4	726				212–2	*Corylus*	27.9
Imst	47.24	10.73	803	207–3	Groundwater	−13			
Imst	47.24	10.73	817				207–2	*Prunus*	28.1
Roppen	47.22	10.81	759	231–2	Groundwater	−13.9	231–3	*Corylus*	29.3
Wenns	47.17	10.73	1020	235–2	Groundwater	−13.6	235–3	*Corylus*	27.9

(continued)

Table 6 (continued)

Site name	Latitude (°N)	Longitude (°E)	Meter a.s.l.	Site code-lab no.	Water	$\delta^{18}O_{water}$ (*VSMOW*)	Site code-lab no.	Cellulose wood	$\delta^{18}O_{cellulose}$ (*VSMOW*)
Matrei	47.16	11.43	963	227–5	Precipitation	−10.7			
Matrei	47.16	11.44	938				227	*Sambucus*	27.4
Matrei/ Brenner	47.13	11.45	993	228–1	Groundwater	−12.2			
Elvas	46.73	11.56	703				312–103	*Ribes*	30.3
Brixen	46.71	11.65	553				302–4	*Corylus*	30.8
Latsch	46.5	10.91	1238	304–104	Groundwater	−12			
Siebeneich	46.51	11.28	366	314–3	Precipitation	−9.5	314–104	*Quercus*	30
Pfatten	46.38	11.28	246				308–106	*Acacia*	29.8
Pfatten	46.41	11.27	214	308–108	Groundwater	−11			
Sanzeno	46.36	11.07	660	310–105	Groundwater	−10.7			
Sanzeno	46.37	11.08	683				310–104	*Corylus*	30.3
Sanzeno	46.37	11.08	683				310–103	*Malus*	26.6
Zambana	46.15	11.07	213	311–106	Groundwater	−10.2			
Zambana	46.15	11.09	200				311–105	*Fraxinus*	28.1

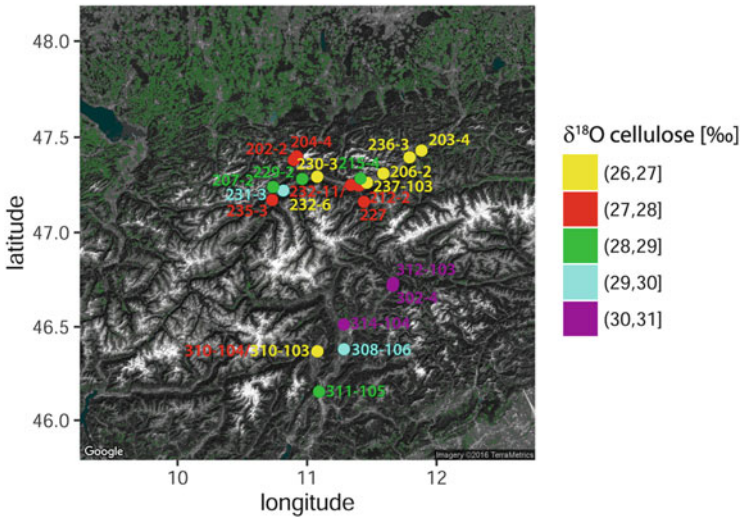

Fig. 5 $\delta^{18}O_{cellulose}$ plotted by latitude and longitude, sampled sites are labelled with site codes. Figure by A. Göhring, created in R

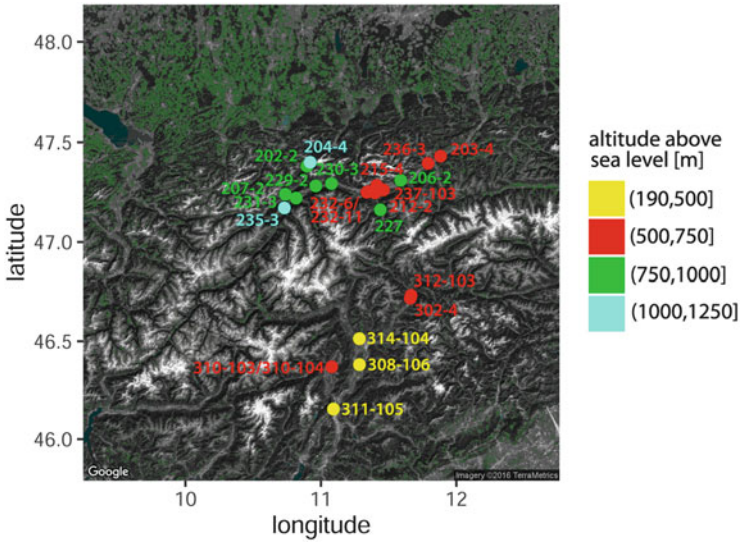

Fig. 6 Altitude of sampling sites for modern reference vegetation samples. Figure by A. Göhring, created in R

Only when the Austrian samples were considered separately, a significant correlation between longitude and $\delta^{18}O_{water}$ becomes evident (Fig. 8; $r = 0.58$, $p = 0.023$) (Göhring et al. 2015). The correlation with altitude however was significant

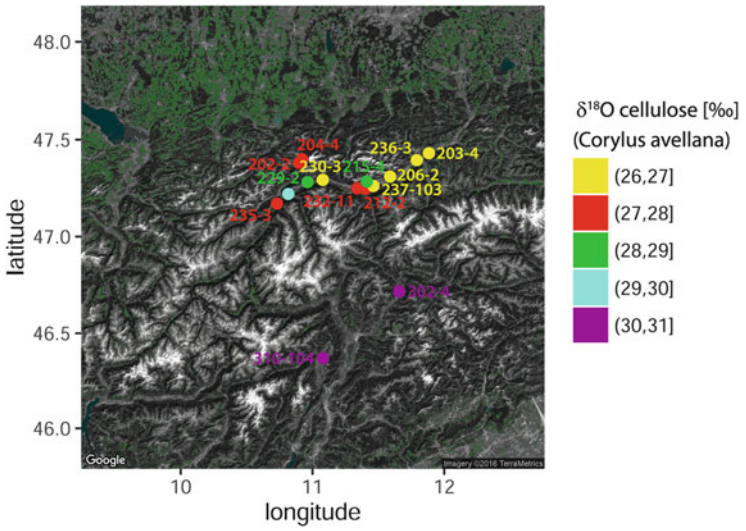

Fig. 7 Latitude effect of $\delta^{18}O_{cellulose}$ in *Corylus avellana*. Figure by A. Göhring, created in R

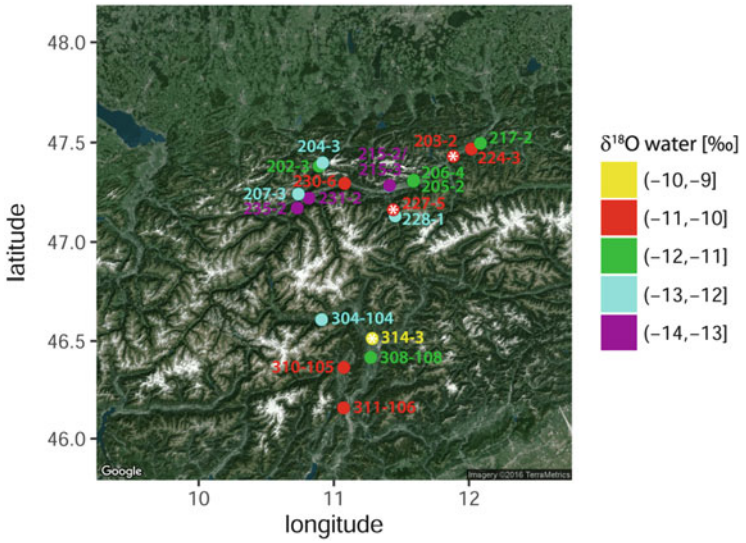

Fig. 8 Spatial distribution of modern $\delta^{18}O_{water}$ with site code labels. Three spring water samples are marked with an asterisk. Figure by A. Göhring, created in R

($r = -0.45$, $p = 0.05$). The general altitude effect between the lowest (Zambana, 213 m a.s.l.) and the highest sampling site (Latsch, 1238 m a.s.l.) is −0.18 ‰ per 100 m and thus in very good agreement with the respective overall gradient published by Humer et al. (1995) but less than the gradient reported by Kern

et al. (2014). Considering the Austrian sites separately, the gradient is much steeper with −0.41 ‰ between the lowest and the highest sampling site (Kirchbichl, 531 m a.s.l., and Wenns, 1020 m a.s.l., respectively) (Göhring et al. 2015).

Both modern α-cellulose and water therefore exhibit $\delta^{18}O$ values that permit a separation between samples taken along the Inn-Eisack-Adige passage that originate in Austria and Italy, respectively. This can be related to the different origin of the precipitating air masses and indicates the potential use of $\delta^{18}O_{cellulose}$ for isotopic mapping of the Alpine transect, whereby a restriction to a single wood species is advisable. Also the negative correlation between $\delta^{18}O_{water}$ and altitude meets expectations. Declining temperatures and the preferential rainout of $H_2{}^{18}O$ (Marshall et al. 2007) lead to ^{18}O depleted meteoric water at higher altitudes. Since altitude rises in Austria from east to west and in Italy from south to north in our reference area, the relationships between $\delta^{18}O_{water}$ and both latitude and longitude are evident. Although no clear correlation was found between $\delta^{18}O_{cellulose}$ and altitude, an indirect altitude effect should nevertheless exist: $\delta^{18}O_{cellulose}$ is negatively correlated with latitude, which in turn is positively correlated with altitude in the Alpine transect. The limited sample size could be responsible for this indirect effect, but also the influence of site-specific climatic parameters such as air humidity and water availability plays a large role as demonstrated by growth chamber experiments (Mayr et al. 2002).

Strontium Stable Isotopes ($^{87}Sr/^{86}Sr_{apatite}$)

The distribution of $^{87}Sr/^{86}Sr$ isotopic ratios per species over all sites is illustrated in Fig. 9. Only a few individuals exhibited particularly high $^{87}Sr/^{86}Sr$ ratios and were identified as mathematical outliers, whereby one cow and four out of five red deer were recovered at the Brixen-Stufels site (see Table 4). The Kernel density plot shows a second peak at $^{87}Sr/^{86}Sr \approx 0.716$, which is largely restricted to the domesticates. Since individual red deer also exhibit such high isotopic ratios, the predominance of domesticates might be due to the smaller sample size of this free-ranging species ($n = 48$ compared to $n > 80$ in cattle and pigs, Table 2). Five mathematical outliers, however, correspond to 10.4 % of the complete red deer data set. The spatial distribution of bone apatite $^{87}Sr/^{86}Sr$ of all species per site is visualized by Fig. 10.

Total variability of $^{87}Sr/^{86}Sr$ along the Alpine transect ranges from 0.7071 (Griesstetten, site code 115) to 0.7207 (Brixen-Stufels, site code 312) which makes a considerable difference of $\Delta = 0.0136$. With regard to the regional median values, a north-to-south trend is recognizable, namely, from 0.7095 (0.7071–0.7135, $\Delta = 0.0064$) in Germany over 0.7120 (0.7092–0.7204, $\Delta = 0.0112$) in Austria to 0.7152 (0.7085–0.7207, $\Delta = 0.0122$) in Italy. Definition of place of origin for those individuals exhibiting a $^{87}Sr/^{86}Sr \leq 0.710$ is however impossible, because such values occur in the north and south and in the inner Alpine regions as well. Nevertheless, low $^{87}Sr/^{86}Sr$ isotopic ratios around 0.7095, coupled with the least variability, are found in the alluvial plains of southern Germany. In

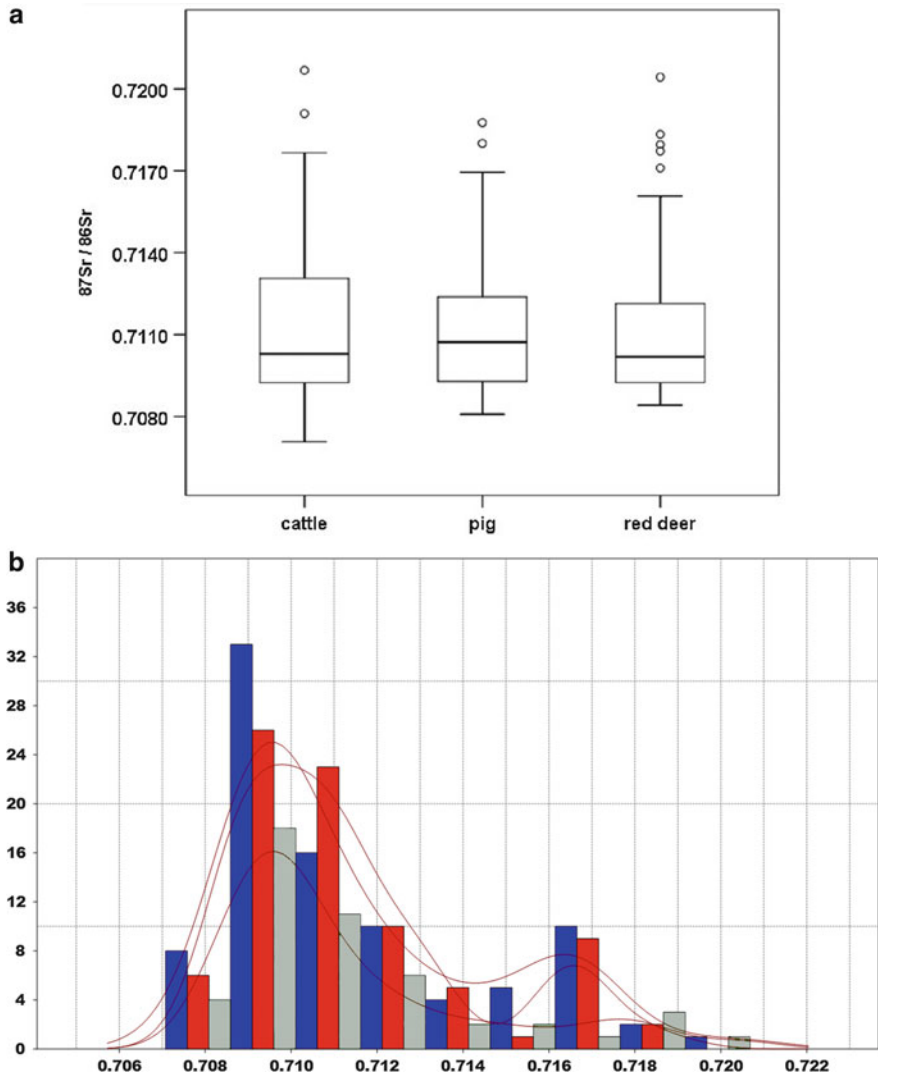

Fig. 9 Measurement data of apatite $^{87}Sr/^{86}Sr$. (**a**) Boxplot (quartiles) of $^{87}Sr/^{86}Sr$ per species and (**b**) $^{87}Sr/^{86}Sr$ Kernel density plot. *Red*: cattle, *blue*: pig, *grey*: red deer

this area, only two out of 106 specimens exhibit a $^{87}Sr/^{86}Sr$ value >0.71 (Manching, site code 127, 0.7135; Schwabmünchen, site code 148, 0.7129); otherwise, an upper limit of 0.7110 is not exceeded by any specimen. Geological variability in present-day Austria and Italy is considerably higher and reflects a broader scatter of the strontium isotopic signatures. Conspicuously high ratios of up to 0.7204 are found at the site "Hohe Birga" (site code 240) which is located in an area dominated by quartz-phyllite and in the Brixen region (site codes 301, 312 and 314) where the

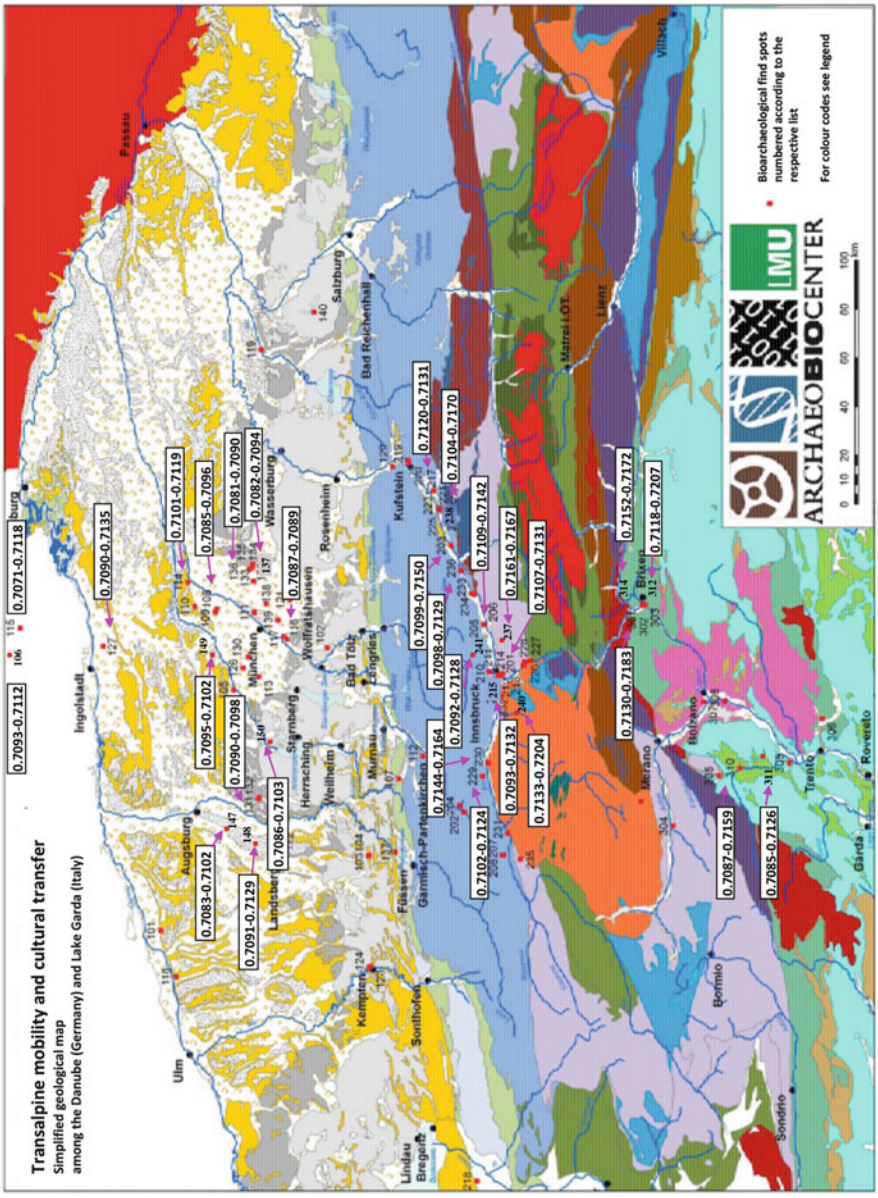

Fig. 10 Spatial distribution of bioavailable $^{87}Sr/^{86}Sr$ isotopic ratios in archaeological animal bone apatite along the Alpine transect

strontium isotopic ratio is related to phyllites and gneisses from the Palaeozoic. On the other hand, lowest bioavailable $^{87}Sr/^{86}Sr$ isotopic ratios in Austria of around 0.7094 were measured in specimens from Innsbruck (site code 215) and Thaur (site code 241), which are located at the foot of the southern slopes of the Northern Calcareous Alps. This meets expectations for this region, because of the occurrence of Mesozoic carbonates and alluvial deposits originating from them in the Inn River valley.

The overall geographic redundancy of bioavailable $^{87}Sr/^{86}Sr$ is also reflected in the considerably high variability of strontium isotopic ratios per site. Only at 8 out of 30 sites is local variability lower than the conservatively defined cut-off of 0.001 between "local" and "non-local" specimens (Grupe et al. 1997), namely, at 149, Erding; 108, Freising; 131, Pestenacker; 136, München-Trudering; 137, Unterhaching; 116, München-Grünwald; 217, Kirchbichl; and 237, Ampass-Widumfeld. Again, the overall homogeneity of the south Bavarian alluvial plains is confirmed. The highest interindividual differences were found at Brixen-Stufels (site code 312, $\Delta = 0.0089$) and Sanzeno and Hohe Birga (site codes 310 and 240, respectively; $\Delta = 0.0072$ each). The fact that not all animal bones might actually originate from truly residential individuals and that the observed variability could be related to osteologically unrecognized imported animals has been mentioned before. Another factor might be related to individual and species-specific dietary preferences and seasonal variations within the transhumant economical system. In sum, while expected relations of individual bioavailable $^{87}Sr/^{86}Sr$ isotopic ratios to the underlying geology of the region are met, the considerable spatial redundancy of strontium isotopic ratios sets obvious limitations to bioarchaeological migration research including provenance analysis.

Model Prediction of Local Bioavailable $^{87}Sr/^{86}Sr$ Isotopic Ratios by Modern Reference Samples

Animal bone specimens are tissue samples that integrate the bioavailable $^{87}Sr/^{86}Sr$ isotopic ratios in the environment in the course of an individual's lifetime. Any individual that exhibits an isotopic signature outside the range of the majority of data measured in the other members of the respective taxon should indicate a non-local individual according to the exclusion principle. Conservatively, and with regard to the measurement precision, a difference of ± 0.001 is considered significant (Grupe et al. 1997; Söllner et al. 2016). Due to the spatial redundancy of $^{87}Sr/^{86}Sr$ (Fig. 10), the place or even the region of origin of this non-local individual cannot be satisfactorily assessed. Migration studies based on a single isotopic ratio such as the most commonly used $^{87}Sr/^{86}Sr$ need both a more precise and site-specific definition of the appropriate cut-off value between a "local" and a "non-local" isotopic signature and a refined method for the assessment of the probable place of origin. Multi-isotope fingerprints would likewise benefit from such cut-off definitions.

In a pilot study focusing on the inner Alpine Inn Valley, where considerable isotopic mixing occurs for obvious topographical reasons, model calculations and

predictions of small-scaled local bioavailable $^{87}Sr/^{86}Sr$ isotopic ratios in prehistory were performed. These model predictions make use of geological mixing diagrams into which isotopic ratios of modern reference samples are entered, namely, groundwater, vegetation and soil (see materials section). Since this approach also monitors the element flux through the biosphere and into the consumer's body, model predictions constitute a step towards the establishment of prehistoric isotopic landscapes (see chapter "The Concept of Isotopic Landscapes: Modern Ecogeochemistry Versus Bioarchaeology").

Vertebrates including humans ingest strontium with food and drinking water, whereby most strontium is supplied by calcium-rich food. Strontium from both food and water mixes in the vertebrate's body, whereby the amount of strontium taken up with the drinking water was most probably highly underestimated for a long time (Crowley et al. 2015). Plants have entirely different strontium sources than animals. They take up the dissolved mineral components in the soil but also absorb considerable amounts of strontium from the atmosphere. In a geological mixing diagram, $^{87}Sr/^{86}Sr$ is plotted against the reciprocal strontium content of the end members. A lesson to learn from our ongoing research is that the Sr concentration (ppm) should be more frequently measured together with the isotopic ratio to permit for a quantification of the various proportions of Sr taken up by plants and vertebrates. For our pilot study, we had to largely rely on published or estimated values.

The $^{87}Sr/^{86}Sr$ of modern ocean water is 0.70924 ± 0.000032 (Veizer 1989), and the amount of strontium in precipitation was estimated to be 0.0013 ppm (Drouet et al. 2005). Since the water samples taken at the archaeological sites were deliberately taken from the bottom of the springs and wells to permit for a measureable uptake of mineral components related to the respective parent rock, $^{87}Sr/^{86}Sr$ of groundwater was approximated by these reference samples. Strontium concentration in groundwater was estimated according to Xin and Hanson (1994), Voerkelius et al. (2010) and Frei and Frei (2011), who showed how strontium concentrations in water adjust to the local geological conditions in relation to the residence time below surface. We therefore estimated a strontium concentration of 0.06 ppm for carbonate soils with $^{87}Sr/^{86}Sr < 0.709$, 0.03 ppm Sr for soils characterized by $0.709 < {}^{87}Sr/^{86}Sr < 0.7135$ and 0.02 ppm Sr for soils with $^{87}Sr/^{86}Sr > 0.7135$. By the use of these data, the stable strontium isotopic ratio of the drinking water [drinking water $X(\text{aq} - f)$] can be calculated, whereby we estimated the proportion of atmospheric water in the drinking water $f(\text{atm,aq} - f)$ to about 30 % (see Xin and Hanson 1994).

Stable strontium isotopic ratios measured in leached soil taken from below the agricultural horizon (Fig. 11) and the vegetation samples were measured, and the respective strontium contents estimated or calculated: With regard to the strontium concentrations in soil [Sr(wea)] and the frequency distribution of the water components in the atmosphere [$f(\text{atm,aq} - f)$] and the fauna [$(\text{aq} - f, \text{fauna})$], variations of 50 % were assumed (for details and complete model calculations step by step, see Söllner et al. 2016). The following data were entered into the mixing diagrams (Figs. 12 and 13), whereby X = correlation of $^{87}Sr/^{86}Sr$ and 1/Sr [1/ppm]

Fig. 11 Taking soil samples during field trips, site code 230 (Pfaffenhofen/Inn). Figure by F. Söllner

for the special case and f = frequency distribution of the water components (standard deviations were taken into account with regard to the measurement error):

f(atm,aq $-$ f) = proportion of the atmospheric water component in drinking water
f(atm,aq $-$ v) = proportion of the atmospheric water component in vegetation water
f(aq $-$ v,veg) = proportion of the vegetation water component in the vegetation
f(aq $-$ f,fauna) = proportion of the drinking water component in faunal bones
$^{87}Sr/^{86}Sr$(atm) = strontium isotopic ratio in the atmosphere (literature, see above)
$^{87}Sr/^{86}Sr$(wat) = strontium isotopic ratio in groundwater (measured)
$^{87}Sr/^{86}Sr$(aq $-$ f) = strontium isotopic ratio of drinking water (mixture of atmospheric and groundwater) incorporated into the fauna
$^{87}Sr/^{86}Sr$(aq $-$ v) = strontium isotopic ratio of vegetation water (mixture of atmospheric and groundwater) assimilated in vegetation
$^{87}Sr/^{86}Sr$(veg) = strontium isotopic ratio of vegetation (measured)
$^{87}Sr/^{86}Sr$(wea) = strontium isotopic ratio of weathered soil (measured)
$^{87}Sr/^{86}Sr$(fauna) = strontium isotopic ratio of faunal bone (calculated)

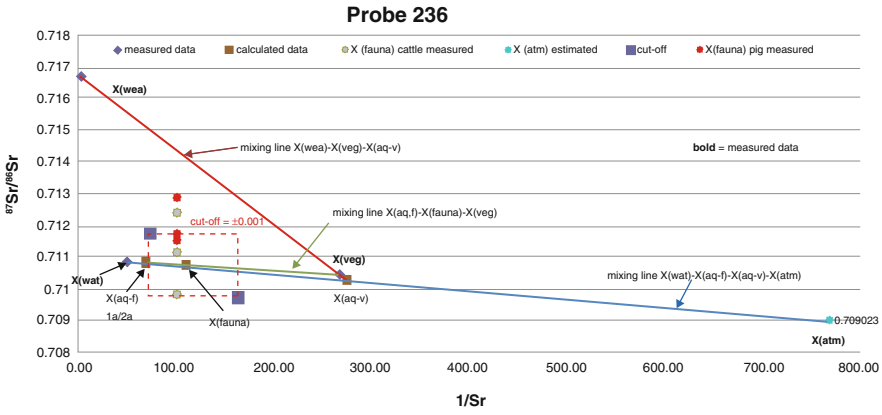

Fig. 12 Model prediction for local bioavailable $^{87}Sr/^{86}Sr$ isotopic ratios at the Wiesing site based on modern reference material (cf. text) and measured data of six archaeological animal bone finds. Figure by F. Söllner

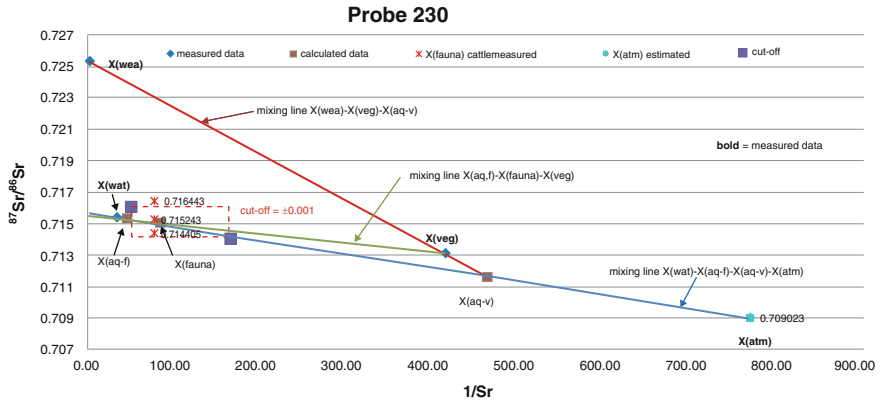

Fig. 13 Model prediction for local bioavailable $^{87}Sr/^{86}Sr$ isotopic ratios at the Pfaffenhofen/Inn site based on modern reference material (cf. text) and measured data of three archaeological animal bone finds. Figure by F. Söllner

Sr(atm) = strontium concentration (ppm) in atmospheric water (literature, see above)

Sr(wat) = strontium concentration (ppm) in groundwater (literature, see above)

Sr(aq − *f*) = strontium concentration (ppm) in drinking water, mixture of atmospheric and groundwater

Sr(aq − *v*) = strontium concentration (ppm) in vegetation water, mixture of atmospheric and groundwater

Sr(fauna) = time-dependent assimilated strontium concentration (ppm) in faunal bone (calculated)
Sr(veg) = time-dependent assimilated strontium concentration (ppm) in vegetation (calculated)
Sr(wea) = strontium concentration (ppm) in weathered soil (literature, see above).

The following two mixing diagrams are chosen as representatives for the general outcome of these model predictions. At Wiesing (site code 236, Fig. 12), the mixing model followed expectations: With the exception of a single cattle bone, all measured $^{87}Sr/^{86}Sr$ isotopic ratios in the faunal bones plot into the triangle delineated by the end members' water, vegetation and leached soil. According to the conservatively defined cut-off value between "local" and "non-local" finds (± 0.001), the pig and the cattle with apatite $^{87}Sr/^{86}Sr$ ratios >0.712 have to be considered primarily non-local to the site of their recovery. According to the univariate statistics, these two animals exhibit no mathematically outlying value (Table 4) and would not have been recognized as import. The distance travelled by these two individuals, however, might have been short (see below). At Pfaffenhofen/Inn (site code 230) in contrast, $^{87}Sr/^{86}Sr$ in leached soil obviously did not contribute to the respective isotopic ratio in consumer tissues (Fig. 13). Both modelled and measured $^{87}Sr/^{86}Sr$ values in the bones are almost exclusively dependent upon drinking water and vegetation moisture. This result is in agreement with the recent study by Crowley et al. (2015) who showed that for a variety of sites in the United States, animal bone $^{87}Sr/^{86}Sr$ isotopic ratios are best predicted by the respective ratio in local water. Unfortunately, only three archaeological cattle bones were available from site number 230. The individual with the highest strontium isotopic ratio has to be considered non-local according to the defined ±0.001 difference, but as all three measured values plot very close to each other, this is debatable (Fig. 13).

Although this pilot study was carried out with the finds from only five selected sites in a consciously chosen region, it was possible to define three geology-related domains in the Inn Valley (Söllner et al. 2016) and to identify individual animal bones which had been assumed to be local according to osteology as non-local. In fact, the majority of the investigated animals had apatite $^{87}Sr/^{86}Sr$ isotopic ratios between 0.709 and 0.7135, implying that they had lived on moraine soil. This comes to no surprise, since glacial and fluvioglacial deposits had filled the Inn Valley to a depth of several hundred meters (Söllner et al. 2016). We conclude that these model predictions open up the possibility for an approximation of an isotopic landscape for bioarchaeology, because they permit for a much finer scaled regional differentiation of local, bioavailable isotopic ratios and the recognition of primarily non-local finds which are by far superior to the traditional exclusion principle. We need to emphasize that the results also imply short-distance mobility rather than long-distance migration. The distance covered between the five selected sites in the Inn Valley is only about 70 km what does by no means prevent a regular mobility, exchange and trade between the sites even in prehistoric times.

Lead Isotopes

Reliable measurements of lead isotopes in archaeological skeletons are less routine in bioarchaeology compared to the measurement of $^{87}Sr/^{86}Sr$ isotopic ratios and also not that easy. This holds especially for the light stable isotope ^{204}Pb because it is of very low abundance in nature (1.4 % only). In addition, although lead is a "bone-seeking" element and bone lead is therefore a very good indicator of long-term lead absorption (Nordberg et al. 1991; Pemmer et al. 2013), skeletal lead content in pre-industrial times is generally low (Grupe 1991). This holds in particular for animal bones. While humans came into contact with heavy metals soon after metal use started in prehistory, domesticates and free-ranging vertebrates were only seldom subject to such direct contamination. Animals take up lead mainly through food and water ingestion but also by inhalation. Unless food was consumed in a contaminated region, for example, in the vicinity of ore deposits or metal smelters, absolute bone lead concentration would hardly be expected to exceed a few ppm. Although it has been strongly advised to consider all four lead isotopes for the scope of georeferencing (Villa 2016), the majority of publications do not rely on ^{204}Pb but rather on the more commonly used ratios $^{208}Pb/^{207}Pb$ and $^{206}Pb/^{207}Pb$. Therefore, the presentation of the results of the isotopic mapping of bioavailable bone lead isotopic signatures along the Inn-Eisack-Adige passage will start with these two ratios. Just as for $^{87}Sr/^{86}Sr$, spatial redundancy of lead isotopes is high along the transect, but in general, a north-to-south gradient is observed. It can be depicted from the following maps that end members for the highest and lowest radiogenic isotopic ratios in this reference area are the German site 206 (Berching-Pollanten) and the Italian site 314 (Brixen-Stufels), respectively. Since to our knowledge a systematic, small-scaled regional mapping of bioavailable lead isotopic ratios has not been performed before, it is not yet possible to define an empirical cut-off-value between "local" and "non-local" finds for a specific site. Modelling bioavailable lead isotopic ratios in order to predict expectations, as demonstrated for $^{87}Sr/^{86}Sr$ in the pilot study (see above), will be a preferred future task.

$^{208}Pb/^{207}Pb_{apatite}$ and $^{206}Pb/^{207}Pb_{apatite}$

The boxplot of $^{208}Pb/^{207}Pb$ (Fig. 14a) shows that isotopic ratios found in red deer are only insignificantly lower than in the domesticates. Mathematical outliers mainly concern $^{208}Pb/^{207}Pb \leq 2.44$ in all three species. This is clearly reflected in the Kernel density plot (Fig. 14b), where the majority of outlying isotopic ratios were again detected in individual domesticates. The spatial distribution of measured $^{208}Pb/^{207}Pb$ isotopic ratios along the Alpine transect does not exhibit any distinct isotopic domain (Fig. 15). Isotopic ratios between 2.454 and 2.472 occur almost everywhere, and also no site-specific trends are detectable. Total variability is from 2.408 (site 106, Berching-Pollanten) to 2.477 (site 314, Brixen-Stufels), which makes a difference of $\Delta = 0.069$. Only a slight north-to-south gradient is observable: To the north of the Alps in Germany, and at the inner Alpine sites in Austria, median $^{208}Pb/^{207}Pb$ values are both 2.461, while to the south of the mountain chains in Italy, median isotopic ratio is 2.466. Variability of

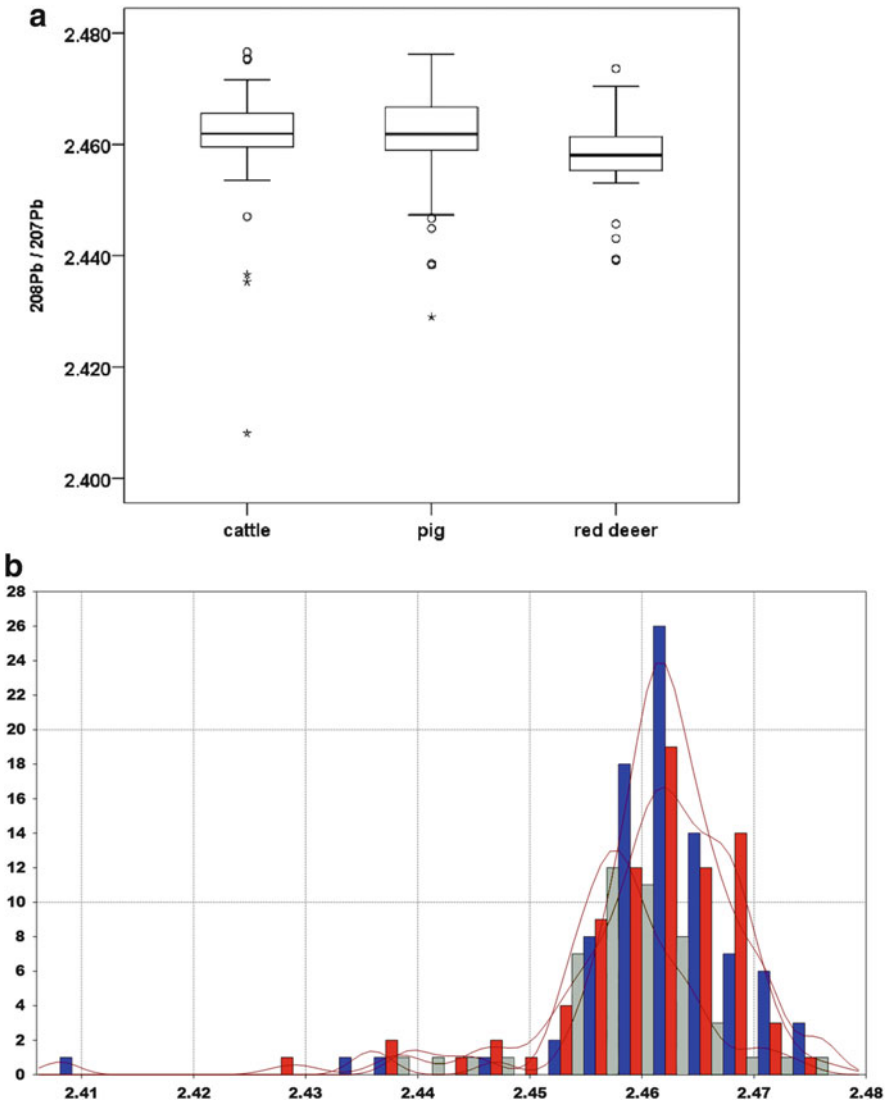

Fig. 14 Measurement data of apatite $^{208}Pb/^{207}Pb$. (**a**) Boxplot (quartiles) of $^{208}Pb/^{207}Pb$ per species and (**b**) $^{208}Pb/^{207}Pb$ Kernel density plot. *Red*: cattle, *blue*: pig, *grey*: red deer

measured values is largest in Germany (2.408–2.472, $\Delta = 0.064$), followed by Austria (2.439–2.475, $\Delta = 0.036$) and Italy (2.454–2.477, $\Delta = 0.023$).

With regard to $^{206}Pb/^{207}Pb$, mathematical outliers are exclusively found among the higher isotopic ratios (Figs. 16a, b). Bioavailable $^{206}Pb/^{207}Pb$ between 1.179 and 1.217 is found both to the north and to the south of the Alps and also in the inner Alpine area (Fig. 17). Total variability along the Alpine transect is from 1.172 (site 312, Brixen-Stufels) to 1.349 (site 106, Berching-Pollanten), which equals a range

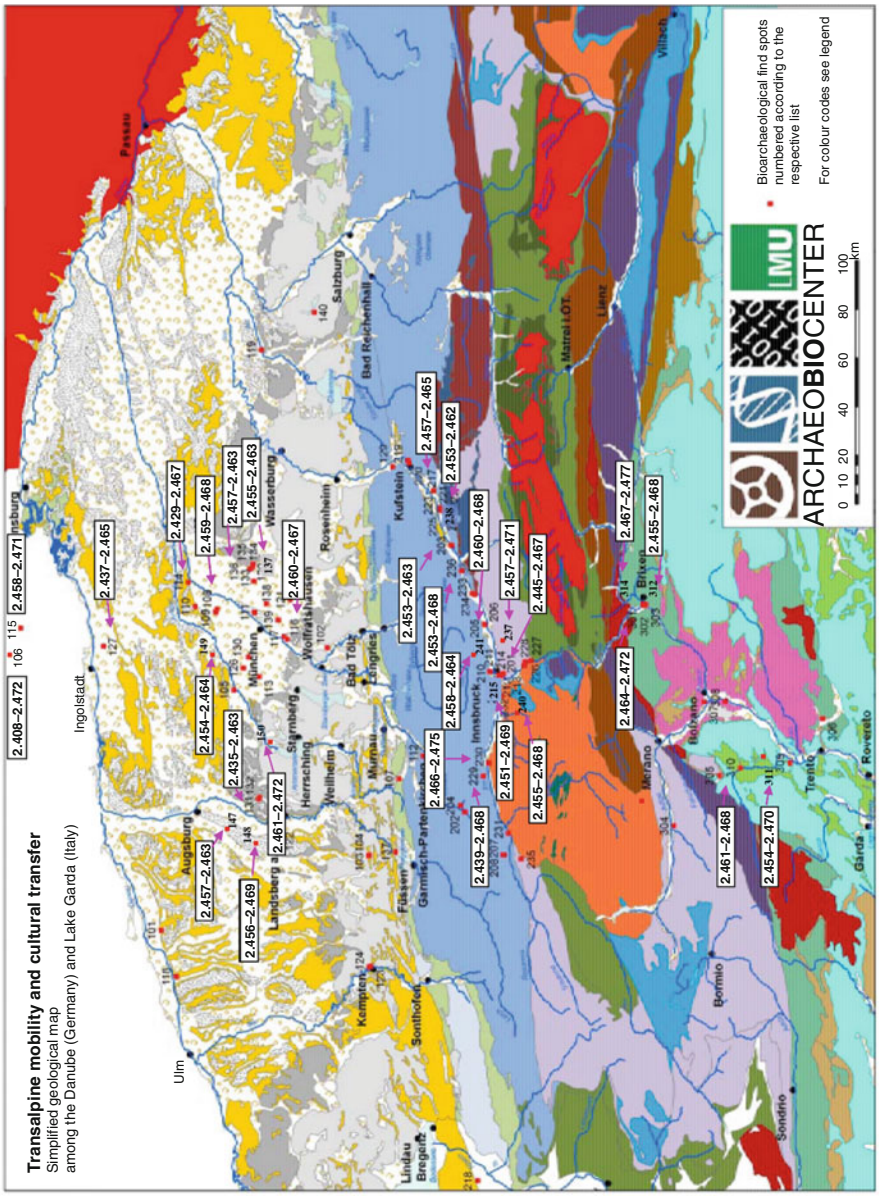

Fig. 15 Spatial distribution of bioavailable $^{208}Pb/^{207}Pb$ isotopic ratios in archaeological animal bone apatite along the Alpine transect

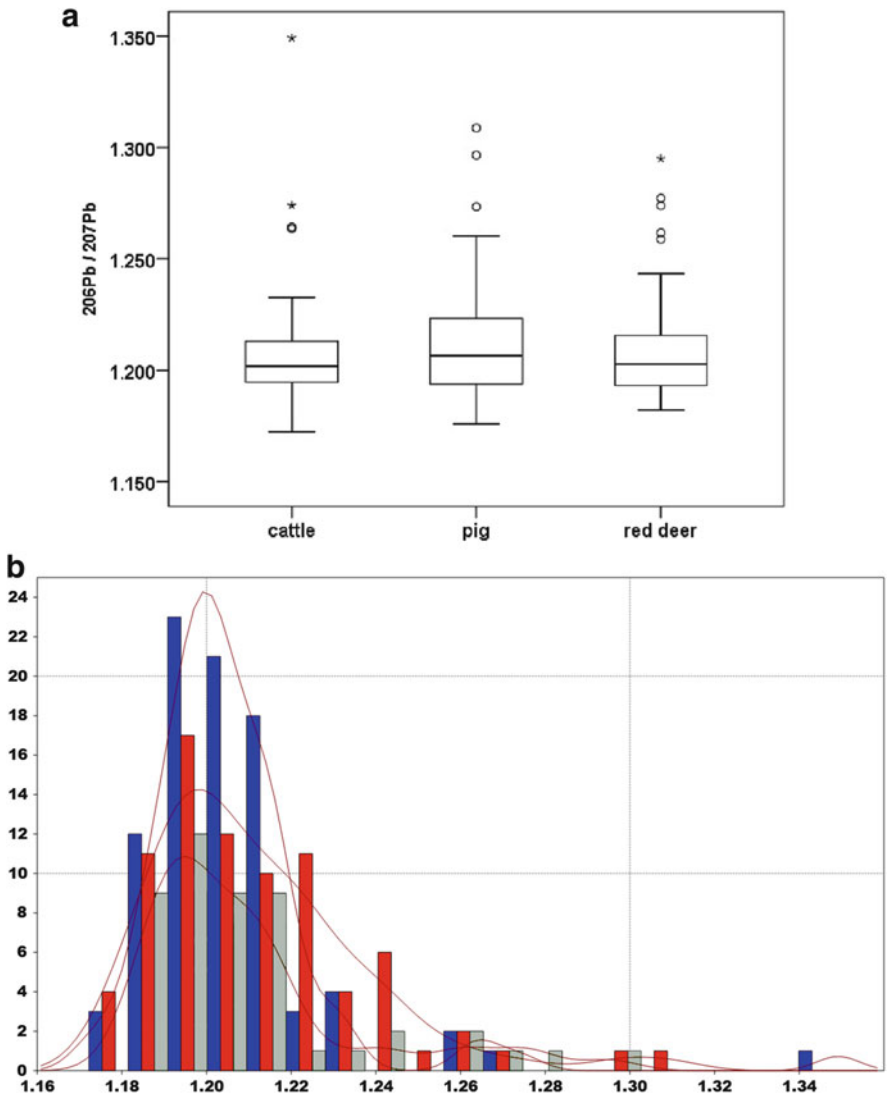

Fig. 16 Measurement data of apatite $^{206}Pb/^{207}Pb$. (**a**) Boxplot (quartiles) of $^{206}Pb/^{207}Pb$ per species and (**b**) $^{206}Pb/^{207}Pb$ Kernel density plot. *Red*: cattle, *blue*: pig, *grey*: red deer

of 0.177. The slight north-to-south gradient of rising $^{208}Pb/^{207}Pb$ isotopic ratios is reflected by parallel declining $^{206}Pb/^{207}Pb$ signatures: The highest median value (1.212) and largest range (1.179–1.349, $\Delta = 0.171$) are found in Germany, followed by a median of 1.198 in Austria and a range from 1.174 to 1.259 ($\Delta = 0.085$) and a median of 1.194 in Italy with the smallest range (1.172–1.217, $\Delta = 0.044$).

The five most radiogenic $^{206}Pb/^{207}Pb$ isotopic ratios >1.277 have all been found to the north of the Alps in Germany, namely, at the sites Berching-Pollanten (site

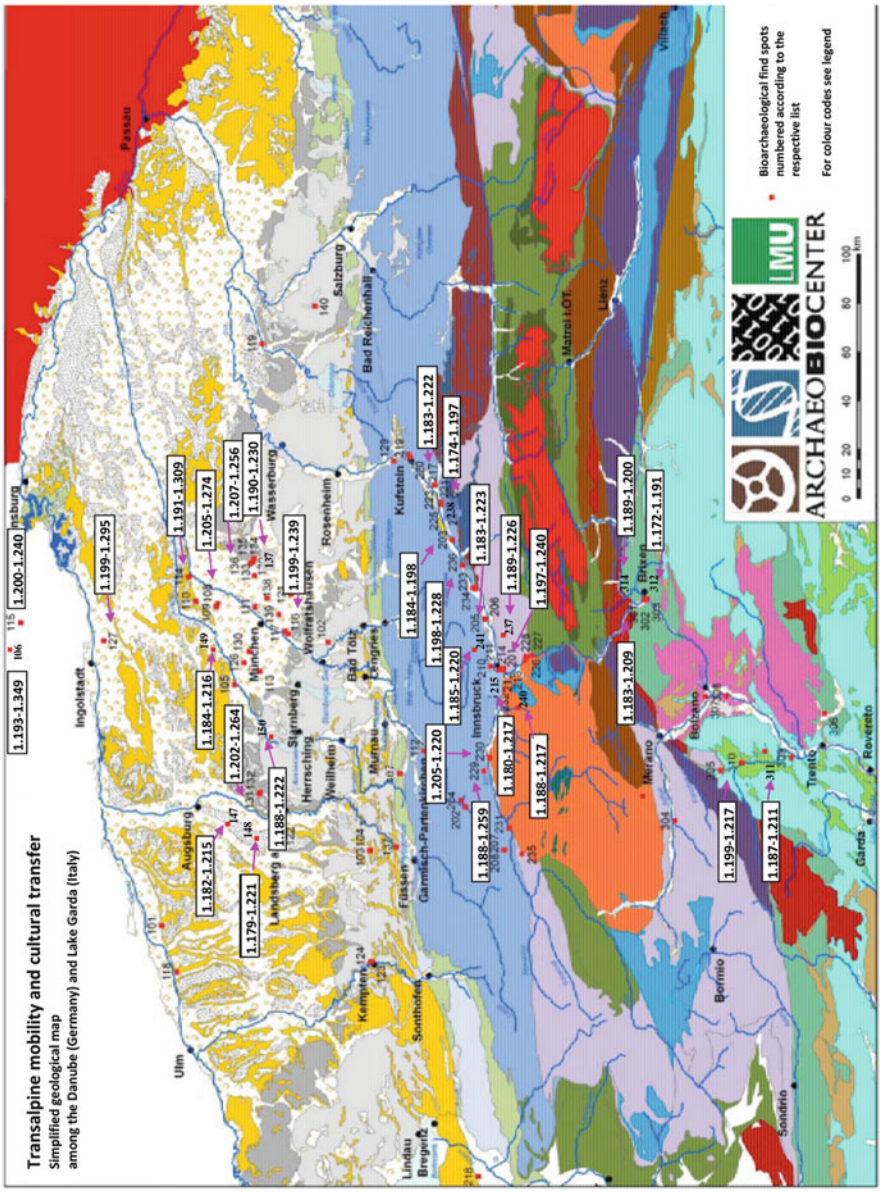

Fig. 17 Spatial distribution of bioavailable $^{206}Pb/^{207}Pb$ isotopic ratios in archaeological animal bone apatite along the Alpine transect

code 106), Freising (site code 114) and Manching (site code 127). Together with Griesstetten (site code 115), these three sites belong to the northernmost locations where animal bones for this isotopic map have been selected. The respective individual animal specimens at the same time exhibit the highest $^{206}Pb/^{204}Pb$ isotopic ratios. Likewise, the animal bones in which the lowest $^{206}Pb/^{207}Pb$ values were measured also exhibit the lowest $^{206}Pb/^{204}Pb$ ratios (see below). With regard to the low abundance of ^{204}Pb and the technical differences accompanying its measurement, the analytically more reliable $^{206}Pb/^{207}Pb$ ratios are helpful in validating isotopic ratios expressed against ^{204}Pb.

$^{208}Pb/^{204}Pb_{apatite}$, $^{207}Pb/^{204}Pb_{apatite}$ and $^{206}Pb/^{204}Pb_{apatite}$

In Fig. 18a, b, the distribution of bioavailable $^{208}Pb/^{204}Pb$ per species over all sites is shown in the form of a boxplot and a Kernel density plot. A single mathematical outlier was found (see Table 4), and just as in Fig. 9b, the Kernel density exhibits a second peak at $^{208}Pb/^{204}Pb \geq 38.6$ which is largely due to the domesticated animals. However, although the sample size of the red deer specimens is much smaller, the trend is also detectable in this free-ranging species. The spatial distribution of measured $^{208}Pb/^{204}Pb$ in archaeological animal bones is shown in Fig. 19. ^{208}Pb, the heaviest stable lead isotope and the end product of the ^{232}Th ($t_{1/2} = 1.4 \times 10^{10}$ years) decay series, has a natural abundance of 52.4 % opposed to only 1.4 % abundance of ^{204}Pb; therefore, for simple fractional arithmetic reasons, the relation between numerator and denominator is not a favourable one.

The spatial redundancy of bioavailable $^{208}Pb/^{204}Pb$ in archaeological animal bones is obvious from Fig. 19, since isotopic ratios between 38.355 and 38.725 are found at many locations along the Alpine transect. Total variability is from 38.188 (site 106, Berching-Pollanten) to 38.827 (site 314, Brixen-Stufels) that is a range of $\Delta = 0.639$. A slight north-to-south gradient is detectable by rising median values by country, namely, from 38.511 in Germany with a range from 38.188 to 38.777 ($\Delta = 0.589$), followed by a median of 38.518 in Austria (range 38.266–38.725; $\Delta = 0.459$) and a median of 38.591 in Italy (range 38.355–38.827, $\Delta = 0.472$). Despite this general trend, certain site specificity is depicted in Fig. 19 since the five most radiogenic $^{208}Pb/^{204}Pb$ ratios >38.750 occur both to the north (German sites 106, Berching-Pollanten, and 108, Eching) and to the south of the Alps (Italian site 314, Brixen-Stufels). Also the five least radiogenic ratios <38.321 exhibit a larger spatial distribution and are found both in the north (German sites 106, Berching-Pollanten, and 137, Unterhaching near Munich) and in the inner Alpine region (Austrian sites 229, Mieming, and 215, Innsbruck).

^{207}Pb is the end product of a uranium-actinium decay series starting with the radioactive ^{235}U atom ($t_{½} = 703.8$ million years). The boxplot distribution (Fig. 20a) exhibits some mathematical outliers exclusively due to more radiogenic isotopic ratios. The Kernel density plot (Fig. 20b) shows that these higher isotopic ratios are encountered in all three species but more clearly in cattle. Along the Alpine transect, $^{207}Pb/^{204}Pb$ isotopic ratios in animal bones vary from 15.604 (site 137, Unterhaching near Munich) to 15.857 (site 106, Berching-Pollanten) (Fig. 21). This difference of 0.253 is thus found between sites which are both located to the

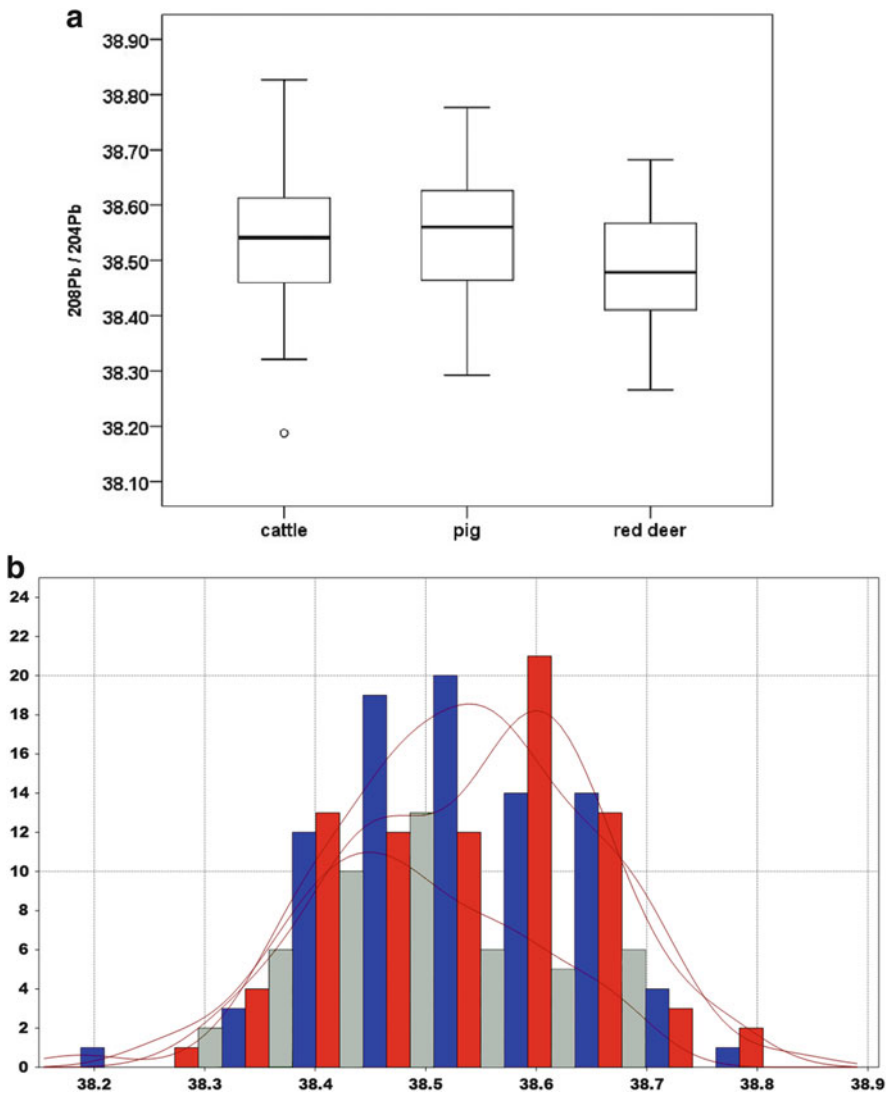

Fig. 18 Measurement data of apatite $^{208}Pb/^{204}Pb$. (**a**) Boxplot (quartiles) of $^{208}Pb/^{204}Pb$ per species and (**b**) $^{208}Pb/^{204}Pb$ Kernel density plot. *Red*: cattle, *blue*: pig, *grey*: red deer

north of the Alps. This in turn implies that the German sites alone cover the total measured variability. The $^{207}Pb/^{206}Pb$ median of the German sites is 15.655 and higher than in the central Alpine and southern Alpine regions. Despite a considerable geological inhomogeneity, total variability is much smaller in Austria (median 15.650, range 15.605–15.705; $\Delta = 0.1$) and smallest in Italy (median 15.654, range 15.614–15.696; $\Delta = 0.082$). Such a relative spatial stability of $^{207}Pb/^{204}Pb$ follows expectations because of the relatively short half-life of the parent isotope ^{235}U.

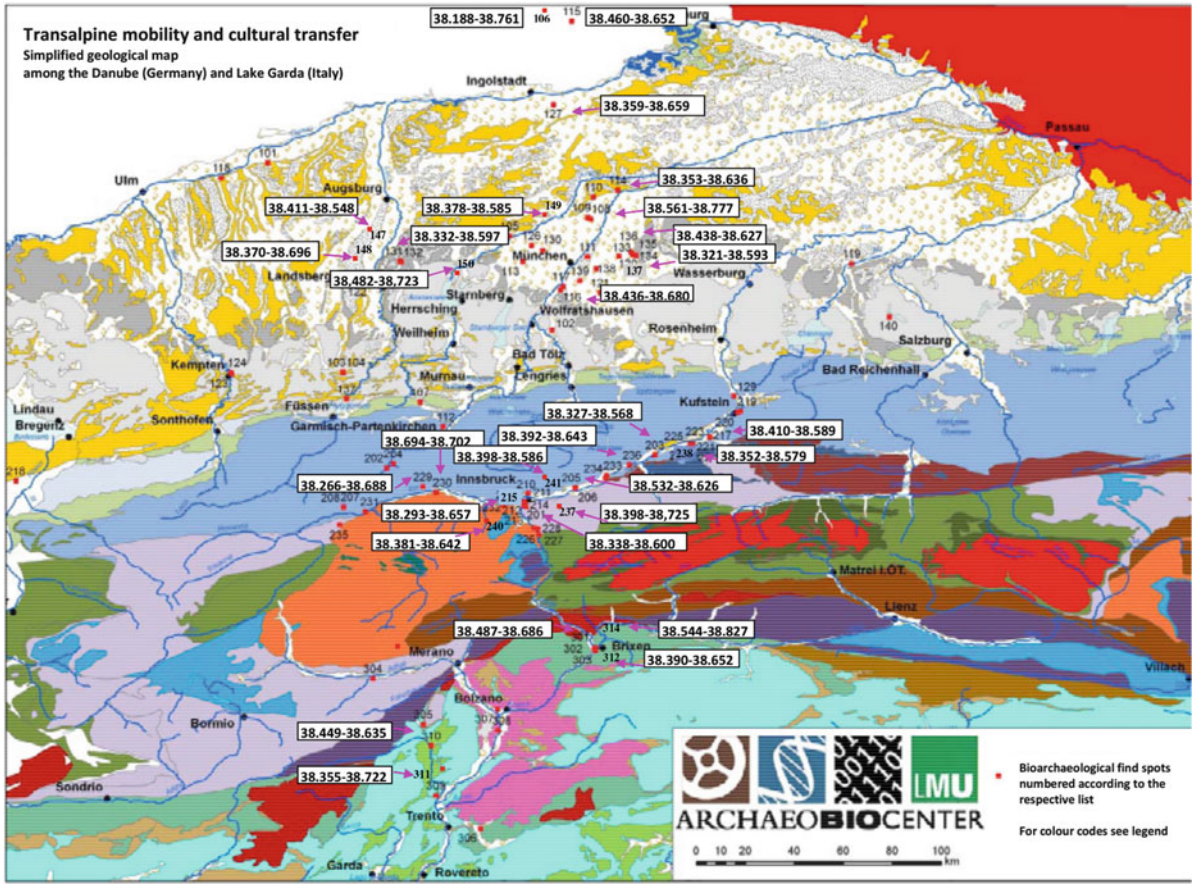

Fig. 19 Spatial distribution of bioavailable $^{208}Pb/^{204}Pb$ isotopic ratios in archaeological animal bone apatite along the Alpine transect

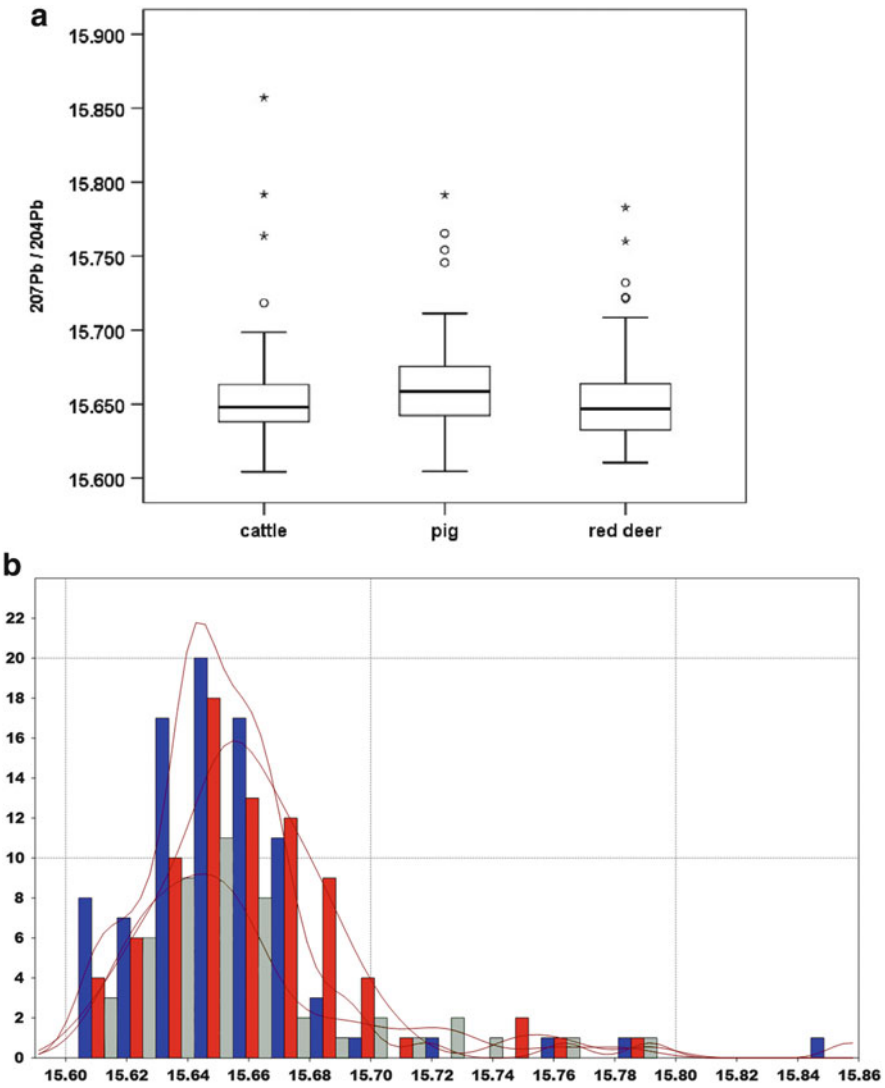

Fig. 20 Measurement data of apatite $^{207}Pb/^{204}Pb$. (**a**) Boxplot (quartiles) of $^{207}Pb/^{204}Pb$ per species and (**b**) $^{207}Pb/^{204}Pb$ Kernel density plot. *Red*: cattle, *blue*: pig, *grey*: red deer

Since locations in the reference area with most radiogenic $^{207}Pb/^{204}Pb$ isotopic ratios also exhibit highest $^{206}Pb/^{204}Pb$ signatures (see below), underlying bedrock should be enriched with uranium compared to the other locations. The ten highest $^{207}Pb/^{204}Pb$ ratios >15.732 were all measured at German sites, namely, at site 114 (Freising, $n = 2$), site 127 (Manching, $n = 6$) and a single individual each at sites 106 (Berching-Pollanten) and 131 (Pestenacker/Lech). Accordingly, site-

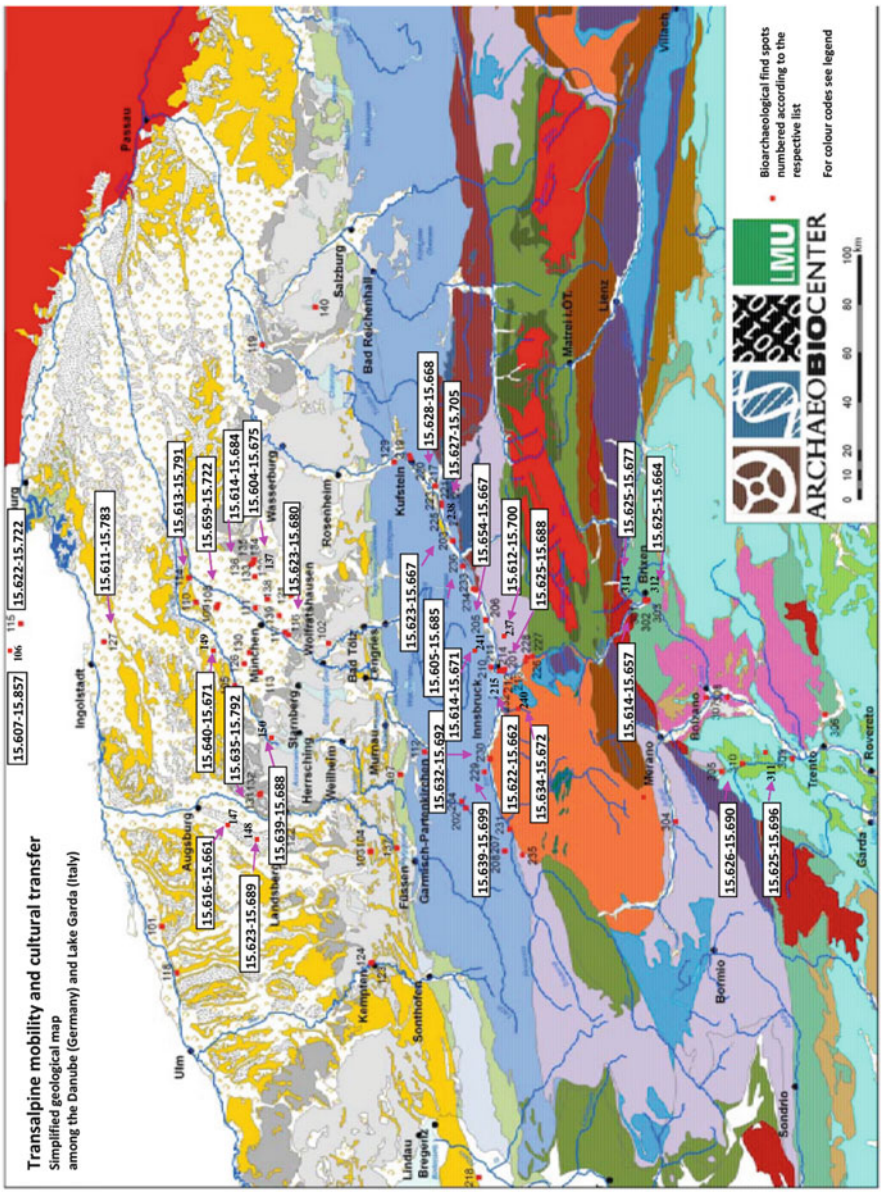

Fig. 21 Spatial distribution of bioavailable $^{207}Pb/^{204}Pb$ isotopic ratios in archaeological animal bone apatite along the Alpine transect

specific variability of $^{207}Pb/^{204}Pb$ is particularly high in Germany. At Berching-Pollanten (site code 106), the variability of 0.250 almost equals the highest Δ measured across the complete data set (0.253, see above). With a Δ of 0.178 and 0.172 at Freising (site code 114) and Manching (site code 127), local variation of $^{207}Pb/^{204}Pb$ is still conspicuously high. Smallest site-specific variations are independent from the geographical location in our reference area.

^{206}Pb finally is the end product of the decay of a uranium-radium series starting with the mother radioisotope ^{238}U ($t_{½} = 4.469 \times 10^9$ years). Mathematical outliers have more radiogenic isotopic ratios (Fig. 22a), whereby the majority of the affected individual bones also constitute mathematical outliers with regard to $^{207}Pb/^{206}Pb$ (see Table 4). Accordingly, also the Kernel density plot (Fig. 22b) is rather similar. Five individuals with the most radiogenic $^{206}Pb/^{204}Pb$ isotopic signatures come from northern Alpine sites in Germany, namely, 106 (Berching-Pollanten), 114 (Freising) and 127 (Manching), which all belong to the northernmost sites where animal bones were sampled for the project. Carbonate rock and related soil frequently exhibit elevated $^{206}Pb/^{204}Pb > 19$ (Köppel and Schroll 1985). Since sandy, clay and carbonate rock are abundant in this micro-region, measured isotopic ratios meet expectations. Although several details about the lead isotope flux from rock into the food chain are still lacking, animals ingest lead mostly with food, and especially grazing herbivores take up lead by soil ingestion (see chapter "The Concept of Isotopic Landscapes: Modern Ecogeochemistry versus Bioarchaeology"). Lead in soil is generally not very mobile (United Nations 2010). Transfer of soil lead into the food chain occurs via the plant roots, but only a small portion of lead is present in soil solution (Hansen et al. 2004), which in turn is responsible for the generally low lead content of food under natural conditions (United Nations 2010).

The total variability of measured $^{206}Pb/^{204}Pb$ along the transalpine passage is 18.330 (site 312, Brixen-Stufels) to 21.397 (site 106, Berching-Pollanten) ($\Delta = 3.067$) with a median of 18.831 (Fig. 23). Again, a weak north-to-south gradient is apparent. The German sites to the north of the Alps exhibit the highest median value (18.969) and the largest variability almost covering the total variation of the complete data set (range 18.421–21.397, $\Delta = 2.976$), followed by the Austrian (median = 18.744, range 18.353–19.748; $\Delta = 1.395$) and Italian sites (median = 18.673, range 18.330–19.088; $\Delta = 0.758$). All countries share bioavailable $^{206}Pb/^{204}Pb$ isotopic ratios between 18.421 and 19.088. With regard to the site-specific "local" variability, highest ranges with an average of 19.090 occur at German sites, a result that corresponds with other bioavailable lead isotopic ratios. Ranges exceeding this average occur at Berching-Pollanten (site 106), Freising (site 114), Eching (site 108), Manching (site 127) and Pestenacker/Lech (site 131). As stated before, the definition of a "local" bioavailable isotopic ratio is complicated by the possibility that some animals or parts of them had not been primarily local to the site of their recovery. A particular example of this is the Iron Age oppidum of Manching (site 127), which was a densely populated town at that time (Sievers 2003). Pestenacker/Lech (site 131), however, was a Neolithic settlement (Bösl et al. 2006) where a considerably smaller catchment area of animals taken to the site is

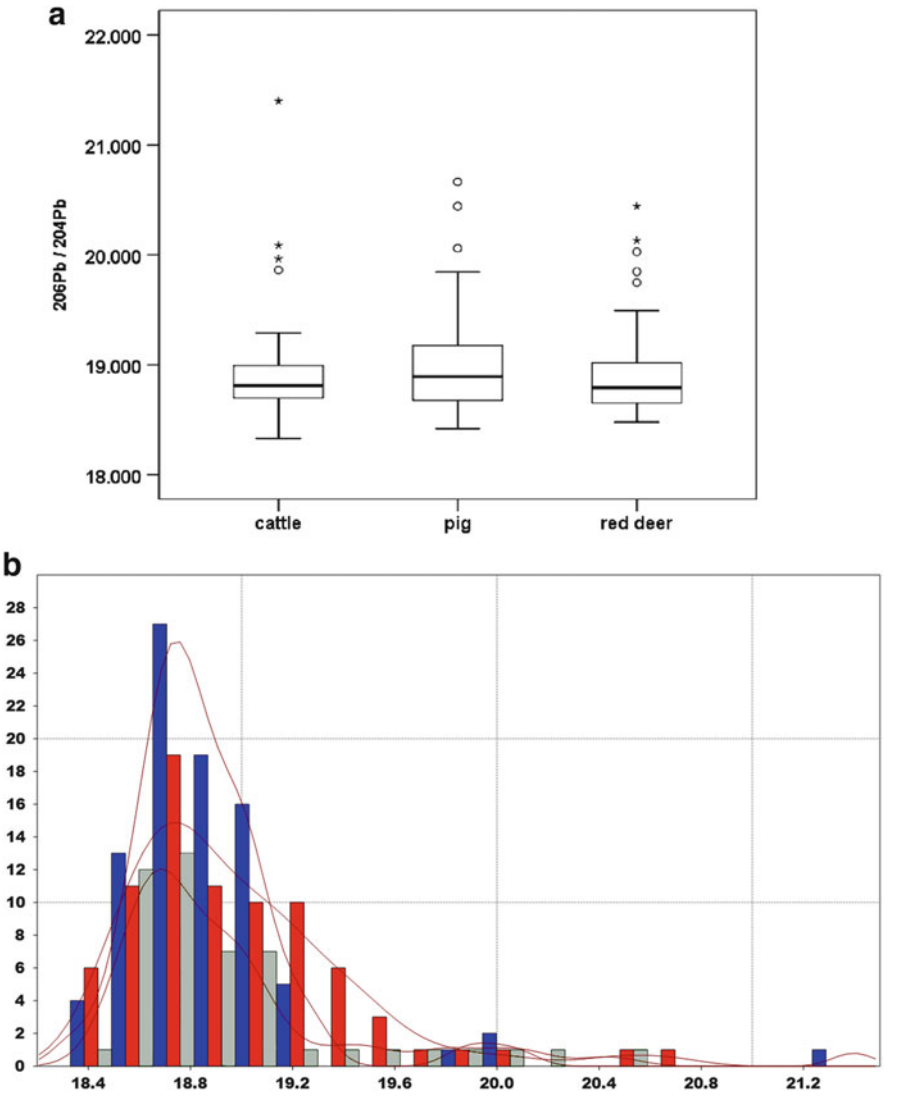

Fig. 22 Measurement data of apatite $^{206}Pb/^{204}Pb$. (**a**) Boxplot (quartiles) of $^{206}Pb/^{204}Pb$ per species and (**b**) $^{206}Pb/^{204}Pb$ Kernel density plot. *Red*: cattle, *blue*: pig, *grey*: red deer

expected. It is therefore impossible to define an empirically based cut-off value between local and primarily non-local finds. Accordingly, sites where the ranges between the measured isotopic ratios were conspicuously small show no relationship to geographical location or geological background (site 314, Brixen-Stufels, $\Delta = 0.122$; site 203, Brixlegg, $\Delta = 0.192$; site 230, Pfaffenhofen/Inn, cattle only, $\Delta = 0.307$; and site 310, Sanzeno, $\Delta = 0.359$).

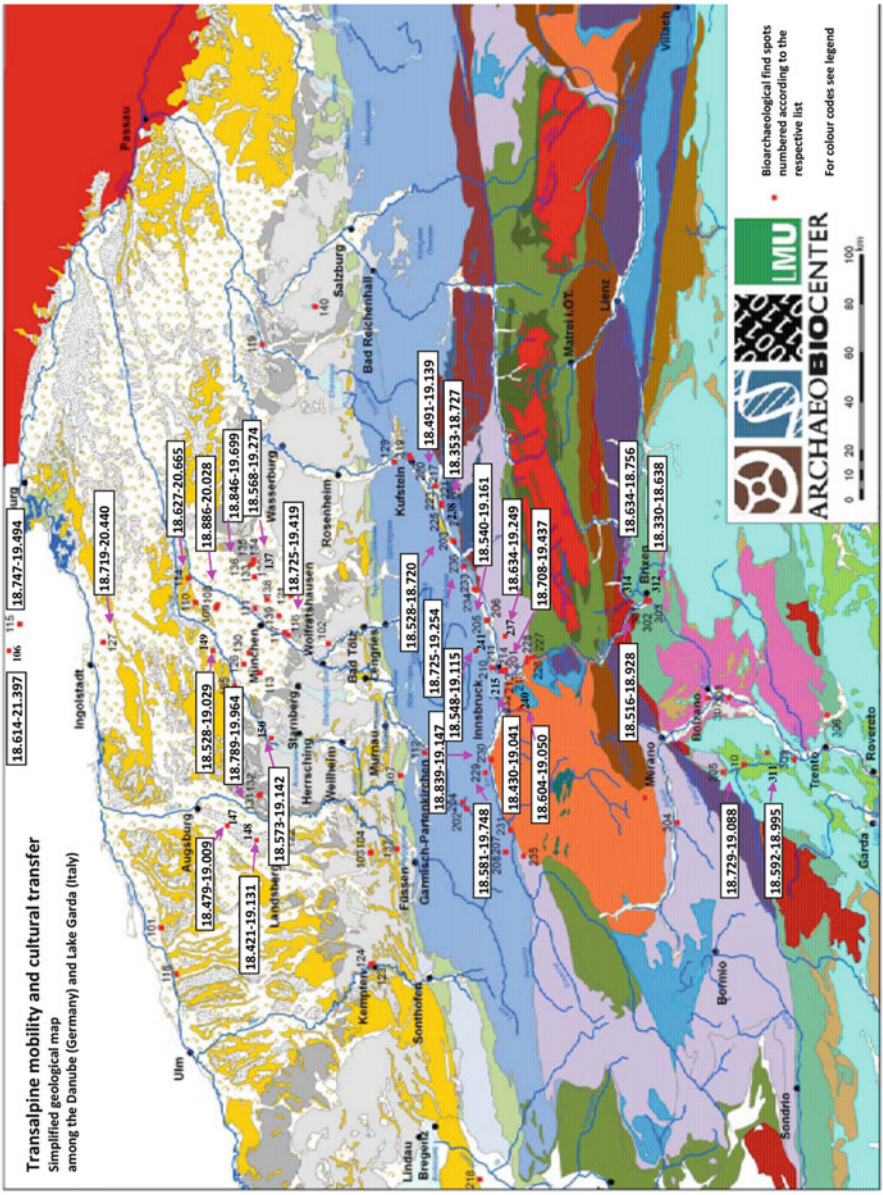

Fig. 23 Spatial distribution of bioavailable $^{206}Pb/^{204}Pb$ isotopic ratios in archaeological animal bone apatite along the Alpine transect

Isotopic Mapping by Multi-isotope Fingerprints in Archaeological Fauna from the Alpine Transect

Without doubt, the five isotopic signatures measured in the apatite of residential archaeological fauna (cattle, pig, red deer) do exhibit some spatial variation, mainly in terms of altitude and latitude (Table 3). While some sites exhibit quite particular isotopic signatures, the overall very high spatial redundancy of single isotopic ratios in this reference area is obvious despite variability with regard to geological background and altitude that meets expectations in most cases. Reliable recognition of "non-local" bioavailable isotopic signatures is possible by the exclusion principle, but the definition of place of origin remains fraught with ambiguity. The question pertaining to how far an imported animal has been transported cannot be answered at all. This, however, constitutes a crucial aspect in the discussion of migration and trade versus normal mobility within the frame of a micro-region. Not all limitations inherent to migration research in prehistory are overcome by the application of novel methods provided by computer sciences with the intention of evaluating the spatial information hidden in a multi-isotope fingerprint. Also, mining of measurement data is not an end in itself – the computer scientist definitely needs contextual input from the domain experts. In this case, the domain experts come from the subjects of biology (metabolical peculiarities, feeding and habitat preferences of vertebrate taxa) and mineralogy (validation of isotopic data, exclusion of decomposition artefacts in archaeological skeletal finds) and naturally from the subject of archaeology (find context). This way, interdisciplinary cooperation is indispensable, which is sometimes time consuming and even tedious.

However, proof that this is worth the effort has been demonstrated in chapter "The Isotopic Fingerprint: New Methods of Data Mining and Similarity Search". Application of data mining methods to the data set led to a much more fine-scaled spatial resolution of the multi-isotope fingerprint on the individual level. Micro-regions are much better defined, and a separate analysis of outlying isotopic signatures according to univariate statistics led to a definition of non-local individuals and possible place of origin with a much higher probability. Research on migration, trade and culture transfer in prehistory will significantly benefit from this research progress.

A second question that still needs to be solved is whether such research based on stable isotopes is still possible with cremated finds. Although the altitude information hidden in $\delta^{18}O_{phosphate}$ is not overwhelming for an individual specimen, it is clearly present and informative. In a fully cremated find, stable oxygen isotopic ratios have been thermally altered. Upon experimental cremation under controlled conditions, the cystallographic unit cell of the bone apatite shows substantial thermal alterations at temperatures exceeding 600–700 °C (Harbeck et al. 2011), a temperature that is easily reached by a prehistoric cremation pyre. Omitting $\delta^{18}O$ from the multi-isotope fingerprint will unavoidably lead to a loss of spatial information. A large sample of human cremations was analysed in order to test whether spatial resolution based on apatite strontium and lead isotopic signatures only is still reliable enough to at least determine the micro-regions identified along the Alpine

transect. The resulting isotopic maps of (1) a traditional spatial plot of the measurement data and (2) after data mining are the subject of the following section.

Migration research and culture transfer in prehistory largely focuses on humans. Population admixture is frequently related to acculturation phenomena. Humans, in the course of domestication, trade and the supply of raw material, mostly force mobility of animals. How does the isotopic map based on fully cremated human skeletal finds agree with the one established on uncremated skeletal remains of residential vertebrates? Do vertebrates integrate the local bioavailable isotopic signatures in a way that the results are compatible with sympatric human finds? If this is the case, then the isotopic maps that are presented in this chapter will be suitable for the majority if not all archaeological strata in the reference region.

Isotopic Fingerprints of Human Cremated Finds from the Reference Area

Cremating the dead before burial was not uncommon in prehistory. For a period of about 1500 years in Central Europe, namely, from the Bronze Age until late Imperial Roman Times (e.g. between about 1300 BC and about 400 AD), cremation was the regular if not exclusive burial practice (Kunter 1989). The reasons for this burial rite should have been manifold; a complete separation of the body and soul of the deceased person might have been only one of them. Fact is that burning a dead appeals to all senses of those attending the ceremony (the smell of the smoke, the light of the fire, the crackle of the burning pyre), who thereby participate at the transformation of the body (Sørensen and Rebay 2007). Cremated animal bones are frequently found comingled with the human bodily remains. These are interpreted as food offerings placed with the dead to nourish them on the way to the afterlife. The anthropological investigation of archaeological cremations necessitates skilled osteologists, not only for the scope of sorting the non-human from the human bone remains but also to gather as much biologically related information to the person as possible.

Depending upon the quality of wood used and oxygen supply, prehistoric cremation pyres could reach temperatures up to 1000 °C (McKinley 2016). Exposure to such high temperatures causes alterations in bone structure leading to a high degree of fragmentation. Since all organic constituents of the skeleton are burnt away, the bones lose their elasticity, making cremated remains very brittle. Every manipulation of a cremation after excavation may lead to further fragmentation and a potential loss of biological information. Macroscopically, it is possible to assess the approximate temperatures to which the bones have been exposed, because oxidation processes and the liberation of carbon are responsible for temperature-dependent colour changes. In general, the bones maintain their original light colour up to temperatures of 200–250 °C, which then changes to brown at 250 °C onwards. Between 300 and 600 °C, the bones turn black and become lighter again via different shades of dark and light grey from 700 °C onwards. Completely cremated bones are chalky white (Wahl 1981; Shipman et al. 1984; Herrmann et al. 1990;

Quatrehomme et al. 1998; Walker et al. 2008; Grupe et al. 2015). A more precise definition of the burning temperatures is not possible visually because of variable parameters such as duration, oxygen availability, etc.

The high degree of fragmentation is both due to the loss of organic tissue components and thermally induced alterations of the crystal structure. Bone is a biomineral in which the mineral components are surrounded and penetrated by organic material, mainly the elastic structural protein collagen. This implies that the mineral crystals have limited contact to each other in the living being. After the organic components are gone in the course of the cremation process, space is supplied that permits growth of the mineral crystals until they fuse with each other. Crystallite size in a cremation can easily exceed 100 nm (Hüls et al. 2010). This process is comparable to a sinter process in the form of a solid-state reaction, which results in a macroscopically visible shrinkage of the skeletal elements. In fully cremated bones, this shrinkage can reach 10 % in every direction. Spherical bones such as the ball joint of the femur can be therefore by one third smaller in the cremated state compared to its original size (Grupe and Herrmann 1983). Since the different parts of a bone are subject to different physical loads (e.g. attachment sites of muscles and tendons induce bending stress), mineral density is not equal throughout the skeleton or even in a single bone. Higher mineral density in vivo only permits less shrinkage during cremation; therefore, the shrinkage of a bone is never homogenous. Fragmentation and change in size and shape are the results.

These thermal alterations are especially destructive for teeth. The composition of the root dentin is very similar to the composition of bone, while mature dental enamel is almost totally devoid of organic material (Hillson 1996). Shrinkage of the root leads to a separation of the crown, whereby the brittle enamel tends to split into smallest fragments. Dental enamel is therefore rarely preserved in cremations, and at best, tooth roots are preserved in only about 45 % of excavated finds (Grosskopf 2004). While even a small tooth root will not escape the eye of a skilled osteologist, it might well have been overlooked by the people who collected the burnt remains of a deceased person for burial, let alone that it is a very common find that not all body parts are represented in a prehistoric cremation.

Burial of a cremation in prehistoric times may follow different customs. Name-giving for a whole time period (the Urnfield culture) was the collection of the cremated bones and their deposition in an urn which was buried. But the cremated bodily relics could also have been simply buried in the soil, either with or without remnants of the cremation pyre. If neither pieces of an urn or relics of the pyre are detected, the cremated bones might have been placed into a container manufactured from organic material (e.g. a leather bag) which had decayed as time went by (Grupe et al. 2015).

Osteologists frequently observe that not all body parts are contained in a cremation. The easiest explanation is that only selected bones had been collected for burial which served as pars pro toto. On the other hand, more than one individual can be represented by a single cremation. If this concerns the majority of the body parts, more than one individual had been cremated at the same time. More often, only single or very few bones indicate the presence of a second

individual. This happens quite frequently when the prehistoric people used the same location for the cremations over and over again.

The anthropological investigation of cremated finds is therefore much more complex and time consuming than the inspection of uncremated inhumations. Under the prerequisite of a good state of preservation and the presence of the majority of body parts, macroscopic inspection augmented by histological and metric analyses leads to an anthropological diagnosis that is not or at least not too inferior to the respective diagnosis of an uncremated skeleton. But these prerequisites can by no means be taken for granted; therefore, for those time periods where inhumations are dominated by cremations, the reconstruction of human population development in time and space is still rather incomplete.

Since organic constituents are no longer or only by chance preserved, important archaeometric approaches such as palaeogenetic analyses are usually no longer possible. But the reconstruction of population admixture, mobility and migration by stable isotope analysis of heavy elements such as strontium and lead which are not subject to thermal alteration is possible and worth the effort, although with inherent limitations. First, the state of preservation must be sufficient for a firm identification of the basic biological parameters such as age at death and sex, and comingled bones of other individuals must be identifiable with certainty. In the case of the human cremations from the Urnfield culture which had been excavated to the north of the Alps, state of preservation was often very poor. Since a systematic investigation of human mobility based on cremated finds was attempted by our research group for the first time, an additional limiting factor was brought about by the mere amount of cremated bone material with regard to the indispensable accompanying mineralogical inspections for a validation of the isotopic date (Fig. 24a, b; see chapter "The Crystalline State of Archaeological Bone Material"). As a result, several cremated finds which should have been included into the project according to the initial plans turned out to be of limited use with regard to the overall research design, and substitutes had to be found.

Second, tooth roots were preserved in the study material only in exceptional cases. This constitutes an insurmountable limitation to migration research based on cremations. As mentioned above, dental enamel is hardly ever preserved, and tooth roots are on average preserved in less than 50 % of the finds. Enamel precipitates during childhood and juvenile age and is not remodelled thereafter. Non-local stable isotopic ratios in dental enamel are therefore unambiguous indicators for an immigrant to the site, because the individual in question must definitely have spent its childhood at a different place. In the absence of dental enamel, root dentin can be analysed alternatively because dentin, once formed, is only remodelled to a minimal extent during lifetime compared to the bone (Walters and Eyre 1983). When the dentition develops, the crown of the tooth is formed first, and the following growth of the root leads to the eruption of the tooth into the mouth cavity (Grupe et al. 2015). Dentin thus precipitates later than enamel but still during childhood and juvenile age. Modern clinical investigations on tissue turnover rates therefore frequently make use of dentin as a "metabolically inactive control material" (e.g. Sivan et al. 2008; Stabler et al. 2009).

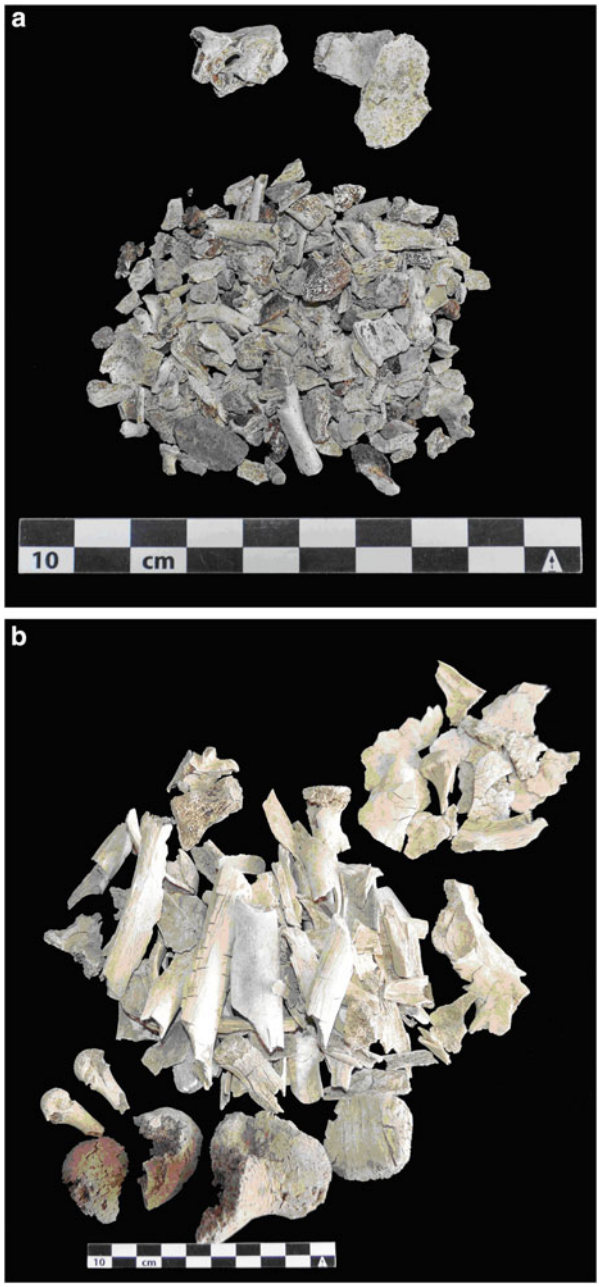

Fig. 24 Human cremations from the Urnfield culture. (**a**) Site 116: München-Grünwald (see Table 7). Fragment size is rather small and hardly meets the preservation criteria for this project. A single fragment has to be available that is large enough to permit for both strontium and lead isotope analyses and a mineralogical investigation. (**b**) Site 111: Englschalking (see Table 7). Almost perfect preservation, not only for the scope of the isotopic analyses but also for the osteological investigation. Photos by D. Wycisk

In cremations where no dentin is preserved, no archaeometric access to childhood conditions including the identification of early immigrants to a site is possible. Migration research based on stable isotopes will be limited to bone, a tissue that

Table 7 Individual cremated human bones analysed, place of recovery with geographical coordinates and all measurement data (the latter established by authors Wycisk, Mayr, Heck and Hölzl). Osteological investigation of the cremations by Dominika Wycisk, with the exception of the specimens from Kleinaitingen (Otto 2015), and 17 cremations from the Inn Valley that were diagnosed by George McGlynn

Site code, site name	Culture	°N	°E	m a.s.l.	Sex	Bone	$\delta^{18}O$	$^{87}Sr/^{86}Sr$	2SE [%]	$^{208}Pb/^{204}Pb$	2SE [%]	$^{207}Pb/^{204}Pb$	2SE [%]	$^{206}Pb/^{204}Pb$	2SE [%]	$^{208}Pb/^{207}Pb$	$^{206}Pb/^{207}Pb$
143, Aubing	Urnfield culture	48.16	11.42	520.9	Female	Cranium	–	0.70914	0.0022	38.7264	0.2080	15.6932	0.1578	19.3005	0.1101	2.4676	1.2298
	Urnfield culture	48.16	11.42	520.9	Indet[a]	Long bone	–	0.70897	0.0020	38.7971	0.2068	15.6978	0.1563	19.4012	0.1070	2.4715	1.2359
	Urnfield culture	48.16	11.42	520.9	Female	Radius	–	0.70908	0.0017	38.7028	0.2023	15.6869	0.1526	19.0855	0.1035	2.4672	1.2167
108, Eching	Urnfield culture	48.30	11.63	496.4	Indet	Femur	–	0.70873	0.0033	38.3827	0.2084	15.6459	0.1584	18.6126	0.1111	2.4533	1.1896
	Urnfield culture	48.30	11.63	496.4	Indet	Long bone	–	0.70850	0.0029	38.5437	0.2055	15.6823	0.1578	18.8812	0.1098	2.4580	1.2040
	Urnfield culture	48.30	11.63	496.4	Indet	Tibia	–	0.70872	0.0021	38.6956	0.2008	15.7068	0.1510	19.8895	0.1009	2.4636	1.2663
	Urnfield culture	48.30	11.63	496.4	Indet	Femur	–	0.70822	0.0026	38.3969	0.2023	15.6366	0.1528	18.5100	0.1035	2.4556	1.1838
	Urnfield culture	48.30	11.63	496.4	Indet	Long bone	–	0.70858	0.0024	38.5201	0.2045	15.6687	0.1558	19.0595	0.1082	2.4584	1.2165
	Urnfield culture	48.30	11.63	496.4	Indet	Femur	–	0.70864	0.0022	38.7198	0.2067	15.7397	0.1587	19.3021	0.1119	2.4600	1.2263
	Urnfield culture	48.30	11.63	496.4	Male	Humerus	–	0.70863	0.0028	38.3792	0.2013	15.6299	0.1512	18.6954	0.1015	2.4555	1.1962
	Urnfield culture	48.30	11.63	496.4	Indet	Humerus	–	0.70932	0.0033	38.3843	0.2015	15.6456	0.1514	18.9106	0.1016	2.4535	1.2087
	Urnfield culture	48.30	11.63	496.4	Indet	Long bone	–	0.70932	0.0031	38.5115	0.2019	15.6667	0.1532	19.0855	0.1049	2.4582	1.2182
	Urnfield culture	48.30	11.63	496.4	Female	Humerus	–	0.70933	0.0047	38.6354	0.2041	15.7116	0.1562	20.0056	0.1073	2.4592	1.2733
	Urnfield culture	48.30	11.63	496.4	Indet	Femur	–	0.70880	0.0054	38.6421	0.2007	15.6975	0.1509	19.6397	0.1011	2.4617	1.2511
	Urnfield culture	48.30	11.63	496.4	Indet	Long bone	–	0.70862	0.0013	38.5971	0.2057	15.7131	0.1571	19.7553	0.1094	2.4564	1.2573
	Urnfield culture	48.30	11.63	496.4	Male	Tibia	–	0.70854	0.0016	38.5886	0.2007	15.6882	0.1508	19.3899	0.1013	2.4597	1.2360
	Urnfield culture	48.30	11.63	496.4	Indet	Long bone	–	0.70960	0.0040	38.4732	0.2010	15.6424	0.1510	18.7076	0.1013	2.4596	1.1959
	Urnfield culture	48.30	11.63	496.4	Female	Femur	–	0.70852	0.0041	38.6019	0.2073	15.6941	0.1580	19.7293	0.1107	2.4596	1.2571

(continued)

Table 7 (continued)

Site code, site name	Culture	°N	°E	m a.s.l.	Sex	Bone	$\delta^{18}O$	$^{87}Sr/^{86}Sr$	2SE [%]	$^{208}Pb/^{204}Pb$	2SE [%]	$^{207}Pb/^{204}Pb$	2SE [%]	$^{206}Pb/^{204}Pb$	2SE [%]	$^{208}Pb/^{207}Pb$	$^{206}Pb/^{207}Pb$
	Urnfield culture	48.30	11.63	496.4	Indet	Humerus	–	0.70861	0.0031	38.3830	0.2039	15.7263	0.1555	19.5678	0.1084	2.4407	1.2441
	Urnfield culture	48.30	11.63	496.4	Indet	Long bone	–	0.70870	0.0027	38.2559	0.2016	15.6514	0.1514	18.6779	0.1020	2.4443	1.1934
	Urnfield culture	48.30	11.63	496.4	Indet	Tibia	–	0.71018	0.0017	38.4793	0.2086	15.6936	0.1600	19.1884	0.1133	2.4519	1.2227
	Urnfield culture	48.30	11.63	496.4	Indet	Femur	–	0.70895	0.0045	38.4210	0.2027	15.6890	0.1524	19.4453	0.1028	2.4489	1.2394
	Urnfield culture	48.30	11.63	496.4	Indet	Tibia	–	0.70872	0.0022	38.6786	0.2012	15.7261	0.1509	20.0348	0.1011	2.4596	1.2740
	Urnfield culture	48.30	11.63	496.4	Indet	Femur	–	0.70874	0.0047	38.7848	0.2066	15.7498	0.1552	19.8953	0.1056		1.2632
111, Englschalking	Urnfield culture	48.15	11.63	521.2	Female	Humerus[c]	–	0.70860	0.0025	38.5705	0.2030	15.6857	0.1533	19.3504	0.1044	2.4590	1.2336
	Urnfield culture	48.15	11.63	521.2	Indet	Femur[c]	–	0.70909	0.0015	38.7649	0.2003	15.6820	0.1503	18.8573	0.1004	2.4720	1.2025
121, Hofoldinger Forst	Urnfield culture	47.95	11.72	641.9	Indet	Long bone	–	0.71153	0.0019	38.6800	0.2053	15.7020	0.1571	19.5870	0.1115	2.4639	1.2473
	Urnfield culture	47.95	11.72	641.9	Indet	Femur[c]	–	0.70890	0.0021							2.4552	
	Urnfield culture	47.95	11.72	641.9	Male	Tibia[c]	–	0.71009	0.0023	38.5913	0.2004	15.6754	0.1505	19.2748	0.1008	2.4619	1.2296
130, Obermenzing	Urnfield culture	48.17	11.47	513.4	Male	Femur	–	0.70960	0.0026	38.6082	0.2018	15.6942	0.1527	19.1415	0.1041	2.4601	1.2197
	Urnfield culture	48.17	11.47	513.4	Indet	Long bone	–	0.70850	0.0017	38.5864	0.2048	15.6816	0.1570	19.0694	0.1107	2.4607	1.2161
	Urnfield culture	48.17	11.47	513.4	Male	Long bone	–	0.70869	0.0037	38.4896	0.2012	15.6571	0.1511	18.8767	0.1013	2.4583	1.2056
	Urnfield culture	48.17	11.47	513.4	Indet	Long bone	–	0.70909	0.0038							2.4587	
	Urnfield culture	48.17	11.47	513.4	Indet	Long bone	–	0.70881	0.0024	38.6920	0.2024	15.6917	0.1535	19.3737	0.1051	2.4659	1.2347
	Urnfield culture	48.17	11.47	513.4	Male	Long bone	–	0.70849	0.0015							2.4549	
	Urnfield culture	48.17	11.47	513.4	Indet	Long bone	–	0.70832	0.0035								1.2021

	Urnfield culture	48.17	11.47	513.4	Male	Long bone	–	0.70827	0.0022							2.4559	
	Urnfield culture	48.17	11.47	513.4	Indet	Long bone	–	0.70844	0.0026	38.4990	0.2058	15.6598	0.1581	19.1342	0.1111	2.4591	1.2220
	Urnfield culture	48.17	11.47	513.4	Male	Long bone	–	0.70847	0.0023	38.3932	0.2065	15.6610	0.1578	18.9365	0.1095	2.4515	1.2091
	Urnfield culture	48.17	11.47	513.4	Indet	Long bone	–	0.70844	0.0018	38.5179	0.2029	15.6655	0.1519	19.2172	0.1018	2.4587	1.2267
	Urnfield culture	48.17	11.47	513.4	Indet	Long bone	–	0.70840	0.0028	38.5689	0.2031	15.6678	0.1525	18.5466	0.1029	2.4617	1.1838
	Urnfield culture	48.17	11.47	513.4	Male	Long bone	–	0.70845	0.0025	38.6103	0.2023	15.6618	0.1527	18.9163	0.1037	2.4653	1.2078
	Urnfield culture	48.17	11.47	513.4	Male	Long bone	–	0.70852	0.0024	38.6103	0.2099	15.6926	0.1618	19.1459	0.1165	2.4605	1.2201
	Urnfield culture	48.17	11.47	513.4	Indet	Long bone	–	0.70798	0.0016	38.4827	0.2106	15.6622	0.1635	18.8675	0.1175	2.4571	1.2045
	Urnfield culture	48.17	11.47	513.4	Male	Long bone	–	0.70873	0.0038	38.3366	0.2089	15.6255	0.1619	18.6529	0.1154	2.4535	1.1937
	Urnfield culture	48.17	11.47	513.4	Indet	Long bone	–	0.70877	0.0018	38.5676	0.2006	15.6782	0.1506	19.2576	0.1008	2.4599	1.2283
	Urnfield culture	48.17	11.47	513.4	Indet	Long bone	–	0.70862	0.0033							2.4471	1.1954
	Urnfield culture	48.17	11.47	513.4	Indet	Long bone	–	0.70839	0.0021	38.4463	0.2004	15.6533	0.1503	18.7222	0.1003	2.4562	1.1961
	Urnfield culture	48.17	11.47	513.4	Female[c]	Long bone	–	0.70867	0.0021							2.4537	
	Urnfield culture	48.17	11.47	513.4	Indet	Long bone	–	0.70863	0.0028							2.4528	
	Urnfield culture	48.17	11.47	513.4	Indet	Long bone	–	0.70914	0.0019	38.2657	0.2055	15.6058	0.1567	18.6637	0.1098	2.4523	1.1959
	Urnfield culture	48.17	11.47	513.4	Indet	Long bone	–	0.70852	0.0013	38.4612	0.2005	15.6267	0.1505	18.5724	0.1007	2.4613	1.1885
138, Waging am See	Urnfield culture	47.93	12.73	463.8	Indet	Cranium	–	0.70851	0.0026	38.7552	0.2005	15.6697	0.1505	18.9989	0.1006	2.4733	1.2124
	Urnfield culture	47.93	12.73	463.8	Indet	Long bone	–	0.70846	0.0026	38.7028	0.2007	15.6778	0.1506	19.1531	0.1007	2.4687	1.2217
	Urnfield culture	47.93	12.73	463.8	Female	Femur	–	0.70868	0.0038	38.4671	0.2051	15.6304	0.1554	18.6873	0.1087	2.4611	1.1955

(continued)

Table 7 (continued)

Site code, site name	Culture	°N	°E	m a.s.l.	Sex	Bone	$\delta^{18}O$	$^{87}Sr/^{86}Sr$	2SE [%]	$^{208}Pb/^{204}Pb$	2SE [%]	$^{207}Pb/^{204}Pb$	2SE [%]	$^{206}Pb/^{204}Pb$	2SE [%]	$^{208}Pb/^{207}Pb$	$^{206}Pb/^{207}Pb$
160, Flintsbach am Inn	Urnfield culture	47.72	12.13	472.9	Indet	Long bone	–	0.70848	0.0017	38.7671	0.2008	15.6769	0.1506	18.7862	0.1008	2.4729	1.1983
	Urnfield culture	47.72	12.13	472.9	Indet	Cranium	–	0.70861	0.0014	38.7834	0.2006	15.6776	0.1506	18.7317	0.1008	2.4738	1.1948
	Urnfield culture	47.72	12.13	472.9	Male	Humerus	–	0.70848	0.0017	38.2311	0.2010	15.6334	0.1508	18.3099	0.1009	2.4454	1.1712
	Urnfield culture	47.72	12.13	472.9	Indet	Long bone	–	0.70832	0.0018	38.5982	0.2007	15.6507	0.1507	18.6459	0.1010	2.4662	1.1914
144, Forstinning	Urnfield culture	48.16	11.91	511.5	Indet	Pars petrosa	–	0.71045	0.0025	38.8027	0.2018	15.7025	0.1520	19.2870	0.1029	2.4713	1.2283
	Urnfield culture	48.16	11.91	511.5	Female	Femur	–	0.70992	0.0032	38.7103	0.2014	15.6940	0.1515	19.2403	0.1019	2.4667	1.2260
116, Grünwald	Urnfield culture	48.04	11.53	593.8	Indet	Cranium	–	0.70926	0.0022	38.7569	0.2003	15.7101	0.1503	19.6556	0.1003	2.4670	1.2511
	Urnfield culture	48.04	11.53	593.8	Female	Femur	–	0.70902	0.0050	38.5659	0.2072	15.6956	0.1572	19.2993	0.1103		1.2296
	Urnfield culture	48.04	11.53	593.8	Indet	Humerus	–	0.70898	0.0014	38.6250	0.2010	15.6807	0.1507	19.2141	0.1009	2.4632	1.2253
	Urnfield culture	48.04	11.53	593.8	Indet	Femur/ humerus	–	0.70962	0.0014	38.6913	0.2005	15.6888	0.1505	19.3953	0.1009	2.4662	1.2362
154, Kleinaitingen	Urnfield culture	48.22	10.84	538.9	Indet	Femur	–	0.70876	0.0021	38.5832	0.2051	15.7471	0.1557	19.9859	0.1064	2.4502	1.2694
	Urnfield culture	48.22	10.84	538.9	Indet	Femur	–	0.70844	0.0016							2.4516	1.1979
	Urnfield culture	48.22	10.84	538.9	Male	Femur	–	0.70851	0.0180	38.3296	0.2086	15.6377	0.1599	18.5826	0.1129	2.4511	1.1885
	Urnfield culture	48.22	10.84	538.9	Indet	Femur	–	0.71011	0.0015	38.4536	0.2030	15.6791	0.1523	19.3698	0.1027	2.4526	1.2354
	Urnfield culture	48.22	10.84	538.9	Indet	Femur	–	0.70826	0.0016	38.5623	0.2006	15.6862	0.1504	19.6945	0.1006	2.4584	1.2555
	Urnfield culture	48.22	10.84	538.9	Indet	Femur	–	0.70903	0.0018	38.3231	0.2016	15.6467	0.1516	18.7613	0.1023	2.4494	1.1991
	Urnfield culture	48.22	10.84	538.9	Female	Femur	–	0.70938	0.0050	38.4399	0.2089	15.6531	0.1615	18.7852	0.1157	2.4560	1.2002
	Urnfield culture	48.22	10.84	538.9	Female	Femur	–	0.70917	0.0016	38.3439	0.2016	15.6812	0.1513	19.1871	0.1013	2.4451	1.2236

	Urnfield culture	48.22	10.84	538.9	Indet	Femur	–	0.70907	0.0026	38.6207	0.2043	15.6814	0.1546	19.3958	0.1069	2.4630	1.2369
	Urnfield culture	48.22	10.84	538.9	Female[c]	Femur	–	0.70912	0.0017	38.4411	0.2024	15.7127	0.1522	19.5624	0.1025	2.4465	1.2450
	Urnfield culture	48.22	10.84	538.9	Female	Femur	–	0.70912	0.0014	38.4211	0.2020	15.6767	0.1519	19.3523	0.1022	2.4509	1.2345
	Urnfield culture	48.22	10.84	538.9	Male	Femur	–	0.70870	0.0036	38.4058	0.2010	15.6468	0.1509	19.0857	0.1011	2.4546	1.2197
	Urnfield culture	48.22	10.84	538.9	Indet	Femur	–	0.70948	0.0029							2.4504	1.1742
	Urnfield culture	48.22	10.84	538.9	Indet	Femur	–	0.70905	0.0027	38.6907	0.2024	15.6920	0.1527	19.1233	0.1036	2.4658	1.2187
	Urnfield culture	48.22	10.84	538.9	Indet	Femur	–	0.70985	0.0018	38.4716	0.2067	15.7271	0.1569	19.6729	0.1077	2.4461	1.2510
	Urnfield culture	48.22	10.84	538.9	Male	Long bone	–	0.70898	0.0019	38.4816	0.2041	15.6756	0.1554	18.9278	0.1083	2.4550	1.2075
	Urnfield culture	48.22	10.84	538.9	Male	Femur	–	0.70898	0.0019	38.4821	0.2060	15.6799	0.1571	19.1894	0.1094	2.4541	1.2237
	Urnfield culture	48.22	10.84	538.9	Male	Femur	–	0.71001	0.0029	38.4179	0.2018	15.6564	0.1516	18.9057	0.1023	2.4538	1.2075
	Urnfield culture	48.22	10.84	538.9	Female	Long bone	–	0.70902	0.0020	38.5559	0.2023	15.6859	0.1529	18.9351	0.1039	2.4582	1.2072
	Urnfield culture	48.22	10.84	538.9	Female	Femur	–	0.70846	0.0025	38.1504	0.2076	15.7329	0.1596	19.7884	0.1168	2.4250	
	Urnfield culture	48.22	10.84	538.9	Male	Femur	–	0.70840	0.0035	38.3843	0.2007	15.6214	0.1506	18.7504	0.1006	2.4571	1.2002
	Urnfield culture	48.22	10.84	538.9	Indet	Femur	–	0.70836	0.0025	38.5363	0.2025	15.6788	0.1520	19.1735	0.1025	2.4578	1.2229
	Urnfield culture	48.22	10.84	538.9	Indet	Femur	–	0.70872	0.0019	38.2298	0.2024	15.6574	0.1532	19.0538	0.1050	2.4417	1.2169
140, Gemlinden	Urnfield culture	48.21	11.30	511.9	Male	Femur	–	0.70874	0.0017	38.6485	0.2039	15.6961	0.1537	19.2405	0.1052	2.4622	1.2258
	Urnfield culture	48.21	11.30	511.9	Male	Femur	–	0.70937	0.0017							2.4613	1.2273
	Urnfield culture	48.21	11.30	511.9	Indet	Humerus	–	0.70868	0.0022	38.5336	0.2122	15.6671	0.1656			2.4598	

(continued)

Table 7 (continued)

Site code, site name	Culture	°N	°E	m a.s.l.	Sex	Bone	$\delta^{18}O$	$^{87}Sr/^{86}Sr$	2SE [%]	$^{208}Pb/^{204}Pb$	2SE [%]	$^{207}Pb/^{204}Pb$	2SE [%]	$^{206}Pb/^{204}Pb$	2SE [%]	$^{208}Pb/^{207}Pb$	$^{206}Pb/^{207}Pb$
141, Unterhaching	Urnfield culture	48.07	11.62	558.0	Male	Femur	–	0.70841	0.0014							2.4455	1.1941
	Urnfield culture	48.07	11.62	558.0	Male	Femur	–	0.70998	0.0023							2.4563	
	Urnfield culture	48.07	11.62	558.0	Indet	Long bone	–	0.70860	0.0017							2.4563	1.1990
125, Langengeisling	Urnfield culture	48.33	11.93	455.8	Male	Humerus	–	0.70980	0.0025	38.2540	0.2035	15.6088	0.1539	18.4248	0.1050	2.4509	1.1803
	Urnfield culture	48.33	11.93	455.8	Male	Femur	–	0.71016	0.0021	38.7762	0.2004	15.6766	0.1505	19.0386	0.1006	2.4736	1.2144
158, Garching an der Alz	Urnfield culture	48.13	12.58	459.0	Indet	Femur	–	0.71002	0.0022	38.4695	0.2018	15.6866	0.1514	19.2861	0.1021	2.4525	1.2295
	Urnfield culture	48.13	12.58	459.0	Male	Femur	–	0.70878	0.0014	38.1564	0.2020	15.6857	0.1519	19.1121	0.1029	2.4326	1.2184
153, Kirchheim	Urnfield culture	48.18	11.76	514.1	Indet	Femur	–	0.70872	0.0040	38.5564	0.2080	15.6587	0.1584	18.9353	0.1099	2.4623	1.2092
156, München-Residenz	Urnfield culture	48.14	11.58	515.3	Female	Femur	–	0.70872	0.0015	38.2510	0.2079	15.6585	0.1576	18.8397	0.1083	2.4429	
155, Königsbrunn-Zeller	Urnfield culture	48.27	10.89	517.0	Indet	Long bone	–	0.70880	0.0018	38.3999	0.2080	15.6710	0.1571	19.0645	0.1084	2.4503	1.2165
							–										
132, Poing	Urnfield culture	48.17	11.81	515.3	Indet	Femur	–	0.70846	0.0016	38.6545	0.2036	15.7067	0.1521	19.3741	0.1024		1.2334
							–										
136, Trudering	Urnfield culture	48.13	11.66	527.5	Male	Femur	–	0.70837	0.0025	38.5458	0.2046	15.7005	0.1539	19.4776	0.1050	2.4550	1.2406
	Urnfield culture	48.13	11.66	527.5	Male[c]	Femur[c]	–	0.71166	0.0021	38.6779	0.2016	15.7011	0.1515	19.5836	0.1019	2.4634	1.2473
	Urnfield culture	48.13	11.66	527.5	Female	long Bone	–	0.70863	0.0021	38.5664	0.2049	15.6918	0.1553	19.3037	0.1061	2.4577	1.2303
249, Ambras	Urnfield culture	47.26	11.43	633.0	Indet	Humerus	–	0.71126	0.0027	38.8333	0.2024	15.6875	0.1529	18.8649	0.1043	2.4754	1.2026
238, Ampaß	Urnfield culture	47.26	11.46	656.1	Indet	Long bone	–	0.713525	0.0035	38.4808	0.2072	15.6667	0.1592	18.5110	0.1135	2.4563	1.1815

246, Ellbögen St. Peter	Urnfield culture	47.19	11.43	1070.9	Female	Humerus	–	0.71272	0.0014	38.7328	0.2019	15.6856	0.1527	18.5619	0.1041	2.4693	1.1834
	Urnfield culture	47.19	11.43	1070.9	Indet	Tibia	–	0.71591	0.0022							2.4675	1.1957
244, Fügen-Kapfing	Urnfield culture	47.33	11.86	563.7	Indet	Femur	–	0.71593	0.0023	38.6965	0.2012	15.6653	0.1511	18.5485	0.1016	2.4701	1.1840
209, Hötting	Urnfield culture	47.27	11.37	663.4	Female	Ulna/radius	–	0.71788	0.0030	38.4810	0.2003	15.6652	0.1503	18.2829	0.1003	2.4565	1.1671
	Urnfield culture	47.27	11.37	663.4	Female	Femur	–	0.70875	0.0031	38.4440	0.2005	15.6636	0.1504	18.7448	0.1006	2.4542	1.1967
	Urnfield culture	47.27	11.37	663.4	Male	femur	–	0.70877	0.0042	38.3476	0.2031	15.6446	0.1524	18.7802	0.1024	2.4513	
	Urnfield culture	47.27	11.37	663.4	Male	Tibia	–	0.70891	0.0029	38.5787	0.2019	15.6645	0.1521	18.6430	0.1030	2.4629	1.1902
	Urnfield culture	47.27	11.37	663.4	Male	Femur	–	0.70889	0.0026	37.9212	0.2019	15.9882	0.1519	22.8229	0.1021	2.3718	1.4274
	Urnfield culture	47.27	11.37	663.4	Male	Femur	–	0.70870	0.0037	38.2032	0.2048	15.6314	0.1553	18.3066	0.1075	2.4441	1.1711
243, Kitzbühel	Urnfield culture	47.45	12.39	757.2	Male	Long bone	–	0.71090	0.0018	38.6106	0.2024	15.6757	0.1522	18.6661	0.1023	2.4630	1.1908
	Urnfield culture	47.45	12.39	757.2	Indet	Femur	–	0.71160	0.0025	38.6830	0.2094	15.7053	0.1620	18.5548	0.1169	2.4631	1.1814
	Urnfield culture	47.45	12.39	757.2	Female	Long bone	–	0.70914	0.0021	38.6669	0.2019	15.6673	0.1516	18.5591	0.1021	2.4680	1.1846
	Urnfield culture	47.45	12.39	757.2	Indet	Long bone	–	0.71113	0.0022	38.7582	0.2004	15.7133	0.1505	18.4053	0.1007	2.4666	1.1713
	Urnfield culture	47.45	12.39	757.2	Indet	Cranium	–	0.71129	0.0023	38.7139	0.2023	15.6708	0.1532	18.6551	0.1047	2.4707	1.1904
	Urnfield culture	47.45	12.39	757.2	Indet	Long bone	–	0.71022	0.0025	38.7371	0.2063	15.6795	0.1591	18.7074	0.1129	2.4708	1.1931
215, Mühlau	Urnfield culture	47.28	11.42	592.2	Female	Humerus	–	0.71189	0.0031	38.4517	0.2013	15.6583	0.1511	18.2872	0.1014	2.4558	1.1679
226, Mühlbachl-Matrei	Urnfield culture	47.14	11.45	1065.5	Female	Radius[c]	–	0.70971	0.0016	38.5349	0.2045	15.6185	0.1541	18.8057	0.1048	2.4600	1.2004
	Urnfield culture	47.14	11.45	1065.5	Female[c]	Humerus[c]	–	0.70982	0.0024	38.4530	0.2117	15.6343	0.1632	18.5390	0.1181	2.4595	1.1858
233, Vomp	Urnfield culture	47.34	11.69	540.3	Indet	Femur	–	0.71042	0.0020	38.6182	0.2019	15.6787	0.1513	18.5738	0.1014	2.4632	1.1846

(continued)

Table 7 (continued)

Site code, site name	Culture	°N	°E	m a.s.l.	Sex	Bone	$\delta^{18}O$	$^{87}Sr/^{86}Sr$	2SE [%]	$^{208}Pb/^{204}Pb$	2SE [%]	$^{207}Pb/^{204}Pb$	2SE [%]	$^{206}Pb/^{204}Pb$	2SE [%]	$^{208}Pb/^{207}Pb$	$^{206}Pb/^{207}Pb$
211, Wilten	Urnfield culture	47.26	11.38	578.3	Male	Femur	–	0.71094	0.0012	38.6790	0.2109	15.6775	0.1626	18.6802	0.1191	2.4668	1.1912
	Urnfield culture	47.26	11.38	578.3	Female	Tibia	–	0.71024	0.0027	38.5134	0.2016	15.6524	0.1516	18.5001	0.1021	2.4606	1.1819
221, Kundl	Fritzens-Sanzeno culture	47.47	11.99	521.0	Male	Long bone	–	0.70907	0.0019	38.3803	0.2001	15.6387	0.1502	18.3528	0.1002	2.4542	1.1735
	Fritzens-Sanzeno culture	47.47	11.99	521.0	Indet	Long bone	–	0.71197	0.0023	38.4711	0.2002	15.6542	0.1502	18.4126	0.1002	2.4576	1.1762
	Fritzens-Sanzeno culture	47.47	11.99	521.0	Male[c]	Femur	–	0.70920	0.0028	38.4992	0.2003	15.6619	0.1502	18.4243	0.1002	2.4581	1.1764
	Fritzens-Sanzeno culture	47.47	11.99	521.0	Indet	Femur	–	0.71070	0.0022	38.3964	0.2001	15.6396	0.1501	18.3664	0.1002	2.4551	1.1743
	Fritzens-Sanzeno culture	47.47	11.99	521.0	Indet	Long bone	–	0.71083	0.0048	38.5140	0.2003	15.6581	0.1502	18.4705	0.1003	2.4598	1.1796
	Fritzens-Sanzeno culture	47.47	11.99	521.0	Male	Long bone	–	0.70929	0.0018	38.2446	0.2006	15.6349	0.1505	18.2740	0.1005	2.4461	1.1688
	Fritzens-Sanzeno culture	47.47	11.99	521.0	Indet[b]	Femur	–	0.71054	0.0020	38.5661	0.2004	15.6695	0.1505	18.4750	0.1006	2.4612	1.1790
	Fritzens-Sanzeno culture	47.47	11.99	521.0	Female	Long bone	–	0.71029	0.0058	38.8297	0.2002	15.7269	0.1502	18.5329	0.1002	2.4691	1.1784
	Fritzens-Sanzeno culture	47.47	11.99	521.0	Indet	Long bone	–	0.71012	0.0023	38.9675	0.2012	15.7393	0.1508	18.7144	0.1006	2.4758	1.1890
	Fritzens-Sanzeno culture	47.47	11.99	521.0	Indet	Long bone	–	0.71094	0.0020	37.9895	0.2001	15.5847	0.1501	18.1376	0.1001	2.4376	1.1638
	Fritzens-Sanzeno culture	47.47	11.99	521.0	Indet	Long bone	–	0.71139	0.0023	38.3824	0.2003	15.6396	0.1503	18.3857	0.1003	2.4542	1.1756

	Fritzens-Sanzeno culture	47.47	11.99	521.0	Female [c]	Femur	–	0.70982	0.0018	38.5737	0.2001	15.6698	0.1501	18.4882	0.1001	2.4616	1.1799
	Fritzens-Sanzeno culture	47.47	11.99	521.0	Indet	Femur/humerus	–	0.71125	0.0017	38.1815	0.2019	15.6248	0.1512	18.2135	0.1010	2.4437	1.1656
	Fritzens-Sanzeno culture	47.47	11.99	521.0	Indet	Long bone	–	0.71131	0.0014	38.5242	0.2012	15.6697	0.1512	18.4590	0.1018	2.4585	1.1780
	Fritzens-Sanzeno culture	47.47	11.99	521.0	Indet	Long bone	–	0.71084	0.0018	38.5631	0.2002	15.6581	0.1503	18.4170	0.1003	2.4628	1.1762
	Fritzens-Sanzeno culture	47.47	11.99	521.0	Indet[a]	Femur	–	0.71123	0.0022	38.4260	0.2014	15.6504	0.1512	18.4032	0.1015	2.4553	1.1759
	Fritzens-Sanzeno culture	47.47	11.99	521.0	Female	Long bone	–	0.71210	0.0014	38.6756	0.2038	15.6699	0.1542	18.6006	0.1058	2.4682	1.1871
	Fritzens-Sanzeno culture	47.47	11.99	521.0	Indet	Long bone	–	0.71113	0.0022	38.3164	0.2006	15.6147	0.1506	18.4447	0.1008	2.4540	1.1812
	Fritzens-Sanzeno culture	47.47	11.99	521.0	Indet	Long bone	–	0.70971	0.0017	38.5585	0.2003	15.6532	0.1502	18.5142	0.1002	2.4634	1.1828
	Fritzens-Sanzeno culture	47.47	11.99	521.0	Indet[a]	Femur	–	0.71025	0.0015	38.3140	0.2021	15.6316	0.1514	18.3392	0.1021	2.4513	1.1733
	Fritzens-Sanzeno culture	47.47	11.99	521.0	Indet[b]	Femur	–	0.71104	0.0020	38.5572	0.2036	15.6784	0.1537	18.4518	0.1051	2.4593	1.1769
	Fritzens-Sanzeno culture	47.47	11.99	521.0	Male	Humerus	–	0.70918	0.0018	38.3771	0.2062	15.6450	0.1577	18.4471	0.1118	2.4530	1.1791
	Fritzens-Sanzeno culture	47.47	11.99	521.0	Male	Femur	–	0.71068	0.0018	38.2069	0.2008	15.6241	0.1507	18.2601	0.1009	2.4453	1.1687
	Fritzens-Sanzeno culture	47.47	11.99	521.0	Indet	Long bone	–	0.71079	0.0018	38.6657	0.2001	15.6452	0.1500	18.7644	0.1001	2.4714	1.1994
	Fritzens-Sanzeno culture	47.47	11.99	521.0	Indet	Femur/humerus	–	0.71077	0.0038	38.3973	0.2005	15.6436	0.1504	18.4348	0.1004	2.4545	1.1784

(continued)

Table 7 (continued)

Site code, site name	Culture	°N	°E	m a.s.l.	Sex	Bone	$\delta^{18}O$	$^{87}Sr/^{86}Sr$	2SE [%]	$^{208}Pb/^{204}Pb$	2SE [%]	$^{207}Pb/^{204}Pb$	2SE [%]	$^{206}Pb/^{204}Pb$	2SE [%]	$^{208}Pb/^{207}Pb$	$^{206}Pb/^{207}Pb$
307, Moritzing	Fritzens-Sanzeno culture	46.50	11.31	251.2	Indet	Long bone	–	0.71199	0.0030	38.8047	0.2001	15.6949	0.1501	18.5600	0.1002	2.4725	1.1826
	Fritzens-Sanzeno culture	46.50	11.31	251.2	Indet	Long bone	–	0.71400	0.0032	38.8643	0.2023	15.7080	0.1517	18.5634	0.1012	2.4743	1.1818
	Fritzens-Sanzeno culture	46.50	11.31	251.2	Indet	Long bone	–	0.71514	0.0029	38.8100	0.2017	15.6993	0.1521	18.6072	0.1029	2.4722	1.1852
	Fritzens-Sanzeno culture	46.50	11.31	251.2	Indet	Femur	–	0.71519	0.0026	38.9103	0.2061	15.7156	0.1581	18.8394	0.1116	2.4759	1.1987
	Fritzens-Sanzeno culture	46.50	11.31	251.2	Indet	Long bone	–	0.71261	0.0018	38.8232	0.2002	15.6732	0.1501	18.6501	0.1002	2.4770	1.1899
	Fritzens-Sanzeno culture	46.50	11.31	251.2	Indet	Humerus	–	0.71283	0.0019	38.8364	0.2001	15.7028	0.1501	18.6273	0.1001	2.4732	1.1862
	Fritzens-Sanzeno culture	46.50	11.31	251.2	Indet	Femur	–	0.71105	0.0023	38.7344	0.2002	15.6723	0.1502	18.5233	0.1003	2.4715	1.1819
	Fritzens-Sanzeno culture	46.50	11.31	251.2	Indet	Long bone	–	0.71307	0.0031	38.8137	0.2008	15.6933	0.1507	18.5943	0.1009	2.4733	1.1849
	Fritzens-Sanzeno culture	46.50	11.31	251.2	Indet	Femur[c]	–	0.71562	0.0036	38.9090	0.2005	15.7230	0.1504	18.5579	0.1003	2.4747	1.1803
	Fritzens-Sanzeno culture	46.50	11.31	251.2	Indet	Femur	–	0.71277	0.0017	38.6687	0.2001	15.6544	0.1501	18.5191	0.1001	2.4701	1.1830
	Fritzens-Sanzeno culture	46.50	11.31	251.2	Indet	Long bone	–	0.71335	0.0021	38.8064	0.2006	15.6940	0.1505	18.6464	0.1004	2.4727	1.1881
308, Pfatten	Fritzens-Sanzeno culture	46.41	11.31	248.3	Indet	Humerus	–	0.71250	0.0015	38.7410	0.2004	15.6724	0.1505	18.7100	0.1007	2.4721	1.1938
	Fritzens-Sanzeno culture	46.41	11.31	248.3	Indet	Femur	–	0.71065	0.0020	38.8792	0.2032	15.6926	0.1536	18.8460	0.1054	2.4774	1.2009

	Fritzens-Sanzeno culture	46.41	11.31	248.3	Male	Rib	–	0.71497	0.0041	38.8043	0.2001	15.6680	0.1501	18.7047	0.1002	2.4767	1.1938
	Fritzens-Sanzeno culture	46.41	11.31	248.3	Female	Femur/humerus	–	0.71276	0.0019	38.8003	0.2009	15.6820	0.1510	18.7744	0.1013	2.4742	1.1972
304, Latsch	Fritzens-Sanzeno culture	46.62	10.86	641.1	Indet	Humerus	13.3	0.71816	0.0019	38.5362	0.2011	15.6493	0.1509	18.7432	0.1012	2.4625	1.1977
	Fritzens-Sanzeno culture	46.62	10.86	641.1	Indet	Humerus	13.6	0.72058	0.0018	38.4894	0.2010	15.6455	0.1510	18.5992	0.1012	2.4601	1.1888
	Fritzens-Sanzeno culture	46.62	10.86	641.1	Indet	Humerus	13.8	0.72167	0.0016	38.5957	0.2013	15.6590	0.1514	18.7497	0.1018	2.4647	1.1974
	Fritzens-Sanzeno culture	46.62	10.86	641.1	Indet	Humerus	13.7	0.72144	0.0017	38.5092	0.2003	15.6497	0.1503	18.6467	0.1003	2.4607	1.1915
	Fritzens-Sanzeno culture	46.62	10.86	641.1	Indet	Humerus	13.9	0.72185	0.0018	38.3693	0.2001	15.6255	0.1502	18.5451	0.1002	2.4556	1.1869
	Fritzens-Sanzeno culture	46.62	10.86	641.1	Indet	Humerus	14.0	0.71925	0.0016	38.5181	0.2003	15.6512	0.1503	18.8594	0.1004	2.4611	1.2050
	Fritzens-Sanzeno culture	46.62	10.86	641.1	Indet	Humerus	15.3	0.71955	0.0024	38.4733	0.2029	15.6427	0.1534	18.6462	0.1045	2.4595	1.1920
	Fritzens-Sanzeno culture	46.62	10.86	641.1	Indet	Humerus	14.5	0.72048	0.0013	38.5716	0.2002	15.6451	0.1502	18.5674	0.1002	2.4654	1.1868
	Fritzens-Sanzeno culture	46.62	10.86	641.1	Indet	Humerus	13.9	0.72147	0.0022	38.5453	0.2005	15.6535	0.1505	18.6984	0.1005	2.4624	1.1946
	Fritzens-Sanzeno culture	46.62	10.86	641.1	Indet	Humerus	14.0	0.72141	0.0017	38.3666	0.2004	15.6185	0.1504	18.4650	0.1006	2.4566	1.1822
	Fritzens-Sanzeno culture	46.62	10.86	641.1	Indet	Humerus	14.4	0.72228	0.0019	38.4996	0.2001	15.6512	0.1501	18.4639	0.1001	2.4599	1.1797
	Fritzens-Sanzeno culture	46.62	10.86	641.1	Indet	Humerus	13.5	0.71832	0.0018	38.6085	0.2003	15.6658	0.1504	18.7170	0.1005	2.4645	1.1948

(continued)

Table 7 (continued)

Site code, site name	Culture	°N	°E	m a.s.l.	Sex	Bone	$\delta^{18}O$	$^{87}Sr/^{86}Sr$	2SE [%]	$^{208}Pb/^{204}Pb$	2SE [%]	$^{207}Pb/^{204}Pb$	2SE [%]	$^{206}Pb/^{204}Pb$	2SE [%]	$^{208}Pb/^{207}Pb$	$^{206}Pb/^{207}Pb$
	Fritzens-Sanzeno culture	46.62	10.86	641.1	Indet	Humerus	12.8	0.71568	0.0017	38.5144	0.2007	15.6310	0.1506	18.5198	0.1006	2.4640	1.1848
	Fritzens-Sanzeno culture	46.62	10.86	641.1	Indet	Humerus	15.9	0.72178	0.0039	38.5489	0.2005	15.6442	0.1505	18.7382	0.1007	2.4641	1.1978
	Fritzens-Sanzeno culture	46.62	10.86	641.1	Indet	Humerus	14.1	0.72148	0.0014	38.5650	0.2012	15.6357	0.1515	18.7286	0.1020	2.4664	1.1978
	Fritzens-Sanzeno culture	46.62	10.86	641.1	Indet	Humerus	12.9	0.72266	0.0030	38.4858	0.2011	15.6332	0.1509	18.6716	0.1010	2.4618	1.1944

[a]Infans II; [b]Infans I; [c]Uncertain, but probably female or male, respectively; *indet* indeterminate. Due to the poor state of preservation, several cremations did not permit a firm sex diagnosis

integrates elemental uptake and respective isotopic signatures over years and even decades. Therefore, while a cremated "non-local" skeleton can be readily identified by its bone isotopic signatures according to the exclusion principle, this individual must have been a late immigrant to the site, because it had died before the bones had adjusted the isotopic signatures to the local ones in the course of the slow tissue turnover. The original extent of population admixture will necessarily remain underestimated. However, in the event that no late immigrants to the site are identified isotopically, this implies that all isotopically "local" individuals must have spent years to decades at or near the site of their recovery, indicative of a stable community.

The following spatial distribution of lead and stable strontium isotopic ratios in human cremations and the results of the data mining procedure are not yet in the state of giving clues to specific archaeological questions. To successfully perform the data mining, a sufficient number of human cremations needed to be analysed. To date, 184 individual human isotopic fingerprints consisting of $^{87}Sr/^{86}Sr$, $^{208}Pb/^{204}Pb$, $^{207}Pb/^{204}Pb$, $^{206}Pb/^{204}Pb$, $^{208}Pb/^{207}Pb$ and $^{206}Pb/^{207}Pb$ are available (Table 7), whereby 16 uncremated individuals from the Latsch site (site code 304) were included to augment the data set. With regard to the further perspective of our project, all human cremations date either into the Urnfield period or are associated with the Fritzens-Sanzeno culture. Also, sample number per site is highly variable because some individual burials, which are of particular archaeological interest, were consciously selected. The first issue that needs to be evaluated is whether the transalpine transect with its isotopic micro-regions as reflected by the isotopic fingerprints of archaeological animal bone finds is also mirrored by the human cremations.

Since lead is a bone-seeking trace element and tends to heavily contaminate bones and teeth (Wittmers et al. 2008), quantitative decontamination of bioarchaeological finds is a necessity for the validation of the isotopic signatures. The mineralogical investigation of the finds confirmed that despite the crystallographic alterations due to the high temperature exposure, no contaminating mineral phases were detectable after completion of the laboratory processing protocol. Also the lead isotopic signatures measured are compatible with pre-industrial lead isotopic ratios (Tables 7, 8). In Europe, soils that are contaminated with industrial lead typically have $^{206}Pb/^{207}Pb$ isotopic ratios <1.16, while uncontaminated soils exhibit ratios >1.20 (Reimann et al. 2012). This difference is largely due to the large-scale introduction of imported lead, mostly in the form of leaded gasoline. All measured isotopic signatures, whether uncremated animal or cremated human bone, are in total agreement with the pre-industrial variability in skeletons as reported by Kamenov and Gulson (2014).

The spatial variability of the isotopic signatures measured in human cremations is plotted into the map and visualized by Figs. 25, 26, 27, 28, 29 and 30. Geographical coordinates and site codes are listed in Table 7. $^{87}Sr/^{86}Sr$ isotopic ratios in the northern Alpine gravel plain are relatively uniform and do not exceed a value of 0.71 with the exception of three individuals (one sample each from sites 144, Forstinning; 121, Hofoldinger Forst; and 136, Trudering). None of the six

Table 8 Comparison of the range of isotopic ratios in archaeological animal bones (uncremated) and human bones (cremated), differentiated per gross geographical region

$^{87}Sr/^{86}Sr$	Animals	Humans	$^{208}Pb/^{204}Pb$	Animals	Humans
Germany			Germany		
Minimum	0.707	0.708	Minimum	38.19	38.15
Maximum	0.714	0.712	Maximum	38.78	38.79
Δ	0.007	0.004	Δ	0.59	0.64
Austria			Austria		
Minimum	0.709	0.708	Minimum	38.27	37.92
Maximum	0.72	0.717	Maximum	38.76	38.96
Δ	0.011	0.009	Δ	0.49	1.04
Italy			Italy		
Minimum	0.709	0.71	Minimum	38.36	38.36
Maximum	0.721	0.722	Maximum	38.83	38.91
Δ	0.012	0.012	Δ	0.47	0.55
$^{208}Pb/^{207}Pb$	Animals	Humans	$^{207}Pb/^{204}Pb$	Animals	Humans
Germany			Germany		
Minimum	2.41	2.42	Minimum	15.6	15.59
Maximum	2.47	2.47	Maximum	15.86	15.75
Δ	0.06	0.05	Δ	0.26	0.16
Austria			Austria		
Minimum	2.44	2.37	Minimum	15.61	15.61
Maximum	2.48	2.47	Maximum	15.71	15.99
Δ	0.04	0.1	Δ	0.1	0.38
Italy			Italy		
Minimum	2.45	2.46	Minimum	15.61	15.61
Maximum	2.48	2.48	Maximum	15.7	15.72
Δ	0.03	0.02	Δ	0.09	0.11
$^{206}Pb/^{207}Pb$	Animals	Humans	$^{206}Pb/^{204}Pb$	Animals	Humans
Germany			Germany		
Minimum	1.18	1.17	Minimum	18.42	18.3
Maximum	1.35	1.27	Maximum	21.4	20.03
Δ	0.17	0.1	Δ	2.98	1.73
Austria			Austria		
Minimum	1.17	1.16	Minimum	18.35	18.28
Maximum	1.26	1.2	Maximum	19.75	18.86
Δ	0.09	0.04	Δ	1.4	0.58
Italy			Italy		
Minimum	1.17	1.17	Minimum	18.33	18.46
Maximum	1.22	1.2	Maximum	19.09	18.84
Δ	0.05	0.03	Δ	0.76	0.38

Since only empirical cut-off values are yet available for the reference area, lead isotopic ratios are listed up to the second decimal place only

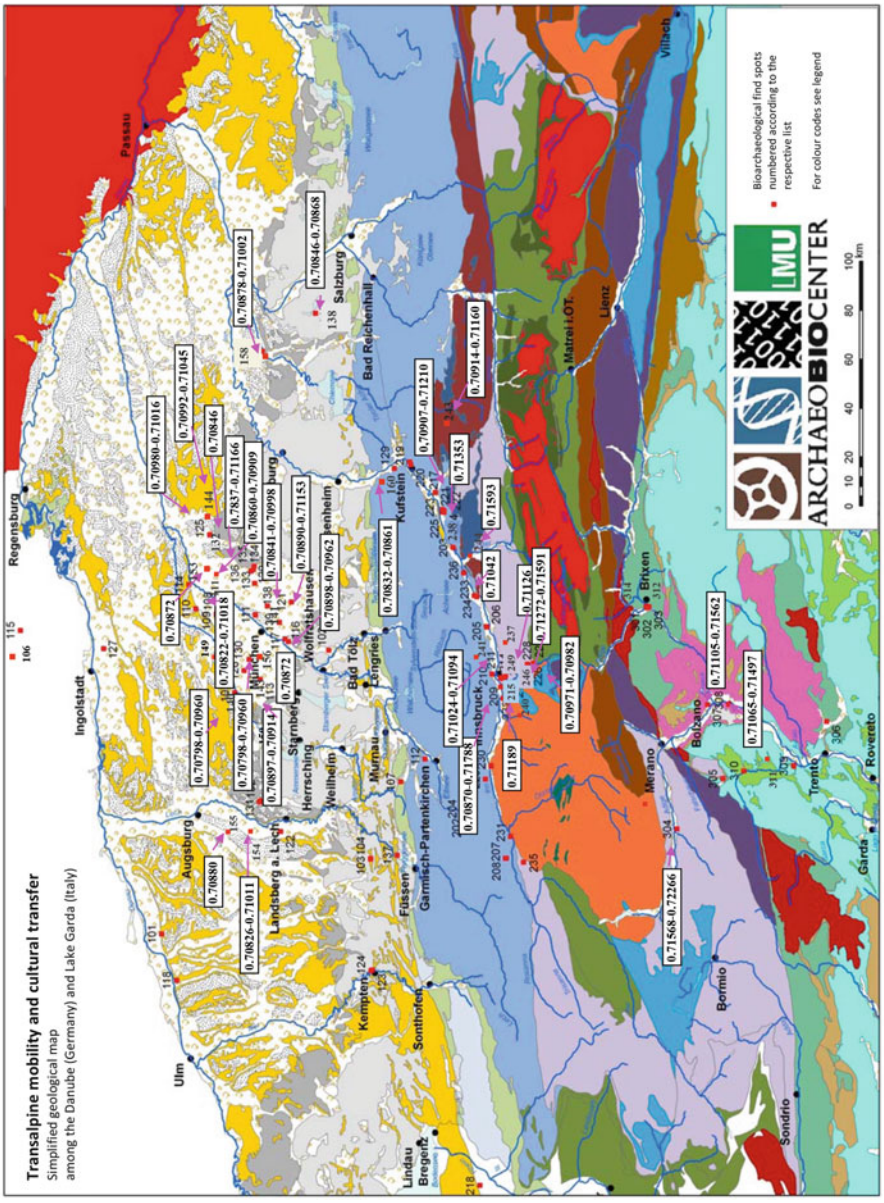

Fig. 25 Spatial distribution of bioavailable $^{87}Sr/^{86}Sr$ isotopic ratios in cremated human bone apatite along the Alpine transect

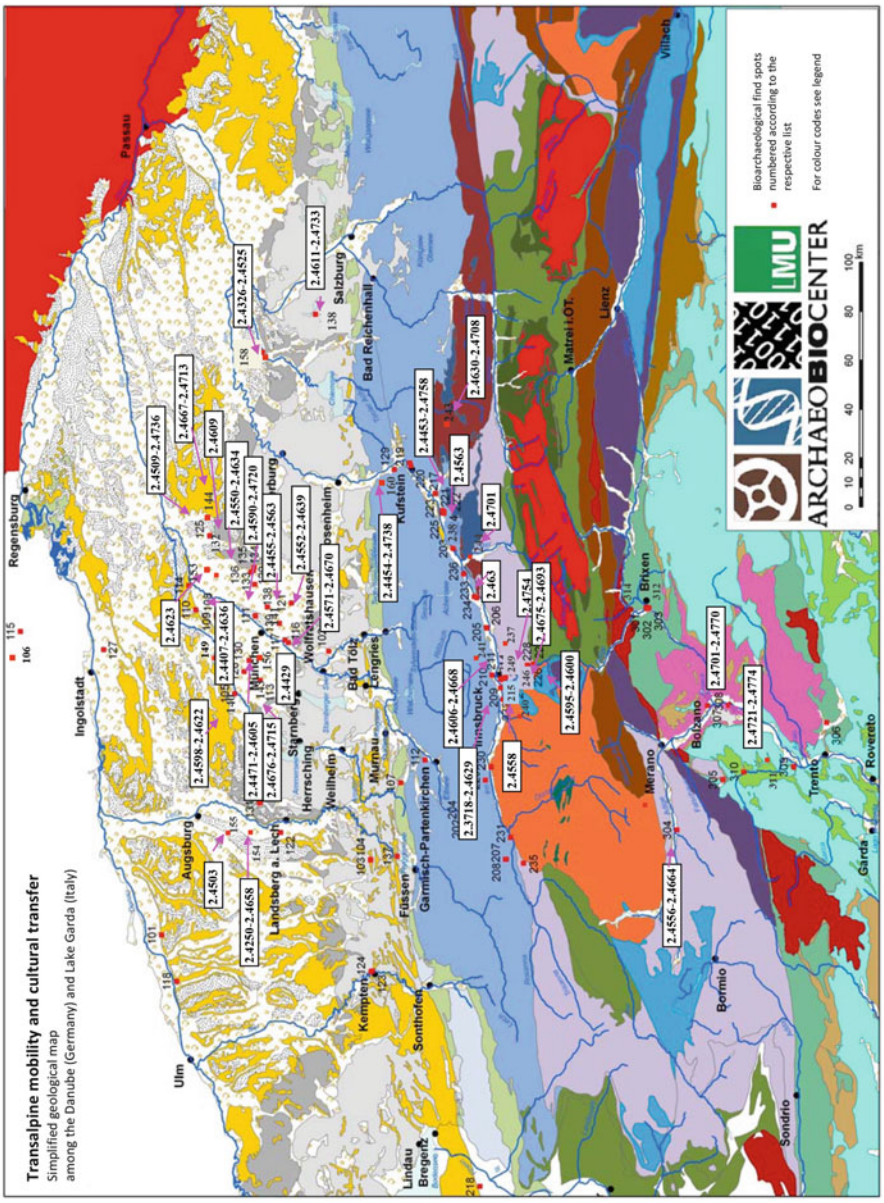

Fig. 26 Spatial distribution of bioavailable $^{208}Pb/^{207}Pb$ isotopic ratios in cremated human bone apatite along the Alpine transect

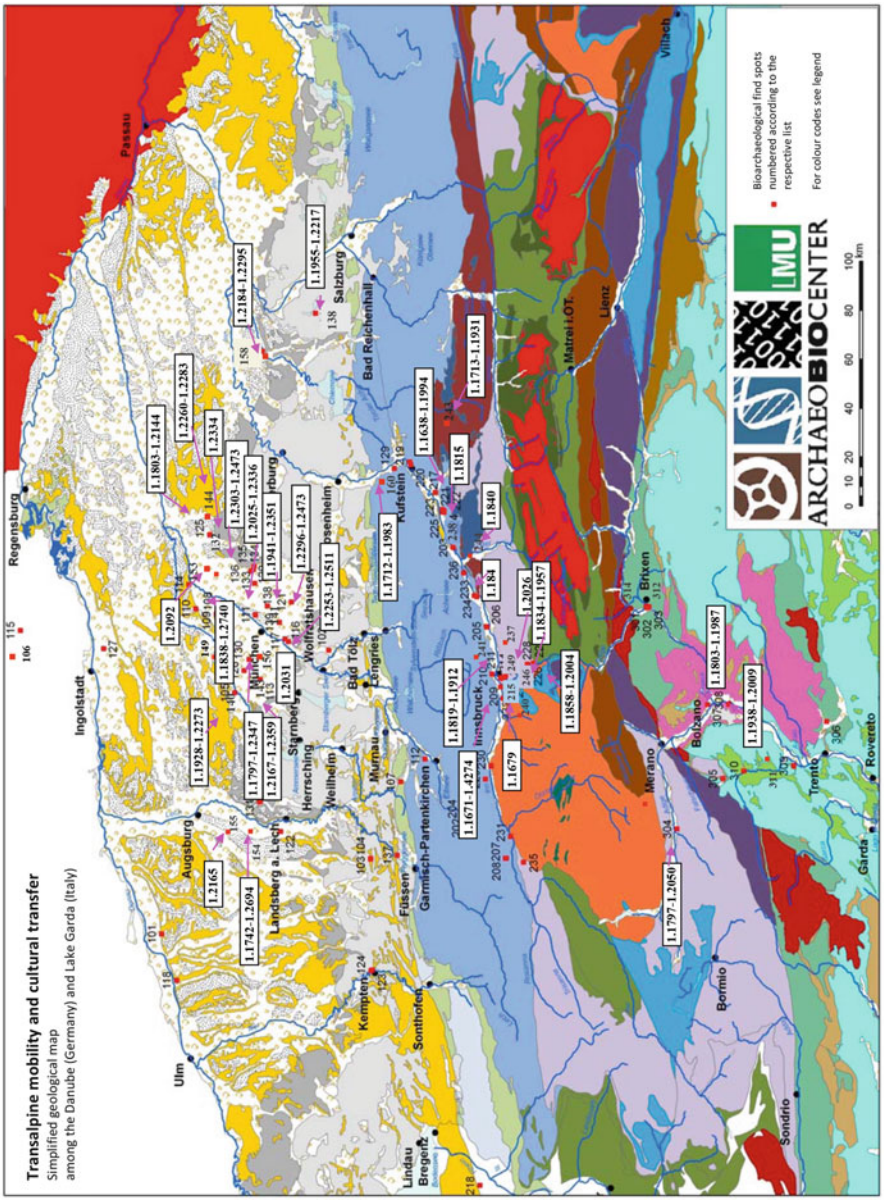

Fig. 27 Spatial distribution of bioavailable $^{206}Pb/^{207}Pb$ isotopic ratios in cremated human bone apatite along the Alpine transect

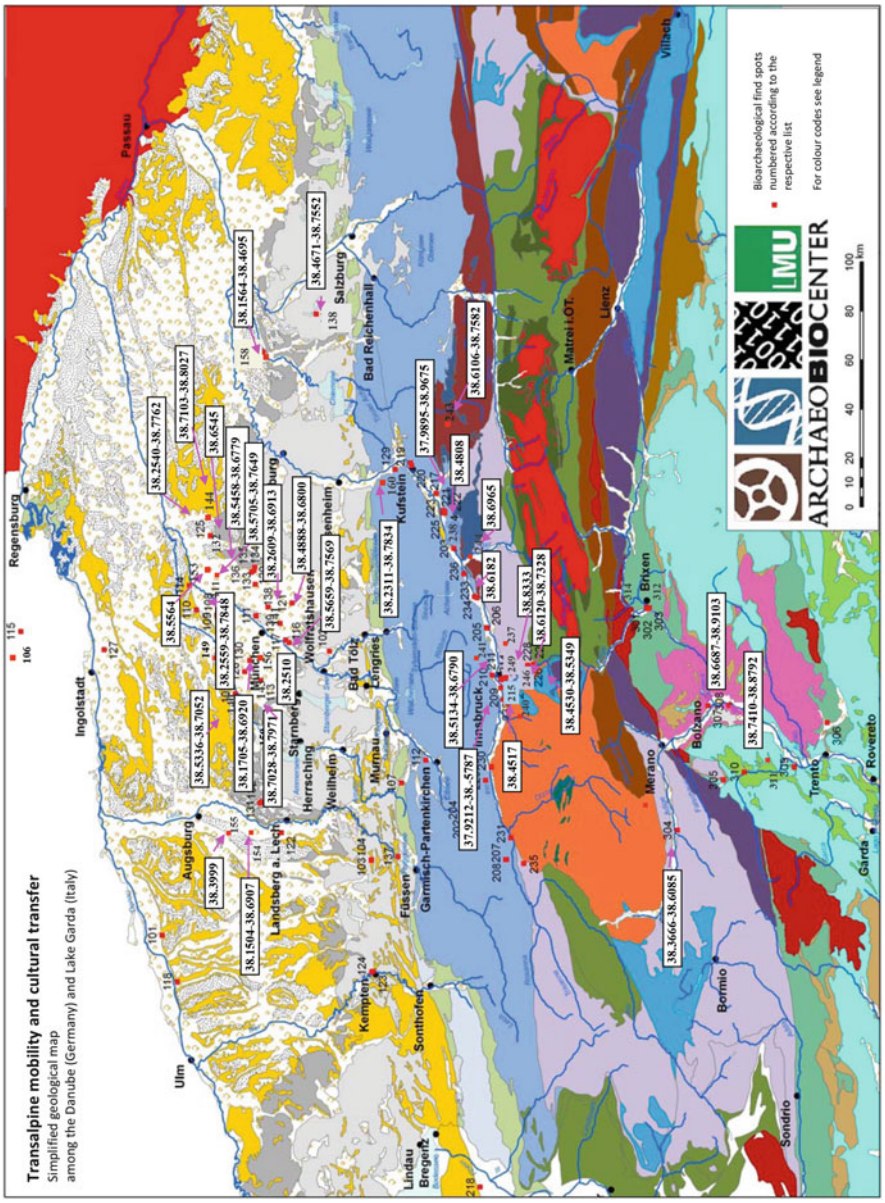

Fig. 28 Spatial distribution of bioavailable $^{208}Pb/^{204}Pb$ isotopic ratios in cremated human bone apatite along the Alpine transect

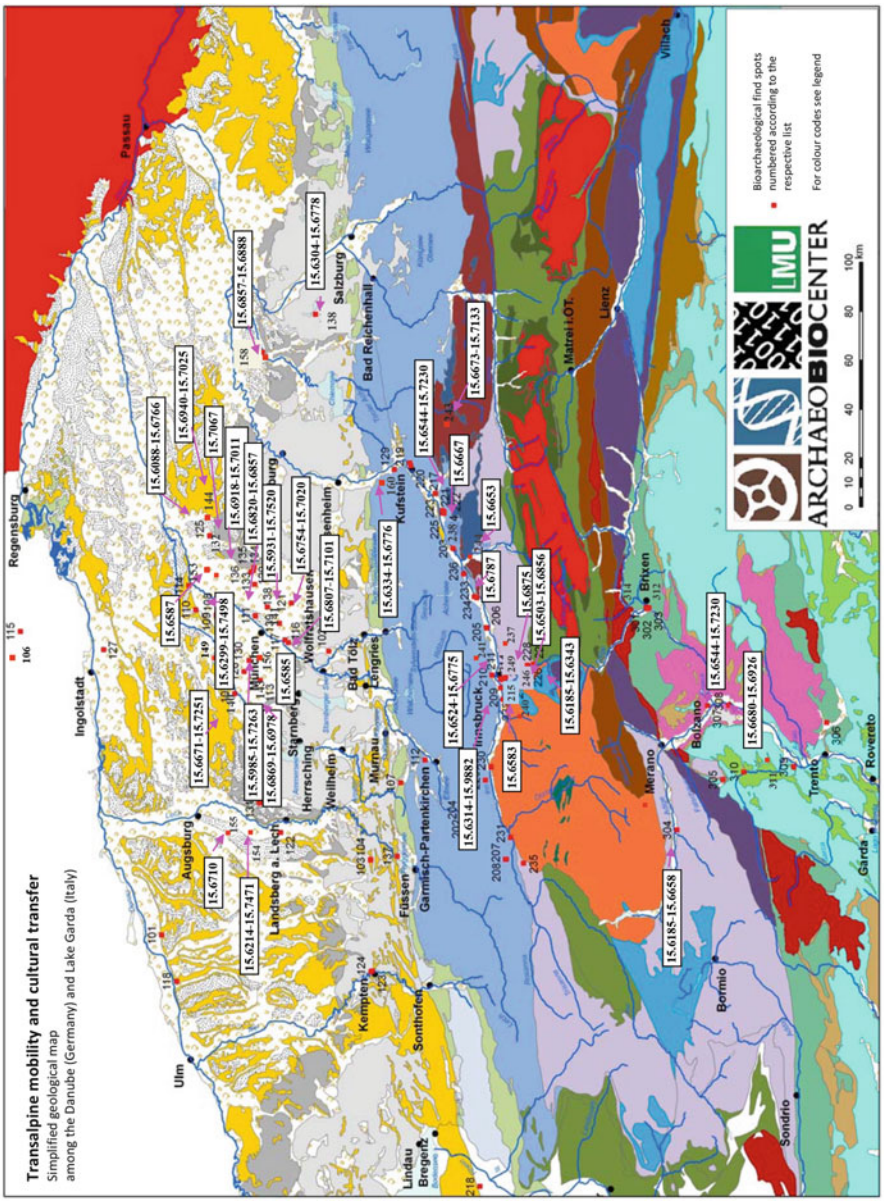

Fig. 29 Spatial distribution of bioavailable $^{207}Pb/^{204}Pb$ isotopic ratios in cremated human bone apatite along the Alpine transect

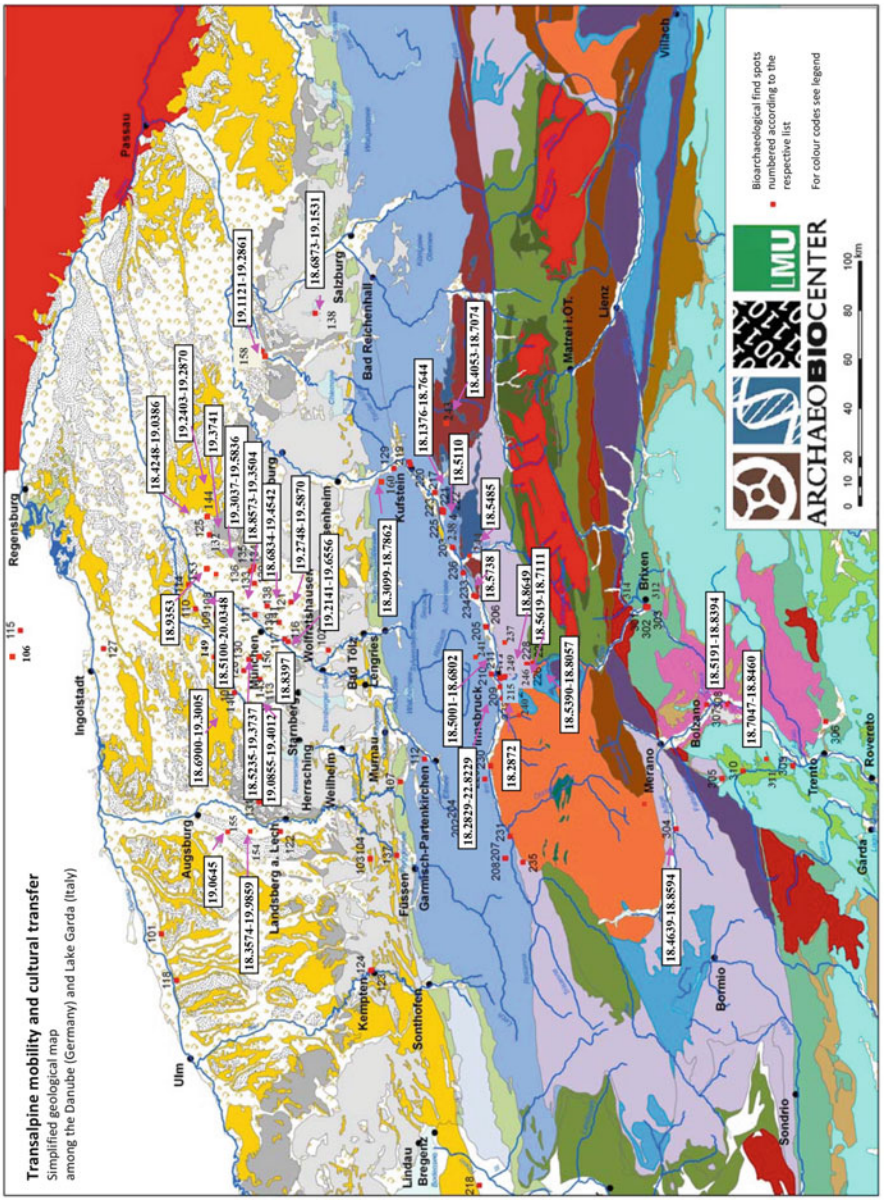

Fig. 30 Spatial distribution of bioavailable $^{206}Pb/^{204}Pb$ isotopic ratios in cremated human bone apatite along the Alpine transect

animal bones recovered at the Trudering site exhibited a $^{87}Sr/^{86}Sr$ isotopic ratio >0.70899; therefore, the single human individual would be cautiously considered as probably not primarily local to the site based on stable strontium isotopic ratios alone. The considerable isotopic mixing due to the topographical particularities of the Inn Valley is reflected in a high $^{87}Sr/^{86}Sr$ variability from 0.708 to 0.717, whereby the Hötting site alone (site code 209) covers the complete range. Most radiogenic ratios up to 0.722 were finally detected at the Italian Latsch site (site code 304).

Interpretation of the human lead isotopic ratios necessitates an in-depth consideration of the find context, archaeological data and all facets of possible relations to early metallurgy. This is beyond the scope of this book, but it can be stated that at least $^{207}Pb/^{204}Pb$ ratios are in total agreement with ore deposits at Schwaz-Brixlegg in the Inn Valley that had been exploited in the regional prehistory (Höppner et al. 2005). The largest inhomogeneity of $^{206}Pb/^{204}Pb$ is found in Upper Bavaria with particular radiogenic isotopic ratios up to 20.03 (site 108, Eching), although ratios ≥20 were occasionally also measured in animal bones from the German sites (Table 1). Radiogenic isotopic ratios are dependent on the age of rock or ores and logically also exhibit a considerable geographical redundancy worldwide. Ore deposits in the European Alps and in several other locations in Central Europe typically have lead isotopic ratios with a low variability, namely, $^{206}Pb/^{204}Pb = 18.3–18.5$, $^{207}Pb/^{204}Pb = 15.6–15.7$ and $^{208}Pb/^{204}Pb = 38.3–38.7$ (Villa 2016). Only slightly different typical ratios have been reported for the entire continent (see chapter "The Concept of Isotopic Landscapes: Modern Ecogeochemistry versus Bioarchaeology"). Provenance analysis by lead isotopes in human skeletal remains is particularly difficult because after metal working had started on a regular scale, airborne lead covered very large distances. This is but one example for the high mobility of lead in nature. While these effects introduced no longer typically "local" but still pre-industrial isotopic signatures into regions even at distances from the location of ores and metal smelting, humans came into daily contact with lead artefacts that might once have been manufactured from distant ore deposits. All these isotopic ratios mix in the consumer's body and incorporate lead into the bone over many years. While in general, the lead isotopic signatures measured in the bioarchaeological finds match the "local" pre-industrial lead composition, radiogenic ratios, e.g. $^{206}Pb/^{204}Pb$ around 20, might therefore not necessarily indicate an immigrant to the site. Blending of different lead sources for the manufacturing of goods of daily life (cauldrons, vessels, pipes, etc.) can totally obscure any local isotopic signature and even the typical signature of the mining districts where the ores had been exploited (Boni et al. 2000; Bray and Pollard 2012; Villa 2016). In times when people deliberately created industrial blends, such as during Imperial Roman Times, provenance analysis by lead isotopes will be extremely tricky, and it is hard to imagine how this can be achieved by univariate statistics alone.

The high spatial redundancy of $^{87}Sr/^{86}Sr$ in human cremated bone is also depicted from Fig. 31: The alluvial sites in Bavaria and the Austrian Inn Valley exhibit an overlap with regard to isotopic ratios between 0.709 and 0.711, while the

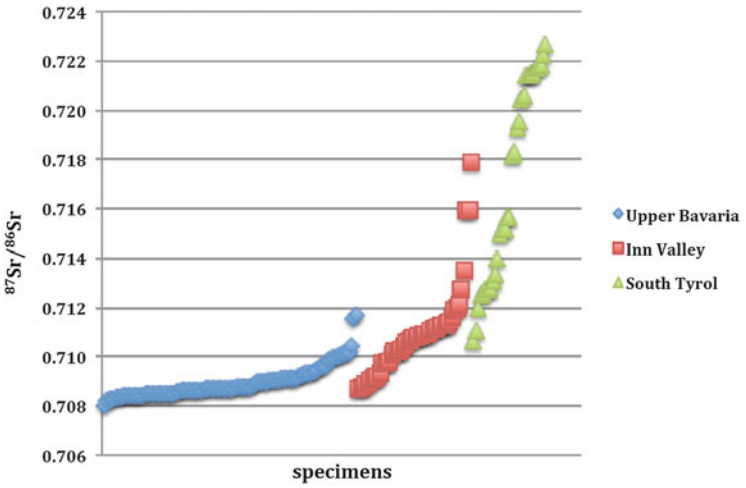

Fig. 31 Distribution of bioavailable $^{87}Sr/^{86}Sr$ in human cremated finds per gross geographical region. Figure by D. Wycisk

Austrian Inn Valley and South Tyrolean alluvial river sites, related to the geology of the adjacent mountain regions, have an overlap of ratios between 0.711 and 0.714. Thus, the general north-to-south gradient is obvious. It does, however, only permit for a firm differentiation between regions with the lowest radiogenic isotopic ratios in Upper Bavaria and highest radiogenic ratios in South Tyrol. The situation becomes much clearer in a bivariate plot, when, for example, $^{206}Pb/^{207}Pb$ is plotted against $^{87}Sr/^{86}Sr$ (Fig. 32). Here, the specimens from South Tyrol are separated from the others, and especially the (uncremated) finds from the Latsch site (code 304) form a distinct cluster. Unfortunately, only human skeletal finds from three southern Alpine sites were available for this first overview of the spatial distribution of isotopic signatures along the Alpine transect. Therefore, it cannot yet be told how significant the isotopic separation of Upper Bavaria and South Tyrol is on the population level.

But to return to the initial question, the answer to whether an isotopic map based on presumably local vertebrate bone finds would be suitable for an isotopic mapping and subsequent migration research with human cremations is "yes". Comparison of the spatial variability of the isotopic ratios in the three main regions (to the north and to the south of the Alps and inner Alpine regions) reveals that the isotopic signatures of cremated human bones readily plot into the variability of bioavailable ratios as established by the use of the uncremated animal bone finds (Table 8). In some cases, total variability of isotopic signals measured in the animal bones exceeds the respective one in the cremated human bones which is most plausibly explained by the fact that for the establishment of the animal data set, members of three different species have been lumped together. Since the human data set is also not uniform in terms of archaeological time frame (see above) and

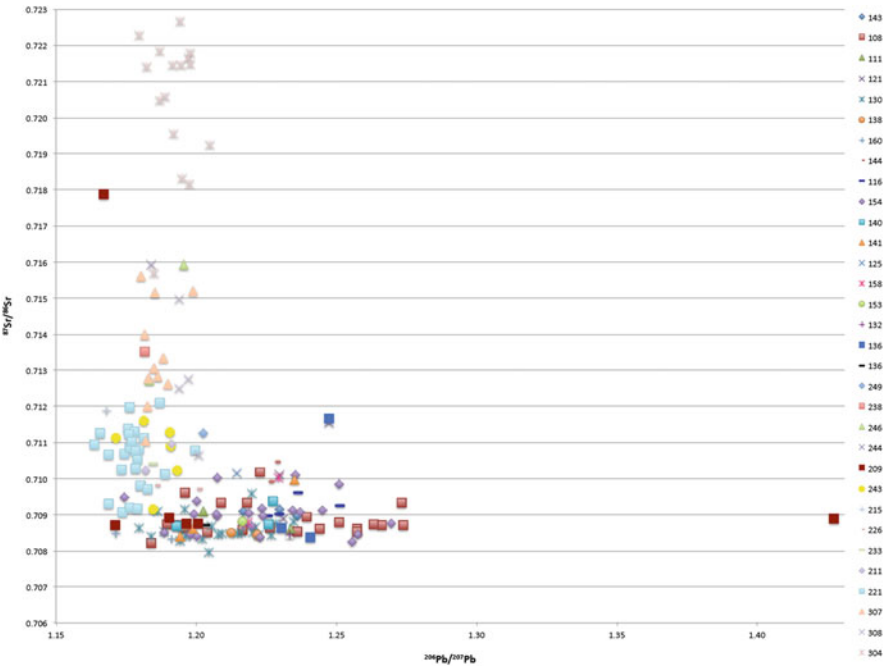

Fig. 32 Bivariate plot of bioavailable $^{206}Pb/^{207}Pb$ versus $^{87}Sr/^{86}Sr$ in human cremated finds. Site labels cf. Table 7. Figure by D. Wycisk

since several cremations have been chosen purposefully for analysis for a variety of reasons and therefore need not be representative for the local, indigenous population, it would be too early at this stage of the project to interpret single individuals with mathematically outlying isotopic signatures as immigrants to the site. It is conspicuous, however, that with regard to the lead isotopes measured in Austrian cremations, total variability exceeds the one of the animal data set. Interestingly, the lowest $^{208}Pb/^{207}Pb$ ratio (2.37), the lowest $^{208}Pb/^{204}Pb$ ratio (37.92) and the highest $^{207}Pb/^{204}Pb$ ratio (15.99) were all measured in one and the same individual from the Hötting site (burial 62; site code 209). In this particular case, it could be concluded that this individual should have been primarily foreign to the site of its recovery and that it immigrated there rather shortly before its death. Archaeologically, however, the grave goods associated with this burial are inconspicuous and do not indicate a primarily non-local individual (S. Reuß, personal communication). Cluster analysis did not identify this particular individual as being totally foreign to the reference area what is in agreement with the archaeological finds.

In a first attempt of GMM clustering of 162 human data, a rather clear separation of a micro-region each to the north (green cluster) and to the south of the Alps (red and pink clusters) results, with some mixing in the Inn Valley (Fig. 33). The individual from the Hötting site with several "non-local" lead isotopic signatures was picked up by the red cluster which also occurs in the Inn Valley. We need to

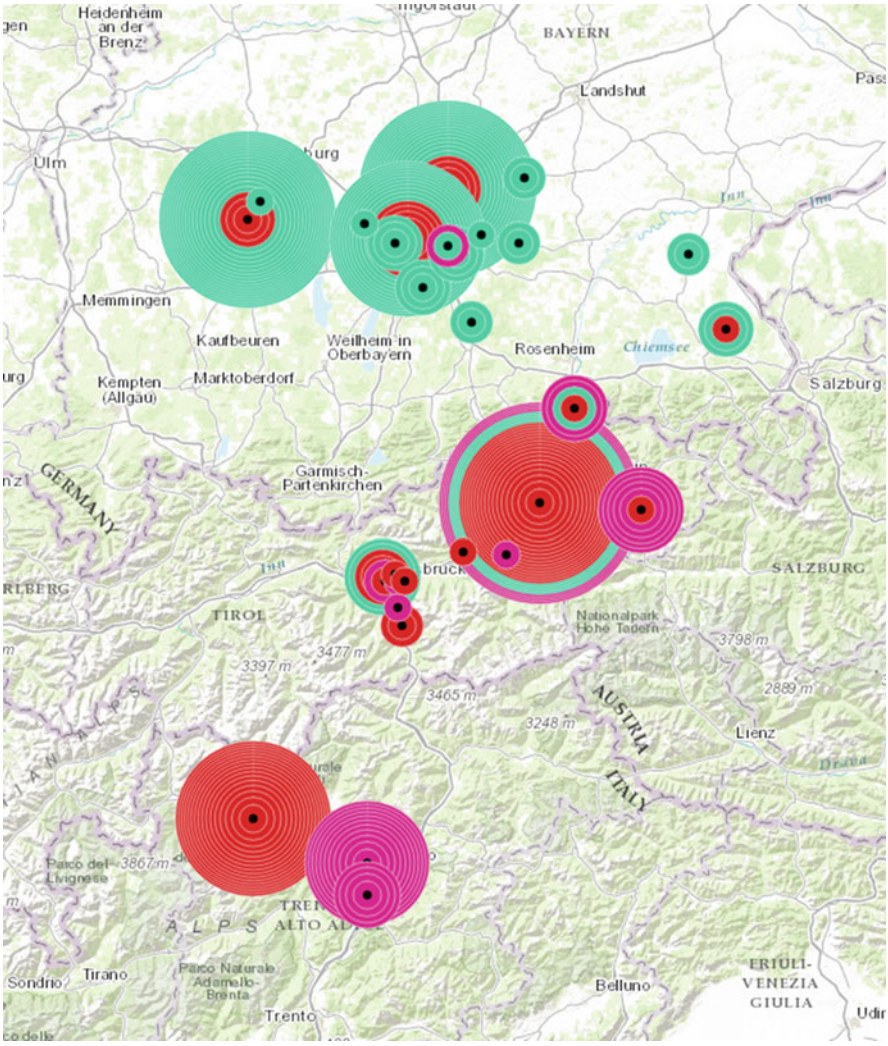

Fig. 33 Result of GMM clustering of apatite strontium and lead isotopic ratios measured in 162 human cremations (see Table 7). The micro-regions to the north and to the south of the Alps are clearly differentiated. Figure by M. Mauder

emphasize at this stage of the project that this initial data mining was performed with minimal contextual information and that data from two different archaeological horizons have been lumped together. This merely represents a pilot study to test whether the human data plot within the isotopic map established on presumably residential vertebrates, and the outcome is positive. The spatial redundancy has been overcome, and migration from north to south or vice versa along the Alpine transect will be detectable with a high certainty. Keeping in mind that only

cremated bones had been analysed and that, therefore, only "late immigrants" are detectable by isotope analysis, the first impression gained from a glimpse at Fig. 33 is that the micro-regions to the south and the north of the Alps seem to have been rather stable with some adult individuals that had migrated from the north into the inner Alpine regions (green cluster) and some others who were recovered in the north or at inner Alpine sites which match the isotopic signatures prevailing in the south (red and pink clusters). Since only bones were available for analysis, nothing can be said about the people who had spent their childhood or juvenile age elsewhere. Therefore, the extent of population admixture cannot be assessed and is most probably underestimated. But one leap forward has been achieved: multi-isotopic fingerprinting and adequate mathematical data analysis are possible for cremated finds, even in a geologically small-scaled region. This enables bioarchaeologists to systematically close the knowledge gap about past human population dynamics revolving around cremation burial rites and practices. Specific archaeological questions about mobility, trade, migration and especially culture transfer in the respective time horizons, however, necessitate adequate find preservation. Only then will it be possible to get access to individual place of residence during childhood and juvenile age. The next tasks to perform will be (1) a similarity search: human multi-isotopic signatures are similar to animal ones, but how similar do they need to be to equally point to a defined region of origin?, and (2), even more importantly, the results need an in-depth evaluation in the frame of the respective archaeological context.

References

Aggarwal PK, Araguás-Araguás LJ, Groening M, Kulkarni KM, Kurttas T, Newman BD, Vitvar T (2010) Global hydrological isotope data and data networks. In: West JB, Bowen GJ, Dawson TE, Tu KP (eds) Isoscapes. Understanding movement, pattern, and process on Earth through isotope mapping. Springer, Dordrecht, pp. 33–50

Blake RE, O'Neil JR, Garcia GA (1997) Oxygen isotope systematics of biologically mediated reactions of phosphate. I. Microbial degradation of organophosphorus compounds. Geochim Cosmochim Acta 61:4411–4422

Blake RE, O'Neil JR, Garcia GA (1998) Effects of microbial activity on the $\delta^{18}O$ of dissolved inorganic phosphate and textural features of synthetic apatites. Am Mineral 83:1516–1531

Boni M, Di Maio G, Frei R, Villa IM (2000) Lead isotopic evidence for a mixed provenance of Roman water pipes from Pompeii. Archaeometry 42:201–208

Bösl C, Grupe G, Peters J (2006) A Late Neolithic vertebrate food web based on stable isotope analyses. Int J Osteoarchaeol 16:296–315

Bray PJ, Pollard AM (2012) A new interpretative approach to the chemistry of copper-alloy objects: source, recycling and technology. Antiquity 86:853–867

Bryant JD, Koch PL, Froelich PN, Showers WJ, Genna BJ (1996) Oxygen isotope partitioning between phosphate and carbonate in mammalian apatite. Geochim Cosmochim Acta 60:5143–5148

Chenery CA, Pashley V, Lamb AL, Sloane HJ, Evans JA (2012) The oxygen isotope relationship between the phosphate and structural carbonate fractions of human bioapatite. Rapid Commun Mass Spectrom 26:309–319

Crowley BE, Miller JH, Bataille CP (2015) Strontium isotopes ($^{87}Sr/^{86}Sr$) in terrestrial ecological and palaeoecological research: empirical efforts and recent advances in continental-scale models. Biol Rev. doi:10.1111/brv.12217

D'Angela D, Longinelli A (1990) Oxygen isotopes in living mammal's bone phosphate: further results. Chem Geol: Isotope Geosci Sec 86:75–82

Drouet T, Herbauts J, Gruber W, Demaiffe D (2005) Strontium isotope composition as a tracer of calcium sources in two forest ecosystems in Belgium. Geoderma 126:203–223

Fischer J, Schneider JW, Voigt S, Joachimski MM, Tichomirowa M, Tütken T, Götze J, Berner U (2013) Oxygen and strontium isotopes from fossil shark teeth: environmental and ecological implication for Late Palaeozoic European basins. Chem Geol 342:44–62

Frei KM, Frei R (2011) The geographic distribution of strontium isotopes in Danish surface waters—a base for provenance studies in archaeology, hydrology and agriculture. Appl Geochem 26:326–240

Fricke HC, Clyde WC, O'Neil JR (1998) Intra-tooth variations in $\delta^{18}O$ (PO_4) of mammalian tooth enamel as a record of seasonal variations in continental climate variables. Geochim Cosmochim Acta 62:1839–1850

Gaudinski JB, Dawson TE, Quideau S, Schuur E, Roden JS, Trumbore SE, Sandquist DR, Oh S-W, Wasylishen RE (2005) Comparative analysis of cellulose preparation techniques for use with ^{13}C, ^{14}C, and ^{18}O isotopic measurements. Anal Chem 77:7212–7224

Göhring AB (2014) Sauerstoff-Isotopiekartierung einer Alpenpassage anhand rezenter botanischer Proben. MSc Thesis, LMU München

Göhring AB, Toncala A, Mayr C, Söllner F, Grupe G (2015) Stable oxygen isotope mapping of the transalpine Inn-Eisack-Etsch passage based on modern α-cellulose and water. Documenta Archaeobiologiae 12:53–80

Grosskopf B (2004) Leichenbrand. Biologisches und kulturhistorisches Quellenmaterial zur Rekonstruktion vor- und frühgeschichtlicher Populationen und ihrer Funeralpraktiken. PhD Thesis, Universität Leipzig

Grupe G (1991) Anthropogene Schwermetallkonzentration in menschlichen Skelettfunden als Monitor früher Umweltbelastungen. USW-Z Umweltchem Ökotox 3:226–229

Grupe G, Herrmann B (1983) Über das Schrumpfungsverhalten experimentell verbrannter spongiöser Knochen am Beispiel des Caput femoris. Z Morph Anthrop 74:121–127

Grupe G, Price TD, Schröter P, Söllner F, Johnson CM, Beard BL (1997) Mobility of Bell Beaker people revealed by strontium isotope ratios of tooth and bone: a study of southern Bavarian skeletal remains. Appl Geochem 12:517–525

Grupe G, Harbeck M, McGlynn GC (2015) Prähistorische Anthropologie. Springer, Berlin

Hansen E, Skårup S, Christensen K, Schmidt A, Hjelmar O, Hauschild M (2004) Life cycle assessment of landfilled waste. Environmental projects 971. Danish Environmental Protection Agency, Copenhagen, Denmark

Harbeck M, Schleuder R, Schneider J, Wiechmann I, Schmahl WW, Grupe G (2011) Research potential and limitations of trace analyses of cremated remains. Forensic Sci Inter 204:191–200

Henningsen D, Katzung G (1998) Einführung in die Geologie Deutschlands, 5th edn. Enke, Stuttgart

Herrmann B, Grupe G, Hummel S, Piepenbrink H, Schutkowski H (1990) Prähistorische Anthropologie. Leitfaden der Feld- und Labormethoden. Springer, Berlin

Hillson S (1996) Dental Anthropology. Cambridge University Press, Cambridge

Höppner B, Bartelheim M, Huisjmas M, Krauss R, Martinek KP, Pernicka E, Schwarz R (2005) Prehistoric copper production in the Inn Valley (Austria), and the earlierst copper in Central Europe. Archaeometry 47:293–315

Hüls CM, Erlenkeuser H, Nadeau MJ, Grootes PM, Andersen N (2010) Experimental study on the origin of cremated bone apatite carbon. Radiocarbon 52:587–599

Humer G, Rank D, Stichler W (1995) Niederschlagsisotopennetzwerk Österreich. Monographien des Bundesministeriums für Umwelt, Band 52. Wien

Iacumin P, Bocherens H, Mariotti A, Longinelli A (1996) Oxygen analyses of co-existing carbonate and phosphate in biogenic apatite: a way to monitor diagenetic alteration of bone phosphate? Earth Planet Sci Lett 142:1–6

Jayme G (1942) Preparation of cellulose with sodium chlorite. Cellulosechemie: Zeitschrift für die gesamte Chemie und Physik der Cellulose sowie der ihr verwandten Stoffe 20:43–49

Kamenov GD, Gulson BL (2014) The Pb isotopic record of historical to modern human lead exposure. Sci Total Environ 490:861–870

Kern Z, Kohán B, Leuenberger M (2014) Precipitation isoscape of high reliefs: interpolation scheme designed and tested for monthly resolved precipitation oxygen isotope records of an Alpine domain. Atmos Chem Phys 14:1897–1907

Köppel V, Schroll E (1985) Herkunft des Pb der triassischen Pb-Zn-Vererzungen in den Ost- und Südalpen, Resultate bleiisotopengeochemischer Untersuchungen. Arch Lagerstättenforsch. Geol Bundesanstalt 6:215–222

Köppel V, Schroll E (1988) Pb-isotope evidence for the origin of lead in strata-bound Pb-Zn deposits in Triassic carbonates of the Eastern and Southern Alps. Mineral Deposita 23:96–103

Kovach A (1968) Blei-Isotopen-Verhältnisse im Raum der alpin-mediterranen Metallogenese. Geolog Rundschau 57:371–385

Kunter M (1989) Leichenbranduntersuchungen in Wederath. In: Haffner A (ed) Gräber-Spiegel des Lebens: zum Totenbrauchtum der Kelten und Römer am Beispiel des Treverer-Gräberfel des Wederath-Belginum. von Zabern, Mainz, pp. 415–432

Lee-Thorp J (2002) Two decades of progress towards understanding fossilization processes and isotopic signals in calcified tissue material. Archaeometry 44:435–446

Lihl CM (2014) Relation zwischen stabilen Sauerstoffisotopen im Phosphat und im strukturellen Karbonat von Tierknochen verschiedener Taxa. MSc Thesis, LMU München

Longinelli A (1984) Oxygen isotopes in mammal bone phosphate: a new tool for paleohydrological and paleoclimatological research? Geochim Cosmochim Acta 48:385–390

Longinelli A, Selmo E (2003) Isotopic composition of precipitation in Italy: a first overall map. J Hydrol 270:75–88

Luz B, Kolodny Y (1989) Oxygen isotope variation in bone phosphate. Appl Geochem 4:317–323

Marshall JD, Brooks JR, Lajtha K (2007) Sources of variation in the stable isotopic composition of plants In: Michener R, Lajtha K (eds) Stable isotopes in ecology and environmental science. Blackwell, Malden, pp 22–60

Mayr C (2002) Möglichkeiten der Klimarekonstruktion im Holozän mit $\delta^{13}C$- und $\delta^{2}H$-Werten von Baumjahresringen auf der Basis von Klimakammerversuchen und Rezentstudien. GSF-Bericht 14/02, Neuherberg

Mayr C, Lücke A, Stichler W, Trimborn P, Ercolano B, Oliva G, Schleser GH, Soto J, Ohlendorf C, Haberzettl T, Schäbitz F, Zolitschka B, Fey M, Janssen S, Wille M (2007) Precipitation orgin and evaporation of lakes in semi-arid Patagonia (Argentina) inferred from stable isotopes ($\delta^{18}O$, $\delta^{2}H$). J Hydrol 335:53–63

Mayr C, Grupe G, Lihl C, Toncala A (2016) Linking oxygen isotopes of animal-bone phosphate with altimetry—results from archaeological finds from a transect in the Alps. In: Grupe G, McGlynn GC (eds) Isotopic landscapes in bioarchaeology. Springer, Berlin, pp. 157–172

McKinley J (2016) Complexities of the ancient mortuary rite of cremation: an osteoarchaeological conundrum. In: Grupe G, McGlynn GC (eds) Isotopic landscapes in bioarchaeology. Springer, Berlin, pp. 17–41

Moebus G (1997) Geologie der Alpen. von Loga, Köln

Nordberg GF, Mahaffey KR, Fowler BA (1991) Introduction and summary. International workshop on bone: implications for dosimetry and toxicology. Environ Health Perspect 91:3–7

Olsen J, Heinemeier J, Bennike P, Krause C, Hornstrup KM, Thrane H (2008) Characterization and blind testing of radiocarbon dating of cremated bone. J Archaeol Sci 35:791–800

Otto L (2015) Anthropologische Bearbeitung des urnenfelderzeitlichen Gräberfeldes Kleinaitingen. MSc-Thesis, LMU München

Park G (2014) Die Geologie Europas. Wissenschaftliche Buchgesellschaft, Darmstadt

Pellegrini M, Lee-Thorp JA, Donahue RE (2011) Exploring the variation of the $\delta^{18}O_p$ and $\delta^{18}O_c$ relationship in enamel increments. Palaeogeogr Palaeoclimatol Palaeoecol 310:71–83

Pemmer B, Roschger A, Wastl A, Hofstaetter JG, Wobrauschek P, Simon R, Thaler HW, Roschger P, Klaushofer K, Streli C (2013) Spatial distribution of the trace elements zinc, strontium and lead in human bone tissue. Bone 57:184–193

Pin C, Joannon S, Bosq C, Fevre BL, Gauthier PJ (2003) Precise determination of Rb, Sr, Ba, and Pb in geological materials by isotope dilution and ICP-quadrupole mass spectrometry following selective separation of the analytes. J Anal Spectrom 18:135–141

Podlesak DW, Torregrossa AM, Ehleringer JR, Dearing MD, Passey BH, Cerling TE (2008) Turnover of oxygen and hydrogen isotopes in the body water, CO_2, hair and enamel of a small mammals. Geochim Cosmochim Acta 72:19–35

Price TD, Burton JH, Bentley RA (2002) The characterization of biologically available strontium isotope ratios for the study of prehistoric migration. Archaeometry 44:117–135

Quatrehomme G, Bolla M, Muller M, Rocca JP, Grevin G, Bailet P, Ollier A (1998) Technical note - Experimental single controlled study of burned bones: contribution of scanning electron microscopy. J Forensic Sci 43:417–422

Reimann C, Flem B, Fabian K, Birke M, Ladenberger A, Négrel P, Demetriades A, Hoogewerff J, The GEMAS Project Team (2012) Lead and lead isotopes in agricultural soils of Europe—the continental perspective. Appl Geochem 27:532–542

Schroll E (1990) Die Metallprovinz der Ostalpen im Lichte der Geochemie. Geol Rundsch 79:479–493

Schroll E, Köppel V, Cerny I (2006) Pb and Sr isotope and geochemical data from the Pb-Zn deposit Bleiberg (Austria): constraints on the age of mineralization. Mineral Petrol 86:129–156

Schurr MR, Hayes RG, Cook DC (2008) Thermally induced changes in the stable carbon and nitrogen isotope ratios of charred bones. In: Schmidt CW, Symes SA (eds) The analysis of burned human remains. Academic Press, London, pp. 95–108

Shipman P, Forster G, Schoeninger M (1984) Burnt bones and teeth: an experimental study of colour, morphology, crystal structure and shrinkage. J Archaeol Sci 11:307–325

Sievers S (2003) Manching—Die Keltenstadt. Theiss, Stuttgart

Sivan SS, Wachtel E, Tsitron E, Sakkee N, van der Ham F, DeGroot J, Roberts S, Maroudas A (2008) Collagen turnover in normal and degenerate human intervertebral discs as determined by racemization of aspartic acid. J Biol Chem 283:8796–8801

Snoeck C, Lee-Thorp JA, Schulting R, Debouge W, de Jong J, Mattielli N (2015) Calcined bone provides a reliable substrate for strontium isotope ratios as shown by an enrichment experiment. Rapid Commun Mass Spectrom 29:107–114

Söllner F, Toncala A, Hölzl S, Grupe G (2016) Determination of geo-dependent bio-available $^{87}Sr/^{86}Sr$ isotopic ratios for archaeological sites from the Inn Valley (Austria)—a model calculation. In: Grupe G, McGlynn GC, (eds) Isotopic landscapes in bioarchaeology. Springer, Berlin, pp. 123–140

Song XIN, Clark KS, Helliker BR (2014) Interpreting species-specific variation in tree-ring oxygen isotope ratios among three temperate forest trees. Plant Cell Environ 37:2169–2182

Sørensen ML, Rebay KC (2007) Changing social practices of death in later European history. Studien zur Kulturgeschichte von Oberösterreich 19:1–5

Stabler TV, Byers SS, Zura RD, Kraus VB (2009) Amino acid racemization reveals differential protein turnover in osteoarthritic articular and meniscal cartilage. Arthritis Res Therapy 11: R34

Thompson M (2006) Representing data distributions with kernel density estimates. Royal Society of Chemistry, Analytical Methods Committee, AMCTB No. 4

Tütken T, Vennemann TW, Pfretzschner H-U (2004) Analyse stabiler und radiogener Isotope in archäologischem Skelettmaterial: Herkunftsbestimmung des karolingischen Maultiers von Frankenthal und Vergleich mit spätpleistozänen Großsäugerknochen aus den Rheinablagerungen. Prähist Z 79:89–110

United Nations (2010) Final review of scientific information on lead. United Nations Environment Progamme, Chemicals Branch, DTIE

Veizer J (1989) Strontium isotopes in seawater through time. Annu Rev Plant Physiol Plant Mol Biol 17:141–167

Vennemann TW, Fricke HC, Blake RE, O'Neil JR, Colman A (2002) Oxygen isotope analysis of phosphates: a comparison of techniques for analysis of Ag_3PO_4. Chem Geol 185:321–336

Villa I (2016) Provenancing bronze: Exclusion, inclusion, uniqueness, and Occam 's Razor. In: Grupe G, McGlynn GC, (eds) Isotopic landscapes in bioarchaeology. Springer, Berlin, pp. 141–154

Voerkelius S, Lorenz GD, Rummel S, Quétel CR, Heiss G, Baxter M, Brach-Papa C, Deters-Itzelberger P, Hölzl S, Hoogewerff J, Ponzevera E, VanBocxstaele M, Ueckermann H (2010) Strontium isotopic signatures of natural mineral waters, the reference to a simple geological map and its potential for authentification of food. Food Chem 118:993–940

Vohberger M (2011) Lokal oder eingewandert? Interpretationsmöglichkeiten und Grenzen lokaler Strontium- und Sauerstoffisotopensignaturen am Beispiel einer Altgrabung in Wenigumstadt. PhD Thesis, Universität München

Wahl J (1981) Beobachtungen zur Verbrennung menschlicher Leichname. Archäologisches Korrespondenzblatt 11:271–279

Walker PJ, Miller KP, Richman R (2008) Time, temperature, and oxygen availability: an experimental study of the effects of environmental conditions on the color and organic content of cremated bone. In: Schmidt CW, Symes SA, (eds) The analysis of burned human remains. Academic Press, London, pp. 129–136

Walters C, Eyre DR (1983) Collagen crosslinks in human dentin: Increasing content of hydroxypyridinium residues with age. Calcif Tissue Int 35:401–405

Wittmers LE, Aufderheide AC, Pounds JG, Jones KW, Angel JL (2008) Problems in determination of skeletal lead burden in archaeological samples: an example from the first African Baptist Church population. Am J Phys Anthrop 136:379–386

Xin G, Hanson N (1994) Strontium isotope study of the Peconic river watershed, Long Island, New York. MSc thesis, State University of New York at Stony Brook

Zazzo A, Lécuyer C, Mariotti A (2004) Experimentally-controlled carbon and oxygen isotope exchange between biapatites and water under inorganic and microbially-mediated conditions. Geochim Cosmochim Acta 68:1–12

Current Synthesis and Future Options

Gisela Grupe, Martin Grünewald, Markus Gschwind, Stefan Hölzl, Peer Kröger, Amei Lang, Christoph Mayr, George C. McGlynn, Carola Metzner-Nebelsick, Ferdinand Neuberger, Joris Peters, Simone Reuß, Wolfgang Schmahl, Frank Söllner, C. Sebastian Sommer, Bernd Steidl, Simon Trixl, and Dominika Wycisk

G. Grupe (✉) • D. Wycisk
Biozentrum, Ludwig-Maximilians-Universität, Martinsried, Germany
e-mail: G.Grupe@lrz.uni-muenchen.de

M. Grünewald
LVR-Amt für Bodendenkmalpflege, Titz, Germany

M. Gschwind • C.S. Sommer
Bayerisches Landesamt für Denkmalpflege, Munich, Germany

S. Hölzl
RieskraterMuseum Nördlingen, Nördlingen, Germany

P. Kröger
Lehr- und Forschungseinheit für Datenbanksysteme, Ludwig-Maximilians-Universität, Munich, Germany

A. Lang • C. Metzner-Nebelsick • S. Reuß
Institut für Vor- und Frühgeschichtliche Archäologie und Provinzialrömische Archäologie, Ludwig-Maximilians-Universität München, Munich, Germany

C. Mayr
Institut für Geographie, Friedrich-Alexander-Universität, Erlangen, Germany

GeoBio-Center & Paläontologie und Geobiologie, Ludwig-Maximilians-Universität, Munich, Germany

G.C. McGlynn
Staatssammlung für Anthropologie und Paläoanatomie, Munich, Germany

F. Neuberger • J. Peters • S. Trixl
Institut für Paläoanatomie, Domestikationsforschung und Geschichte der Tiermedizin, Ludwig-Maximilians-Universität, Munich, Germany

W. Schmahl
Sektion Kristallographie, Ludwig-Maximilians-Universität, Munich, Germany

F. Söllner
Department für Geo- und Umweltwissenschaften, Ludwig-Maximilians-Universität, Munich, Germany

B. Steidl
Archäologische Staatssammlung, Munich, Germany

G. Grupe et al. (eds.), *Across the Alps in Prehistory*,
DOI 10.1007/978-3-319-41550-5_7

Abstract

Provenance analysis for the scope of quantifying the extent of population admixture and the direction of migration and trade will remain an important topic in the future and is not restricted to bioarchaeological science. We understand the maps as a starting point for the generation of an ecogeographic "isotopic landscape", which can be of benefit for other sciences as well, such as ecology, biodiversity and forensic sciences. As outlined in chapter "The Isotopic Fingerprint: New Methods of Data Mining and Similarity Search", identification of the structural importance and structural redundancy of single isotopic signatures within a multi-isotope fingerprint will significantly contribute to the probability with which a region of provenance can be identified for non-local individuals. While the results reported in this book are specific for the chosen reference region, the general methodological approach may be suitable for other regions as well.

One of the major results achieved is that provenance analysis of fully cremated finds in the region is possible by measuring apatite lead and strontium isotopic ratios. Ongoing research concentrates on defined archaeological projects related to transalpine mobility and culture transfer where provenance analysis by multi-isotope fingerprints of cremated finds is specifically targeted and to which the isotopic map is applied. Aims and scopes of these archaeological projects that address periods from the Urnfield Period until Imperial Roman times are briefly outlined. Specifically, these projects concentrate on "Mobility and social dynamics in Southern Bavaria and the eastern Central Alps in the Late Bronze Age (1300–800 BCE)", "Migration or acculturation—the genesis and spread of the early Fritzens-Sanzeno culture (fifth/fourth century BCE)", "Population and domestic animals of the Raetian Alps and Alpine foreland during the first century CE" and "Gontia as melting pot? The composition of the population during Günzburg's Roman military period, as reflected by its graves".

The Isotopic Map: Future Options

The isotopic map of the reference region has been generated, but this was not an end in itself. Provenance analysis for the scope of quantifying the extent of population admixture and the direction of migration and trade will remain an important topic in the future, and this is also not restricted to bioarchaeological sciences. We understand this map as a starting point for the generation of an "isotopic landscape": Entering more data into the database will naturally lead to a further refinement of both the map and the clustering procedure. We also cannot fully exclude that the map presented in this volume may be subject to some revision. It needs to be tested for every new entry into the database by which of the existent clusters this individual isotopic fingerprint will be caught or whether additional clusters will arise. As outlined in chapter "The Isotopic Fingerprint: New Methods of Data Mining and Similarity Search", identification of structural importance and structural redundancy of single isotopic signatures within the multi-isotope fingerprint will

significantly contribute to the probability with which a region of provenance can be identified for non-local individuals, be it man or animal.

It is expected that the structural importance/redundancy of isotopic ratios of specific elements may change over time. For instance, metal working, even to a small extent, produces airborne metals and aerosols which can be distributed over long distances and will alter the natural regional isotopic patterning of lead (e.g. Kamenov and Gulson 2014). Metal working in preindustrial times had to exclusively rely on wood as fuel, whereby the clearing of woods and the removal of roots rendered the soils prone to substantial erosion with the consequence of long-distance transport of pollutants by rain, rivers and mudslides. Analysis of archaeological finds from different time horizons are suitable for an assessment and quantification of the regional and even supraregional anthropogenic input of metal sources through time, such as the global aerosol transport is assessed by analyzing ice cores (e.g. Hong et al. 1994) or peat bogs (e.g. Shotyk et al. 1996; Dunlap et al. 1999). Lead concentrations and lead isotopic ratios in archaeological skeletal finds are very good indicators for these processes (Grupe 2016) and give clues by which extent the consumer was affected, since anthropogenic lead is more soluble and more readily incorporated into the mineralized tissues than mineral-bound lead (Budd et al. 2000). This way, deliberate analysis of bioarchaeological finds excavated from specific time horizons will shed light on important aspects of environmental history and the generation of anthropogenic landscapes.

Modern biodiversity research is confronted with a rapid decline of the number of extant species, and one can only estimate how many species become extinct before they have even been discovered. Biodiversity research through time may also benefit substantially from bioarchaeological isotopic maps. The reconstruction of dietary and habitat preferences by use of stable isotopes of light elements such as carbon and nitrogen from bone collagen has already shown how the home ranges of some vertebrate species have become considerably smaller from preindustrial times until today (e.g. Becker and Grupe 2012). Additional information on the place of provenance and hence the firm differentiation between local game and imported animals, what cannot always be assessed morphologically, would contribute significantly to the current efforts with regard to landscape protection.

Let alone that multi-isotope fingerprints have also become routine in forensic sciences (Lehn and Graw 2014) and the prosecution of legal cases including the application of multivariate statistics to unravel the geographically defined data structure for provenance analysis (e.g. Ziegler et al. 2016). New methods of data mining applied to large databases are likely to reduce the overall global redundancy of regional single isotopic patterns, which is today substantially higher because of the global transport of food, beverages and pollutants.

This volume, however, focuses on the isotopic mapping of a specific geographical reference area with the scope of a better approach to time-related isotopic landscapes and a quantification of population admixture, migration and trade in the past—topics which belong to the driving forces of human history and are major determinants of human population development in time and space. While the results achieved so far are specific for this reference region, the general

methodological procedure is applicable to other regions of interest as well. The application of data mining methods proved suitable for the contextual resolution of the multi-isotope fingerprint and constitutes a leap forward with regard to the generation of a bioarchaeological isoscape, but it needs to be emphasized that a pre-evaluation of the data set by conventional univariate statistics remains indispensable (see chapter "Isotopic Map of the Inn-Eisack-Adige-Brenner Passage and its Application to Prehistoric Human Cremations"). A major option for the future is continuing with and refining the model calculations for local isotopic ratios based on modern reference samples, not only because this constitutes a step forward towards predictability but is at the same time highly informative for the data mining community. It seems that the interdependencies of soil, water and vegetation with regard to bioavailable trace elements for the consumer are much more complex than previously assumed and that the analysis of radiogenic isotopes in bioapatite has been too much focussed on underlying bedrock and soil properties.

Also, the computer scientists necessarily rely on a substantial contextual input by the domain experts, such as information on mineral metabolism. The other side of the medal, however, is that data mining depends on a minimum number of individual data sets, the establishment of which is both time and money intensive. With regard to the benefits for several academic and applied sciences, from cultural heritage via biodiversity and forensic studies, this might be worth the efforts.

One of the major results achieved is that provenance analysis of fully cremated finds is possible by measuring apatite lead and strontium isotopic ratios, however with some contextual *caveat*. The isotopic map has been purposefully established by analyzing compact bone, a tissue that integrates small-scale variability of regional isotopic signatures over years and decades, if not the lifetime of an animal. This way, local isotopic fingerprints were defined. Mobility, migration and trade on the other hand necessitate at least one residence change during an individual life, and its recognition depends on the adequate choice of mineralized tissue for analysis. In uncremated finds, this is usually tooth enamel or dentin which precipitates during childhood and juvenile age. Any non-local isotopic signal detected in dental tissue is a firm proof for an individual residence change between childhood and death/burial. The majority of cremated finds however lacks any such tissue, and the analyses are restricted to the bone. The quantification of the extent of population admixture by immigration is thus restricted to "late immigrants", that is, people that migrated to their place of recovery at some time during adult age. Difficult to resolve are mixed isotopic signatures in the bone which are generated when an immigrant did not spend sufficient time at the new place of residence to permit the skeleton to adjust to the local isotopic fingerprint in the course of tissue remodelling. The in-depth interpretation of mixed isotopic fingerprints, both in cremated and uncremated finds, will explicitly constitute a major research topic in the future, and we expect that, again, GMM clustering can be beneficial. Trace elements in biominerals exhibit a reservoir effect that depends on tissue turnover, but data on such effects are relatively scarce (e.g. Rabinowitz et al. 1976; Leggett 1993; Gulson 2008; Montgomery et al. 2010; Keller et al. 2016).

An additional task to fulfil in the near future is a similarity search, again aided by computer scientists. Isotopic maps for bioarchaeological purposes are mainly based on the isotopic analysis of residential bone finds, and the a priori generation of a spatial map was also the method of choice in this study. However, food, beverages, inhalation, etc. always produce mixed isotopic ratios in the consumer's tissue without exception. Therefore, a local human isotopic fingerprint will be similar to a local isotopic fingerprint established on an animal skeleton, but since feeding habits substantially differ between taxa, the term "similar" needs quantification. For instance, pigs living from human food leftovers are probably more similar to humans in their isotopic composition than free ranging deer. Which species matches the humans best is currently under study. After this will be worked out, provenance analysis can proceed to a next step when similarity search through the database will be capable of giving answers to questions such as "find any individual within a distance of 50 km from a certain site that belongs to the same species and shares the same isotopic fingerprint".

When the project has come to an end, the database established so far will be augmented by a large number of new data sets established by the archaeological research projects which rely on the isotopic map (see below) and will be made public in the form of a worldwide data sharing. For a sustainable storage and long-term availability of the produced data, the IT infrastructure is hosted by the Munich Leibniz-Rechenzentrum (LRZ) and will be curated by the ArchaeoBioCenter of the Ludwig-Maximilians-Universität (LMU). It will be accessible through a web interface available on the homepage of the ArchaeoBioCenter (http://www.archaeobiocenter.uni-muenchen.de).

At present, ongoing research concentrates on defined archaeological projects related to transalpine mobility and culture transfer where provenance analysis by multi-isotope fingerprints of cremated finds is specifically targeted and to which the isotopic map is applied.

Mobility and Social Dynamics in Bavaria and the Eastern Central Alps in the Late Bronze Age (1300–800 BCE)

Passages connecting the Italian Peninsula with Central Europe and beyond through the central Eastern Alps belong to the most important long-distance contact routes in Europe and are thus well suited for assessing the role of migration or mobility in prehistoric communities. For this particular area, both concepts have always played an important role in explaining cultural and demographic change.

Our project concentrates on periods in which the prevailing burial custom was cremation, paying tribute to the anthropological methods applied. Cremation was practiced in the late Bronze Age, the Iron Age as well as in Roman times.

Looking first at the Bronze Age segment of the research group, the late Bronze Age or Urnfield Period provided an ideal study area. Although immigration processes of the Northern Alpine population groups of the early Bronze Age (ca. 2150–1600 BCE) belonging to the so-called Straubing group located in

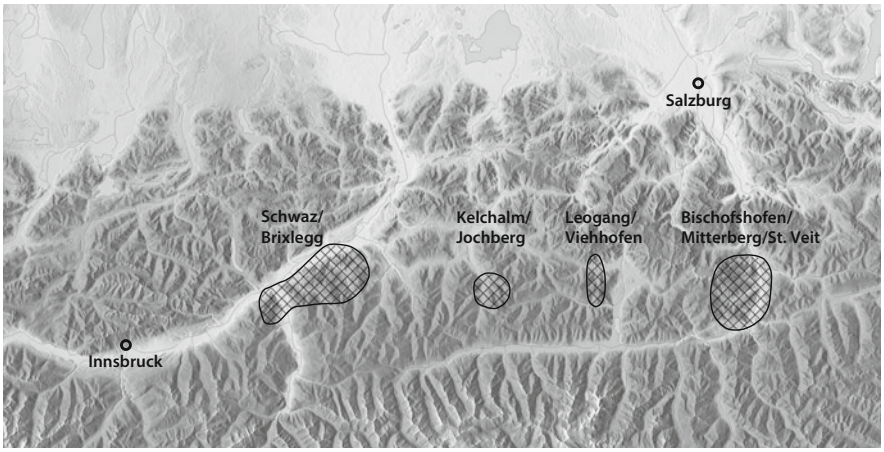

Fig. 1 Location of the main copper deposits and Bronze Age metal working districts in the central eastern Alps (graphic: Reuß)

southern Bavaria (Ruckdeschel 1978; Massy 2016) and reaching into the Tyrolean Inn Valley have been suggested recently (Sölder 2002; Töchterle 2015), the persisting absence of graves in this area makes it impossible to test this hypothesis on the basis of anthropological analyses.

The north Tyrolean Inn Valley lost its interregional significance due to the replacement of fahlore copper by a new copper type of sulphidic chalcopyrite (Kupferkies), the so-called East Alpine copper, in the early Middle Bronze Age at around 1500 BCE (Fig. 1) (Stöllner 2015a). The abundant chalcopyrite deposits of the Mitterberg region in the Austrian Salzach Valley and Saalfelden Basin were exploited during the Middle and Late Bronze Age (1600–800 BCE) on a large scale by deep mining and surface shaft working (Shennan 1995; Kienlin 2013; Stöllner 2015b).

The Inn Valley regained its importance as a mining and metal-producing area during the last phase of the Bronze Age, the so-called Urnfield Period dating between 1300 and 800/750 BCE. In the 13th and 12th centuries BCE, we observe a significant increase in burial and also mining and metal-processing activities (Goldenberg 2015). New cemeteries were founded with significantly more graves than in the middle Bronze Age (Kossack 1993; Sperber 1992, 1997, 2004). What is equally important is the fact that grave constructions display a new design with well-equipped urn-burials or long stone cists, in which the cremated bones of the deceased were sometimes strewn in the form of the actual body with the attire in place of the imagined body parts. Secondly a couple of artefact types themselves mirror a spectrum which is alien to the local Middle Bronze Age alpine cultural environment but match perfectly with grave inventories in southern Bavaria (Fig. 2).

These significant similarities of burial rites and the material culture between southern Bavaria and the north Tyrolean Inn Valley exhibit tight cultural

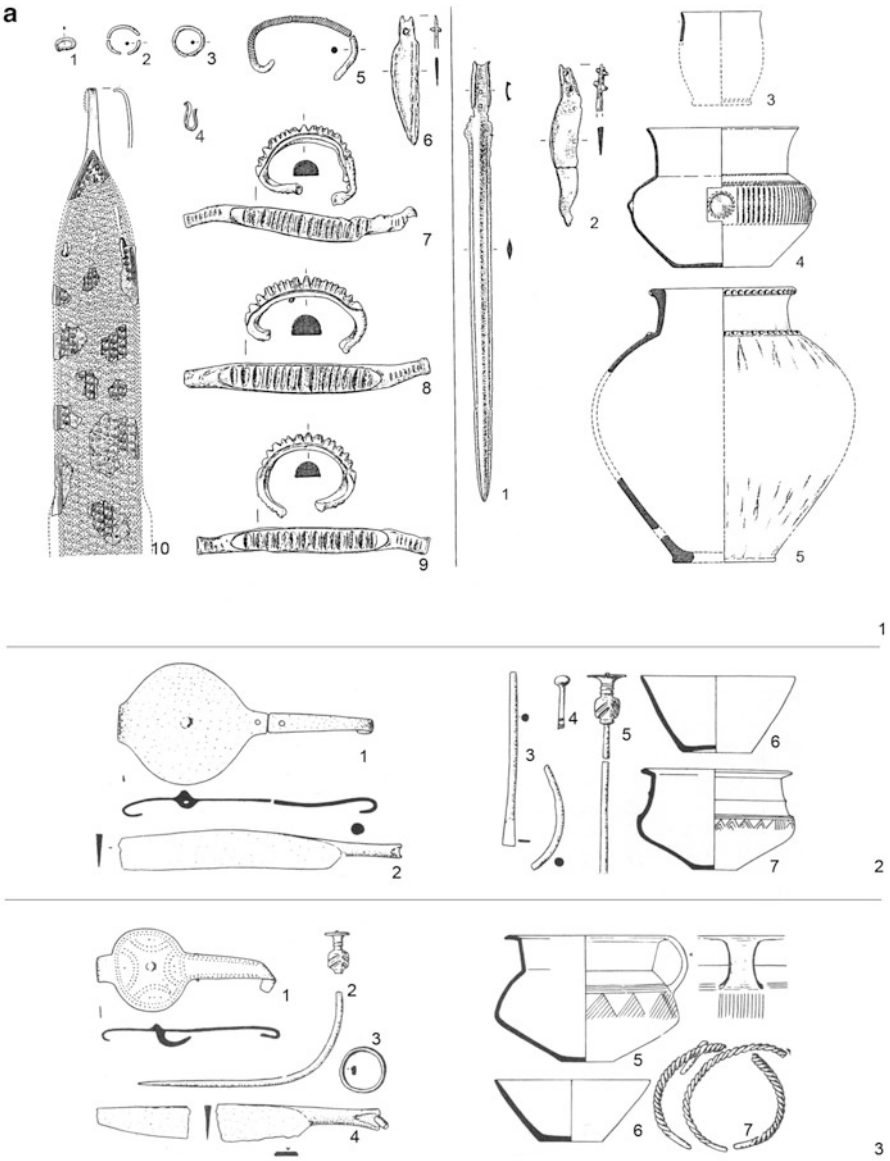

Fig. 2 Grave assemblages of the early Urnfield Period (13th–12th century BCE) from the north Alpine piedmont zone and the north Tyrolean Inn Valley in comparison. *Left:* Bavarian sites: 1. Riegsee, tumuli 25 and 23; 2. München-Grünwald, grave 12; 3. München-Grünwald, grave 32; *Right:* North Tyrolean sites: 1.-2. Selection of artefacts from the cemetery of Volders; 3. Wilten, grave 68 (after Koschik 1981, pl. 132–133; Müller-Karpe 1957, pl. 8 H, 10 A; ibid. 1980, pl. 411 B–C; 409C)

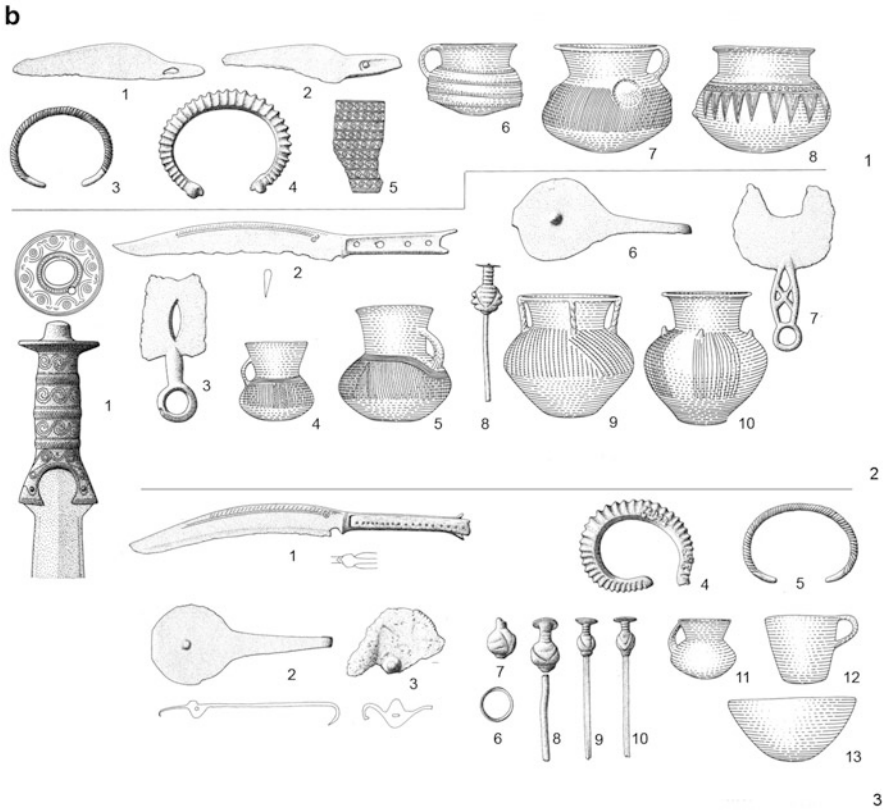

Fig. 2 (continued)

relationships between these two regions. While the cultural development in southern Bavaria in the Late Bronze Age, i.e. Urnfield Period (1300–800 BCE), is derived from a local substrate (Koschik 1981; Müller-Karpe 1957, 1959), the contemporary burial customs in Tyrol differ substantially from the Middle Bronze Age traditions (Müller-Karpe 1959; Moosleitner 1991; Tomedi et al. 2006). This supports the model of immigrants from south Central Europe as founders of the specific Tyrolean Urnfield communities (Sperber 1992, 1997, 2004). New studies focusing on archaeometallurgy, mining activities and settlement structure even speak of colonization by newcomers (Staudt and Tomedi 2015). The reason for this occupation was seen in the intention to exploit the copper ore deposits of the Inn Valley (Rieser and Schrattenthaler 1998/99; Goldenberg and Rieser 2004; Goldenberg 2013) and to control the trade of copper ores or ingots to the north (Winghart 1999; Möslein and Winghart 2002).

Although a thorough analysis of cultural traits and customs is applied, the question whether the described processes of new burial practices and increased burial activity can be explained by the immigration of people from southern Bavaria, as has been argued, or whether they were the result of cultural adaptation

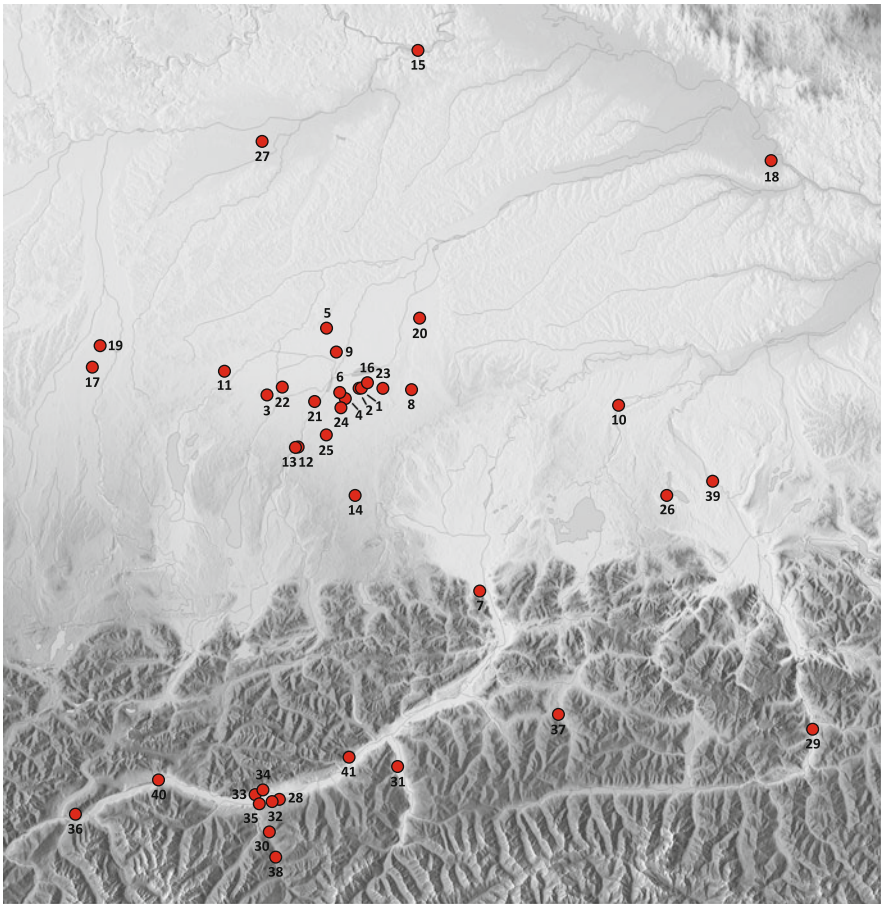

Fig. 3 Distribution of the cemeteries from which graves of Late Bronze Age/Urnfield Period date were sampled: most sites are located in the north Tyrolean Inn Valley, the Salzach Valley—both in Austria—and the area around Munich; others in the Lech Valley and along the Danube in southern Bavaria (graphic: Reuß)

and appropriation processes is evaluated by stable strontium and lead isotopes in human cremations. The isotopic signature of each individual can be assessed, and local and foreign individuals can in effect be distinguished from one another.

In combination of archaeological with anthropological investigations of the cremation burials, the focus of our project lies in the definition of the kind and extent of mobility, migration processes and cultural transfer (Fig. 3).

That southern Bavaria played a key role in this scenario and profited immensely by the control of the copper exchange is supported by the fact that in the 13th and 12th centuries BCE, emerging hierarchies became evident in new behavioural patterns of the social elites (i.e. Winghart 1998). In the archaeological context, these changes are displayed in the equipment of ostentatious graves, some of which

contain the first bronze-clad four-wheeled vehicles in Central Europe (Pare 1987) and lavish metal drinking sets (Müller-Karpe 1956; Nebelsick 2016) as supreme status markers of a sword-fighting warrior elite.

The newly discovered cremation cemetery of Vomp near Innsbruck with presently 467 cremations in stone cists and in urns is the largest cemetery ever discovered in the area (Sölder 2015). Its rich equipment with bronze objects and the high percentage of north alpine-type warrior graves strongly suggest migration of population groups from Northern Alpine areas. Within our project, cremated bones from a series of burials from Vomp will be analysed. So far comparatively few graves have been restored; thus, an evaluation of the extent of non-local and local elements is difficult to conduct. What is already clear however and also supported by the evidence of previously excavated burials such as Volders and others (Kasseroler 1959; Sperber 1992, 1997, 1999) is the fact that many graves contain pottery exhibiting local styles or a mixture of local and non-local pots or other artefact types. Thus, it is of particular interest to test the hypothesis of an immigration event in Vomp and other places or the model of possibly lifelong mobility patterns or perhaps exchange processes by local people, indicating modes of cultural transfer and cultural appropriation.

In order to pursue this objective, 250 burials from cemeteries in Bavaria and the Tyrolean Inn Valley have been or are currently being sampled (analyses by Dominika Wycisk). Although the artefacts from burials of the southern Bavarian or Munich Urnfield group from the period spanning between 1300 and 1100 BCE (early to middle Urnfield culture) are considered key for the proposed immigration events, a thorough evaluation of the burial rituals in Northern Alpine cemeteries has only been undertaken on a broader level (Falkenstein 2005; Wiesner 2009). A detailed analysis, however, including the spatial arrangements of grave goods, the treatment of dress accessories or other personal equipment such as weapons or tools, and analysis of quality and quantity of grave goods in regard to sex and age for this catchment area, will be focused on within a doctoral dissertation (Simone Reuß). The comparison not only of quality but also quantity of grave goods is essential to understand cultural affiliations, social dynamics as well as mobility and exchange patterns. Of equal importance is the comparison of ritual components such as the treatment of the cremated bones and occurring selection processes in a post-cremation state (Fig. 4).

First results indicate that the number of non-local individuals in the Inn Valley seems to be less significant than assumed; secondly, there seems to be no significant influx of people from the inner Alps into the north alpine areas, hinting that dual exchange by mobile people appears to be at least of marginal importance in the context of the burial record. This may support the idea that putative settlers or their descendants, who originally came to the Tyrolean Inn Valley in search of copper, did not go back to the areas in the north where they came from. However, cultural contacts between different micro-regions are closest between the Inn Valley and the Urnfield cemeteries around Munich (the so-called Munich Urnfields) as has been shown by statistical analyses of grave inventories in different catchment areas north of the Alps and in Tyrol (Reuß and Metzner-Nebelsick in press).

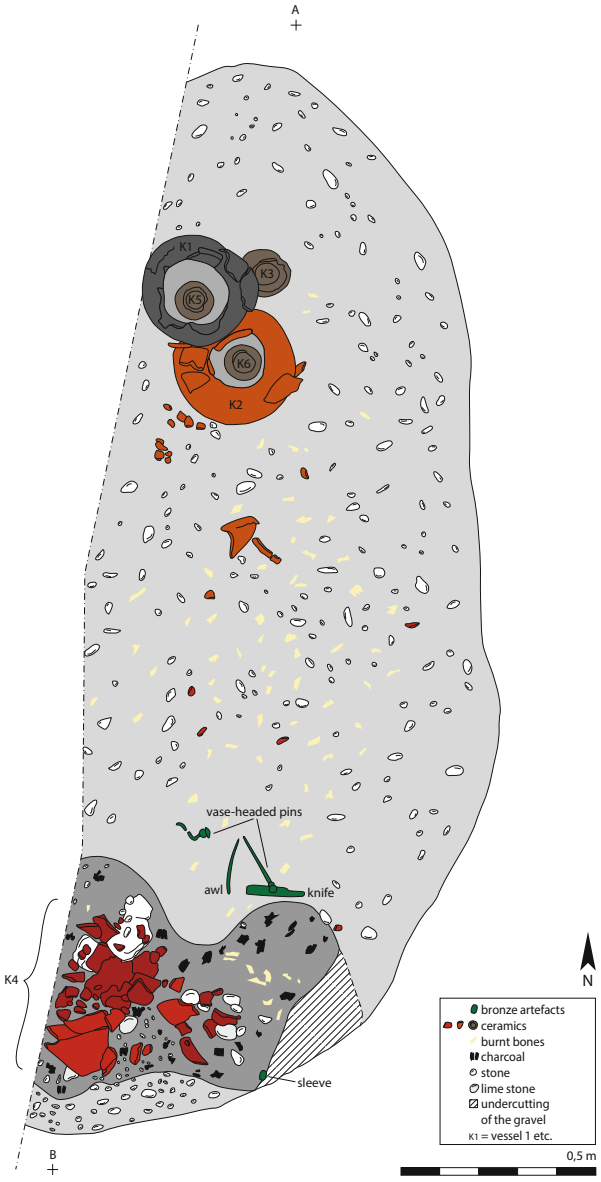

Fig. 4 Cremation grave of the early Urnfield Period, ca. 1300 BCE, from the Munich Residence. As typical for the period the cremated bones were strewn all over the grave pit. The pottery was divided into a set of grave offerings in the north of the grave pit and a secondary set of pots of different ritual purpose. They were smashed after use and burnt on the pyre (graphic: Reuß)

That the picture of late Bronze Age, i.e. Urnfield Period connectivity in the east Central Alpine region, is not a static one, but rather dynamic, is clearly represented by changing exchange networks and/or mobility patterns as represented by the evidence of cemeteries and graves from the younger and late Urnfield Period (ca. 1000–800 BCE). At around 1000 BCE, large cemeteries along the Salzach Valley are founded. In this timeframe the Salzach Valley and the ore deposits of the

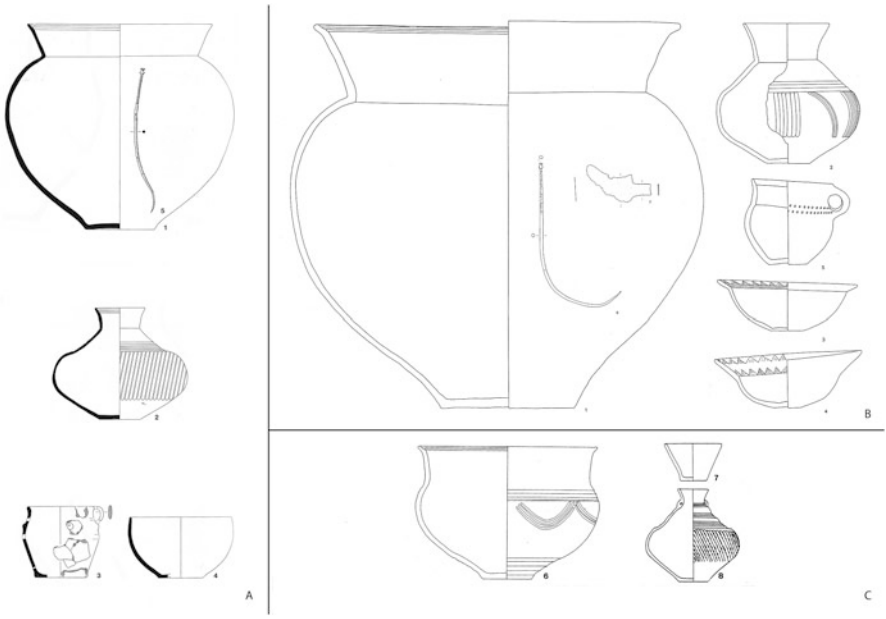

Fig. 5 Grave inventories of the late Urnfield Period (9th century BCE) from the Salzach Valley (**a**) and the Bavarian Danube region (**b–c**) in comparison (after Höglinger 1993; Schopper 1995; Pfauth 1998)

Mitterberg region south of Salzburg regain importance (Stöllner 2015a). Urnfield cemeteries like Obereching and Bischofshofen along the Salzach River starting in the younger and late Urnfield Period (9th to 10th century BCE) (Höglinger 1993; Lippert and Stadler 2009) display a multitude of culturally differently connotated traits indicating contacts with various geographical areas. Among the grave goods, mainly pottery displays a varied picture. In some graves, local types are present, in others non-local forms and yet in others both local and non-local (Fig. 5).

Next to eastern connections to Lower Austria or the southeastern Alps, pottery types indicate strong affiliations to stylistic expressions which can be found in the area of Danube bound Lower Bavaria between Straubing and Kelheim and beyond the Upper Palatinate, those forms are standing in a local tradition. This phenomenon seems to be analogous to the events in the catchment area of Schwaz-Brixlegg in the north Tyrolean Inn Valley that took place three hundred years before during the early Urnfield Period. After about 1000 BCE, the latter region and the Munich gravel plain no longer seem to have benefitted substantially from interregional exchange processes. While fewer burial sites are attested for in the Inn Valley, the Salzach region by contrast shows newly established graveyards that hint at an increase in population. The settlement processes and settlement structures as such are still insufficiently investigated; the heterogeneous styles of the grave goods within these newly founded cemeteries, however, suggest intensified mobility and cultural transfer or migration. Because of obvious similarities in pottery styles as

well as other artefact types, the lower Bavarian Danube region (Müller-Karpe 1952; Pfauth 1998; Schopper 1995) seems to have been an important starting point for contacts with the Salzach Valley in the 9th to 10th century BCE. Possibly, it was again the search for copper which was the driving force for the Northern Alpine communities to seek exchange and establish contacts with areas rich in ore deposits—this time the Mitterberg region in the Salzach Valley.

Migration or Acculturation: The Genesis and Spread of the Early Fritzens-Sanzeno Culture (Fifth/Fourth Century BCE)

Around 450 BCE, the Fritzens-Sanzeno culture emerged in North Tyrol, South Tyrol and Trentino. This formation was supported by the extensive use of the Inn-Eisack-Adige passage and created a unified inner-alpine cultural group, characterized, for example, by similarities in material culture, house construction, metallurgic technology and religious beliefs including the practice of cremation and use of sacrificial sites for burnt offerings (Fig. 6a).

The onset of the early Fritzens-Sanzeno culture is generally defined by the appearance of specific types of ceramics, namely the so-called Fritzener bowls (Fig. 6b) and bowls with a compressed S-shaped profile and comb stamped ornamentation (Fig. 6c). However it still remains a matter of debate whether these artefacts in fact indicate the emergence, existence and distribution in time and space of a unique cultural group.

Gamper (2006) postulates a regional and chronological sequence starting from the Adige Valley (Sanzeno group) and spreading north. The genesis of the Fritzens-Sanzeno culture should therefore have taken place in the south, and its characteristic features (ceramics, fibula types, house construction) were transferred to the north. The spread from the Adige Valley into the Brixen region could well be explained by culture transfer.

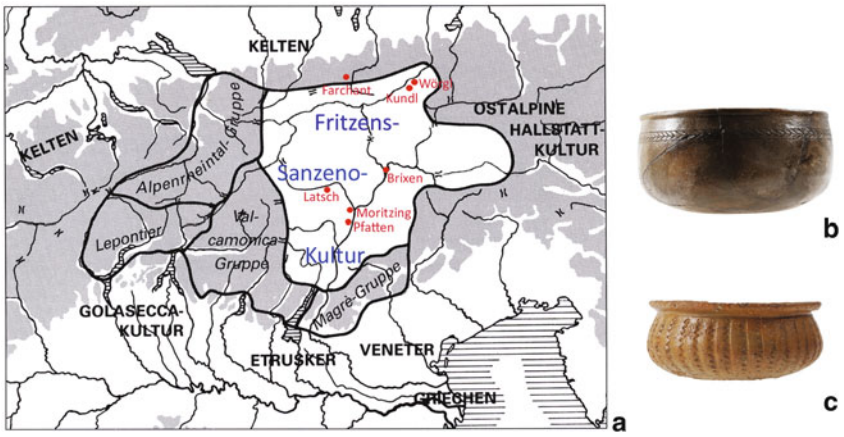

Fig. 6 (**a**) Distribution area of Fritzens-Sanzeno-Culture and the sites to be analyzed. (**b**) Fritzener bowl from Vill, Goarmbichl, North Tyrol. Photo: Tiroler Landesmuseum Ferdinandeum Innsbruck. (**c**) Bowl with comb stamped ornamentation from Telfes, North Tyrol. Photo: Tiroler Landesmuseum Ferdinandeum Innsbruck

An alternative explanation is suggested by the Fritzens-Sanzeno chronology in the Southern Alps established by Lang (1998) and Marzatico (2001). The onset of the culture in the lower Inn Valley took place as early as the latest Hallstatt Period/early La Tène. The time of emergence is based on a securely dated sacrificial site of burnt offerings at Farchant (Lang 2016) and also on graves documented in Kundl. A simultaneous development of the characteristic ceramic types of the early Fritzens-Sanzeno culture is evidenced both north and south of the Alpine range. There is no evidence to support a formation independent of one another. A highly efficient and rapid communication network across the Alps existed, resulting in the quick transfer of stimuli from the one side to the other. Stilistic concepts concerning artefacts, behavioral patterns, ritual practices and religious beliefs were transferred and implemented within such a short span of time that it is impossible to differentiate them archaeologically. This was either due to human mobility or to an intensification of contacts between people of both sides of the Brenner Pass. The question arises whether the genesis of this culture resulted from migratory events or if it is the result of an acculturation process by culture transfer.

The Brixen-Stufels settlement in the Eisack Valley played a central role in mobility across the Brenner Pass during the late Hallstatt and early Fritzens-Sanzeno period. It is located at the intersection between the north-south Brenner route and the east-west route through the Puster Valley in the direction of East Tyrol. Brixen-Stufels was a centre of innovation and pivotal point of dissemination for early Fritzens-Sanzeno culture ceramics. The oldest known Fritzener vessels were found there (Dal Ri 1985; Pezzo 2004). The impulse to adopt this ceramic form in the Inn Valley likely originated there. This further led to the uniform manifestation of the Fritzens-Sanzeno culture on both sides of the Brenner Pass.

Mobility and culture transfer are hotly debated topics (e.g. Prien 2005). Archaeological tools such as the comparative analysis of artefacts and their respective dates cannot solve all relevant questions centred around these topics, and the cooperation with natural sciences such as physical anthropology and archaeometry is indispensable (Grupe et al. 2015).

Discerning between migration and acculturation is only possible through the isotopic analysis of cremated human remains and human skeletons dating to the beginning of the Fritzens-Sanzeno culture and the late Hallstatt period.

Potential places of origin are determined by creating a multi-isotope fingerprint (Sr, Pb, O). The application of two isotope systems of heavy elements (Sr, Pb), which do not entail thermally induced isotopic fractionation, will for the first time permit an isotopic analysis of cremated bones.

Both cremated and uncremated human skeletal remains are available for the time period marking the formation of this specific culture, thus providing the opportunity of detecting possible migration events. Isotopic analysis will be conducted on a total of 120 individuals stemming from the early Fritzens-Sanzeno culture. Presently, approximately 25 % of the data have already been established. Cremated samples are available from the Kundl (Lang 1998) and Wörgl (unpublished) sites in North Tyrol (late Hallstatt and early Fritzens-Sanzeno culture and late Hallstatt period, respectively) and from Moritzing (Steiner 2002) and Pfatten (Alberti 2007) in South Tyrol (early Fritzens-Sanzeno culture).

In the early Fritzens-Sanzeno culture, inhumations were the exception to the rule, which involved cremating the dead. Among the burial sites which have been sampled, a small group of 19 uncremated skeletons, 16 of which are partial inhumations, come from Latsch in the Vinschgau (Steiner 2007). With respect to burial customs, types of grave goods and their isotopic fingerprint (analyses D. Wycisk), the group from Latsch represents an ensemble not yet seen in the Fritzens-Sanzeno culture. One remarkable feature is the topographical location, which is situated at a main Fritzens-Sanzeno culture traffic and communication route leading through the Adige Valley.

An isotopic analysis conducted on two individuals whose hands had been tied and were buried in a double grave discovered in Brixen Oberegger, room B, should reveal whether these victims of violence belonged to the Latsch group.

Isotopic analyses of animal remains from burials, settlements (Brixen) and a sacrificial site for burnt offerings (Farchant) should provide information on the import and export of animals and their impact on livestock farming and farm animals with respect to local livestock breeding.

Furthermore, for the first time, it is possible to determine the catchment area of wild animals not under wide human influence. Beyond its special scientific scopes, this project therefore also has implications for modern biodiversity research and the reconstruction of anthropogenic environment genesis.

Population and Domestic Animals of the Raetian Alps and Alpine Foreland During the First Century CE

The conquest of the Alps and its northern piedmont region by Rome in 15 BCE had a strong impact on the region's cultural development. Archaeologically unsolved for the moment are the cultural histories of the autochthonous Celtic and Raetian populations and their role in the nascent province of Raetia. Of particular interest is the so-called Heimstetten Group (c. 30–60 CE), confined to the region between the rivers Lech and Inn. Characterized by inhumation burials with the dead richly dressed in traditional clothing and accessories, this culture is only tangible for slightly more than a single generation. Controversy surrounds the existing interpretations for this culture's advent and departure: Roman-controlled immigration from the Tyrolean Inn Valley or cultural development of autochthonous origin (Mackensen 1978; Keller 1984)?

A comprehensive archaeological, archaeozoological, palaeobotanical and anthropological examination of finds originating from settlements under Roman-Mediterranean influence (e.g. Langweid) as well as settlements and graves from the Heimstetten Group (e.g. Heimstetten, Aubing) was conducted within the framework of the project "Population and domestic animals of the Raetian Alps and Alpine foreland during the first century CE". This study revealed marked differences between the "Roman" and local societies, their settlements and building style, economies, diet and manner in which they disposed of their refuse. Thus, we interpret these findings as evidence that the Heimstetten Group was the

autochthonous population of the Alpine foreland and also postulate a continuous development from the Iron Age to Roman times. At the same time, it is apparent that the Roman military presence and early imperial process of Romanization both boosted the trade of wares and animals stemming from the Mediterranean (see chapter III, this volume).

The goal of the archaeological and archaeozoological examinations conducted up to now in this project was to create a foundation for further archaeometric analyses helpful in assaying and improving already existing models for the Romanization of Raetia. Emphasis is placed on the mobility of humans and animals across the Alps and tested using strontium, lead and oxygen isotope analysis of bones from cattle, red deer and pig collected in early Roman archaeological contexts. This method proved useful with respect to the question of provenance of the early imperial inhabitants of settlements displaying Roman-Mediterranean influence (e.g. Cambodunum/Kempten), since, according to their material culture and burial rituals, they likely originated from populations stemming from upper Italy and Gaul (Mackensen 1978). This of course leads to the direct comparison with the Heimstetten Group. In addition to changes in the composition of the human population, that of the cattle herds is also affected (Peters and Manhart 2004; Trixl et al. in press). Early imperial archaeofauna show evidence for the importation of stock used to meliorate local domestic breeds. The possibility that allochthonous draught and pack animals were brought to Raetia during military movements and civilian trade traffic must also be taken into consideration. The planned isotopic analyses should help provide a better understanding of the currently documented use of domestic animals than now exists, which is presently based solely on archaeozoological examinations.

On the whole and by incorporating the isotopic map introduced in chapter "Isotopic Map of the Inn-Eisack-Adige-Brenner Passage and its Application to Prehistoric Human Cremations", the possibility of identifying signatures as local or foreign is given. Determining the time and perhaps even the intensity of human migration and animal importation will be provided at least to some extent by way of this approach. We expect to generate a clearly detailed and regionally differential picture of how local cattle breeding evolved during the Roman period between the Alpine divide and Danube River. Provided the necessary results are available, this interdisciplinary project should contribute significantly to understanding the processes driving the provincialization of Raetia's rural regions in the first century CE.

Gontia as Melting Pot? The Composition of the Population during Günzburg's Roman Military Period, as Reflected by its Graves

Where did the Roman population in the Northern Alpine foothills come from? This question will be addressed in part within the framework of this archaeological project, which is made up of researchers specializing in Roman archaeology and

physical anthropologists with expertise in cremated ossified remains. The focus of this examination will be on one of the largest Roman cemeteries in Germany, the well-documented Günzburg site. Several aspects of the Günzburg necropolis are quite unique and have the potential for providing needed information in order to determine the place of origin of its former inhabitants. For example, the sheer size of the cemetery, which contained more than 1800 burials consisting of very well-preserved cremations, will not only provide an excellent opportunity to establish various biological and demographic parameters of the once living population, but it also represents a good indicator of population makeup and the changes occurring within it over time. It was also recently investigated by application of modern archaeometric methods, yielding information to the settlement area important for generating a clearer picture of past environmental and geological circumstances. However two prerequisites must be fulfilled. An archaeological examination of the enormous amount of artefacts, which are contained in over 2700 boxes, must be conducted as well as a dating of the burials.

Specifically, this project hopes to elucidate whether the people at Günzburg were native to the region (Hüssen et al. 2004) or if Günzburg was settled by foreign migrants that came as a result of the Roman occupation (cf. Chap. "Transalpine Mobility and Trade Since the Mesolithic"). It is assumed that the soldiers in Günzburg during this period were members of a special cavalry unit: the *ala II Flavia pia fidelis milliaria* (Czysz 2002). Totalling 1000 men, this was the largest military unit at the time in the province of *Raetia*. Second only to the provincial governor, the *praefectus* was the highest ranking person of *Raetia* (Scholz 2009). Civilians may have moved together with the military unit to their new locations (see chapter "Transalpine Mobility and Trade Since the Mesolithic"; Sommer 1990; Grünewald submitted 2).

The Roman cemetery at Günzburg was used continuously from the second half of the first century CE into the fifth century CE. The research concentrates on the graves of Günzburg's early phase of occupation in the decades around 100 CE (Grünewald submitted 1 and 2; for late Antiquity: Hüdepohl in preparation). The largest burial area of the cemetery was examined in order to discern graves stemming from this earlier period. A total of 364 burials were selected and are the focus of study. Chronological dating is based to a large extent on the presence of Samian ware from La Graufesenque, Banassac, and also the early pottery from central Gaul. Terra nigra, early fibulae and lamps are also decisive for detecting early burials. Grave goods including a large number of mirrors and also balsamaria indicate the presence of women. Numerous inhumations belonging to children were found among the cremations (anthropological considerations concerning inhumations are already published by Gerstmann et al. 2015). Both observations verify the presence of civilian burials inside the Günzburg cemetery at Ulmer Street. An anthropological study of the buried will shed light on these individuals and possible differences to the military personnel.

According to archaeological examinations conducted at the cemetery as well as on the artefacts recovered there, the different burial rites and grave goods documented indicate a very heterogeneous population at Günzburg and Raetia.

Both suggest that the provenance of the people there was likely also diverse. Hypotheses to the probable places of origin based on the archaeological analyses will be compared with those established by stable isotope analyses of the cremated remains. This archaeometric analysis is specifically implemented here to determine the origin of non-local individuals. Together the modern archaeological and archaeometric examinations of this burial ground presents an especially informative foundation of information from which our research can profit.

To date, there has been no evidence for a rapid influx of large numbers of people from Günzburg's surrounding areas. Despite some indication for Celtic or Germanic traditions (Czysz 2002; Grünewald submitted 1), evidence for migration predominates. Objects were imported from Italy and Gaul (cf. chapter "Early Roman Transfer of Animals Across the Alps: Setting the Stage for Interpreting the Results of Isotope Fingerprinting") and were later produced in the region. Among other finds, more than 650 lamps used as grave goods are proof for a massive cultural impact from the Mediterranean. This cultural influence is also indicated by evidence for libation rites, which are seldom detected north of the Alps (Grünewald 2016). Fibulae suggest migration from Gaul, but evidence for contacts to the Eastern Alpine region and even Britain also exists (Grünewald submitted 1). The relationship with the Heimstettener group is also a focus of investigation. An analysis of the names of people from the later *ala II* garrison in Heidenheim reveals probable African, German, French and Spanish origins (Scholz 2009, 143; Farkas 2015, 128 f.). It thus appears that the oldest burials at the Günzburg garrison containing soldiers, their family members and also tradesmen are comprised of people who came from regions further away.

Following the departure of the Roman military unit, a reduction of Günzburg's civilian settlement area is very likely. This is supported by the finding of graveyard expansion into parts formerly settled (Grünewald 2016). Mass migration to the Roman frontier can be detected by contextualizing the graves from Günzburg with the known dated cemeteries of other forts at the Roman frontier region in Germany (Grünewald submitted 2). Compared with prehistoric epochs, a very high percentage of people that migrated through the transalpine region seems probable.

At present, examinations of the graves appear to indicate that the population during Günzburg's Roman military period was very diverse and that Günzburg was a melting pot for different cultural attributes and peoples. A further examination of the grave goods and burial customs of the Günzburg cemetery and other similar burial grounds is requisite to acquire more knowledge about the genesis of the Roman population in the Northern Alpine foothills in the Roman province of *Raetia*. The ongoing osteological investigation is indispensable for all further archaeological interpretation and a prerequisite for subsequent archaeometric analyses (Grupe et al. 2015). A selection of graves for this analyses based on the immense archaeological data has been made. A comparison of the archaeological interpretation with the data from about 100 strontium and lead isotope analysis of the cremated bones will provide further insights about the origin of the deceased.

References

Alberti A (2007) La necropoli protostorica di Vadena. Tesi di laurea in protostorica europea. Unpublished thesis, Università di Roma La Sapienza, Roma

Becker C, Grupe G (2012) Archaeometry meets archaeozoology: Viking Haithabu and medieval Schleswig reconsidered. Archaeol Anthropol Sci 4:241–262

Budd P, Montgomery J, Evans J, Barreiro B (2000) Human tooth enamel as a record of the comparative lead exposure of prehistoric and modern people. Sci Tot Environ 263:1–10

Czysz W (2002) Gontia. Günzburg in der Römerzeit. Likias, Friedberg

Dal Ri L (1985) Scavo di una casa dell'Età del Ferro a Stufles, quartiere di Bressanone (Stufles B). Denkmalpflege in Südtirol, pp. 195–237

Dunlap CE, Steinnes E, Flegal AR (1999) A synthesis of lead isotopes in two millennia of European air. Earth Planet Sci Lett 167:81–88

Falkenstein F (2005) Aspekte von Alter und Geschlecht im Bestattungsbrauchtum der nordalpinen Bronzezeit. In: Müller J (ed) Alter und Geschlecht in ur- und frühgeschichtlichen Gesellschaften. Tagung Bamberg 2004. Universitätsforschungen zur Prähistorischen Archäologie 126. Rudolf Habelt Verlag, Bonn, pp. 73–90

Farkas IG (2015) The dislocation of the Roman Army in Raetia. BAR International Series 2723

Gamper P (2006) Die latènezeitliche Besiedlung am Ganglegg in Südtirol. Neue Forschungen zur Fritzens-Sanzeno-Kultur. Internationale Archäologie 91. Verlag Marie Leidorf, Rahden

Gerstmann A, Lex M, Rodschinka G, Sebald S, Stenzel L, Hüdepohl S, McGlynn GC, Grupe G (2015) The Roman cemetery of Günzburg/site Ulmer Straße—The uncremated skeletal finds. Documenta Archaeobiologiae 12:81–168

Goldenberg G (2013) Prähistorischer Fahlerzbergbau im Unterinntal—Montanarchäologische Befunde. Montanwerke Brixlegg. In: Oeggl K, Schaffer V (eds) Cuprum Tyrolense. 5550 Jahre Bergbau und Verhüttung in Tirol. Edition Tirol, Brixlegg, pp. 89–122

Goldenberg G (2015) Prähistorische Kupfergewinnung aus Fahlerzen der Lagerstätte Schwaz-Brixlegg im Unterinntal, Nordtirol. In: Stöllner T, Oeggl K (eds) Bergauf Bergab. 10.000 Jahre Bergbau in den Ostalpen. Deutsches Bergbau Museum, Bochum, pp. 151–163

Goldenberg G, Rieser B (2004) Die Fahlerzlagerstätten von Schwaz/Brixlegg (Nordtirol). Ein weiteres Zentrum urgeschichtlicher Kupferproduktion in den österreichischen Alpen. In: Weisgerber G, Goldenberg G (eds) Alpenkupfer—Rame delle Alpi. Der Anschnitt, Beiheft 17, pp. 37–52

Grünewald M (submitted 1) *Gontia* as a melting pot. The composition of the population during Günzburg's early Roman military period, as reflected by its graves. Thoughts about a model for *Raetia*. In: Matešic S, Sommer CS (eds) XXIII. Limes. Proceedings of the 22nd International Congress of Roman Frontier Studies, Ingolstadt

Grünewald M (submitted 2) Migration zur Grenze. Überblick anhand ausgewählter Gräberfelder Obergermaniens und Raetiens

Grünewald M (2016) Studien zur Herkunft der Bevölkerung in Raetien am Beispiel der frühen römischen Bestattungen von Günzburg. In: Grabherr G, Kainrath B, Kopf J, Oberhofer K (eds) Der Übergang vom Militärlager zur Zivilsiedlung. Akten des internationalen Symposiums vom 23.–25. Oktober 2014 in Innsbruck. IKARUS 10. Universität Innsbruck, Innsbruck, pp 171–191

Grupe G, Grünewald M, Gschwind M, Hölzl S, Kocsis B, Kröger P, Lang A, Mauder M, Mayr C, McGlynn GC, Metzner-Nebelsick C, Ntoutsi E, Peters J, Renz M, Reuß S, Schmahl WW, Söllner F, Sommer CS, Steidl B, Toncala A, Trixl S, Wycisk D (2015) Networking in bioarchaeology: the example of the DFG Research Group FOR 1670 "Transalpine Mobility and Culture Transfer". Documenta Archaeobiologiae 12:13–51

Grupe G (2016) Bioarchäologie des Abfalls. Ein Schlüssel zur Alltagsgeschichtsforschung. In: Kersten J (ed) Inwastement. Abfall in Umwelt und Gesellschaft. Transcript, Bielefeld, pp. 247–268

Gulson B (2008) Stable lead isotopes in environmental health with emphasis on human investigations. Sci Tot Environ 400:75–92

Höglinger P (1993) Das urnenfelderzeitliche Gräberfeld von Obereching. Archäologie in Salzburg 2. Amt der Salzburger Landesregierung, Salzburg
Hong S, Candelone JP, Patterson CC, Boutron CF (1994) Greenland ice evidence of hemispheric lead pollution two millennia ago by Greek and Roman civilizations. Science 265:1841–1843
Hüdepohl S (in preparation) Das spätrömische Guntia/Günzburg. Die Gräberfelder an der Ulmer Straße und in der Oberstadt und das spätrömische Kastell. PhD thesis, Ludwig-Maximilians-Universität München
Hüssen C-M, Irlinger W, Zanier W (eds) (2004) Spätlatènezeit und frühe römische Kaiserzeit zwischen Alpenrand und Donau. Akten des Kolloquiums in Ingolstadt am 11. und 12. Oktober 2001. Kolloquien zur Vor- und Frühgeschichte 8, Bonn
Kamenov GD, Gulson BL (2014) The Pb isotopic record of historical to modern human lead exposure. Sci Tot Environ 490:861–870
Kasseroler A (1959) Das Urnenfeld von Volders. Schlern-Schriften 204, Innsbruck
Keller AT, Regan LA, Lundstrom CC, Bower NW (2016) Evaluation of the efficacy of spatiotemporal Pb isoscapes for provenancing of human remains. Forensic Sci Int 261:83–92
Keller E (1984) Die frühkaiserzeitlichen Körpergräber von Heimstetten bei München und die verwandten Funde aus Südbayern. Münchner Beiträge zur Vor- und Frühgeschichte 37, CH Beck, München
Kienlin TL (2013) Copper and bronze: bronze age metalworking in context. In: Harding A, Fokkens H (eds) The Oxford Handbook of the European Bronze Age. Oxford University Press, Oxford, pp. 414–436
Koschik H (1981) Die Bronzezeit im südwestlichen Oberbayern. Materialhefte zur Bayerischen Vorgeschichte, Reihe A 50. Verlag Michael Lassleben, Kallmünz/Opf
Kossack G (1993) Die Zentralalpen und das bayerische Vorland in prähistorischer Zeit. In: Ammann G, Pizzini M (eds) Bayerisch-Tirolsche G'schichten . . . eine Nachbarschaft. Tiroler Landesausstellung 1993. Festung Kufstein 19. Mai bis 31. Oktober 1993. II Beiträge. Tiroler Landesmuseum Ferdinandeum, Innsbruck, pp. 7–26
Lang A (1998) Das Gräberfeld von Kundl im Tiroler Inntal. Studien zur vorrömischen Eisenzeit in den zentralen Alpen. Frühgeschichtliche und Provinzialrömische Archäologie Materialien und Forschungen 2. Verlag Marie Leidorf, Rahden
Lang A (2016) Der Brandopferplatz auf dem Spielleitenkopf bei Farchant, Lkr. Garmisch-Partenkirchen. In: ZwischenWelten. Naturheilige Plätze in vorgeschichtlicher Zeit, Nürnberg, pp. 183–200
Lehn C, Graw M (2014) Stabilisotopenanalysen an Körpergeweben von unbekannten Personen. Rechtsmedizin 24:129–143
Leggett RW (1993) An age-specific kinetic model of lead metabolism in humans. Environ Health Perspect 101:598–616
Lippert A, Stadler P (2009) Das spätbronze- und früheisenzeitliche Gräberfeld von Bischofshofen-Pestfriedhof. Universitätsforschungen zur Prähistorischen Archäologie 168. Rudolf Habelt Verlag, Bonn
Mackensen M (1978) Das römische Gräberfeld auf der Keckwiese in Kempten. I. Gräber und Grabanlagen des 1. und 4. Jahrhunderts. Materialhefte zur bayerischen Vorgeschichte A 34. Lassleben, Kallmünz/Opf
Marzatico F (2001) La seconda età del ferro. In Lanzinger M, Marzatico F, Pedrotti A (eds) Storia del Trentino I: La Preistoria e la Protostoria. Il Mulino, Bologna, pp. 479–573
Massy K (2016) Die Gräber der Frühbronzezeit zwischen Nördlinger Ries, Lech und Alpen. Untersuchungen zu den Bestattungs- und Beigabensitten sowie gräberfeldimmanenten Strukturen, PhD Thesis, Ludwig-Maximilians-Universität München 2016. book version in print (Materialhefte zur Bayerischen Archäologie)
Möslein S, Winghart S (2002) Produktion, Verarbeitung und Verteilung von Kupfer—Die Beziehungen der alpinen Lagerstätten und der Handel in Südbayern. In: Über die Alpen—Menschen, Wege, Waren. Ausstellungskatalog. Folio, Stuttgart, pp. 137–143
Montgomery J, Evans JA, Horstwood MSA (2010) Evidence for long-term averaging of strontium in bovine enamel using TIMS and LA-MC-ICP-MS strontium intra-molar profiles. Environ Archaeol 15:32–42

Moosleitner F (1991) Bronzezeit im Saalfeldener Becken. Archäologie in Salzburg 1. Amt der Salzburger Landesregierung, Salzburg

Müller-Karpe H (1952) Das Urnenfeld von Kelheim. Materialhefte zur Bayerischen Vorgeschichte 1. Verlag Lassleben, Kallmünz/Opf

Müller-Karpe H (1956) Das urnenfelderzeitliche Wagengrab von Hart a.d. Alz, Oberbayern. Bayerische Vorgeschichtsblätter 21:46–75

Müller-Karpe H (1957) Münchner Urnenfelder. Kataloge der Prähistorischen Staatssammlung München. Prähistorische Staatssammlung, München

Müller-Karpe H (1959) Beiträge zur Urnenfelderkultur nördlich und südlich der Alpen. Römisch-Germanische Forschungen 22. de Gruyter, Berlin

Nebelsick LD (2016) Drinking sets in ostentatious tombs in the Late Bronze and Early Iron Ages in the western Carpathian Basin. In: Nebelsick LD (ed) Drinking against Death. Warszawa. Monographs of the Institut of Archaeology, UKSW

Pare CEF (1987) Der Zeremonialwagen der Bronze- und Urnenfelderzeit: Seine Entstehung, Form und Verbreitung. In: Barth FE (ed) Vierrädrige Wagen der Hallstattzeit. Römisch-Germanisches Zentralmuseum, Monographien 12. Verlag des Römisch-Germanischen Zentralmuseums, Mainz, pp. 25–67

Peters J, Manhart H (2004) "... und jegliches heimische Rind ist weit besser als ein auswärtiges..." Zur Frage der Kontinuität keltischer Viehwirtschaft im süddeutschen Raum. In: Hüssen CM, Irlinger W, Zanier W (eds) Spätlatène- und frühe römische Kaiserzeit zwischen Alpenrand und Donau. Akten des Kolloquiums in Ingolstadt am 11- und 12. Oktober 2001. Kolloquien zur Vor- und Frühgeschichte 8. Rudolf Habelt Verlag, Bonn, pp. 39–52

Pezzo MI (2004) Neue dendrochronologische Untersuchungen in Brixen/Stufels. Schlernmitteilungen 7:45–48

Pfauth U (1998) Beiträge zur Urnenfelderzeit in Niederbayern. Materialien zur Bronzezeit in Bayern 2. Universitätsverlag Regensburg, Regensburg

Prien R (2005) Archäologie und Migration. Universitätsforschungen zur Prähistorischen Archäologie 120. Rudolf Habelt Verlag, Bonn

Rabinowitz MB, Wetherill GW, Kopple JD (1976) Kinetic analysis of lead metabolism in healthy humans. J Clin Invest 58:260–270

Reuß S, Metzner-Nebelsick C (in print) Mobility and Social Dynamics in Bavaria and North Tyrol in the Urnfield Culture. In: Scharl S, Gehlen B, Zimermann A (eds) Mobilität in sesshaften Gesellschaften. Beiträge eines Workshops des SFB 'Our Way to Europe' 26.–27. Juni 2015 in Köln

Rieser B, Schrattenthaler H (1998/99) Urgeschichtlicher Kupferbergbau im Raum Schwaz-Brixlegg, Tirol. Archaeologia Austriaca 82(83):135–179

Ruckdeschel W (1978) Die frühbronzezeitlichen Gräber Südbayerns. Ein Beitrag zur Kenntnis der Straubinger Kultur. Antiquitas 11. Rudolf Habelt Verlag, Bonn

Scholz M (2009) Das Reiterkastell Aquileia/Heidenheim. Die Ergebnisse der Ausgrabungen 2000–2004. Forschungen und Berichte zur Vor- und Frühgeschichte in Baden-Württemberg 110

Schopper F (1995) Das urnenfelder- und hallstattzeitliche Gräberfeld von Künzing, Lkr. Deggendorf (Niederbayern). Materialhefte zur Bronzezeit in Bayern 1. Universitätsverlag Regensburg, Regensburg

Shennan S (1995) Bronze Age copper production of the eastern Alps: Excavations at St. Veit-Klingelberg. Universitätsforschungen zur Prähistorischen Archäologie 27. Rudolf Habelt Verlag, Bonn

Shotyk W, Cheburkin AK, Appleby P, Fankhauser A, Kramers JD (1996) Two thousand years of atmospheric arsenic, antimony, and lead deposition recovered in ombrotrophic peat bog profile, Jura mountains, Switzerland. Earth Planet Sci Lett 145:E1–E7

Sommer CS (1990) Das römische Militär und sein Einfluss auf die Bevölkerung in Obergermanien und Raetien rechts des Rheins und nördlich der Donau. In: Vetters H, Kandler M (eds) Akten des 14. Internationalen Limeskongresses 1986 in Carnuntum. VÖAW, Wien, pp. 121–131

Sölder W (2002) Zur Urgeschichte und Römerzeit in Nordtirol. In: Sölder W (ed) Zeugen der Vergangenheit. Archäologisches aus Tirol und Graubünden. Ausstellungskatalog Tiroler Landesmuseum Ferdinandeum. Tiroler Landesmuseum Ferdinandeum. Innsbruck, pp. 19–76

Sölder W (2015) Das Brandgräberfeld Vomp—Fiecht—Au im Unterinntal und die Nordtiroler Urnenfelderzeit. In: Stöllner T, Oeggl K (eds) Bergauf Bergab. 10.000 Jahre Bergbau in den Ostalpen. Deutsches Bergbau Museum, Bochum, pp. 273–277

Sperber L (1992) Bemerkungen zur sozialen Bewertung von goldenem Trachtschmuck und Schwert in der Urnenfelderkultur. Archäologisches Korrespondenzblatt 22:63–77

Sperber L (1997) Zur Demographie des spätbronzezeitlichen Gräberfeldes von Volders in Nordtirol. In: Rittershofer KF (ed) Demographie der Bronzezeit. Paläodemographie—Möglichkeiten und Grenzen, Internationale Archäologie 36. Verlag Marie Leidorf, Rahden, pp 105–124

Sperber L (1999) Zu den Schwertträgern im westlichen Kreis der Urnenfelderkultur: Profane und religiöse Aspekte. In: Eliten der Bronzezeit. Teil 2. Monographien Römisch-Germanisches-Zentralmuseum Mainz 43,2. Römisch-Germanisches Zentralmuseum, Mainz, pp. 605–659

Sperber L (2004) Zur Bedeutung des nördlichen Alpenraumes für die spätbronzezeitliche Kupferversorgung in Mitteleuropa. In: Weisgerber G, Goldenberg G (eds) Alpenkupfer—Rame delle Alpi. Der Anschnitt, Beih, 17, pp. 303–345

Staudt M, Tomedi G (2015) Zur Besiedlungsgeschichte der Ostalpen in der Mittel- bis Spätbronzezeit: Bestand, Kolonisation und wirtschaftlicher Neuanfang in der mittleren und späten Bronzezeit in Nordtirol. In: Stöllner T, Oeggl K (eds) Bergauf Bergab. 10.000 Jahre Bergbau in den Ostalpen. Deutsches Bergbau Museum, Bochum, pp. 135–143

Steiner H (2002) Das jüngereisenzeitliche Gräberfeld von Moritzing, Gemeinde Bozen (Südtirol). In: Tecchiati U (ed) Der Heilige Winkel. Der Bozner Talkessel zwischen Später Bronzezeit und der Romanisierung (13.-1. Jh. v. Chr.). Schriften des Südtiroler Archäologiemuseums. Folio, Bozen/Wien, 2, pp. 155–358

Steiner H (2007) Staatsstraße. In: Denkmalpflege in Südtirol 2007, pp. 231–234

Stöllner T (2015a) Die alpinen Kupfererzreviere: Aspekte ihrer zeitlichen, technologischen und wirtschaftlichen Entwicklung im zweiten Jahrtausend vor Christus. In: Stöllner T, Oeggl K (eds) Bergauf Bergab. 10.000 Jahre Bergbau in den Ostalpen. Deutsches Bergbau Museum, Bochum, pp. 99–105

Stöllner T (2015b) Der Mitterberg als Großproduzent für Kupfer in der Bronzezeit. In: Stöllner Th, Oeggl K (eds) Bergauf Bergab. 10.000 Jahre Bergbau in den Ostalpen. Deutsches Bergbau Museum, Bochum, pp. 175–185

Töchterle U (2015) Die Besiedlung der Ostalpen in der Früh- und Mittelbronzezeit: Kolonisation und wirtschaftlicher Neuanfang. Teil 2. In: Stöllner T, Oeggl K (eds) Bergauf Bergab. 10.000 Jahre Bergbau in den Ostalpen. Deutsches Bergbau Museum, Bochum, pp. 129–134

Tomedi G, Töchterle U, Altenburger A (2006) Ein neu entdecktes Gräberfeld der Bronzezeit in Weer-Stadlerhof. ArchaeoTirol Kleine Schriften 5:65–73

Trixl S, Steidl B, Peters J (in press). Archaeology and zooarchaeology of the La Tène-Roman transition in the Province Raetia (100 BC–100 AD). Eur J Archaeol

Wiesner N (2009) Grabbau und Bestattungssitten während der Urnenfelderzeit im südlichen Mitteleuropa. Internationale Archäologie 110. Verlag Marie Leidorf, Rahden

Winghart S (1998) Produktion, Verarbeitung und Verteilung. Überlegungen zur Bedeutung metallischer Rohstoffe bei der Ausbildung politischer Systeme im südbayerischen Alpenvorland während der Bronzezeit. Vorträge des 16. Niederbayerischen Archäologentages 1998:99–113

Winghart S (1999) Die Wagengräber von Poing und Hart a. d. Alz. Evidenz und Ursachen spätbronzezeitlicher Elitenbildung in der Zone nordwärts der Alpen. In: Eliten in der Bronzezeit. Ergebnisse zweier Kolloquien in Mainz und Athen. Monographien Römisch-Germanisches-Zentralmuseum Mainz 43,2. Römisch-Germanisches Zentralmuseum, Mainz, pp. 515–532

Ziegler S, Streit B, Jacob DE (2016) Assigning elephant ivory with stable isotopes. In: Grupe G, McGlynn GC (eds) Isotopic landscapes in bioarchaeology. Springer, Berlin, pp. 213–220

Index

A
Adjusted Rand Index, 111
Aerosol, 231
Alpine war, 16, 50
Alps, 3, 4, 6, 7, 9–11, 15–17, 19, 39, 50–67, 76, 106, 113, 123, 124, 128–131, 134, 136, 146, 147, 158, 176, 181, 182, 184, 186, 187, 191, 197, 219–223, 233–241
Altitude, 7, 63, 66, 113, 130, 134, 153, 155, 156, 163, 164, 171, 173, 194
Altitude effect, 163–164, 168, 172, 173
Ambras, 204
Ampass, 14, 15, 146, 148, 163, 167, 169, 176
Amphorae, 57, 60–62, 65
Animal, 4, 8, 11, 13, 15, 28, 29, 33–35, 37 39, 41, 49–68, 82, 84, 86, 106–108, 113, 122–124, 134–136, 147, 153–155, 158, 163–168, 175–177, 179–181 183, 185, 186, 188–191, 193–195 211, 212, 219–221, 223, 231–233, 243–244, 246
Animal transfers, 62–64
Apatite, 33, 76, 77, 79, 86–88, 96, 97, 100, 128, 148–151, 164, 165, 168, 173–175, 180, 182, 184, 185, 187–190, 192–194, 213–218, 222, 232
Archaeofauna, 57, 136, 163, 244
Aubing, 55, 57, 243
Austria, 124, 158, 173, 174, 176, 181, 184, 186, 187, 212, 240

B
Bavaria, 4, 6, 7, 9, 11, 14, 82, 86, 100, 219, 220, 233–241
Berching-Pollanten, 146, 163, 181, 182, 184, 186, 189, 191
Bergisel, 146, 163, 165, 167
Bieberwier, 169
Bioapatite, 31–34, 76–81, 83, 88, 128, 134, 150–152, 168, 232
Bioarchaeology, 28–42, 106, 107, 180, 181
Biodiversity, 231, 232, 243
Biomineral, 30, 42, 77, 196, 232
Body mass, 54
Bone, 4, 29, 54, 76, 106, 128, 231
Bone remodelling, 62
Breeding history, 55
Brenner pass, 4, 9–11, 13, 50, 59, 76, 106, 128, 130, 134–136, 146–153, 155, 156, 158, 163–165, 168, 172–174, 176–181, 184, 186, 189, 191, 192, 194–197, 211, 219–221, 223
Brixen, 6, 7, 10, 14, 15, 134, 147, 163, 167, 170, 173, 174, 176, 181, 182, 186, 191, 192, 241–243
Brixlegg/Inn, 146
Bronze Age, 2, 5, 7–11, 77, 82, 92, 128, 163, 195, 233–241

C
Calcite, 78, 84, 85, 97, 100
Calcium, 30, 32, 36, 38, 39, 41, 77, 78, 148, 153, 177
Carbonate, 30–32, 35, 36, 77–79, 81, 86–88, 100, 130, 147–149, 164, 165, 168, 176, 177, 191
Carbonated hydroxyapatite, 30, 77, 78, 81, 88, 100
Cat, 56
Cattle, 38, 54, 55, 64, 65, 113, 134–136, 153–159, 163–167, 173, 174, 180, 182, 184, 186, 187, 192, 194, 244
α-cellulose, 148, 150, 168–173
Chalcopyrite, 234
Chicken, 56, 66
Cluster analysis, 155, 221

G. Grupe et al. (eds.), *Across the Alps in Prehistory*,
DOI 10.1007/978-3-319-41550-5

Clustering algorithm, 108, 109, 121, 122, 124
Collagen, 29–33, 35, 77, 78, 80, 87, 106 196, 231
Contamination, 39, 40, 76, 84, 87, 181
Copper, 2, 3, 6–9, 57, 234, 236–238, 241
Cremation, 9, 79, 81, 82, 87–91, 93, 96, 98–101, 128, 130, 134–136, 146–153, 155, 156, 158, 163–165, 168, 172–174, 176–181, 184, 186, 189, 191, 192, 194–197, 211, 219–221, 223, 233, 237, 238, 241, 245
Crystallite, 77, 79–81, 83, 88, 89, 96, 97, 100
Crystallite size, 80, 84–86, 88, 89, 96–98, 100, 196
Culture transfer, 30, 42, 76, 128, 136, 194, 195, 223, 233, 241, 242
Cut-off value, 135, 176, 180, 181, 192

D
Danube, 16, 17, 51, 134, 240, 244
Data mining, 42, 106, 108–116, 118–124, 158, 194, 195, 211, 222, 231, 232
Data structure, 110, 231
Database, 40, 230, 231, 233
Dentin, 30, 65, 196–198, 232
Deuterium, 33
Diffusion fractionation, 28
Dog, 55

E
Eching, 82, 92, 93, 96, 100, 146, 163, 186, 191, 219
Ehrwald, 169
Ellbögen, 15
Enamel, 30, 31, 36, 62, 63, 65, 66, 77, 196, 197, 232
Englschalking, 198
Equilibrium fractionation, 28
Erding, 146, 176
Exclusion principle, 37, 176, 194, 211
Expectation-maximization algorithm, 42
Experimental cremation, 82, 87–91, 194

F
Feature selection, 109–119, 123
Feeding behaviour, 63, 64
Flintsbach/Inn, 9
Forensic sciences, 29, 231
Forstinning, 211
Founder individuals, 66
Fourier Transform Infrared Spectroscopy (FTIR), 79, 82, 89, 92, 96, 98, 100, 101, 150
Freising, 146, 163, 165, 166, 176, 186, 189, 191
Fritzens, 12–14, 146, 147, 169
Fritzens-Sanzeno culture, 12–14, 16, 211, 241–243
Fügen, 205

G
Garching/Alz, 204
Gaul, 16, 19, 50, 51, 57, 58, 60–62, 64, 65, 244–246
Gaussian mixture model, 42, 109, 110, 121, 122, 124
Geological map, 29, 36, 37, 106, 131
Geology, 63, 176, 220
Germany, 4, 6, 16, 19, 56, 58, 106, 130, 158, 173, 181, 184, 186, 191, 212, 245, 246
Gernlinden, 203
Glass, 60, 149
GMM clustering, 221, 222, 232
Gneiss, 176
Grave goods, 11, 221, 238, 240, 243, 245, 246
Griesstetten, 146, 163, 166, 173, 186
Groundwater, 148, 163, 168–170, 177, 178
Grünwald, 146, 163, 176, 198
Günzburg, 19, 244–246

H
Hallstatt period, 11, 12, 56, 242
Hazelnut, 147, 148, 168
Heimstetten Group, 51, 55, 67, 243, 244, 246
Hofoldinger Forst, 211
Hohe Birga, 146, 174, 176
Horse, 54, 56, 57, 65
Hötting, 169, 219, 221
Human, 2, 29, 50, 76, 106, 128, 231
Hydrogen, 28, 31–34
Hydroxyapatite, 30, 31, 38, 77–79, 81, 86, 88, 100

I
Immigration, 6, 7, 232, 233, 236, 238, 243
Imperial Roman Times, 77, 128, 195, 219
Imst, 4, 169
Infrared spectroscopy, 77, 81

Inn-Eisack-Adige, 5–7, 11, 76, 106, 107, 113, 123, 128, 130, 134–136, 146–153, 155, 156, 158, 163–165, 168, 172–174, 176–181, 184, 186, 189, 191, 192, 194–197, 211, 219–221, 223, 232, 241, 244
Innsbruck, 5, 9, 10, 15, 146, 147, 176, 186, 238
Introduced stock, 54, 66
Isoscape, 29, 106, 232
Isotopic fingerprint, 40–42, 106, 108–116, 118–124, 130, 135, 136, 195–223, 230, 232, 233, 243
Isotopic fractionation, 28, 34, 242
Isotopic landscape, 3, 28–42, 177, 180, 230, 231
Isotopic map, 28, 37, 40, 42, 106, 108–113, 120–123, 128, 130, 134–136, 146–153, 155, 156, 158, 163–165, 168, 172–174, 176–181, 184, 186, 189, 191, 192, 194–197, 211, 219–221, 223, 230–233, 244
Isotopic mixing, 130, 176, 219
Italy, 4, 6, 11, 15, 16, 50, 51, 57–62, 64, 106, 123, 130, 158, 173, 174, 181, 184, 186, 187, 212, 244, 246

J
Julio-Claudian period, 57, 61

K
Kernel density, 153, 155, 156, 158, 159, 173, 174, 181, 182, 184, 186, 187, 191, 192
Kinetic fractionation, 28
Kirchbichl, 146, 169, 173, 176
Kirchheim, 204
Kitchenware, 51
Kitzbühel, 205
Kleinaitingen, 199, 202
Königsbrunn, 204
Kundl, 11, 14, 169, 242

L
Langengeisling, 204
Latitude, 113, 146, 153, 155, 156, 168, 171–173, 194
Latsch, 170, 172, 211, 219, 220, 243
Lattice parameter, 79, 80, 86, 87, 97, 100
Lead, 4, 28, 62, 79, 106, 128, 230
Livestock, 19, 52, 62, 66, 67, 243
Livestock husbandry, 54
Livestock melioration, 52, 54, 67
Local, 7, 29, 52, 81, 106, 128, 231
Longitude, 113–115, 118, 119, 153, 155, 156, 168, 171, 173

M
Manching, 146, 163, 174, 186, 189, 191
Mass spectrometry, 149–151
Mathematical outlier, 155, 173, 181, 182, 186, 191
Matrei, 7, 9, 170
Mediterranean foodstuff, 51, 57
Mediterranean lifestyle, 50, 57, 64
Meteoric water, 164, 168, 173
Micro-region, 30, 135, 191, 194, 211, 221–223, 238
Microstrain, 80, 82, 87, 98
Midden deposits, 57
Mieming, 146, 163, 169, 186
Migration, 2–4, 9, 16, 29, 30, 32–33, 35, 37, 39–41, 50, 67, 76, 107, 128, 130, 134–136, 164, 176, 180, 194, 195, 197, 198, 220, 222, 223, 230–233, 237, 238, 240–244, 246
Mineralogy, 194
Mining, 6, 7, 9, 15, 42, 106, 108–116, 118–124, 158, 194, 195, 211, 219, 222, 234, 236
Mixing diagram, 177, 180
Mixing model, 180
Mobility, 2–4, 6–17, 19, 30, 35, 37, 39–41, 53, 62–64, 66, 67, 106, 107, 109, 135, 136, 155, 180, 194, 195, 197, 219, 223, 232–242, 244, 245
Model prediction, 176–180
Modelling, 3, 29, 34, 181
Modern ocean water, 36
Moritzing, 242
Mühlau, 147
Mule, 56, 57, 65, 66
Multivariate analysis, 108
München, 146, 163, 176, 198

N
NBS 120c, 34, 149
NBS 982, 152
Nitrogen, 29, 32, 33, 35, 106, 231
Non-local, 3, 30, 36, 37, 40, 55, 62, 66, 67, 106, 108, 109, 113, 114, 121, 128, 135, 155, 176, 180, 181, 192, 194, 197, 211, 221, 231, 232, 238, 240, 246

O
Obermenzing, 200
$\delta^{18}O_{carbonate}$, 134, 164–168
Ocean water, 113, 177
$\delta^{18}O_{cellulose}$, 168, 171–173
$\delta^{18}O_{phosphate}$, 33, 34, 128, 134, 135, 149, 153, 155, 158, 159, 161, 163–168
$\delta^{18}O_{precipitation}$, 130, 158, 164
Ore deposits, 39, 134, 181, 219, 236, 239, 241
$\delta^{18}O_{water}$, 34, 153, 155, 158, 163, 164, 171–173
Oxygen, 28, 32–34, 40–42, 62–64, 108, 109, 113–120, 122, 124, 128, 130, 135, 148–150, 153, 158–165, 168, 194–196, 244

P
Pack animal, 15, 53, 54, 56, 65–67, 244
Palaeoclimate, 34
Palaeodiet, 29, 35, 106, 164
Pasturing, 63, 64
$^{206}Pb/^{204}Pb$, 39, 42, 134, 151, 152, 155, 186, 189, 191–193, 211, 218, 219
$^{206}Pb/^{207}Pb$, 39, 42, 134, 151, 152, 155, 181, 182, 184–186, 211, 215, 220, 221
$^{207}Pb/^{204}Pb$, 39, 42, 134, 151, 186, 187, 189–191, 211, 217, 219, 221
$^{208}Pb/^{204}Pb$, 39, 42, 134, 151, 186–188, 211, 216, 219, 221
$^{208}Pb/^{207}Pb$, 42, 134, 151, 155, 181, 182, 184, 211, 214, 221
Pestenacker/Lech, 146, 189, 191
Pfaffenhofen/Inn, 146, 147, 178–180, 192
Pfatten, 8, 15, 170, 242
Phosphate, 30–32, 41, 77, 79, 89, 92, 93, 99, 100, 106, 149, 150, 164, 165, 168
Phosphorus, 165
Photosynthesis, 28, 34
Phyllite, 174
Physiology, 63
Pig, 38, 64, 113, 134–136, 153–157, 159, 163, 164, 166, 167, 173, 174, 180, 182, 184, 187, 194, 233
Poing, 204
Population admixture, 42, 128, 195, 197, 211, 223, 230–232
Potter stamps, 57, 59
Precipitation, 28, 33, 34, 41, 113, 130, 135, 147–149, 163, 164, 168–170, 177
Prediction, 29, 34, 37, 106, 109, 177, 179, 180
Probability density function, 122
Profile analysis, 81
Provenance analysis, 29, 33, 41, 61, 106, 108, 109, 113, 121–124, 136, 155, 176, 219, 230–233

Q
Quartz, 84, 97, 151, 174

R
Radfeld-Mauken, 146
Raetia, 16, 19, 51–62, 64–68, 243–246
Recrystallization, 78, 79, 81
Red deer, 38, 64, 113, 134–136, 153–159, 163, 164, 166, 167, 173, 174, 181, 182, 184, 186, 187, 194
Reference clustering, 110–112, 114–120
Rietveld analysis, 96
Roman conquest, 19, 50, 52, 56, 57, 67
Roman times, 19, 50, 52, 54, 55, 61, 163, 233, 244
Roppen, 169

S
Sanzeno, 12, 147, 163, 167, 168, 170, 176, 192, 241–243
Schwabmünchen, 146, 174
Secondary phase, 84, 100
Shoulder height, 54, 55
Siebeneich, 167, 170
Similarity search, 106, 108–116, 118–124, 223, 233
Sires, 52, 65, 66
Skeleton, 30–33, 35, 38, 39, 41, 42, 100, 128, 130, 153–158, 181, 195–197, 211, 232, 233, 242, 243
Skull morphology, 54
Soil, 28, 29, 31, 34–40, 63, 76, 78, 84–86, 100, 107, 130, 134, 135, 147, 148, 152, 155, 177, 178, 180, 191, 196, 211, 231, 232
Soil admixture, 63
Spatial clustering, 109, 121–123
Spatial redundancy, 37, 42, 176, 181, 186, 194, 219, 222
Spectral decomposition, 79, 82, 89, 93
SRM 1400, 149, 151, 152
SRM 987, 33, 151
$^{87}Sr/^{86}Sr$, 29, 32, 35–38, 41, 42, 106, 128, 130, 134, 147, 148, 151, 153, 155, 173–181, 211, 213, 219–221
Straubing group, 233

Strontium, 29, 62, 79, 106, 128, 232
Structural carbonate, 32, 35, 79, 148, 149, 164, 165, 168
Structural redundancy, 112, 116–120
Structural relevance, 112, 116–120
Sulfur, 32, 33
Supply patterns, 61

T
Tablewares, 57–59, 61, 65
Terra Sigillata, 58–61, 65
^{232}Th, 38, 186
Thaur, 6, 7, 146, 176
Tooth, 30, 31, 41, 62, 63, 65, 77, 151, 196, 197, 232
Trade, 2–4, 6–17, 19, 29, 30, 33, 37, 40, 50, 52, 53, 56–62, 64, 65, 76, 106, 107, 109, 128, 135, 136, 180, 194, 195, 223, 230–232, 236, 244
Transhumance, 15, 64, 66
Trudering, 146, 176, 211

U
^{235}U, 38, 186, 187
^{238}U, 38, 191
Unit cell, 79, 81, 86, 87, 194
Univariate statistics, 29, 135, 153, 155, 157, 180, 194, 219, 232
Unsupervised learning, 110
Unterhaching, 146, 163, 165, 166, 176, 186
Urnfield Period, 9, 211, 233, 234, 236, 239, 240

V
Vegetation, 34, 35, 37, 38, 147, 171, 177, 178, 180, 232
Via *Claudia Augusta*, 51, 54, 59–62, 64, 65, 67
Völs, 169
Vomp, 238

W
Waging am See, 201
Wehringen, 146
Wenns, 8, 14, 169, 173
Wiesberg, 148
Wiesing, 14, 146, 163, 167, 169, 179, 180
Wilten, 169
Wood, 98, 147, 148, 150, 168, 173, 195, 231
Wörthsee, 146

X
X-ray diffraction (XRD), 77, 79–82, 84, 86, 88, 93, 96–101

Z
Zambana, 147, 163–165, 167, 170, 172